Détermination de la composition en acyles gras des glycérolipides et glycérophospholipides par techniques séparatives couplées à la spectrométrie de masse haute résolution

Sonia Abreu

▶ **To cite this version:**

Sonia Abreu. Détermination de la composition en acyles gras des glycérolipides et glycérophospholipides par techniques séparatives couplées à la spectrométrie de masse haute résolution. Chimie analytique. Université Paris-Saclay, 2023. Français. NNT : 2023UPASF033 . tel-04279242

HAL Id: tel-04279242
https://theses.hal.science/tel-04279242

Submitted on 10 Nov 2023

HAL is a multi-disciplinary open access archive for the deposit and dissemination of scientific research documents, whether they are published or not. The documents may come from teaching and research institutions in France or abroad, or from public or private research centers.

L'archive ouverte pluridisciplinaire **HAL**, est destinée au dépôt et à la diffusion de documents scientifiques de niveau recherche, publiés ou non, émanant des établissements d'enseignement et de recherche français ou étrangers, des laboratoires publics ou privés.

THÈSE DE DOCTORAT

NNT : 2023UPASF033

université PARIS-SACLAY

Détermination de la composition en acyles gras des glycérolipides et glycérophospholipides par techniques séparatives couplées à la spectrométrie de masse haute résolution

Thèse de doctorat de l'université Paris-Saclay

École doctorale n° 571, Sciences chimiques : molécules, matériaux, instrumentation et biosystèmes (2MIB)
Spécialité de doctorat : Chimie
Graduate School : Chimie. Référent : Faculté de pharmacie

Thèse préparée dans l'unité de recherche **Lipides : Systèmes Analytiques et Biologiques - Lip(Sys)^2 (Université Paris-Saclay)**
sous la direction de **Pierre CHAMINADE**, Professeur des Universités

Thèse soutenue à Orsay, le 12 juin 2023, par

Sonia ABREU

Composition du Jury

Juliette JOUHET Directrice de recherche, Laboratoire de Physiologie Cellulaire & Végétale, CNRS, INRAE, CEA, Université de Grenoble Alpes	Rapporteur
Philippe SOUDANT Directeur de recherche, Laboratoire des Sciences de l'Environnement Marin, CNRS, Université de Bretagne Occidentale	Rapporteur
Corinne BURE Ingénieure de recherche HDR, Institut européen de chimie et biologie, CNRS, Inserm, Université de Bordeaux	Examinatrice
Christophe JUNOT Directeur de recherche, Département Médicaments et Technologies pour la Santé, CEA, INRAE, Université Paris-Saclay	Président du jury

Titre : Détermination de la composition des acyles gras des glycérolipides et glycérophospholipides par techniques séparatives couplées à la spectrométrie de masse haute résolution..... ....

Mots clés : acyles gras ; triacylglycérols ; phospholipides ; lipides ; chromatographie ; spectrométrie de masse

Résumé : Les acyles gras (FAs) représentent le principal élément constitutif des lipides complexes (glycérolipides / phospholipides / sphingolipides). Leur structure varie en fonction de leur fonctionnalisation, nombre de carbones, nombre et position d'insaturations. Cette variété est à l'origine du très grand nombre d'espèces lipidiques et de la complexité de leur analyse.

Les travaux menés au cours de cette thèse ont démontré, au travers de trois publications, que l'évaluation de la distribution FAs des glycérolipides et phospholipides était accessible grâce à l'intensité des ions fragments $[monoacylglycérol+H- H_2O]^+$ (ions B) produits en source APPI/APCI-HRMS, lors du couplage à la FIA ou la NPLC.

Les bases de ce nouveau concept ont été posées via l'étude des triglycérides d'huiles végétales.
Il a été observé que la distribution des intensités des ions B était directement reliée à la distribution des FAs, sauf pour le FA polyinsaturé C18:3.
Des coefficients de pondération des intensités des ions B ont été calculés pour compenser les différences d'ionisation. Globalement, un coefficient deux fois plus important a été appliqué aux intensités des ions B(18 :3) pour compenser sa plus faible intensité.

Le concept a ensuite été étendu aux phospholipides (PLs). Pour les extraits contenant uniquement des diacyl-PLs, la transposition est également directe. La nature de la tête polaire n'a pas eu d'influence sur la formation des ions B.

Pour les extraits contenant à la fois des diacyl-PLs et des plasmalogènes (fonction éther vinylique) une séparation préalable doit être réalisée. En effet, la formation des ions B n'a pas lieu au même degré pour ces deux sous-classes.
Une hydrolyse par des vapeurs d'acide chlorhydrique a permis de rompre spécifiquement les liaisons éthers vinyliques. Les plasmalogènes sont alors transformés en Lyso-PLs et aldéhydes.
Ces extraits ont également la particularité de contenir des teneurs importantes de FAs polyinsaturées. Par analogie avec l'étude des TGs, un coefficient pondérateur de deux a été appliqué aux intensités des ions B de ces FAs.

Pour accéder à la distribution des alkényls gras des plasmalogènes, un concept similaire à celui des ions B a été mis en œuvre avec succès.
De plus, un schéma de fragmentation a été proposé pour les plasmalogènes PC lors de l'utilisation de la source APCI.

Enfin, notre nouveau concept a été mis en œuvre sur des extraits lipidiques de souches *Yarrowia Lipolytica* (levure oléagineuse) modifiées pour favoriser la production de FAs à chaînes impaires. La distribution des FAs au sein de chaque classe de lipides a été évaluée et le concept a été étendu à deux autres classes de lipide (Diglycérides-DG et glucuronosyl diacylglycerol-GlcADG).

Title : Determination of the fatty acyl composition of glycerolipids and glycerophospholipids by separation techniques coupled with high resolution mass spectrometry ....

Keywords : fatty acyls; triacylglycerols; phospholipids; lipids; chromatography; mass spectrometry

Abstract : Fatty acyls (FAs) represent the main constituent element of complex lipids (glycerolipids / phospholipids / sphingolipids). Their structure varies according to their functionalization, number of carbons, number and position of unsaturations. This variety is at the origin of the very large number of lipid species and the complexity of their analysis.

The work carried out during this thesis has demonstrated, through three publications, that the evaluation of the FAs distribution of glycerolipids and phospholipids was accessible thanks to the intensity of the fragment ions $[monoacylglycerol+H-H2O]^+$ (B ions) produced in APPI/APCI-HRMS source, during coupling to the FIA or the NPLC.

The foundations of this new concept were laid through the study of vegetable oil triglycerides.

It was observed that the intensity distribution of B ions was directly related to the distribution of FAs, except for the polyunsaturated FA C18:3.

Weighting coefficients of the intensities of the B ions have been calculated to compensate for the differences in ionization. Overall, a coefficient twice as large was applied to the intensities of the B(18:3) ions to compensate for its lower intensity.

The concept was later extended to phospholipids (PLs). For extracts containing only diacyl-PLs, the transposition is also direct. The nature of the polar head had no influence on the formation of B ions.

For extracts containing both diacyl-PLs and plasmalogens (vinyl ether function) a prior separation must be carried out. Indeed, the formation of B ions does not take place to the same degree for these two subclasses.

Hydrolysis by hydrochloric acid vapors made it possible to specifically break the vinyl ether bonds. The plasmalogens are then transformed into Lyso-PLs and aldehydes.

These extracts also have the particularity of containing high levels of polyunsaturated FAs. By analogy with the study of TGs, a weighting coefficient of two was applied to the intensities of the B ions of these FAs.

To access the fatty alkenyl distribution of plasmalogens, a concept similar to that of B ions has been successfully implemented.

Additionally, a fragmentation scheme has been proposed for PC plasmalogens when using the APCI source.

Finally, our new concept was implemented on lipid extracts of Yarrowia Lipolytica strains (oleaginous yeast) modified to promote the production of odd-chain FAs. The distribution of FAs within each lipid class was evaluated and the concept was extended to two other lipid classes (Diglycerides-DG and glucuronosyl diacylglycerol-GlcADG).

COLLABORATIONS

❖ Université Paris-Saclay - IUT d'Orsay

13 Av. des Sciences, 91190 Gif-sur-Yvette

❖ UMS IPSIT, Service d'Analyse des Médicaments et Métabolites (SAMM)

17 Av. des Sciences, 91400 Orsay

❖ Institut des Corps Gras et produits apparentés (ITERG)

ZA PESSAC, 11 Rue Gaspard Monge CS 20428, 33610 Canéjan

❖ Plate-forme de Métabolomique et fluxomique de Toulouse (METATOUL)

135 Av. de Rangueil, 31077 Toulouse

❖ Institut national de recherche pour l'agriculture, l'alimentation et l'environnement (INRAE)

Imp. Yvette Cauchois, 44300 Nantes

ENCADREMENT

Ce projet de thèse a été réalisé sous la direction du Professeur Pierre CHAMINADE au sein du laboratoire de recherche - Lipides : Systèmes Analytiques et Biologiques - Lip(Sys)², Faculté de Pharmacie, Université Paris Saclay

17 Av. des Sciences, 91400 Orsay

FINANCEMENT

Ce projet a été réalisé dans le cadre de mon activité d'ingénieure d'étude au sein du laboratoire Lip(Sys)².

Remerciements

Au Docteur Juliette JOUHET ainsi qu'au Docteur Philippe SOUDANT, pour avoir accepté de juger la qualité de mes travaux de thèse en tant que rapporteurs.

Au Docteur Corinne BURE ainsi qu'au Docteur Christophe JUNOT pour avoir accepté d'examiner ces travaux.

A l'Université Paris-Saclay et la Faculté de Pharmacie à travers le Professeur Marc PALLARDY (Doyen de la Faculté), Madame Sylvie ETIEMBLE (Déléguée de la Directrice Générale des Services), Madame Lorraine THIRION (responsable du Service du Personnel) et le Professeur Gilles PONCHEL (responsable de la filière VAE) pour m'avoir permis de réaliser mon projet de thèse en parallèle de mon activité d'Ingénieure d'Etudes.

Au Professeur Gilles PONCHEL pour avoir accepté d'être membre extérieur de mon comité de suivi de thèse ainsi que pour votre gentillesse et votre bienveillance lors de nos échanges.

Au Professeur Pierre CHAMINADE pour m'avoir fait l'honneur d'encadrer ce travail de thèse. Vous m'avez transmis un savoir et un savoir-faire précieux qui m'ont permis d'être là où je suis aujourd'hui. Votre confiance et la liberté scientifique que vous m'accordez me permettent de m'épanouir dans mon travail. Je vous remercie également pour vos conseils et votre soutien tout au long de ces années.

Au Docteur Sylvie HERON ainsi qu'au Professeur Alain TCHAPLA pour nos échanges scientifiques, vos relectures et votre bienveillance à mon égard. C'est un honneur pour moi d'avoir mon nom à côté des vôtres sur ces travaux. J'ai également une pensée chaleureuse pour l'équipe du LETIAM qui m'a toujours bien accueillie, notamment Myriam, Marine, Kaouther et Jean.

Au Docteur Marie-Joëlle VIROLLE ainsi qu'au Docteur Jean-Marc NICAUD et leurs équipes (Clara et Young-Kyoung) pour leur gentillesse, nos échanges et de m'avoir permis de mettre en œuvre notre méthode sur vos bactéries et levures de prédilection. Cela est très gratifiant pour moi de voir l'apport de mon travail dans vos thématiques de recherches.

Au Docteur Florent JOFFRE, au Docteur Justine BERTRAND-MICHEL, à Jessica DALLOUX-CHIOCCIOLI, au Docteur Anne MEYNIER et à Alice KERMARREC pour m'avoir aidé à réaliser ce travail. Votre expertise dans l'analyse des FAs par GC-FID a été un prérequis à ce travail, sans vous ce travail n'aurait pas pu se faire.

Au Docteur Audrey SOLGADI et Bastien PROST pour votre précieuse aide scientifique et technique en spectrométrie de masse, lors de ces travaux et de tous les autres. Vous êtes toujours enthousiastes pour relever de nouveaux défis et c'est un plaisir de travailler avec vous.

A l'ensemble de mes collègues pour tous les moments partagés depuis ces nombreuses années.

Aux étudiants qui ont partagé un bout de chemin avec notre équipe et avec qui j'ai beaucoup appris, notamment Laurent, Ricardo, Benoit, Nolwenn, Spiro, Kodjo…

A Marie-France et Jean, ma famille de cœur, pour m'avoir permis de poursuivre mes études.

A ma famille, celle de mon conjoint et à mes amis pour tout votre soutien.

A Ralph pour m'avoir supporté dans cette aventure et dans toutes les autres aventures de la vie.

A ma fille, Fanny.

TABLE DES MATIERES

INTRODUCTION GENERALE 21

PARTIE I : ETUDE BIBLIOGRAPHIQUE 27

Chapitre I. Généralités sur les lipides 27

1. Définition 29
2. Classification 30
   - 2.1 Acyles gras 31
   - 2.2 Glycérolipides 32
   - 2.3 Glycérophospholipides 33
   - 2.4 Sphingolipides 37
   - 2.5 Stérols 38
3. Fonctions biologiques 39
   - 3.1 Membranes cellulaires 39
   - 3.2 Messagers cellulaires 41
   - 3.3 Stockage d'énergie 41

Chapitre II. Analyse lipidomique 43

1. Introduction 45
2. Extraction 47
3. Séparations par chromatographie en phase liquide et supercritique 48
4. Spectromètres de masse 53
   - 4.1 Sources d'ionisation 53

4.2 Mobilité ionique 59

4.3 Analyseurs 60

4.4 Modes d'acquisition de données en spectrométrie de masse 64

4.4.1 L'acquisition par balayage MS 64

4.4.2 Modes de fragmentation 65

4.4.3 Modes d'acquisition MS^2 66

4.5 Traitement des données 67

4.5.1 Traitement des données brutes 67

4.5.2 Identification et annotations 69

4.5.3 Quantification 73

5. Exemples d'approches lipidomiques 77

Chapitre III. Optimisation des conditions chromatographiques en phase normale pour l'analyse des lipides et techniques de détection associées 85

1. Introduction 87

2. Publication numéro 1 87

3. Conclusion 107

Chapitre IV. Acyles gras et voies metaboliques 109

1. Introduction 111

2. Voies métaboliques des acides gras libres (FFA) 111

3. Voies métaboliques des glycérolipides et des PLs 112

4. Lipidome et pathologies 113

5. Lipidome, nutrition et santé 114

Chapitre V. Analyse des acyles gras : méthodes usuelles 117

1. Analyse des FAMEs par GC-FID et GC-MS 119

1.1 Séparation et isolement 119

1.2 Conversion des FAs en FAMEs 122

1.3 Conversion des chaînes alkényles en DMAs 127

1.4 Séparation des FAMEs et DMAs par GC 127

1.5 Couplage de la GC au FID et à la MS 129

2. LC-MS/MS 131

PARTIE II : RESULTATS 133

INTRODUCTION : ANALYSE DES ACYLES GRAS PAR LES IONS B 135

1. Origine du concept 135

2. Fragmentation des TGs et PLs en mode positif 136

Chapitre VI. Evaluation de la distribution des acyles gras des triacylglycérols par les ions B 141

1. Introduction 143

2. Publication 2 144

3. Conclusion 155

Chapitre VII. Evaluation de la distribution des acyles gras des phospholipides et des plasmalogènes par les ions B 159

1. Introduction 161

2. Publication 3 162

3. Conclusion 179

Chapitre VIII. Réajustement des lipides dans les souches productrices d'acides gras à chaînes impaires de *Yarrowia lipolytica* 181

1. Introduction 183

2. Publication 4 183

3. Conclusion 204

DISCUSSION ET CONCLUSION GENERALE 207

REFERENCES BIBLIOGRAPHIQUES 217

ANNEXES

ANNEXE I. Supplémentaires publication 1 235

ANNEXE II. Supplémentaires publication 2 249

ANNEXE III. Supplémentaires publication 3 267

ANNEXE IV. Supplémentaires publication 4 279

Collaboration sur l'étude des lipides chez les bactéries du genre Streptomyces 305

ANNEXE V. Impact de la disponibilité du phosphate sur la teneur en lipides membranaires des souches modèles, *Streptomyces lividans* et *Streptomyces coelicolor* 309

1. Introduction 311
2. Publication 5 312
3. Conclusion 326

ANNEXE VI. Corrélation négative entre la teneur en lipides et l'activité antibiotique chez *Streptomyces* : règle générale et exceptions 327

1. Introduction 329
2. Publication 6 329
3. Conclusion 349

ANNEXE VII. L'inhibition de la production d'antibiotiques chez *Streptomyces coelicolor* surexprimant le régulateur TetR SCO3201 est corrélée aux modifications du lipidome de la souche 351

1. Introduction 353
2. Publication 7 353
3. Conclusion 370

Liste de figures

Figure 1: Classification des lipides [31]. 30
Figure 2: Exemples de structures d'acyles gras. 32
Figure 3: Exemples de structures de glycérolipides. 33
Figure 4: Exemples de structures de glycérophospholipides. 35
Figure 5: Exemples de structure de plasmalogènes et de plasmanyl. 36
Figure 6: Teneur en plasmalogène dans différents tissus de mammifères [35]. 36
Figure 7: Exemples de sphingolipides. 37
Figure 8: Structure du noyau de base des stérols et exemples de stérols. 38
Figure 9: Représentation schématique d'une membrane. 39
Figure 10: Membranes cellulaires : Synthèse lipidique et composition à l'état d'équilibre (A) ; Mécanismes générant une distribution lipidique asymétrique (B) [11]. 40
Figure 11: Schéma des domaines de recherche omiques [36]. 45
Figure 12: Analyse lipidomique basée sur la LC-MS [17]. 46
Figure 13: Focus sur les études lipidomiques basées sur la LC-MS : matrices analysées (A) et protocoles d'extraction (B) [17]. 47
Figure 14: Utilisation de systèmes chromatographiques (A), de modes d'ionisation (B) et d'analyseurs de masse (C) dans des papiers lipidomiques à base de LC-MS [17]. 48
Figure 15: Principe de séparation des lipides utilisant différentes techniques chromatographiques : RPLC (A), NPLC (B) et HILIC (C) [47]. 49
Figure 16 : Espace chimique des lipides [47]. 50
Figure 17 : Séparations de lipide en mode HILLIC [49]. 51
Figure 18 : Séparation d'un mélange de standards de lipides par UHPSFC/ESI^{+}-MS [52]. 52
Figure 19 : Exemple de schémas de sources APCI, APPI et ESI ainsi que leur domaine d'application [54]. 53
Figure 20 : Espèces ioniques majoritaires dans une source APCI : en l'absence de vapeurs de solvants LC (A) et en présence de vapeurs de solvants LC (B) [55]. 55
Figure 21 : Source APPI, effets de la phase mobile sur : la surface du pic (a), l'intensité de base (b) et le rapport signal sur bruit (S/N) de l'ester méthylique d'EPA (m/z 317) (c) [58]. 57
Figure 22 : Source ESI : interface (A) et mécanismes d'ionisation (B) [56]. 58
Figure 23 : Schéma de l'instrument Agilent IM-QTOF [65]. 59
Figure 24 : Analyses IM-MS de standards d'acides gras avec différents emplacements et orientations de doubles liaisons [64]. 59
Figure 25 : Schémas des principaux analyseurs utilisés pour l'analyse des lipides [71]. 60
Figure 26: Comparaison de la résolution à R = 25 000 et à R = 100 000 à m/z 200 (A) et variation de la résolution en fonction du rapport m/z (B) [73]. 62
Figure 27: Représentation de l'exactitude et de la précision [74]. 62
Figure 28: Schéma du Thermo Orbitrap Velos Pro LC-MS [75]. 63
Figure 29: Photographie et spécifications du Thermo Orbitrap Velos Pro Orbitrap [75]. 63
Figure 30: Modes de détection MS : analyse complète (full scan), surveillance des ions sélectionnés (SIM), surveillance des réactions multiples (MRM) & (SRM) et surveillance de réaction parallèle (PRM) [77]. 64
Figure 31: Figure schématique des voies de dissociation en mode CID et HCD [79]. 65
Figure 32: Schémas des modes d'acquisition: DDA (a) ; AIF, MS^{E} (b) et SWATH (c) [81]. 67
Figure 33: Flux de travail en lipidomique non ciblé et flux de travail de traitement de données basé sur le logiciel open source MS – DIAL [81]. 70

Figure 34: Schéma de la combinaison d'une correspondance 4D (m/z ; RT ; CCS (collision cross-section) et MS/MS) pour l'identification des lipides dans la lipidomique non ciblée basée sur IM-MS [91]. 71
Figure 35: Niveaux de résolution structurale et nomenclatures associées [92]. 72
Figure 36 : Effet de la concentration de PC saturées (A et B) et insaturés © sur la réponse de l'instrument (trappe ionique) [108]. 76
Figure 37: Distribution de lipides dans des extraits de deux microalgues et d'une plante supérieure. Chaque classe de lipides a été quantifiée par TLC-GC-FID, LC-MS/MS-Stds et LC-MS /MS -QC [19]. 77
Figure 38: Distribution des FAs des MGDG, PC et TG issues des extraits de deux microalgues et d'une plante supérieure. La distribution a été calculée suivant la méthode TLC plus GC-FID et la méthode MS/MS-QC [19]. 78
Figure 39: Composition lipidique du NIST SRM 1950, selon le nombre d'espèces lipidiques (A) et la concentration (B) [115]. 80
Figure 40: Comparaison des quantités des classes de lipides les plus concentrées (A) et les moins concentrées (B) entre l'étude de Bowden et al. [115] et l'étude LIPID MAPS [14]. Figure extraite de l'étude [115]. 81
Figure 41: Exactitude des données de l'essai inter-laboratoire utilisant le kit p400HR par rapport aux données consensuelles pour le NIST SRM-1950 [117]. 83
Figure 42: Séparation de lipides par classe [20]. Sont indiqués en bleu les lipides étudiés pour le développement du nouveau concept et en vert les lipides auquel le concept pourrait être étendu. 107
Figure 43: Biosynthèse des acides gras à longue et très longue chaîne chez les mammifères [144]. 112
Figure 44: Synthèse des glycérolipide et PLs à partir d'acides gras à longue chaîne [145]. .. 113
Figure 45: Localisation de la voie des espèces lipidiques dérégulées détectées dans le LCR post-mortem dans la maladie de Parkinson [154]. 114
Figure 46: Bioactivités des PLs enrichis en DHA/EPA dans les aliments marins [161]. 116
Figure 47: Instruments CAMAG® pour analyses HPTLC (https://anchrom.in). 120
Figure 48: Séparation de lipides sur plaque TLC bidimensionnelle [165]. 120
Figure 49: Illustration schématique d'une procédure de séparation de lipide par classe réalisée par SPE [169]. 121
Figure 50: Image d'une plaque HPTLC utilisée pour séparer des extraits de lipides totaux (a) et leurs FAMEs correspondant (b) [172]. 124
Figure 51: Comparaison de l'efficacité de trois méthodes de dérivatisation pour la génération de FAMEs par HPTLC [172]. 125
Figure 52: Comparaison de l'efficacité de six méthodes de dérivatisation pour la génération de FAMEs par GC-FID [173]. 126
Figure 53: Séparation de FAMEs et de DMAs par GC-FID réalisée sur une colonne CP-Sil 88 - site internet Restek. 128
Figure 54: Séparation de DMAs et FAMEs issue de graisse intramusculaire d'agneau par GC-FID [178]. 129
Figure 55: Gauche : courbes d'étalonnage du FAME 18:0 obtenue par GC-FID (a), QP-MS (b) et IT-MS (c). Droite : facteurs de réponse pour une série de FAMEs saturés (a) et une série de FAMEs insaturés (b) obtenus par GC-FID et QP-TIC/QP-SIM/IT-TIC/IT-SIE [179]. IT, ion trap; QP, quadrupole; SIE, selected ion extraction; SIM, selective ion monitoring; TIC, total ion count. 130
Figure 56: Comparaison des méthodes LC-MS et GC-FID pour l'obtention de la distribution des FAs. Préparation des échantillons (a). Variabilité intra- et inter-journalière de la

concentration en FAs selon les deux méthodes dans : le plasma humain (b) ; l'huile de tournesol (c) et l'huile de lin (d) [182]. 131
Figure 57: Gauche : schéma de fragmentation des TGs [186]. Droite : schéma de fragmentation des PC [187]. Des illustrations ont été ajoutées aux schémas d'origine. 137
Figure 58: Spectre full scan des TGs issus de l'huile d'olive (a) ; zoom dans la gamme m/z correspondante aux ions B (b) ; pourcentage des FAs obtenus par GC-FID et par les intensités des ions B (c). 138
Figure 59: Spectre full scan des PC extraits du cerveau de bœuf (a) ; zoom dans la gamme m/z correspondante aux ions B (b) ; distribution en pourcentage des FAs par GC-FID et par les intensités des ions B (c). 138
Figure 60: Biosynthèse des lipides d'ornithine (OL) chez *S. coelicolor* [195]. 311

Liste des tableaux

Table 1 : Réactions d'ionisation dans la source APCI : en mode d'ionisation positif (A) et en mode d'ionisation négatif (B) [57]. 55
Table 2 : Energies d'ionisation de gaz API, solvants LC, dopants, et énergies émises par les lampes UV utilisées en APPI [55].API- ionisation à pression atmosphérique ; IE- ionisation électronique ; PA- affinité protonique. 55
Table 3 : Réactions d'ionisation dans la source APPI : en mode d'ionisation positif (A) et en mode d'ionisation négatif (B) [57]. 57
Table 4 : Comparaison des caractéristiques et spécifications des analyseurs de masse couramment utilisés pour la protéomique [72]. 61
Table 5: Comparaison des logiciels d'identification des lipides [87]. 68
Table 6: Conditions d'affectation régiochimique des FAs aux positions sn-1, sn-2 et sn-3 des PLs et glycérolipides [19]. 72
Table 7: Synthèse des méthodes de transméthylation décrites dans la norme NF EN ISO 12966-2. 123

Abréviations

ACT	Actinorhodine
ADN	Acide DésoxyriboNucléique
AIF	Fragmentation des ions de toute la gamme de masse / All Ion Fragmentation
ANR	Agence Nationale de la Recherche
APCI	Ionisation chimique à pression atmosphérique / Atmospheric Pressure Chemical Ionisation
APPI	Ionisation par photoionisation à pression atmosphérique / Atmospheric Pressure PhotoIonisation
ARN	Acide RiboNucléique
ATP	Adénosine TriphosPhate
CCS	Collision Cross-Section
CE	Esters de cholestérol
CID	Dissociation induite par collision après activation résonnante / Collision Induced Dissociation
Corona-CAD®	Détecteur d'aérosol chargé
CV	Coefficient de Variation
DDA	Acquisition des données dépendantes / Data Dependent Acquisition
DEDL	Détecteur Evaporatif à Diffusion de la Lumière
DG	Diacylglycerols
DHA	Acide docosahexaénoïque
DIA	Acquisition données indépendante / Data Independent Acquisition
DMAs	Diméthylacétals
DMS	Spectrométrie de mobilité différentielle
EPA	Acide eicosapentaénoïque
ESI	Ionisation par électrospray / Electrospray Ionisation
FAMEs	Acides gras d'ester méthylés / Fatty Acid Methyl Esters
FAs	Acyles gras / Fatty Acyls
FFAs	Acides gras libres / Free Fatty Acids
FIA	Analyse par injection en flux continu, Flow Injection Analysis
FID	Détecteur à ionisation de flamme
FT-ICR	Résonance Cyclotronique des ions à transformée de Fourier / Fourier-Transform Ion-Cyclotron Resonance
FWHM	Largeur à mi-hauteur / full width at half maximum
GC	Chromatographie en phase gazeuse / Gas Chromatography
GlcADG	Glucuronosyl diacylglycérol
GlcCers	GlucosylCéramides
GSLs	Glycosphingolipides
HCD	Dissociation induite par collision à haute énergie après activation non-résonnante/Higher energy Collision induced Dissociation
HILIC	Chromatographie liquide d'interactions hydrophiles / Hydrophilic Interaction Liquid Chromatography
HPTLC	High Performance Thin Layer Chromatography

HRMS	Spectrométrie de masse à haute résolution / High Resolution Mass Spectrometry
Ions A	$[DG+H-H2O]^+$
Ions B	$[MG+H-H2O]^+$
IM	Mobilité ionique / Ion Mobility
IT	Trappe ionique / Ion trap
LC	Chromatographie en phase liquide / Liquid Chromatography
LC-MS	Chromatographie Liquide couplée à la Spectrométrie de Masse
LCR	Liquide CéphaloRachidien
LIT	Trappe ionique linéaire / Linear Ion Trap
LOD	Limite de détection
LOL	Lyso Ornithines Lipides
LOQ	Limite de quantification
LPA	Acide lysophosphatidique
LPC	Lysophosphatidylcholine
LPE	Lysophosphatidyléthanolamine
LPS	Lysophosphatidylserine
m/z	Rapport masse/charge
MG	Monoacylglycerols
MP	Maladie de Parkinson
MRM	Multiple Reaction Monitoring
MS	Spectrométrie de masse / Mass Spectrometry
MS^1	Full scan
MS^2 (MS/MS)	Spectrométrie de masse en tandem / Tandem Mass Spectrometry
NAPE	N-Acylphosphatidylethanolamines
NPLC	Chromatographie Liquide à polarité de Phase Normale
OL	Ornithines lipides
PA	Acide phosphatidique
PC	Phosphatidylcholine
PE	Phosphatidyléthanolamine
PG	Phosphatidylglycérol
PI	Phosphatidylinositol
PIMs	Phosphatidylinositol mannosides
PIP	Phosphatidylinositol phosphates
PLs	Phospholipides
P-PLs	Plasmalogènes
PRM	Parallel Reaction Monitoring
PS	Phosphatidylsérine
PUFAs	Acides gras polyinsaturés / Polyunsaturated Fatty Acids
Q	Quadripôle
QC	Contrôle qualité / Quality Control
QqQ	Triple quadripôle
RED	Undecylprodigiosin
RMN	Résonance Magnétique Nucléaire

RPLC	Chromatographie Liquide à polarité de Phases Inversée / Reverse Phase Liquid Chromatography
RT	Temps de rétention / retention time
SE	Esters de stérol
SFC	Chromatographie en phase supercritique / Supercritical Fluid Chromatography
SIM	Selective Ion Monitoring
SM	Sphingomyélines
SPE	Extraction sur phase solide / Solid Phase Extraction
SQDG	SulfoQuinovosylDiacylGlycerols
SRM	Selected Reaction Monitoring
SWATH	Acquisition séquentielle de toutes les fenêtres de masse / Sequential Window Acquisition of all THeoretical fragment-ion spectra
TGs	Triglycérides
TLC	Thin layer chromatography / chromatographie sur couche mince
TOF	Temps de vol / Time Of Flight
UPLC	Chromatographie liquide ultra performance / Ultra Performance Liquid Chromatography
UV	Ultraviolet

INTRODUCTION GENERALE

Les lipides sont des substances composant les matières grasses, dans lesquelles les acides gras et le glycérol sont les éléments prédominants [1]. La relation entre les lipides et la santé humaine a été explorée dès les années 1900, où les lipides ont été notés comme des facteurs nutritionnels importants [2,3] et se sont fréquemment avérés être modifiés par rapport aux concentrations homéostatiques dans des conditions physiopathologiques [4–6].

Sur le plan alimentaire, tous les lipides ne représentent pas le même apport, notamment par leur composition en acides gras [7]. Plusieurs sources d'information suggèrent que les êtres humains ont évolué avec un régime oméga-6 (œuf, viande, fromage, huile de tournesol…) et oméga-3 (poissons gras, noix, huile de cameline…) dans un rapport ~ 1 :1 alors que dans les régimes occidentaux, le rapport est de 15 :1 à 16,7 :1 [8]. Ces deux familles d'acides gras sont métabolisées par des enzymes communes et se trouvent ainsi en compétition. Ce fort ratio en faveur des oméga-6 favorise la pathogenèse de nombreuses maladies, notamment les maladies cardiovasculaires, les cancers, les maladies inflammatoires et auto-immunes [8].

Les acides gras *trans* peuvent être d'origine naturelle (produits issus de ruminants tels que le lait et la viande) [9]. Cependant, ils peuvent également être issus du chauffage à haute température des huiles végétales ou issus de procédés industriels d'hydrogénation des acides gras insaturés (chips, viennoiserie, pizza, gâteaux, etc.) [10]. La consommation d'acides gras *trans* d'origine industrielle est considérée comme présentant un risque accru de maladies cardio-vasculaires.

Les lipides exercent également des rôles majeurs au sein des organismes vivants. Ils sont les principaux constituants des membranes cellulaires (phospholipides ou PLs), permettent le stockage d'énergie (triglycérides ou TGs) et sont impliqués dans les voies de signalisation grâce

auxquelles les cellules communiquent entre elles et avec leur environnement [11]. Là encore, la nature des acides gras substitués sur les lipides complexes (PLs, TGs…) influe directement sur les fonctions cellulaires. Par exemple, les PLs polyinsaturés favorisent la fluidité des membranes, alors que des PLs saturés les rendent rigides [12].

Un déséquilibre des acyles gras (FAs) est observé dans certaines pathologies telles que les cancers, les maladies cardiovasculaires ou dans divers troubles neurologiques [13].

Parmi les quatre types de molécules biologiques qui composent le corps humain, c'est-à-dire les acides nucléiques, les acides aminés (protéines), les glucides (sucres) et les lipides (graisses), les lipides se distinguent des divers métabolites cellulaires par le simple nombre de molécules distinctes [14].

La base de données LIPID MAPS [15] recense à ce jour 47 704 structures lipidiques uniques et biologiquement pertinentes, regroupées en 8 catégories [16]. La première catégorie regroupe les acyles gras (10 509), la deuxième les glycérolipides (7 731) et la troisième les glycérophospholipides (10 064). Ces 3 catégories représentent 60% des lipides inventoriés à ce jour par cette base de données.

Les glycérolipides et les PLs contiennent une structure glycérol sur laquelle est substitué un, deux ou trois FAs. La variabilité structurelle des FAs (fonctionnalisation, longueur de chaîne, nombre et position des insaturations) confère à ces deux catégories de lipides une grande diversité d’espèces moléculaires, généralement retrouvée dans les extraits lipidiques d’origine naturelle.

Les analyses lipidomiques visent à étudier l’ensemble des lipides d’un système (organisme, cellule, tissus ou encore fluide biologique) afin de mieux comprendre les variations de composition occasionnées par différentes situations physiologiques et pathologiques. Ces analyses sont principalement réalisées par chromatographie liquide couplée à la spectrométrie de masse (LC-MS), mais de nombreux défis restent encore à relever pour l’obtention de

données quantitatives fiables [17]. Les difficultés de la lipidomique quantitative, dont les principes reposent sur les techniques d'étalonnage classiques, s'expliquent d'une part par la très grande diversité des lipides à quantifier à mettre en regard avec la faible disponibilité des standards commerciaux et, d'autre part aux variations de réponse des spectromètres de masse en fonction de la nature des espèces moléculaires de lipides [18].

L'analyse des esters méthyliques d'acides gras (FAMEs) par chromatographie en phase gazeuse couplée au détecteur à ionisation de flamme (GC-FID) est une technique bien établie qui permet d'accéder quantitativement à la distribution des FAs. L'obtention de la distribution des FAs par classe, nécessite néanmoins une étape de séparation contraignante et est de ce fait peu usitée [19].

Dans ce travail, nous avons développé un nouveau concept d'évaluation de la distribution des FAs, intermédiaire entre la lipidomique quantitative et l'analyse des FAMEs par GC-FID. Pour cela, nous avons utilisé la méthode utilisant la chromatographie liquide à polarité de phase normale couplée au spectromètre de masse (NPLC-MS) permettant la séparation des lipides par classes, que nous avons publiée en 2017 dans Journal of Chromatography A [20]. Cette méthode permet une approche lipidomique, puisque l'ensemble des espèces moléculaires des extraits lipidiques sont accessibles. L'originalité du travail réside dans l'investigation des intensités des ions fragments monoacylglycérol $[MG+H-H_2O]^+$ produit par les glycérolipides et les PLs lors de l'utilisation des sources d'ionisation par photoionisation à pression atmosphérique (APPI) et d'ionisation chimique à pression atmosphérique (APCI) pour l'obtention de la distribution des FAs. L'étude de nos spectres de masse a mis en exergue une similitude entre la distribution des ions $[MG+H-H_2O]^+$ et la distribution des FAs obtenue par GC-FID. Dans ce travail, nous avons donc étudié la faisabilité d'utiliser ces ions pour évaluer la distribution en FAs.

Les chapitres I à V rassemblent les différents aspects de l'état de l'art sur les lipides et leur analyse en lien avec le sujet de cette thèse.

Le chapitre I présente la classification des lipides ainsi que leurs fonctions biologiques. Les notions de catégories, de classes et de sous-classes de lipides étant fréquemment utilisées dans le manuscrit, ces notions y sont détaillées.

Le chapitre II est consacré aux analyses lipidomiques menées par LC-MS. Les étapes d'extraction de lipides, de séparations par LC, de détection MS et de traitement des données sont passées en revue. Les difficultés rencontrées lors des études lipidomiques quantitatives sont présentées au travers de plusieurs exemples. Ces éléments permettent de situer notre approche par rapport à ce type d'analyse.

Le chapitre III est consacré à la méthode séparative, publiée antérieurement aux travaux de thèse [20]. C'est à partir des spectres de masse obtenus par le couplage de cette méthode avec les sources APCI/APPI-MS qu'est née l'idée d'investiguer les ions $[MG+H-H_2O]^+$ pour accéder à la distribution des FAs. Cette méthode est le support de toutes les analyses LC-MS réalisées durant la thèse. Il nous a donc semblé important d'incorporer cette publication au manuscrit.

Le chapitre IV présente les acyles gras dans leur contexte biologique, de leur synthèse à leur influence sur notre santé.

Le chapitre V détaille l'analyse des FAMEs par GC-FID et MS, principales techniques utilisées pour accéder à la distribution des FAs. Un exemple d'analyse des FAs, issus de l'hydrolyse des lipides, par LC-MS/MS est également abordé.

Les chapitres VI à VIII détaillent, à travers trois publications, les différentes étapes du développement de notre approche pour l'évaluation de la distribution des FAs des glycérolipides et PLs.

Dans **le chapitre VI**, les bases de notre nouveau concept sont posées à travers l'étude des TGs issus d'huiles végétales [21].

Dans **le chapitre VII**, le concept a été étendu aux classes des PLs. Cette étude nous a conduit à développer une stratégie particulière pour prendre en compte la présence de plasmalogènes [22].

Dans **le chapitre VIII** nous avons mis en œuvre notre nouveau concept sur des souches *Yarrowia Lipolytica* (levure oléagineuse) modifiées pour favoriser la production d'acyle gras à chaînes impaires [23].

Les annexes I à IV correspondent aux données supplémentaires (supplementary) des quatre publications intégrées au manuscrit.

Les annexes V à VII rassemblent trois publications qui, elles aussi, découlent de la publication de notre méthode NPLC d'analyse des lipides par classe [20] et qui présentent, à ce titre, un lien avec ce travail de thèse. Ces trois articles [24–26] concrétisent notre participation à l'étude du métabolisme lipidique de souches de *Streptomyces* génétiquement modifiées menées dans le cadre d'une collaboration avec l'équipe du Dr. M.J. Virolle (I2BC/Université Paris-Saclay). Dans ces travaux, nous n'avons pas exploité l'approche décrite dans les chapitres VI~VIII pour la mesure de la distribution des FAs qui était alors en cours de développement. Il s'agit cependant d'un travail connexe, effectué conjointement à mes travaux de thèse dans le cadre de mes activités d'Ingénieure d'Etudes d'où sa présence dans le manuscrit sous forme d'annexes.

PARTIE I : ETUDE BIBLIOGRAPHIQUE

CHAPITRE I. GENERALITES SUR LES LIPIDES

1. Définition

Selon l'IUPAC (International Union of Pure and Applied Chemistry) « lipides » correspond à un « terme vague désignant des substances d'origine biologique solubles dans des solvants non polaires. Ils sont constitués de lipides saponifiables, tels que les glycérides (graisses et huiles) et phospholipides, ainsi que des lipides insaponifiables, principalement des stéroïdes » [27].

Les progrès de la spectrométrie de masse au cours des deux dernières décennies a permis le développement d'approches « omiques » [28]. Ces approches ont pour objectif d'appréhender la complexité du vivant dans son ensemble [29]. Cependant, ces nouvelles technologies génèrent un volume considérable de données, qu'il est impératif d'organiser et de traiter.

C'est pourquoi, en 2005, l'ILCNC (International Lipid Classification and Nomenclature Comittee) sous le parrainage du consortium LIPID Metabolites and Pathways Strategy (LIPID MAPS), a développé un système de classification globalisé des lipides en se basant sur la définition proposée par Fahy et al [30]. Les lipides y sont définis comme « de petites molécules hydrophobes ou amphipathiques qui peuvent provenir entièrement ou en partie de condensations à base de carbanions de thioesters (acyles gras, glycérolipides, glycérophospholipides, sphingolipides, saccharolipides et polycétides) et/ou par condensations à base de carbocations d'unités d'isoprène (lipides de prénol et lipides de stérol) ». Une mise à jour a étendu la classification, initialement basée sur les lipides présents chez les espèces mammifères, à ceux présents chez les plantes, bactéries et champignons d'après les travaux de Fahy et al. publiés en 2009 [16].

2. *Classification*

Le consortium LIPID MAPS met à disposition via son site internet [15] la plus grande base de données sur les lipides ainsi que des outils associés. Les lipides y sont classés suivant 8 grandes catégories : les acyles gras, les glycérolipides, les glycérophospholipides, les sphingolipides, les stérols, les prénols, les saccharolipides et les polycétides. Chaque catégorie de lipides est divisée en classes, elles-mêmes divisées en sous-classes. Sur la Figure 1, les 8 catégories sont présentées en rouge et les principales classes de lipides (des cellules eucaryotes) associées sont notées en noir.

Les catégories se différencient par leurs motifs structuraux au niveau de leurs chaînes lipidiques principales. Les classes se différencient par la nature et le nombre des groupements polaires. Les sous-classes se différencient par la structure des chaînes acyles fixées sur la chaîne principale (ramification, longueur des chaînes carbonées, présence et position d'insaturations, présence d'hétéroatomes).

Dans le cadre de ce travail, seules les cinq premières catégories ainsi que leurs classes associées seront abordées. La nomenclature est reprise de LIPID MAPS, à l'exception de l'abréviation phospholipides (PLs) usuellement employée pour désigner la catégorie des glycérophospholipides (GPs).

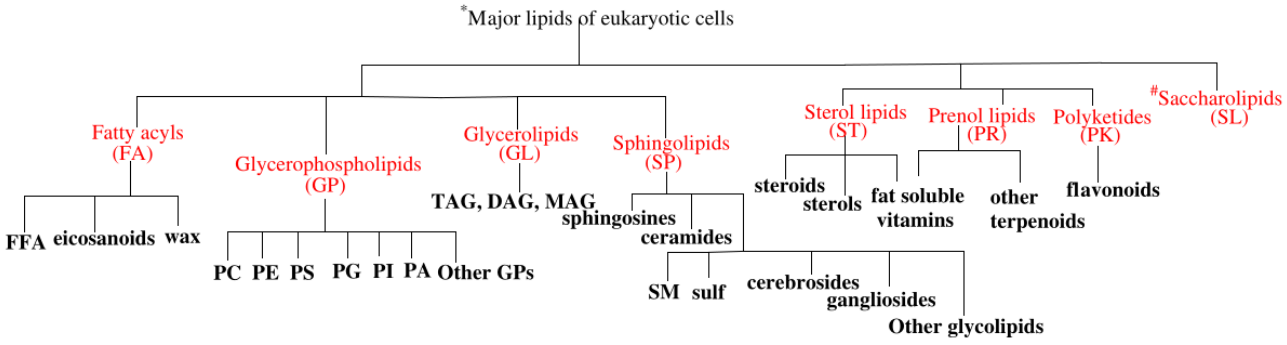

Figure 1: Classification des lipides [31].

Les structures des lipides présentées ci-après sont reprises du site internet LIPID MAPS.

2.1 Acyles gras

La structure des acyles gras représente le principal élément constitutif des lipides complexes, c'est donc l'une des catégories fondamentales des lipides biologiques. Cette catégorie comporte 13 classes :

- [FA01] Les acides gras (FAs) et dérivés, constitués d'une succession de groupements méthylène ainsi que d'un acide carboxylique terminal.
- [FA02] Les octadécanoïdes, composés dérivant d'acides gras à 18 atomes de carbone.
- [FA03] Les eicosanoïdes, composés dérivant de l'acide arachidonique.
- [FA04] Les docosanoïdes, composés dérivant de l'acide docosahexaénoïque.

Le groupement carboxylique peut-être remplacé par différents groupements définissant ainsi les classes des :

- [FA05] Alcools gras (-OH)
- [FA06] Aldéhydes gras (-CH=O)
- [FA07] Esters gras (R-CO-O-R')
- [FA08] Amides gras (-CONH2)
- [FA09] Nitriles gras (-C≡N)
- [FA10] Ethers gras (-C-O-R)

A ces classes s'ajoutent les classes des :

- [FA11] Hydrocarbonés gras
- [FA12] Hydrocarbonés gras oxygénés
- [FA13] Acyles gras glycosylés

Des exemples d'acyles gras sont présentés sur la Figure 2.

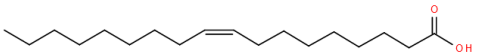

FAs : acide oléique

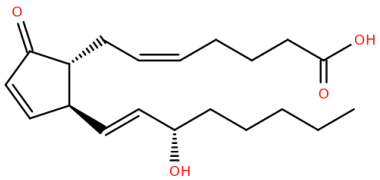

Eicosanoïdes : prostaglandine A2

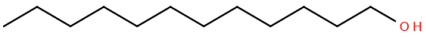

Alcools gras : dodecanol

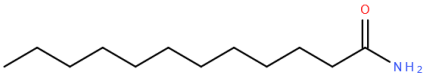

Amides gras : dodecanamide

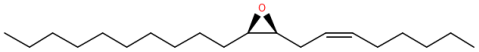

Hydrocarbonées gras oxygénés :

9R,10S-Epoxy-6Z-eicosene

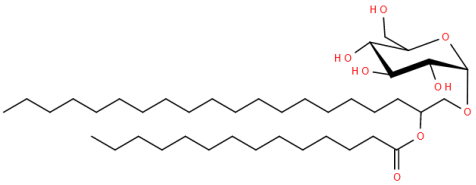

Acyles gras glycosilés :

1-O-α-D-glucopyranosyl-(2-tetradecanoyloxy)-eicosan-1-ol

Figure 2: Exemples de structures d'acyles gras.

2.2 Glycérolipides

Les glycérolipides englobent les lipides contenant du glycérol, hormis les glycérophospholipides. Cette catégorie comporte 5 classes numérotées GL01 à GL05.

Les classes les plus abondantes sont les glycérols mono-, di- et tri-substitués, les plus connus étant les esters d'acides gras du glycérol (acylglycérols) :

- [GL01] Monoacylglycérols
- [GL02] Diacylglycérols
- [GL03] Triacylglycérols

Deux autres classes supplémentaires sont caractérisées par la présence d'un ou plusieurs résidus de sucre attachés au glycérol via une liaison glycosidique :

- [GL04] Glycosylmonoradylglycérols
- [GL05] Glycosyldiradylglycérols

Des exemples de structures de glycérolipides sont présentés sur la Figure 3.

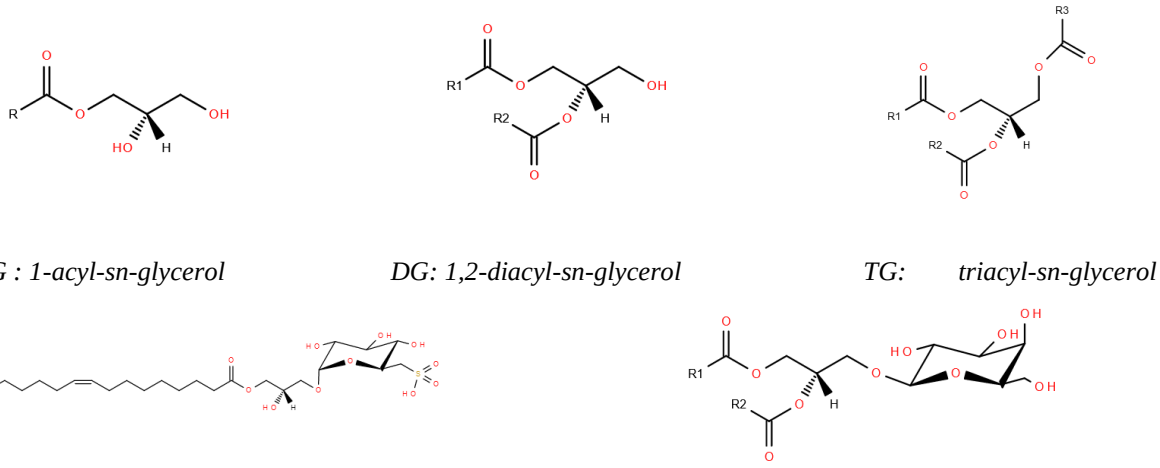

Figure 3: Exemples de structures de glycérolipides.

2.3 Glycérophospholipides

Les glycérophospholipides sont les principaux lipides des membranes cellulaires. Leurs structures amphotères permettent une organisation lipidique, notamment en bicouches.

Les glycérophospholipides sont divisés en fonction de la nature de leur tête polaire en position *sn*-3 du squelette glycérol (hors archéobactéries, en position *sn*-1).

Cette catégorie comporte 20 classes :

- [GP01] Glycérophosphocholines (PC)
- [GP02] Glycérophosphoethanolamines (PE)
- [GP03] Glycérophosphoserines (PS)
- [GP04] Glycérophosphoglycerols (PG)
- [GP05] Glycérophosphoglycerophosphates (PGP)
- [GP06] Glycérophosphoinositols (PI)
- [GP07] Glycérophosphoinositol monophosphates (PIP)
- [GP08] Glycérophosphoinositol bisphosphates (PIP2)
- [GP09] Glycérophosphoinositol trisphosphates (PIP3)
- [GP10] Glycérophosphates (PA)
- [GP11] Glycéropyrophosphates (PPA)
- [GP12] Glycérophosphoglycerophosphoglycerols (CL)
- [GP13] CDP-Glycérols
- [GP14] Glycosylglycérophospholipids
- [GP15] Glycérophosphoinositolglycans
- [GP16] Glycérophosphonocholines
- [GP17] Glycérophosphonoethanolamines
- [GP18] Di-glycerol tetraether phospholipids (caldarchaeols)
- [GP19] Glycerol-nonitol tetraether phospholipids
- [GP20] Glycérophospholipids oxydés

Les principales classes de glycérophospholipides sont présentées sur la Figure 4.

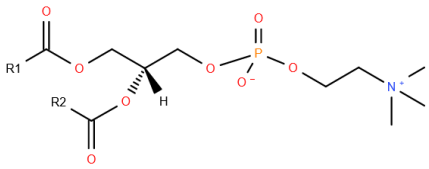

PC: 1,2-diacyl-sn-glycero-3-phosphocholine

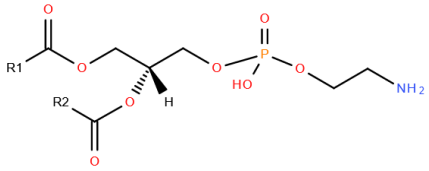

PE :1,2-diacyl-sn-glycero-3-phosphoethanolamine

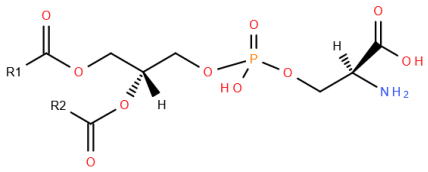

PS : 1,2-diacyl-sn-glycero-3-phosphoserine

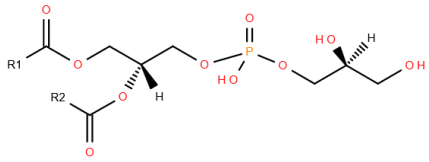

PG : 1,2-diacyl-sn-glycero-3-phosphoglycerol

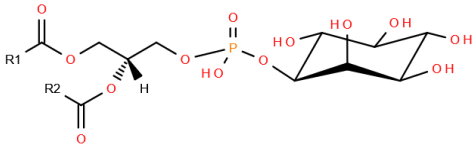

PI: 1,2-diacyl-sn-glycero-3-phosphoinositol

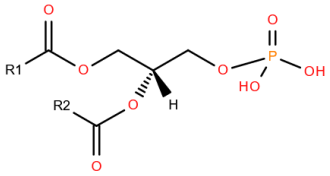

PA : 1,2-diacyl-sn-glycero-3-phosphate

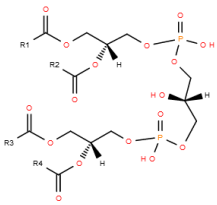

CL: 1',3'-Bis-(1,2-diacyl-sn-glycero-3-phospho)-sn-glycerol

Figure 4: Exemples de structures de glycérophospholipides.

Les sous-classes de cette catégorie, abordées dans ce travail de thèse, correspondent aux diacyl-PLs, monoacyl-PLs (lyso-PLs), 1-O-alkényl-PLs (plasmalogènes ou P-PLs) et 1-O alkyl-PLs (plasmanyls).

Dans le cas des 1-O-alkényl-PLs, un alcool vinylique gras est substitué en *sn*-1 du glycérol pour former une liaison éther vinylique. Dans le cas des 1-O alkyl-PLs un alcool gras (non vinylique) est substitué en *sn*-1 du glycérol pour former une liaison éther, un exemple de ces deux sous-classes est présenté sur la Figure 5.

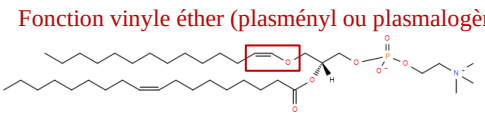

PC(P-14:0/18:1(9Z)): 1-O-(1Z-tetradecenyl)-2-(9Z-octadecenoyl)-sn-glycero-3-phosphocholine

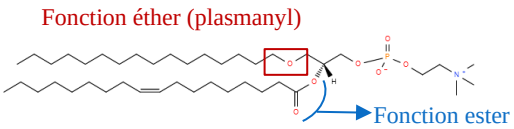

PC(O-16:0/18:1(9Z)): 1-hexadecyl-2-(9Z-octadecenoyl)-sn-glycero-3-phosphocholine

Figure 5: Exemples de structure de plasmalogènes et de plasmanyl.

Les éthers lipides sont principalement rencontrés dans les membranes cellulaires inflammatoires [32]. Les plasmalogènes (P-PLs) sont quant à eux essentiellement rencontrés dans la classe des PE et PC à l'état basal de certains tissus comme le cœur [33] ou le cerveau [34]. Les plasmalogènes jouent un rôle d'antioxydant vis-à-vis des FAs polyinsaturés généralement substitués en position *sn*-2. La Figure 6 illustre la teneur de ces plasmalogènes dans différents tissus de mammifères.

Species	Tissue	PlsEtn (%GPEtn)	PlsCho (%GPCho)	PlsEtn (%total PL)[a]	PlsCho (%total PL)[a]	Plasmalogen (% total PL)[a]	Reference[b]
Human	Brain	58	1	20, 22.4	0.8, 0.9	22	[111], [112]
	Heart	53	26	15, 17	11, 16		
	Kidney	46	5	14	4.7		
	Skeletal muscle	48	19	14	6.5		
	Liver	8	3	4.7	3.4		
	Gray matter						[6], [113]
	Frontal cortex	57				54	
	Parietal cortex	58				51	
	Temporal cortex	56					
	Cerebellum	63					
	White matter						
	Frontal cortex	84				76	
	Parietal cortex	81				100	
	Temporal cortex	83					
	Cerebellum	78					
Mouse	Cortex	46					
	Cerebellum	53					
Rat	Cerebellum			26.2			[114]
	Cortex			21.8			
	Hippocampus			23.4			
	Brainstem			31.9			
	Midbrain			23.8			
	Kidney	20	2.3			12	[113], [115]
	Liver	3.3	0.4			3.4	
	Lung	42	1.6			16	
Human	Neutrophils	68	3.6				[116]
	Eosinophils	72	4				[117]
	Erythrocytes			20			[105]
	Lens	70		14			[118]
Rat	Plasma	36					[8]
	LDL	32.2	1.9				
	HDL	46.3	2.4				
	VLDL	14	1.6				
Mouse	Surfactant	38				1.5	[73]
Rat	Brain synaptic vesicles			16			[119]
Dog	Heart sarcolemma	73	57			53	[120]
Rat	Mature spermatozoa	42	52			38	[121]
Hamster	CHO cells	35	0	11	0	11	[7], [65]

[a] Total phospholipid content includes cardiolipin, GPEtn, PlsEtn, GPCho, PlsCho, GPIns, GPser, and sphingomyelin.
[b] Methods to measure plasmalogens include thin layer chromatography, gas chromatography, NMR, and mass spectroscopy.

Figure 6: Teneur en plasmalogène dans différents tissus de mammifères [35].

2.4 Sphingolipides

Les sphingolipides sont caractérisés par la présence d'un squelette commun appelé « base sphingoïde ». Cette catégorie se divise en neuf classes :

- [SP01] Bases sphingoïdes et leurs dérivés simples (comme le 1-phosphate)
- [SP02] Céramides (bases sphingoïdes avec un acide gras lié par une liaison amide)
- [SP03] Phosphosphingolipides (liaisons phosphodiester)
- [SP05] Glycosphingolipides neutres (liaisons glycosidiques)
- [SP06] Glycosphingolipides acides (liaisons glycosidiques)
- [SP07] Glycosphingolipides basiques (liaisons glycosidiques)
- [SP08] Glycosphingolipides amphotères (liaisons glycosidiques)
- [SP04] Phosphonosphingolipides (autres liaisons)
- [SP09] Arsenosphingolipides (autres liaisons)

Des exemples de sphingolipides sont présentés sur la Figure 7.

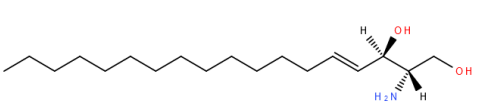

Bases sphingoïdes : Sphingosine

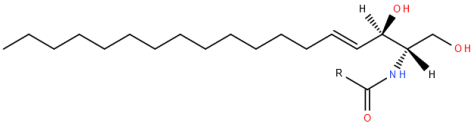

Céramide

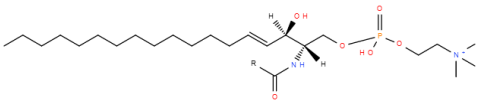

Phosphosphingolipides : Sphingomyéline

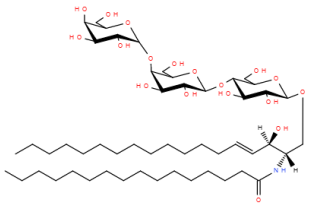

Neutral glycosphingolipids : Galα1-4Galβ1-4Glcβ-Cer(d18:1/16:0) (Gb3(d18:1/16:0))

Figure 7: Exemples de sphingolipides.

2.5 *Stérols*

Les stérols résultent d'une structure à quatre noyaux fusionnés, hydroxylée sur le carbone n°3, appelé noyau stérane. Cette catégorie se divise en cinq classes, principalement en fonction de la fonction biologique :

- [ST01] Les stérols englobent le cholestérol et ses dérivés (issus de sources végétales, fongiques et marines). Cette classe joue un rôle essentiel dans les lipides membranaires chez les mammifères.
- [ST02] Les stéroïdes comprennent des stérols intervenant en tant qu'hormones et molécules de signalisation, par exemple les œstrogènes et la testostérone.
- [ST03] Les secostéroïdes comprennent les diverses formes de vitamine D, et sont caractérisées par le clivage de l'anneau B du noyau stérane.
- [ST04] Les acides biliaires et dérivés.
- [ST05] Les stéroïdes conjugués.

La structure du noyau de base des stérols ainsi que des exemples de stérols sont présentés sur la Figure 8.

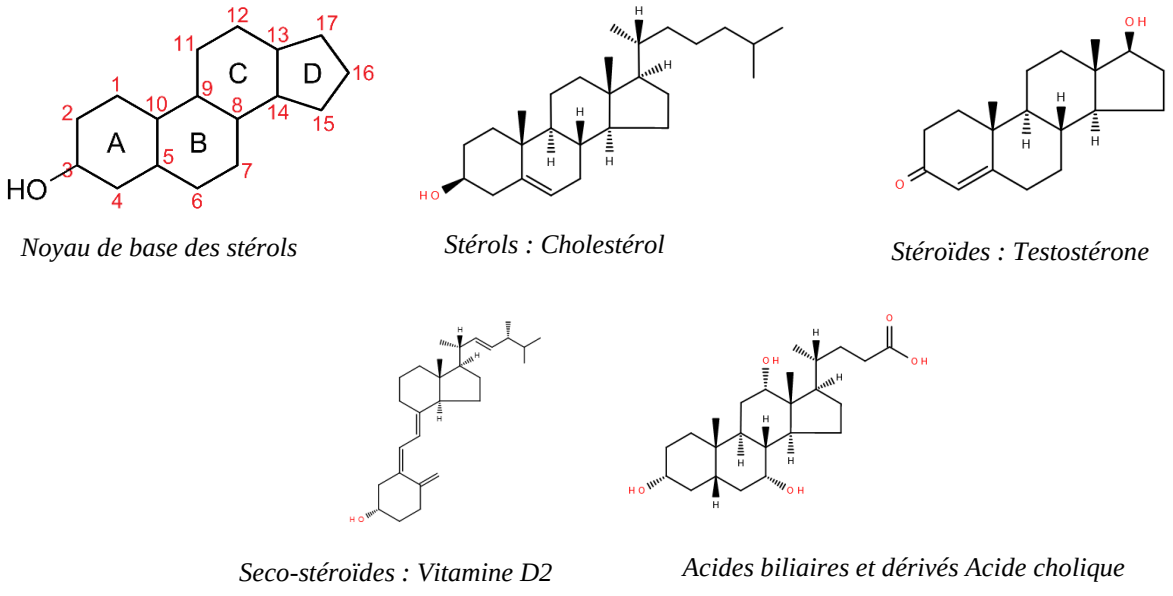

Figure 8: Structure du noyau de base des stérols et exemples de stérols.

3. *Fonctions biologiques*

Les lipides ont trois fonctions biologiques principales. Ce sont les constituants majoritaires des membranes cellulaires, ils interviennent en tant que messagers dans la signalisation et sont utilisés pour le stockage d'énergie métabolique.

3.1 Membranes cellulaires

Les membranes cellulaires sont constituées principalement de phospholipides, molécules amphiphiles composées d'une tête polaire et d'une ou de deux chaînes aliphatiques [11]. Un schéma communément utilisé pour représenter les membranes biologiques est présenté sur la Figure 9. En plus des phospholipides, des stérols, des sphingolipides, des glycolipides et des protéines sont insérés dans la membrane.

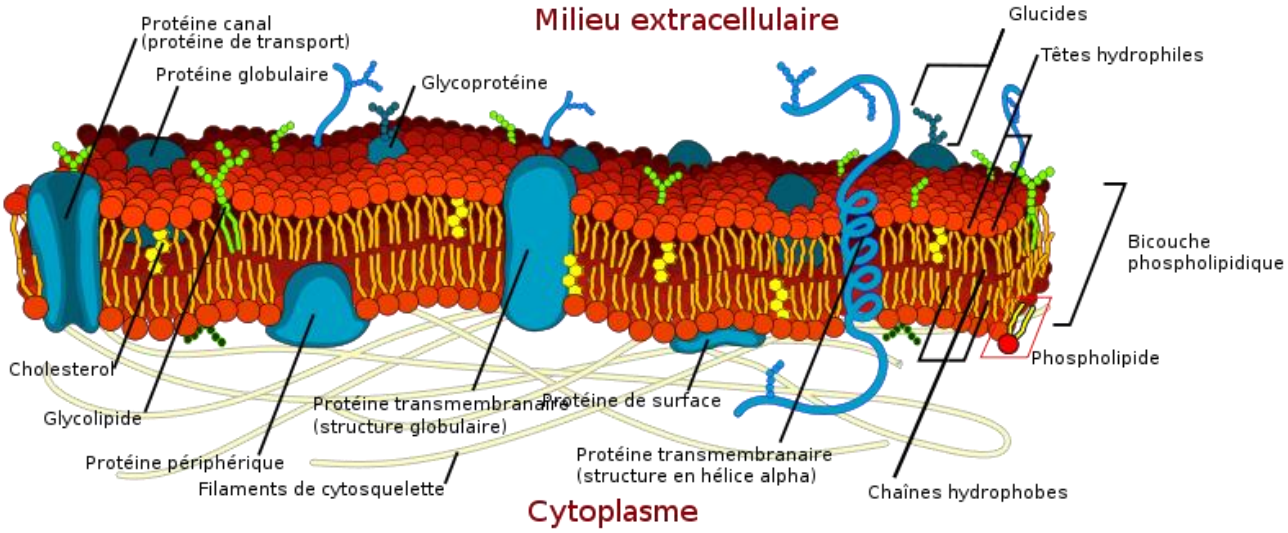

Figure 9: Représentation schématique d'une membrane.

La composition des bicouches lipidiques varie suivant la membrane (plasmique et organite) et présente souvent une asymétrie, Figure 10.

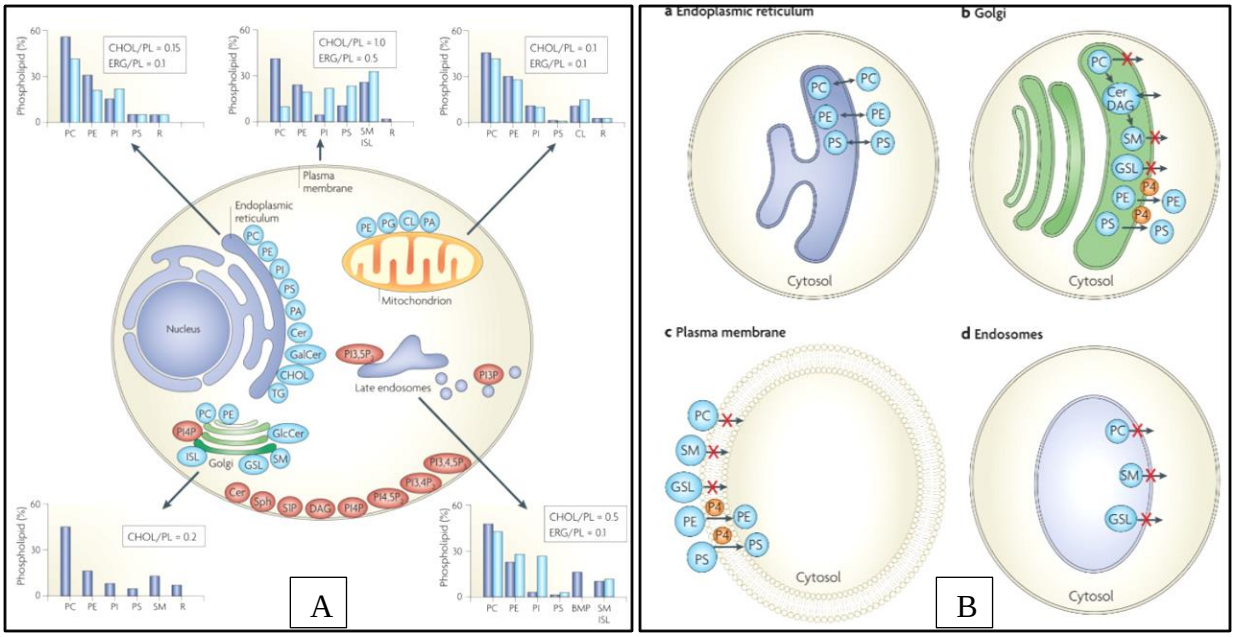

Figure 10: Membranes cellulaires : Synthèse lipidique et composition à l'état d'équilibre (A) ; Mécanismes générant une distribution lipidique asymétrique (B) [11].

Les histogrammes, Figure 10 A, permettent de comparer les pourcentages de PLs chez les mammifères (bleu) et chez la levure (bleu clair). Suivant les membranes étudiées, les pourcentages en PLs peuvent être plus ou moins différents. Le panneau principal montre le site de synthèse des principaux PLs (bleu) et des lipides impliqués dans les voies de signalisation et de reconnaissance des organites (rouge). Le réticulum endoplasmique est le principal organite de biosynthèse lipidique.

La Figure 10 B, présente la distribution des lipides de part et d'autre des membranes biologiques. Le réticulum endoplasmique possède une distribution lipidique symétrique. Cependant, la membrane plasmique présente une asymétrie due à la présence ou à l'absence de transporteurs permettant de franchir la bicouche (noté P4). Le PE et le PS traversent la bicouche et sont présents très majoritairement dans la couche interne de la membrane plasmique.

Le PC, la SM et les glycosphingolipides (GSLs) restent très majoritairement, voire exclusivement (pour les GSLs), sur la couche externe de la membrane.

3.2 Messagers cellulaires

Les produits de dégradation des lipides membranaires servent de seconds messagers lipidiques. Ainsi, les PLs vont produire par dégradation des LPC, LPA, PA et DG. Les sphingolipides vont produire par dégradation la sphingosine-1-phosphate, le Cer-1-phosphate et des céramides. L'acide arachidonique produit les eicosanoïdes et les endocannabinoïdes de signalisation. Les phosphatidylinositol phosphates (PIP) sont également produits, ils marquent les membranes cellulaires pour le recrutement des protéines. Ces messagers sont présentés en rouge sur la Figure 10 A.

Les lipides de signalisation et de reconnaissance représentent moins de 1% des PLs totaux, à l'exception des céramides.

3.3 Stockage d'énergie

Les FAs sont la principale source d'énergie métabolique, ils sont stockés par l'organisme sous forme de TGs. Lors de l'hydrolyse des TGs, les FAs libérés sont dégradés dans la mitochondrie, suivant le schéma de la β-oxydation appelé également « tour d'hélice de Lynen ». À chaque tour de l'hélice de Lynen, le FA perd deux carbones, sous la forme d'une molécule d'acétyl-CoA. Puis, l'acétyl-CoA entre dans le cycle de Krebs, ce qui permet de produire de l'ATP, molécule énergétique utilisée par les cellules.

CHAPITRE II. ANALYSE LIPIDOMIQUE

1. Introduction

Le domaine des sciences « omiques » comprend la génomique, la transcriptomique, la protéomique et la métabolomique qui élucident les marqueurs ADN, les transcrits d'ARN, les protéines et les métabolites produits, comme illustré sur la Figure 11. Toutes ces approches offrent une opportunité remarquable pour la découverte de nouveaux biomarqueurs pour le pronostic et le diagnostic de pathologies. Ces sciences contribuent à concevoir de nouvelles stratégies thérapeutiques [36].

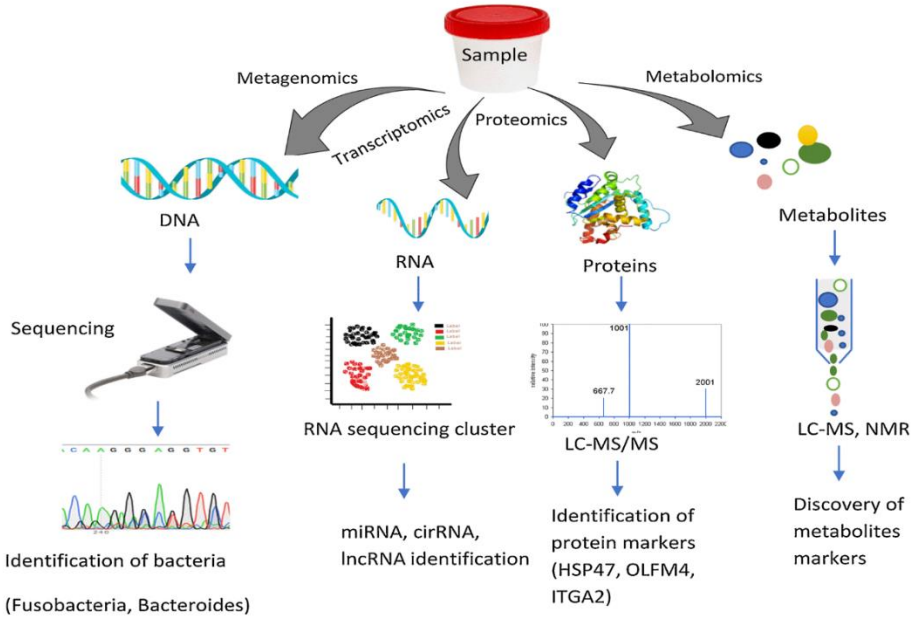

Figure 11: Schéma des domaines de recherche omiques [36].

La lipidomique est une sous partie de la métabolomique. La compréhension du métabolisme lipidique est un champ de recherche important, avec des applications dans les domaines tels que la santé [37–40], l'alimentation, les biocarburants, la chimie verte et bien d'autres [41,42]. Il existe différentes techniques analytiques pour explorer le lipidome. Les plus utilisées sont la LC-MS et l'introduction directe (infusion-MS), couramment appelé « shogun », mais d'autres techniques comme la GC, chromatographie sur couche mince (TLC) et la résonance magnétique nucléaire (RMN) sont également utilisées [17].

Le principal avantage de l'infusion-MS par rapport à la LC-MS est le temps d'analyse réduit au minimum. La LC-MS permet la séparation des lipides, ce qui limite les effets de suppression d'ionisation et facilite l'interprétation grâce à l'information sur les temps de rétention. La Figure 12 extraite de la revue de Tomas Cajka et Olivier Fiehn (2014) [17] présente les différentes étapes lors des études lipidomiques, ainsi que les principales techniques utilisées par LC-MS. Chaque étape de cette figure est détaillée ci-après.

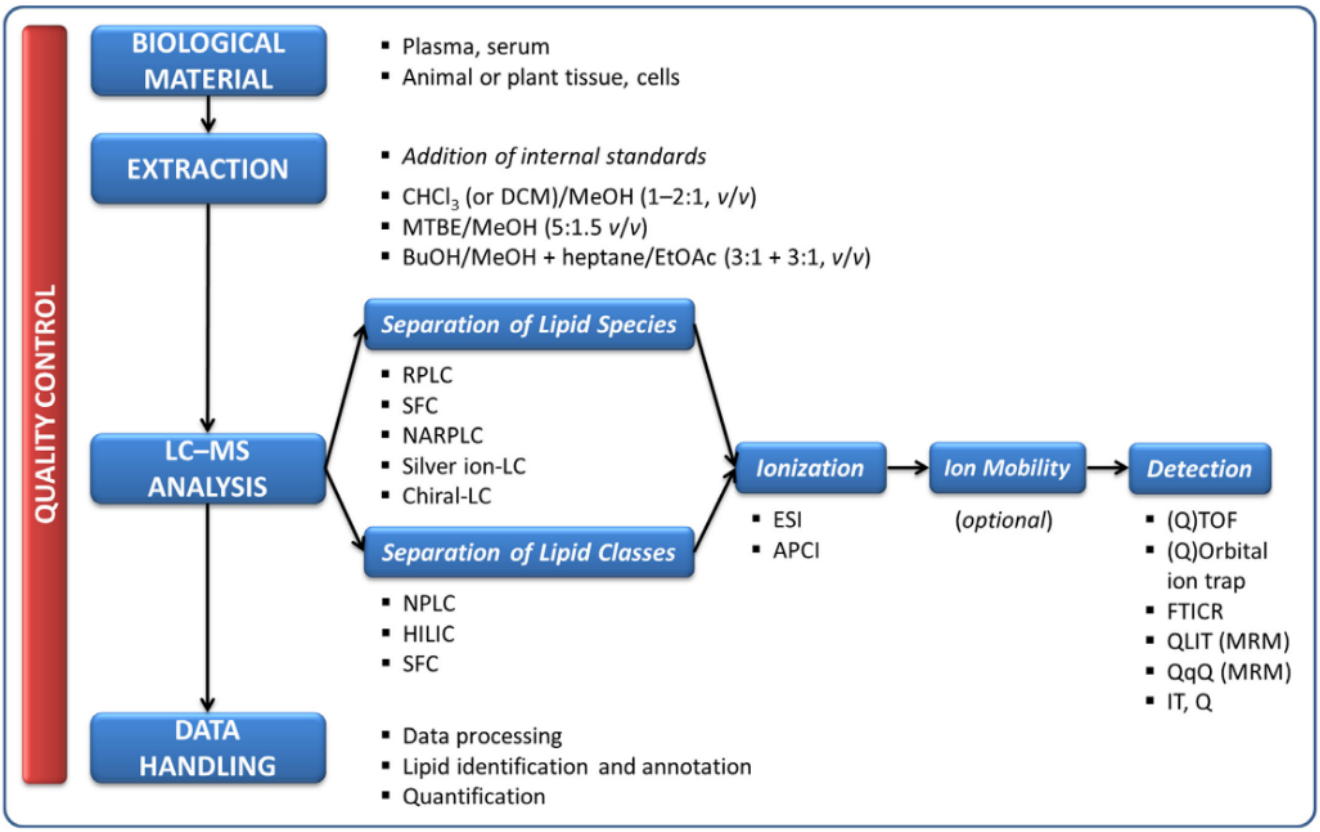

Figure 12: Analyse lipidomique basée sur la LC-MS [17].

2. *Extraction*

L'extraction des lipides est la 1ère étape lors du processus d'analyse. L'extraction permet de séparer les lipides d'intérêt du reste des constituants d'un matériel biologique. Le protocole d'extraction doit être adapté en fonction du matériel biologique et des lipides cibles. La plupart des études lipidomiques utilisent des extractions générales, souvent modifiées, telles que la méthode de Folch [43], de Bligh and Dyer [44], de Matyashetal [45] ou BUME [46]. Les solvants utilisés et les proportions sont décrits respectivement sur la Figure 13. En 2014, l'analyse du plasma et du sérum représentait 39% des matrices étudiées en lipidomique, les matrices animales 23% et les cellules 22%, Figure 13 A. Les extractions sont réalisées en grande majorité avec un mélange de chloroforme/méthanol, Figure 13 B.

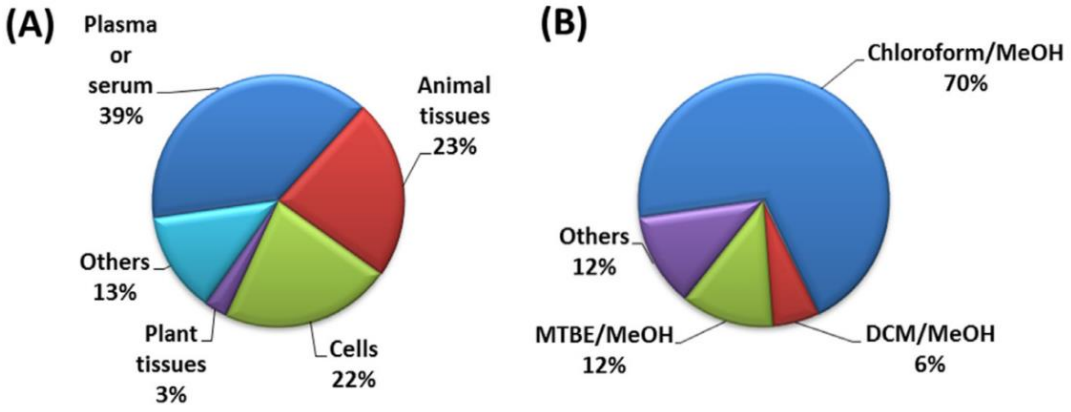

Figure 13: Focus sur les études lipidomiques basées sur la LC-MS : matrices analysées (A) et protocoles d'extraction (B) [17].

3. *Séparations par chromatographie en phase liquide et supercritique*

La répartition des systèmes chromatographiques dans les études lipidomiques est présentée sur La Figure 14 A.

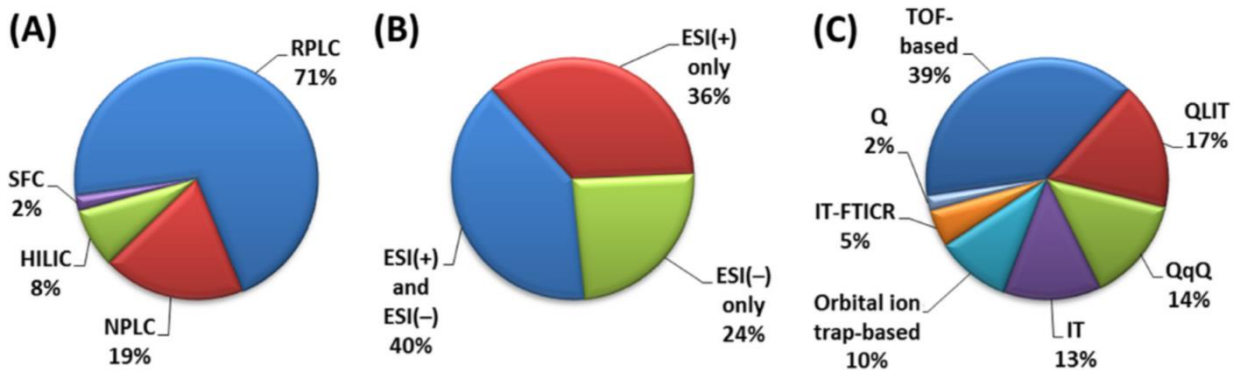

Figure 14: Utilisation de systèmes chromatographiques (A), de modes d'ionisation (B) et d'analyseurs de masse (C) dans des papiers lipidomiques à base de LC-MS [17].

La chromatographie liquide à polarité de phases inversée (RPLC) est la méthode séparative de loin la plus utilisée (71%). Elle permet une séparation par espèces moléculaires. Ensuite, arrivent la chromatographie en phase normale (NPLC, 19%) et la chromatographie liquide d'interactions hydrophiles (HILIC, 8%), ces deux méthodes conduisent à une séparation de lipides par classe. La chromatographie en phase supercritique (SFC) est encore peu utilisée, elle permet, suivant le type de colonne mise en œuvre, de séparer les lipides par espèces moléculaires ou par classes. Le principe de séparation par RPLC, NPLC et HILIC est présenté sur la Figure 15.

Le PC(16 :0/18 :2) est symbolisé par le rond rouge, correspondant à sa partie hydrophobe (chaînes grasses), et par le rond bleu, correspondant à sa partie hydrophile (tête polaire).

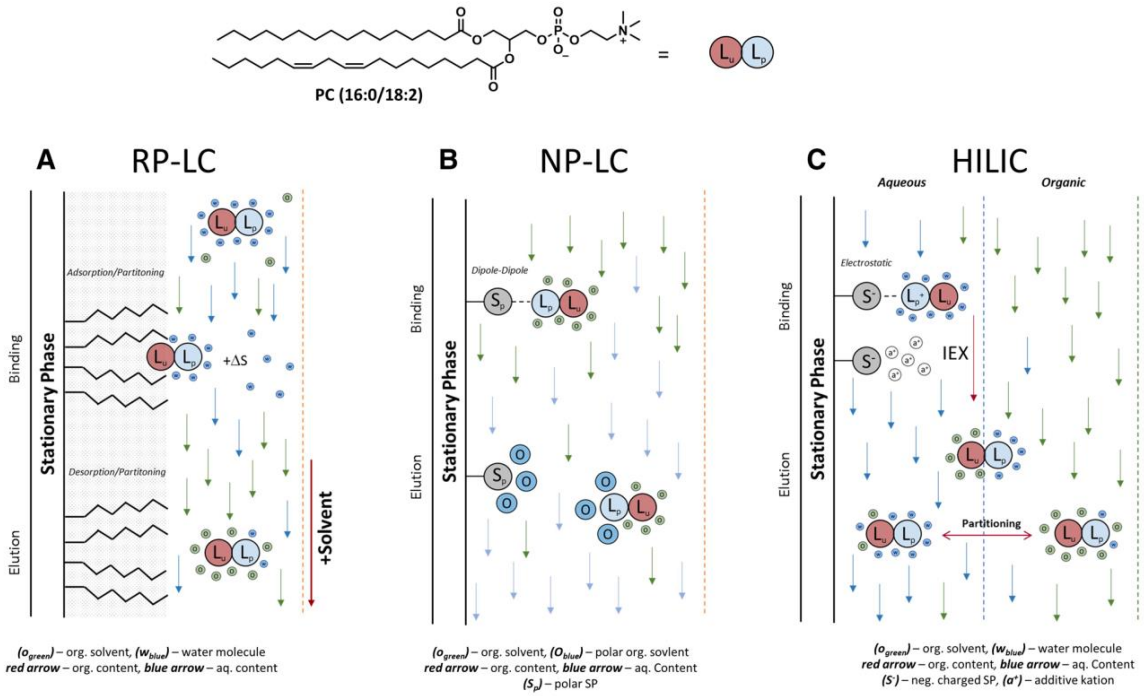

Figure 15: Principe de séparation des lipides utilisant différentes techniques chromatographiques : RPLC (A), NPLC (B) et HILIC (C) [47].

En RPLC, la phase stationnaire est constituée, la plupart du temps, par des silices greffées apolaires (C8, C18, etc.). La phase mobile utilisée en début d'analyse contient une proportion importante d'eau (flèches bleues). Les lipides sont retenus sur la phase stationnaire par des interactions hydrophobes. L'élution est déclenchée par l'augmentation du solvant organique (flèches vertes).

En NPLC, la phase stationnaire est constituée de silice vierge (chromatographie d'adsorption) ou de silice greffée polaire (exemple : PVA - polyvinyle-alcool). La phase mobile utilisée en début d'analyse contient une proportion importante de solvant apolaire (flèches vertes). La rétention des lipides par la phase stationnaire se fait principalement grâce aux liaisons hydrogènes et aux forces de van der Waals (interactions dipolaires) engagées par les groupements polaires des lipides. L'augmentation de la polarité du solvant (flèches bleues) entre en concurrence avec les sites polaires de la phase stationnaire et conduit à l'élution des lipides.

La Figure 16 illustre sur un même graphique, la séparation par espèces moléculaires (RPLC) et la séparation par classe (NPLC). Chaque point correspond à une espèce moléculaire. Cette figure met en exergue le potentiel que peut avoir une séparation bidimensionnelle (combinaison des deux modes de séparation). La compatibilité des solvants pour passer d'un mode de séparation à l'autre est toutefois problématique. La revue [48], propose un tutoriel pour les analyses bidimensionnelles à partir des données recueillies dans la littérature.

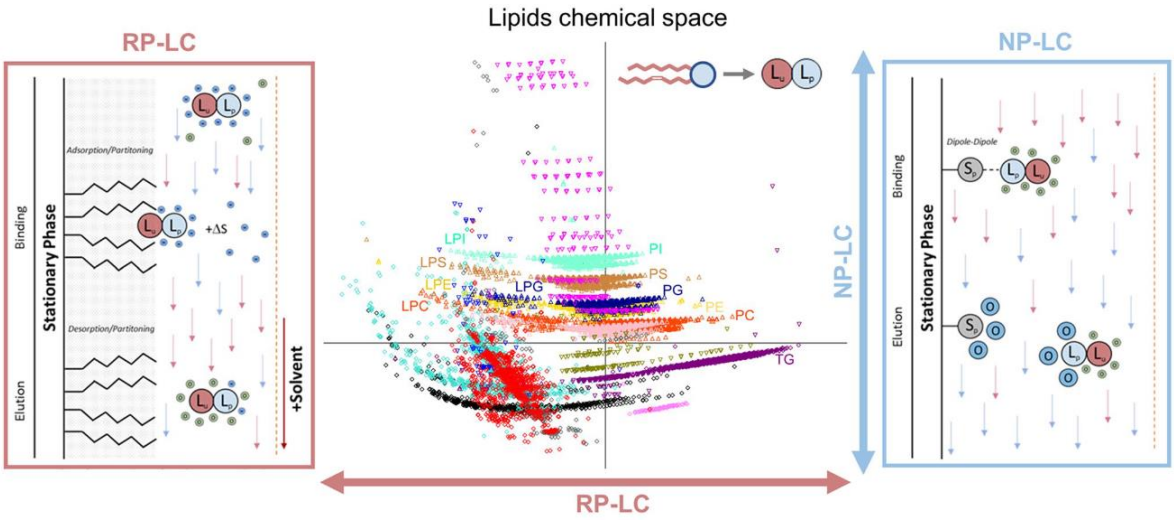

Figure 16 : Espace chimique des lipides [47].

L'**HILIC** se différencie de la NPLC par une teneur importante en eau de la phase mobile, de sorte à maintenir une couche d'eau à la surface de la phase stationnaire. La rétention des lipides est basée sur les interactions électrostatiques des fractions lipidiques chargées. L'élution est obtenue de trois manières différentes : (1) gradient de pH ou de force ionique, (2) augmentation du pH entraînant un changement de l'état de dissociation, (3) augmentation de la teneur en eau, atténuant ainsi les interactions électrostatiques. Dans l'étude [49], les auteurs ont optimisé la séparation chromatographique des lipides acides (PA, LPA, PS, LPS), ainsi que celles d'autres classes de lipides. Les principaux paramètres inclus dans l'optimisation ont été le type de phases stationnaires HILIC (9 colonnes testées), le pH de la phase mobile, le type et la concentration des additifs de la phase mobile.

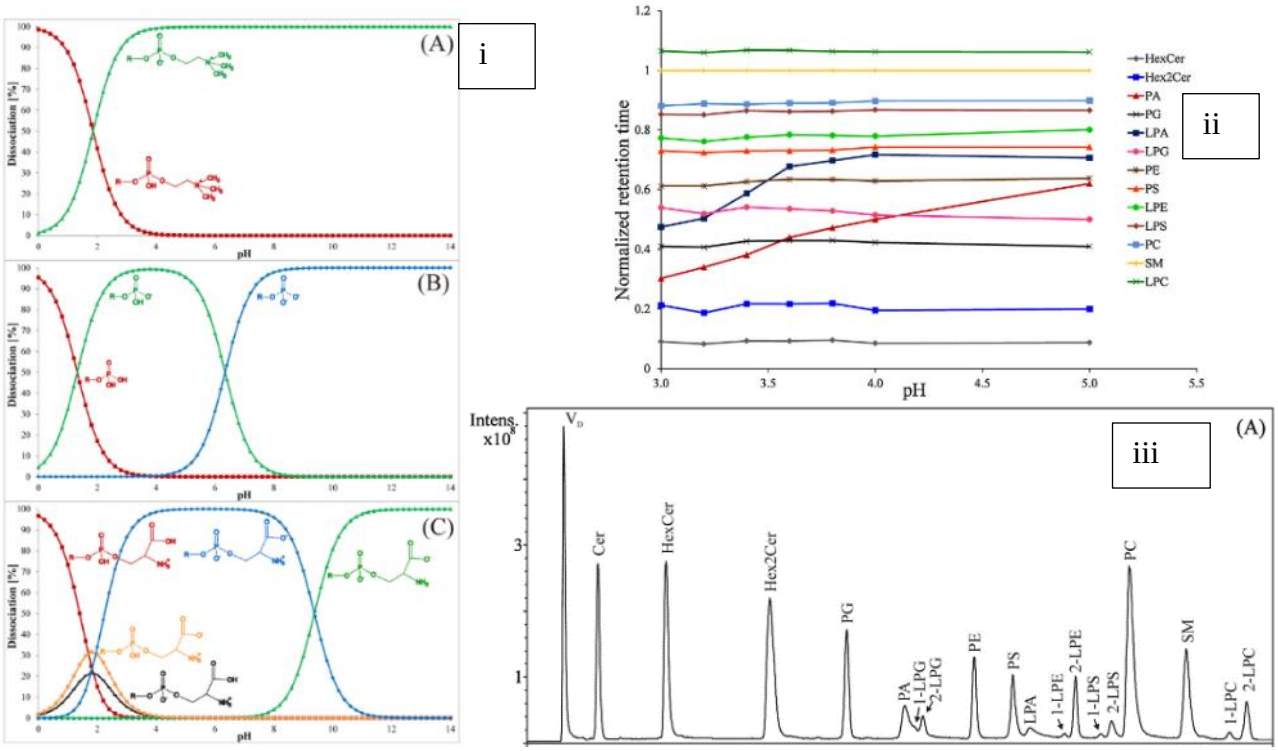

Figure 17 : Séparations de lipide en mode HILLIC [49].

Les lipides acides, tels que le PA et le PS, ont plusieurs pKa, Figure 17 i. En fonction du pH, ces lipides peuvent donc changer d'état d'ionisation, entraînant ainsi des changements de rétention sur les phases stationnaires, Figure 17 ii. Cela explique pourquoi ces lipides sont particulièrement difficiles à analyser. Un exemple de séparation de standards de lipides dans les conditions optimisées est présenté sur la Figure 17 iii.

La SFC a connu un renouveau ces dernières années grâce au développement de systèmes commerciaux robustes et performants [50]. Les fluides supercritiques possèdent des propriétés « hybrides » entre celles des liquides et celles des gaz. Leur densité est proche de celle du liquide, mais leur faible viscosité et haute diffusivité, se rapprochent des caractéristiques du comportement des gaz. Les séparations par SFC présentent de nombreux avantages, tels qu'une efficacité de séparation élevée, une faible consommation de solvant organique (SFC subcritique) et un court temps d'analyse. Le dioxyde de carbone (CO_2) est usuellement utilisé en SFC car son point supercritique est aisément atteignable (température : 31°C ; pression : 73.8 bars). Le CO_2 supercritique est un solvant non polaire, souvent comparé à l'hexane [51], bien adapté à l'analyse de composés de faible polarité. Des co-solvants et des additifs peuvent être mélangés au CO_2 supercritique afin de moduler la polarité de la phase mobile et permettre l'élution de l'ensemble des lipides. Lísa et Holčapek ont publié en 2015 [52] une séparation de lipides de moins de 6 min, illustrée sur la Figure 18.

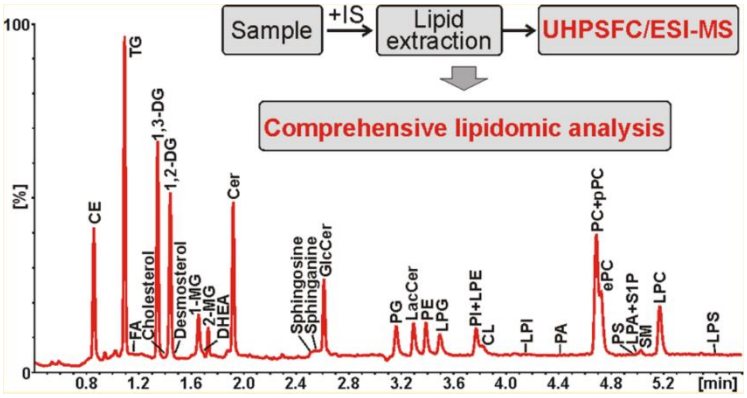

Figure 18 : Séparation d'un mélange de standards de lipides par UHPSFC/ESI$^+$-MS [52].

La SFC peut également être utilisée en chromatographie bidimensionnelle associée avec la RPLC. Dans l'étude [53], menée sur du plasma humain de patientes atteintes d'un cancer du sein *vs* témoins sains, 370 espèces lipidiques provenant de dix classes différentes ont été identifiées et 20 biomarqueurs lipidiques du cancer du sein ont été trouvés.

4. *Spectromètres de masse*

Après leurs séparations sur colonne chromatographique, les lipides arrivent dans le spectromètre de masse. Les lipides sont alors ionisés dans la source, puis transférés vers l'analyseur et envoyés vers le détecteur.

4.1 *Sources d'ionisation*

L'ionisation par électrospray (ESI) est la principale source utilisée, cela explique pourquoi cette source est la seule à être représentée sur la Figure 14 B [17]. L'ESI est compatible avec les solvants polaires utilisés lors des séparations par RPLC et présente l'avantage de produire peu de fragments. Les sources APCI et APPI sont adaptées pour des solvants les moins polaires tels que ceux utilisés en NPLC. Un schéma de ces trois sources est proposé sur la Figure 19. Le principe de fonctionnement est détaillé ci-après.

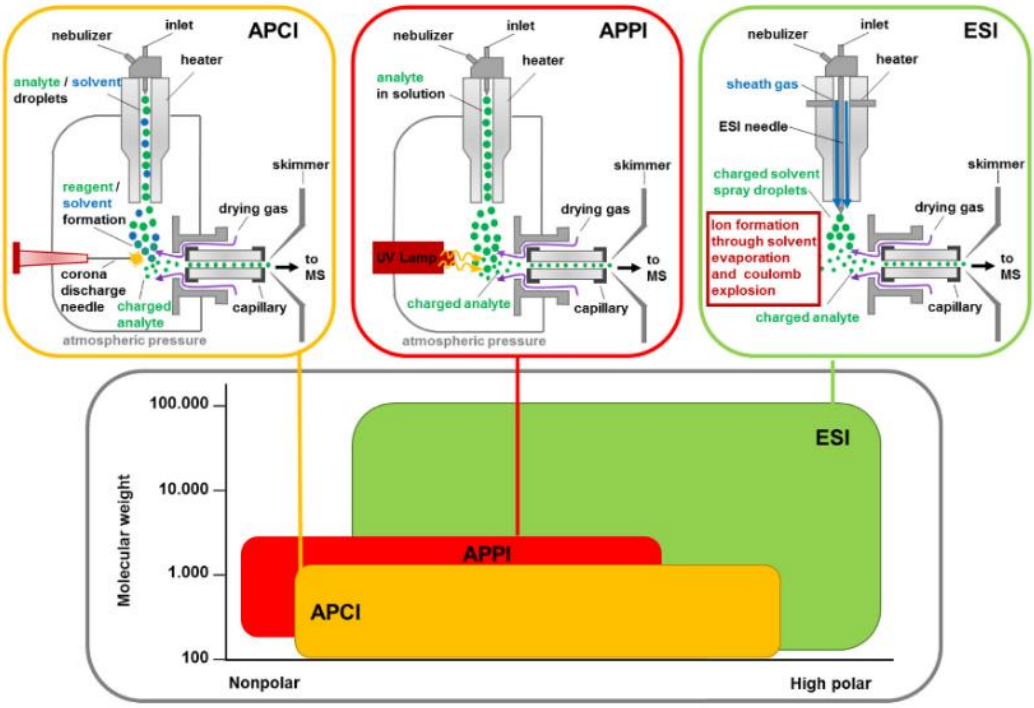

Figure 19 : Exemple de schémas de sources APCI, APPI et ESI ainsi que leur domaine d'application [54].

Dans les « Techniques de l'Ingénieur », le principe de fonctionnement des sources APCI et APPI est détaillé par Patrick Arpino [55], et celui de la source ESI par Bertrand Monégier [56]. Ces deux articles constituent le principal support de la partie ci-après.

Il existe des similitudes entre les sources APCI et APPI, ce qui permet aux fournisseurs de proposer des sources avec les deux modes d'ionisation simultanément. Dans nos travaux, les études en APPI ont été menées en introduisant la lampe Krypton dans la source APCI, cependant que l'aiguille corona avait été désactivée.

Ceci est possible car les processus mis en jeu au niveau du nébuliseur sont identiques. Le nébuliseur est chauffé à haute température (200-500°C) et parcouru par un gaz de nébulisation (généralement N_2), ce qui permet aux analytes accompagnés de leur solvant d'être nébulisés puis évaporés. L'étape d'ionisation diffère entre les deux sources.

En APCI, « les ions réactants présents dans le plasma activé par les électrons de la décharge couronne sont dominés par les espèces positives ou négatives les plus stables » [55].

En absence de vapeurs de solvants, les molécules présentes sont celles provenant de l'air atmosphérique (N_2, O_2, CO_2 et H_2O) et celles du gaz ajouté.

En mode positif, la première espèce réactive produite est $N_2^{+\bullet}$, mais elle est très rapidement remplacée par des clusters majoritaires $(H_2O)_nH_3O^+$, l'eau étant la molécule de l'air avec la plus forte affinité protonique.

En mode négatif, l'anion superoxyde $O^{-\bullet}$ est formé en premier. Il est rapidement remplacé par des clusters majoritaires $(H_2O)_nO^{-\bullet}$. Un schéma simplifié est présenté sur la Figure 20 A.

En présence de vapeurs de solvants, l'affinité protonique la plus forte est celle des solvants notés [S_1 et S_2]. Cela conduit à l'ionisation du solvant tel que présenté sur la Figure 20 B. Les solutés sont ensuite ionisés par des réactions classiques d'ionisation chimique en phase gazeuse, lors de collisions avec les espèces réactives dans la source [55]. Les réactions

chimiques en mode positif et négatif sont détaillées sur la Table 1. Des exemples de valeurs d'affinité protonique sont présentés sur la Table 2.

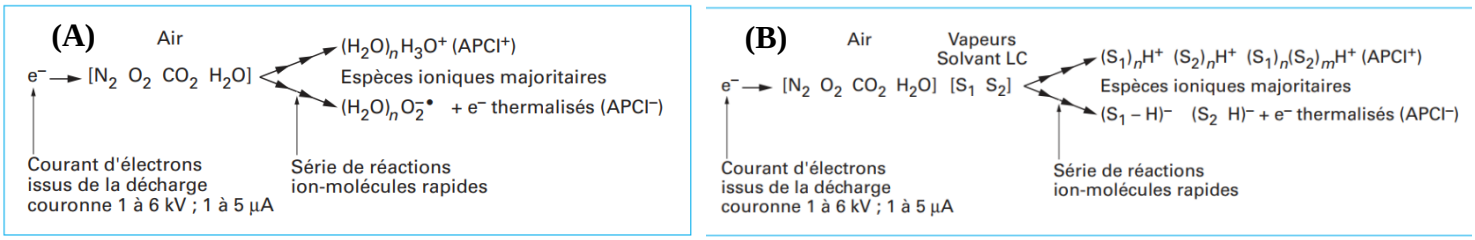

Figure 20 : Espèces ioniques majoritaires dans une source APCI : en l'absence de vapeurs de solvants LC (A) et en présence de vapeurs de solvants LC (B) [55].

(A)

$N_2 + e^- \rightarrow N_2^{+\bullet} + 2e^-$	(1)
$N_2^{+\bullet} + 2N_2 \rightarrow N_4^{+\bullet} + N_2$	(2)
$H_2O^{+\bullet} + H_2O \rightarrow H_3O^+ + HO^\bullet$	(3)
$H_3O^+ + H_2O + N_2 \rightarrow H^+(H_2O)_2 + N_2$	(4)
$H^+(H_2O)_{n-1} + H_2O + N_2 \rightarrow H^+(H_2O)_n + N_2$	(5)
$A + B^{+\bullet} \rightarrow A^{+\bullet} + B$	(6)
$A + BH^+ \rightarrow AH^+ + B$	(7)

(B)

$M + e^- \rightarrow M^{-\bullet}$, if $EA(M) > 0$	(1)
$O_2 + e^- \rightarrow O_2^{-\bullet}$, since $EA(O_2) = 0.48$ eV	(2)
$O_2^{-\bullet} + M \rightarrow M^{-\bullet} + O_2$, if $EA(M) > EA(O_2) = 0.48$ eV	(3)
$HA + O_2^{-\bullet} \rightarrow A^- + HO_2^\bullet$, if $\Delta G_{acid}(HA) < \Delta G_{acid}(HO_2^\bullet)$	(4)
$A + [B-H]^- \rightarrow [A-H]^- + B$, if $\Delta G_{acid}(A) < \Delta G_{acid}(B)$	(5)
$M + O_2^{-\bullet} \rightarrow [M-X+O]^- + OX^\bullet$, where X = halogen, NO_2 or H	(6)
$M^{-\bullet} + O_2 \rightarrow [M-X+O]^- + OX^\bullet$	(7)

Table 1 : Réactions d'ionisation dans la source APCI : en mode d'ionisation positif (A) et en mode d'ionisation négatif (B) [57].

Tableau 4 – Énergies d'ionisation de gaz API, solvants LC, dopants, et énergies émises par les lampes UV utilisées en APPI

Atmosphère API		Solvants LC			Dopants			Lampe UV	
Air	IE (eV)	S	IE (eV)	PA (kJ · mol⁻¹)	D	IE (eV)	PA (kJ · mol⁻¹)	Gaz	IE (eV)
N_2	15,58								
CO_2	13,78								
H_2O	12,62	H_2O	12,62	691					
		CH_3CN	12,20	779					
O_2	12,07							Ar	11,8
		$CHCl_3$	11,37	–					11,6
		CH_2Cl_2	11,33	–					
		HCO_2H	11,33	742					
		CH_3CO_2H	10,65	784					
		CH_3OH	10,84	754				Kr	10,64
		C_2H_5OH	10,48	776					
		i-C_3H_7OH	10,17	793					
		n-C_6H_{14}	10,13	665					
		NH_3	10,07	854					
		n-C_7H_{16}	9,93	–					
		i-C_8H_{18}	9,89	–				Kr	10,03
					Acétone	9,70	812		
					THF	9,40	822		
					Benzène	9,24	750		
					DMSO	9,10	884		
					Chlorobenzène	9,07	753		
					Bromobenzène	9,00	754		
					Toluène	8,83	784	Xe	8,4
					Anisole	8,20	840		

Table 2 : Energies d'ionisation de gaz API, solvants LC, dopants, et énergies émises par les lampes UV utilisées en APPI [55]. API- ionisation à pression atmosphérique ; IE- ionisation électronique ; PA- affinité protonique.

En APPI, une lampe UV émet des photons d'énergie *hv*. Ces photons interagissent avec les molécules (M) qui passent dans un état excité. Les molécules peuvent se désexciter par différents processus, dont la photoionisation : $M^* \rightarrow M^{+\bullet} e^-$.

La photoionisation n'intervient que si l'énergie du photon est supérieure à l'énergie d'ionisation de la molécule. Les valeurs des énergies d'ionisation et d'émission des lampes UV sont présentées sur la Table *2*. La lampe krypton émet deux raies d'énergies proches à 10,0 et 10,6 eV, dans un rapport d'intensité 4 :1. Ces énergies sont suffisamment importantes pour ioniser les analytes et suffisamment faibles pour ne pas ioniser la plupart des solvants utilisés. La lampe krypton est la seule à être utilisée dans les appareils commerciaux [55].

Les solvants (heptane, isooctane et acétone) dont l'énergie d'ionisation est légèrement inférieure à l'énergie émise par les photons de la lampe Krypton, permettent de jouer un rôle de dopant sans induire un bruit de fond important. Ces solvants peuvent être utilisés dans les phases mobiles ou être ajoutés en complément. Cai et Syage [58] ont étudié l'influence du solvant sur l'ionisation de l'ester méthylique de l'acide eicosapentaénoïque (EPA) (Figure 21 a), l'intensité du bruit de fond (Figure 21 b) et le rapport signal sur bruit (Figure 21 c). Les expérimentations mettent en exergue que l'hexane et le chloroforme induisent chacun peu de bruit de fond. Cependant, lors de leur utilisation en mélange, le bruit de fond devient important. Dans ces conditions, le rapport signal sur bruit (S/N) de l'ester méthylique de l'EPA devient très faible. Les réactions chimiques en mode positif et négatif mis en jeu avec la source APPI sont détaillées sur la Table 3.

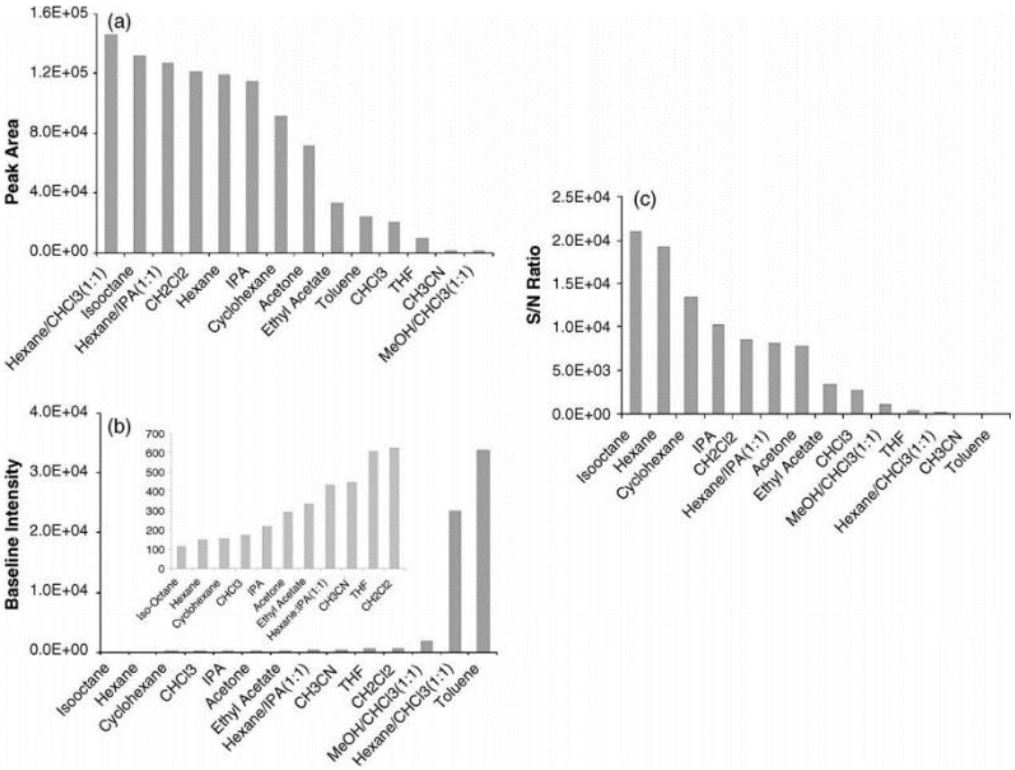

Figure 21 : Source APPI, effets de la phase mobile sur : la surface du pic (a), l'intensité de base (b) et le rapport signal sur bruit (S/N) de l'ester méthylique d'EPA (m/z 317) (c) [58].

(A)

$M + h\nu \rightarrow M^{+\bullet} + e^-$	(1)
$M^{+\bullet} + S \rightarrow MH^+ + [S-H]^\bullet$	(2)
$D(\text{dopant}) + h\nu \rightarrow D^{+\bullet} + e^-$	(3)
$D^{+\bullet} + M \rightarrow M^{+\bullet} + D$, if $IE(M) < IE(D)$	(4)
$D^{+\bullet} + S(\text{solvent molecule}) \rightarrow [D-H]^\bullet + SH^+$, if $PA(S) > PA([D-H]^\bullet)$	(5)
$SH^+ + M \rightarrow MH^+ + S$, if $PA(M) > PA(S)$	(6)
$S + h\nu \rightarrow S^{+\bullet} + e^-$	(7)

(B)

$D + h\nu \rightarrow D^{+\bullet} + e^-$	(1)
$O_2 + e^- \rightarrow O_2^{-\bullet}$	(2)
$M + e^- \rightarrow M^{-\bullet}$, if $EA(M) > 0\,eV$	(3)
$M + O_2^{-\bullet} \rightarrow M^{-\bullet} + O_2$, if $EA(M) > EA(O_2) = 0.451\,eV$	(4)
$M + O_2^{-\bullet} \rightarrow [M-H]^- + HO_2^\bullet$, if $\Delta G_{acid}(M) < \Delta G_{acid}(HO_2^\bullet)$	(5)
$S + O_2^{-\bullet} \rightarrow [S-H]^- + HO_2^\bullet$, if $\Delta G_{acid}(S) < \Delta G_{acid}(HO_2^\bullet)$	(6)
$M + [S-H]^- \rightarrow [M-H]^- + S$, if $\Delta G_{acid}(M) < \Delta G_{acid}(S)$	(7)
$M + O_2^{-\bullet} \rightarrow [M-H+O]^- + OH^\bullet$	(8)
$M^{-\bullet} + O_2 \rightarrow [M-H+O]^- + OH^\bullet$	(9)

Table 3 : Réactions d'ionisation dans la source APPI : en mode d'ionisation positif (A) et en mode d'ionisation négatif (B) [57].

L'ESI, est également une source à pression atmosphérique. Les analytes et le solvant entrent dans la source via un capillaire. Ce capillaire traverse une aiguille métallique dont le potentiel est généralement compris entre 3 à 5 kV. Il se forme alors un cône de Taylor à la sortie du capillaire. De fines gouttelettes chargées en surface sont produites, ce phénomène est appelé *nébulisation électrostatique* [59]. Le solvant contenu dans les gouttelettes s'évapore progressivement, grâce à l'azote chauffé circulant à contre-courant, jusqu'à atteindre la limite

de Rayleigh. Puis, la répulsion électrostatique des charges de même signe à la surface provoquent une succession d'explosions coulombiennes [60]. La désolvatation se poursuit jusqu'à la formation d'ions en phase gazeuse. Une illustration de l'interface ESI et du mécanisme d'ionisation est présenté sur la Figure 22.

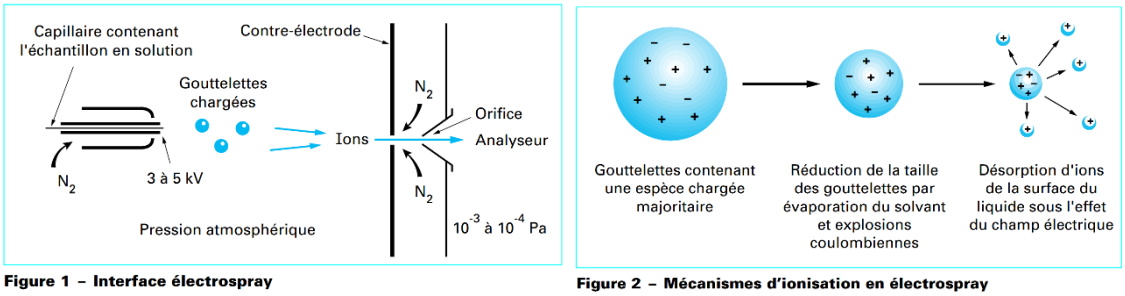

Figure 22 : Source ESI : interface (A) et mécanismes d'ionisation (B) [56].

La différence de potentiel entre la tension au niveau de l'orifice et le premier potentiel appliqué dans l'enceinte de l'appareil influence l'allure des spectres. Une différence de potentiel de quelques volts, n'est pas suffisante pour éliminer totalement les adduits formés avec le solvant. Une différence de potentiel de 30 V permet d'éliminer ces adduits au profit des adduits $[M+H]^+$ et $[M+Na]^+$. Une différence de potentiel de 120 V, favorise la fragmentation en source, liée aux collisions avec l'azote circulant. Cette fragmentation s'apparente à celle pouvant être obtenue par spectrométrie de masse en tandem (SM/SM) [56]. Le principal inconvénient de cette source est la suppression d'ionisation en présence d'autres composés ou lors de concentrations importantes [61,62]. Ce phénomène est moins important avec la source APCI [62,63] car les analytes ne sont pas en compétition pour entrer dans la phase gazeuse et le nombre maximal d'ions formés en phase gazeuse est beaucoup plus élevé, les ions réactifs étant formés de manière continue.

Dans l'étude [20], nous avons comparé l'ionisation de 22 standards de lipides lors du couplage de la NPLC à ces trois sources d'ionisation. Ces travaux sont présentés dans le chapitre III et en Annexe I de ce manuscrit.

4.2 Mobilité ionique

Les spectromètres de masse peuvent être équipés d'une mobilité ionique (IM), comme dans le schéma de l'instrument Agilent IM-QTOF présenté sur la Figure 23. La mobilité ionique, située après la source d'ionisation, est un module permettant d'obtenir une séparation des ions par la taille, la forme, la charge et la masse en fonction de leurs différentes mobilités dans des champs électriques faibles ou élevés. Cette technologie est particulièrement intéressante pour l'étude d'espèces moléculaires isobares, la détermination des positions *sn*-1/*sn*-2 des FAs sur le glycérol, la position de double liaison ainsi que leur configuration (cis/trans) et la chiralité (R/S) [64]. Un exemple de séparation d'acides gras obtenue par mobilité ionique est présenté sur la Figure 24.

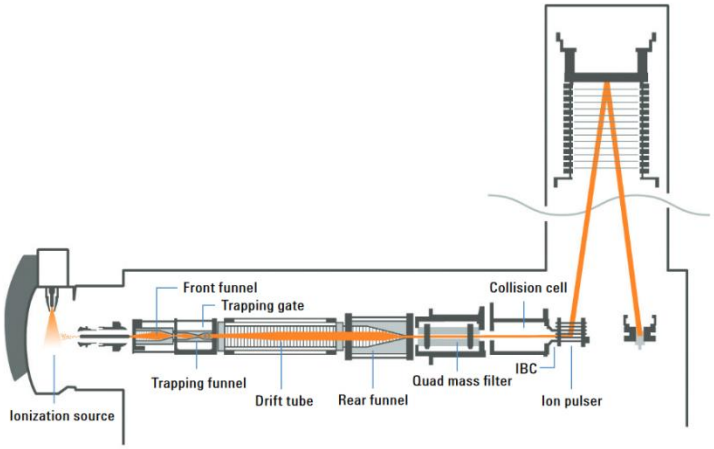

Figure 23 : Schéma de l'instrument Agilent IM-QTOF [65].

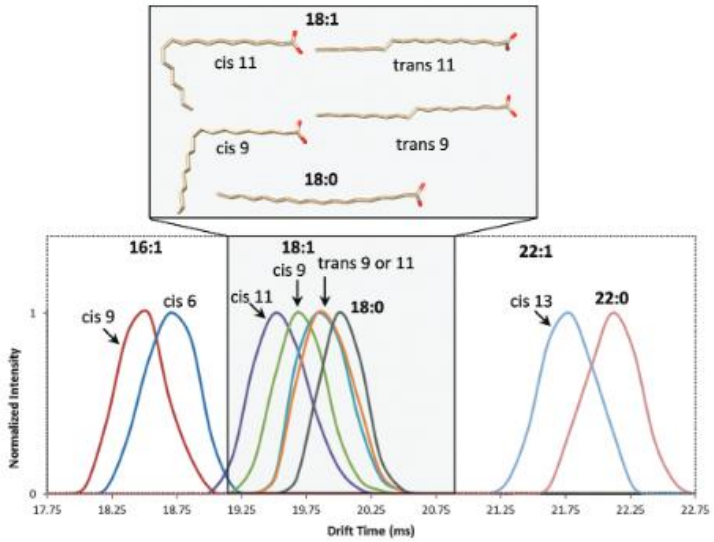

Figure 24 : Analyses IM-MS de standards d'acides gras avec différents emplacements et orientations de doubles liaisons [64].

4.3 Analyseurs

Les analyseurs se différencient par leur principe de sélection des ions :

- Quadripôle (Q) : transmission des ions traversant un champ électrodynamique [66].
- Trappe ionique (IT) : mouvement périodique dans un champ magnétique ou électrodynamique [67].
- Temps de vol (TOF) : séparation dans le temps, fondée sur la vitesse des ions [68].
- Trappe orbitale : dispersion des ions, fondée sur leur moment ou leur énergie cinétique, instruments à secteur électrique [69].
- Résonance Cyclotronique des ions à transformée de Fourier (FT-ICR) : Dispersion des ions, fondée sur leur moment ou leur énergie cinétique, instruments à secteur magnétique [70].

Le schéma de ces analyseurs, extrait du livre de Schuchardt et al. [71] sont présentés sur la Figure 25. Comme indiqué sur le schéma, la trappe ionique linéaire (LIT) est une synthèse simplifiée d'un quadripôle et d'une trappe ionique (flèches de connexion) avec des performances améliorées.

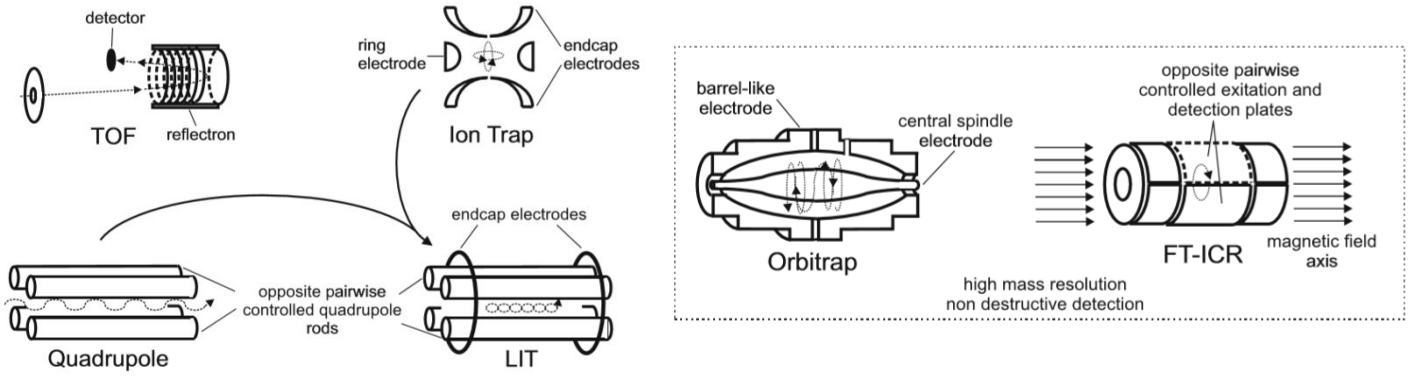

Figure 25 : Schémas des principaux analyseurs utilisés pour l'analyse des lipides [71].

Les spectromètres de masse couplant différents analyseurs sont dits hybrides. La répartition des analyseurs dans les études lipidomiques est présentée sur la Figure 14 C. Le principal analyseur utilisé est le TOF (39%), suivi du QLIT (17%), QqQ (14%), IT (13%), trappe orbitale (10%), IT-FTICR (5%) et Q (2%).

Les spécifications des analyseurs varient suivant leurs technologies, comme détaillé sur la Table 4. Les analyseurs de type FTICR sont ceux qui possèdent les meilleures performances de résolution et d'exactitude (accuracy) suivi des trappes orbitales et des TOF, ces trois analyseurs sont dits à haute résolution.

Comparison of the features and specifications of the mass analyzers commonly used for proteomics

Mass analyzer	Mass resolution[a]	Mass accuracy (ppm)	Sensitivity	*m/z* range	MS/MS capability	Ion source
IT	1000–1500	100–1000	Picomole	50–2000; 200–4000	MS^n	ESI
LTQ (LIT)	2000	100–500	Femtomole	50–2000; 200–4000	MS^n	ESI
Q-q-Q	1000	100–1500	Attomole	50–4000	MS/MS	ESI
TOF	10 000–20 000	5–50	Femtomole	No upper limit	n/a	MALDI
TOF-TOF	10 000–40 000	5–50	Femtomole	No upper limit	MS/MS	MALDI
Q-q-TOF	10 000–40 000	5–50	Attomole	No upper limit	MS/MS	ESI; MALDI
LTQ-FTICR	50 000–800 000	1–2	Femtomole	50–2000; 200–4000	MS^n	ESI; MALDI
LTQ-Orbitrap	50 000–500 000	<5	Femtomole	50–2000; 200–4000	MS^n	ESI; MALDI

[a]Mass resolution at full width half maximum.

Table 4 : Comparaison des caractéristiques et spécifications des analyseurs de masse couramment utilisés pour la protéomique [72].

La résolution correspond au rapport entre la masse mesurée (m) de l'ion et la largeur à mi-hauteur du pic (Δm). $R=m/\Delta m$

Plus la résolution d'un analyseur est grande, plus le Δm est petit, comme illustré sur la Figure 26 A. La résolution d'un analyseur est toujours définie pour une masse donnée, car elle varie en fonction de celle-ci. Par exemple, la résolution d'une trappe orbitale (Q exactive HF MS ou MS) diminue lorsque la masse de l'ion analysé augmente, Figure 26 B. Les quadripôles et les trappes ioniques sont des analyseurs à basse résolution.

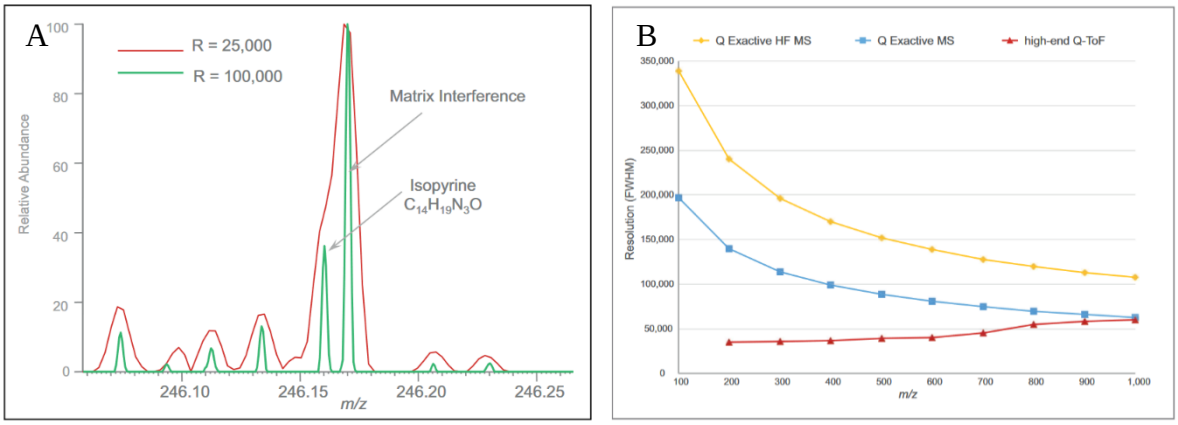

Figure 26: Comparaison de la résolution à R = 25 000 et à R = 100 000 à m/z 200 (A) et variation de la résolution en fonction du rapport m/z (B) [73].

L'exactitude de masse (accuracy) correspond à l'écart entre la masse mesurée et la masse exacte. Cette valeur s'accompagne d'une autre valeur qui rend compte de la dispersion des mesures expérimentales, appelée « précision ». Ces deux termes sont illustrés sur la Figure 27 A et B. Une mesure peut être exacte et précise (i), exacte mais non précise (ii), précise mais non exacte (iii) ou non exacte et non précise (iv).

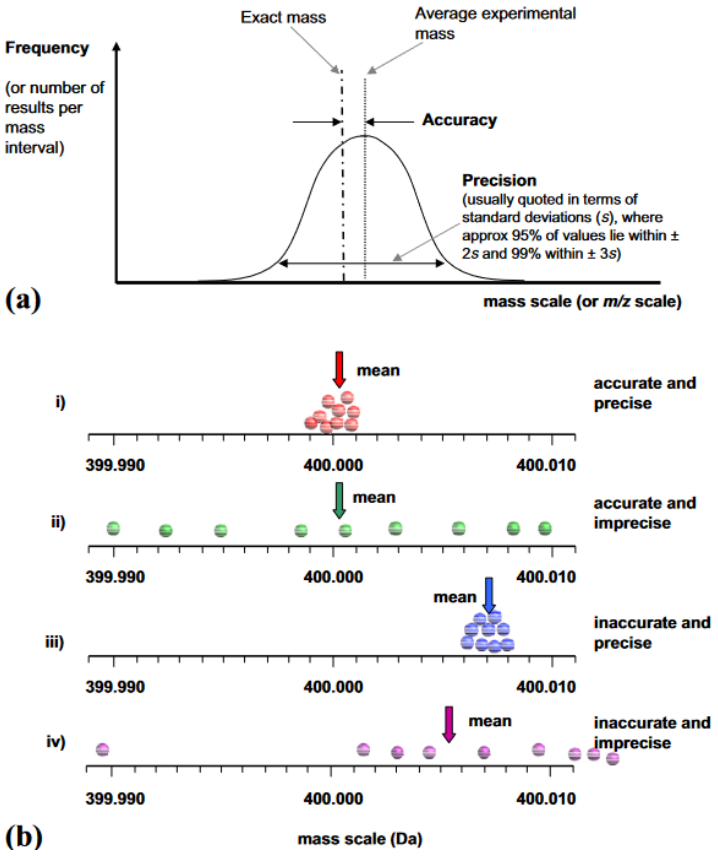

Figure 27: Représentation de l'exactitude et de la précision [74].

Le schéma du spectromètre de masse hybride Thermo Orbitrap Velos Pro, utilisé durant les travaux de thèse est présenté sur la Figure 28. Une photographie de cet équipement ainsi que ses spécifications sont présentées sur la Figure 29.

Cet équipement possède un analyseur de type LTQ, équivalent à la trappe ionique linéaire (LIT). Les cellules (haute et basse pression) du LTQ permettent de réaliser des expérimentations en MS^2 et en MS^3. Les ions issus de la MS, MS^2 et MS^3 peuvent être détectés en basse résolution via les deux détecteurs positionnés de part et d'autre du LTQ. Ces ions peuvent être également transmis jusqu'à l'Orbitrap pour une séparation des ions à haute résolution.

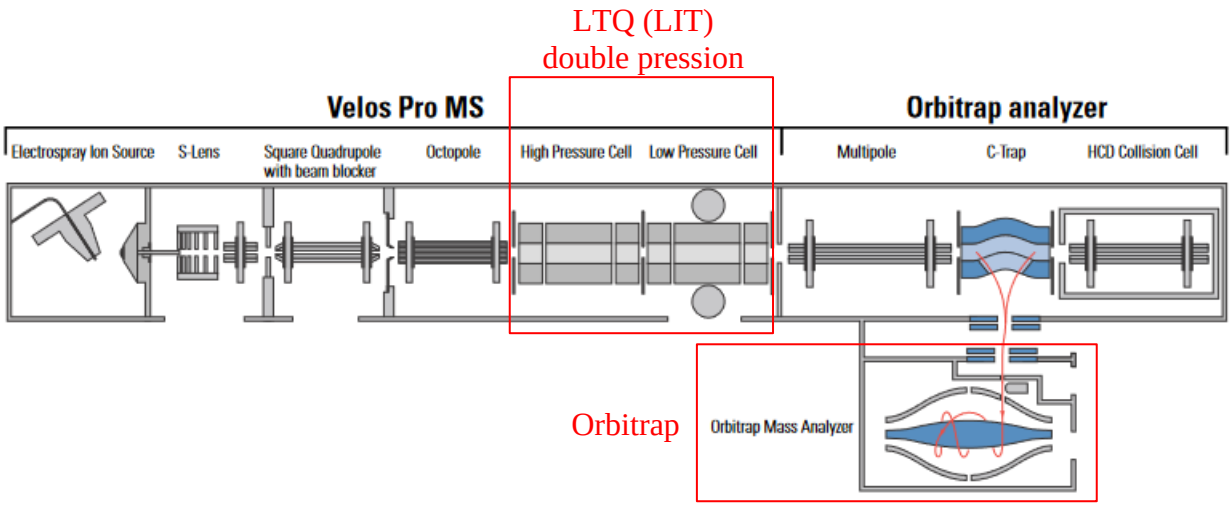

Figure 28: Schéma du Thermo Orbitrap Velos Pro LC-MS [75].

The Orbitrap Velos Pro mass spectrometer has the following measuring specifications:

Resolution	60000 (FWHM) @ *m/z* 400 with a scan repetition rate of 1 second Minimum resolution 7500, maximum resolution 100000 @ *m/z* 400
Cycle Time	1 scan at 60000 resolution @ m/z 400 per second
Mass Range	m/z 50–2000; m/z 200–4000
Mass Accuracy	<3 ppm RMS for 2 h period with external calibration using defined conditions, <1 ppm RMS with internal calibration
Dynamic Range	>10000 between mass spectra, >5000 between highest and lowest detectable ion signal in one spectrum
MS/MS	MS/MS and MS^n scan functions

Figure 29: Photographie et spécifications du Thermo Orbitrap Velos Pro Orbitrap [75].

4.4 Modes d'acquisition de données en spectrométrie de masse

4.4.1 L'acquisition par balayage MS

L'acquisition MS^1 (full scan), consiste à enregistrer simultanément l'ensemble des ions produits en source dans la gamme de masse sélectionnée, comme illustré sur le premier cadran de la Figure 30. Ce mode d'acquisition, non ciblé, est particulièrement intéressant pour mettre en évidence, en première intention, des signaux discriminants entre différents groupes d'échantillons. En 2012, notre laboratoire a ainsi comparé le profil des PLs de souche de *Leishmania donovani* non traités, traités et résistants à la miltéfosine [76]. Une fois les signaux discriminants mis en évidence, grâce à des outils chimiométriques, l'identification des lipides est réalisée par l'investigation des acquisitions MS^n.

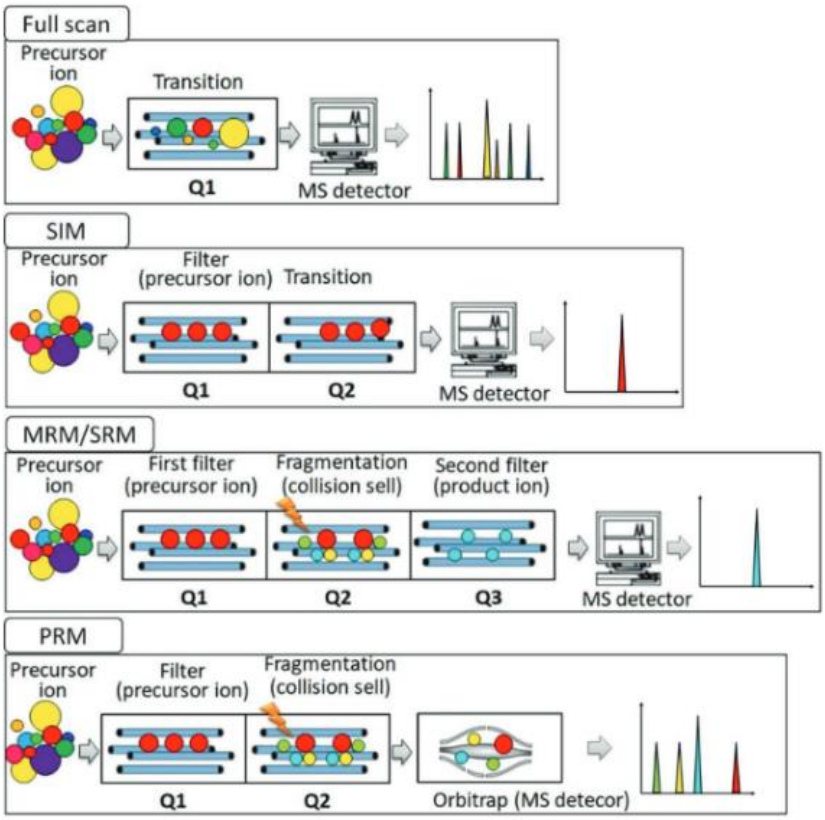

Figure 30: Modes de détection MS : analyse complète (full scan), surveillance des ions sélectionnés (SIM), surveillance des réactions multiples (MRM) & (SRM) et surveillance de réaction parallèle (PRM) [77].

4.4.2 Modes de fragmentation

Lors de l'utilisation des sources d'ionisation à pression atmosphérique, deux modes de fragmentation sont principalement rencontrés [78], le mode de dissociation induite par collision (CID) après activation résonnante et le mode de dissociation induite par collision à haute énergie (HCD) après activation non-résonnante. Un schéma des voies de dissociation en mode CID et HCD est présenté sur la Figure 31. La Figure 31 A permet de comparer la gamme *m/z* des deux techniques de fragmentation. En mode CID, la fenêtre d'isolation *m/z* est égale à la fenêtre d'excitation résonnante. Le mode HCD utilise la même fenêtre d'isolement, cependant l'excitation est appliquée de manière non résonnante sur toute la gamme de masse. La Figure 31 B présente la généalogie des ions précurseurs et descendants. En mode CID, seul le précurseur est excité au-dessus du seuil de dissociation. Toute la fragmentation qui en résulte est alimentée par ce transfert d'énergie. En mode HCD, des réactions consécutives sont alimentées par une excitation non sélective de toutes les espèces ioniques. Le mode CID et HCD permettent d'obtenir des spectres de masse différents [78].

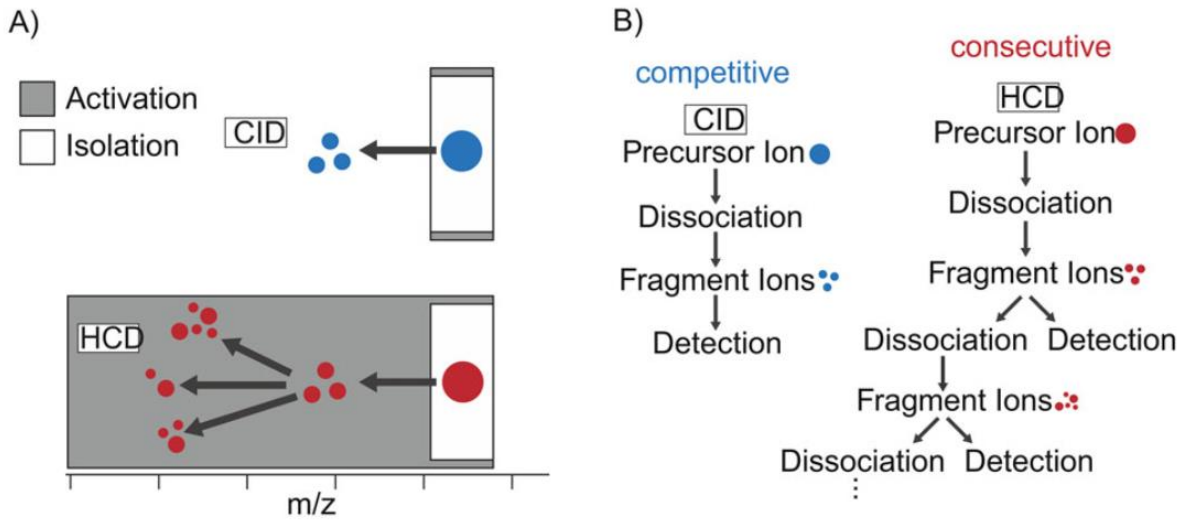

Figure 31: Figure schématique des voies de dissociation en mode CID et HCD [79].

4.4.3 Modes d'acquisition MS²

Le mode d'acquisition ciblé permet de suivre de manière très spécifique des composés d'intérêts. Il existe le mode « Selected Ion Monitoring » (SIM) ; le mode « Multiple Reaction Monitoring » (MRM) équivalent au mode « Selected Reaction Monitoring » (SRM) et le mode « Parallel Reaction Monitoring » (PRM). Ces différents modes sont présentés sur la Figure 30.

En mode SIM, un seul ion est filtré. En mode MRM/SRM et PRM, un ion précurseur est sélectionné par le Q1, la fragmentation de cet ion est réalisée par le Q2, la différence entre les deux modes apparaît à l'étape suivante. En mode MRM/SRM un ion fragment est sélectionné par le Q3, ce mode permet de suivre une seule transition. En mode PRM l'ensemble des ions fragments sont dirigés vers la trappe orbitale.

En mode d'acquisition non ciblé, l'ensemble des ions sont pris en compte. Il existe le mode « Data Dependent Acquisition » (DDA) et le mode « Data-Independent Acquisition » (DIA). Ces deux modes se distinguent par la mise en œuvre de la MS^2.

En mode DDA, l'analyseur sélectionne les ions les plus intenses, afin de les fragmenter et les analyser de manière indépendante. Ainsi, le spectre de masse de chacun de ces ions est accessible.

En mode DIA, la MS^2 est réalisée sur l'ensemble des ions produit en MS^1, « All-Ion Fragmentation » (AIF). Cette fragmentation globale des ions rend difficile l'interprétation. Pour pallier cette difficulté, le mode « Sequential Window Acquisition of all Theoretical fragment-ion mass spectra » (SWATH) [80] a été développé. Le mode SWATH réalise des spectres MS^2 par segments de *m/z*, de manière indépendante. Un schéma des différents modes d'acquisition non ciblé est présenté sur la Figure 32.

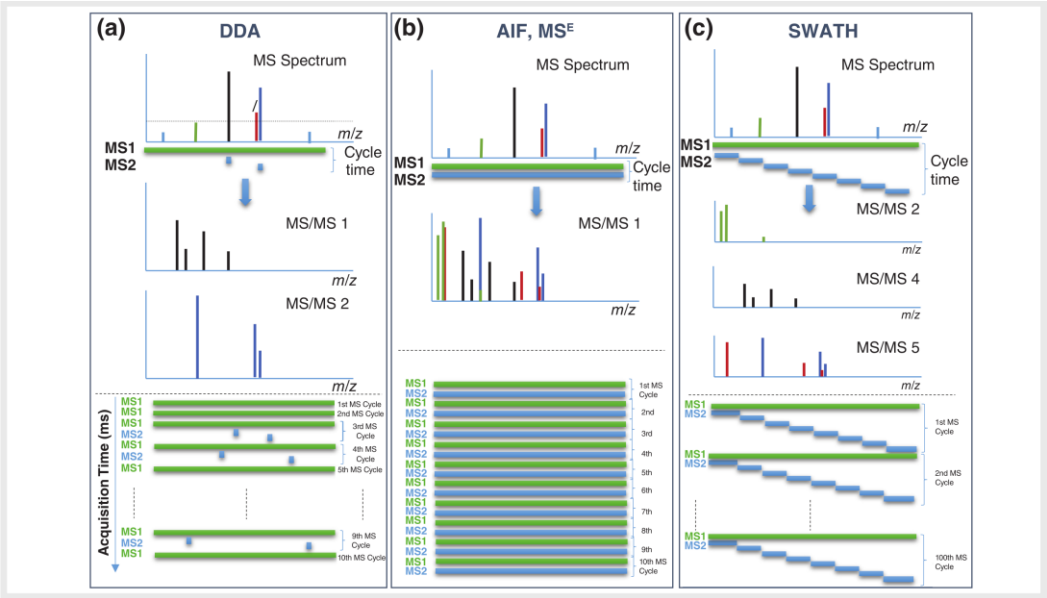

Figure 32: Schémas des modes d'acquisition: DDA (a) ; AIF, MS^E (b) et SWATH (c) [81].

4.5 Traitement des données

4.5.1 Traitement des données brutes

L'analyse LC-MS comporte trois dimensions: le temps de rétention, la valeur *m/z* et l'intensité du signal. Le format des données issu des instruments doit être généralement converti au format des logiciels de traitement de données avant de pouvoir les importer.

Par exemple, Reifycs converti les données au format ABF (http://www.reifycs.com/AbfConverter/index.html) et *ProteoWizard* [82] converti les données aux formats mzML, mzXML etc.

Certains logiciels de traitement de données, comme *XCMS* [83] ou *Workflow4Metabolomics* [84], permettent l'exécution de quatre étapes :

(1) Le filtrage ; (2) la détection de signaux (features), (3) l'alignement et (4) la normalisation.

Les méthodes de filtrage permettent d'éliminer le bruit de fond. La détection de signaux consiste à éliminer les signaux interférents comme ceux des motifs isotopiques par une méthode de déconvolution, par exemple. Les méthodes d'alignement corrigent les différences de temps de rétention. Enfin, la normalisation correspond à une correction des signaux pour pallier les différences dans la nature ou dans la préparation des échantillons.

Des tests statistiques sont proposés pour établir des comparaisons de données. Il est toutefois important de garder un regard critique sur les résultats obtenus. Une étude sur des biomarqueurs plasmatiques chez des rats nourris et à jeun, a mis en évidence des différences plus grandes entre les outils de traitement des données que les différences liées aux échantillons [85].

Ce type de logiciels ne permet pas de gérer l'ensemble des données acquises lors des analyses, notamment les informations issues de la MS^2, indispensables à l'identification. Pour cela, il est possible d'utiliser d'autres logiciels librement accessibles comme MS-DIAL [86], LipidMatch [87], Greazy (pour les PLs) [82] ou des logiciels sous licence constructeurs comme LipidSearch de ThermoFisher Scientific. Une comparaison de ces logiciels est présentée sur la Table 5. Le site web de LIPID MAPS propose également un guide des outils pour la lipidomique (disponible sous l'onglet « Mass Spectrometry Tools » puis « Lipidomics Tools Guide »).

	LipidMatch	MS-DIAL	GREAZY	LipidSearch 4.1
Identification (ID) Strategy*	Rules	Similarity	Similarity	Rules & Similarity
Fragment Intensity for ID*	Yes (ranking)	Yes	No	Yes
in-silico Library (Types)	56	34	24	59
User Developed Libraries	Yes	Difficult	Difficult	Difficult
Programming Language	R	C#	C++	Java
Restrictions	None	None	None	Purchase License
Multiple Vendor Formats	Yes (.ms2)	Yes (.abf)	Yes (.mzML)	Yes (vendor DLL)
Data Independent Analysis**	Yes	Yes	No	No
MS^3 analysis	No	No	No	Yes
Multiple Hits in Final Report	Yes (ranked)	No	No	Yes (ranked)
Structural Resolution***	Correct	Over Reports	Over Reports	Correct
Identifiers (eg. LipidMaps)	No	Yes	No	No
Computational time (HR data)	Slow	Medium	Fast	Fast
Employs False Discovery	No	No	Yes	No

Table 5: Comparaison des logiciels d'identification des lipides [87].

4.5.2 Identification et annotations

L'utilisation d'échantillons de contrôles qualité (QC) est essentielle pour une annotation correcte des données lipidomiques [88]. Le QC est injecté au début d'une séquence d'analyse puis à intervalles réguliers pour suivre les performances de l'instrumentation et détecter d'éventuelles dérives [89]. Le QC doit être représentatif de la composition à la fois quantitative et qualitative des échantillons. De ce fait, le QC est obtenu par le mélange de tous les échantillons. Son injection à différents niveaux de concentration permet de déterminer pour chaque variable le coefficient de corrélation, le coefficient de variation (CV) et les ratios QC/blanc.

Le traitement du flux d'information par le logiciel MS-DIAL est présenté sur la Figure 33. Ce logiciel prend en compte les modes d'acquisition précédemment détaillés (DDA, DIA…) mais également la mobilité ionique. La déconvolution des pics est effectuée en tirant parti des spectres MS^2. Pour l'identification des composés, le logiciel compare les spectres MS^2 à ceux de bases de données en accès libre tels que LipidBlast (in silico) [90], MassBank of North America (MoNa), etc. Les spectres de masse, « in silico » ou réalisés avec des paramètres différents, peuvent générer des spectres MS^2 avec des intensités différentes ou avec des *m/z* manquants ou supplémentaires. De plus, lors de l'analyse de matrices complexes, il peut y avoir des coélutions de plusieurs isomères, ce qui rend l'identification difficile et oblige à une vérification manuelle [88]. L'annotation du logiciel est faite sur la base de plusieurs scores. La problématique du « scoring » intervient lorsqu'il y a trop de différences par rapport aux spectres expérimentaux ou les spectres de référence.

Pour des analyses faites dans certaines conditions préalablement définies, il existe des pipelines en téléchargement facilitant l'identification. Le temps de rétention des lipides ainsi que leurs adduits sont déjà définis. Généralement, ces pipelines sont établis en RPLC avec une

source ESI. Il est toutefois possible de créer sa propre base de données en définissant ces données, mais cela peut s'avérer difficile [87].

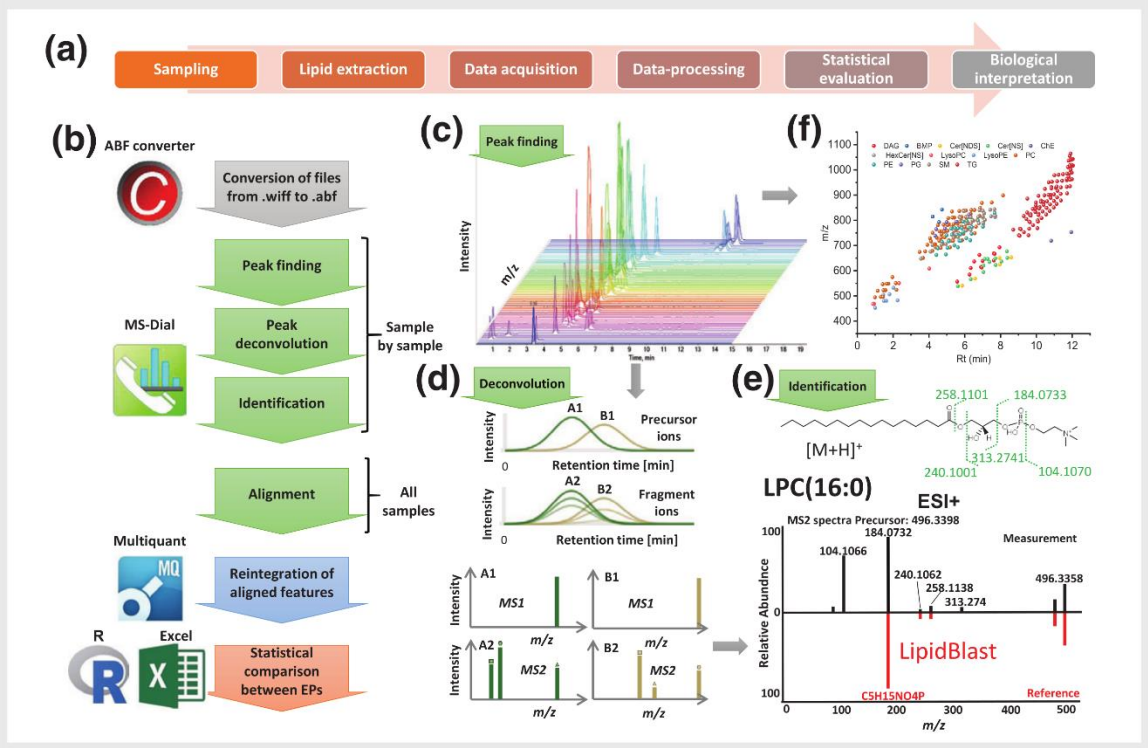

Figure 33: Flux de travail en lipidomique non ciblé et flux de travail de traitement de données basé sur le logiciel open source MS – DIAL [81].

L'annotation des lipides peut être faite à plusieurs niveaux, en fonction des données expérimentales et de leurs correspondances avec les bases de données. La Figure 34, illustre cet aspect. Si les fragments acyles sont trouvés, une information sur les FAs peut être donnée. Suivant le ratio entre les ions fragments, la position des FAs (*sn*-1/*sn*-2) peut être déterminée.

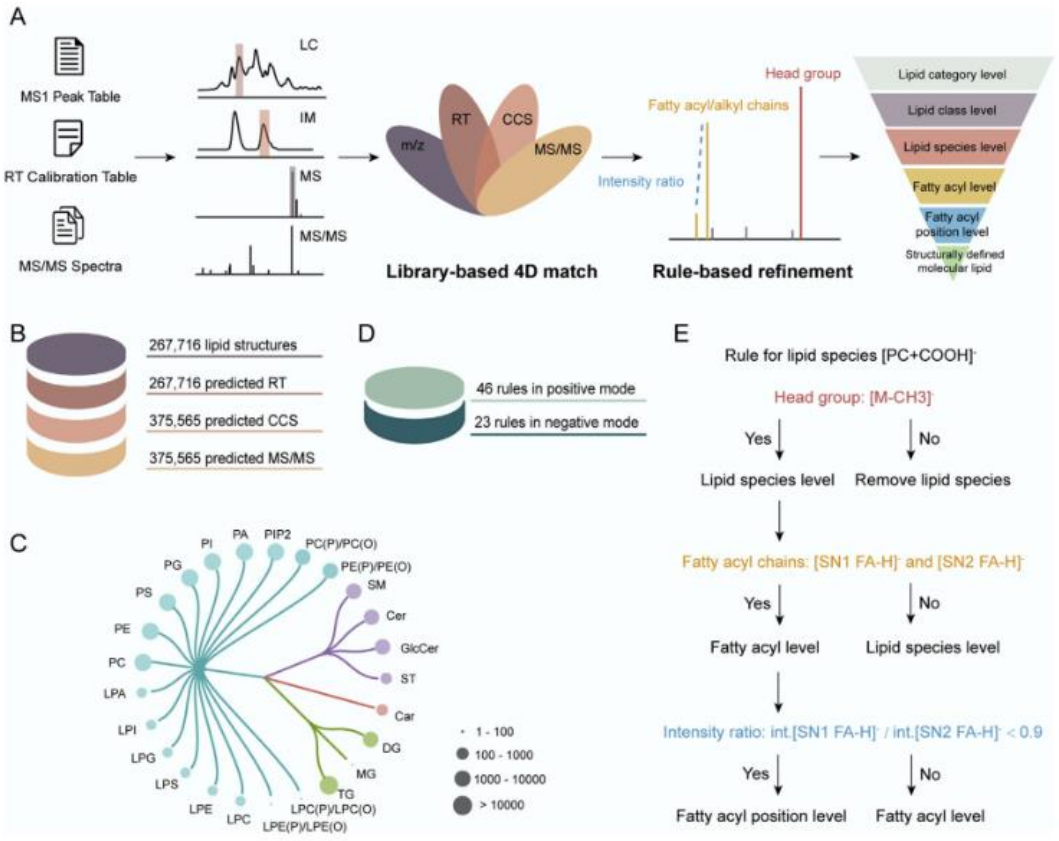

Figure 34: Schéma de la combinaison d'une correspondance 4D (m/z ; RT ; CCS (collision cross-section) et MS/MS) pour l'identification des lipides dans la lipidomique non ciblée basée sur IM-MS [91].

Un exemple de résolution structurale est présenté sur la Figure 35. Lorsque la position des FAs n'est pas connue, le symbole « _ » est placé entre les FAs. Si leurs positions sont connues, le symbole « / » est utilisé.

Les logiciels de traitement des données peuvent également générer des réseaux moléculaires permettant d'établir un lien entre des molécules proches.

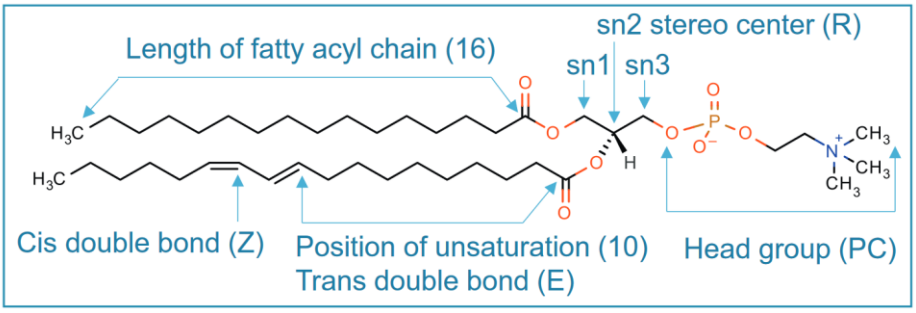

Structural resolution	Annotation
Carbons and double bonds	PC(34:2)
Fatty acyl constituents	PC(16:0_18:2)
Positional isomers	PC(16:0/18:2)
Double bond position	PC(16:0/18:2(10,12))
Double bond Cis/Trans	PC(16:0/18:2(10E,12Z))
Stereochemistry	PC(16:0/18:2(10E,12Z)[R])

Figure 35: Niveaux de résolution structurale et nomenclatures associées [92].

La Table 6, présente des propriétés sur les ions fragments MS^2 permettant de déterminer la position des FAs sur le glycérol.

Analyzed lipids	Parental ion to be fragmented	MS2 fragments properties	References	Références thèse
Phospholipids				
phosphatidylcholines (PC)	$[M+H]^+$	$[M+H-R_2CH=C=O]^+ > [M+H-R_1CH=C=O]^+$	[31]	[62]
Phosphatidylethanolamines (PE)	$[M-H]^-$	$[R_2COO]^- > [R_1COO]^-$	[32]	[63]
phosphatidylglycerols (PG)	$[M-H]^-$	$[M-H-R_2COOH]^- > [M-H-R_1COOH]^-$	[33]	[64]
phosphatidylinositols (PI)	$[M-H]^-$	$[M-H-R_2COOH]^- > [M-H-R_1COOH]^-$	[34]	[65]
Phosphatidic acids (PA)	$[M-H]^-$	$[M-H-R_2COOH]^- > [M-H-R_1COOH]^-$	[35]	[66]
Cardiolipins (DPG)	$[M-H]^-$	MS2 produced the corresponding PA	[36]	[67]
Non phosphorus glycerolipids				
sulfoquinovosyldiacylglycerols (SQDG)	$[M-H]^-$	$[M-H-R_1COOH]^- > [M-H-R_2COOH]^-$	[37]	[68]
Monogalactosyldiacylglycerols (MGDG)	$[M+Na]^+$	$[M+Na-R_1COO^-]^+ > [M+Na-R_2COO^-]^+$	[38]	[69]
digalactosyldiacylglycerols (DGDG)	$[M+Na]^+$	$[M+Na-R_1COO^-]^+ > [M+Na-R_2COO^-]^+$	[38]	[69]
diacylglyceryl-hydroxymethyl-N,N,N-trimethyl-β-alanine (DGTA)	$[M+H]^+$	$[M+H-R_2COOH]^+ > [M+H-R_1COOH]^+$	By analogy with phospholipid diacylglycerol moiety	
diacylglyceryl-hydroxymethyl-N,N,N-trimethyl-homoserine (DGTS)	$[M+H]^+$	$[M+H-R_2COOH]^+ > [M+H-R_1COOH]^+$ Can be differentiated from DGTA by a neutral loss of *m/z* 87	By analogy with phospholipid diacylglycerol moiety	
Neutral lipids				
Diacylglycerol (DAG)	$[M+NH_4]^+$	$[M+NH_4-R_1COONH_4]^+ > [M+NH_4-R_2COONH_4]^+$	[39]	[70]
Triacylglycerol (TAG)	$[M+NH_4]^+$	$[M+NH_4-R_{1/3}COO^-]^+ > [M+NH_4-R_2COO^-]^+$	[40]	[71]

https://doi.org/10.1371/journal.pone.0182423.t001

Table 6: Conditions d'affectation régiochimique des FAs aux positions sn-1, sn-2 et sn-3 des PLs et glycérolipides [19].

4.5.3 Quantification

Une quantification fiable est essentielle, pour que le développement de la lipidomique progresse durablement dans les applications biologiques et biomédicales [93].

La quantification « absolue » de toutes les espèces moléculaires présentes dans le lipidome d'un organisme vivant est impossible d'un point de vue pratique. Le très grand nombre d'espèces moléculaires présentes, l'hétérogénéité chimique des lipides, la présence de nombreux isomères, la présence d'espèces isobares et la large gamme de concentrations des lipides dans les échantillons empêchent la mesure de profils lipidiques complets [18].

A cela, s'ajoutent de nombreuses sources d'erreurs pouvant influer les résultats (prélèvement, extraction, traitement de l'échantillon, effet matrice, nature et pureté des standards utilisés, dérive de l'instrument, erreurs systématiques, etc. [94]).

Les résultats quantitatifs doivent par ailleurs être associés à une méthode dont certains paramètres doivent être déterminés (limite de détection (LOD), limite de quantification (LOQ), gamme dynamique d'analyse, exactitude, précision de la méthode, etc.) [95].

Le groupe de travail « Lipidomique-Standards-Initiative (LSI) » [96], en collaboration avec LIPID MAPS, propose des lignes directrices concernant les principaux flux de travail en lipidomique.

Concernant la quantification par spectrométrie de masse, le consortium indique que celle-ci n'est pas possible sans étalons internes. Les exigences sur ces étalons sont nombreuses. Les étalons doivent être ajoutés dans les échantillons avant l'étape d'extraction, mais ne doivent pas être présent naturellement dans celui-ci. Il est recommandé d'avoir au minimum un étalon par classe de lipide. Les étalons doivent présenter une similitude structurale élevée avec les analytes (nombre similaire de carbones et de doubles liaisons, même types de liaisons : ester *vs* éther) et une ionisation simultanée avec l'analyte. L'utilisation d'étalons marqués par des isotopes stables de structure identique est actuellement considérée comme la meilleure approche.

Les lipides peuvent être séparés en deux groupes : les « lipides simples » et les « lipides complexes ». Les lipides simples correspondent aux stérols, FAs et leurs dérivés, tandis que les lipides complexes correspondent aux sphingolipides, glycérolipides et glycérophospholipides [18]. Dans le cas des lipides simples, il est possible de trouver des standards internes et une quantification « absolue » est de ce fait possible. Dans le cas des lipides complexes, la diversité de structures est telle, que la disponibilité commerciale de toutes les espèces moléculaires n'est pas possible, la quantification ne peut être que « relative » par rapport au standard pris en référence [97].

Le fournisseur Avanti Polar Lipids a commercialisé à cet égard des mélanges de standards deutérés. Le mélange de standards SPLASH® LIPIDOMIX® contient 14 espèces lipidiques deutérées appartenant toutes à des classes lipidiques différentes. De nombreuses études utilisent ce mélange pour la quantification [98–101]. Avanti Polar Lipids a également commercialisé récemment le mélange de standard UltimateSPLASH® contenant 69 étalons internes deutérés couvrant les phospholipides, les lipides neutres, la sphingomyéline et les céramides. Ce mélange contient plusieurs espèces moléculaires pour chaque classe (3à 9 selon la classe). La diversité des FAs (longueur de chaîne et nombre d'insaturations) au sein de chaque classe, permet de mieux corriger le rendement d'extraction ainsi que l'ionisation des composés [102]. Ces deux mélanges de standards ont été optimisés pour les analyses de plasma, représentant en 2014, 39% des matrices étudiées en lipidomique, Figure 13 A. La revue de Lippa et al. (2022) [103] présente les différents matériaux de référence pour l'assurance qualité et le contrôle qualité des analyses métabolomiques et lipidomiques non ciblées.

L'une des méthodes couramment utilisées pour la quantification des lipides est l'introduction directe en continu de l'échantillon dans le spectromètre de masse appelée « shotgun lipidomics » [104,105]. Ce terme a été employé pour la première fois par Han et Gross [106,107]. L'échantillon est soumis à différentes conditions d'ionisation (mode

positif/négatif, énergie de collision, ajout de sel…). Ainsi chaque classe de lipides est analysée dans ses conditions optimales d'ionisation. Toutes les espèces lipidiques d'une même classe sont donc affectées de la même manière par les différents paramètres pouvant influencer leur ionisation (environnement chimique, suppression d'ionisation, concentration…). Les standards internes de chaque classe sont utilisés pour normaliser les réponses.

La revue [31] porte un regard critique sur cette méthode et présente les nombreuses difficultés rencontrées en shotgun lipidomics, (large gamme de concentration des analytes, nombreux adduits (créant parfois des ions isobares), chevauchement isotopique, suppression d'ionisation, artéfacts liés à des ions fragments communs (PA, Lyso-PLs, DG, MG, FAs, etc.).

L'influence de la composition des PLs sur la réponse de l'instrument en ESI-MS, a fait l'objet de plusieurs études [61,108,109]. Il en ressort que la classe de lipide à plus d'influence sur l'intensité des ions que les variations de structure au sein d'une même classe (longueur de la chaîne acyle, nombre d'insaturations, etc.). Il apparaît également que la concentration des analytes est un paramètre impactant fortement l'ionisation et qu'il est important de la contrôler, comme illustré sur la Figure 36. Lorsque les analytes sont faiblement concentrés (0.1-0.5 pmol/µl) les espèces moléculaires d'une même classe ont des intensités globalement proches, même si une diminution de l'intensité est observée avec l'augmentation du nombre de carbones.

Les séparations de lipides par classe (NPLC [110], HILIC [111] ou la SFC [52]) permettent également des analyses lipidomiques quantitatives car elles suivent la même stratégie que celle mise en œuvre en shotgun lipidomics. Autrement dit, ces techniques chromatographiques conduisent à la coélution d'espèces moléculaires d'une même classe, elles sont donc ionisées à l'entrée du spectromètre de masse dans les mêmes conditions. Les effets de suppression d'ionisation consécutifs à la présence d'autres classes sont éliminés et l'assignation des ions fragments communs (PA, Lyso-PL, DG, MG, FAs…) ne constitue pas une difficulté. D'autre part, la détection d'espèces moléculaires minoritaires est favorisée.

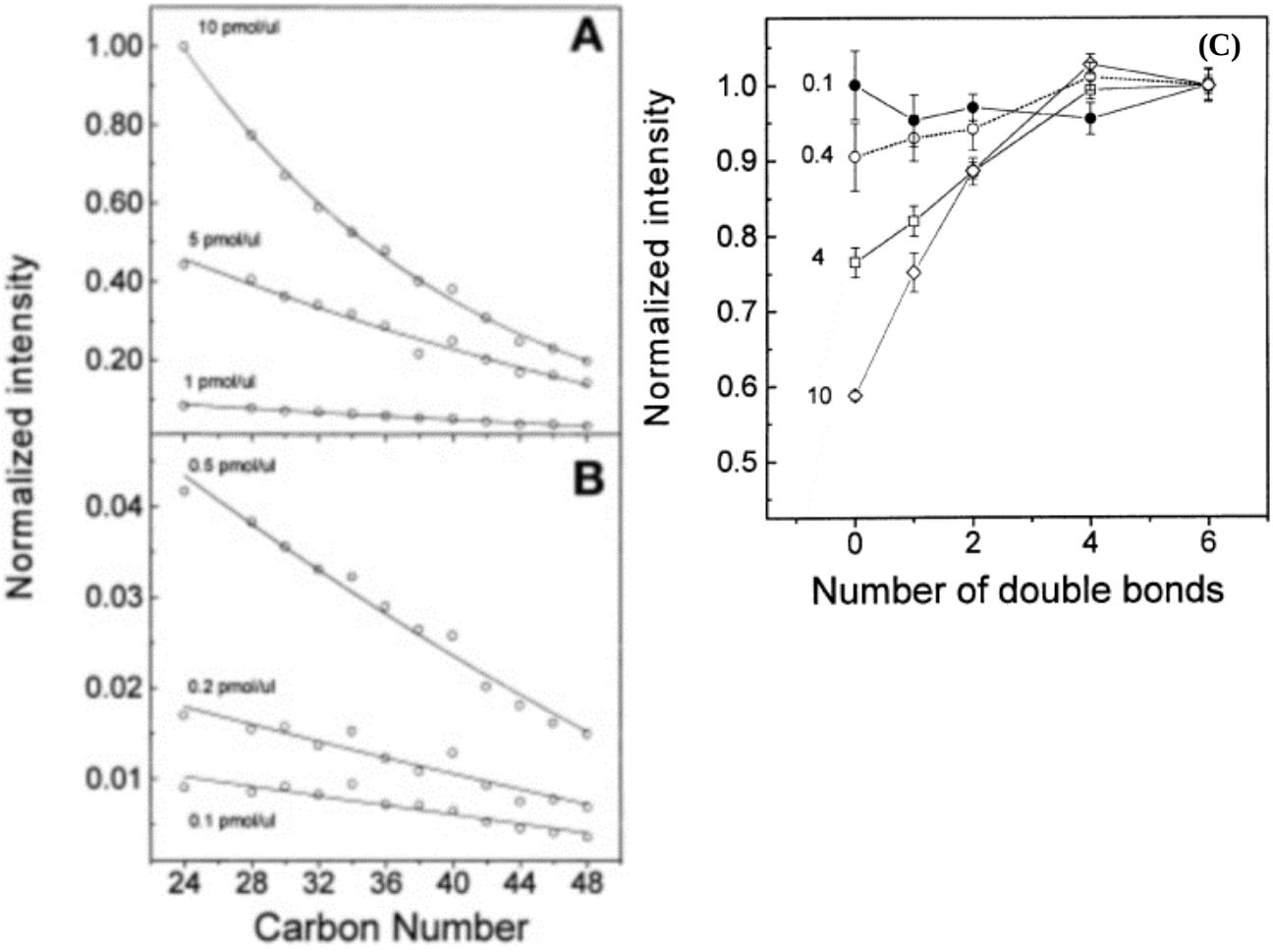

Figure 36 : Effet de la concentration de PC saturées (A et B) et insaturés © sur la réponse de l'instrument (trappe ionique) [108].

Du fait que les espèces moléculaires d'une même classe sont séparées sur le chromatogramme, la RPLC ne suit pas le concept de la co-ionisation du standard interne et de l'ensemble des analytes qu'il représente. De ce fait, il n'est pas recommandé de l'utiliser pour des analyses lipidomiques quantitatives, sauf pour des échantillons comportant un nombre important d'espèces lipidiques isobares comme les eicosanoïdes [112], oxylipines [113] ou oxystérol [114].

5. *Exemples d'approches lipidomiques*

Pour illustrer la complexité des analyses lipidomiques quantitatives, des exemples d'études sont présentés ci-après.

Jouhet et al. (2018) [19] ont comparé la distribution des classes lipidiques de deux microalgues et d'une plante supérieure par TLC-GC-FID, LC-MS/MS-Stds et par LC-MS/MS-QC. La méthode LC-MS/MS-Stds, adaptée de l'article [174], utilise un standard interne par classe de lipides, avec principalement des FAs saturés car ceux-ci sont quasi inexistants dans les échantillons. La méthode LC-MS/MS-QC utilise un contrôle qualité représentatif des échantillons et préalablement analysé par TLC-GC-FID. Le QC est utilisé comme étalon externe pour la quantification. Les analyses LC-MS/MS sont réalisées sur un triple quadripôle muni d'une source d'ionisation ESI et utilisent le mode MRM. Les résultats obtenus sont présentés sur la Figure 37.

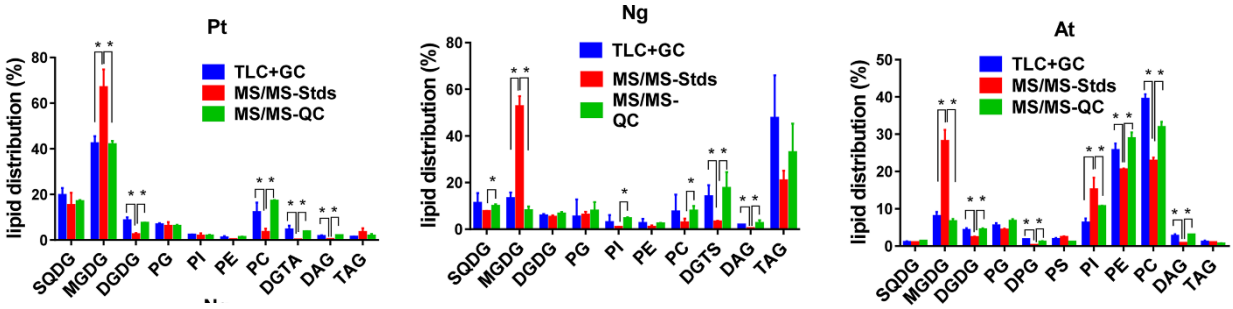

Figure 37: Distribution de lipides dans des extraits de deux microalgues et d'une plante supérieure. Chaque classe de lipides a été quantifiée par TLC-GC-FID, LC-MS/MS-Stds et LC-MS /MS -QC [19].

La méthode LC-MS/MS-Stds conduit à des résultats significativement différents des deux autres méthodes. L'inexactitude de cette méthode est expliquée par la différence d'ionisation en source des espèces moléculaires saturées prises comme standards et des espèces moléculaires insaturées présentes dans les échantillons.

La méthode LC-MS/MS-QC a ensuite été utilisée pour évaluer la distribution des FAs par classes, les résultats sont présentés sur la Figure 38.

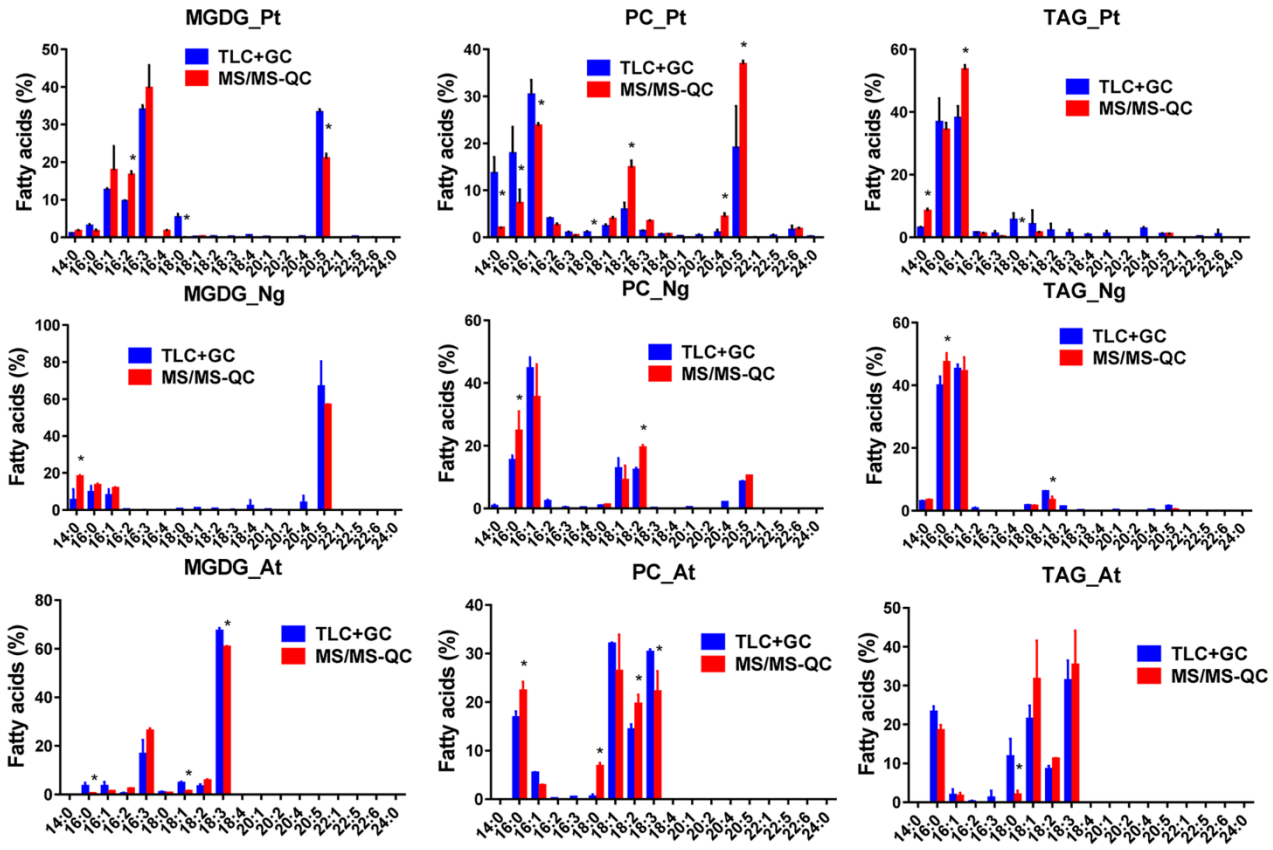

Figure 38: Distribution des FAs des MGDG, PC et TG issues des extraits de deux microalgues et d'une plante supérieure. La distribution a été calculée suivant la méthode TLC plus GC-FID et la méthode MS/MS-QC [19].

Les résultats sont globalement cohérents avec ceux obtenus par TLC-GC-FID. Certains écarts observés sont expliqués par des difficultés de prélèvements des spots de lipides sur la plaque TLC. Par exemple, pour l'échantillon noté (Pt), le PC contient des sulfoquinovosyldiacylglycerols (SQDG). Des différences sont également observées pour des FAs présent en très faible quantité comme le C18 :0. Les auteurs expliquent qu'il est probable que ces molécules soient difficilement piégées au niveau de la trappe et que leurs masses et transitions MRM n'ont sans doute pas été introduites dans le logiciel d'analyse MS/MS. La

difficulté de calculer toutes les combinaisons possibles associées à une classe spécifique de glycérolipide sans trop augmenter le temps nécessaire a été évoquée.

En prenant des standards internes saturés pour quantifier des lipides polyinsaturés, l'étude [19] se positionne dans une configuration défavorable pour la quantification relative. Dans le cas de certains échantillons, le choix des standards internes peut s'avérer plus simple. Par exemple, dans l'étude de **Buré et al. [50]**, des standards de PLs saturés impairs ont été utilisés pour étudier les PLs extraits de levures *S. cerevisiae*. Les PLs de ces levures sont principalement saturés ou monoinsaturés avec un nombre de carbones proche de ceux des standards. Dans ces conditions, la correction des intensités par les standards choisis est dans une configuration plus favorable que dans l'étude précédemment détaillée.

En 2010, **LIPID MAPS** a formé un consortium pour définir les constituants du lipidome des mammifères à l'aide du matériau NIST SRM 1950 – Metabolites in Frozen Human Plasma du National Institute of Standards and Technology (NIST) [14], disponible commercialement. Lors de cette étude, un total de 588 espèces de lipides a été décrit pour ce lipidome. Plusieurs laboratoires ont contribué avec comme principale technologie des spectromètres de masse de type triple quadripôle pour des mesures ciblées des classes de lipides. Depuis, ce standard sert de référence à l'échelle de la communauté pour le contrôle qualité intra et inter laboratoire et la validation des méthodes comme illustrés dans les trois études détaillées ci-après.

Dans l'étude de **Bowden et al. (2017)** [115], 31 laboratoires utilisant un flux de travail lipidomique différent ont analysé le NIST SRM 1950. Un total de 1 527 lipides uniques a été mesuré par tous les laboratoires. Des estimations consensuelles, avec les incertitudes associées ont été déterminées pour 339 de ces lipides, par cinq laboratoires. La composition lipidique du NIST SRM 1950, est présentée sur la Figure 39. Ces données mettent en exergue que le NIST SRM 1950 contient principalement des esters de cholestérol (CE) (47%), des PC (18%) du

cholestérol (12%) et des TGs (9%), les autres classes lipidiques représentent moins de 5%. La plus grande diversité d'espèce moléculaire est obtenue pour le PC (63), puis les TGs (59), la sphingomyéline (SM) (38), le PE (35), les autres classes lipidiques contiennent un nombre d'espèces inférieur ou égal à 25.

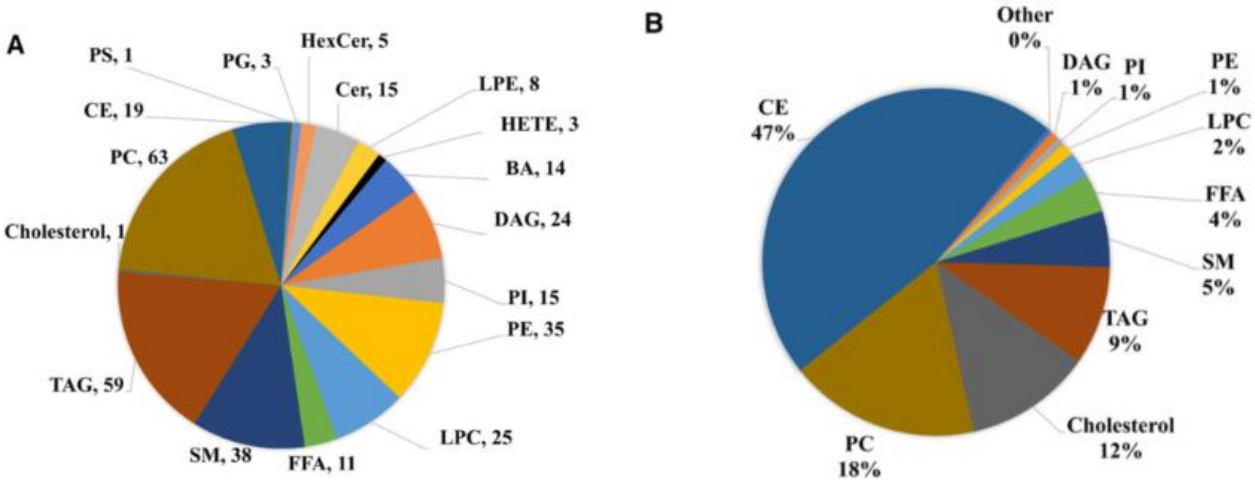

Figure 39: Composition lipidique du NIST SRM 1950, selon le nombre d'espèces lipidiques (A) et la concentration (B) [115].

Les valeurs obtenues ont été comparées à celles publiées précédemment par LIPID MAPS [14]. Les comparaisons concernent uniquement les lipides mesurés par les deux études, les résultats sont présentés sur la Figure 40.

Des écarts significatifs pour des classes de lipides spécifiques entre les deux études ont été trouvées, notamment pour les PE. Les auteurs indiquent qu'une attention supplémentaire est nécessaire pour comprendre les raisons de cette différence. L'étude a également fourni des informations précieuses sur les forces et les faiblesses potentielles des mesures lipidomiques actuelles. Les auteurs soulignent la nécessité de réaliser d'autres études inter-laboratoires avec la mise à disposition des données à la communauté et d'examiner l'influence de la méthodologie.

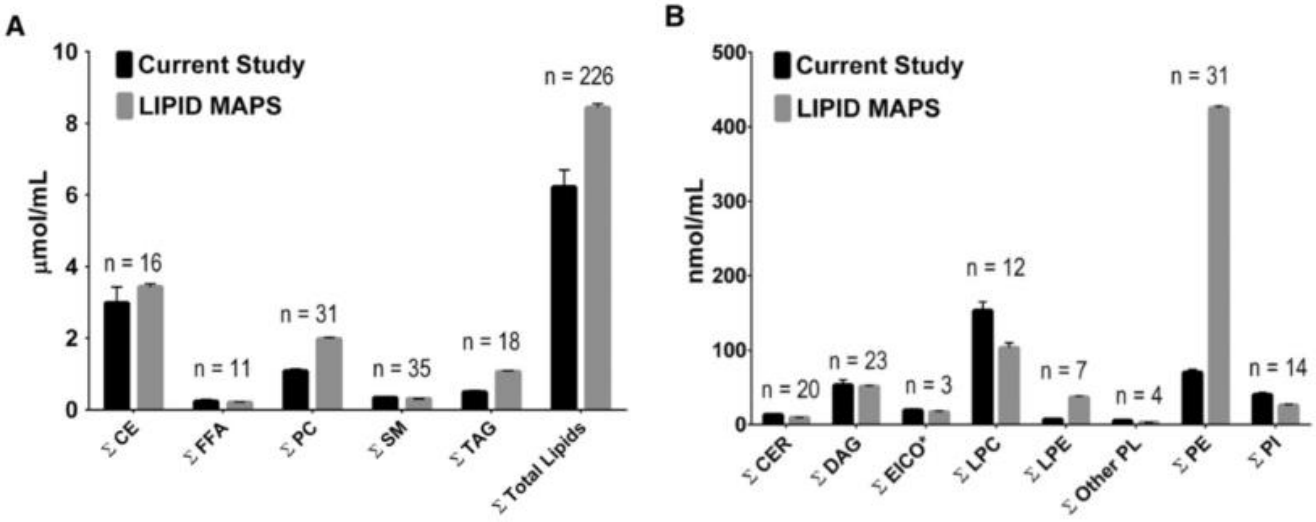

Figure 40: Comparaison des quantités des classes de lipides les plus concentrées (A) et les moins concentrées (B) entre l'étude de Bowden et al. [115] et l'étude LIPID MAPS [14]. Figure extraite de l'étude [115].

Dans l'étude de **Ghorasaini et al. (2021)** [116] les performances de la plateforme « Lipidyzer » sont évaluées sur différents matériaux dont le NIST SRM 1950 au travers de 14 laboratoires. Les auteurs expliquent que l'inexactitude de la quantification causée par le chevauchement des espèces lipidiques isomères et isobares lors des analyses shotgun est surmontée sur la plateforme Lipidyzer grâce à l'utilisation de la spectrométrie de mobilité différentielle (DMS) et la surveillance de réactions multiples (MRM) sur un spectromètre de masse QTRAP et en appliquant 54 étalons internes marqués.

Les données ont été comparées aux données de LIPID MAPS [14] et à celles de Bowden et al. (2017) [115]. La comparaison met en exergue le meilleur accord de leurs données avec celles de l'étude [115]. Les auteurs affirment avoir attribué un nombre sans précédent de valeurs consensuelles de lipides pour ce standard, 704 espèces de lipides mesurées avec un CV ≤ 20 %.

Contrairement aux deux précédentes études citées [14] et [115] qui présentent les résultats des espèces moléculaires sous forme : nombre de carbones/nombre d'insaturations, cette étude [116] présente dans son « suppementary data » les espèces moléculaires en précisant la nature des FAs sauf pour les TGs. Pour les TGs l'information est donnée comme dans l'exemple : « TA G36:0-F A12:0 ».

Thompson et al. (2019) [117] ont étudié le flux de travail métabolomique et lipidomique via un protocole expérimental commun fourni avec le kit Biocrates AbsoluteIDQ p400HR, pour quantifier jusqu'à 408 métabolites. 14 laboratoires utilisant des instruments Orbitrap ont analysé divers échantillons de sang (plasma/sérum) dont le NIST SRM 1950.

La variance inter-laboratoires pour le NIST SRM-1950 a une médiane de 10 % pour les acides aminés, 24 % pour les amines biogènes, 38 % pour les acylcarnitines, 25 % pour les glycérolipides, 23 % pour les glycérophospholipides, 16 % pour les esters de cholestérol, 15 % pour les sphingolipides et 9 % pour les hexoses. Par rapport aux valeurs consensuelles du NIST SRM-1950, près de 80 % des analytes comparables ont démontré un biais < 50 % par rapport à la valeur de référence comme illustré sur la Figure 41. Cependant, certains coefficients de variation sont élevés, jusqu'à 306 % pour les TGs et 181 % pour les PLs.

De meilleures performances en termes de précision et d'exactitude ont été observés pour les analytes mesurés à l'aide d'un étalonnage externe par LC-HRMS par rapport à ceux mesurés avec une quantification par dilution isotopique stable (point unique) par FIA-HRMS. Les auteurs suggèrent que des courbes d'étalonnage et des séparations chromatographiques doivent être utilisées pour obtenir les données les plus précises, lorsque cela est faisable d'un point de vue analytique et financier.

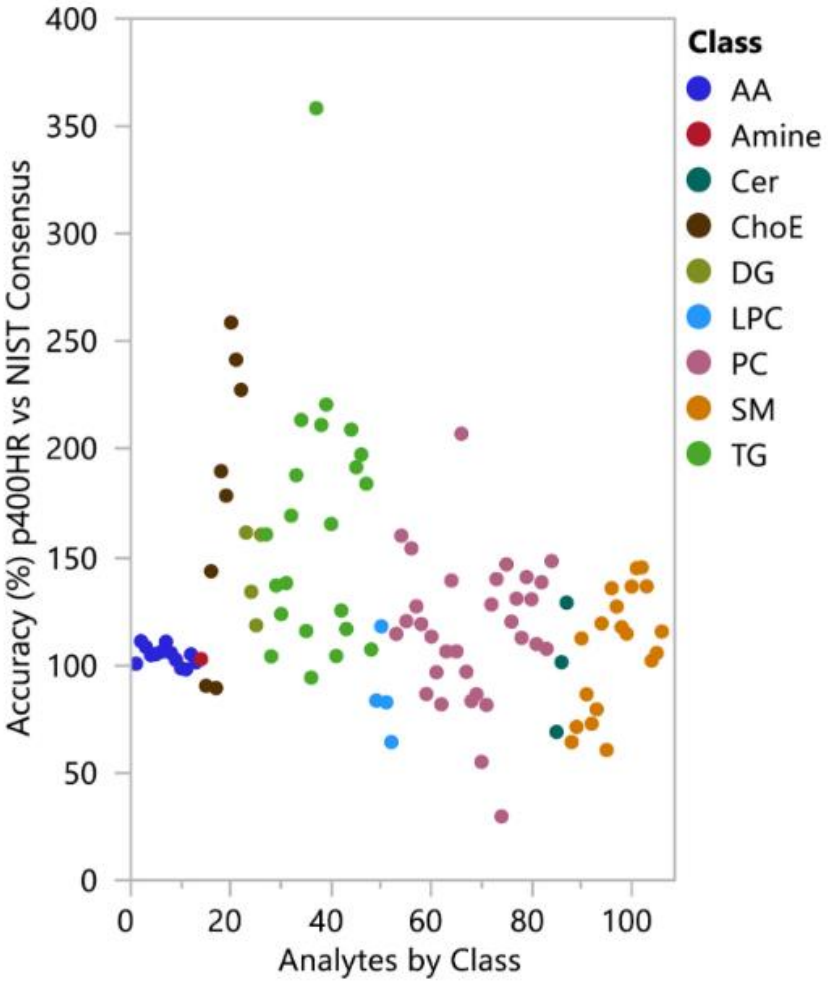

Figure 41: Exactitude des données de l'essai inter-laboratoire utilisant le kit p400HR par rapport aux données consensuelles pour le NIST SRM-1950 [117].

Même si les méthodes lipidomiques quantitatives représentent un fort potentiel, notamment dans le domaine de la santé humaine, les études mettent en évidence des divergences dans les résultats malgré tous les efforts déployés. L'origine de ces différences reste à élucider pour l'obtention de résultats quantitatifs fiables.

CHAPITRE III. OPTIMISATION DES CONDITIONS CHROMATOGRAPHIQUES EN PHASE NORMALE POUR L'ANALYSE DES LIPIDES ET TECHNIQUES DE DETECTION ASSOCIEES

1. Introduction

Ce chapitre est consacré à l'article : « Optimization of normal phase chromatographic conditions for lipid analysis and comparison of associated detection techniques » publié en 2017 (antérieur au début de la thèse). Ce travail est incorporé dans la partie I du manuscrit, car il constitue le principal support de ces travaux de thèse.

Les séparations menées par NPLC sont reconnues pour être difficiles à mettre en œuvre. Le grand écart de polarité entre le début et la fin de gradient impose des conditions de travail rigoureuses pour obtenir une bonne reproductibilité. D'autres difficultés peuvent s'ajouter, comme des défauts de pompage des solvants ayant une forte pression de vapeur saturante (heptane et isooctane) ainsi que la présence d'impuretés dans les solvants commerciaux. Dans cet article, des solutions techniques sont apportées pour résoudre ces difficultés.

D'autre part, une optimisation de la séparation des lipides par classe est réalisée par NPLC à partir de sept extraits lipidiques d'origines différentes (animales, végétales, bactéries et levures), afin de proposer une séparation la plus exhaustive possible.

Enfin, le couplage de la séparation à différents détecteurs (DEDL, Corona-CAD$^{@}$ et ESI/APPI/APCI-LTQ-Orbitrap) est également étudié.

L'originalité du travail de thèse, repose sur le traitement des données acquises par APPI/APCI-LTQ-Orbitrap obtenue avec cette méthode séparative.

2. Publication numéro 1

Les données supplémentaires liées à cette publication sont présentées en Annexe I.

Journal of Chromatography A, 1514 (2017) 54–71

Contents lists available at ScienceDirect

Journal of Chromatography A

journal homepage: www.elsevier.com/locate/chroma

Optimization of normal phase chromatographic conditions for lipid analysis and comparison of associated detection techniques

Sonia Abreu[a], Audrey Solgadi[b], Pierre Chaminade[a,*]

[a] Lip(Sys)[2], Chimie Analytique Pharmaceutique (FKA EA4041 Groupe de Chimie Analytique de Paris-Sud), Univ. Paris-Sud, Université Paris-Saclay, F-92290 Châtenay-Malabry, France
[b] SAMM, UMS IPSIT, Université Paris Sud, Université Paris-Saclay, Chatenay-Malabry, France

ARTICLE INFO

Article history:
Received 7 November 2016
Received in revised form 7 July 2017
Accepted 18 July 2017
Available online 24 July 2017

Keywords:
Lipids
Normal-phase liquid chromatography
Evaporative light scattering detector
Charged aerosol detector
Atmospheric pressure photoionization
LC/MS

ABSTRACT

One important challenge in lipid class analysis is to develop a method suitable or, at least adaptable, for a vast diversity of samples. In the current study, an improved normal-phase liquid chromatography (NPLC) method allowed analyzing the lipid classes present in mammalian, vegetable as well as microorganism (yeast and bacteria) lipid samples. The method effectively separated 30 lipid classes or subclasses with a special focus on medium polarity lipids. The separation was carried out with bare silica stationary phase and was coupled to evaporative light scattering detection (ELSD), charged aerosol detection (Corona-CAD®) and mass spectrometry. Solutions are provided to circumvent technical issues (such as pumping solvents of low viscosity, solvent purity, rinsing step). The influence of mobile phase composition and addition of ionic modifiers on the chromatographic behavior of particular lipid classes is documented. A comparison between ELSD and Corona-CAD® confirmed the interest of this later detector for samples with a wide range of concentration of different lipids. Three common atmospheric pressure ionization interfaces were used for coupling the NPLC separation to a LTQ Velos Pro® mass spectrometer. The comparison of the chromatographic profiles showed that atmospheric pressure chemical ionization (APCI) and atmospheric pressure photoionization (APPI) are both suitable to detect the different lipid classes whereas APPI allows a better sensitivity for lipids at low-concentration.

© 2017 Elsevier B.V. All rights reserved.

1. Introduction

Lipidomics has emerged with the growing progress in mass spectrometry and bioinformatics. This is a complex field of activity since more than 40 000 unique lipid structures are listed in the LIPIDMAPS database nowadays [1,2]. Analytical techniques for lipidomics represent a very dynamic and motivating area as the lipid composition of animal or vegetal tissue is influenced by external factors (such as metabolic state or diet) and as research methods have still to be developed. New technologies and/or new developments in analytical sciences are now addressing lipid analysis to promote alternative and original separation techniques coupled with mass spectrometry. An important review about LC/MS based lipid analysis was published by Cajka & Fiehn [3] in 2014. They analyzed 185 original research papers and covered the technical approaches involved in lipidomics. The scope ranges from sample preparation to data treatment and encompasses mass spectrometry and separation techniques.

Several interesting findings can be extracted from this article. First, the diversity of the biological samples addressed by these 185 studies: plasma and serum represent 39% of the samples, animal tissue 23% and cells 22%, only 3% are plant tissues and other matrix represent 13%. Second, when LC/MS is used, reversed-phase liquid chromatography (RPLC), normal phase liquid chromatography (NPLC) and hydrophilic interaction chromatography (HILIC) are the most important techniques and correspond respectively to 71, 19 and 8% of the studies. It is worthy to note that RPLC and HILIC take advantage of improved sub-2-μm or fused core 2.6–2.8 μm particle size stationary phases whereas NPLC methods use classical 3–5 μm. In the vast majority of cases, narrow bore columns (2.1 mm I.D.) are used whatever is the retention mechanism. RPLC and HILC benefit from the high water content and water miscible solvents used as mobile phase that facilitate the coupling with MS. HILIC is presented as an alternative to NPLC with a better reproducibility and a better compatibility with MS. Finally, this review pointed out the dominant position of electrospray ionization mass spectrometry (ESI) in lipidomic studies, most of time used in positive mode.

* Corresponding author.
E-mail address: pierre.chaminade@u-psud.fr (P. Chaminade).

http://dx.doi.org/10.1016/j.chroma.2017.07.063
0021-9673/© 2017 Elsevier B.V. All rights reserved.

At the opposite, atmospheric pressure chemical ionization (APCI) appears to be limited to nonpolar lipids (mainly triacylglycerols).

With regard to separation techniques, the recent trends in lipidomic analysis can be illustrated by four impressive studies issued by Holčapek's group. Two of them concern alternative retention mechanisms (namely HILIC) or separation techniques i.e. supercritical fluid chromatography (SFC) and their coupling to MS. The two remaining studies take advantage of multidimensional techniques such as LCxLC or LCxIon Mobility to deal with sample complexity.

In a recent work (2016) [4], a considerable effort was made to optimize the HILIC separation of acidic phospholipids. This separation appears to be also suitable for medium polarity lipids (such as ceramides) but, in case of a total lipid extract, both NPLC and HILIC must be employed to accommodate the sample complexity and polarity [5]. The most nonpolar lipids cannot be retained in HILIC conditions.

SFC offers both efficiency and analysis speed when used with modern sub 2 μm particles. A high-throughput method by UHPSFC coupled with electrospray ionization mass spectrometry (ESI–MS) with a chromatography column packed with silica particles of less than 2 μm (2015) [6] was proposed. 24 classes of lipids were separated in 6 min and 436 lipid species were identified in a porcine brain extract. The CO_2 co-solvents used were only water and methanol.

When the lipid sample is extremely complex, one-dimensional analysis becomes insufficient. The second trend is to enhance the discriminating power of the chromatographic system by adding a supplementary separation step before the mass spectrometer entry. Two-dimensional liquid chromatography-electrospray ionization mass spectrometry (2D LCxLC ESI–MS) was developed for the comprehensive and simultaneous separation of classes and species of lipids (2015) [7]. The authors used RPLC with a C18 column in the first dimension (150 min), and HILIC with a silica column in the second dimension (1 min). Finally, in a study dealing with the complex analysis of the regioisomers of triacylglycerol by differential mobility ESI–MS (2016) [8], the authors describe how ionic mobility permits the separation of compounds which are chromatographically co-eluted.

All these recent studies take advantage of recent sub 2 μm or fused core particles that allow fast and efficient separations. This trend is only scarcely represented when considering normal phase separations. In 2011, McLaren [9], adapted the separation of total lipids to a Fused-Core particle column using UHPLC. He used an Halo HILIC column with 2.7 μm particle, but carried out the separation in normal-phase mode with evaporative light scattering detection (ELSD). The separation of the main lipids found in plasma, liver and heart was realized in 10 min. The method was developed with only 7 different lipid standards; however it is advisable form the chromatogram that more lipid classes could be separated using this method. The solvent program appears to be very similar to the one proposed by Christie [10] for mammalian lipid class analysis.

Thus, despite of its typically longer analysis time, NPLC remains attractive for the analysis of a total lipid extract and the objective of a complete separation of lipid classes. Method development is more complex in NPLC than in RPLC. The mobile phases are usually made of solvent mixtures to ensure miscibility and to encompass a wide range of polarity. The main advantage of NPLC is the elution of lipids according to their polar moieties or "head group" which also define their family or "lipid class". Even complex lipid mixtures lead to easily interpretable chromatograms where molecular species of the same class co-elute within a single peak. Mass spectrometry is the usual way to access the molecular species identification and relative distribution.

In most studies, the chromatographic technique is developed to resolve the lipid classes present in a sample or a group of samples. For example some method are designed to address animal tissues (heart, liver, brain, kidney...) but only few studies are assessed with samples of various origin (such as animal and vegetal).

In chronological order, Graeve's method [11], initially devoted to zooplankton analysis was further adapted by Gerits [12] for wheat lipids analysis during bread making. Graeve's method [11] is particularly effective for the analysis of nonpolar lipids. At the opposite, Gerits' solvent conditions offer a better separation for lipids of intermediate polarity such as glycolipids. Both these methods where derived from the work of Homan and Anderson [13] which studied lipids from animal tissues. Homan and Anderson, themselves, adapted the pioneering work of Christie issued in 1985 [10]. By comparing all these publications, one can easily notice the changes operated by theses authors and the subsequent tailoring of the separation to assess the complexity of specific samples. However, solvent programs are complex and it is difficult and almost impossible to synthetize all these experimental conditions to arrive at a compromise gathering the strength of both methods.

In this publication, our objective was to develop an almost universal method for the overall evaluation of the lipid classes present in natural samples regardless of their origin. Further, as NPLC is rather complex to develop due to subtle interactions between analytes and mobile and stationary phases, we tried to exemplify the effect of changes in the solvent program on the lipid class separation. Ref [9] shows that even in NPLC, the solvent program can be adapted from conventional LC to UHPLC and, we can expect the solvent conditions we propose should be transposable as well.

As already pointed out, ESI is the most represented ionization interface in lipidomic studies, presumably because RPLC and HILIC represent nearly 80% of the chromatographic separations and are known to be compatible with this interface. Mobile phase compatibility with atmospheric pressure ionization (API) sources depends on the API source and the solvent [14]. We investigated coupling our separation with ESI and APCI but also atmospheric pressure photoionization (APPI) in order to select the most appropriate interface. Finally, and because ELSD and corona charged aerosol detection (Corona-CAD®) are useful to monitor the separation in parallel with MS, a short comparison between those two detectors is provided.

2. Experimental

2.1. Chemicals

Isooctane, ethyl acetate, acetone (all HPLC grade), acetic acid (AA) and trimethylamine (TEA) were all purchased from Sigma-Aldrich. Chloroform and water (all HPLC grade) were obtained from VWR (Fontenay-sous-Bois, France). Isopropanol (IPA) (ULC/MS grade) was from Biosolve (Dieuze, France). Isooctane was purified prior analysis by pumping the solvent through a semi preparative column packed with Lichroprep Si 60 5–20 μm silica (Merck KGaA, Darmstadt, Germany).

2.2. Standards

Phosphatidylglycerols (PG), phosphatidylethanolamines (PE), phosphatidic acids (PA), phosphatidylcholines (PC), sphingomyelins (SM), lysophosphatidylcholines (LPC) from egg yolk, phosphatidylinositols (PI) from bovine liver, phosphatidylserines (PS) from bovine brain, Cardiolipins (CL) from bovine heart, squalene (SQ), cholesteryl palmitic acid (CE(16:0)), methyl-nonadecanoic acid (FAME), tristearic acid triglyceride (TG(18:0/18:0/18:0)), cholesterol (Chol), diacylglycerols (DG(18:2/0:0/18:2) and DG(16:0/16:0/0:0)), stearic acid (FA(18:0)), monoacylglycerol (MG(18:0/0:0/0:0)) were purchased from Sigma-Aldrich (St. Quentin Fallavier, France).

Table 1
Information about the lipid species composition of standards. SQ-squalene, CE-cholesteryl esters, FAME-fatty acids methylesters, TG-triacylglycerols, Chol-cholesterol, DG-diacylglycerols, FA-fatty acids, MG-monoacylglycerols, Ceramides(CerII (Cer(d18:1/18:0)), CerIIIb (Cer(t18:0/18:1)), CerV (Cer(d18:1/18:0(2OH)) and CerVI (Cer(t18:0/18:0(2OH)))), ASG-acylated steryl glycosides, MGDG-monogalactosyldiglycerols, SG-steryl glycosides, GlcCer-glucosylceramides, DGDG-digalactosyldiglycerols, NAPE-N-Acylphosphatidylethanolamines, PG-phosphatidylglycerols, PE-phosphatidylethanolamines, PA-phosphatidic acids, PI-phosphatidylinositols, CL-cardiolipins, PS-phosphatidylserines, PC-phosphatidylcholines, SM-sphingomyelins, LPC-lysophosphatidylcholines.

A

Monomolecular lipids standards

Lipid Class	Isoprenoids	ST	FA	TG	DG	MG	Cer
Subclasses (species)	SQ	CE(16:0)	FAME(methyl-nonadecanoic acids)	TG (18:0/18:0/18:0)	DG (18:2/0:0/18:2)	MG (18:0/0:0/0:0)	Cer(d18:1/18:0)
		Chol ASG (18:2-Glc-Sitosterol)	FA(18:0)		DG (16:0/16:0/0:0)		Cer(t18:0/18:1) Cer(d18:1/18:0(2OH)) Cer(t18:0/18:0(2OH))

B

Composition of natural PL standards (typical composition provided by Avanti Polar)

Lipid Class FA%\origin	PG egg yolk chicken	PE egg yolk chicken	PA egg yolk chicken	PI bovine liver	CL bovine heart	PS bovi ne brain	PC egg yolk chicken	SM egg yolk chicken	LPC egg yolk chicken
16:0	32.9	17.3	34.2				32.7	86	69
18:0	12.2	24.2	11.5	46		42	12.3	6	24.6
18:1	30.2	18.1	31.5	8	5	30	32		3.4
18:2	18.7	14	18.5	6	90		17.1		0.3
20:3				13					
20:4	3.5	16	2.7	17		2	2.7		
22:6		4.2				11			

C

Natural lipids standards (typical composition provided by Avanti Polar)

Lipid Class FA\origin	DGDG plant	MGDG plant	Neutral glycosphingolipids wheat
18:3–18:3	44.5	14.1	GlcCer(d18:2/16:0(OH))
18:2–18:3	10.7	3.2	GlcCer(d18:1/16:0(OH))
16.3–18:3	21.3	66.8	GlcCer(d18:1/20:0(OH))
16:3–18:2	7	12.9	
16:1–18:3	6.9	3	
16:0–18:3	9.7		

D

Other subclasses of lipids found in samples

Lipid Class origin	Quinones and hydroquinones brain	ST Wheat	Neutral glycosphingolipids brain	PE Wheat
Subclasses	coenzyme Q10	SG	HexCer HexCer(OH)	NAPE

Monogalactosyldiglycerols (MGDG) and digalactosyldiglycerols (DGDG) (vegetable origin) was from Avanti Polar (Coger, Paris, France). Wheat Glucosylceramides (GlcCer) were purchased from Extrasynthese (Genay, France). Acylated steryl glycosides (ASG (18:2-Glc-Sitosterol)) came from Larodan (Limhamn,Sweden) Ceramides: CerII (Cer(d18:1/18:0)), CerIIIb (Cer(t18:0/18:1)), CerVI (Cer(t18:0/18:0(2OH))), were purchased from Degussa (Hanau, Germany) and CerV (Cer(d18:1/18:0(2OH))) from Matreya (State College, PA USA). Stock solutions (5 g/L) of each standard compound were prepared in chloroform.

Table 1 presents detailed information about the lipid species composition of standards.

The lipid nomenclature follows the LIPID MAPS system and the shorthand notation for lipid structures [15]. When no abbreviation can be found for a specific lipid class or subclass in the LIPID MAPS nomenclature, commonly used abbreviation was employed (squalene (SQ), cholesterol (Chol), fatty acids methyl esters (FAME)). A list of abbreviations is proposed in Table S-1.

2.3. Samples

Total lipid extracts from heart, brain and liver (all from bovine origin), *Escherichia coli*, yeast (*Saccharomyces cerevisiae*) and soybean were purchased from Avanti Polar (Coger, Paris, France).

Lipowheat® oil is the food grade ingredient from ROBERTET Health & Beauty (Formerly HITEX, Vannes, France). This sample comes from the ethanolic extraction of bakery wheat gluten.

Each sample is prepared in chloroform at the concentration of 5 g/L for analysis and storage.

2.3.1. Lipid test mixtures

Test mixture 1 is composed by 22 lipid standards: SQ, CE, FAME, TG, Chol, DG 1–3, DG 1–2, FA, MG, ASG, MGDG, GlcCer, DGDG, PG, PE, PA, PI, CL, PS, PC, SM and LPC at an individual concentration of 0.5 g/L.

Table 2
Quaternary gradient mobile phase composition. A, isooctane:ethyl acetate (99.8:0.2, v/v); B, acetone:ethyl acetate (2:1, v/v) containing 0.15% acetic acid (v/v); C, 2-propanol:water (85:15, v/v) containing 0.043% acetic acid (v/v) and 0.104% trimethylamine (v/v); D, ethyl acetate.

Time (min)	Percent solvent				Flow-rate (mL/min)
	A	B	C	D	
0	100	0	0	0	0.8
1.5	100	0	0	0	0.8
1.6	97	3	0	0	0.8
9	94	6	0	0	0.8
11	70	30	0	0	0.8
14	45	55	0	0	0.8
15	45	55	0	0	0.8
16	40	55	5	0	0.8
20	35	55	10	0	0.8
20.1	33	50	17	0	0.8
25	38	45	17	0	0.8
25.1	48	35	17	0	0.8
30	53	30	17	0	0.8
40	40	0	60	0	0.8
40.1	0	100	0	0	0.8
42	0	100	0	0	0.8
42.1	50	0	0	50	0.8
45	50	0	0	50	0.8
47	100	0	0	0	0.8
53	100	0	0	0	0.8

Test mixture 2 is a mixture of wheat oil (Lipowheat® oil) and soya lecithin supplemented with Chol in (9:9:0.6, v/v) proportion with a total lipid concentration of 10 g/L.

Ceramides test mixture 3 is made of CerII, CerIIIb, CerV and CerVI sub-classes at an individual concentration of 0.5 g/L.

Test mixture 1, 2 and 3 were prepared by mixing the appropriate stock solutions. After mixing all standards, the solution is evaporated under a stream of nitrogen and dissolved in mobile phase A: chloroform (4:1 v/v)

2.4. Apparatus

Separation of lipids was performed with an Inertsil Si 5 μm (150 mm × 2.1 mm I.D.) column (GL Sciences Inc., Tokyo, Japan) thermostated at 40 °C. The HPLC instrumentation consisted of an Agilent system, 1050 injector and a 1260 pump (Agilent Technologies, Santa Clara, CA, USA). An overpressure of 0.2 bar was applied to the mobile phase A reservoir. The 0.2 bar overpressure is set by a pressure regulator and the nitrogen line connected to the solvent bottle via a solvent pressurization kit obtained from Thermo Fischer Scientific. This kit consists in an adapted bottle cap and all necessary connections.

Two universal detectors, ELSD (Eurosep, Cergy, France) and Corona CAD® systems (both from ESA, Chelmsford, MA, USA) are compared; the signal was acquired with a Chromeleon data station (Thermo Fisher Scientific, Villebon-sur-Yvette, France). ELSD settings: nebulizer temperature 35 °C, drift tube 45 °C, photomultiplier 600 and air pressure 1.5 bar. Corona-CAD® settings: range 500pA, filter none and air pressure 35 psi.

MS analyses were performed with a LTQ-Orbitrap Velos Pro (Thermo Fisher Scientific). The MS^2 and MS^3 spectra were obtained in data dependent acquisition (DDA) mode. The LTQ-Orbitrap Velos Pro mass spectrometer was equipped with an H-ESI II probe/and a combined APCI/APPI ion source.

2.5. Chromatographic method

The mobile phases and the solvent program are presented in Table 2. The flow rate was set at 0.8 ml min^{-1}. The injected volume was 2 μl.

2.6. MS method

2.6.1. H-ESI II probe

Spray voltage was set at 3.3 kV. Heater temperature of the probe was set at 300 °C. Sheath gas, auxiliary gas, and sweep gas flow rates were set at 40, 20, and 0 (arbitrary unit) respectively. Capillary temperature was set at 350 °C and S-lens RF level at 60%. Analysis was performed in negative and positive ion mode.

2.6.2. APCI/APPI ion source

Corona needle voltage in APCI mode was set at 6 kV. Vaporizer temperature of the probe was set at 400 °C. Sheath gas, auxiliary gas, and sweep gas flow rates were set at 40, 10, and 0 (arbitrary unit) respectively. Capillary temperature was set at 325 °C and S-lens RF level at 60%. Analyses were performed in negative and positive ion mode.

3. Results and discussion

There are two ways to understand the different NPLC methods developed for lipid class analysis and their progress over time: either by the sample origin or by the stationary phase and solvent program.

Table 3 summarize the successive evolutions of Christie's method by the authors quoted in the introductive part of the manuscript. Chloroform, a CMR (carcinogenic, mutagenic, or toxic for reproduction) solvent was replaced by dichloromethane, itself substituted by the less toxic and peek-tubing compatible ethyl acetate. IPA was replaced by acetone to improve the sterols (ST)/DG chromatographic selectivity. AA and TEA were added at the end of the gradient program to enhance phospholipids (PL) analysis. In the same way, the addition of 0.2% (v/v) of ethyl acetate in isooctane appeared to improve the separation of early eluting lipids. Other modifications/improvements were made to help instrument performances. IPA was used as a rinsing solvent, prior the equilibration with isooctane and to avoid pumping failure with this low viscosity solvent that can be encountered with some pumping devices.

The mobile phases used in Graeve's [11] and Gerits' [12] methods differ by the presence of 0.2% (v/v) of ethyl acetate in isooctane, the ionic modifiers concentration and the addition of IPA as rinsing solvent (Table 3). In the present study, we intended to appreciate and exemplify the impact of these differences on the chromatographic separation of lipid classes. The main goal being to achieve the highest degree of separation allowing the characterization of biological lipid extracts from various origins (animal, vegetal, yeast, bacteria). For this purpose, test mixture 1 composed of 22 lipid standards and test mixture 2 were systematically chromatographed. Ceramides are biologically relevant lipids which have not been considered in Refs. [11,12]. We used test mixture 3, to appreciate the impact of the changes in chromatographic conditions on the retention of several compounds of this class.

The different methods listed in Table 3 use ELSD as detection principle. In this study, we compared the chromatographic profiles achieved by both ELSD and Corona-CAD®. Those two quasi-universal detectors allow quantitation but are unable to provide any structural information. As this later aspect is mandatory in lipidomic profiling of biological extracts, we assessed the MS response when coupling our separation through three ionization sources, namely ESI, APCI and APPI.

Table 3
Changes and evolution of the lipid class analysis method from Christie to this work. Abbreviation: acetic acid (AA), 2-propanol (IPA), ethanolamine (EA), trimethylamine (TEA), tetrahydrofuran (THF). The full name of lipids can be retrieved in table S-1. SQ-squalene, SE-sterol ester, CE-cholesteryl esters, FAME-fatty acids methylesters, DGE- diacylglycerol ethers, TG-triacylglycerols, Chol-cholesterol, DG-diacylglycerols, FA-fatty acids, FAlc- fatty acids alcohol, MG-monoacylglycerols, ceramides (CerII (Cer(d18:1/18:0)), CerIIIb (Cer(t18:0/18:1)), CerV (Cer(d18:1/18:0(2OH)) and CerVI (Cer(t18:0/18:0(2OH)))), ASG-acylated steryl glycosides, MGDG-monogalactosyldiglycerols, SG-steryl glycosides, GlcCer-glucosylceramides, HexCER- hexosylceramide, DGDG-digalactosyldiglycerols, NAPE-N-Acylphosphatidylethanolamines, PG-phosphatidylglycerols, DPG- diphosphatidylglycerol, PE-phosphatidylethanolamines, PA-phosphatidic acids, PI-phosphatidylinositols, CL-cardiolipins, PS-phosphatidylserines, PC-phosphatidylcholines, SM-sphingomyelins, LPC-lysophosphatidylcholines.

Author (year)	Christie [10] (1985)	Homan [13] (1998)	Graeve [11] (2009)	Gerits [12] (2013)	McLaren [9] (2011)	Present study (2017)
Column	Spherisorb 3 μm Si 100 × 5 mm	Spherisorb 5 μm Si 100 × 4.6 mm	Chromolith Si 100 × 4.6 mm	Chromolith Si 100 × 4.6 mm	Halo HILIC 2.7 μm 50 × 2.1 mm	Inertsil 5 μm Si 150 × 2.1 mm
Temperature		45 °C	40 °C	40 °C		40 °C
Analysis time	30 min	30 min	35 min	35 min	10.5 min	53 min
Flow rate	2 ml/min	1.6–2 ml/min	1.4–3 ml/min	1.4–3 ml/min	1.2 ml/min	0.8 ml/ min
injected Volume	5 μl	10 μl	2–60 μl	1–50 μl	2 μl	2 μl
injection Solvent	Chloroform:isooctane (1:1, v/v)	Isooctane:THF (9:1, v/v)	Isooctane:ethyl acetate (9:1, v/v) or Dichloromethane:methanol (2:1, v/v)	Isooctane	Isooctane:THF:methanol (9:1:1, v/v/v)	Isooctane:chloroform (4:1, v/v)
Detector	ELSD	ELSD	ELSD	ELSD	ELSD	ELSD/CAD/ESI/APCI/APPI
Solvent A	Isooctane:THF (99:1, v/v)	Isooctane:THF (99:1, v/v)	Isooctane:ethyl acetate (99.8:0.2, v/v)	Isooctane	Isooctane:THF (99:1, v/v)	Isooctane:ethyl acetate (99.8:0.2, v/v) pressurized
Solvent B	IPA:chloroform (4:1, v/v)	Acetone:dichnloromethane	Acetone:ethyl acetate (2:1, v/v) + AA (0.02% (v/v))	Acetone:ethyl acetate (2:1, v/v) + 70 mM AA	Acetone:dichnloromethane (4:1, v/v)	Acetone:ethyl acetate (2:1, v/v) + 35 mM AA
Solvent C	IPA:water (1:1, v/v)	IPA:water (85:15, v/v) + 7.5 mM AA + 7.5 mM EA	IPA:water (85:15, v/v) + 7.5 mM AA + 7.5 mM EA	IPA:water (85:15, v/v) + 7.5 mM AA + 7.5 mM TEA	IPA:chloroform (80:20, v/v)	IPA:water (85:15, v/v) + 7.5 mM AA + 7.5 mM TEA
Solvent D				IPA	IPA:water (1:1, v/v)	Ethyl acetate
Samples investigated	heart, erythrocytes, plasma	heart, liver, brain, Kidney	marine zooplankton	wheat	plasma, liver, heart	heart, liver, brain, yeast, *E. coli*, soy, wheat
Standards used to optimize the analytical method	CE, TG, Chol, DG, FA, DPG, PE, PI, PS, PC, SM, LPC	CE, TG, Chol, DG, FA, MG, HexCer, HexCer(OH), CL, PE, PI, PS, PC, SM, LPC	SQ, SE, WE, FAME, DGE, TG, FAlc, ST, DG, FA, HexCer, CL, PE, PI, PS, PC, LPC	TG, Chol, DG, FA, MG, MGDG, DGDG, NAPE, PE, PA, PG, NALPE, PI, PC, LPC	CE, TG, FA, Chol, DG, PE, PC	SQ, CE, FAME, TG, Chol, DG, FA, MG, CerII, CerIII, CerV, CerVI, ASG, MGDG, GlcCer, DGDG, PG, PE, PA, PI, CL, PS, SM, LPC
Lipids classes and subclasses identified in samples	CE, TG, Chol, DG, FA, DPG, PE, PI, PS, PC, SM, LPC	CE, TG, Chol, HexCer, HexCer(OH), CL,PE, PI, PS, PC, SM	Sql, WE, DGE, TG, FAlc, ST, FA, HexCer, CL, PE, PI, PS, PC, LPC	TG, Chol, DG, FA, MG, MGDG, DGDG, NAPE, PE, NALPE, PI, PC, LPC	CE, TG, FA, Chol, PE, PC, CL	SQ, SE, Coenzyme, TG, ST, Chol, DG, FA, MG, Cer, ASG, MDGD,SG, GlcCer, HexCer, HerCer(OH), DGDG, NAPE, PG, PE, PA, PI, CL, PS, PC, SM, LPC

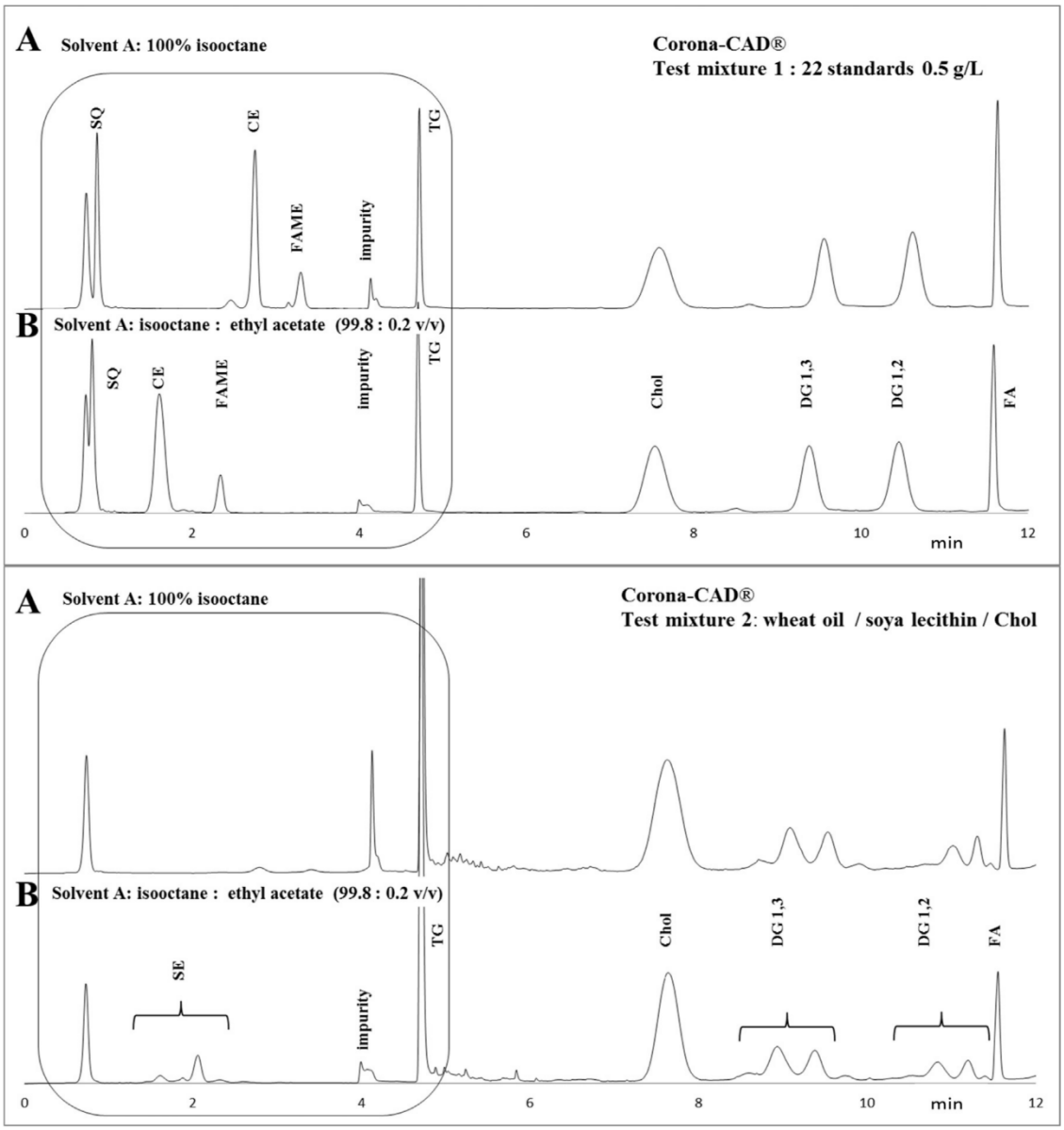

Fig. 1. Influence of the initial mobile phase composition on the first part of the chromatogram (0–12 min) for test mixtures 1 (top) and 2 (bottom). (A) 100% isooctane (B) isooctane:ethyl acetate (99.8:0.2, v/v). The other mobiles phases of the solvent program are as indicated in Table 2. SQ-squalene, SE-sterol ester, CE-cholesteryl esters, FAME-fatty acids methylesters, TG-triacylglycerols, ST-sterols, Chol-cholesterol, DG-diacylglycerols, FA-fatty acids. Detector: Corona-CAD®.

Finally, 7 total lipid extracts from different origins (3 animal, 2 vegetal, 1 from yeast and 1 from bacteria) were analyzed with the method presenting the best resolution between the lipid classes. In order to appreciate the versatility of the method we briefly compared the results obtained with each extract to information from the literature.

3.1. Mobile phase composition

3.1.1. Mobile phase A

3.1.1.1. Isooctane purification. In an attempt to reduce the impurity level, isooctane was flowed through a semi-preparative column packed with Lichrospher Si-60, 5–20 μm bare silica prior its use in mobile phase [16–18].

3.1.1.2. Eluent pressurization. Gerits introduced the IPA rinsing to prevent pressure fluctuation encountered at the beginning and at the end of the solvent program. From our experience, such phenomenon is more or less pronounced depending on the equipment used and is encountered with highly compressible and low viscosity solvents such as alkanes. A slight pressurization (0.2 bar) of the solvent reservoir minimize the pumping difficulties encountered with alcanes.

3.1.1.3. Ethyl acetate. Graeve's method [11] allows the best separation of the most nonpolar lipids (SQ, SE (sterol ester), WE (wax ester), FAME, DAGE (diacylglycerol ethers) and TG). Mobile phase A composition is isooctane:ethyl acetate (99.8:0.2, v/v). Ethyl acetate was preferred to tetrahydrofuran (THF) initially proposed by Christie or Homan since it is compatible with peek tubing [19]. The lower polarity and the selectivity change induced by this solvent allow an improved separation of SQ, SE and WE.

Gerits [12] uses pure isooctane. Unfortunately, the most nonpolar lipids cannot be seen on its chromatograms that start at 5 min

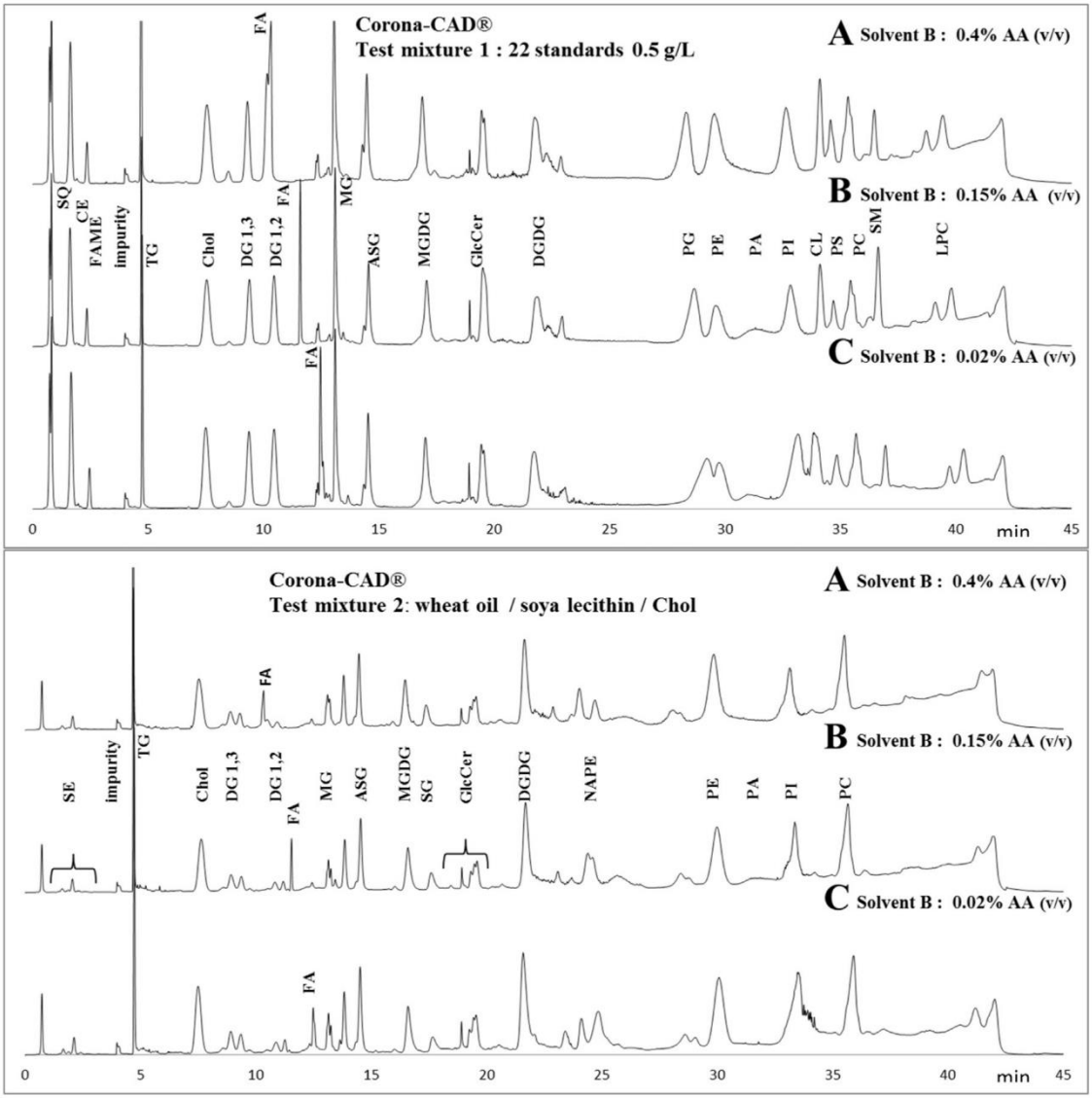

Fig. 2. Influence of the amount of acetic acid in the B phase of the solvent program on the chromatogram of test mixtures 1 (top) and 2 (bottom). (A) 0.4%, (B) 0.15% (C) 0.02% acetic acid (v/v) in acetone:ethyl acetate (2: 1, v/v). The other mobiles phases of the solvent program are as indicated in Table 2. SQ-squalene, SE-sterol ester, CE-cholesteryl esters, FAME-fatty acids methylesters, TG-triacylglycerols, Chol-cholesterol, DG-diacylglycerols, FA-fatty acids, MG-monoacylglycerols, ASG-acylated steryl glycosides, MGDG-monogalactosyldiglycerols, SG-steryl glycosides, GlcCer-glucosylceramides, DGDG-digalactosyldiglycerols, NAPE-N-Acylphosphatidylethanolamines, PG-phosphatidylglycerols, PE-phosphatidylethanolamines, PA-phosphatidic acids, PI-phosphatidylinositols, CL-cardiolipins, PS-phosphatidylserines, PC-phosphatidylcholines, SM-sphingomyelins, LPC-lysophosphatidylcholines. Detector: Corona-CAD®.

after the injection. In order to appreciate the exact role of the 0.2% (v/v) ethyl acetate addition in mobile phase A, test mixtures 1 and 2 were analyzed with a pure or modified phase A (Fig. 1). Adding 0.2% (v/v) ethyl acetate only influences the selectivity between lipid classes eluted during the first 5 min of the chromatogram. Both SE and FAME are less retained and show a broader peak. Additionally, the resolution between the dead volume and SQ decreases. The chromatograms from natural samples mixture show an improved separation of nonpolar compounds eluted during the 5 first minutes. Co-elutions with solvent impurities are also limited.

To summarize, the addition of 0.2% (v/v) ethyl acetate enhances the discrimination of nonpolar lipids. Alternatively, when SQ is a compound of interest, only pure isooctane used as initial mobile phase allows its retention.

3.1.2. Mobile phase B

The mobile phase B, as optimized by Gerits for the analysis of medium polarity lipids (MG, MGDG and DGDG), contains 20 fold more AA than the mobile phase proposed by Graeve [11]. In order to highlight the effect of AA on lipid classes retention, three levels were compared and presented in Fig. 2: 0.02% (Graeve), 0.15% (v/v) (this work) and 0.4% (Gerits).

The retention of FA decreases with increasing concentration in AA in the mobile phase. This is probably due to the competition between AA and FA for the adsorption onto the stationary phase. With 0.02% AA (v/v), the FA peak co-elutes with a system peak and at 0.4% (v/v) FA and DG 1,3 co-elute. Among the tested concentrations, 0.15% AA (v/v) offers the best compromise for the elution of FA and their resolution with adjacent peaks.

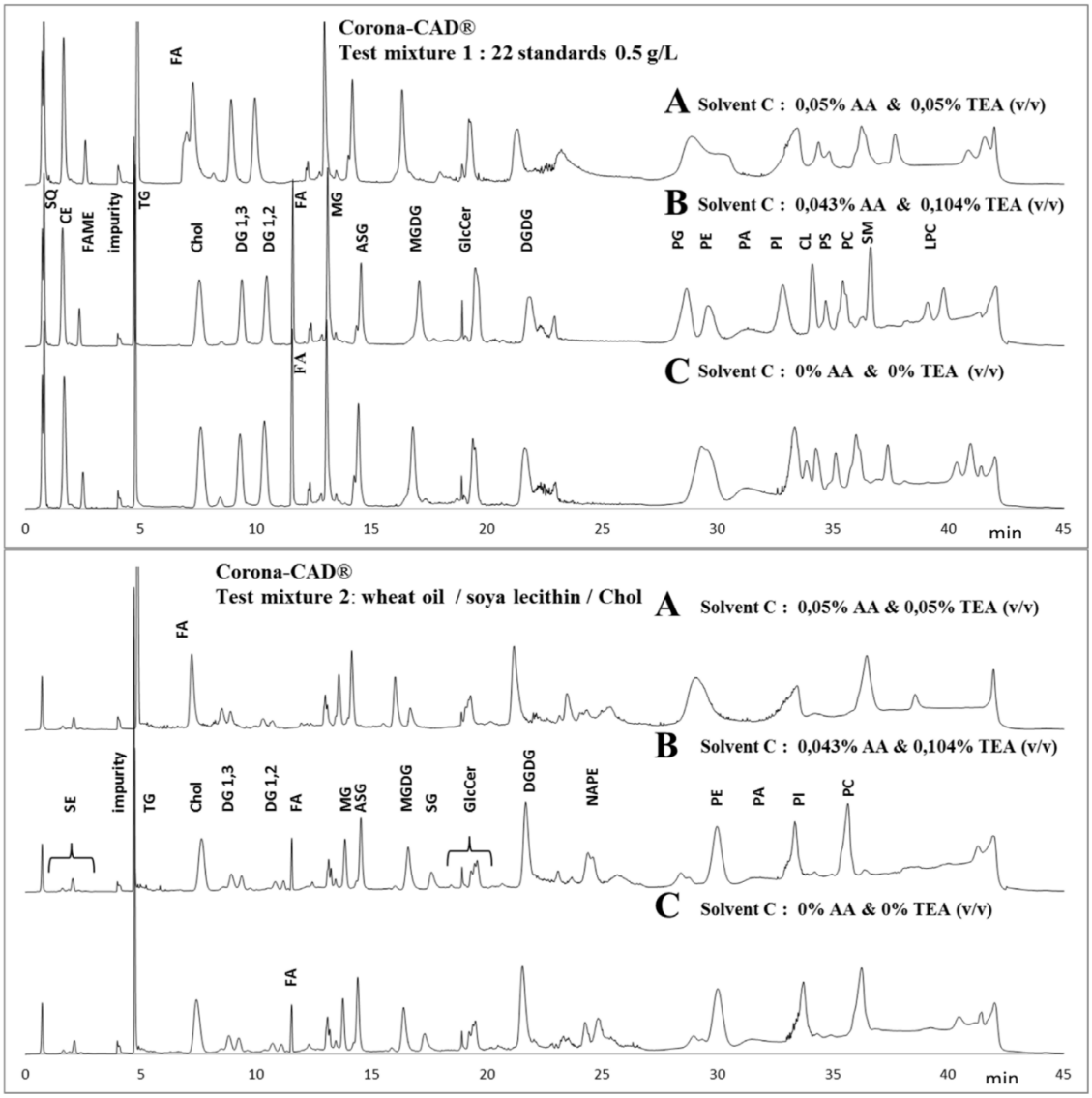

Fig. 3. Influence of the amounts of acetic acid and trimethylamine in the C phase of the solvent program on the chromatogram of test mixtures 1 (top) and 2 (bottom). (A) 0.05% AA & TEA (v/v), (B) 7.5 mM AA & TEA (0.043% AA & 0.104% TEA) and (C) without AA or TEA. The other mobiles phases of the solvent program are as indicated in Table 2. SQ-squalene, SE-sterol ester, CE-cholesteryl esters, FAME-fatty acids methylesters, TG-triacylglycerols, Chol-cholesterol, DG-diacylglycerols, FA-fatty acids, MG-monoacylglycerols, ASG-acylated steryl glycosides, MGDG-monogalactosyldiglycerols, SG-steryl glycosides, GlcCer-glucosylceramides, DGDG-digalactosyldiglycerols, NAPE-N-Acylphosphatidylethanolamines, PG-phosphatidylglycerols, PE-phosphatidylethanolamines, PA-phosphatidic acids, PI-phosphatidylinositols, CL-cardiolipins, PS-phosphatidylserines, PC-phosphatidylcholines, SM-sphingomyelins, LPC-lysophosphatidylcholines. Detector: Corona-CAD®.

In addition, AA concentration in mobile phase B has a noticeable impact on the second part of the chromatogram. 0.15% AA (v/v) is also an optimum concentration for the elution of PL at the end of the chromatogram as advisable from chromatographic profile of test mixture 1 in Fig. 2. Alternatively, using 0.4% AA (v/v) is interesting to improve the chromatographic profile of lipids eluting between DGDG and PL.

We decided to favor FA retention and PL separation and thus, to use the intermediate 0.15% AA (v/v) concentration in the solvent program.

3.1.3. Mobile phase C

Homan [13] first introduced a mobile phase C composed by IPA and water (85:15, v/v) with an equimolar amount of AA and ethanolamine (EA) at 7.5 mM. The same C mobile phase is used by Graeve [11]. The experimental conditions of Gerits [12] are close to those of Homan, except EA is replaced by TEA. The mobile phases proposed by Homan [6] don't incorporate any ionic modifier. In order to understand the influence of the ion pair concentration and volume ratio in mobile phase C, a separation of test mixtures 1 and 2 with A: 0.05% (v/v) AA and TEA, B: 7.5 mM AA and TEA (0.043% (v/v) AA and 0.104% (v/v) TEA) C: neither AA nor TEA is presented in Fig. 3.

The AA/TEA relative amounts do not affect the lipids eluted at the beginning of the chromatogram with the notable exception of FA. When absent or in equimolar ratio, FA retention is unaffected.

When the same volume of AA and TEA e.g. 0.05% (v/v) is added, the molar excess of AA represents the addition of 0.025% (v/v) AA in the mobile phase. Although being present in the C mobile phase and despite of the rinsing phase D, the AA amount influences the FA retention at the beginning of the chromatogram. In these conditions, the AA amount in phase C is responsible for the co-elution of FA and Chol.

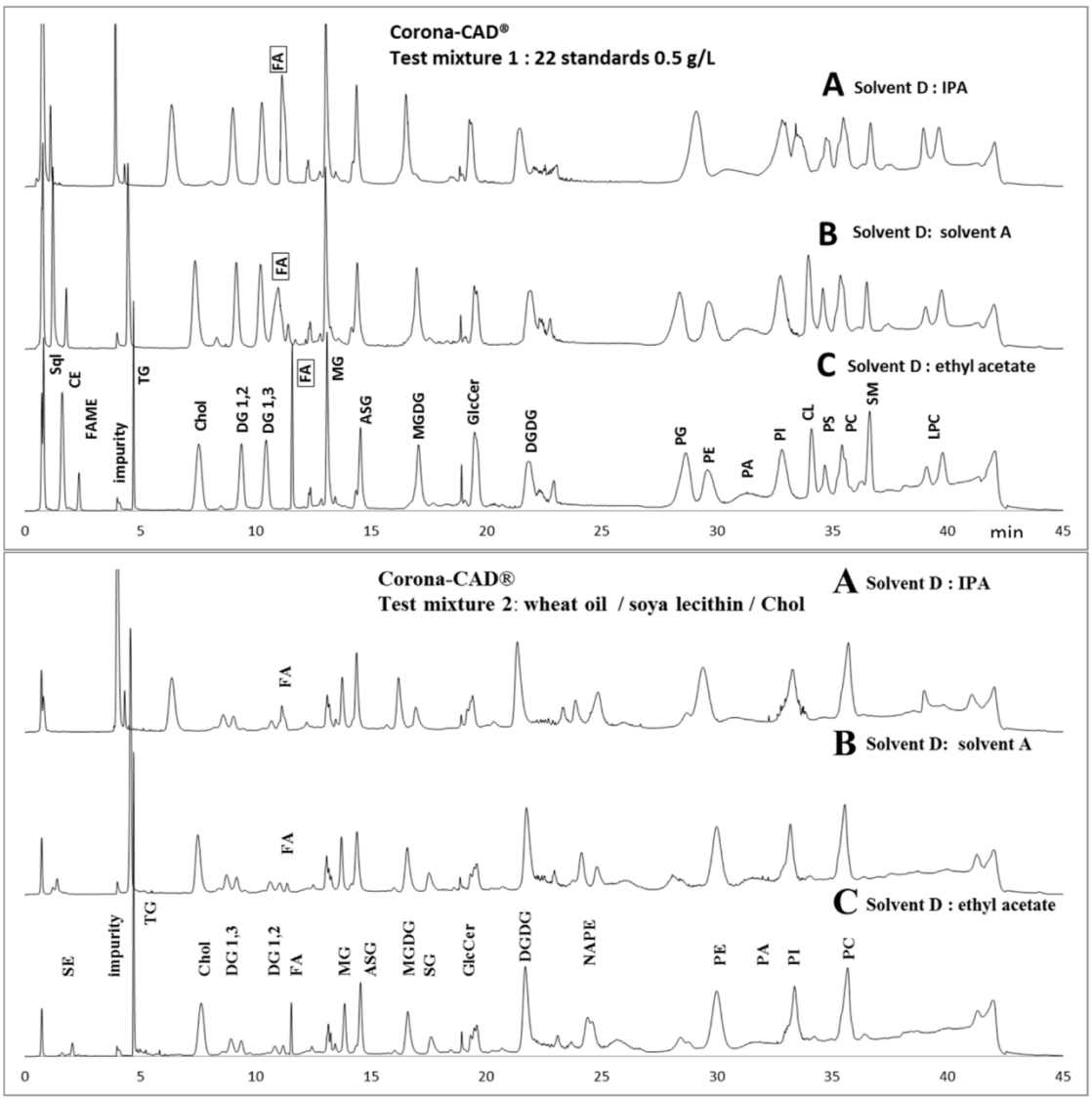

Fig. 4. Influence of the rinsing step (mobile phase D) on the chromatogram of test mixture 1 (top) and 2 (bottom): (A) isopropanol (B) isooctane: ethyl acetate (99.8: 0.2, v/v) (C) ethyl acetate (C). The other mobiles phases of the solvent program are as indicated in Table 2. SQ-squalene, SE-sterol ester, CE-cholesteryl esters, FAME-fatty acids methylesters, TG-triacylglycerols, Chol-cholesterol, DG-diacylglycerols, FA-fatty acids, MG-monoacylglycerols, ASG-acylated steryl glycosides, MGDG-monogalactosyldiglycerols, SG-steryl glycosides, GlcCer-glucosylceramides, DGDG-digalactosyldiglycerols, NAPE-N-Acylphosphatidylethanolamines, PG-phosphatidylglycerols, PE-phosphatidylethanolamines, PA-phosphatidic acids, PI-phosphatidylinositols, CL-cardiolipins, PS-phosphatidylserines, PC-phosphatidylcholines, SM-sphingomyelins, LPC-lysophosphatidylcholines. Detector: Corona-CAD®.

The relative amounts of AA and TEA influence polar lipid (PL) retention and selectivity. The best separation is obtained with an equimolar amount of AA/TEA in phase C.

3.1.4. Mobile phase D

Graeve's method [11] doesn't make use of a particular rinsing solvent at the end of the solvent program. After the phase C step, the solvent program goes back to the B phase and then re-equilibration is performed using the A phase. The low viscosity of isooctane together with the high permeability of monolithic silica, allow doubling the flow rate during the equilibration step. Gerits [12] introduced IPA as rinsing solvent and indicated that this rinsing step improves the subsequent pumping of isooctane. As already underlined, this step influences the first part of the chromatogram.

In this study, a rinsing step was introduced with ethyl acetate, an intermediate polarity solvent, in order to facilitate equilibration while favoring the retention of nonpolar lipids at the beginning of the chromatogram. As indicated in Table 2, the rinsing step consists in a 50:50 mixture between mobile phase A and D. The chromatograms of test mixtures 1 and 2 obtained with 3 rinsing conditions are presented in Fig. 4. When no rinsing is performed (Fig. 4B), mobile phase D composition is identical to mobile phase A. In Fig. 4A and C, IPA and ethyl acetate are respectively used.

As seen in Fig. 4A the use of IPA as rinsing solvent is not compatible with a proper retention of neutral lipids at the beginning of the chromatogram. Indeed, we can hypothesize that the IPA adsorption energy is so high that this solvent cannot be readily driven out the silanols of the silica by isooctane.

Repeated experiments have shown that the ethyl acetate rinsing step (Fig. 4C) gives a superior result compared to an increase in equilibration time performed with mobile phase A (Fig. 4A). In the first part of the chromatogram, SQ, CE, FAME and TG are more retained. The retention time of FA is slightly increased but the influ-

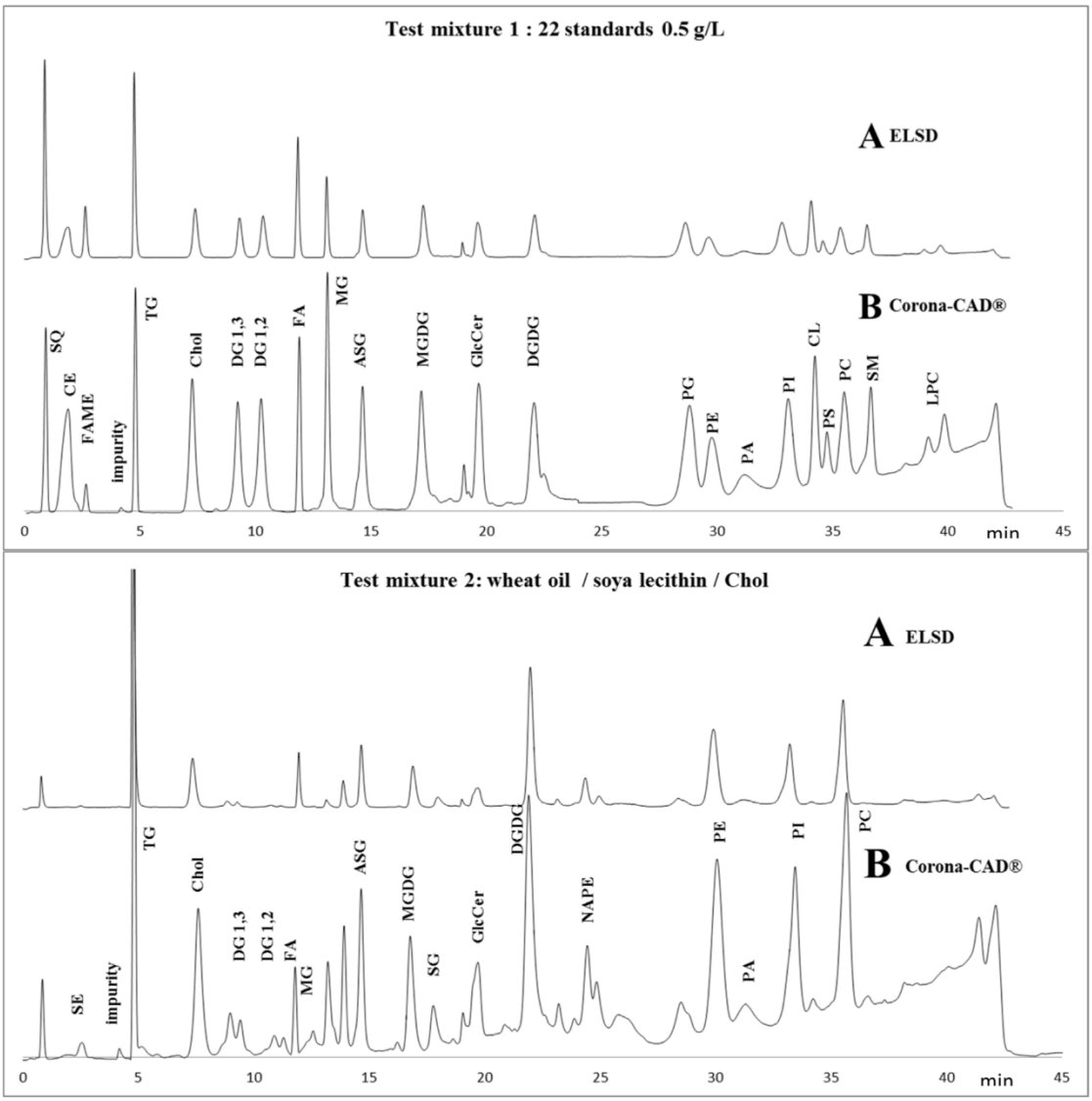

Fig. 5. Chromatographic profiles of test mixtures 1 (top) and 2 (bottom) obtained with (A) ELSD and (B) Corona-CAD® detection. SQ-squalene, SE-sterol ester, CE-cholesteryl esters, FAME-fatty acids methylesters, TG-triacylglycerols, Chol-cholesterol, DG-diacylglycerols, FA-fatty acids, MG-monoacylglycerols, ASG-acylated steryl glycosides, MGDG-monogalactosyldiglycerols, SG-steryl glycosides, GlcCer-glucosylceramides, DGDG-digalactosyldiglycerols, NAPE-N-Acylphosphatidylethanolamines, PG-phosphatidylglycerols, PE-phosphatidylethanolamines, PA-phosphatidic acids, PI-phosphatidylinositols, CL-cardiolipins, PS-phosphatidylserines, PC-phosphatidylcholines, SM-sphingomyelins, LPC-lysophosphatidylcholines. Detector: Corona-CAD®.

ence of the ethyl acetate rinsing step is especially noticeable on peak geometry with FA eluting as a sharp and intense peak.

It is also important to note that the rinsing step can have an influence on the most polar lipids of the chromatogram. The PL profile in Fig. 4A using IPA is noticeably different than the profiles obtained with mobile phase A (Fig. 4B) and ethyl acetate (Fig. 4C).

Solvent consumption is directly impacting analysis cost and solvent rejection being an environmental and safety issue, it is worthy to note that the method we propose use about 40% less solvent than refs [10,11]. The total solvent volume of our method is 42 ml, 32 ml for the solvent program plus 10 ml for rinsing and equilibration whereas it is 68 ml when using the methods described in Refs. [10,11].

Medium polarity lipids (Ceramides) The aforementioned publications do not relate to ceramides.This lipid class is frequently investigated in lipidomic studies, especially in skin research where a vast diversity is encountered [23–26]. We considered important to evaluate the elution window of the ceramide subclasses and to assess the possible co-elution with other lipid classes. Cer elute in the area of medium polarity lipids with retention times intermediate between MG and MGDG (Fig. 6). ASG co-elutes with the first peak of CerVI. CerV elutes as a double peak. CerV, a synthetic ceramide, is a racemic mixture of two epimers N-(R,S)-alpha-Hydroxyoctadecanoyl-D-erythro-sphingosine. These two peaks presumably correspond to the epimers. Bare silica had already proven to separate epimers, as for example sterols [27]. No information is available about the stereochemistry of CerVI, but, as for CerV, its elution as two distinct peaks may be due to the occurrence of two epimeric forms. Unlike in CerV and CerVI, carbon at position 2 of the fatty acyl chain of CerII is not a chiral center. The double peak encountered with this compound is presumably due to the Z and E configuration of the double bound of the fatty base moiety. To facilitate understanding, drawings of the chemical structures are presented in figure S-1. The MS spectra of the 3 couples of peaks are commented further in the document (ESI, APCI and APPI comparison).

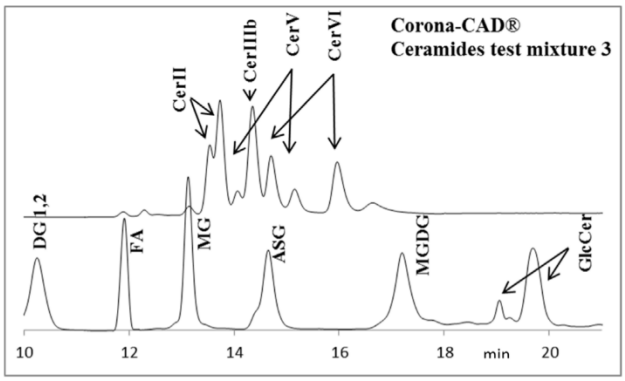

Fig. 6. Superimposition of chromatographic profiles of ceramides subclasses (test mixture 3) and chromatographic profile of standards (test mixture 1) obtained with Corona-CAD®. Ceramides (CerII(Cer(d18:1/18:0)), CerIIIb (Cer(t18:0/18:1)), CerV (Cer(d18:1/18:0(2OH)) and CerVI (Cer(t18:0/18:0(2OH)))), DG-diacylglycerols, FA-fatty acids, MG-monoacylglycerols, ASG-acylated steryl glycosides, MGDG-monogalactosyldiglycerols, SG-steryl glycosides, GlcCer-glucosylceramides. Detector: Corona-CAD®.

3.2. ELSD/Corona-CAD® comparison

ELSD has gained a wide acceptance in lipid class analysis since the pioneering work of Robinson and Macrae [20] at the beginning of the '80s. Indeed, ELSD is a nebulization-based detector that is compatible with gradient elution and allows detecting any solute less volatile than the mobile phase. The Corona-CAD®, introduced in 2004 [21], shares the same operating principle except aerosol charging is used instead of the light diffusion exploited in the ELSD.

Fig. 5 presents the chromatograms of test mixtures 1 & 2 at 0.5 g/L (2 μl injected) using both detectors. Corona-CAD® appears to be more sensitive to the baseline drift phenomenon occurring from the gradient program. The chromatogram of lipid standard at equal concentration (test mixture 1) shows more consistent peak heights with Corona-CAD® than with ELSD. This can be explained by the typical response functions of both detectors [22]. With ELSD, when Rayleigh scattering is the dominant phenomenon, the sensitivity increases with increasing amount of solutes. From our experience, this is the case when narrow bore column and reduced flow rates are used. Consequently, the peak intensities of minor compounds appear to be less than their actual quantity. At the opposite, major compounds benefit from the increased sensitivity and their peak intensities dominate the chromatogram. The response function of the Corona-CAD® is more consistent among injected quantities and, at least, the sensitivity decreases for high solute amounts. Therefore, with the Corona-CAD®, the chromatographic profile is more likely to reflect the relative amounts of solutes involved in complex samples such as mixture 2.

3.3. ESI, APCI and APPI comparison

Although combined positive-negative ionization mode could be achieved by the mass spectrometer, distinct positive and negative profiles where recorded with the three ion sources to highlight the different behavior of some lipid classes (Fig. 7).

ESI does not give any signal at the beginning of the chromatogram in either positive or negative ionization mode. Only polar lipids are detected but with an unfavorable background noise. Coupling the present NPLC method with ESI cannot be recommended.

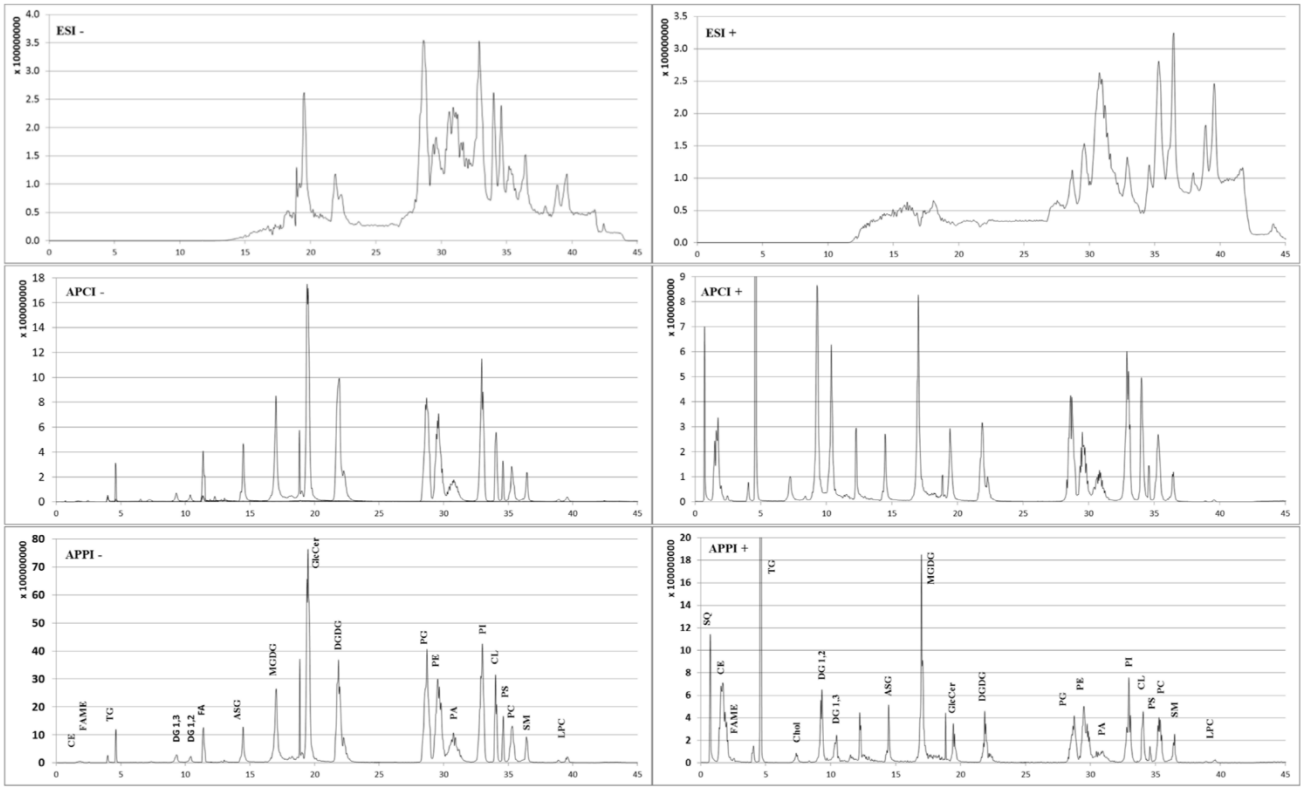

Fig. 7. LC/MS chromatographic profile of mixture 1, using three different ion sources: ESI (top), APCI (middle) and APPI (down), in negative ion mode (left) and positive ion mode (right). SQ-squalene, CE-cholesteryl esters, FAME-fatty acids methylesters, TG-triacylglycerols, Chol-cholesterol, DG-diacylglycerols, FA-fatty acids, ASG-acylated steryl glycosides, MGDG-monogalactosyldiglycerols, GlcCer-glucosylceramides, DGDG-digalactosyldiglycerols, PG-phosphatidylglycerols, PE-phosphatidylethanolamines, PA-phosphatidic acids, PI-phosphatidylinositols, CL-cardiolipins, PS-phosphatidylserines, PC-phosphatidylcholines, SM-sphingomyelins, LPC-lysophosphatidylcholines.

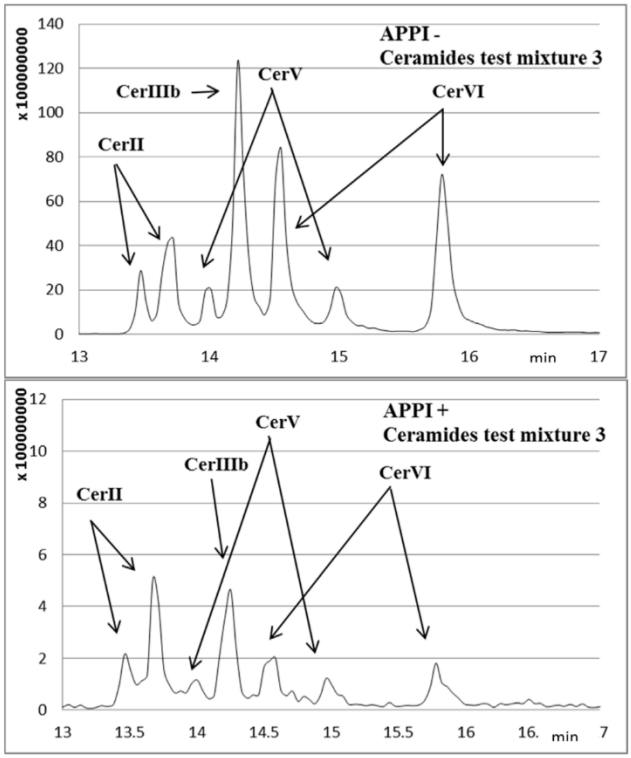

Fig. 8. LC/MS chromatographic profile of test mixture 3, using APPI, in negative ion mode (top) and positive ion mode (down). Ceramides (CerII (Cer(d18:1/18:0)), CerIIIb (Cer(t18:0/18:1)), CerV (Cer(d18:1/18:0(2OH)) and CerVI (Cer(t18:0/18:0(2OH)))).

The chromatograms acquired with either APCI or APPI showed similar profiles. In positive ion mode, peak intensities of ionized lipid classes appeared to be similar. On the contrary, APPI delivered a 4 fold more important signal than APCI in negative mode. APCI is much more readily available in mass spectrometry platforms than APPI and can conveniently be used with this method. However, APPI will be preferred if available. For example, the Cer class is detected with a ≈20 fold more intense response in negative APPI detection compared to positive APPI (Fig. 8). This finding corroborates the fact that APPI appears to be particularly interesting for lipid analysis [29], well suited to NPLC solvent conditions [30] and offering a high sensitivity for lipid analysis [31].

The three API sources were compared by Imbert et al. [14] by coupling the Graeve's method [11] to mass spectrometry for the analysis of *Leishmania donovani* lipids. In this previous study from our group, the number of lipids classes was twice as less. In addition, when comparing chromatographic profiles, the separation appears to be poorer than in the present study. It is worthy to note that mobile phases contain AA and TEA in proportions that are different from the present study and this presumably influence ionization. In addition, Imbert and al. employed an acetone post-column addition as dopant for APPI ionization. In the present study, such addition did not improve ionization. The presence of 0.2% (v/v) ethyl acetate in the initial mobile phase presumably plays this role. The effect of eluent composition on the ionization efficiency of ESI, APCI and APPI in LC–MS was studied in [32].

Fig. 9 contains a selection of MS spectra obtained for 4 standards that illustrate characteristic ions obtained with the 3 API sources. Supplementary figure S-2 presents the LC/MS full scan spectra of all standards considered in this study in either positive or negative ionization mode with ESI, APCI and APPI interfaces.

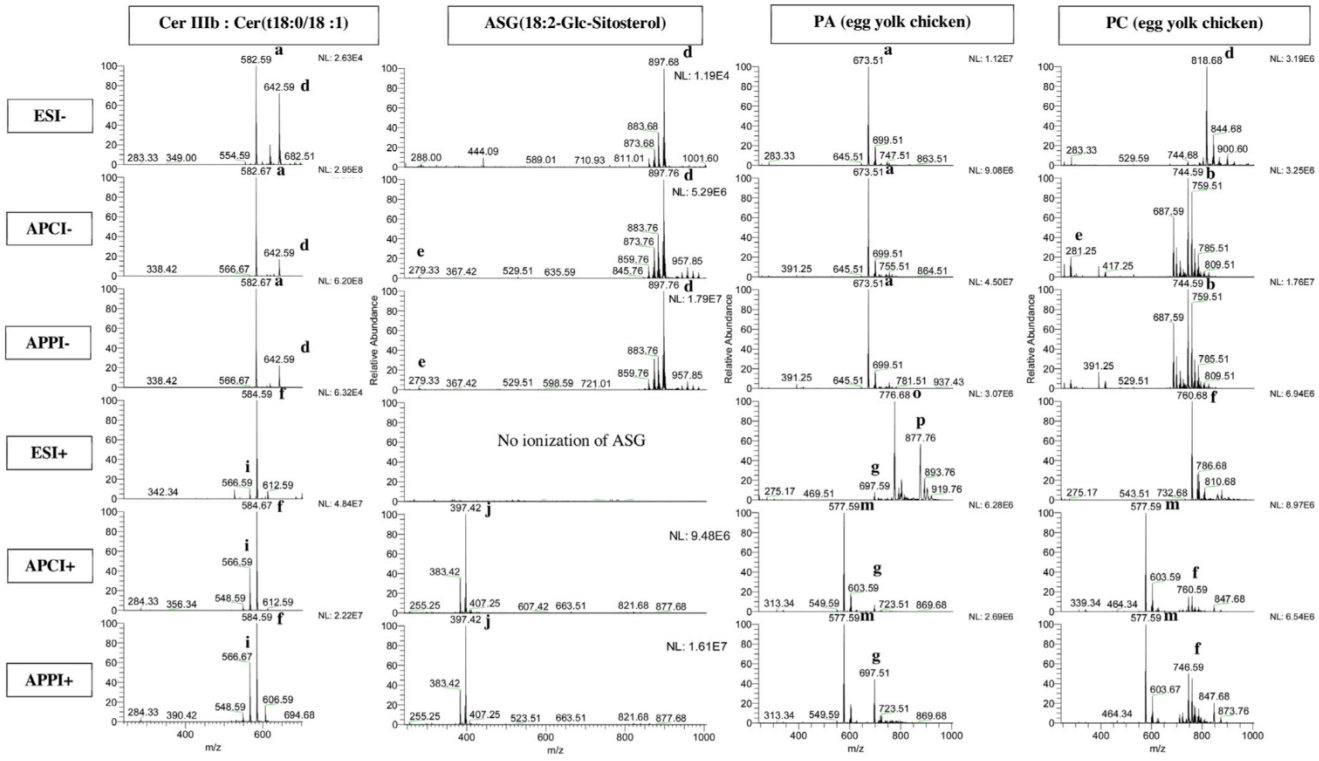

Fig. 9. LC/MS full scan spectra obtained with the 3 API sources in positive and negative mode. a: $[M-H]^-$, b: $[M-CH3]^-$, c: $[M^\circ]^-$, d: $[M-H+CH_3COOH]^-$, e: $[FA-H]^-$, f: $[M+H]^+$, g: $[M+Na]^+$, h: $[M+H-FA]^+$, i: $[M+H-H_2O]^+$, j: [M-FA-sugar+H+H2O]$^+$, k: [Aglycone+H−H2O]$^+$, l: [Aglycone+H]$^+$, m: [M+H-polar Head]$^+$, n: Diglyceride like ion, o: [M+H+TEA]$^+$ and p: [M+H+2TEA]$^+$.

3.3.1. CerIIIb:Cer(t18:0/18:1)

The three API sources produced similar ions for CerIIIb. The full scan spectra of other Cer standards presented similar ionization patterns.

In negative mode [33,34], the most abundant ion was $[M-H]^-$ whereas the AA adduct $[M-H+CH_3COOH]^-$ was also observed. With ESI, the AA adduct represented 80% relatively to the $[M-H]^-$ but only 20% when APCI and APPI were used. The total ion count (TIC) was low with ESI^- (2.6E4) whereas it was more important with APCI and APPI. APPI provided a 2 fold more intense signal than APCI.

In positive mode, the most abundant ion was $[M+H]^+$ and was accompanied by the $[M+H-H_2O]^+$ that correspond to the loss of a water molecule. This in source fragmentation was more pronounced with APPI and less important with ESI. The TIC remained low in ESI (6.3E4) and more important with APCI and APPI. At the opposite of the negative mode, the TIC was 2 fold more important with APCI than APPI.

The MS spectra obtained in full scan, MS^2 and MS^3 for each couple of peaks encountered with CerV and CerVI were identical (Figure S-3). The MS spectra of the two peaks of CerII showed the same ions but with different relative intensities. This supposes quasi-identical structures and reinforces the hypothesis of the epimeric forms separation or CerV and CerVI and the stereoisomerism of CerII.

3.3.2. ASG(18:2-Glc-Sitosterol)

In negative mode, the base peak was $[M-H+CH_3COOH]^-$ with the 3 ionization sources. Here also, APPI provided a 3 fold more intense signal than APCI, whereas ESI exhibited a low TIC (1.2E4).

In positive mode [35], the ASG ions could not be retrieved from the ESI LC/MS profile. The most abundant ion corresponds to [M-FA-sugar + H + H2O]$^+$ and was 3 fold more intense with APPI compared to APCI.

3.3.3. PA from egg yolk, PA(16:0_18:1) as most abundant specie

The adducts and fragmentation patterns observed with PA were also encountered with other PL (PG, PE, PI and PS) [36,37].

In negative mode, the base peak was $[M-H]^-$ with all API sources. The TIC was comparable between ESI and APCI (about 1E7) and 4 fold more abundant with APPI.

In positive mode, the observed ions with ESI were different from the two other sources. TEA adducts were observed with ESI as $[M+TEA+H]^+$ et $[M+2TEA+H]^+$. With both APCI and APPI, the major ion corresponded to the loss of the polar head of the PL $[M+H\text{-polar head}]^+$ and a $[M+Na]^+$ of lesser intensity was also observed.

3.3.4. PC from egg yolk, PC(16:0_18:1) as most abundant specie

The adducts and fragmentation patterns observed with PC were also encountered with other PL (SM and LPC) [36,37].

In negative mode, ESI spectra were different from the two others and exhibited a predominant AA adduct. With APCI and APPI, a radical ion $[M^\circ]^-$ was observed together with a $[M-CH_3]^-$ that correspond to the loss of a methyl group. The signal intensity was comparable between ESI and APCI (about 3E6) and 5 fold more intense with APPI.

In positive mode, the major ion was [M+H]+ with ESI and no fragment ion was observable. With APCI and APPI, the major ion was a $[M+H\text{-polar Head}]^+$ and $[M+H]^+$ was also observed. The signal intensity was comparable between the 3 API sources.

It is important to note that, whereas APCI and APPI induce more fragments than ESI, the structural information is preserved by combining both positive and negative mode of ionization.

3.3.5. The particular case of TG

Tristearin or TG(18:0/18:0/18:0) was arbitrary chosen to represent the TG class. The LC/MS tristearin spectra obtained with APCI and APPI in positive mode showed an unique $[M+H-FA]^+$ ion whereas in TG spectra from lipid samples, the $[M+H-FA]^+$ coexisted with the $[M+H]^+$. TG from natural oils are often characterized using the $[M+H]^+$ ion [38,39]. In most publications, saturated TG are not reported. Saturated TG are indeed only present in very low amount in natural oils. A systematic study of TG fragmentation patterns using LC/APCI-MS shows that for saturated TG the $[M+H]^+$ ion is not observed [40]. For TG(18:1/18:1/18:1) or TG(16:1/16:1/16:1) the $[M+H]^+$ is weak and accounts for only 7% of the base peak $[M+H-FA]^+$. The $[M+H]^+$ ion becomes the major ion of the spectrum when the degree of unsaturation increases.

To summarize, APPI appeared to be the best-suited interface for coupling the present NPLC lipid classes separation to mass spectrometry. A simplified list of ions encountered in positive and negative ion mode APPI is presented in Table 4. This table was built to facilitate the identification of lipid classes in different sample types. In most cases, the lipid classes correspond to analytical standard. In some instances, when the standards are not readily available, the reported ions correspond to lipid structures identified in natural samples. For each lipid class or subclasses, the ions observed for a representative specie are reported together with its molecular mass, retention time and adduct(s) observed. By working with the two ionization modes, all the lipid classes studied herein could be detected. It is easily possible to trace back to the lipid specie parent structure despite of the in source fragmentation.

3.4. Chromatographic profiles of 7 total lipid extracts from differerent samples

All total lipid extracts available from Avanti Polar were studied: 3 from animal, 2 from plants and one from yeast and bacterium (Fig. 10).

3.4.1. Heart/Liver/Brain

Homan [13] studied the three animal tissues, Christie [10] and McLaren [9] studied the heart and liver, and Holčapek's group [6] the brain. The three animal samples exhibit similar lipid profiles. TG, Chol, FA are found in variable quantities according to the animal tissue considered. PE and PC are the major phospholipids. Heart shows a higher amount of CL whereas brain contains high quantities of cerebrosides (HexCer and HexCer(OH)) that are not present in other tissues. The lipid profiles obtained in the present study are similar to those shown by Christie [10] or Homan [13]. The method proposed in herein presents a better retention of CE and allows quantifying them if needed. In McLaren's study, the aim was to analyze the major lipids with the shortest possible analysis time. Consequently, the chromatogram duration is only 10 min but low concentration lipids are not observable in the chromatograms of real samples. This is possibly a consequence of the reduced amount of sample injected. As the method was developed with only 7 different lipid standards, it is difficult to appreciate the real ability of this method to separate a complex total lipid extract. In contrast, the UHPSFC-MS profile of pork brain presented by [6], shows a very detailed separation. All the lipids we evidenced in our profiles (except SQ) were found and additional lipids in low amount were identified.

UHPSFC-MS appears to be a very promising technique for total lipid extract analysis together by its high efficiency and high throughput. It is also worthy to note that this technique only uses supercritical CO2 with methanol and water as co-solvent or make-up fluid and is much more environment friendly than usual NP-HPLC methods. At the present time, this equipment is scarcely

Table 4
APPI negative and positive mode: characteristics ions of some lipid species encountered in lipid standards and samples (see text for details). A retention time noted x-y indicates a broad peak and x;y indicates a dual peak. Ions between brackets have an intensity of less than 5.10^6 counts. For PL, the FA indication is not positional. SQ-squalene, CE-cholesteryl esters, FAME-fatty acids methylesters, TG-triacylglycerols, Chol-cholesterol, DG-diacylglycerols, FA-fatty acids, MG-monoacylglycerols, Ceramides (CerII (Cer(d18:1/18:0)), CerIIIb (Cer(t18:0/18:1)), CerV (Cer(d18:1/18:0(2OH)) and CerVI (Cer(t18:0/18:0(2OH)))), ASG-acylated steryl glycosides, MGDG-monogalactosyldiglycerols, SG-steryl glycosides, GlcCer-glucosylceramides, DGDG-digalactosyldiglycerols, NAPE-N-Acylphosphatidylethanolamines, PG-phosphatidylglycerols, PE-phosphatidylethanolamines, PA-phosphatidic acids, PI-phosphatidylinositols, CL-cardiolipins, PS-phosphatidylserines, PC-phosphatidylcholines, SM-sphingomyelins, LPC-lysophosphatidylcholines.

Lipid species	Rt. (min)	Molecular mass (g/mol)	APPI −					APPI +					
			$[M-H]^-$	$[M-CH3]^-$	$[M^{\bullet-}]^-$	$[M-H+CH_3COOH]^-$	$[FA-H]^-$	$[M+H]^+$	$[M+Na]^+$	$[M+H-FA]^+$			
											$[M+H-H_2O]^+$	**[M-FA-sugar+H +H2O]$^+$**	**[Aglycone+H−H2O]$^+$**	**[Aglycone +H]$^+$**
SQ	0.7	410.4	(409.4)					411.4						
CE(16:0)	1.7–2.8	624.6					(255.2)			369.4				
FAME(methyl-nonadecanoic acids)	2.5	312.3					(297.3)	(313.3)						
TG(18:0/18:0/18:0)	4.6	890.8	(889.8)				283.3			607.6				
Coenzyme Q10	4.6	862.7	(861.7)					(863.7)						
Chol	7.4	386.4								(369.4)				
DG(18:2/0:0/18:2)	9.3	616.5	(615.5)			(675.5)		279.2	617.5	599.5				
DG(16:0/16:0/0:0)	10.4	568.5				(627.5)		255.2		551.5				
FA(18:0)	11.4	284.3	283.3					283.3						
Cer II: Cer(d18:1/18:0)	13.4; 13.7	567.6	566.6			626.6			568.7	550.7				
Cer IIIb: Cer(t18:0/18:1)	14.2	583.6	582.5			642.6			584.6	566.6				
Cer V: Cer(d18:1/18:0(2OH))	14.0; 14.9	581.5	580.6			(640.5)				564.6				
Cer VI: Cer(t18:0/18:0(2OH))	14.5; 15.8	599.5	598.5			(658.5)			600.6	582.5				
MG(18:0/0:0/0:0)	13	358.3				(417.3)		(283.3)	(359.3)	(341.3)				
ASG(18:2-Glc-Sitosterol)	14.5	838.7				897.7		279.2			397.3			
MGDG(18:3/16:3)	17	746.5	745.5			805.5		249.2/277.2		769.5			585.5	
SG(Sitosteryl glucoside)	17.6	576.4				(635.5)							(397.3)	
GlcCer(d18:2/20:0(OH))	19.5	771.6	770.6							(794.6)			(610.6)	
HexCer	19	809.7	808.8								792.8			
HexCer(OH)	19.5	827.7	826.8								810.8			
DGDG(18:3/18:3)	21.8	936.6	935.6			995.6		(277.2)		(959.6)				(613.4)
NAPE(18:2-16:0-N18:2)	24.4	977.7	(976.7)					(255.2)/(297.3)		(1000.7)	**[M+H-polar Head]$^+$**		**Diglyceride like ion** (575.6)	
PC(16:0.18:1)	28.7	748.5	747.5					(255.2)/(281.2)		771.5	[M+H-172]$^+$=	577.5		
PE(18:2.18:0)	29.5	743.5	742.5					(279.2)/(283.3)		(766.5)	[M+H-141]$^+$=	(603.5)		
PA(16:0.18:1)	30.7	674.5	673.5					(255.2)/(281.2)		(697.5)	[M+H- 98]$^+$=	577.5		
PI(18:0.20:4)	33	886.6	885.5					(283.3)/(303.2)		(909.5)	[M+H-260]$^+$=	627.6		
CL([18:2/18:2],-[18:2/18:2])	34	1449.0	1448.0					279.2		1472.0			599.6	
PS(18:0.18:1)	34.6	789.6	788.5					(280.2)/(283.3)		812.5	[M+H-185]$^+$=	605.7		
PC(16:0.18:1)	35.3	759.6		744.6	759.6			(255.2)/(281.2)	(760.6)		[M+H-183]$^+$=	577.5		
SM(d18:1/16:0)	36.4	702.6		687.5	(702.6)				(703.6)		[M+H-183]$^+$=	(520.5)		
LPC(0:0/18:0)	38.9	523.4		(508.4)	(523.4)			283.3	(524.4)					
LPC(16:0/0:0)	39.6	495.3		(480.3)	(495.3)			(255.2)	(496.3)					

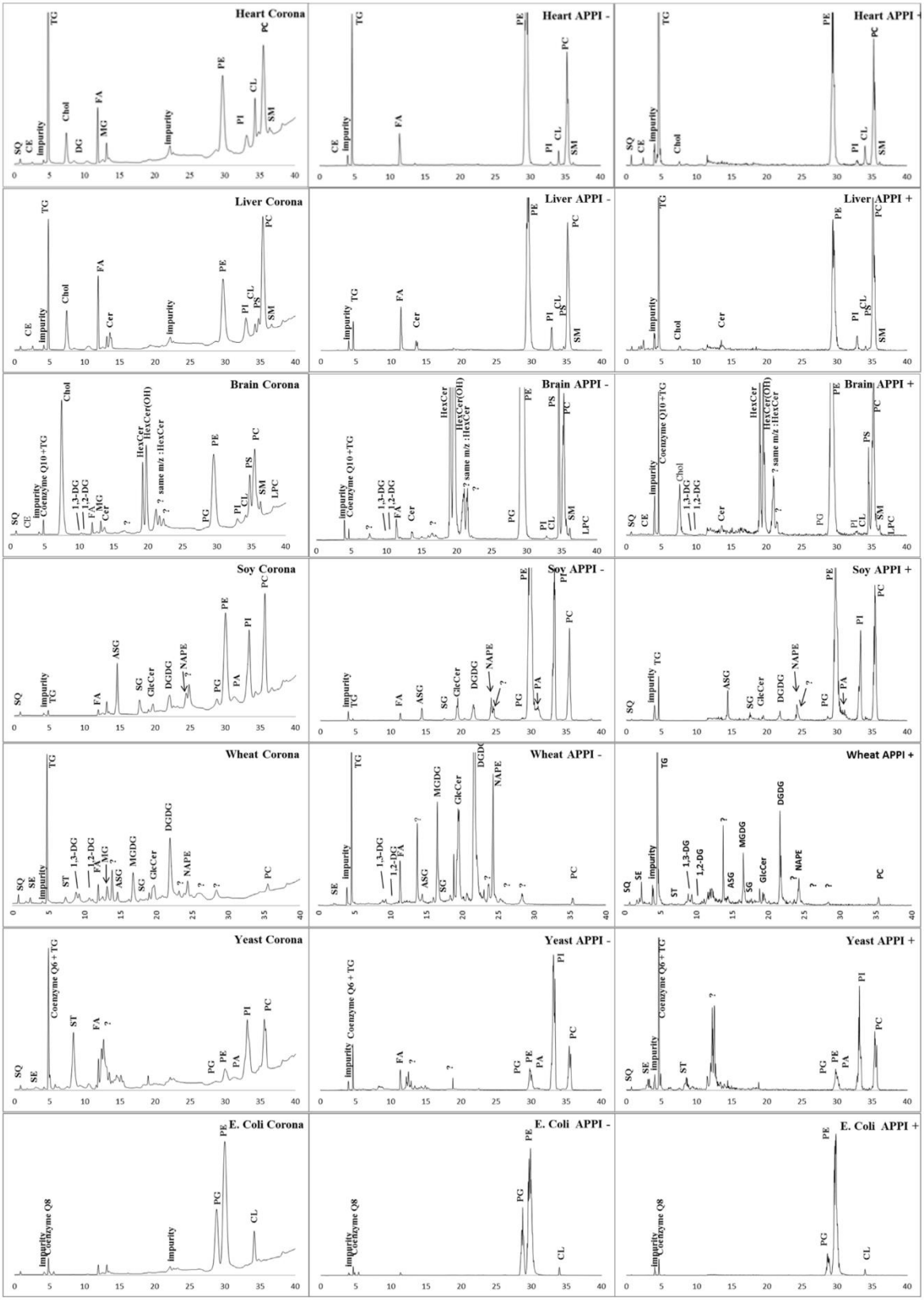

Fig. 10. Chromatograms of 7 total lipid extracts, obtained by LC- Corona-CAD® (left), LC-APPI negative ion mode (middle) and LC-APPI positive ion mode (right). SQ-squalene, SE-sterol ester, CE-cholesteryl esters, TG-triacylglycerols, ST-sterols, Chol-cholesterol, DG-diacylglycerols, FA-fatty acids, MG-monoacylglycerols, ASG-acylated steryl glycosides, MGDG-monogalactosyldiglycerols, SG-steryl glycosides, GlcCer-glucosylceramides, HexCer-hexosylceramide, DGDG-digalactosyldiglycerols, NAPE-N-Acylphosphatidylethanolamines, PG-phosphatidylglycerols, PE-phosphatidylethanolamines, PA-phosphatidic acids, PI-phosphatidylinositols, CL-cardiolipins, PS-phosphatidylserines, PC-phosphatidylcholines, SM-sphingomyelins, LPC-lysophosphatidylcholines.

present in the laboratories but these uses should grow for both high throughput and extensive analysis.

3.4.2. Soybean/Wheat

The two vegetal samples soya and wheat are also the most complex samples involved in this study in term of lipid composition. They are particularly rich in lipid of intermediate polarity typical from vegetal such as ASG, SG, GlcCer and DGDG. Soya lecithin and wheat were already extensively studied in our laboratory while developing separations with the poly(vinyl)alcool stationary phase [41] and ASG, SG, GlcCER, DGDG, PI, PE and PC were identified.

Soya lecithin is particularly rich in PL and most studies focus on these classes. An example of extensive characterization using phosphorus 31 nuclear magnetic resonance can be found in [42] and the lipid classes reported are PC, PE, PI, PA, PG, N-acylphosphatidylethanolamines (NAPE), LPC, diphosphatidylglycerol (DPG), PS and lysophosphatidic acids (LPA) (by increasing order of magnitude in the sample). The chromatographic profiles in Fig. 10 show that, whereas the main classes are identified, our method only fails at detecting the quantitatively minor lipid classes. Those minor classes (LPC, DPG, PS and LPA) are less than 0.8% mol/100 mol of phosphorylated lipids.

Concerning wheat lipids, the entirety of the lipid classes involved in Gerits' publication [12] are resolved in our conditions. In addition, 6 extra lipids are identified (SQ, SE, ST, ASG, SG and GlcCer) and 4 unknown peaks are resolved from the lipid classes. Compared to previously published solvent programs, the present chromatographic conditions allow an appropriate retention of the nonpolar lipid classes (SQ and SE) together with an improved separation in the intermediate polarity lipids area which allows to detect ST, ASG, SG and GlcCer while preserving the resolution of PL classes.

*3.4.3. Yeast (*Saccharomyces cerevisiae*)*

Saccharomyces cerevisiae is often used as a model organism and there is abundant information concerning its metabolism. The lipid profile of yeast (*Saccharomyces cerevisiae*) was not studied by the authors we comparedwith and we referred to other bibliographical sources to ascertain the level of information provided by our method. The yeast lipidome was investigated by shotgun mass spectrometry in Ref. [43] with a special attention paid to lyso forms of the PL classes. Ref. [44] also examines yeast lipidome and presents consistent results (only Cer are found in addition to the lipids of Ref. [43]). The main lipid classes highlighted in these articles were TG, DG, Cer and ST and the phospholipids PA, PS, PE, PC, PI, PG, CL together with their lyso forms. Inositol phosphoceramide (IPC) derivatives (IPC, Mannosylated-IPC and Man(IP)$_2$C) were found in notable but also variable amount in *S. cerevisiae* wildtype stains.

Our method allowed identifying the main lipid classes (except PS and the lyso-forms, which was not in noticeable quantity in our sample) but not the IPC derivatives. This result compared favorably with the NPLC/Corona-CAD® of ref [45]. SQ, coenzyme Q6 and PG are detected in our chromatographic profile and are not reported in [45].

Neither our method nor [45] allow to detect IPC derivatives. Except in the 12–14 min range no unidentified peak could be detected and this elution window does not correspond to the IPC derivatives that, from our experience [46], should elute near the PL elution windows. We unsuccessfully performed an in depth examination of the APPI profiles searching for the quasi-molecular and possible adduct ions of the main species of IPC and its derivatives. IPC derivatives are cell messengers and appear to increase dramatically as a response to a stress or a change in the culture media (temperature for [44], AA for [47]). Their levels are possibly too low to be detected in our sample. These compounds are also ionized very differently according to the ionic modifiers added to the mobile phase both with respect to the adducts observed and their intensities [48]. A detailed investigation of IPC derivatives detection under our mobile phase composition conditions would be necessary but is out of the scope of this work.

*3.4.4. Bacteria (*Escherichia coli*)*

As for yeast, no NPLC of the *E. coli* lipids was found and the characteristic composition of these bacteria had to be retrieved from the literature. The typical composition as mentioned by the lipid standard supplier Avanti Polar is rather simple and *E.coli* extract contains 57.5% PE, 15.1% PG, 9.8 CL and 17.6% of non-identified lipids. Coenzyme Q8 [49] is not listed but is also present and signaled as being obtained from *E. coli* extract by the same supplier. Lipid A which is involved in the toxicity of Gram negative bacteria is also present in *E. coli* but wasn't detected in our experimental conditions as the *m*/*z* of its molecular ion is beyond the mass range of the full scan detection (*m*/*z* 1700). This lipid composition was confirmed by different publications using mass spectrometry [50–52] and our separation appeared to highlight the main component of the *E. coli* extract.

4. Conclusions

Most of NPLC methods for lipid classes analysis where developed to separate lipids issued from animal samples. Fewer methods were developed to assess the higher complexity of vegetal samples. Some plant lipids such as ASG, MGDG, SG and DGDG present an intermediate polarity and increase the sample complexity in this region of the chromatogram.

The method we propose compares favorably with those developed for animal tissues [9–11,13] and presents an improved separation for vegetal samples [12]. This method, developed using lipid classes of intermediate polarity is also interesting to separate ceramides.

NPLC method development is generally considered as difficult and requiring a specific skill. We decided to add information about the different issues solved during this development. Particularly the use of nonpolar, low viscosity solvent such as isooctane and the use of a pressurized solvent tank to circumvent the pumping difficulties encountered. In addition, the presence of impurities in isooctane led us to re-purify this solvent using a semi-preparative silica column. We also focused on the rinsing step and the importance of using ethyl acetate to both eliminate the C mobile phase from the stationary phase and favor the re-equilibration.

NPLC solvent programs frequently incorporate complex mobile phases. In this study, we documented the importance of adding 0.2% (v/v) ethyl acetate in the initial mobile phase. Also, the importance of the relative amounts of AA and TEA in the mobile phase on the retention of some specific lipid classes such as FA in the first part of the chromatogram but also the PL classes at the end and the compromise to be found to ensure a correct selectivity.

The comparison of the detection systems that are both heavily solvent dependent reinforce the interest of the Corona-CAD® thanks to its increased sensitivity at low concentration compared to the commonly used ELSD. When comparing the API interfaces under NPLC conditions, ESI did not succeed at detecting the whole lipids in the chromatogram as signal extinction occurs at the beginning of the chromatogram. We have shown that for lipids such as PL, in positive mode APCI and APPI present more in source fragmentation compared with ESI. In negative mode, the in source fragmentation is comparable with the three API sources. By using both positive and negative mode, structural information is visible in full scan spectra. Coupling with APCI provided satisfactory results but APPI is generally more sensitive and does not require any dopant make-up in our chromatographic conditions.

Appendix A. Supplementary data

Supplementary data associated with this article can be found, in the online version, at http://dx.doi.org/10.1016/j.chroma.2017.07.063.

References

[1] S. Subramaniam, E. Fahy, S. Gupta, M. Sud, R.W. Byrnes, D. Cotter, A.R. Dinasarapu, M.R. Maurya, Bioinformatics and systems biology of the lipidome, Chem. Rev. 111 (2011) 6452–6490.
[2] E. Fahy, S. Subramaniam, R.C. Murphy, M. Nishijima, C.R.H. Raetz, T. Shimizu, F. Spener, G. van Meer, M.J.O. Wakelam, E.A. Dennis, Update of the LIPID MAPS comprehensive classification system for lipids, J. Lipid Res. 50 (2008) S9–S14.
[3] T. Cajka, O. Fiehn, Comprehensive analysis of lipids in biological systems by liquid chromatography-mass spectrometry, TrAC Trends Anal. Chem. 61 (2014) 192–206.
[4] E. Cífková, R. Hájek, M. Lísa, M. Holčapek, Hydrophilic interaction liquid chromatography-mass spectrometry of (lyso)phosphatidic acids, (lyso)phosphatidylserines and other lipid classes, J. Chromatogr. A 1439 (2016) 65–73.
[5] M. Holčapek, E. Cífková, B. Červená, M. Lísa, J. Vostálová, J. Galuszka, Determination of nonpolar and polar lipid classes in human plasma, erythrocytes and plasma lipoprotein fractions using ultrahigh-performance liquid chromatography-mass spectrometry, J. Chromatogr. A. 1377 (2015) 85–91.
[6] M. Lísa, M. Holčapek, High-Throughput and comprehensive lipidomic analysis using ultrahigh-performance supercritical fluid chromatography–mass spectrometry, Anal. Chem. 87 (2015) 7187–7195.
[7] M. Holčapek, M. Ovčačíková, M. Lísa, E. Cífková, T. Hájek, Continuous comprehensive two-dimensional liquid chromatography-electrospray ionization mass spectrometry of complex lipidomic samples, Anal. Bioanal. Chem. 407 (2015) 5033–5043.
[8] M. Šala, M. Lísa, J.L. Campbell, M. Holčapek, Determination of triacylglycerol regioisomers using differential mobility spectrometry, Rapid Commun. Mass Spectrom. RCM 30 (2016) 256–264.
[9] D.G. McLaren, P.L. Miller, M.E. Lassman, J.M. Castro-Perez, B.K. Hubbard, T.P. Roddy, An ultraperformance liquid chromatography method for the normal-phase separation of lipids, Anal. Biochem. 414 (2011) 266–272.
[10] W.W. Christie, Rapid separation and quantification of lipid classes by high performance liquid chromatography and mass (light-scattering) detection, J. Lipid Res. 26 (1985) 507–512.
[11] M. Graeve, D. Janssen, Improved separation and quantification of neutral and polar lipid classes by HPLC–ELSD using a monolithic silica phase: application to exceptional marine lipids, J. Chromatogr. B 877 (2009) 1815–1819.
[12] L.R. Gerits, B. Pareyt, J.A. Delcour, Single run HPLC separation coupled to evaporative light scattering detection unravels wheat flour endogenous lipid redistribution during bread dough making, LWT – Food Sci. Technol. 53 (2013) 426–433.
[13] R. Homan, M.K. Anderson, Rapid separation and quantitation of combined neutral and polar lipid classes by high-performance liquid chromatography and evaporative light-scattering mass detection, J. Chromatogr. B. Biomed. Sci. App. 708 (1998) 21–26.
[14] L. Imbert, M. Gaudin, D. Libong, D. Touboul, S. Abreu, P.M. Loiseau, O. Laprévote, P. Chaminade, Comparison of electrospray ionization, atmospheric pressure chemical ionization and atmospheric pressure photoionization for a lipidomic analysis of Leishmania donovani, J. Chromatogr. A. 1242 (2012) 75–83.
[15] G. Liebisch, J.A. Vizcaino, H. Kofeler, M. Trotzmuller, W.J. Griffiths, G. Schmitz, F. Spener, M.J.O. Wakelam, Shorthand notation for lipid structures derived from mass spectrometry, J. Lipid Res. 54 (2013) 1523–1530.
[16] S. Williams, Ghost peaks in reversed-phase gradient HPLC: a review and update, J. Chromatogr. A. 1052 (2004) 1–11.
[17] T.J. Leiker, R.M. Barkley, R.C. Murphy, Analysis of diacylglycerol molecular species in cellular lipid extracts by normal-phase LC-electrospray mass spectrometry, Int. J. Mass Spectrom. 305 (2011) 103–108.
[18] X. Guo, A.P. Bruins, T.R. Covey, Characterization of typical chemical background interferences in atmospheric pressure ionization liquid chromatography-mass spectrometry, Rapid Commun. Mass Spectrom. 20 (2006) 3145–3150.
[19] S. Altmaier, K. Cabrera, Structure and performance of silica-based monolithic HPLC columns, J. Sep. Sci. 31 (2008) 2551–2559.
[20] J.L. Robinson, R. Macrae, Comparison of detection systems for the high-performance liquid chromatographic analysis of complex triglyceride mixtures, J. Chromatogr. 303 (1984) 386–390.
[21] R.W. Dixon, D.S. Peterson, Development and testing of a detection method for liquid chromatography based on aerosol charging, Anal. Chem. 74 (2002) 2930–2937.
[22] R.G. Ramos, D. Libong, M. Rakotomanga, K. Gaudin, P.M. Loiseau, P. Chaminade, Comparison between charged aerosol detection and light scattering detection for the analysis of Leishmania membrane phospholipids, J. Chromatogr. A 1209 (2008) 88–94.
[23] D. Kauhanen, M. Sysi-Aho, K.M. Koistinen, R. Laaksonen, J. Sinisalo, K. Ekroos, Development and validation of a high-throughput LC–MS/MS assay for routine measurement of molecular ceramides, Anal. Bioanal. Chem. 408 (2016) 3475–3483.
[24] J. van Smeden, W.A. Boiten, T. Hankemeier, R. Rissmann, J.A. Bouwstra, R.J. Vreeken, Combined LC/MS-platform for analysis of all major stratum corneum lipids, and the profiling of skin substitutes, Biochim. Biophys. Acta BBA Mol. Cell Biol. Lipids 1841 (2014) 70–79.
[25] A. Tfayli, F. Bonnier, Z. Farhane, D. Libong, H.J. Byrne, A. Baillet-Guffroy, Comparison of structure and organization of cutaneous lipids in a reconstructed skin model and human skin: spectroscopic imaging and chromatographic profiling, Exp. Dermatol. 23 (2014) 441–443.
[26] L. Quinton, K. Gaudin, A. Baillet, P. Chaminade, Microanalytical systems for separations of stratum corneum ceramides, J. Sep. Sci. 29 (2006) 390–398.
[27] A. Sunde, P. Stenstad, K.B. Eik-Nes, Separation of epimeric 3-hydroxyandrostanes and 3-hydroxyandrostenes by thin-layer chromatography on silica gel, J. Chromatogr. A 175 (1979) 219–221.
[29] I. Marchi, S. Rudaz, J.-L. Veuthey, Atmospheric pressure photoionization for coupling liquid–chromatography to mass spectrometry: a review, Talanta 78 (2009) 1–18.
[30] S.-S. Cai, J.A. Syage, Comparison of atmospheric pressure photoionization atmospheric pressure chemical ionization, and electrospray ionization mass spectrometry for analysis of lipids, Anal. Chem. 78 (2006) 1191–1199.
[31] S.-S. Cai, J.A. Syage, Atmospheric pressure photoionization mass spectrometry for analysis of fatty acid and acylglycerol lipids, J. Chromatogr. A 1110 (2006) 15–26.
[32] R. Kostiainen, T.J. Kauppila, Effect of eluent on the ionization process in liquid chromatography–mass spectrometry, J. Chromatogr. A 1216 (2009) 685–699.
[33] M.H. Lee, G.H. Lee, J.S. Yoo, Analysis of ceramides in cosmetics by reversed-phase liquid chromatography/electrospray ionization mass spectrometry with collision-induced dissociation, Rapid Commun. Mass Spectrom. RCM 17 (2003) 64–75.
[34] F.-F. Hsu, J. Turk, Characterization of ceramides by low energy collisional-activated dissociation tandem mass spectrometry with negative-ion electrospray ionization, J. Am. Soc. Mass Spectrom. 13 (2002) 558–570.
[35] R. Rozenberg, N.L. Ruibal-Mendieta, G. Petitjean, P. Cani, D.L. Delacroix, N.M. Delzenne, M. Meurens, J. Quetin-Leclercq, J.-L. Habib-Jiwan, Phytosterol analysis and characterization in spelt (Triticum aestivum ssp. spelta L.) and wheat (T. aestivum L.) lipids by LC/APCI-MS, J. Cereal Sci. 38 (2003) 189–197.
[36] M. Pulfer, R.C. Murphy, Electrospray mass spectrometry of phospholipids, Mass Spectrom. Rev. 22 (2003) 332–364.
[37] R.C. Murphy, Tandem Mass Spectrometry of Lipids, 2014, http://pubs.rsc.org/en/content/ebook/978-1-84973-827-9#!divbookcontent. (Accessed 22 February2017).
[38] E. Kofroňová, J. Cvačka, P. Jiroš, D. Sýkora, I. Valterová, Analysis of insect triacylglycerols using liquid chromatography-atmospheric pressure chemical ionization-mass spectrometry, Eur. J. Lipid Sci. Technol. 111 (2009) 519–525.
[39] M. Fasciotti, A.D. Pereira Netto, Optimization and application of methods of triacylglycerol evaluation for characterization of olive oil adulteration by soybean oil with HPLC–APCI-MS–MS, Talanta 81 (2010) 1116–1125.
[40] M. Holčapek, P. Jandera, P. Zderadička, L. Hruba, Characterization of triacylglycerol and diacylglycerol composition of plant oils using high-performance liquid chromatography–atmospheric pressure chemical ionization mass spectrometry, J. Chromatogr. A 1010 (2003) 195–215.
[41] F.S. Deschamps, P. Chaminade, D. Ferrier, A. Baillet, Assessment of the retention properties of poly(vinyl alcohol) stationary phase for lipid class profiling in liquid chromatography, J. Chromatogr. A 928 (2001) 127–137.
[42] L. Yao, S. Jung, 31P NMR phospholipid profiling of soybean emulsion recovered from aqueous extraction, J. Agric. Food Chem. 58 (2010) 4866–4872.
[43] C.S. Ejsing, J.L. Sampaio, V. Surendranath, E. Duchoslav, K. Ekroos, R.W. Klemm, K. Simons, A. Shevchenko, Global analysis of the yeast lipidome by quantitative shotgun mass spectrometry, Proc. Natl. Acad. Sci. 106 (2009) 2136–2141.
[44] C. Klose, M.A. Surma, M.J. Gerl, F. Meyenhofer, A. Shevchenko, K. Simons, Flexibility of a eukaryotic lipidome –insights from yeast lipidomics, PLoS One 7 (2012) e35063.
[45] S. Khoomrung, P. Chumnanpuen, S. Jansa-Ard, M. Ståhlman, I. Nookaew, J. Borén, J. Nielsen, Rapid quantification of yeast lipid using microwave-Assisted total lipid extraction and HPLC-CAD, Anal. Chem. 85 (2013) 4912–4919.
[46] L. Imbert, R.G. Ramos, D. Libong, S. Abreu, P.M. Loiseau, P. Chaminade, Identification of phospholipid species affected by miltefosine action in Leishmania donovani cultures using LC-ELSD LC-ESI/MS, and multivariate data analysis, Anal. Bioanal. Chem. 402 (2012) 1169–1182.
[47] L. Lindberg, A.X. Santos, H. Riezman, L. Olsson, M. Bettiga, Lipidomic profiling of saccharomyces cerevisiae and zygosaccharomyces bailii reveals critical changes in lipid composition in response to acetic acid stress, PLoS One 8 (2013) e73936.
[48] C.S. Ejsing, T. Moehring, U. Bahr, E. Duchoslav, M. Karas, K. Simons, A. Shevchenko, Collision-induced dissociation pathways of yeast sphingolipids and their molecular profiling in total lipid extracts: a study by quadrupole TOF and linear ion trap?orbitrap mass spectrometry, J. Mass Spectrom. 41 (2006) 372–389.
[49] W. Xu, S. Yang, J. Zhao, T. Su, L. Zhao, J. Liu, Improving coenzyme Q8 production in Escherichia coli employing multiple strategies, J. Ind. Microbiol. Biotechnol. 41 (2014) 1297–1303.

[50] A. Laganowsky, E. Reading, T.M. Allison, M.B. Ulmschneider, M.T. Degiacomi, A.J. Baldwin, C.V. Robinson, Membrane proteins bind lipids selectively to modulate their structure and function, Nature 510 (2014) 172–175.
[51] D. Oursel, C. Loutelier-Bourhis, N. Orange, S. Chevalier, V. Norris, C.M. Lange, Lipid composition of membranes of Escherichia coli by liquid chromatography/tandem mass spectrometry using negative electrospray ionization, Rapid Commun. Mass Spectrom. 21 (2007) 1721–1728.
[52] J. Gidden, J. Denson, R. Liyanage, D.M. Ivey, J.O. Lay, Lipid compositions in escherichia coli and bacillus subtilis during growth as determined by MALDI-TOF and TOF/TOF mass spectrometry, Int. J. Mass Spectrom. 283 (2009) 178–184.

3. *Conclusion*

La méthode NPLC-DEDL [20] est régulièrement mise en œuvre par d'autres laboratoires, sur des extraits lipidiques, pour déterminer la composition des lipides par classes [118–128]. Dans de nombreux cas, une analyse des FAMEs par GC est associée pour accéder à la distribution des FAs [124–128]. L'objectif de cette thèse est de permettre d'accéder rapidement à cette information, en couplant la méthode séparative à l' $APPI^+$/$APCI^+$-HRMS.

Parmi les 30 classes de lipides séparées, la moitié correspond soit à des glycérolipides (TG, DG, MG, MGDG, DGDG) soit à des glycérophospholipides (NAPE, PG, PE, PA, PI, CL, PS, PC, LPC). Tous ces lipides contiennent un squelette glycérol sur lequel sont estérifiés un ou plusieurs FAs, comme illustré sur la Figure 42. L'ensemble de ces classes constitue le glycérolipidome.

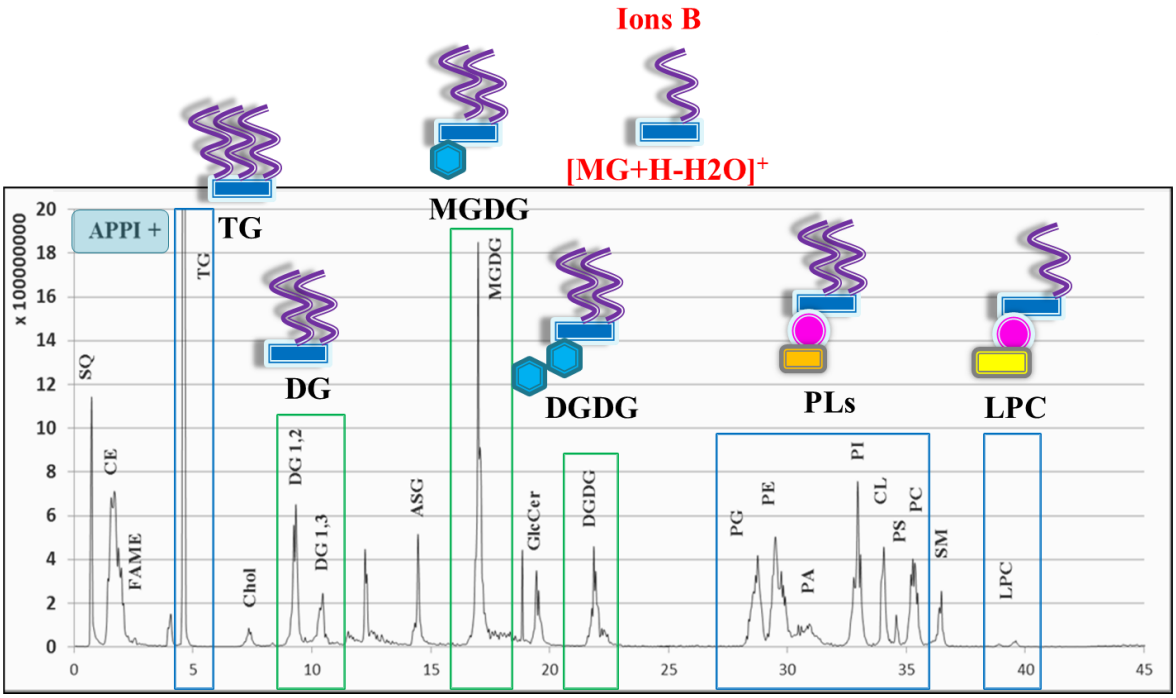

Figure 42: Séparation de lipides par classe [20]. Sont indiqués en bleu les lipides étudiés pour le développement du nouveau concept et en vert les lipides auquel le concept pourrait être étendu.

Cet article est également à l'origine de l'étude collaborative sur des souches de *Yarrowia lipolytica* (levure), présentée dans le chapitre VIII et de trois études sur des souches de *Streptomyces* (bactérie), présentées en Annexe V-VII.

CHAPITRE IV. ACYLES GRAS ET VOIES METABOLIQUES

1. Introduction

La structure des FAs représente le principal élément constitutif des lipides complexes. Certaines études se focalisent de manière spécifique sur ces catégories de lipides. Cela est notamment le cas, des études portant sur le phospholipidome [129,130] ou sur le glycérolipidome [131–138].

Le **glycérolipidome**, également appelé **profil glycérolipidique** [137,139–142], regroupe à la fois la catégorie des PLs et la catégorie des glycérolipides. L'emploi de ces deux termes dans la littérature reste cependant, très confidentiel, ils sont essentiellement utilisés dans quelques études portant sur des plantes (*Arabidopsis thaliana*, blé, soja), des algues ou des protistes (eucaryote unicellulaire).

2. Voies métaboliques des acides gras libres (FFA)

Chez les mammifères, la majorité des FFA sont exogènes. Néanmoins, leurs métabolismes sont capables de synthétiser de novo le C16 :0 à partir de l'acétyl-CoA, dans le cytosol. Le système enzymatique (élongase et désaturase) permet de synthétiser à partir du C16 :0 d'autres FFA tel que les FFA n-7 et n-9 ainsi que les FFA saturés (Figure 43 a). En revanche, le métabolisme des mammifères ne possède pas le système enzymatique capable de synthétiser le C18 :2, C18 :1 et C18 :3, précurseurs des FFA n-3, n-6 et n-12. Ces FFA, sont dits « indispensables » et doivent être apportés par l'alimentation. Seuls les végétaux et les bactéries peuvent les synthétiser. Les mammifères peuvent cependant synthétiser les FFA « essentiels » issus des FFA « indispensables ». Le schéma de synthèse est présenté sur la Figure 43 b. A noter que le taux de conversion du C18 :3 n-3 en C22 :6 n-3 est trop faible pour couvrir les besoins de l'homme en C22 :6 n-3, cet FFA est donc également considéré comme indispensable [143].

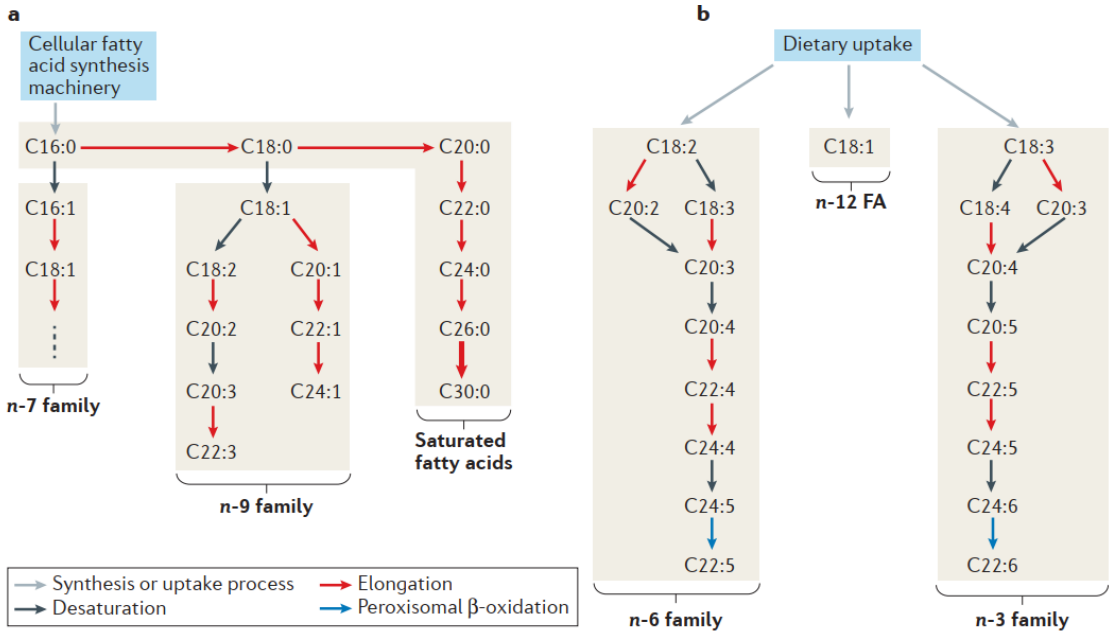

Figure 43: Biosynthèse des acides gras à longue et très longue chaîne chez les mammifères [144].

3. *Voies métaboliques des glycérolipides et des PLs*

Les FFA à longues chaînes sont ensuite utilisés par l'organisme pour synthétiser les glycérolipides et les PLs, tel que schématisé sur la Figure *44*. Les FFA sont transformés de manière successive en Acyl-CoA, LPA et PA. Le PA est le précurseur du PI, CL et DG. Le DG est lui-même précurseur du PE, PC, PS et TG.

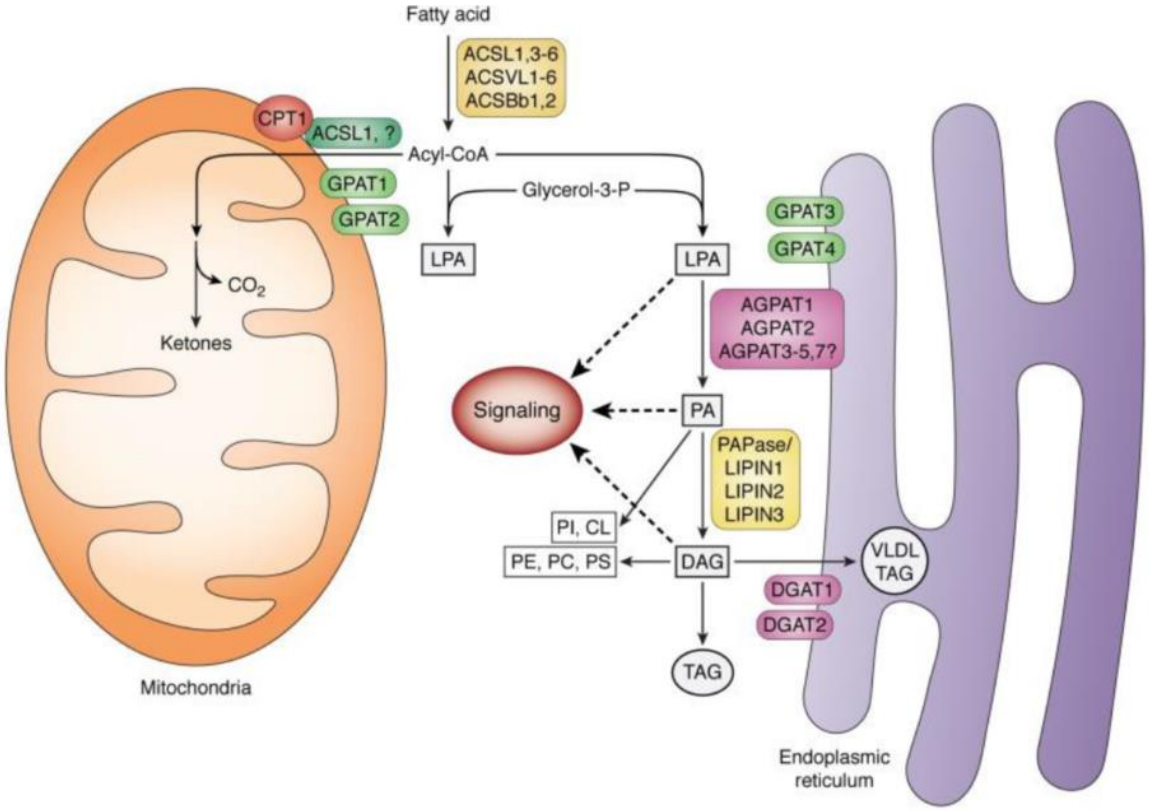

Figure 44: Synthèse des glycérolipide et PLs à partir d'acides gras à longue chaîne [145].

4. Lipidome et pathologies

Diverses maladies ont été rapportées comme étant en corrélation avec le métabolisme des lipides (cancers, maladie d'Alzheimer, maladie de Parkinson, diabète…) [35,146–149] et plusieurs études ont révélé des changements dans la régulation des lipides dans les tissus animaux et humains [148,150–153].

Par exemple, dans le cadre de la maladie de Parkinson (MP), une étude récente [154] a analysé le liquide céphalo-rachidien (LCR) prélevé post mortem sur des témoins neurologiquement sains et malades. Les analyses réalisées par UPLC-ESI-qToF-MS/MS ont permis de suivre 257 espèces lipidiques. L'analyse des données multivariées et univariées a mis en évidence une augmentation significative des glycérolipides, PLs, sphingolipides, N-acyléthanolamines et des stérols dans le groupe atteint de la MP par rapport au groupe témoin, comme illustré sur la

Figure 45. Ces résultats ont également mis en évidence une dyshoméostasie lipidique du LCR suivant le stade neuropathologique et la durée de la maladie. Le lipidome du LCR pourrait selon les auteurs, être un outil prometteur pour identifier les marqueurs lipidiques potentiels ainsi que les espèces lipidiques discriminantes entre la MP et d'autres parkinsonismes atypiques.

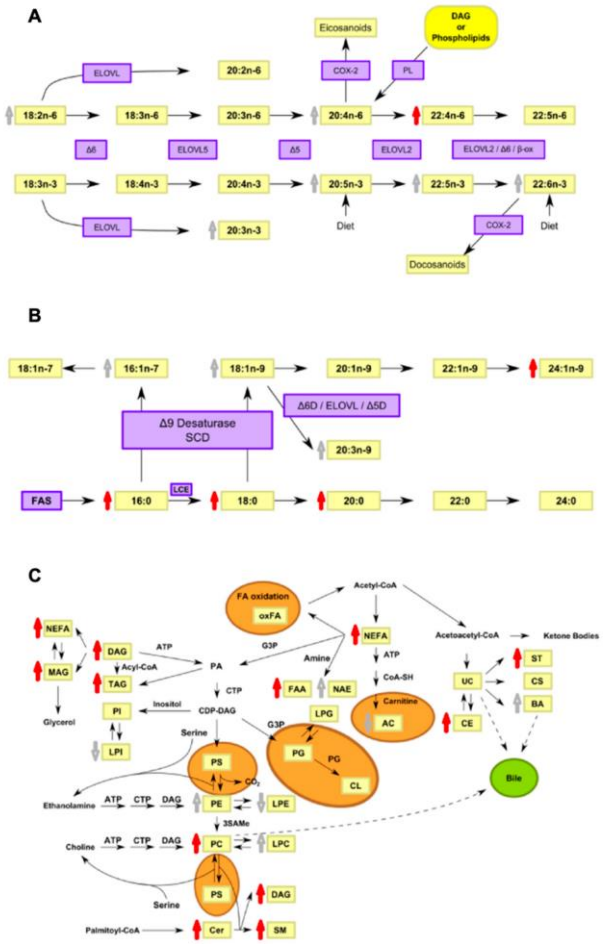

Figure 45: Localisation de la voie des espèces lipidiques dérégulées détectées dans le LCR post-mortem dans la maladie de Parkinson [154].

5. *Lipidome, nutrition et santé*

La découverte des bénéfices du C22 :6 n-3 (acide docosahexaénoïque - DHA), 20 :5 n-3 (acide eicosapentaénoïque - EPA) et C18 :3 n-3 (acide alpha-linolénique - ALA) sur la santé des Inuits du Groenland en 1975 [155] a été le point de départ d'un fort intérêt pour les acides gras polyinsaturés (PUFAs) n-3. De nombreuses études ont été menées sur le sujet, mais les

avis sur leurs bienfaits sont restés longtemps divergents [156]. Aujourd'hui, l'Agence nationale de sécurité sanitaire de l'alimentation, de l'environnement et du travail (ANSES) affirme clairement leur apport favorable sur la santé (https://www.anses.fr/fr/content/les-acides-gras-om%C3%A9ga-3). Les effets bénéfiques du DHA et de l'EPA sont mis en avant dans des pathologies affectant le cœur, le sang et les vaisseaux, les yeux, les os, le cerveau, l'inflammation, les cancers, etc. [157].

Les micro-organismes sont utilisés en biologie de synthèse dans de nombreux domaines (médecine, industrie, énergie…) pour la production de molécules d'intérêts. Ces micro-organismes sont également modifiés génétiquement pour l'obtention de lipides riches PUFAs n-3 [158,159]. C'est notamment le cas de la levure *Yarrowia lipolytica* et des bactéries du genre *Streptomyces coelicolor* [160] que nous avons étudiées durant cette thèse, à d'autres fins.

Les organismes marins sont également très étudiés pour leur teneur en PUFAs n-3. Les microalgues et le krill (petit crustacé), riches en PUFAs n-3, sont au début de la chaîne alimentaire du monde marin. Ces organismes contribuent aux teneurs importantes de DHA et EPA dans les poissons et les crustacés que nous consommons.

Dans l'étude [128], les auteurs ont étudié la cinétique de digestion in vitro de différentes huiles marines commerciales contenant différentes classes de lipides (cires - huile de calanus, TGs - huile de foie de morue, ester éthylique - huiles de poissons purifiées et estérifiées, TG/PC - huile de krill et DG/MGDG/PG - huile de *Porosira glacialis*). **La cinétique de digestion a été réalisée avec la méthode séparative issue de nos travaux** [20] **et complétée par une analyse des FAMEs réalisée par GC-FID pour obtenir la cinétique de la composition des FAs totaux**. Les auteurs ont montré une dépendance de la cinétique de l'hydrolyse des FAs par la pancréatine porcine avec l'huile étudiée. Cela implique que la cinétique de digestion des FAs est dépendante de la classe des lipides sur lesquels les FAs sont fonctionnalisés.

Cet aspect est étudié dans la revue [161] car de récentes découvertes ont suggéré que les DHA/EPA-PL alimentaires sont supérieurs aux formes de TG ou d'ester éthylique dans l'exercice de leurs propriétés fonctionnelles par le biais de mécanismes d'action spécifiques. Les DHA et EPA, comme illustré Figure 46 contenus dans les PLs sont principalement estérifiés en position *sn-2* des plasmalogènes (P-PLs). La liaison éther vinylique joue un rôle de protection des FAs polyinsaturés grâce à ses propriétés antioxydantes.

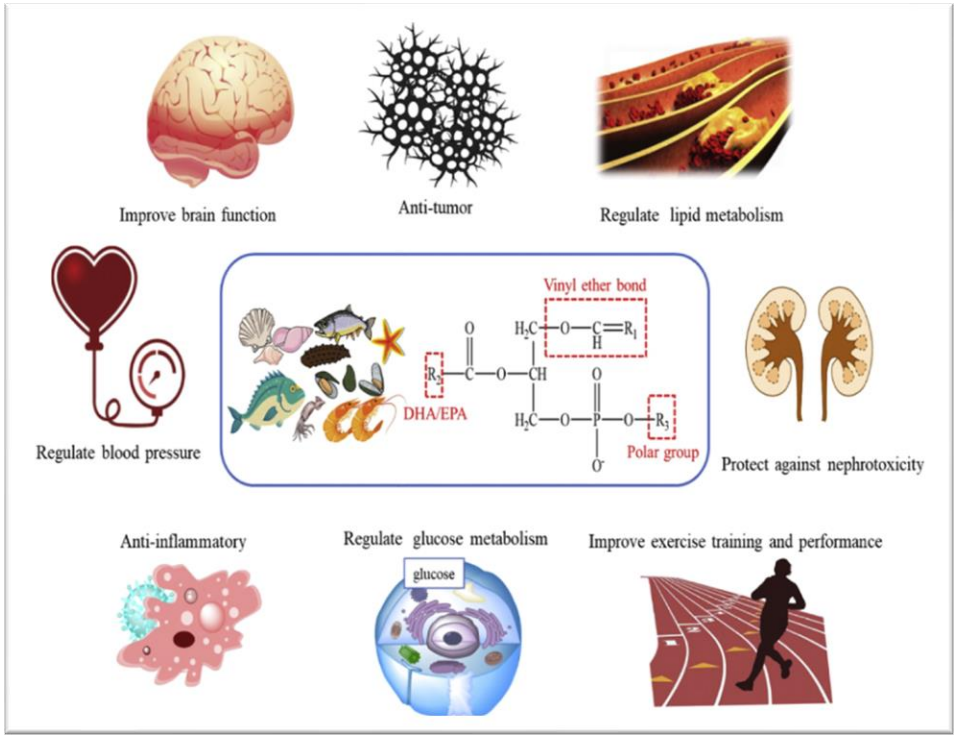

Figure 46: Bioactivités des PLs enrichis en DHA/EPA dans les aliments marins [161].

Les P-PLs sont beaucoup moins étudiés que les PLs, pourtant leurs teneurs dans certains organes nobles tels que le cerveau et le cœur peuvent représenter jusqu'à 50 % des PLs [35]. Certaines pathologies affectant ces deux organes ont été rapportées comme étant en corrélation avec le métabolisme des P-PLs [35,148,162,163], d'autres organes peuvent être également affectés comme le système gastro-intestinal [146].

CHAPITRE V. ANALYSE DES ACYLES GRAS : METHODES USUELLES

1. Analyse des FAMEs par GC-FID et GC-MS

La GC permet de séparer les composés gazeux ou susceptibles d'être vaporisés par chauffage, lorsque ceux-ci ne se décomposent pas sous l'effet de la chaleur. Cette technique est fréquemment utilisée pour étudier **la distribution des FAs totaux** dans les échantillons. Pour cela, les extraits lipidiques (dans leur globalité) sont soumis à une transestérification. Tous les lipides estérifiables sont alors convertis en esters, facilement analysables par GC-FID ou GC-MS.

Il est également possible d'obtenir **la distribution des FAs par classe**. Pour cela, les classes de lipides doivent être préalablement séparées et isolées. Ensuite, chaque classe de lipide est transestérifiée et analysée individuellement par GC-FID ou MS. La mise en œuvre est beaucoup plus lourde que la méthode donnant accès à la distribution des FAs totaux, ce qui limite son utilisation. Cependant, cette méthode est considérée comme robuste et reste encore très largement employée [19].

1.1 Séparation et isolement

La séparation des lipides est généralement réalisée par TLC ou HPTLC sur gel de silice à une dimension [164] ou deux dimensions [165,166]. L'identification des lipides est réalisée par comparaisons aux caractéristiques de migration de lipides témoins. Des systèmes automatisés sont disponibles commercialement pour réaliser les différentes étapes de l'analyse. A titre d'exemple, la Figure 47 présente différents équipements commercialisés par la société CAMAG®.

Le dépôt d'échantillons peut se faire de manière reproductible grâce à un échantillonneur automatique. La migration peut être réalisée avec un gradient d'élution utilisant plusieurs phases mobiles. La dérivatisation et la détection sont adaptables aux propriétés

physicochimiques des analytes. Une interface MS permet le couplage TLC-MS, ce dispositif permet aussi de collecter l'éluat pour des analyses hors lignes.

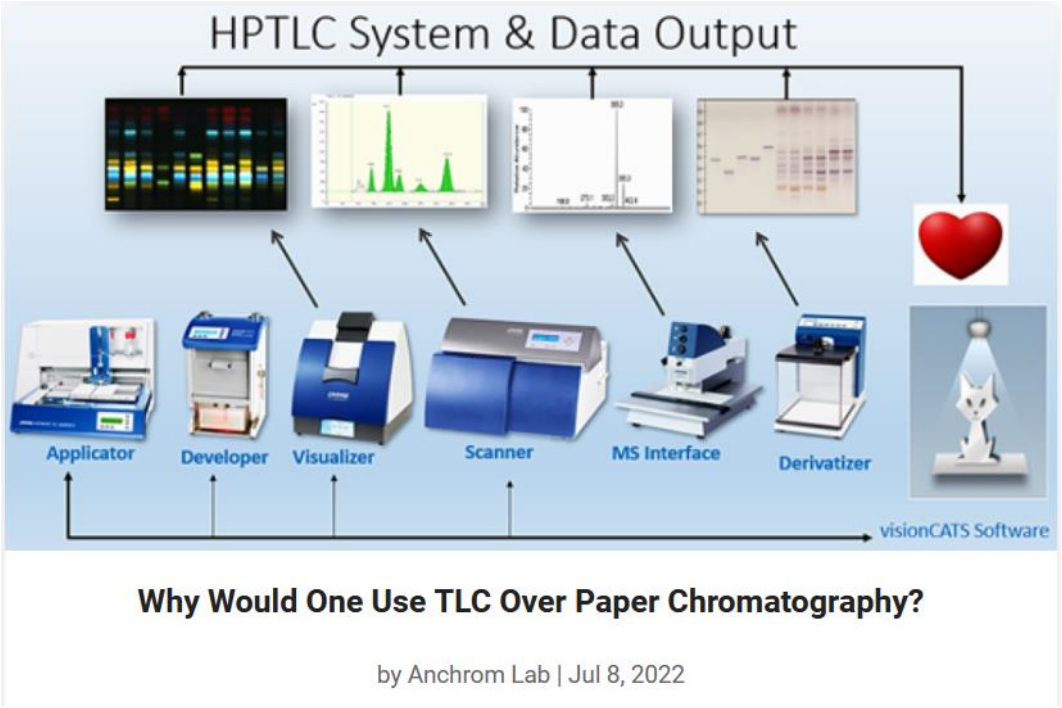

Figure 47: Instruments CAMAG® pour analyses HPTLC (https://anchrom.in).

Tous les laboratoires ne disposent pas d'appareillages aussi performants. Les analyses sont encore souvent réalisées manuellement, ce qui limite la reproductibilité et les performances des analyses. Un exemple de séparation bidimensionnelle [165] (non automatisée) est présenté sur la Figure 48.

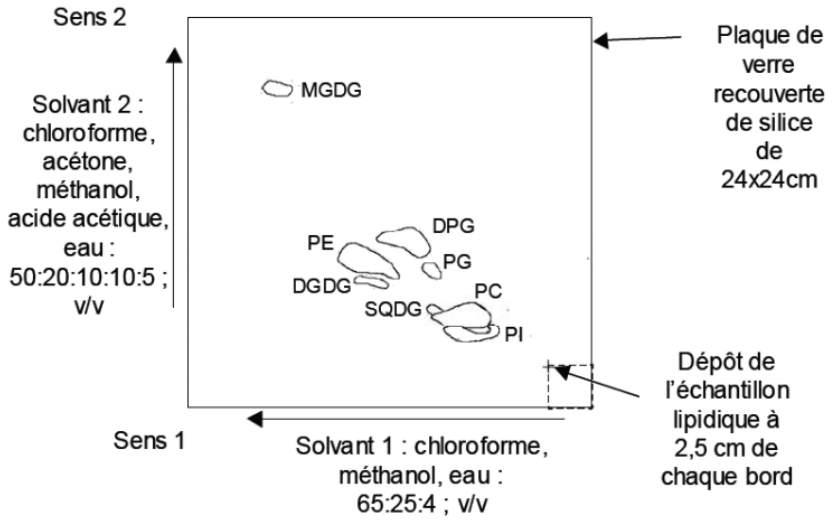

Figure 48: Séparation de lipides sur plaque TLC bidimensionnelle [165].

Malgré des phases éluantes optimisées, la PC est partiellement coéluée avec le SQDG. Le prélèvement par grattage, de la PC et du SQDG conduit inévitablement à des fractions adultérées.

La TLC est parfois utilisée pour isoler un ou plusieurs mélanges de lipides d'intérêt avant leur analyse par GC-FID. Par exemple, dans l'étude [167] portant sur les effets des régimes enrichis en PUFAs n–3 ou n–6 sur les métabolites lipidiques musculaires de porc, deux fractions ont été récupérées, l'une contenant l'ensemble de PLs et l'autre la classe des TGs.

La séparation et l'isolement des lipides peuvent également être réalisés par SPE [139,168–170], comme illustré sur la Figure 49. Suivant le support de la cartouche et les solvants utilisés, il est possible de récolter sélectivement les différentes classes de lipides. Cependant, la mise en œuvre n'est pas forcément simple. Dans les travaux de thèse de Guillaume Sayet, la SPE a été utilisée pour isoler l'ensemble des PLs. Un contrôle des éluats avait été mené avec notre méthode NPLC-DEDL [20], avant leur analyse par GC-MS. Cela a permis une optimisation du protocole afin d'obtenir des fractions de pureté acceptable.

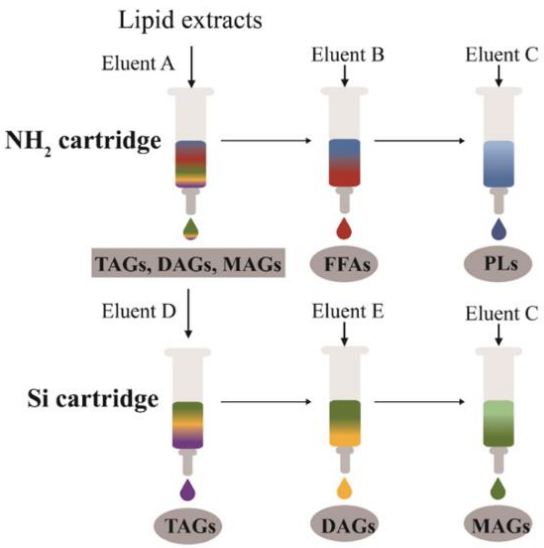

Figure 49: Illustration schématique d'une procédure de séparation de lipide par classe réalisée par SPE [169].

1.2 Conversion des FAs en FAMEs

Lorsque les FAs sont associés à des lipides complexes telles que les glycérolipides, PLs, esters de cholestérol, les cires ou glycosphingolipides, ils peuvent être obtenus libres par saponification (solution basique) ou hydrolyse acide, puis dérivatisés pour l'obtention d'esters, le plus souvent des FAMEs. Les FAMEs peuvent également être obtenus directement par transestérification (appelé aussi méthanolyse).

Il existe de nombreuses méthodes d'estérification. Le choix s'effectue en fonction de la classe de lipide et la nature des FAs (longueurs des chaînes et insaturations). La plupart des méthodes sont réalisées avec un excès d'alcool, généralement du méthanol pour l'obtention des FAMEs. Les réactions peuvent aussi être réalisées avec d'autres alcools (éthylique, propylique, isopropylique…), les températures d'ébullition des esters formés sont alors plus élevées. Quatre méthodes sont décrites dans la norme NF EN ISO 12966-*2 (Corps gras d'origines animale et végétale : chromatographie en phase gazeuse des esters méthyliques d'acides gras – Partie 2 : préparation des esters méthyliques des acides gras)*. L'article [171] issus des Techniques de l'Ingénieur (2015) résume ces méthodes. Ces informations ont été regroupées dans la Table 7. **La méthode 1 a été utilisée par l'Institut des Corps Gras (ITERG) lors de notre travail collaboratif sur les huiles végétales** [21]**.**

La partie 3 de la norme (ISO 12966-**3**) détaille la préparation des esters méthyliques par l'hydroxyde de triméthyl sulfonium (TMSH) équivalent à $(CH3)_3S(OH)$.

Les méthodes normalisées sont recommandées pour des applications spécifiques. Cependant, des études évaluent la possibilité d'utiliser des méthodes générales capables de transméthyler l'ensemble des lipides. C'est le cas des études [172] et [173] détaillées ci-après.

Méthode	Principe	Application	Réactifs	Réactions
1	Transméthylation rapide à température ambiante en conditions alcalines	- Echantillons dont l'acidité libre est inférieure ou égale à 0,5 % (recommandée). - Huiles d'olive vierges dont l'acidité est de l'ordre de 3 % ; – Corps gras comportant des triglycérides possédant des acides gras à chaîne courte ; – Corps gras comportant des triglycérides possédant des acides gras trans (E).	Potasse méthanolique **2 M (KOH/MeOH)**	Les triglycérides sont transméthylés en esters méthyliques.
2	Méthode générale de transméthylation/ méthylation à chaud	Cette méthode exclut les matières grasses laurique et les matières grasses à chaîne courte.	Hydroxyde de sodium méthanolique **0,2 M (NaOH/MeOH)** ************** Catalyse acide à l'acide sulfurique méthanolique **1 M (H_2SO_4/MeOH)**	Transméthylation des esters glycériques en esters méthyliques d'acides gras. Les acides gras libres sont convertis en savon. ************** Les savons sont convertis en esters méthyliques des acides gras.
3	Méthode de transméthylation par le méthanol à l'aide d'un catalyseur	Triglycérides avec présence d'acides gras libres	Hydroxyde de sodium méthanolique **0,5 M (NaOH/MeOH)** ************** Trifluorure de bore (acide de Lewis)/méthanol **12 à 15 % (BF3/MeOH)**	Les triglycérides sont transméthylés en esters méthyliques. Les acides gras libres sont convertis en savon. ************** Les savons sont convertis en esters méthyliques des acides gras.
4	Méthode de transméthylation par catalyse acide des glycérides	Glycérolipides	Acide sulfurique méthanolique **(H_2SO_4/MeOH)**	Transméthylation des esters glycériques en esters méthyliques d'acide gras. Le réactif de méthylation convertit également les acides gras libres en esters méthyliques d'acide gras.

Table 7: Synthèse des méthodes de transméthylation décrites dans la norme NF EN ISO 12966-2.

Dans l'étude [172] trois méthodes de transméthylation adaptées de Morrison and Smith [174] (1), Castro-Gómez et al. [175] (2) et Christie et al. [176] (3) sont comparées. Les auteurs souhaitent sélectionner la méthode la plus adaptée à l'analyse des espèces lipidiques riches en PUFAs n-3 à longue chaîne couramment rencontrés dans les matrices alimentaires et biologiques.

Pour cela, quatre classes de lipides (TG, PL, FFA et SE), issus d'extraits naturels, ont été soumis à ces trois méthodes de transméthylation. Ces classes ont ensuite été séparées par HPTLC pour évaluer leur taux de conversion en FAMEs. La séparation de lipides obtenue avec la méthode Castro-Gómez et al. (2) est présentée sur la Figure 50.

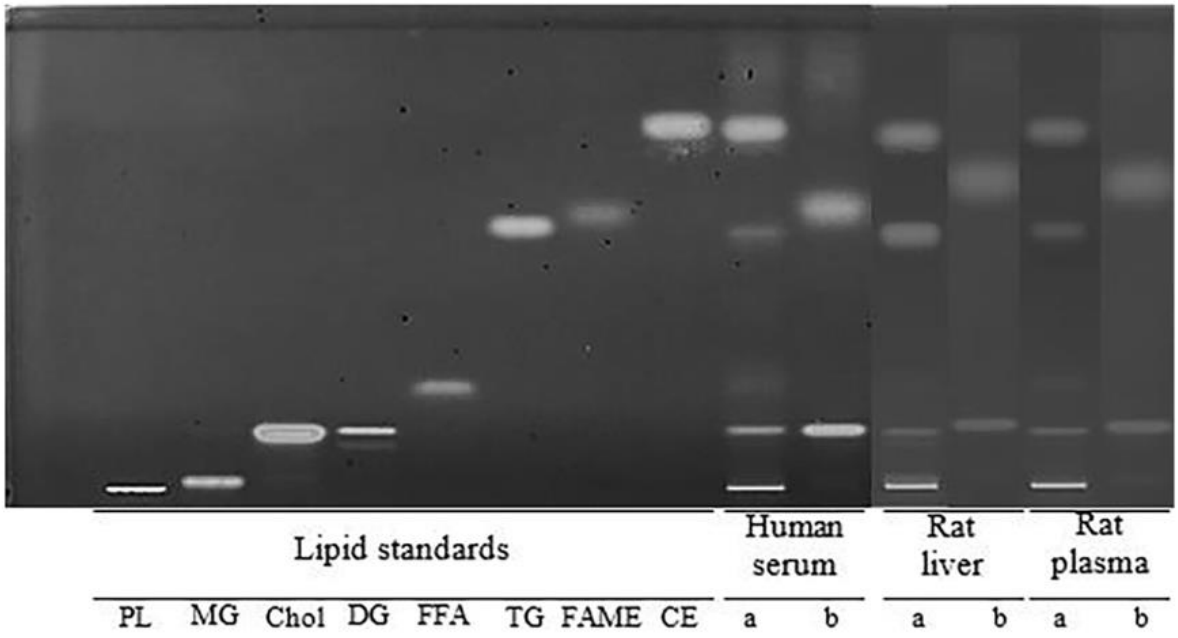

Figure 50: Image d'une plaque HPTLC utilisée pour séparer des extraits de lipides totaux (a) et leurs FAMEs correspondant (b) [172].

Les dépôts « a » correspondent à la séparation des lipides avant transméthylation et les dépôts « b » après transméthylation. Dans l'exemple, tous les lipides estérifiables (PL, FFA, TG et CE) ont disparu aux profits des FAMEs.

La lecture de la plaque HPTLC par le scanner permet de visualiser le résultat par luminescence, Figure 51. Les FAMEs produits ont également été analysés par GC-FID pour comparer l'efficacité des méthodes sur la nature des FAs.

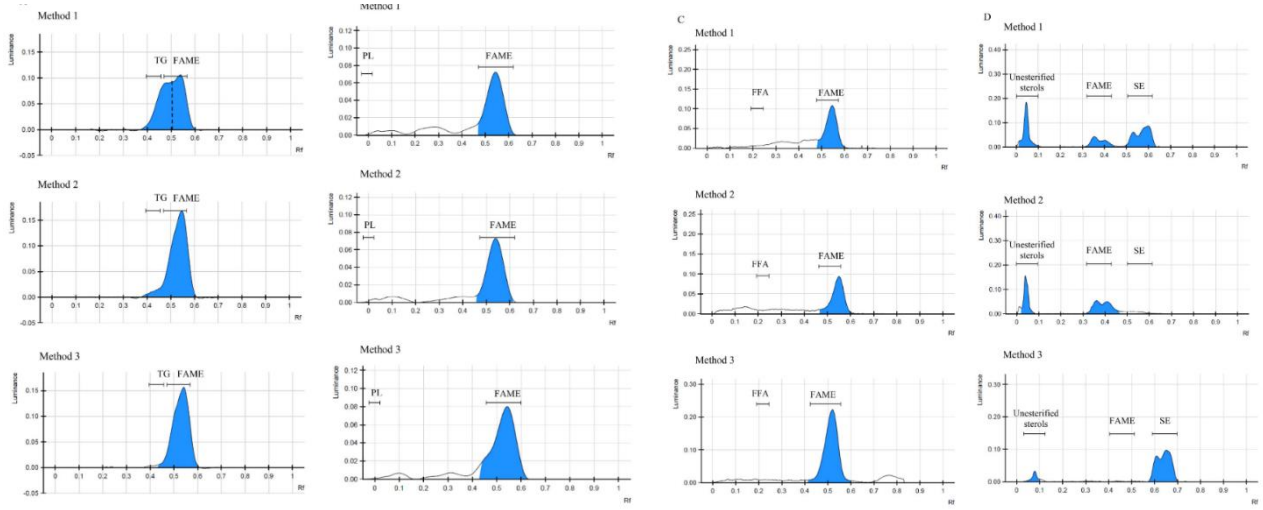

Figure 51: Comparaison de l'efficacité de trois méthodes de dérivatisation pour la génération de FAMEs par HPTLC [172].

Le **BF_3/MeOH (+ NaOH/MeOH** pour les PLs) **(**1) a permis de transméthyler les PLs et les FFA mais pas les TG et les SE. La méthode de Morrison and Smith a été utilisée par l'INRAe de Nantes lors de notre travail collaboratif sur les PLs [22]**.**

Le **CH_3ONa/H_2SO_4/MeOH (**2) a été efficace sur l'ensemble des classes de lipides prises individuellement ou en milieu complexe.

Le **CH_3ONa + BF_3/MeOH (**3) à température modérée (50°C contre 100°C pour les deux autres méthodes) a été efficace sur les TG, PL, FFA mais pas sur les SE. De plus, cette méthode a conduit à un profil de FAMEs altéré pour les PLs. Cela a été expliqué par la présence de sphingomyéline riche en C24:1n-9 (42%). Le C24:1n-9 n'ayant pas été retrouvé sur les résultats de la GC-FID.

Dans l'étude [173] le rendement de 6 protocoles de dérivatisation couramment utilisés sont comparés à travers 2 FFA saturés, 3 FFA insaturés, le PC(21 :0), le CE(17 :0), le TG(18 :1) et le TG(19 :0), les résultats sont présentés sur la Figure 52.

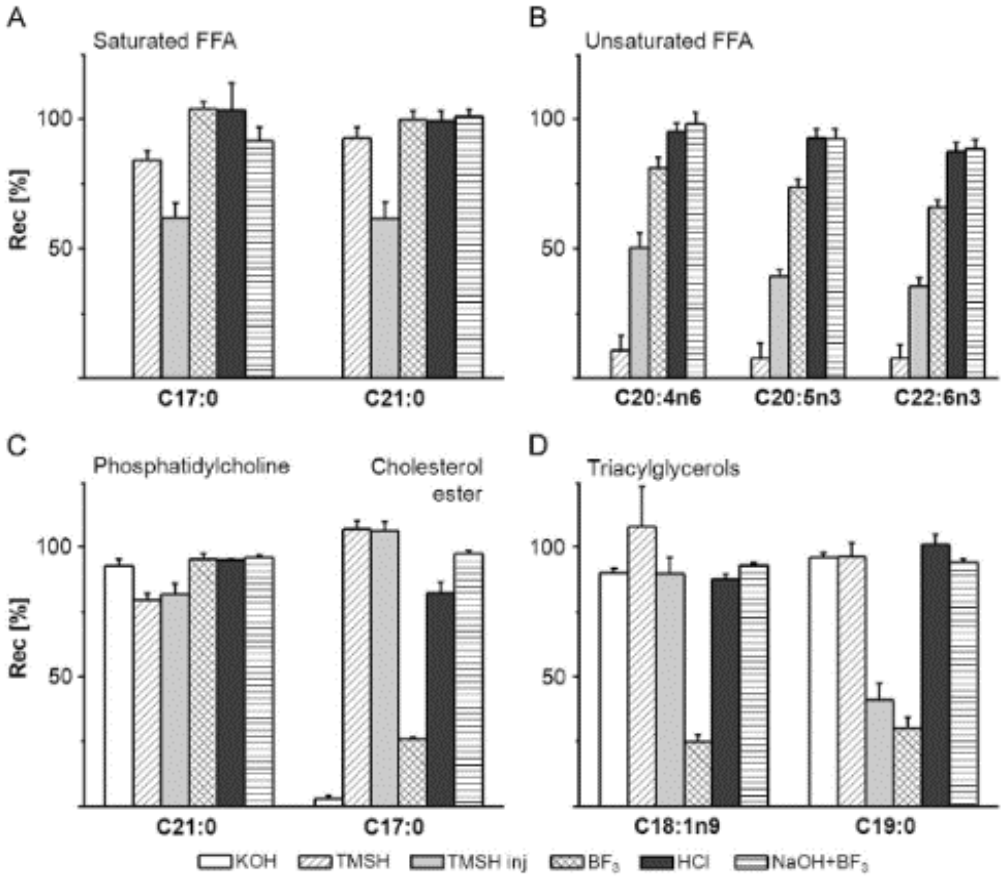

Figure 52: Comparaison de l'efficacité de six méthodes de dérivatisation pour la génération de FAMEs par GC-FID [173].

Le **KOH/MeOH** a permis la transestérification des TGs, conformément à la Table 7 (méthode 1). Cette méthode a également permis la transestérification des PLs, mais pas celles des CE et FFA.

Le **TMSH/MeOH** a donné de bons résultats uniquement pour les CE.

Le **BF_3/MeOH** seul, a permis la méthylation des FFA saturés mais pas celles des FFA insaturés. Il a aussi permis la transméthylation des PLs mais pas celles des CE et TGs.

Le **HCl/MeOH** a donné de bons résultats sur l'ensemble des lipides.

Le **NaOH/BF_3/MeOH** a permis la transestérification des TGs, conformément à la Table 7 (méthode

3). Il a été également efficace sur l'ensemble des autres lipides étudiés. Cette méthode a été utilisée par la plateforme MetaToul lors de notre travail collaboratif sur les PLs [22].

La durée et la température d'incubation des réactifs de dérivatisation ont également un impact sur l'obtention des FAMEs.

Le **BF_3/MeOH** a permis une bonne méthylation de tous les FFA dans la 1ère étude [172] et un rendement incomplet pour les FFA polyinsaturés dans la 2ème étude [173]. Dans le 1er cas, l'incubation est réalisée à 100°C pendant 15min et dans le 2ème cas à 90-95°C durant 1h. Les FFA polyinsaturés se sont peut-être oxydés sous l'effet d'une exposition trop longue à la chaleur.

1.3 Conversion des chaînes alkényles en DMAs

Comme décrit par Morrison and Smith [174], lors de la transestérification, les chaînes alkényles des P-PLs produisent des diméthylacétals (DMAs). Dans les conditions usuelles de séparation des FAMEs par GC, les DMAs sont élués juste avant leurs homologues FAMEs [177]. Les DMAs doivent être impérativement identifiés afin de ne pas les confondre avec des FAMEs [178].

Par ailleurs, cette méthode est recommandée pour l'étude de la distribution des chaînes alkényles des P-PLs [178].

1.4 Séparation des FAMEs et DMAs par GC

La séparation des FAMEs est généralement faite sur une phase polaire (FAMEWAX (polyéthylèneglycol) ; DB 225MS ((50%-cyanopropylphenyl) -methylpolysiloxane) …). Dans ces conditions de polarité, le temps de rétention des FAMEs augmente avec le nombre de carbones. Pour un même nombre de carbones, la rétention augmente avec le nombre de doubles liaisons. Les colonnes très polaires permettent de séparer les FAMEs isomères (isomérie de configuration (Z et E) et de position) [171].

Un exemple de séparation réalisé sur une colonne RT-2330 (90% biscyanopropyl/10% phenylcyanopropyl polysiloxane) est présenté sur la Figure 53, issue du site internet du fabricant Restek (https://www.restek.com/fr/documentation-technique/articles/analysis-of-FAMEs-in-biodiesel-fuel-pro-EZGC-modeling-software-ensures-proper-column-selection/). Les isomères trans sont élués avant les isomères cis.

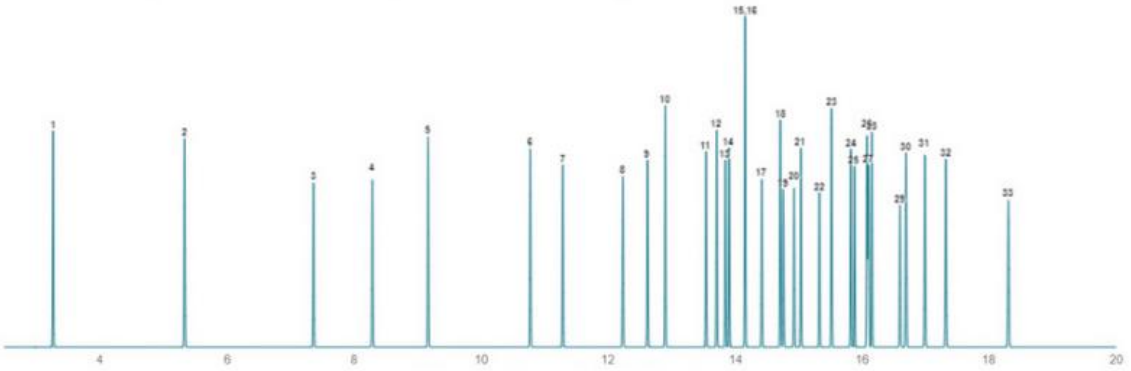

Peaks	t_R (min)	R_S	Peak Width (min)	T_{peak} (°C)
1. C6:0	3.25	73.9	0.028	72.5
2. C8:0	5.32	66.4	0.031	93.2
3. C10:0	7.35	30.4	0.031	113.5
4. C11:0	8.28	28.8	0.031	122.8
5. C12:0	9.16	28.8	0.031	131.6
6. C14:0	10.77	17.1	0.030	147.7
7. C14:1 (cis-9)	11.28	17.1	0.030	152.8
8. C16:0	12.23	13	0.030	162.3
9. C16:1 (cis-9)	12.62	9.2	0.030	166.2
10. C17:0	12.89	9.2	0.030	168.9
11. C18:0	13.54	5.6	0.029	175.4
12. C18:1 (trans-9)	13.71	4.6	0.030	177.1
13. C18:1 (cis-9)	13.84	1.9	0.030	178.4
14. C18:1 (cis-11)	13.90	1.9	0.030	179.0
15. C18:2 (all-trans-9,12)	14.15	--	0.030	181.5
16. C19:0	14.15	--	0.029	181.6
17. C18:2 (all-cis-9,12)	14.41	8.8	0.030	184.2
18. C18:3 (all-cis-6,9,12)	14.71	1.5	0.030	187.1
19. C20:0	14.76	1.5	0.029	187.6
20. C18:3 (all-cis-9,12,15)	14.93	3.4	0.031	189.3
21. C20:1 (cis-11)	15.03	3.4	0.030	190.3
22. C21:0	15.32	6.5	0.029	193.3
23. C20:2 (all-cis-11,14)	15.52	6.5	0.030	195.2
24. C20:3 (all-cis-8,11,14)	15.82	1.8	0.030	198.2
25. C22:0	15.88	1.8	0.029	198.8
26. C20:3 (all-cis-11,14,17)	16.07	0.7	0.030	200.4
27. C20:4 (all-cis-5,8,11,14)	16.10	0.7	0.031	200.5
28. C22:1 (cis-13)	16.15	1.7	0.030	200.8
29. C22:2 (all-cis-13,16)	16.59	2.9	0.032	203.0
30. C20:5 (all-cis-5,8,11,14,17)	16.69	2.9	0.033	203.4
31. C24:0	16.99	8.8	0.033	204.9
32. C24:1 (cis-15)	17.32	10.2	0.034	206.6
33. C22:6 (all-cis-4,7,10,13,16,19)	18.30	28.7	0.039	211.5

Column:	**Rt®-2330**, 30.00 m, 0.25 mm ID, 0.25 µm
Carrier Gas:	Hydrogen, Constant Flow @ 1.75 mL/min
Average Velocity:	48.32 cm/sec
Outlet Pressure (abs):	14.70 psi (Atmospheric Pressure)
Oven Temp:	60 °C (hold 2 min) to 200 °C @ 10 °C/min to 240 °C @ 5 °C/min

Figure 53: Séparation de FAMEs et de DMAs par GC-FID réalisée sur une colonne CP-Sil 88 - site internet Restek.

Un exemple de séparation de FAMEs et de DMAs issus de la transestérification de la graisse intramusculaire d'agneau sur une colonne CP-Sil 88 est présentée sur la Figure 54.

Comme décrit précédemment, les DMAs sont élués avant leurs homologues FAMEs. Les isomères iso sont élués avant les isomères anteiso (cas des FAs branchées).

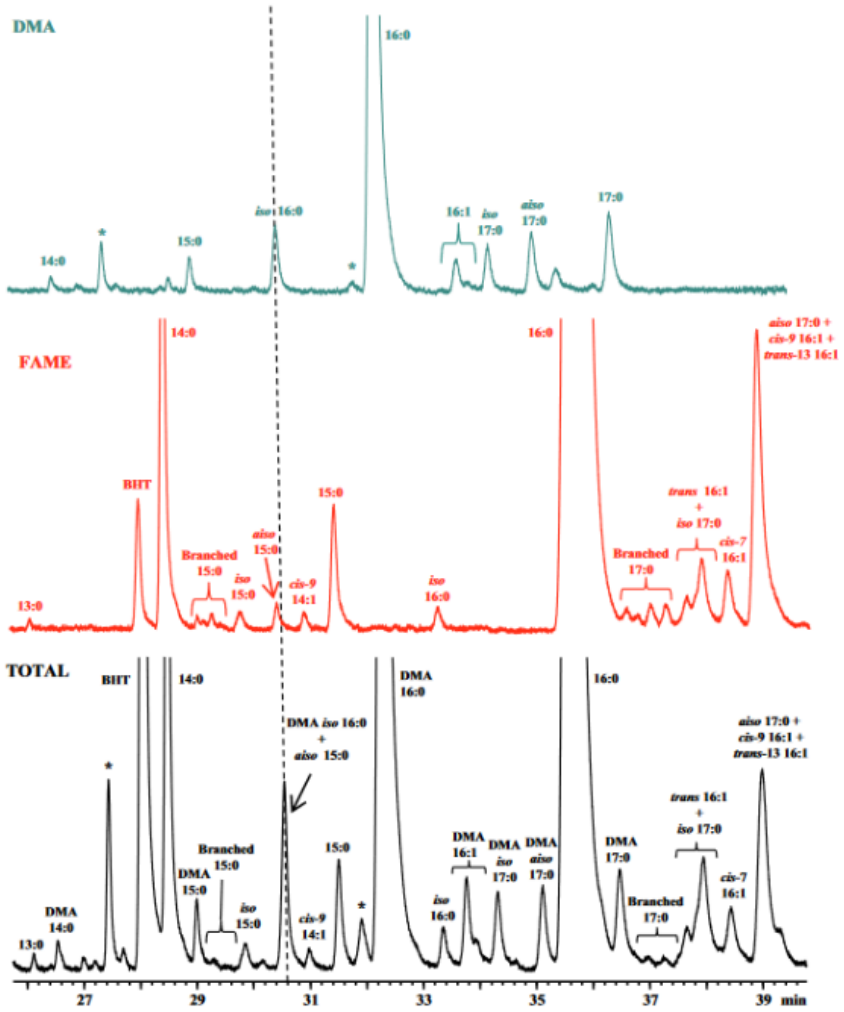

Figure 54: Séparation de DMAs et FAMEs issue de graisse intramusculaire d'agneau par GC-FID [178].

1.5 Couplage de la GC au FID et à la MS

Le couplage de la GC au FID permet d'obtenir des données quantitatives et le couplage à la MS permet d'obtenir des données quantitatives et qualitatives (identification/caractérisation).

Dodds et al. (2005) [179] ont comparé la réponse du FID à celles obtenues par deux analyseurs MS (un Quadripôle (PQ) et une Trappe ionique (IT)) couplés à une source d'impact électronique (EI).

Les résultats montrent que le FID a une réponse linéaire sur l'ensemble des points de gamme du C18 :0, ce qui n'est globalement pas le cas des deux détecteurs MS, sauf lors de l'utilisation du QP en

mode SIM, Figure 55 (a). D'autre part, les FAMEs ont des coefficients de réponse beaucoup plus homogènes avec le FID par rapport aux détecteurs MS, Figure 55 (b). Ces deux spécificités expliquent pourquoi les analyses quantitatives sont plus fréquemment faites par GC-FID. Néanmoins, la GC-MS offre deux principaux avantages par rapport au FID, la capacité à confirmer l'identité des analytes sur la base d'informations spectrales en plus du temps de rétention et la possibilité de séparer les pics du bruit de fond ou d'une coélution de pics si des ions spécifiques sont disponibles.

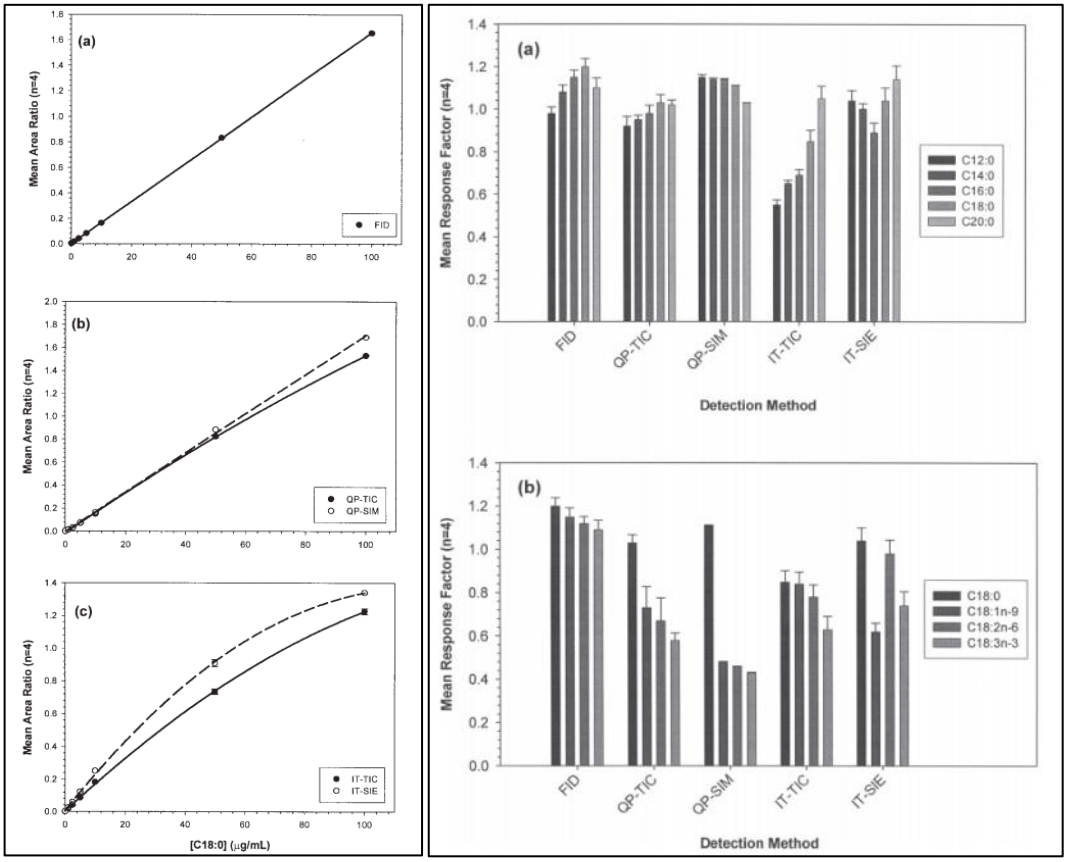

Figure 55: Gauche : courbes d'étalonnage du FAME 18:0 obtenue par GC-FID (a), QP-MS (b) et IT-MS (c). Droite : facteurs de réponse pour une série de FAMEs saturés (a) et une série de FAMEs insaturés (b) obtenus par GC-FID et QP-TIC/QP-SIM/IT-TIC/IT-SIE [179].

IT, ion trap; QP, quadrupole; SIE, selected ion extraction; SIM, selective ion monitoring; TIC, total ion count.

2. LC-MS/MS

La distribution des FAs totaux peut également être déterminée par LC-MS/MS [180–182]. Le principe consiste à hydrolyser les lipides et à analyser les FFA produits par RPLC-MS/MS. Dans l'étude [182], 41 FFA (dont des isomères) ont été séparés sur une colonne C8. Onze FFA marqués ont été utilisés comme standards internes. Les concentrations déterminées par cette méthode sont proches de celles obtenues par GC-FID, Figure 56.

Selon les auteurs, les atouts de cette méthode sont : la rapidité de préparation des échantillons par hydrolyse et dilution ; la combinaison possible avec l'analyse des produits d'oxydation des PUFAs (eicosanoïdes et autres oxylipines) [183] et la quantification des FAs non estérifiée en présence de triacylglycérols.

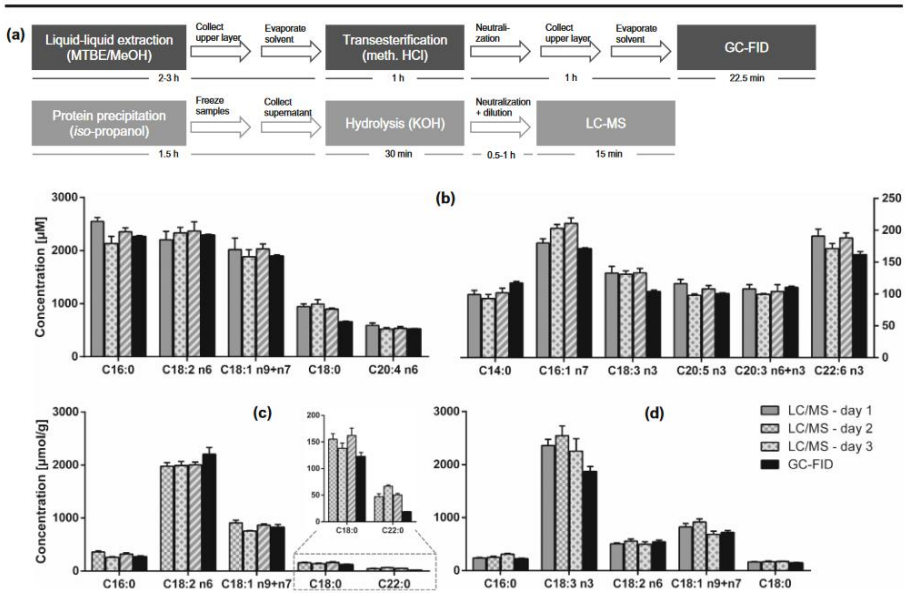

Figure 56: Comparaison des méthodes LC-MS et GC-FID pour l'obtention de la distribution des FAs. Préparation des échantillons (a). Variabilité intra- et inter-journalière de la concentration en FAs selon les deux méthodes dans : le plasma humain (b) ; l'huile de tournesol (c) et l'huile de lin (d) [182].

PARTIE II : RESULTATS

INTRODUCTION :

ANALYSE DES ACYLES GRAS PAR LES IONS B

1. Origine du concept

Lors de notre participation à l'ANR Omegasomes (2012-2015) nous avons été confrontés à la difficulté d'obtenir une estimation fiable de la distribution des FAs dans les différentes classes de lipides issus d'échantillons naturels.

Dans ce projet, des sous-produits alimentaires riches en PUFAs n-3 (tourteaux oléagineux et noix de Saint-Jacques) ont été choisis pour formuler des éthosomes en vue d'applications nutritionnelles ou topiques. Les éthosomes sont des capsules de taille colloïdale, résultant de l'assemblage spontané des phospholipides en présence d'eau et d'éthanol.

L'un des objectifs était de déterminer la distribution des PUFAs n-3 au sein des différentes classes de lipides, notamment dans celles des PLs utilisées pour former les éthosomes. Ce projet a donné lieu à l'article [184] dans lequel les espèces moléculaires des PLs ont été déterminées par shotgun-MS, RPLC-MS/MS et NPLC-MS. Il a également donné lieu à l'article [185] dans lequel la distribution des FAs totaux a été déterminée par GC-FID. Dans cet article, la fraction des PLs a également été isolée par TLC avant d'être analysée par RMN. L'utilisation de la ^{31}P RMN a permis de déterminer la distribution des PLs par classe et l'utilisation de la ^{1}H RMN a permis de déterminer la teneur globale des PLs en PUFAs n-3.

A l'issue du projet ANR, la composition en FAs déterminée par les autres laboratoires nous a permis d'obtenir une base de comparaison avec nos données NPLC-APPI-MS, obtenues à partir des mêmes échantillons.

La NPLC permet de séparer les lipides par classe, ainsi l'ensemble des TGs sont élués vers 5 min et les différentes classes de la catégorie des PLs sont éluées entre 24 et 40 min. En étudiant le spectre de

masse sous le pic de la classe des TGs, nous avons observé que la distribution des intensités des ions fragments $[MG+H-H_2O]^+$ produits en source coïncidait avec la distribution en % des FAs déterminée pendant l'étude ANR par les autres laboratoires. La même observation a été faite lors de l'étude des pics de chaque classe de PLs. **Cette observation est uniquement possible si une classe de lipide est éluée sous un pic unique et sans autre coélution**. Il n'est donc pas possible de faire cette observation lors d'une séparation par RPLC, par exemple.

L'énergie des sources APPI et APCI (Thermo Fisher) a permis d'induire des ions fragments $[MG+H-H_2O]^+$ à partir de glycérolipides ou de PLs. Cette observation n'a pas été faite lors de l'utilisation de la source ESI de ce même constructeur, cette source étant moins énergétique. Nous apportons une précision sur le fabricant, car la géométrie de la source peut influencer l'ionisation.

Les ions étudiés dans ce travail de thèse sont exclusivement issus de la fragmentation en source APPI ou APCI, ils ne sont pas issus de la fragmentation MS/MS.

2. Fragmentation des TGs et PLs en mode positif

Le schéma de fragmentation en mode positif des TGs et des PLs (exemple du PC) sont présentés sur la Figure 57. Les TGs se fragmentent en perdant une chaîne grasse et les PLs en perdant leur tête polaire. Dans les deux cas, ces fragmentations aboutissent à la formation d'un ion commun équivalent à l'ion $[DG+H-H_2O]^+$. Cet ion se fragmente à nouveau, en perdant une chaîne grasse, pour former un ion équivalent à l'ion $[MG+H-H_2O]^+$. **Ces deux ions, $[DG+H-H_2O]^+$ et $[MG+H-H_2O]^+$, sont nommés respectivement ions A et B dans l'étude Holčapek et al. (2003)** [186]. Cette notation a été conservée dans nos travaux.

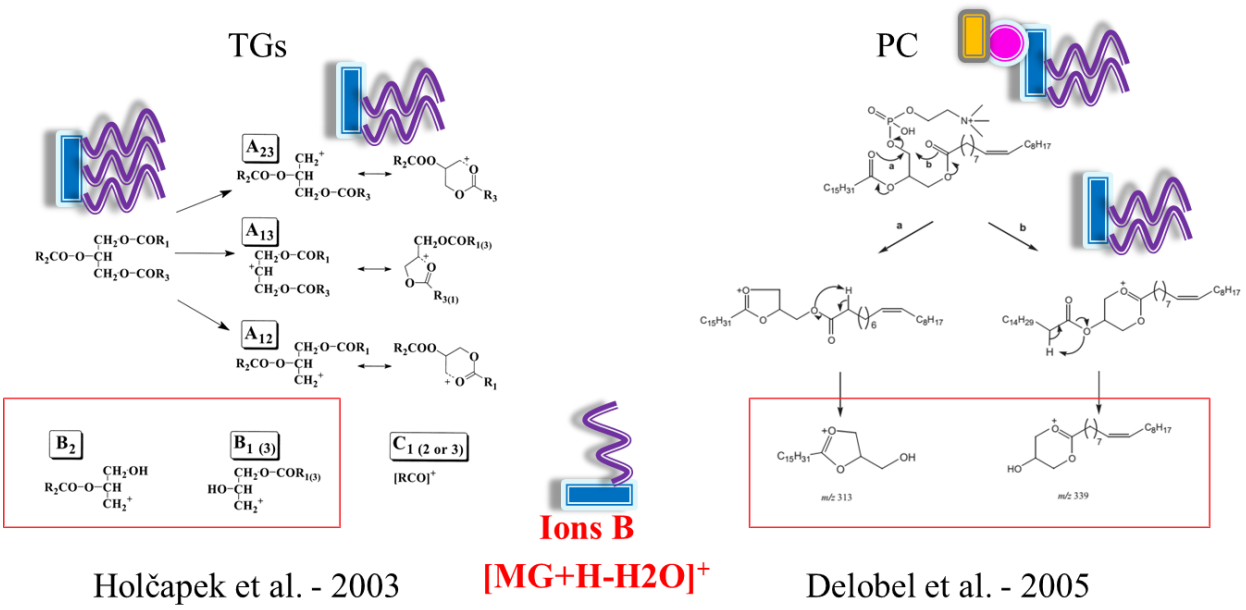

Figure 57: Gauche : schéma de fragmentation des TGs [186]. Droite : schéma de fragmentation des PC [187]. Des illustrations ont été ajoutées aux schémas d'origine.

Pour illustrer ces schémas de fragmentation, les spectres de masse en mode « full scan » des TGs issus de l'huile d'olive et des PC extraits du cerveau de bœuf (standard Sigma-Aldrich) obtenus lors de nos premiers essais sont présentés respectivement sur la Figure 58 (a) et sur la Figure 59 (a).

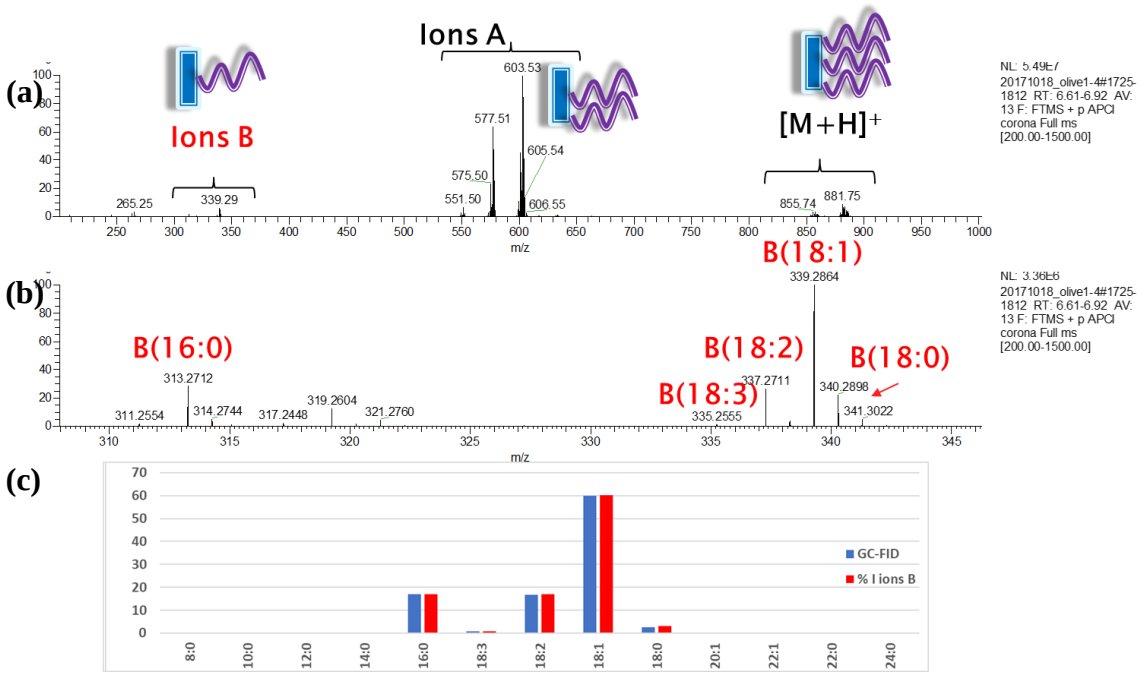

Figure 58: Spectre full scan des TGs issus de l'huile d'olive (a) ; zoom dans la gamme m/z correspondante aux ions B (b) ; pourcentage des FAs obtenus par GC-FID et par les intensités des ions B (c).

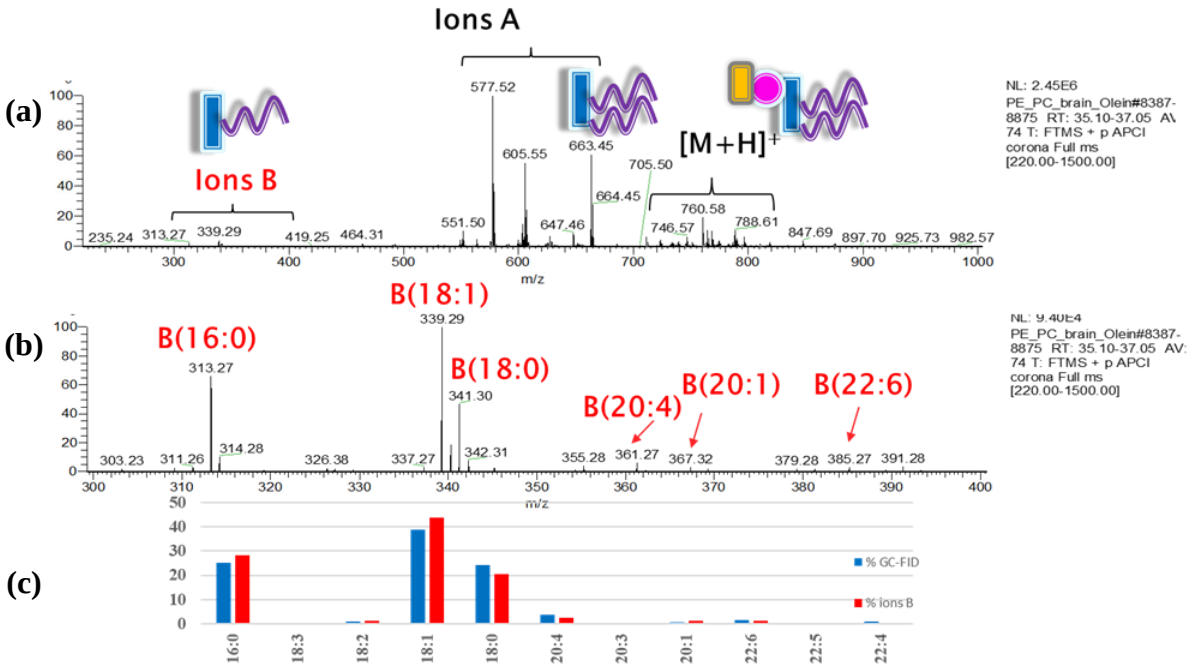

Figure 59: Spectre full scan des PC extraits du cerveau de bœuf (a) ; zoom dans la gamme m/z correspondante aux ions B (b) ; distribution en pourcentage des FAs par GC-FID et par les intensités des ions B (c).

Dans les deux cas, l'intensité des ions A est très majoritaire par rapport à celles des autres ions. Les intensités des ions B représentent moins de 5% de l'intensité de l'ion A le plus abondant. Cette faible intensité relative des ions B, contribue sans doute à une sous exploitation de ces ions dans les études. Pour mieux visualiser les ions B, un zoom est présenté sur la Figure 58 (b) et la Figure 59 (b). Les ions B présentent l'avantage d'être composés d'une seule partie variable, correspondant au FA, leurs *m/z* sont donc très simples à identifier. L'identification des ions contenant 2 ou 3 FAs (ions A et ions $[M+H]^+$) n'est pas directe à cause du nombre important de combinaisons de FAs possibles.
Sur la Figure 58 (c) et la Figure 59 (c), les intensités relatives des ions B sont converties en pourcentages et comparées aux pourcentages des FAs obtenus par GC-FID. Les résultats des deux approches sont comparables. Cette observation est à l'origine de notre hypothèse de travail.

Pour objectiver la possibilité d'utiliser les ions B pour prédire la distribution des FAs, nous avons réalisé deux études. Dans la 1ère étude, les bases et les limites du concept ont été définies au travers de la classe des TGs. Dans la 2nd étude le concept a été étendu aux classes des PLs (dont les plasmalogènes).
Cette méthode a pu être valorisée au travers d'un travail collaboratif portant sur le réajustement des lipides dans les souches productrices d'acides gras à chaînes impaires de *Yarrowia lipolytica*. Ces trois études font l'objet des trois chapitres suivants.

CHAPITRE VI. EVALUATION DE LA DISTRIBUTION DES ACYLES GRAS DES TRIACYLGLYCEROLS PAR LES IONS B

1. Introduction

Cette première étude a pour but d'évaluer la possibilité d'utiliser les ions B, produits en sources APPI et APCI, pour prédire la distribution des FAs des glycérolipides et PLs. Pour cela, deux prérequis à la mise en œuvre de ce nouveau concept ont dû être étudiés.

Tout d'abord, les ions B doivent être toujours formés en source, quelle que soit la nature des espèces moléculaires. D'autre part, les ions B doivent être spécifiques des FAs, pour une résolution de spectromètre de masse donnée.

Il a également fallu trouver un support (échantillons/standards) pour le développement du concept. L'utilisation exclusive de standards mono-moléculaires a été rapidement écartée. Leur disponibilité commerciale est limitée et leur coût élevé. Nous nous sommes donc orientés également vers l'utilisation de standards issus d'extraits naturels. Le développement sur des extraits naturels permet d'appréhender au mieux les défis analytiques sur des cas d'études concrets.

Ayant travaillé sur des extraits de lipides totaux dans l'article de 2017, nous avons pensé à leur utilisation. Ces échantillons présentent l'avantage de contenir différentes classes de lipides simultanément. Cependant, nous n'avons pas retenu cette idée, car la détermination de la distribution des FAs par la GC-FID aurait nécessité la séparation et l'isolement des différentes classes de lipides, ce qui aurait complexifié les expérimentations. De ce fait, nous avons choisi de travailler avec des extraits lipidiques naturels contenant une seule classe de lipide. Un nombre limité de standards de PLs issus d'extraits naturels sont disponibles commercialement chez Avanti Polar Lipids, Inc et Sigma-Aldrich, mais aucun extrait n'est disponible pour la classe des TGs.

Fort de notre expérience sur les huiles végétales lors du projet ANR Omegasomes, nous avons pensé à utiliser des huiles végétales comme standards. Aroma-Zone commercialise à des fins cosmétiques un grand nombre d'huiles avec un bulletin d'analyse relativement détaillé concernant la composition en FAs. Les huiles ont pu être sélectionnées pour balayer la plus large gamme (nature et concentration)

de FAs. De plus, les huiles sont constituées à plus de 95% de TGs ce qui permet de considérer ces échantillons comme quasi purs par rapport aux besoins de notre expérimentation.
Vingt huiles ont été sélectionnées pour étudier la classe des TGs et dix-sept standards de PLs ont été sélectionnés pour étudier la catégorie des PLs. Pour simplifier les expérimentations, seule la classe des TGs est étudiée dans ce premier travail.

Les huiles étant considérées dans cette étude comme quasi pures en TGs, il a été possible de réaliser des analyses très rapides par FIA-HRMS. Ce mode d'introduction permet une élution de l'ensemble des TGs au temps mort du système (environ 1 min).
L'analyse des huiles a également été réalisée par NPLC-HRMS, pour étudier le potentiel de la méthode à être utilisée sur des échantillons contenant plusieurs classes de lipides.

Le choix de la source d'ionisation s'est porté sur l'APPI, pour ses intensités plus importantes que celles de l'APCI (Abreu et al. 2017) [20].

Nous avons également initié une collaboration avec l'ITERG, laboratoire expert dans l'analyse des FAs par GC-FID, afin d'obtenir des valeurs de références fiables de la distribution des FAs de ces huiles.

Ce travail a donné lieu à l'article « Rapid assessment of triacylglycerol fatty acyls composition by LC-APPI^{+}-HRMS using monoacylglycerol like fragments intensities » publié dans le journal Analytica Chimica Acta, présenté ci-après.

2. Publication 2

Les données supplémentaires liées à cette publication sont présentées en Annexe II.

Analytica Chimica Acta 1178 (2021) 338809

Contents lists available at ScienceDirect

Analytica Chimica Acta

journal homepage: www.elsevier.com/locate/aca

Rapid assessment of triacylglycerol fatty acyls composition by LC-APPI$^+$-HRMS using monoacylglycerol like fragments intensities

Sonia Abreu [a], Sylvie Heron [b, 1], Audrey Solgadi [c], Florent Joffre [d], Alain Tchapla [b, 1], Pierre Chaminade [a, *]

[a] Université Paris-Saclay, Lipides: Systèmes Analytiques et Biologiques, 92290, Chatenay-Malabry, France
[b] Université Paris-Saclay, ICP – CNRS UMR 8000, (LETIAM), 91400, Orsay, France
[c] Université Paris-Saclay, Inserm, CNRS, Ingénierie et Plateformes Au Service de L'Innovation Thérapeutique, IPSIT-SAMM, 92290, Chatenay-Malabry, France
[d] ITERG, 33610, Canejan, France

HIGHLIGHTS

- Fatty acyls distribution of triacylglycerols is estimated from their APPI $^+$ -HRMS spectra.
- Monoacylglycerol like fragments (Ions B) are produced by in source fragmentation of triacylglycerols.
- The fatty acyls composition of triacylglycerols (TG) can be deduced from Ion B intensities.
- Coupling with flow injection (TG in plant oils) or NPLC (TG in complex samples) is achieved without prior sample preparation.

GRAPHICAL ABSTRACT

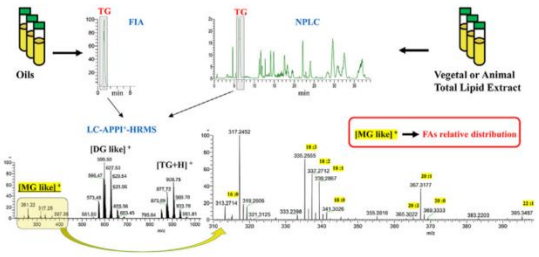

ARTICLE INFO

Article history:
Received 19 May 2021
Accepted 27 June 2021
Available online 1 July 2021

Keywords:
Lipids
Triacylglycerols
Fatty acids composition
Normal phase chromatography
Orbitrap mass spectrometry
Atmospheric pressure photoionization

ABSTRACT

We present a new analytical approach for the analysis of triacylglycerol fatty acyls distribution by normal phase liquid chromatography (NPLC) coupled with APPI$^+$-HRMS. The NPLC method used allows the separation of more than 30 classes of lipids. The energy of the APPI$^+$ source enables the formation of low-intensity ions B fragments ($[RC = O+74]^+$ <3%), characteristic of lipids with a glycerol esterified by one or more fatty acyls. We found the relative intensities of ions B were close to the fatty acyl distribution. To establish the proof of concept, we decided to focus on the triacylglycerols (TGs) class, the major component of plant oils. By either NPLC or FIA, the TGs class appeared as a single peak. In our experimental conditions, ions B are always present in the mass spectra of TGs and each ion B is specific to a fatty acyl group. The Orbitrap mass spectrometer featured high enough resolution and accuracy to identify ions B and distinguish them from other TG fragment ions. A further adjustment of the fatty acyls relative quantities calculation from ions B intensities was computed using weighting coefficients of ions B response. The methodology was developed and validated using plant oils characterized by a GC-FID reference method. NPLC-APPI$^+$-HRMS method offers the advantage of analyzing the fatty acyl composition of complex lipid extracts without the need for sample preparation.

© 2021 Elsevier B.V. All rights reserved.

1. Introduction

Fatty acids consist of an aliphatic hydrocarbon chain, variable in

* Corresponding author.
E-mail address: pierre.chaminade@universite-paris-saclay.fr (P. Chaminade).
[1] Former address: Université Paris-Saclay, EA 7357, Lip(Sys)^2, LETIAM, IUT Orsay, Plateau de Moulon, 91400, Orsay, France.

https://doi.org/10.1016/j.aca.2021.338809
0003-2670/© 2021 Elsevier B.V. All rights reserved.

length and unsaturation degree, terminated by a carboxylic acid group. They can be used in various metabolic pathways to synthesize more complex lipids, including glycerolipids and glycerophospholipids (PLs) [1]. As a result, fatty acids contribute to the vast structural diversity of the cell lipid pool, which in turn serves to regulate several biochemical processes. These include the synthesis of biological membranes and the modulation of their fluidity, the production of secondary messengers in signaling pathways to maintain homeostasis [2] and serve as a form of energy storage [3,4]. One of the current challenges is to understand the mechanics and function of lipids. For this, some studies are interested in glycerolipidome through experiments on model bacteria [5–7], plants [8,9] or algae [10–13]. As discussed in several recent publications [11,14,15] quantitative analysis of lipid species in biological samples remains an analytical challenge. Numerous LC-MS methods have been published in the last decades, but quantification is however difficult because the ionization efficiency depends on several parameters including the nature of the molecule to be analyzed and the chemical environment of this molecule.

The transesterification of fatty acyls (FAs) to fatty acid methyl esters (FAMEs) followed by their analysis by gas chromatographic coupled to flame ionization detector (GC-FID) still remains the main method used to assess the FA content and the composition of a lipid extract. This method is widely recognized as reliable and frequently used as reference when developing new methods [11,16–19]. When the sample contains several lipid classes, the method provides a global information concerning FA composition. The access to the FA composition of lipid classes needs a fractionation of lipid classes of interest before applying the method. This step is generally performed by solid phase extraction (SPE) [20–22] or thin layer chromatography (TLC) [16,22–24]. Depending on the number of lipid classes under investigation and/or sample complexity, this fractionation step may increase dramatically the sample processing time.

In a former study [25], we published a normal-phase liquid chromatography (NPLC) coupled with APPI$^+$-HRMS method geared towards the analysis of most lipid classes encountered in natural extracts. Total lipid extracts of heart, liver, brain, soya, wheat, yeast and bacteria were analyzed. An in-depth re-examination of mass spectra from glycerolipids and PLs suggest that fragmented ions $[RC=O+74]^+$ intensities reflect the relative quantities of FAs present in these classes. 74 represents the glyceryl moiety C3H6O2 and R an acyl chain, as presented Fig. 1. These ions will be designated as "ions B″ to reproduce the same terminology as in other studies [26,27]. Ions B are issued from in-source fragmentation of glycerolipids or PLs.

The present work focuses on the TG class. We propose developing a treatment of HRMS data issued from FIA or NPLC-APPI$^+$-HRMS [25] able to assess the TGs primary composition i.e. the FA composition of the TG class, using the intensities of the ions B formed. In order to simplify the study implementation, plant oils are used as they contain more than 90% TG. Even though they contain a single lipid class, samples we analyzed by NPLC, as the objective is to propose a methodology able to accommodate samples that are more complex. In that way, the method we propose can be used with total lipid extract without prior fractionation.

2. Experimental section

2.1. Chemicals

Isooctane, ethyl acetate, acetone (all HPLC grade), acetic acid, trimethylamine, sulfuric acid and anhydrous sodium sulfate were all purchased from Sigma-Aldrich (St Louis, MO, USA). Chloroform and water (all HPLC grade) were obtained from VWR (Radnor, Pennsylvania, USA). Isopropanol (UHPLC/MS grade) was from Biosolve (Dieuze, France). Isooctane was purified prior analysis by pumping the solvent through a semi preparative column packed with Lichroprep Si 60 5–20 μm silica (Merck KGaA, Darmstadt, Germany).

2.2. Standards

Trilaurin (LaLaLa), tripalmitin (PPP), trilinolenin (LnLnLn), trilinolein (LLL), triolein (OOO), tristearin (SSS), triarachidin (AAA) and trierucin (ErErEr) were purchased from Sigma-Aldrich. Each TG stock solution is prepared in isooctane or in isooctane: chloroform 1:1 depending on the TG solubility at the concentration of 5 g/l. LaLaLa, PPP, SSS and AAA could not be adequately solubilized in isooctane. 5 dilutions levels were prepared from the stock solution: 0.05; 0.25; 0.5; 0.75 and 1 g/l. Nu-Check Prep GLC 36 FAME mixtures was obtained from Nu-Chek-Prep (Elysian, MN, USA).

2.3. Sample preparation

Total lipid extracts from bovine heart were purchased from Avanti Polar Lipids (Alabaster, AL, USA). Lipowheat® oil is a food grade ingredient from Robertet Health & Beauty (Formerly HITEX, Vannes, France). This sample comes from the ethanolic extraction of bakery wheat gluten. Each sample is prepared in chloroform at the concentration of 5 g/L for analysis and storage.

Calibration set oils (coconut, babassu, bay laurel, macada-mia, piqui, blackcurrant, shea olein, camelina, pracaxi and mustard) and validation set oils (wheat germ, oats, olive, inca inchi, hemp, evening primrose, borage, sesame, hazelnut, and broccoli) were purchased from Aroma-Zone (Paris, France). Each oil is prepared in isooctane at the concentration of 0.75 g/l for storage and analysis.

2.4. GC-FID apparatus

GC (Thermo Electron Corporation, Thermofisher, Waltham, Massachusetts, USA) equipped with a split/splitless injector and a FID. Separation of FAMEs was performed with a CPSil88-fused silica capillary column (100 m length × 0.25 mm internal diameter, 0.2 μm film thickness). The hydrogen inlet pressure was 200 kPa. The injector and detector temperatures were at 250 and 280 °C, respectively. The oven was at 60 °C for 2 min, increased to 165 °C at a rate of 15 °C/min with a 1-min hold, increased to 225 °C at a rate of 1 °C/min and then left at this temperature for 1min.

2.5. GC-FID method

TGs are transmethylated according to the NF EN ISO 12966 method (Animal and vegetable fats and oils Gas chromatography of fatty acid methyl esters) part 2 for the preparation of methyl esters and part 4 for the GC-FID analysis. Briefly, 100 mg of oil are dissolved in 2 ml of isooctane. The alkaline transesterification is carried out by the addition of 0.1 ml of KOH/MeOH solution (2 N) and vortexing for 1 min. The reaction is stopped with 2 ml of saturated NaCl solution. After decantation, the upper phase is collected and 1 g of anhydrous sodium bisulfate is added to remove any trace of water that would disrupt the chromatographic analysis. After centrifugation, 1 μl of isooctane which contains the FAMEs is analyzed on a FOCUS GC. FAMEs were identified by making a comparison of the retention time with commercial standards (Nu-Check Prep GLC 36).

The GC method was validated and meets the following performance criteria: global composition uncertainty of measurement 8% with a minimum of 0.5% and a maximum of 3.5% on individual FA. The limit of quantification is validated at 0.05% for each FA in plant

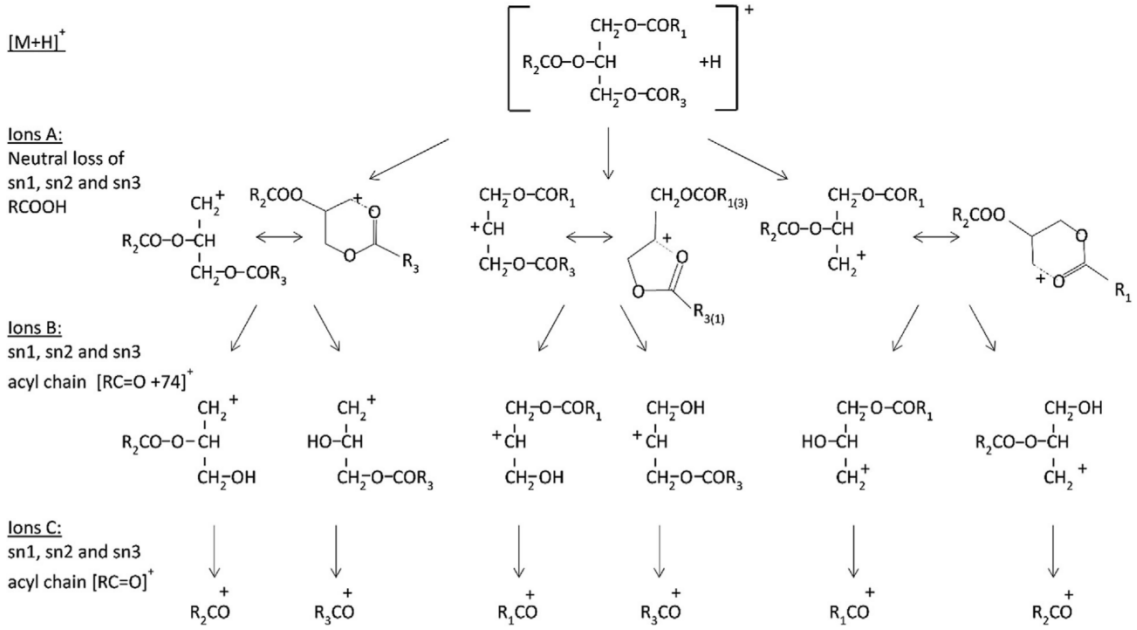

Fig. 1. Triacylglycerols structures and fragment ions.

oil (except in Olive oil where the mandatory value of 0.02% in met).

2.6. FIA and NPLC-APPI$^+$-HRMS apparatus

FIA and NPLC-APPI$^+$-HRMS analyses were performed with a LTQ-Orbitrap Velos Pro (Thermofisher, Waltham, Massachusetts, USA) instrument coupled to a LC system (Dionex U-3000 RSLC, Thermofisher, Waltham, Massachusetts, USA) both controlled through Thermo Xcalibur (version 2.2) software.

The LTQ-Orbitrap Velos Pro mass spectrometer was equipped with an APPI ion source with a krypton PKS 100 lamp (Cathodeon, Cambridge, England) that generates a continuous flow of 10.0 and 10.6eV photons.

APPI ion source: Vaporizer temperature of the probe was set at 400 °C. Sheath gas, auxiliary gas, and sweep gas flow rates were set at 40, 10, and 0 (arbitrary unit) respectively. Capillary temperature was set at 325 °C and S-lens RF level at 60%. Analyses were performed in positive ion mode. The data was acquired in the mass range *m/z* [200–1500] at the maximum resolution of 100000 @ *m/z* 400.

2.7. NPLC method

Two lipid extracts were analyzed with a previously published NPLC method [25]. In the case of oils, an adaptation of the method has been made, because the original method lasts 53 min, while the peak of TGs is eluted in less than 5 min. The adapted NPLC method corresponds to the first 9 min of the original solvent program described in Ref. [25], followed by a 5 min equilibration with mobile phase A.

Mobile phase A consists in isooctane: ethyl acetate (99.8 : 0.2, v/v) and mobile phase B is composed of acetone: ethyl acetate (2 : 1,v/v) with 0.15% acetic acid (v/v). The solvent program is as follow: 0 min, 0% B; 1.5 min, 0% B; 1.6 min, 3% B; 9 min, 6% B; 10 min, 0% B; 15 min 0% B. Separation was performed with an Inertsil Si 5 μm (150 mm × 2.1 mm I.D.) column (GL Sciences Inc., Tokyo, Japan) thermostated at 40 °C. The flow rate was set at 0.8 ml/min. The injected volume was 2 μl. Repeatability was assessed by calculating the standard deviation of ion B intensities measured from six injections of hemp oil.

2.8. FIA method

The FIA conditions were selected to be as close as possible from the NPLC elution of the TG class in Ref. [25], the mobile phase composition corresponds to 96% of mobile phase A and 4% of mobile phase B. An inox tubing of narrow diameter was added to achieve a 33 bars counter pressure. Repeatability was assessed by calculating the standard deviation of ion B intensities measured from three consecutive injections of each oil.

2.9. Statistical analysis

The comparison of % FA values calculated from ion B intensities with reference values obtained by GC-FID was performed using the Real Statistics Resource Pack for Excel available at https://www.real-statistics.com/.

3. Results and discussion

3.1. TGs fragmentation in positive mode mass spectrometry

The fragmentation principles of TGs are well documented [26–28]. The structure of TGs fragment ions and the corresponding notation used in the present work are adapted from Ref. [26] and presented in Fig. 1. Starting from the $[M+H]^+$ adduct, ion A and ion B correspond to the loss of one or two acyl chains respectively. Ion C is the acylium ion issued from ion B. Ions $[M+H]^+$, ions B and ions C can undergo dehydration to form the corresponding $[M+H-H_2O]^+$, B–H_2O and C–H_2O ions (not presented in Fig. 1). To represent an ion B or C containing one FA or an ion A (two FAs) the notation will be A(FA/FA), B(FA) or C(FA).

A combination of three acyl chains is present in $[M+H]^+$ TG ions whereas ions A incorporate two acyl chains. Isobaric $[M+H]^+$ or ions A can be encountered that incorporate different FA combinations. For example, TG(18:0/18:0/18:0) and TG(18:0/16:0/20:0) or A(18:1/20:0) and A(18:0/20:1). Such isobaric ions can be distinguished by examining their fragment ions. The situation is much simpler with ions B where a single acyl chain is linked to the $C_3H_6O_2$ group originating from glycerol. Ions B allow a direct identification of their FA moiety.

Table 1 shows a list of 41 FAs frequently encountered in natural lipid extract. This list was established using LIPIDMAPS "Predict MS/MS spectrum and generate a list of commonly occurring product ions for a glycerolipid (positive ion mode)" [29]. FAs isomers, of identical molecular weight, are gathered on the same line, for example 18:1 (n-9), 18:1 (n-7) and 18:1 (trans). Only the name and abbreviation of the most frequently encountered isomer is reported for sake of simplification in column 1 and 2. This corresponds to the 1st isomer column 3. The other possible isomers are shown next to. The double bonds positions and trans isomerism are indicated between brackets. The exact masses of characteristic ions and fragment ions issued from homotriacylglycerols corresponding to those 41 FAs are also reported in Table 1.

3.2. Ions B specificity

Since this study aims at predicting the TGs primary composition from the intensities of ions B produced by in-source fragmentation, it is of critical importance to verify the absence of interfering isobaric ions. Thanks to the NPLC method used herein [25], TGs are separated from other lipid classes present in complex lipid extracts. An example of Lipowheat® and bovine heart lipid extract is presented in Fig. S1. In oil samples and/or when a lipid classes separation is performed, only ions originating from TGs themselves or TGs fragment ions have to be considered as possible interfering ions.

Table 1 is non-exhaustive since TGs may contain three different FAs. From the 41 FAs listed and taking into account all the FA isomers [30], it is statistically possible to compose 68921 TGs (41 [3]) and 1681 ions A (41 [2]).

Starting from Table 1, we looked for the smallest mass differences between the ions B and the other ions in the table. The corresponding formulas are presented in Table S1. To be more extensive, a Python code was written to calculate the exact mass of the 68921 TG structures and the *m/z* values of all corresponding ions and fragments. In addition to structures containing only ^{12}C, the occurrence of up to three ^{13}C were accounted for in the calculations. The difference in *m/z* values between each ion B and each

Table 1
Calculated exact mass of in-source ions arising from the corresponding **homotriacylglycerols** species (possible isomers of mainly encountered FA are between brackets).

Fatty acyls			Homotriacylglycerols						
Trivial Name	Symbol	FA	$[M+H]^+$	$[M+H-H2O]^+$	Ion A	Ion B	Ion B − H2O	Ion C	Ion C − H2O
Acetic	Ac	2:0	219.08632	201.07575	159.06519	117.05462	99.04406	43.01784	25.00728
Butyric	Bu	4:0	303.18022	285.16965	215.12779	145.08592	127.07536	71.04914	53.03858
Caproic	Co	6:0	387.27412	369.26355	271.19039	173.11722	155.10666	99.08044	81.06988
Caprylic	Cy	8:0	471.36802	453.35745	327.25299	201.14852	183.13796	127.11174	109.10118
Capric	C	10:0	555.46192	537.45135	383.31559	229.17982	211.16926	155.14304	137.13248
Lauric	La	12:0	639.55582	621.54525	439.37819	257.21112	239.20056	183.17434	165.16378
Tridecylic		13:0	681.60277	663.59220	467.40949	271.22677	253.21621	197.18999	179.17943
Myristoleic	My	14:1 (n-5)	717.60277	699.59220	491.40949	283.22677	265.21621	209.18999	191.17943
Myristic	M	14:0	723.64972	705.63915	495.44079	285.24242	267.23186	211.20564	193.19508
Baustoroleic		15:1 (n-6)	759.64972	741.63915	519.44079	297.24242	279.23186	223.20564	205.19508
Baustoric	Bo	15:0	765.69667	747.68610	523.47209	299.25807	281.24751	225.22129	207.21073
Palmitoleic	Po	16:1 (n-7) or (n-9)	801.69667	783.68610	547.47209	311.25807	293.24751	237.22129	219.21073
Palmitic	P	16:0	807.74362	789.73305	551.50339	313.27372	295.26316	239.23694	221.22638
Margarolenic		17:2 (n-5)	837.69667	819.68610	571.47209	323.25807	305.24751	249.22129	231.21073
Margaroleic	Mr	17:1 (n-8)	843.74362	825.73305	575.50339	325.27372	307.26316	251.23694	233.22638
Margaric	Ma	17:0	849.79057	831.78000	579.53469	327.28937	309.27881	253.25259	235.24203
Stearidonic	St	18:4 (n-3)	867.64972	849.63915	591.44079	333.24242	315.23186	259.20564	241.19508
α-Linolenic	Ln	18:3 (n-3) or (n-6)	873.69667	855.68610	595.47209	335.25807	317.24751	261.22129	243.21073
Linoleic	L	18:2 (n-6) trans	879.74362	861.73305	599.50339	337.27372	319.26316	263.23694	245.22638
Oleic	O	18:1 (n-9) or (n-7) trans	885.79057	867.78000	603.53469	339.28937	321.27881	265.25259	247.24203
Stearic	S	18:0	891.83752	873.82695	607.56599	341.30502	323.29446	267.26824	249.25768
Nonadecylic		19:0	933.88447	915.87390	635.59729	355.32067	337.31011	281.28389	263.27333
Timnodinic	EPA	20:5 (n-3)	945.69667	927.68610	643.47209	359.25807	341.24751	285.22129	267.21073
Arachidonic	Ao	20:4 (n-6) or (n-3)	951.74362	933.73305	647.50339	361.27372	343.26316	287.23694	269.22638
Biotaic	Bi	20:3 (n-3) or (n-6) or (n-9)	957.79057	939.78000	651.53469	363.28937	345.27881	289.25259	271.24203
Dihomolinoleic	Dh	20:2 (n-6)	963.83752	945.82695	655.56599	365.30502	347.29446	291.26824	273.25768
Gondoic	Go	20:1 (n-9) or (n-11)	969.88447	951.87390	659.59729	367.32067	349.31011	293.28389	275.27333
Arachidic	A	20:0	975.93142	957.92085	663.62859	369.33632	351.32576	295.29954	277.28898
Heneicosylic		21:0	1017.97837	999.96780	691.65989	383.35197	365.34141	309.31519	291.30463
Cervonic	DHA	22:6 (n-3)	1023.74362	1005.73305	695.50339	385.27372	367.26316	311.23694	293.22638
Clupanodonic	DPA	22:5 (n-3) or (n-6)	1029.79057	1011.78000	699.53469	387.28937	369.27881	313.25259	295.24203
Adrenic	Ad	22:4 (n-6)	1035.83752	1017.82695	703.56599	389.30502	371.29446	315.26824	297.25768
Behelonelic	Bq	22:3 (n-6) or (n-3)	1041.88447	1023.87390	707.59729	391.32067	373.31011	317.28389	299.27333
Diplotaxic	Di	22:2 (n-6)	1047.93142	1029.92085	711.62859	393.33632	375.32576	319.29954	301.28898
Erucic	Er	22:1 (n-9) or (n-7) or (n-11)	1053.97837	1035.96780	715.65989	395.35197	377.34141	321.31519	303.30463
Behenic	B	22:0	1060.02532	1042.01475	719.69119	397.36762	379.35706	323.33084	305.32028
Tricosylic	Tr	23:0	1102.07227	1084.06170	747.72249	411.38327	393.37271	337.34649	319.33593
Nervonic	Ne	24:1 (n-9)	1138.07227	1120.06170	771.72249	423.38327	405.37271	349.34649	331.33593
Lignoceric	Lg	24:0	1144.11922	1126.10865	775.75379	425.39892	407.38836	351.36214	333.35158
Hyenic	Hn	25:0	1186.16617	1168.15560	803.78509	439.41457	421.40401	365.37779	347.36723
Cerotic	Ce	26:0	1228.21312	1210.20255	831.81639	453.43022	435.41966	379.39344	361.38288

other ion was computed, and the minimal $\Delta m/z$ appeared to be 0.0065. The quasi-isobaric interference occurs between ions B from C13:0, C15:0 and C15:1 FAs and the isotope cluster of ion $C-H_2O$ from C20:4, C22:4 and C22:5 respectively. More precisely, the third isotopic ion of $C-H_2O$ involving two ^{13}C. This third ion of the isotopic cluster accounts for about 2.2–2.7% of the intensity of the corresponding monoisotopic $C-H_2O$ ions. Hence, this $\Delta m/z$ appear to be the practical limit and corresponds to a minimal resolution (FWHM) of about 60 000 @m/z 400 that is required to separate ions B from other ions issued from the in-source fragmentation of TGs.

3.3. Working concentrations range

The working range was determined from 8 homotriacylglycerols standards over 5 concentrations ranging from 0.05 to 1 g/l (0.05; 0.25; 0.5; 0.75 and 1 g/l), analyzed by FIA and presented in Fig. S2. Ions B intensities increase with the homotriacylglycerols concentrations. The 4 darker curves represent the ions B most often encountered in the selected oil set (P, Ln, L and O). It is worthy to note that the detector saturation occurs at the concentration of 1 g/l for La, L and O. The best working range appears to be between 0.25 and 0.75 g/l (0.5 and 1.5 μg injected). In this mass range the response can be considered as almost linear.

3.4. In-source FIA-APPI$^+$-HRMS ionization of homotriacylglycerols standards

The 8 homotriacylglycerols standards at the concentration of 0.75 g/l were used to evaluate the relative abundance of each characteristic ion, the results are given in Table S2. The results obtained were found to be consistent with the work of Holčapek et al. [26] using non-aqueous reversed-phase (NARP) coupled to APCI$^+$. In brief, ions [M+H]+are inconstantly observed. Ions A intensity diminishes with the growing number of unsaturation whereas adduct ion [M+H]+increases (and can represent the base peak). At the opposite, ions B intensities appear to be less variable. Ion B intensity is always non-zero whatever is the FA and should then be exploitable. Moreover, ions B relative intensities range between 1.11 and 1.96% and are thus relatively homogenous.

3.5. Plant oils selection and analysis by GC-FID

The oils were selected to cover the greatest diversity and percentage of FAs. To determine the exact composition of the oil samples used in this study, the FA composition of the plant oils was determined by GC-FID. The results are presented in Table S3. These results are used as reference values throughout the article. The oils are ordered according to increasing average molecular weight of the FAs.

Values from this table were included in the calculation with the following changes. First, as positional isomers of unsaturated FAs correspond to the same ion B their respective percentages were summed. Second, since the working range of the mass spectrometer was set between m/z 200 and 1500, B(6:0) at m/z 173.11722 was excluded. Hence, 20 FAs measured by GC-FID in plant oil samples were considered in the calculations.

3.6. Calibration and validation sets

It is well known that certain FAs are predominantly esterified in a preferred position (*sn*-1/3 or 2). For example, unsaturated fatty acyls tend to occupy the middle *sn*-2 position, especially the linoleoyl in plant oils [26]. On the other hand, it is also known that, the loss of RCOOH from the equivalent side positions *sn*-1 and *sn*-3 is preferred comparing to the cleavage from the middle position *sn*-2 [31,32]. This specificity is used for the determination of the positions *sn*-1/3 and *sn*-2. Indeed, the A_{12} and A_{23} are more abundant than the A_{13} ion [26].

It is mainly for these two reasons that the choice to use plant oils as a calibrator rather than synthetic standards. We hypothesize that the influence of the position of FAs on glycerol is compensated by the use of natural standards of origin close to the samples to be analyzed. This strategy also has the advantage of being less expensive.

The 20 plant oils are separated in two distinct sets. The calibration and validation set, each set gathering 10 oils. The oils selected for the calibration set were chosen according to 2 criteria: the greatest diversity of FA and the widest FA percent range.

3.7. Ions B extraction

A flowchart of this step is presented Fig. S3. The intensities of the 500 most abundant ions are collected in the [200–460] m/z range for each plant oil samples, corresponding to the mass range of ions B in Table 1 (B(8:0)-B(26:0)). Before extracting the intensity of each ion B form the MS data, a correction is applied to the m/z values to account for the spectrometer mass accuracy. This correction (of about 0.002 u) is calculated as the mean difference observed between exact mass and measured mass of ion B corresponding to the 3 or 4 most frequent FA encountered in each oil samples.

The exact m/z values of the 20 selected FAs rounded to the fourth decimal place are then compared to experimental values issued from mass spectra using a lab made python code presented Fig. S4. The matching algorithm selects the ions with an m/z value tolerance of ±0.002 u to account for mass spectrometric precision.

3.8. Comparisons: % FAs vs % intensities of ions B

A comparison between the FAs relative composition of the calibration set and validation set oils as measured by GC-FID and the relative intensities of the corresponding ions B obtained from either FIA or NPLC is shown in Fig. 2. To simplify, only the FAs representing 3% or more are presented. The distribution profiles based on ions B intensities appear to be fairly comparable to the primary composition of TGs as measured by the GC-FID reference method. Only C18:3 rich oils (sacha inchi, cassis, hemp, borage, camelina) show a more marked difference. The ions B(18:3) intensities are systematically lower than expected. Apart C18:3, no systematic trend is observed for the other FAs. The prediction of the FAs composition from the ions B intensities thus needs the calculation of weighting coefficients to account for their response characteristics.

3.9. Weighting coefficient calculation and validation

The calibration set was used to calculate the coefficients to be applied for each ion B. These coefficients are then validated by the prediction of the FA composition of TG of validation set.

The following formula expresses the percentage $\widehat{\%FA_i}$ of the ith FA over the n FA to be calculated using the ion B intensities:

$$\widehat{\%FA_i} = w_i IB_i \frac{\sum_{i=1}^{n} \%FA_i}{\sum_{i=1}^{n} w_i IB_i} \quad (1)$$

where w_i is the weighting coefficient to be applied to the corresponding ion B intensity (I_{Bi}) and $\%FA_i$ is the percentage of the ith FA in the composition of the oil considered as measured by the reference method (GC-FID).

w_i are calculated using Microsoft Excel Solver using the

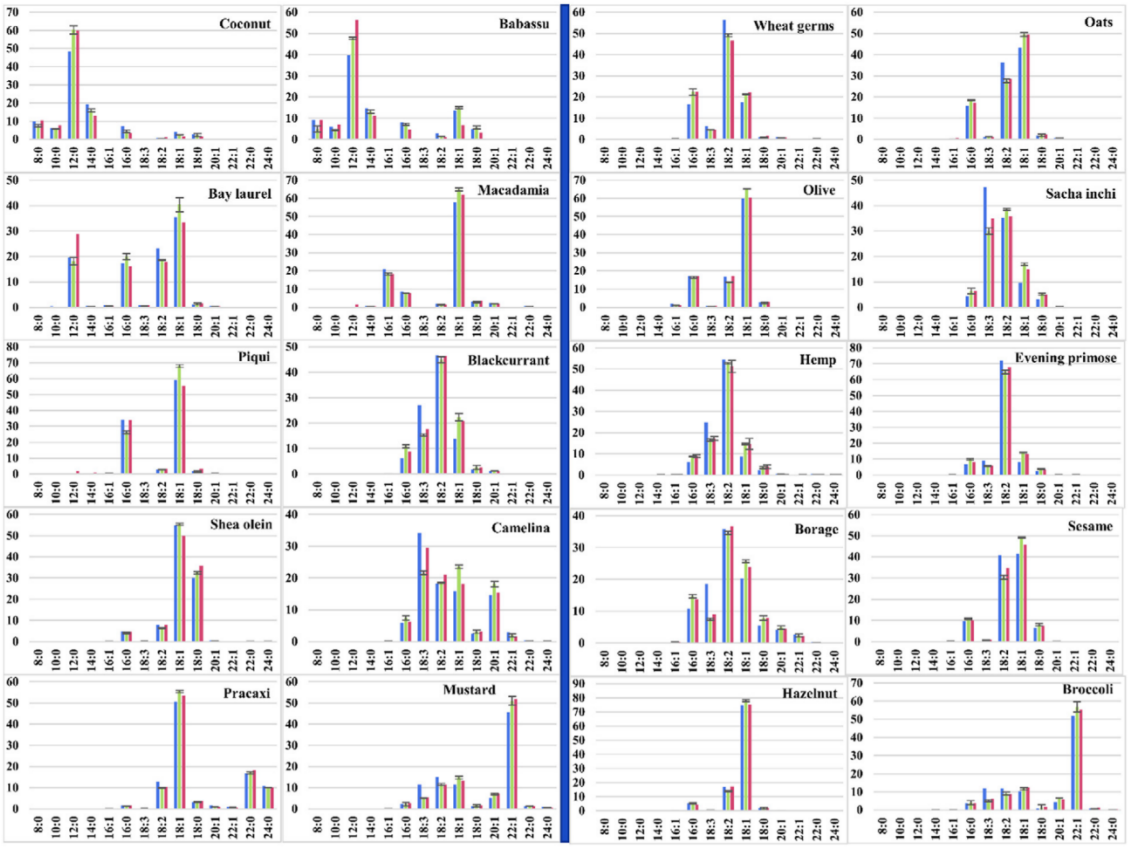

Fig. 2. Relative FA composition of calibration set oils (left) and validation set oils (right) measured by GC-FID (blue) compared to relative ion B intensities obtained by FIA (green) or NPLC (red). Error bars represent two standard deviations of the mean. (For interpretation of the references to colour in this figure legend, the reader is referred to the Web version of this article.)

Evolutionary Solving method. The constrains applied to the w_i coefficient are $0.05 \leq w_i \leq 1.0$. The solver minimizes the sum of the squared differences (SSD) between the reference values (GC-FID) of FA composition and values calculated through eqn (1). The SSD is the sum of the individual SSD calculated for each of the plant oils. There is as much w_i as FA to calculate, and the corresponding model involves a significant degree of complexity.

Eqn (1) is used to predict the FA composition of the validation set. The sum of the % FA is set to 100 as the ion B list is representative of the FA diversity in the validation set. The w_i coefficients are the values calculated from the calibration set. The organization of the Excel spreadsheet is presented in Fig. S5.

3.10. Weighting coefficient

All values of w_i are presented in Fig. S6 together with the occurrence of the corresponding FAs in oil samples from the calibration set (FA% measured by GC-FID). The w_i calculated from a large number of values and a wide % range are presumably the most relevant. This is the case for the w_i of the most abundant FAs such as C16:0, C18:3, C18:2, C18:1, C18:0.

w_i is inversely proportional to its response coefficient FAs. The C18:3 FA was found underestimated in Fig. 2 and S5 when assessed from the corresponding ion B intensity. Accordingly, w_i for C18:3 FA is the largest of the dataset and reaches the maximum value of 1.0. Other C18 FAs show decreasing values of w_i as their number of double bounds decreases. No noticeable trends appear for other FAs whose w_i range from 0.4 to 0.7.

Differences appear between w_i calculated from FIA or NPLC ions B intensities. When calculated from FIA, short chain FAs (C8:0 to C14:0) show higher w_i coefficients data compared to w_i obtained from NPLC. At the opposite, longer FAs (C16 and upper) show slightly higher w_i coefficients issued from NPLC.

The relevance of the calculation has been verified from two angles. First, for each individual FA, by evaluating the relationship between the predicted concentrations and GC-FID reference values. In a second step, the evaluation is carried out on the basis of the natural oil samples FA distribution by comparing the FA composition of TGs estimated based on ions B intensities with GC-FID data.

3.11. Individual FA prediction and testing

Fig. 3 presents the scatter plots of the $\widehat{\%FA_i}$ predictions from FIA/APPI$^+$ HRMS data vs GC reference values for the calibration (blue square points) and validation (red points) sets. Except for two FAs (C18:4 and C20:3) scarcely abundant in both sets, the scatter plots suggest a good agreement between prediction and reference data as trend lines pass through the origin and the slopes appear close to one. A similar tendency can be seen for the $\widehat{\%FA_i}$ predictions issued form NPLC/APPI$^+$ HRMS data in Fig. S7.

As both reference and test method are subject to random error, a

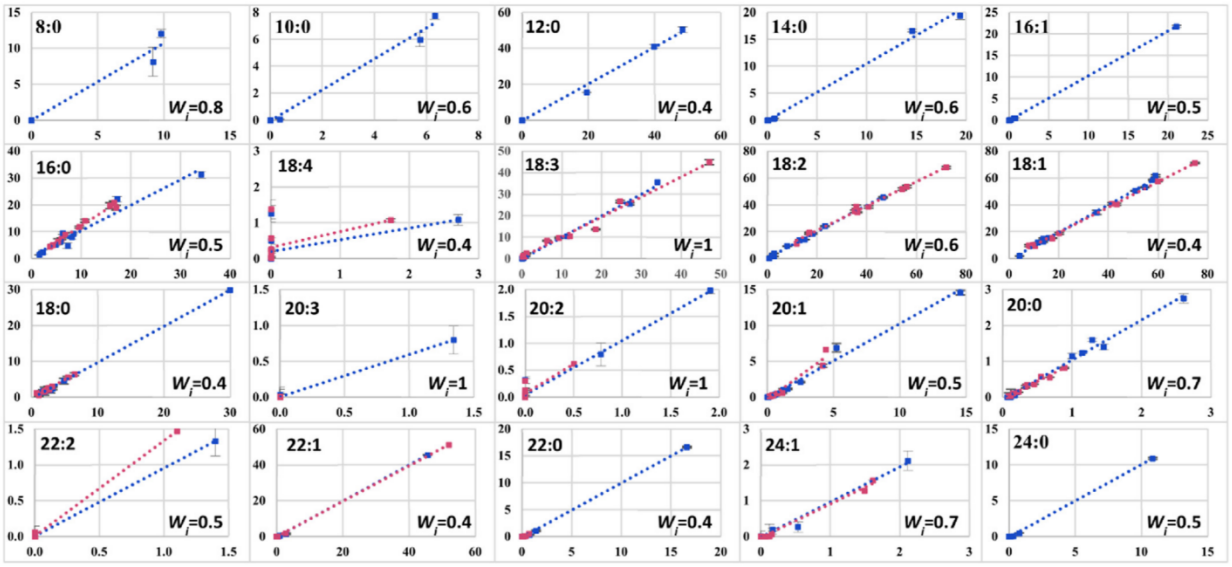

Fig. 3. FIA-APPI + -HRMS individual FA prediction and validation. Regression lines for predicted (Y-axis) vs GC-FID (X-axis). Blue lines are for the calibration set and red lines for the validation set. (For interpretation of the references to colour in this figure legend, the reader is referred to the Web version of this article.)

deeper examination the agreement between the FA prediction and GC-FID reference was realized by applying Deming Regression [33] with $\lambda = 4$. Table S4 summarizes the results obtained for 10 FAs retrieved in sufficient number and quantity in both sets to calculate the regressions statistics. Among them, C16:0, C18:0, C18:1, C18:2 and C18:3 appeared to be ubiquitous and present over a wide range of percentage in both calibration and validation set samples. Consequently, their statistical figures of merit are thought to be the most relevant for both FIA and NPLC issued predictions.

For those 5 FAs and in both calibration or validation sets, the adjustment quality of the linear model as measured by the determination coefficient (R^2) is high, standing at 0.9430 in the worst case and being most of time $\geq$ 0.98. For the calibration set, the intercept and the slope of the regression lines meet the criteria of being non-significantly different from zero or unity, respectively. At first glance, this last criterion is not met for C18:2 and C18:1 in the FIA/APPI$^+$HRMS validation set where slopes of 0.91 and 0.94 deviate from unity. This is also the case for C18:1 slope (0.94) in the NPLC/APPI$^+$HRMS validation set. A closer examination of the corresponding data shows that the validation set contains C18:1 and C18:2 in extreme proportions, superior to that of the calibration set. When removing the data point 72% corresponding to the C18:2% contained in evening primrose or 74.8% corresponding to C18:1 in hazelnut, both of these two FAs present slopes not differing from unity. It is of common practice to place the extreme values in the calibration set, but the natural origin of the oil samples did not allow this criterion to be met for all FAs. Despite their lesser abundance of the remaining FAs (in number and quantity), the statistics calculated for C16:1, C20:0, C20:1, C22:0 and C24:0 support the same conclusions.

At this stage and within the limits of our experiments, we can conclude that the two methods, GC-FID or the $\widehat{\%FA_i}$ predictions from FIA or NPLC APPI$^+$HRMS provide equivalent results and should be applicable whatever is the FA structure.

3.12. Natural oil samples FA distribution

In Fig. 4, the FAs relative quantities measured by GC-FID are compared to those predicted from ions B intensities measured from FIA and NPLC- APPI$^+$-HRMS and corrected by applying the w_i coefficients. As for Fig. 2, only FAs of more than 3% in Table S5 are reported. Compared to Fig. 2 and S5, Fig. 4 shows a much closer agreement between GC-FID data and FIA or NPLC. The C18:3 FA that was constantly underestimated when using ion B intensity in Fig. 2 and S5 is now close to the reference values.

Table S5 allows a comparison of the relative composition of oil samples over all 20 FAs. In the case of quantitatively major lipids, such as linoleic acid (C18:2), differences of up to 6% are observed. Thus, even though the FA composition results of the oils differ between the two methods, the composition profile is almost similar.

3.13. Limit of detection and quantification

C18:4 and C20:2 are two FAs reported as minor constituents (<3% et < 2% respectively) in a limited number of plant oils. Nevertheless, in the whole oils set, C18:4 is reported 17 times by FIA, 13 times by NPLC and only 2 times in the reference GC-FID data (blackcurrant 2.71% and hemp1.73%). C20:2 is reported 13 times by FIA, 9 times by NPLC and only 3 times by GC-FID (camelina 1.91%, mustard 0.78% and broccoli 0.5%).

In the literature, C18:4 was reported in borage [34–36] and primrose [36] oils. Similarly, C20:2 occurs in hemp and borage oils [37] and was measured in blackcurrant (0.07%), primrose (0.004%) and wheat (0.05%) oils by NARP-APCI [38].

The FIA or NPLC-APPI$^+$-HRMS methods we propose, appear to present a more favorable LOD/LOQ than the GC-FID for C18:4 and C20:2. At the opposite, with long to very long FAs (C20:1, 20:0, C22:1, C22:0, C24:1, C24:0) the ions B are sometimes not retrieved whereas they are quantified by the GC-FID method. However, those cases appear for low values ($\leq$0.18%).

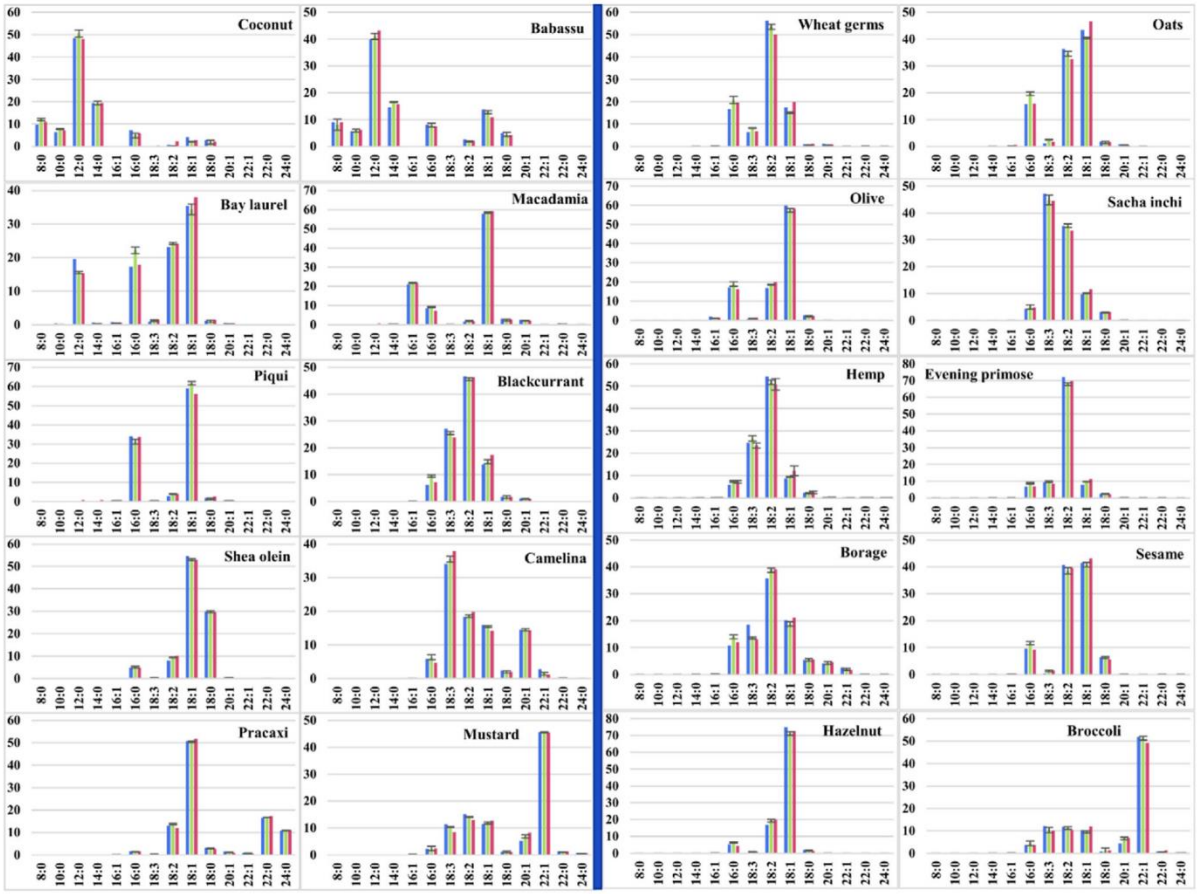

Fig. 4. Relative FAs compositions measured by GC-FID (blue) compared to predicted values obtained by FIA (green) or NPLC-HRMS (red) using w_i coefficients. Error bars represent two standard deviations of the mean. Calibration set at the left of the figure and validation set at right. (For interpretation of the references to colour in this figure legend, the reader is referred to the Web version of this article.)

4. Conclusion

Ions B issued from the TGs $APPI^+$ in-source fragmentation are always observed in our analysis conditions. By considering the 41 most frequently observed FAs, all possible combinations of TGs and their fragment ions were calculated. As a result, ions B *m/z* values are specific of their constituting FA provided that the mass spectrometer is capable of distinguishing ions differing by about 0.0065 amu through the ion B measuring region.

Ions B relative intensities measured by FIA and NPLC-$APPI^+$-HRMS in TGs mass spectra issued from 20 plant oil samples are close from the relative FAs quantities determined by GC-FID. This observation allows a rapid estimate of the FAs distribution in the TGs lipid class. However, it should be noted that for C18:3 rich oils, GC-FID and ions B intensity diverge. This is due to the response coefficient of B(C18:3) which appears to be half that of the other ions B.

Weighting coefficients w_i are computed to account for the ions B response characteristics. The calculation process makes uses of a calibration set of 10 plant oils. A validation set made up of 10 other plant oils is used to evaluate the model fit. Both sets are fully characterized by GC-FID. After applying the w_i weighting coefficients, the FAs distribution profiles are close to the FAs relative composition measured by GC-FID.

The results achieved for the most frequently encountered FAs in our samples (C16:0, C18:0, C18:1, C18:2, C18:3, C20:0) show a wide dynamic range. The precision of the FIA or NPLC method appears to be of the same order of magnitude than the GC-FID method. The limits of detection and quantification appear to be of the same order of magnitude than the GC-FID and all FAs reported at more than 0.20% by the reference method are detected.

A key point of the method is that there is almost no need for sample preparation since the only prerequisite is to solubilize the sample. Retrieval of ions B intensities from HRMS data together with the calculation of FAs relative composition can be readily automated for a quick and reliable data treatment.

Ions B are present in the mass spectra of lipids that includes a glycerol backbone esterified by at least one FA. This is the case of, for example, PLs. The full potential of this method remains to be studied for these other lipid classes. This opens the perspective of a rapid assessment of the FAs composition for these lipid classes within a single analysis of a total lipid extract.

CRediT authorship contribution statement

Sonia Abreu: Conceptualization, Methodology, Validation, Formal analysis, Investigation, Writing – original draft, Visualization. **Sylvie Heron:** Manuscript review and scientific discussion.

Audrey Solgadi: Instrumental assistance in mass spectrometry, manuscript review. **Florent Joffre:** GC/MS FAMES analysis. **Alain Tchapla:** Manuscript review and scientific discussion. **Pierre Chaminade:** Resources, Project administration, Supervision, Chemometrics, Writing – review & editing.

Declaration of competing interest

The authors declare that they have no known competing financial interests or personal relationships that could have appeared to influence the work reported in this paper.

Appendix A. Supplementary data

Supplementary data to this article can be found online at https://doi.org/10.1016/j.aca.2021.338809.

References

[1] P. Fagone, S. Jackowski, Membrane phospholipid synthesis and endoplasmic reticulum function, J. Lipid Res. 50 (Supplement) (2009) S311–S316, https://doi.org/10.1194/jlr.R800049-JLR200.

[2] G. van Meer, D.R. Voelker, G.W. Feigenson, Membrane lipids: where they are and how they behave, Nat. Rev. Mol. Cell Biol. 9 (2) (2008) 112–124, https://doi.org/10.1038/nrm2330.

[3] E. Tvrzicka, L.-S. Kremmyda, B. Stankova, A. Zak, Fatty acids as biocompounds: their role in human metabolism, Health and disease - a review. Part 1: classification, dietary sources and biological functions, Biomed. Pap. 155 (2) (2011) 117–130, https://doi.org/10.5507/bp.2011.038.

[4] L.-S. Kremmyda, E. Tvrzicka, B. Stankova, A. Zak, Fatty acids as biocompounds: their role in human metabolism, Health and disease - a review. Part 2: fatty acid physiological roles and applications in human Health and disease, Biomed. Pap. 155 (3) (2011) 195–218, https://doi.org/10.5507/bp.2011.052.

[5] M. David, C. Lejeune, S. Abreu, A. Thibessard, P. Leblond, P. Chaminade, M.-J. Virolle, Negative correlation between lipid content and antibiotic activity in streptomyces: general rule and exceptions, Antibiotics 9 (6) (2020) 280, https://doi.org/10.3390/antibiotics9060280.

[6] J. Zhang, Q. Liang, Z. Xu, M. Cui, Q. Zhang, S. Abreu, M. David, C. Lejeune, P. Chaminade, M.-J. Virolle, D. Xu, The inhibition of antibiotic production in streptomyces coelicolor over-expressing the TetR regulator SCO3201 IS correlated with changes in the lipidome of the strain, Front. Microbiol. 11 (2020) 1399, https://doi.org/10.3389/fmicb.2020.01399.

[7] A. Millan-Oropeza, R. Rebois, M. David, F. Moussa, A. Dazzi, J. Bleton, M.-J. Virolle, A. Deniset-Besseau, Attenuated total reflection fourier transform infrared (ATR FT-IR) for rapid determination of microbial cell lipid content: correlation with gas chromatography-mass spectrometry (GC-MS), Appl. Spectrosc. 71 (10) (2017) 2344–2352, https://doi.org/10.1177/0003702817709459.

[8] S. Wu, C. Hu, X. Yang, Q. Tan, S. Yao, Y. Zhou, X. Wang, X. Sun, Molybdenum induces alterations in the glycerolipidome that confer drought tolerance in wheat, J. Exp. Bot. 71 (16) (2020) 5074–5086, https://doi.org/10.1093/jxb/eraa215.

[9] T. Liu, J. Chen, F. Xu, X. He, S. Yang, Y. Zhu, W. Li, G. Zheng, Analysis of changes in the panax notoginseng glycerolipidome in response to long-term chilling and heat, Plant Divers 42 (2) (2020) 102–110, https://doi.org/10.1016/j.pld.2019.11.002.

[10] L. Dalheim, J.B. Svenning, H.C. Eilertsen, T. Vasskog, R.L. Olsen, Stability of lipids during wet storage of the marine diatom porosira glacialis under semi-preserved conditions at 4 and 20 °C, J. Appl. Phycol. (2020), https://doi.org/10.1007/s10811-020-02292-0.

[11] J. Jouhet, J. Lupette, O. Clerc, L. Magneschi, M. Bedhomme, S. Collin, S. Roy, E. Maréchal, F. Rébeillé, LC-MS/MS versus TLC plus GC methods: consistency of glycerolipid and fatty acid profiles in microalgae and higher plant cells and effect of a nitrogen starvation, PloS One 12 (8) (2017), e0182423, https://doi.org/10.1371/journal.pone.0182423.

[12] C. Degraeve-Guilbault, C. Bréhélin, R. Haslam, O. Sayanova, G. Marie-Luce, J. Jouhet, F. Corellou, Glycerolipid characterization and nutrient deprivation-associated changes in the green picoalga *Ostreococcus tauri*, Plant Physiol. 173 (4) (2017) 2060–2080, https://doi.org/10.1104/pp.16.01467.

[13] Y. Meng, X. Cao, C. Yao, S. Xue, Q. Yang, Identification of the role of polar glycerolipids in lipid metabolism and their acyl attribution for TAG accumulation in nannochloropsis oceanica, Algal Res. 24 (2017) 122–129, https://doi.org/10.1016/j.algal.2017.03.004.

[14] S. Khoury, C. Canlet, M. Lacroix, O. Berdeaux, J. Jouhet, J. Bertrand-Michel, Quantification of lipids: model, reality, and compromise, Biomolecules 8 (4) (2018) 174, https://doi.org/10.3390/biom8040174.

[15] X. Han, H. Ye, Overview of lipidomic analysis of triglyceride molecular species in biological lipid extracts, J. Agric. Food Chem. (2021), https://doi.org/10.1021/acs.jafc.0c07175 acs.jafc.0c07175.

[16] T.L. Nguyen, D. Hlangothi, M.A. Saleh, Characterization of silybum marianum triacylglycerol regioisomers using accurate mass quadrupole time of flight mass spectrometry, Cogent Chem. 4 (1) (2018), https://doi.org/10.1080/23312009.2018.1477246.

[17] V. Guarrasi, M.R. Mangione, V. Sanfratello, V. Martorana, D. Bulone, Quantification of underivatized fatty acids from vegetable oils by HPLC with UV detection, J. Chromatogr. Sci. 48 (8) (2010) 663–668, https://doi.org/10.1093/chromsci/48.8.663.

[18] M. Li, E. Baughman, M.R. Roth, X. Han, R. Welti, X. Wang, Quantitative profiling and pattern analysis of triacylglycerol species in arabidopsis seeds by electrospray ionization mass spectrometry, Plant J. 77 (1) (2014) 160–172, https://doi.org/10.1111/tpj.12365.

[19] A. Acheampong, N. Leveque, A. Tchapla, S. Heron, Simple complementary liquid chromatography and mass spectrometry approaches for the characterization of triacylglycerols in pinus Koraiensis seed oil, J. Chromatogr. A 1218 (31) (2011) 5087–5100, https://doi.org/10.1016/j.chroma.2011.05.064.

[20] M.Á. Rincón-Cervera, V. González-Barriga, R. Valenzuela, S. López-Arana, J. Romero, A. Valenzuela, Profile and distribution of fatty acids in edible parts of commonly consumed marine fishes in Chile, Food Chem. 274 (2019) 123–129, https://doi.org/10.1016/j.foodchem.2018.08.113.

[21] J.L. Slater-Jefferies, S.P. Hoile, K.A. Lillycrop, P.A. Townsend, M.A. Hanson, G.C. Burdge, Effect of sex and dietary fat intake on the fatty acid composition of phospholipids and triacylglycerol in rat heart, Prostaglandins Leukot. Essent. Fat. Acids PLEFA 83 (4–6) (2010) 219–223, https://doi.org/10.1016/j.plefa.2010.07.006.

[22] G.C. Burdge, P. Wright, A.E. Jones, S.A. Wootton, A Method for Separation of Phosphatidylcholine, Triacylglycerol, Non-esterified Fatty Acids and Cholesterol Esters from Plasma by Solid-phase Extraction, vol. 7, 2000.

[23] J. Zou, Q. Zhang, Z. Zhu, L. Gao, Y. Zheng, D. Li, Embryogenic callus induction and fatty acid composition analysis of oil palm (elaeis guineensis cv. Tenera), Sci. Hortic. 245 (2019) 125–130, https://doi.org/10.1016/j.scienta.2018.10.014.

[24] V.J. Sinanoglou, D. Meimaroglou, S. Miniadis-Meimaroglou, Triacylglycerols and their fatty acid composition in edible mediterranean molluscs and Crustacean, Food Chem. 110 (2) (2008) 406–413, https://doi.org/10.1016/j.foodchem.2008.02.035.

[25] S. Abreu, A. Solgadi, P. Chaminade, Optimization of normal phase chromatographic conditions for lipid analysis and comparison of associated detection techniques, J. Chromatogr. A (2017), https://doi.org/10.1016/j.chroma.2017.07.063.

[26] M. Holčapek, P. Jandera, P. Zderadička, L. Hruba, Characterization of triacylglycerol and diacylglycerol composition of plant oils using high-performance liquid chromatography–atmospheric pressure chemical ionization mass spectrometry, J. Chromatogr. A 1010 (2) (2003) 195–215.

[27] M. Holčapek, P. Jandera, J. Fischer, B. Prokeš, Analytical monitoring of the production of biodiesel by high-performance liquid chromatography with various detection methods, J. Chromatogr. A 858 (1) (1999) 13–31, https://doi.org/10.1016/S0021-9673(99)00790-6.

[28] P. Geng, J.M. Harnly, P. Chen, Differentiation of whole grain from refined wheat (T. Aestivum) flour using lipid profile of wheat bran, germ, and endosperm with UHPLC-HRAM mass spectrometry, J. Agric. Food Chem. 63 (27) (2015) 6189–6211, https://doi.org/10.1021/acs.jafc.5b01599.

[29] LIPID MAPS Lipidomics Gateway http://www.lipidmaps.org/tools/structuredrawing/GL_p_form.php (accessed Feb 12, 2019).

[30] D. Libong, S. Héron, A. Tchapla, P. Chaminade, Lipid analysis with the corona CAD, in: Charged Aerosol Detection for Liquid Chromatography and Related Separation Techniques, John Wiley & Sons, Ltd, 2017, pp. 221–287, https://doi.org/10.1002/9781119390725.ch5.

[31] A. Jakab, K. Heberger, E. Forgacs, Comparative analysis of different plant oils by high-performance liquid chromatography–atmospheric pressure chemical ionization mass spectrometry, J. Chromatogr. A 976 (1) (2002) 255–263.

[32] W.E. Neff, W.C. Byrdwell, Characterization of model triacylglycerol (triolein, trilinolein and trilinolenin) autoxidation products via high-performance liquid chromatography coupled with atmospheric pressure chemical ionization mass spectrometry, J. Chromatogr. A 818 (2) (1998) 169–186, https://doi.org/10.1016/S0021-9673(98)00553-6.

[33] C. Wu, J.Z. Yu, Evaluation of linear regression techniques for atmospheric applications: the importance of appropriate weighting, Atmospheric Meas. Technol. 11 (2) (2018) 1233–1250, https://doi.org/10.5194/amt-11-1233-2018.

[34] E.A. Miles, T. Banerjee, M.M.B.W. Dooper, L. M'Rabet, Y.M.F. Graus, P.C. Calder, The influence of different combinations of γ-linolenic acid, stearidonic acid and EPA on immune function in healthy young male subjects, Br. J. Nutr. 91 (6) (2004) 893, https://doi.org/10.1079/BJN20041131.

[35] J.P. Arm, J.A. Boyce, L. Wang, H. Chhay, M. Zahid, V. Patil, U. Govindarajulu, P. Ivester, K.L. Weaver, S. Sergeant, E. Israel, F.H. Chilton, Impact of botanical oils on polyunsaturated fatty acid metabolism and leukotriene generation in mild asthmatics, Lipids Health Dis. 12 (1) (2013) 141, https://doi.org/10.1186/

1476-511X-12-141.
[36] L. Sabikhi, M.H. Sathish Kumar, Fatty acid profile of unconventional oilseeds, in: Advances in Food and Nutrition Research, vol. 67, Elsevier, 2012, pp. 141–184, https://doi.org/10.1016/B978-0-12-394598-3.00004-6.
[37] A. Bialek, M. Bialek, M. Jelinska, A. Tokarz, Fatty acid composition and oxidative characteristics of novel edible oils in Poland, CyTA - J. Food 1–8 (2016), https://doi.org/10.1080/19476337.2016.1190406.
[38] M. Lísa, M. Holčapek, Triacylglycerols profiling in plant oils important in food industry, dietetics and cosmetics using high-performance liquid chromatography–atmospheric pressure chemical ionization mass spectrometry, J. Chromatogr. A 1198–1199 (Supplement C) (2008) 115–130, https://doi.org/10.1016/j.chroma.2008.05.037.

3. Conclusion

L'ionisation en source de la classe des TGs a été étudiée à l'aide de huit standards mono-moléculaires. Les résultats obtenus sont comparables (Table S2) à ceux d'Holčapek et al. [186]. L'ion $[M+H]^+$ n'est pas formé en source lors de l'ionisation des TGs saturés. Son intensité augmente avec le nombre d'insaturations. L'ion $[M+H]^+$ devient majoritaire à partir de 6 insaturations. Cette particularité explique pourquoi les TGs sont rarement analysés sans adduit. L'intensité de tous les autres ions formés en source ont également été étudiés. L'ion A et l'ion B sont les seuls ions à être toujours observés quel que soit le standard utilisé. L'intensité des ions B correspond de manière très stable à 1 à 2 % de l'ion majoritaire.

L'intensité des ions B a également été étudiée en fonction de la concentration en standards mono-moléculaires de TGs (Figure S2). Les résultats montrent une croissance quasi linéaire de l'intensité des ions B avec l'augmentation de la concentration entre 0 et 0,75 g/L. Ces premières données ont conforté notre hypothèse de travail.

Une liste de FAs d'intérêts a été établie d'après les outils de spectrométrie de masse sur le site LIPID MAPS. Cette liste de 41 FAs, les plus couramment rencontrées dans les échantillons naturels, est apparue suffisamment complète par rapport au besoin de l'étude.

Pour vérifier que les ions B sont spécifiques de chaque FAs, un fichier Excel particulièrement volumineux a été créé. A partir des 41 FAs sélectionnés, il est théoriquement possible de former 68921 TGs (41^3). Ainsi, tous les ions pouvant être théoriquement formés en source à partir de ces 68921 TGs ont été édité sur le tableau Excel, en y ajoutant les ions issus de la contribution isotopique du ^{13}C (jusqu'à deux atomes ^{13}C).

Ensuite, le *m/z* de chacun des 41 ions B a été comparé à l'ensemble des *m/z* édités précédemment. Cette comparaison sous forme de soustraction entre les *m/z* a permis de déterminer la résolution minimale nécessaire du spectromètre de masse pour différencier les

ions B de tous les autres ions. Un Δ *m/z* minimal de 0.0065 a été trouvé, ce qui implique une résolution minimale de (FWHM) 60 000 @ *m/z* 400. Le nouveau concept doit donc être mis en œuvre sur des spectromètres de masse ayant un pouvoir de résolution supérieur ou égal à la valeur calculée.

Il a fallu également développer un logiciel sous Python, capable d'extraire de manière automatique les intensités des ions B. Ce logiciel a dû intégrer une fonctionnalité de tolérance des *m/z* pour prendre en compte la précision du spectromètre de masse ainsi que son exactitude.

Les résultats ont montré que pour des huiles contenant peu ou pas de C18 :3, la distribution des intensités des ions B était directement corrélée à la distribution des % de FAs. Pour les huiles riches en C18 :3, comme la cameline, les intensités des ions B étaient systématiquement sous-estimées.

Il a donc été nécessaire de corriger l'intensité des ions B, via un coefficient de pondération. Pour cela, dix huiles ont été utilisées pour la calibration de la méthode et les dix autres huiles pour la validation. L'utilisation de la fonction « Solver » sur le logiciel Excel a permis d'automatiser les ajustements de pondérations de l'intensité des ions B lors de l'étape de calibration. Globalement, l'intensité des ions B(C18 :3) ont été multipliées par 2.

La validation de la méthode a été réalisée selon la régression de Deming. Cette régression permet de prendre en compte les incertitudes expérimentales liées également aux valeurs prises en références. Les résultats statistiques ont montré que pour les FAs dont le nombre de données était suffisants, les régressions issues des courbes de calibration et de validation n'étaient pas statistiquement différentes.

La limite de détection du nouveau concept est comparable à celle pouvant être obtenue par GC-FID. Globalement, tous les FAs détectés à plus de 0,2% par GC-FID ont également été

détectés par les ions B. Le seuil de détection du C18 :4 et C20 :2 semble être plus favorable avec notre méthode et le seuil de détection du C20 :1, C20 :0, C22 :1, C22 :0, C24 :1 et C24 :0 semble être plus favorable avec la méthode GC-FID.

Cette étude a permis de valider le nouveau concept ainsi que d'en poser les bases et les limites. Elle ouvre également la perspective à sa transposition aux classes des PLs.

CHAPITRE VII. EVALUATION DE LA DISTRIBUTION DES ACYLES GRAS DES PHOSPHOLIPIDES ET DES PLASMALOGENES PAR LES IONS B

1. Introduction

Les bases du concept, permettant d'évaluer la distribution des FAs des glycérolipides et des PLs, via l'intensité relative des ions B, ont été posées dans l'étude précédente à travers la classe des TGs contenues dans les huiles végétales. Le choix de ces échantillons a été effectué par rapport aux besoins de la preuve de concept. Cependant, l'évaluation des FAs des huiles végétales par les ions B présente en réalité un avantage limité par rapport à l'utilisation classique de la GC-FID. La méthode de l'ion B devient réellement compétitive lors de l'étude d'extraits lipidiques comprenant plusieurs classes de lipides. Pour ce type d'échantillons, une séparation de lipides par classe est nécessaire avant la mise en œuvre de l'analyse de FAMEs par GC-FID, ce qui limite son emploi.

Cette étude évalue la transposition de la méthode des ions B à la catégorie des PLs. Précédemment, une seule classe de lipides était analysée, alors que dans la présente étude, toutes les classes des PLs sont étudiées. Cela conduit à appliquer la méthode des ions B a des classes de lipides ayant des groupements de têtes polaires différents et des temps d'élution également différents. Il est donc nécessaire d'étudier l'impact de la structure chimique des PLs (groupement polaire/distribution des FAs) et du gradient d'élution sur la formation des ions B.

Pour cela, dix-sept standards issus d'extraits naturels de PLs ont été sélectionnés pour couvrir l'ensemble des classes. Cinq extraits d'origine différente ont pu être sélectionnés pour le PE et PC du fait de leur plus grande disponibilité commerciale.

La source d'ionisation APPI utilisée lors de l'étude précédente, n'était pas disponible pour cette seconde étude. Cela nous a conduits à utiliser la source APCI, plus fréquemment utilisée dans les laboratoires. Cette contrainte a permis de proposer une alternative à l'utilisation de l'APPI pour la mise en œuvre des ions B.

Comme précédemment, l'ensemble des extraits a été analysé par GC-FID pour l'obtention de valeurs de référence. Pour cela, nous avons collaboré avec Justine Bertrand-Michel, Directrice de la plateforme lipidomique MetaToul. La plateforme permet aux utilisateurs de se former aux différentes techniques disponibles, à partir de leurs propres échantillons.

L'estimation de la distribution des FAs des PLs par les ions B et par la GC-FID s'est avérée différente pour quatre extraits (trois extraits de PE et un extrait de PC). Pour comprendre l'origine de ces écarts, nous avons collaboré avec Alice Kermarrec et Anne Meynier de l'INRAe de Nantes. Leur expertise nous a orienté vers une difficulté d'analyse liée à la présence de P-PLs dans ces quatre extraits. Cela nous a amené à développer une stratégie d'analyse spécifique pour les extraits contenant simultanément des diacyl-PLs et des P-PLs.

Ce travail a donné lieu à l'article « Rapid assessment of fatty acyls chains of phospholipids and plasmalogens by atmospheric pressure chemical ionization in positive mode and high-resolution mass spectrometry using in-source generated monoacylglycerol like fragments intensities » publié dans *Journal of Chromatography A*, présenté ci-après.

2. Publication 3

Les données supplémentaires liées à cette publication sont présentées en Annexe III.

Journal of Chromatography A 1673 (2022) 463093

Contents lists available at ScienceDirect

Journal of Chromatography A

journal homepage: www.elsevier.com/locate/chroma

Rapid assessment of fatty acyls chains of phospholipids and plasmalogens by atmospheric pressure chemical ionization in positive mode and high-resolution mass spectrometry using in-source generated monoacylglycerol like fragments intensities

Sonia Abreu[a], Sylvie Héron[b], Audrey Solgadi[c], Bastien Prost[c], Jessica Dalloux-Chioccioli[d,e], Alice Kermarrec[f], Anne Meynier[f], Justine Bertrand-Michel[d,e], Alain Tchapla[b], Pierre Chaminade[a,*]

[a] Lipides: Systèmes Analytiques et Biologiques, Université Paris-Saclay, Chatenay-Malabry 92290, France
[b] ICP - CNRS UMR 8000, (LETIAM), Université Paris-Saclay, Orsay 91400, France
[c] Inserm, CNRS, Ingénierie et Plateformes Au Service de l'Innovation Thérapeutique, IPSIT-SAMM, Université Paris-Saclay, Chatenay-Malabry 92290, France
[d] I2MC, INSERM, Université Toulouse III -Paul Sabatier (UPS), Université de Toulouse, Toulouse, France
[e] MetaboHUB-MetaToul, National Infrastructure of Metabolomics and Fluxomics, Toulouse 31077, France
[f] INRAE, UR BIA, Nantes F-44316, France

ARTICLE INFO

Article history:
Received 2 March 2022
Revised 23 April 2022
Accepted 25 April 2022
Available online 27 April 2022

Keywords:
Phospholipids
Plasmalogens
Fatty acyls composition
Normal phase chromatography
Atmospheric pressure chemical ionization

ABSTRACT

We recently published a new concept using monoacylglycerol-like fragments $[MG+H-H_2O]^+$ (ions B) produced in-source by atmospheric pressure photoionization in positive mode and high-resolution mass spectrometry for the determination of the fatty acyl (FA) composition of triacylglycerols (TGs) from plant oils. This study extends the concept to the phospholipids (PLs) category and shows that the $APCI^+$ source can also be used. Moreover, the coupling with NP-LC allows to simultaneously analyze different PLs classes in the same sample. We compared the relative intensities of the ions B produced in-source to the % composition of FAs determined by GC-FID. In the case of PLs from natural extracts composed exclusively of diacyl-PLs, the relative intensities of ions B are close to the % of the FAs obtained by GC-FID. This approach is not directly useable for extracts containing plasmalogens (P-PLs). For these PLs, acidic hydrolysis by HCl fumes allows hydrolyzing selectively vinyl ether functions to form lyso-PLs. The analysis of hydrolyzed extracts makes it possible to obtain the composition of P-PLs FAs thanks to the lyso-PLs thus formed, while the diacyl-PLs composition remains unchanged. Unlike GC-FID FAs determination, this approach allows a distinction between the diacyl-PLs and P-PLs FAs composition. We also found that the ion B intensities were consistent among the PL classes (PG, PE, PA, PI, CL, PS and PC) and lyso- forms (LPE and LPC). In the case of the diacyl-PLs extracts analyzed, no statistically significant differences were found between the PLs FAs compositions calculated from ion B intensities and the corresponding GC-FID data. A weighting coefficient was applied to correct ion B intensities issued from polyunsaturated FAs with three or more double bonds. The fatty alkenyls composition of P-PLs could also be calculated from the % intensities of specific ions.

© 2022 Elsevier B.V. All rights reserved.

1. Introduction

Phospholipids (PLs) are a family of lipids (termed as the glycerophospholipids category in the Lipidmaps Lipid Classification System [1]), composed of a glycerol skeleton substituted in position *sn*-1 by a radyl, in *sn*-2 by a fatty acyl (FA) and in position *sn*-3 by a phosphate ester group [2]. The polar head in *sn*-3 defines the PL class. The type of radyl in *sn*-1 (ester, vinyl ether or ether) defines the subclass. The structure, name, and abbreviation of the different PL classes and the *sn*-1 and *sn-2* substituents are shown in Fig. 1.

PLs are the main constituents of biological membranes (cells and organelles), but their role in biochemistry is only partially understood [3]. Diacyl-PLs are the most abundant in living beings and are the most commonly studied [4] for this reason.

* Corresponding author.
E-mail address: pierre.chaminade@universite-paris-saclay.fr (P. Chaminade).

https://doi.org/10.1016/j.chroma.2022.463093
0021-9673/© 2022 Elsevier B.V. All rights reserved.

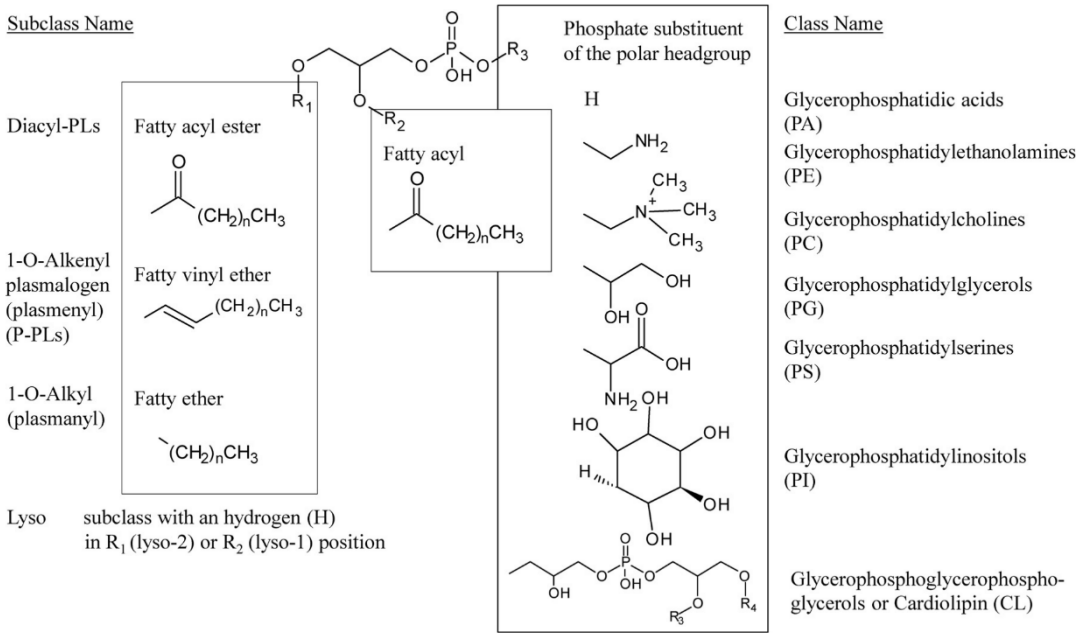

Fig. 1. Structural presentation of the glycerophospholipids (PLs) category. The abbreviations used in the figure are those used in the text. Note that the fatty radyl substituent may present a variable degree of unsaturation.

Plasmalogens (P-PLs), also called plasmenyls, present a vinyl ether bound in *sn*-1 position instead of the ester bound encountered in diacyl-PLs. The long-chain fatty alkenyl R_1 consists almost exclusively of P-16:0, P-18:0, and P-18:1 [5], while the chain R_2 is esterified mainly with n-6 or n-3 polyunsaturated FAs [6]. According to the nomenclature [7], the prefix "P-" before the designation of the fatty alkenyl chain implicitly indicates the occurrence of the vinyl ether double bond. P-PLs represent about 18 to 20% of the total PLs in the cell membranes of almost all mammals [6,8]. Among P-PLs, P-PE is the most commonly encountered [6,9]. P-PC's significant contents are also found, especially in the heart [9]. Other P-PLs are seldomly encountered, such as P-PS in retina tissues [9,10]. P-PLs are involved in neuronal development, immune response (macrophages), cell signaling (lyso-P-PLs) and are also endogenous antioxidants [10,11]. Many pathologies such as neurodegenerative diseases [11,12], obesity [13], diabetes [13], cardiovascular [11], respiratory [9] and ocular [9,10,14] diseases involve a decrease of the P-PLs levels. It is important to note that P-PLs are also present in some anaerobic microorganisms but absent in fungi or plants [15].

Ether PLs are common in inflammatory cell membranes [16]. They are also called plasmanyls and exhibit a fatty alcohol linked through an ether bound to the glycerol phosphate skeleton. The PAF (platelet activation factor) is part of this subclass, and it intervenes in cell signaling [12]. Studies have shown PAF accumulation in Alzheimer's disease and epilepsy [12]. It is complicated to differentiate plasmanyls from plasmalogens by LC-MS. Indeed, when two isobar species belong to these two subclasses, they cannot be distinguished by their exact masses and fragmentation patterns. This issue can be solved by chromatographic separation [17,18] or a specific derivatization method before MS/MS analysis [19].

Shotgun [20] or LC/MS lipidomics [21,22], are able to characterize PLs at the molecular species level but at the cost of a considerable analytical data treatment [23]. Therefore, in studies of PLs metabolism, the most frequently used method intended to measure the FA composition is to separate the lipid classes by TLC, then to collect the PL classes to achieve a transesterification of the FAs. The fatty acids methyl esters (FAMEs) are then analyzed by GC-FID [24]. This method is known for robustness but remains difficult to reconcile with lipidomic analyses consisting of a large number of samples.

We recently published a study [25] showing that the FAs composition of the triacylglycerol (TG) class can be determined from monoacylglycerol-like ions, $[MG+H-H_2O]^+$ also called ions B. These ions, produced in the APPI source in positive mode, are specific to the acyl moiety and present relatively homogeneous response factors. Their relative intensities allow a rapid estimate of the FAs composition of TGs.

In the present study, we propose extending the principle of the FAs composition estimation from the ions B intensities to the glycerophospholipids category. Ions B are characteristic fragments of lipids in which FAs esterify the glycerol backbone. These ions are observed in source, in positive mode, when analyzing PLs by $APPI^+$ [26–28] and $APCI^+$ /MS [26]. The current methodology was developed with APCI as it is more frequently available than APPI when coupling NP-LC methods to MS.

As stated previously for the TG class [25], the FAs composition estimation using ion B is only applicable when the lipid classes are eluted as peaks or bands without co-eluting compounds. The NP-LC method, developed with a silica stationary phase and used in this study, was already published by our group [26] and was designed to accommodate a vast diversity of samples. It allows to separate thirty lipid classes and, among them, glycerolipids and phospholipids classes. An example chromatogram is shown in Fig. S1.

We considered several PLs classes to determine whether each class is to be considered individually or whether the interclass response of the ions B is homogeneous. We also considered the case of plasmalogen-rich samples as these subclasses may be present in mammalian samples. Specific ions were researched to access the fatty alkenyls composition of P-PLs. As for ion B intensities, the same methodology was applied with those ions.

2. Experimental

2.1. Chemicals

Isooctane, ethyl acetate, acetone (all HPLC grade), acetic acid, trimethylamine, tridecanoic acid, boron trifluoride-methanol solution (14% in methanol), sulfuric acid, and anhydrous sodium sulfate were all purchased from Sigma-Aldrich (St. Louis, MO, USA). Chloroform and water (all HPLC grade) were obtained from VWR (Radnor, Pennsylvania, USA). Isopropanol (UHPLC/MS grade) was from Biosolve (Dieuze, France) and cyclohexane from Carlo Erba (Milan, Italy).

2.2. Phospholipids (PLs)

The study was conducted on seventeen PLs commercial natural extracts. As PE and PC are the naturally most abundant, it was possible to obtain extracts from five animal or tissue sources. Commercial availability is more limited for the other classes, and only one source was included in the study.

Phosphatidylcholines (PC) from bovine heart, bovine liver, porcine brain, and soy; phosphatidylethanolamines (PE) from bovine heart, bovine liver, and porcine brain; phosphatidylinositols (PI) from soy and phosphatidylserines (PS) from porcine brain were purchased from Avanti Polar Lipids, Inc. (Alabaster, AL, USA). PC, PE, phosphatidylglycerols (PG), phosphatidic acid (PA), lysophosphatidylcholines (LPC), and lysophosphatidylethanolamines (LPE) from yolk egg; PE from soy and cardiolipins (CL) from bovine heart were purchased from Sigma-Aldrich.

PC P-18:0/18:1 was purchased from Avanti Polar Lipids.

2.3. Standards for GC analysis

Trinonadecanoate (TG 19:0) and tridecanoic acid (C13:0), approx. 99%, methyl palmitate (FAME 15:0) ≥ 99% (capillary GC) and methyl stearate (FAME 17:0) ~99% (GC) were purchased from Sigma-Aldrich. C16:0 and C18:0 dimethylacetal (DMA) were purchased from Avanti polar lipids, Inc. (Alabaster, AL, USA).

2.4. Apparatus and method

2.4.1. FAMEs analysis (laboratory 1)

An aliquot of 10 µL of PLs solution (5 µg/µL in chloroform) was mixed with 10 µL of internal standard solution (TG 19:0 at 0.4 µg/µL). PLs were hydrolyzed with 1 mL KOH (0.5 M methanol) at 55 °C for 30 min and transmethylated in boron trifluoride-methanol (1mL BF_3 14%) and heptane (1 mL) at 80 °C for 1 h. After water addition (1 mL), methylated total FAs were extracted with heptane (2 mL), evaporated to dryness, and dissolved in ethyl acetate (20 µL).

FAMEs (1 µL) were analyzed on a Clarus 600 Perkin Elmer (Shelton, CO, USA) equipped with a split (10:1) injector and a flame ionization detector. FAMEs were separated on a Famewax RESTEK (Bellefonte, PA, USA) fused silica capillary columns (30 m × 0.32 mm i.d., 0.25 µm film thickness). The oven temperature was programmed as follows: the initial temperature of 130 °C was held for 1 min, increased to 250 °C at 6 °C/min, and held for 5 min. The carrier gas hydrogen was set at a constant flow rate of 1.5 mL/min. The injector and the detector temperatures were set to 220 and 230 °C, respectively.

FAs were identified by comparing their retention time with those of a standard mixture (FAME Mix; Supelco, Sigma-Aldrich). Results were expressed as %FA/Total FA ratio with the internal standard.

2.4.2. FAMEs and dimethylacetals (DMAs) analysis (laboratory 2)

FAs and alkenyl composition of PLs and P-PLs were determined by GC respectively as methyl esters and DMAs after transmethylation, according to Paul et al. [29].

An aliquot of 0.5 mg of lipids was mixed with 50 µg of internal standard (C13:0) and evaporated to dryness under nitrogen. Then 1 mL of BF_3 – methanol (14%) was added. The tube was hermetically capped, briefly mixed, heated at 100 °C for 30 min and finally cooled at room temperature. FAMEs and DMAs were extracted after adding 1 mL of cyclohexane and 0.5 mL of water. The tubes were then briefly shaken, and the upper layer (cyclohexane phase) was transferred into a vial.

FAMEs and DMAs (1 µL) were analyzed by GC on a Clarus 690 Perkin Elmer, equipped with a splitless injector and a flame ionization detector. FAMEs and DMAs were separated on a capillary column (DB 225MS, 30 m x 0.32 mm, film thickness 0.25 µm, Agilent Technologies, Santa Clara, CA, USA). The oven temperature was programmed as follows: the initial temperature of 50 °C was held for 1 min, increased to 180 °C at 15 °C/min and held for 1 min, increased to 220 °C at 5 °C/min and held for 10 min. The carrier gas hydrogen was set at a 2 mL/min constant flow rate. The detector and injector temperature was maintained at 250 °C. The air and hydrogen flow rates were set at 350 and 35 mL/min, respectively.

FAs were identified by comparing their retention time with those of a standard mixture (FAME Mix; Supelco, Sigma-Aldrich). Peak surfaces were integrated and corrected by response factors of individual FAs. Results were expressed as the percentage of each FA corrected surface relative to the sum of FAs corrected surfaces. For DMAs identification and quantification, an equimolar standard composed of DMA 16:0; DMA 18:0; FAME 16:0 and FAME 18:0 was prepared. Response factors of individual DMAs were calculated from the comparison of DMAs peak surfaces with that of FAME 18:0 whose response factor is 1. This allows DMAs to be analyzed in the same way as FAMEs.

The percentage of P-PL is estimated from percent total DMA ($\%S_{DMA}$) and FAME ($\%S_{FAME}$) corrected areas according to the following equation: $\%P_PL = 100x \frac{\%S_{DMA}}{\frac{(\%S_{FA} - \%S_{DMA})}{2} - \%S_{DMA}}$

2.4.3. NP-LC-APCI$^+$-HRMS apparatus

Lipids were separated with an Inertsil Si 5 µm (150 mm × 2.1 mm I.D.) column (GL Sciences Inc., Tokyo, Japan). HRMS analyses were performed with a LTQ-Orbitrap Velos Pro coupled to a LC system Dionex U-3000 RSLC instrument both controlled through Thermo Xcalibur (version 2.2) software (all Thermofisher, Waltham, MA, USA).

The mass spectrometer was equipped with an APCI ion source. Corona needle voltage in APCI mode was set at 4 µA. The vaporizer temperature of the probe was set at 400 °C. Sheath gas, auxiliary gas, and sweep gas flow rates were set at 40, 10, and 0 (arbitrary unit), respectively. The capillary temperature was set at 325 °C and S-lens RF level at 60%. Analyses were performed in positive ion mode. The data was acquired in the mass range of *m/z* 220 – 1 500 at the maximum resolution of 100000 at *m/z* 400.

2.4.4. NP-LC method

The NP-LC method was as described in REF [26] with slight modifications in the solvent program as presented in Table S1, where two isocratic steps were introduced to improve PLs separation.

The column temperature was set at 25 °C (instead of 40 °C) for the same purpose. The flow rate was set at 0.8 mL/min. The injected volume was 2 µl, except for LPC natural extract and LPC from acid hydrolysis (20 µL). The volume of the LPC was multiplied by ten to compensate for its very low ionization [26,30].

2.4.5. Acid hydrolysis of plasmalogens

60 µL of each PLs (5 g/L) were evaporated under a stream of nitrogen. Then, the test tubes were placed inverted over five drops of concentrated HCl in a test tube cap for 5 min. This caused the complete hydrolysis of the vinyl ether bond of the P-PLs while acyl ester bonds remained intact [31]. Lipids extraction was achieved by a mixture of 2 mL of chloroform: methanol (2:1,v/v) and 0.5 mL of 0.88% KCl (wt/v in water). The chloroform layer was retrieved and dried under a stream of nitrogen [32] before dissolution in 60 µL of injection solvent.

3. Theory: summary of PLs fragmentation in positive mode

Most PLs extracts studied are composed exclusively of diacyl-PLs. However, it is anticipated that some PE from animal origins (heart, brain, and liver) and PC from the heart contain a mixture of diacyl-PLs and P-PLs [9]. The in-source fragmentation of these two subclasses differs as documented in the literature and summarized hereafter.

3.1. Case of diacyl-PLs

In positive ionization mode, APPI and APCI produce more in-source fragmentation than ESI [26] (corresponding spectra in supplemental information [26]). The primary in-source fragment ions of diacyl-PLs are ions A ($[M+H\text{-polar headgroup}]^+$ that are equivalent to $[DG+H\text{-}H_2O]^+$) [26–28]. The ESI ion source favors adduct formation and generates few fragment ions. This is the principal reason this source is hugely exploited in lipidomic studies [4].

Ions A can be observed after CID-MS^2 fragmentation of the diacyl-PLs $[M+H]^+$ obtained by ESI^+ except in the specific case of PC. The PC $[M+H]^+$ ion rearranges to form the ionized polar head (phosphocholine) at *m/z* 184 [27] and does not provide information about the glycerol substituents. This specific behavior of PC is not observed when using $APPI^+$ or $APCI^+$.

Fig. S2 shows an $APPI^+/APCI^+$ in-source fragmentation scheme of PLs inspired by [27,33]. The $[M+H]^+$ ion loses the polar group after rearrangement to form the ion A. The resulting ion A undergoes two competitive dissociations reactions leading to the loss of ketene molecules from the lateral FAs to form two ions B (equivalent to $[MG+H\text{-}H2O]^+$). It is worth noting that acylium ions C ($[RCO]^+$) are not produced in the source. Ions C are only observed under collisional activation conditions [27].

3.2. Case of P-PLs

Studies using $APCI^+$ or $APPI^+$ for P-PLs analysis are much less abundant than ESI^+. Only one publication from the late 90s was found for P-PLs analysis by $APCI^+$-MS [34]. Unfortunately, the spectra presented correspond to P-PLs mixtures that prevent any in-depth interpretation of the fragmentation of P-PE and P-PC. We thus took advantage of ESI^+-MS^2 fragmentation information available in different publications to understand the in-source generated fragments observed with $APCI^+$.

3.2.1. P-PE

The P-PE is the most abundant P-PL subclass in natural extracts [6,9]. In ESI^+, P-PE FAs related ions A and B are observable from MS^2 of the $[M+H]^+$ ion [35,36] together with ions specific to fatty alkenyls. These ions, presented in Fig. S3 (adapted from [5]), include the phosphoethanolamine (PEA) headgroup and the fatty alkenyl linked by a vinyl ether bond. Multiple Reaction Monitoring (MRM) experiments intended to study P-PE in samples exploit these ions [37].

In natural extracts, the diversity of fatty alkenyls is limited to P-16:0, P-18:1, P-18:0, P-20:1 and P-20:0 [17]. Additionally, P-17:0 and P-18:2 were also reported in low quantities [38]. The exact masses calculated for the frequently occurring $[\text{fatty alkenyl PEA} + H]^+$ ions are presented in Table 1.

Table 1
Exact masses for $[\text{fatty alkenyl PEA} + H]^+$ and ions P.

	P-PE	P-PE and P-PC
sn-1 substituent	m/z $[\text{fatty alkenyl PEA} + H]^+$	m/z Ion P
P-16:1	362.24547	277.25259
P-16:0	364.26112	279.26824
P-17:0	380.29242	295.29954
P-18:2	388.26112	303.26824
P-18:1	390.27677	305.28389
P-18:0	392.29242	307.29954
P-20:1	418.30807	333.31519
P-20:0	420.32372	335.33084

A critical feature concerning diacyl-PLs and P-PLs mixtures was described by K.A.Z Berry and R.C. Murphy [5]. Briefly, the neutral loss corresponding to the loss of the polar head (PEA, 141 Da), commonly used to determine the PE content in lipid mixtures, cannot be applied if the lipid extract contains a combination of diacyl-PE and P-PE. Diacyl-PE and P-PE do not experience neutral loss to the same degree. The authors showed that P-PE has a lower neutral loss during CID-MS^2. This implies that the degree of formation of ions A is influenced by the presence of the vinyl ethers function. We can anticipate that such phenomena also occur during the $APCI^+$ in-source fragmentation when diacyl- and P-PLs co-exist and that ions B formation is also influenced.

4. Results and discussion

4.1. P-PC fragmentation in $APCI^+$ ionization mode

To the best of our knowledge, no specific literature is available about P-PC ionization with $APCI^+$ or $APPI^+$ ion sources. We thus decided to investigate the fragmentation of PC P-18:0/18:1 in $APCI^+$ ionization mode. The full scan $APCI^+$ spectrum of PC P-18:0/18:1 is presented in Fig. 2a and shows the $[M+H]^+$ at *m/z* 772.61 together with fragment ions and ions of higher *m/z*. As for diacyl-PLs, ion A(P18:0/18:1) at *m/z* 598.55 and ion B(18:1) at *m/z* 339.29 can be identified among the fragment ions. In contrast, the base peak at *m/z* 445.27 does not correspond to a previously encountered fragment ion.

As shown in Fig. 2b, the MS^2 of the $[M+H]^+$ ion produces the ion A(P18:0/18:1). In Fig. 2c, the MS^3 of ion A @772.61→@598.55 produces a fragment ion at *m/z* 571.55 (ion A–H_2O) and an ion at *m/z* 307.30. It is worth noting that both ion B and the ion at *m/z* 445.27 only appear in the full scan $APCI^+$ spectra and not under CID conditions. Those ions are then only produced under the in-source specific ionization conditions offered by the APCI.

In the case of P-PC, the fragmentation pathway of diacyl-PLs [27] as reproduced in Fig. S2 can explain how ion A can be produced from the $[M+H]^+$, but the alkenyl ether function instead of a carbonyl group needs another fragmentation mechanism to be proposed to describe the further fragmentation of ion A into ion B. In the case of P-PC, it could be suggested that a hydrogen transfer on the oxygen of the ether bound with a simultaneous release of the alkenyl chain as an alkyne produces the ion B as illustrated in the pathway i of Fig. 3. Ion at *m/z* 307.30 formation (pathway ii) would arise from an open form of ion A as an allylic carbocation by loss of the C18:1 fatty acid. We propose giving the name “ion P” to this fragment to emphasize that it is characteristic of fatty alkenyls. The ion A-H_2O would also come from the open form of ion A by dehydration of its enol form. The structure of the ions at *m/z* 445.27 was determined with the software "CFM-ID 3.0" available at https://cfmid.wishartlab.com/predict. This ion results from a re-

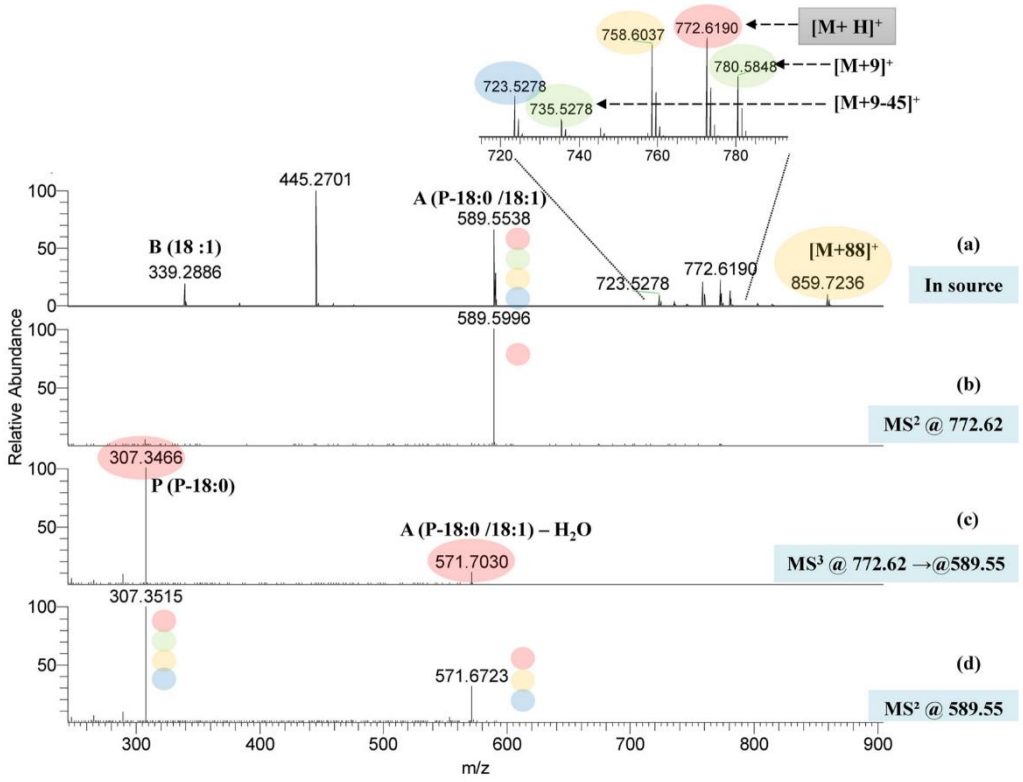

Fig. 2. Mass spectrum of the PC P-18:0 /18:1 obtained by NP-LC-APCI$^+$-HRMS. (a) Full scan; (b) MS^2 of the $[M+H]^+$ ion; (c) MS3 of $[M+H]^+$ → ion A and (d) MS^2 of the ion A. The color code indicates fragment ions and their precursor.

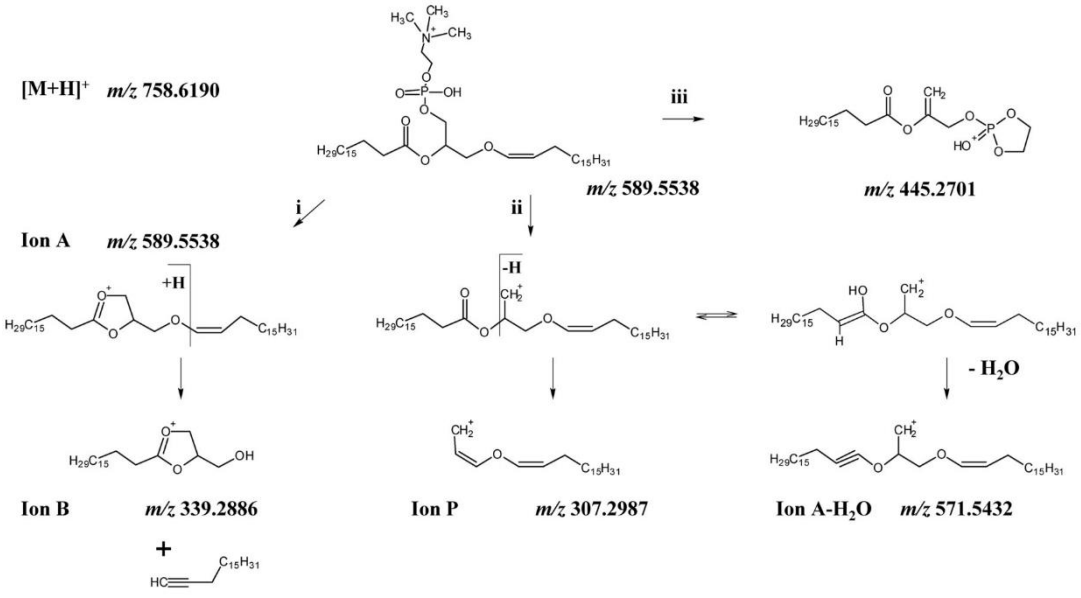

Fig. 3. Proposed fragmentation scheme from the $[M+H]^+$ ion of PC P-18:0/18:1.

arrangement between the polar headgroup and the alkenyl chain. It still contains the phosphate group, suggesting a third pathway of fragmentation of the $[M+H]^+$ ion, as shown in Fig. 3, pathway iii.

Ion P is also present as an in-source fragment but with a relative intensity of only 0.8%. As this ion is a product ion of ion A, it is anticipated as characteristic of all P-PLs. Indeed, although the literature does not mention it explicitly for P-PE, our experimental data show that they are found in our samples. The exact masses of the main ion P are presented in Table 1.

An investigation was conducted to try to understand the nature of the ions whose *m/z* are higher than 700 Da, visible on the full scan mass spectrum. The MS^2 and MS^3 spectra of the ions at

Table 2
Percent FAs composition of PLs extracts as measured by GC-FID. An asterisk at the end of the sample name indicates that the results are from laboratory 2 (samples containing P-PLs and diacyl-PLs mitures).

	PC					PE					PI	PS	CL	PG	PA	LPC	LPE
FA	Egg	Brain	Soy	Heart*	Liver	Egg	Brain*	Soy	Heart*	Liver*	Soy	Brain	Heart	Egg	Egg	Egg	Egg
8:0																	
10:0																	
11:0																	
12:0															0.1		
13:0																	
14:1																	
14:0	0.2	0.4	1.3	0.1	0.1	0.8		0.1		0.3	0.2	0.2	0.4	0.6	0.2	0.3	
15:1																	
15:0			0.1	0.2	0.1	0.1				0.1			0.1				
16:4					0.1												
16:3		0.3	0.1		0.3	0.3		0.1					0.1				
16:2																	
16:1	0.1	0.8	0.2	0.2	0.4		0.6	0.1	0.1	0.2		0.1		0.2	0.2		34.2
16:0	29.1	25.3	18.9	22.2	12.7	21.6	5.0	17.9	1.3	6.5	32.1	1.9	3.0	30.9	31.2	60.6	
17:1										0.1							0.6
17:0	0.2	0.5	0.5	0.2	1.1	0.5	0.2	0.1	0.3	0.1	0.3	0.2	0.1	0.3	0.2	0.4	
18:4		0.3			0.2									0.1			
18:3	0.1	0.1	4.5	0.6	0.8			6.4	0.2	0.6	5.5		0.7	0.1	0.2		
18:2	16.7	0.9	46.7	42.0	10.8	10.7	0.4	63.7	25.2	9.6	46.6	0.2	82.3	12.8	15.8		2.1
18:1	32.5	38.9	15.0	10.5	17.6	20.5	31.4	7.8	3.1	10.1	6.4	25.9	6.4	31.1	36.0	1.5	60.0
18:0	14.8	24.3	11.9	6.8	35.3	30.6	18.0	2.9	30.6	38.9	8.9	47.6	4.4	19.3	13.2	36.9	
20:5				0.3	0.7				1.0	0.4							
20:4	3.7	3.8	0.1	7.1	6.6	11.0	13.2	0.1	30.9	16.2		2.4	0.9	2.7	2.0		
20:3	0.3	0.3		3.0	7.3	0.5	0.7		2.8	3.6		0.5	0.8	0.3	0.2		
20:2	0.2	0.2		0.2	0.4	0.5			0.1	0.1		0.6	0.4	0.2	0.2		
20:1	0.2	0.8	0.1	0.4			3.4		0.1	0.3		1.5	0.1	0.1	0.1		
20:0		0.2	0.2	0.3			0.5	0.2	0.2	0.2		0.3	0.1	0.1	0.0	0.2	
21:0										0.2							
22:6	1.6	1.7			1.0	2.1	7.1	0.1	0.1	1.4		12.0		1.0	0.5		
22:5	0.1	0.1	0.2	1.4	4.3	0.1	9.3		1.9	8.4		0.3		0.1			
22:4	0.2	0.9				0.5	4.2	0.1	0.1	0.7		5.5					
22:3																	
22:2							1.3										3.0
22:1		0.2	0.1	3.0			2.8		1.0	1.2		0.4				0.1	
22:0		0.1	0.1				0.4	0.5				0.3					
23:0																	
24:1																	
24:0		0.1	0.1	1.3			1.4		0.9	0.8			0.1	0.1	0.1		

m/z 859.72, at *m/z* 780.60, at *m/z* 723.53 are presented in Figs. S4, S5 and S6. Overall, the fragmentation of these ions results in the formation of the ions already observed during the fragmentation of $[M+H]^+$ ions. In Fig. 2, an affiliation between the ions is represented by a color code. The fragment ion A produced in-source was also refragmented in MS^2; its spectrum is presented in Fig. 2d.

We failed to highlight common adducts that could explain the ions observed at *m/z* 859.72 and at *m/z* 780.60. However, the common fragments between these ions and the $[M+H]^+$ ion suggest this hypothesis.

4.2. Analysis of PLs by GC-FID

Methylation procedures generate FAMEs from FAs esterifying the glycerol backbone and DMAs from fatty alkenyls of P-PLs [29]. In the GC chromatogram, DMAs elute slightly before their FAMEs homolog. Laboratory 1 assessed the FAs composition of P-PLs free samples, whereas samples with P-PLs were evaluated by laboratory 2. Both results are presented in Table 2.

Since the method using B ions could not differentiate between the n-3 or n-6 series, the results obtained by GC-FID for the two isomers had to be grouped. FAs are ranked by increasing molecular weight in the following tables and figures. Detailed results (with double bond position and %DMA) from Laboratories 1 and 2 are provided in Tables S2 and S3.

Accounting for the DMAs percent together with FAMEs allowed to determine the part of P-PLs present in samples. A content of 69% brain P-PE was measured, this value is far from the average value estimated at 50% by the supplier. This discrepancy may be related to the sample batch. A content of 44% heart P-PC was measured, agreeing with the 40%, announced by the supplier's batch analysis. A content of 48% of heart P-PE was found, in line with the content of 45.0 ± 3.7% obtained by [3]. An amount of 9% was found for P-PE in the bovine liver. We did not find a similar extract in the literature; alternatively, a value of 9% P-PE in human liver was reported [9]. The values measured are close to those announced by the supplier and the literature.

4.3. FAs composition prediction for diacyl-PLs

4.3.1. Comparisons: % FAs vs % ions B intensities

The relative intensities of the ions B, of all PLs, are compared with the % FAs composition obtained by GC-FID in Fig. 4. The liver PC mass spectrum in the ion B region is also presented to illustrate that relative ions B intensities closely match the %FA composition.

As anticipated earlier in the text, results from PL samples with plasmalogen-rich tissues (heart PE and heart PC, brain PE) exhibit a discrepancy between GC-FID measured and ion B intensities predicted FAs composition. This divergence in FAs composition strongly diminishes for lower P-PL sample content such as liver PE, where P-PE accounts for ≈ 9% of the total PE. Thus, when the samples contain a large predominance of diacyl-PLs, the relative intensities of ions B correspond to the relative compositions of the FAs as obtained in GC-FID. This observation also suggests

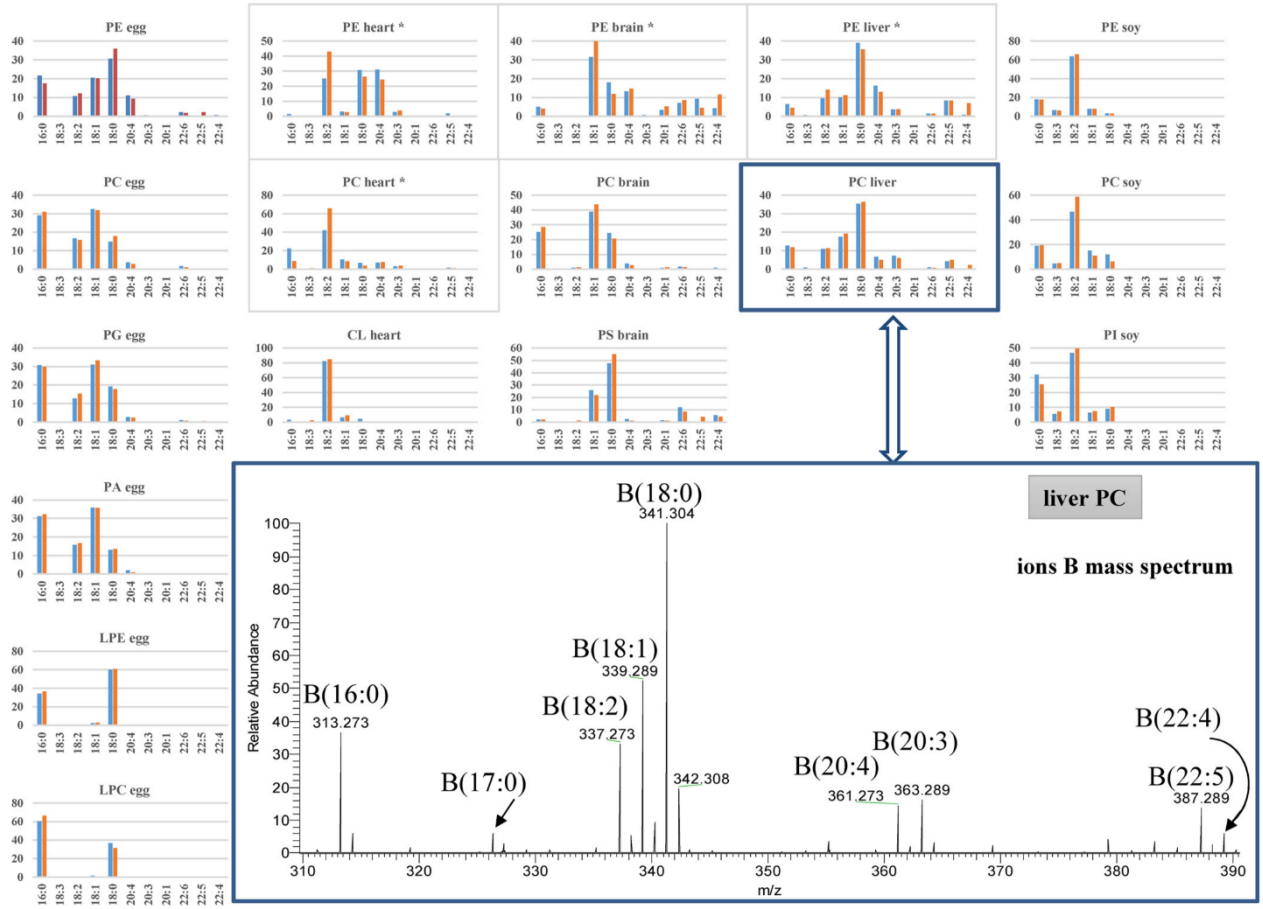

Fig. 4. Relative FA distribution of PLs: measured by GC-FID (blue); % ion B intensities obtained by NP-LC-APCI$^+$-HRMS (orange). The liver PC extract spectrum zoomed in the ion B region is provided for direct comparison of ions B intensities and FAs distribution.

that the fragmentations yields leading to ions B are comparable among the same PLs class. This hypothesis can also be made between the PE and PC classes and with a little more reserve given the lower number of samples, for the other classes presented in Fig. 4.

4.3.2. Deming regression

For extract containing only diacyl-PLs (samples without an asterisk in Table 2 or Fig. 4), a Deming regression was used to relate the FAs percentage predicted using the ions B intensities and the values measured by GC-FID. This type of regression has been preferred over simple linear regression since both dependent, and independent variables contain a certain degree of experimental error.

As shown in Fig. 5, some FAs are frequently encountered and with extended percentages, including C16:0, C18:2, C18:1, C18:0. In these cases, the experimental values are distributed over the entire measurement domain, and the statistical analysis of the regression model presented in Table 3 can provide us with relevant information. The R^2 range from 0.96 to 0.98, which testifies to the very high proportion of variance of the dependent variables explained by the regression model. For C20:1, C22:4 and C22:5, experimental values are rarer and cover a restricted domain. For these FAs, except for one measurement, all values are $\leq$ 1%, and these are inconstantly detected by either method. The corresponding R^2 are low (0.14 to 0.74); we have included the regression statistics of these FAs only for clarity. The C18:3, C20:4, C20:3, and C22:6 are in an intermediate situation since, although not the majority, the observed values make it possible to calculate a regression with R^2 between 0.98 and 0.99. As in the case of C16:0, C18:2, C18:1, C18:0, the examination of the significance of the regression coefficients can be performed.

Table 3 shows that all intercepts of the different regression lines are not significantly different from zero, with various significance thresholds but always greater than 5%. There is, therefore, a direct proportionality between the percentage of an FA measured by GC-FID and the predicted value using the intensities of the ions B. In the same table, the probability threshold is given for comparing the slopes of the regression lines with the value 1.0. Here too, none of the slopes differs statistically from the unit at risk 5% (and this even if the C22:6 approaches it). Except for C20:1, C22:5 and C22:4 where the limited amount of data does not allow us to be affirmative, we can therefore conclude that the determination of the FAs composition using the intensity of the ions B of the PLs produced in the source and their measurement by GC-FID after transformation into FAMEs give statistically equivalent results.

In this article, given the more limited number of samples and the results preceding the statistical analysis, we can consider that the ions B intensities are a valid approach to evaluate the relative composition of FAs in a complex sample containing diacyl-PLs. In this context, it does not seem necessary to calculate weights *Wi*, as achieved in [25].

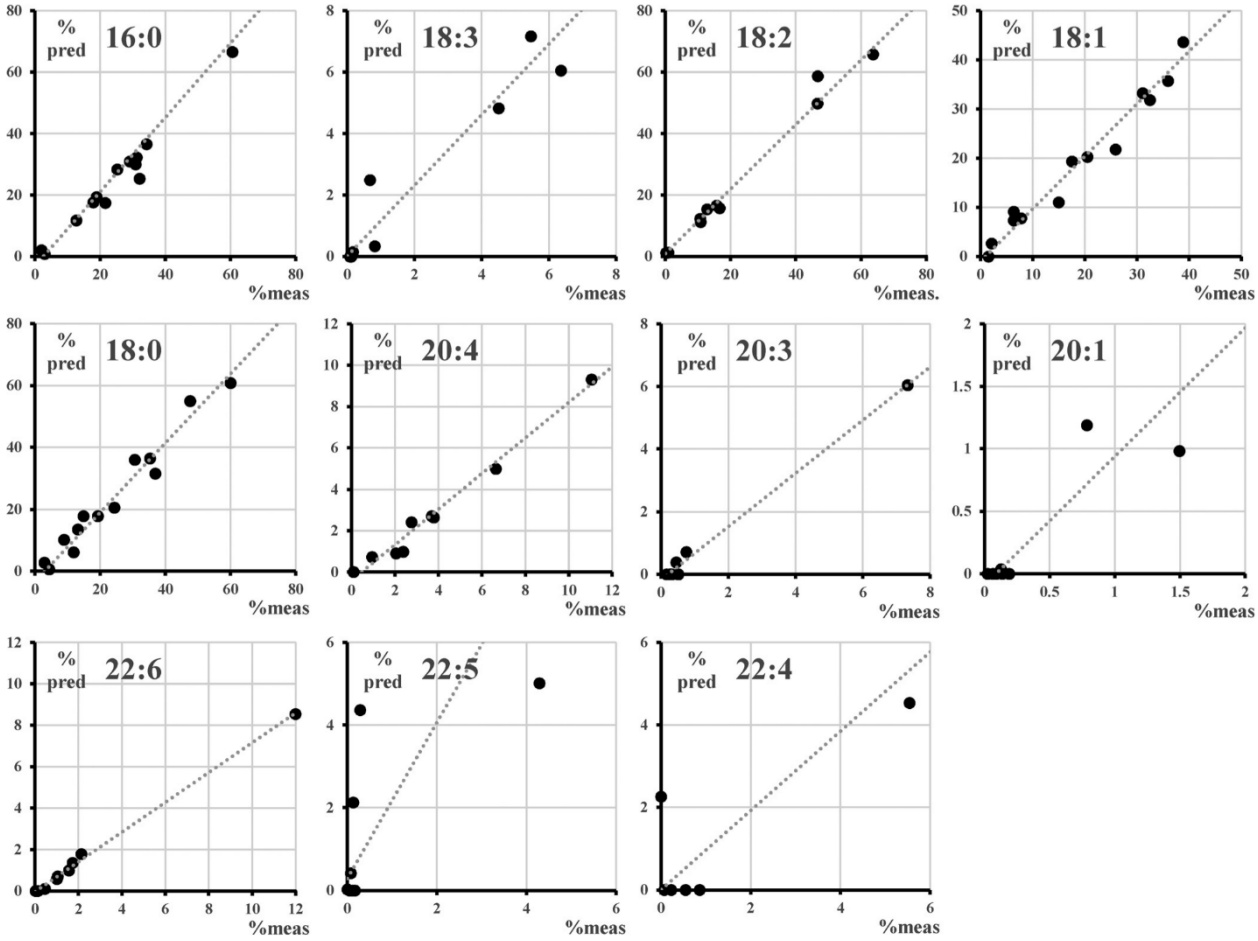

Fig. 5. Predicted vs. measured %FA distribution. Black circles are experimental values and lines correspond to the Deming regression whose coefficients presented in Table 3.

Table 3
Deming regression statistics for each FA. Std err indicates the standard error of the intercept and the slope of the regression equation. Pr(> |t|) is the significance threshold for comparing the intercept with zero and the slope with unity. R^2 is the determination coefficient and df is the degree of freedom.

FA	df	Intercept	std err	Pr(>|t|)	Slope	std err	Pr(>|t|)	R^2
16:0	**11**	**-3.08**	**1.68**	**0.09**	**1.21**	**0.07**	**0.10**	**0.9705**
18:3	**7**	**0.02**	**0.32**	**0.94**	**1.15**	**0.18**	**0.43**	**0.9780**
18:2	**9**	**1.00**	**0.69**	**0.18**	**1.05**	**0.05**	**0.30**	**0.9884**
18:1	**11**	**-0.98**	**1.19**	**0.42**	**1.07**	**0.07**	**0.33**	**0.9671**
18:0	**11**	**-3.33**	**1.80**	**0.09**	**1.12**	**0.08**	**0.16**	**0.9604**
20:4	**8**	**-0.39**	**0.23**	**0.13**	**0.86**	**0.07**	**0.07**	**0.9816**
20:3	**6**	**-0.17**	**0.30**	**0.59**	**0.85**	**0.72**	**0.84**	**0.9942**
20:1	**6**	**-0.09**	**0.06**	**0.21**	**1.03**	**0.67**	**0.96**	**0.7392**
22:6	**8**	**-0.03**	**0.10**	**0.76**	**0.72**	**0.12**	**0.05**	**0.9972**
22:5	**7**	**0.29**	**1.54**	**0.85**	**1.89**	**17.35**	**0.96**	**0.1443**
22:4	**4**	**0.01**	**1.82**	**0.99**	**0.96**	**4.31**	**0.99**	**0.6230**

4.4. FAs composition prediction in extracts containing P-PLs

Ions B ionization depends on the subclass (diacyl-PLs and P-PLs). It is therefore imperative to separate these subclasses before using ions B to evaluate the FAs composition. We chose to add a sample preparation step that hydrolyzes specifically the vinyl-ether bonds in P-PLs [31]. The reaction scheme is presented in Fig. 6, where P-PLs are hydrolyzed to form their lyso-PLs counterpart (substituted by the acyl chain) plus a fatty aldehyde. These compounds and their corresponding ions being separated chromatographically does not interfere with ions B from PLs. As the content of lyso-PLs is usually less than 1% in cell membranes [3], this strategy can be applied to total lipid extracts.

This approach then requires two analyses. The first analysis is performed on the total lipid extract, and the second is performed on the lipid extract after acid hydrolysis. The first analysis allows detecting P-PLs via specific ions ([fatty alkenyl PEA + H]$^+$ and ions P). It also allows analyzing the lyso-PE /PC naturally present in the case of total lipid extracts. The diacyl-PLs and lyso-PLs from acid hydrolysis can be studied during the second analysis. The informa-

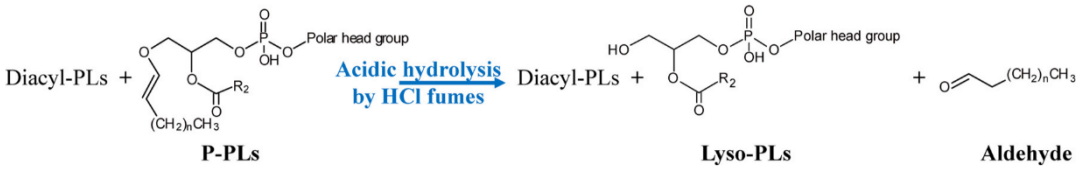

Fig. 6. Acid hydrolysis of plasmalogens by HCl fumes.

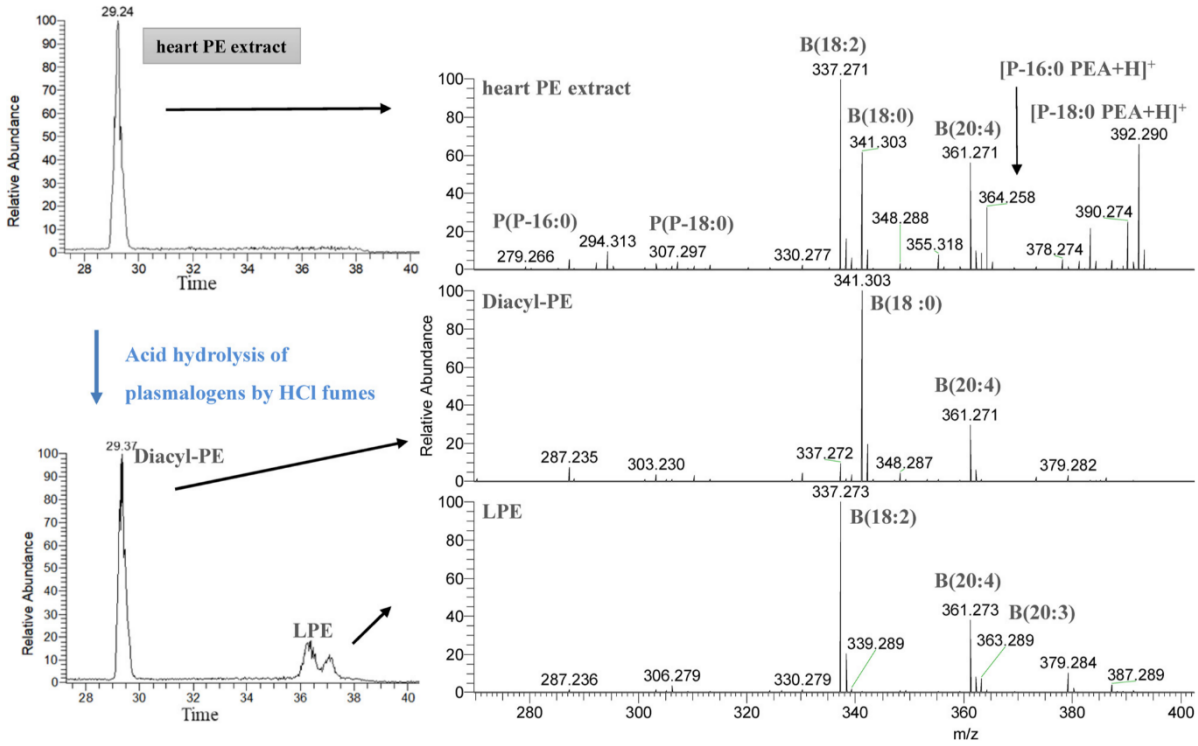

Fig. 7. NP-LC-APPI$^+$-HRMS chromatogram and spectra (m/z [270–400]) of heart PE before and after acid hydrolysis.

tion extracted from the lyso-PLs thus formed by hydrolysis of plasmalogens provide information on the FAs in position *sn*-2 of the P-PLs from which they are derived.

The NP-LC-APPI$^+$-HRMS analysis of heart PE extract according to the previously mentioned procedure is presented in Fig. 7. Before acid hydrolysis, all PE molecular species elute as a single peak at 29.24 min. Ions P are observables from the corresponding mass spectrum, indicating the occurrence of P-PE. Hence ions B intensities cannot be exploited to assess the FAs composition since they originate from both diacyl- and P-PE. After acid hydrolysis, the chromatogram still shows the intact diacyl-PE peak at 29.37 min, plus a double peak between 36 and 38 min corresponding to lyso-PE. FAs C18:0 and C20:4 are the majority in diacyl-PE, whereas C18:2 and C20:4 predominate in lyso-PE.

The lyso-PE double peak is explained by the presence of both 1-lyso-PE and 2-lyso-PE. Since fatty acyls are exclusively located at the *sn*-2 position of the P-PE glycerol backbone, only 2-lyso-PE are expected. 1-Lyso-PE formation is explained by an acyl-group migration catalyzed by the bare silica used in NP-LC [39]. This phenomenon can be observed with other lipid classes that present a free hydroxyl group on the glycerol skeleton, such as MG and DG.

The assessment of the FAs composition in heart, brain, and liver PE and heart PC extracts was carried out with the method using ions B [25]. In these extracts, the fraction of polyunsaturated FAs (PUFAs) with an unsaturation number ≥ 3 can be significant (30% of C20:4 in heart PE). In our previous study based on plant oils [25] we noticed that the intensity of ion B(18:3) was two times less than those of other FAs. PUFAs with more than three double bonds are indeed unusual in plant samples [40]. In the 20 plant oils set studied in [25], only 1.3% of C20:3 was found in cameline oil. To account for the response variability of PUFAs derived ions B, weighting coefficients (W*i*) were calculated. Compared to ion B of other FAs the W*i* of ion B(18:3) is two times higher.

In the present study, the small number of extracts studied does not allow us to reliably calculate weighting coefficients for these FAs. Based on our previous study [25], and by analogy with ions B issued from TGs which share the same precursor (ion A), we have chosen to apply a W*i* coefficient two times higher for ions B from PUFAs with an unsaturation number ≥ 3 compared with saturated or mono- or di-unsaturated FAs. This W*i* multiplicative factor is applied to correct ion B(18:3) intensities for their lower response factor. This is a simplified version of the calculation detailed in our TG study [25]. The results are shown in Fig. 8.

$$\text{Let}: \ \%L_3 = \frac{2(\%\ \text{diacyl}_{PL}) \times \%L_1 + (\%P_PLs) \times \%L_2}{2(\%\text{diacyl}_P L) + (\%P_PLs)}$$

where L_3 is the % of FA considered, $\%L_1$, $\%L_2$ are the % of FA in diacyls-PL and lyso-PL, respectively, %P-PLs and %diacyl-PL are the total % of P-PL and diacyl-PL, respectively.

$$\text{Brain PE example}: \ \%L_3 = \frac{2 \times 31 \times \%L_1 + 31 \times \%L_1}{2 \times 31 + 69}$$

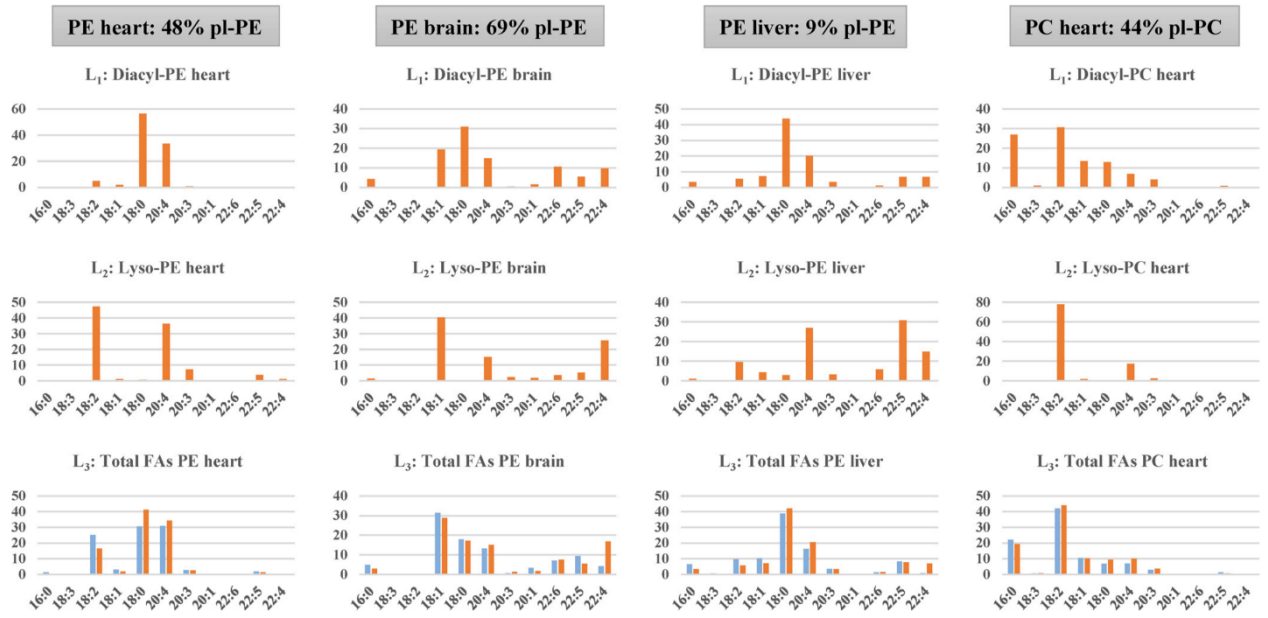

Fig. 8. Relative FAs distribution: % Ions B intensities (Wi corrected) obtained by NP-LC-APCI$^+$-HRMS (orange), and relative FAs distribution obtained by GC-FID (laboratory 2) (blue). L_1 corresponds to diacyl-PLs remained intact after acid hydrolysis; L_2 corresponds to Lyso-PLs obtained by acid hydrolysis of P-PLs; L_3 corresponds to the global FAs distribution (obtained by combining L_1 and L_2).

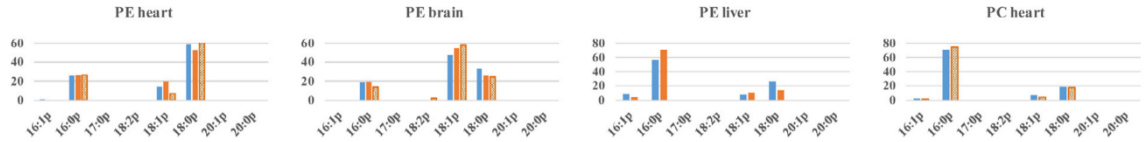

Fig. 9. Fatty alkenyls distribution: % DMAs as obtained by GC-FID (blue); [fatty alkenyl PEA + H]$^+$ intensities (dark orange); % ions P intensities (light orange). .

The reconstructed overall compositions are shown in row 3 (L3), orange histograms. The blue histograms represent the FAs composition obtained by GC-FID.

The results show that the *sn*-2 FAs in P-PLs are almost exclusively mono- or polyunsaturated. This result agrees with the literature [6], as numerous studies reported high levels of PUFAs in P-PL compared to diacyl-PLs. Consistently, saturated FAs are quasi exclusively encountered in diacyl-PLs, whereas they also contain some extent of mono or polyunsaturated FAs. The overall composition of FAs by both methods (line 3) is essentially similar. In the literature, a study of PE extracted from bovine heart [38], carried out by shotgun lipidomics, also presents compositions of FAs (diacyl-PE and P-PL) close to those found here. Therefore, the developed method allows quick access to an estimate of the composition of FAs of diacyl-PL and FAs of P-PL.

If the % of P-PL in the samples is known, it is also possible to calculate an estimate of the total FAs, as usually provided by GC-FID. This data is less informative but allows a comparison of the results. The method does not allow the calculation of the % P-PL versus % diacyl-PL. This information is usually obtained by GC-FID through % DMA and % FAMEs [41] or in LC-MS/MS in MRM mode using internal standards [5,42].

4.5. P-PLs fatty alkenyls composition prediction

4.5.1. P-PE

Study [5] presents the ESI$^+$-CID-MS^2 mass spectra of PE P-18:0-18:1, PE P-18:0-20:4, PE P-18:0-22:6, PE P-16:0-20:4 and PE P-18:1-20:4. Two major ions have been identified, corresponding to a B ion and the [fatty alkenyl PEA + H]$^+$ ion. The spectra show a similar intensity of these two ions, except PE P-18:0-22:6. For PE P-18:0-22:6, the intensity of P-18:0-PEA is about half as intense as the B(22:6) ion. As C22:6 is not very abundant in our extracts (maximum 7% in brain PE), we tested the transposition of the B ion method to evaluate the fatty alkenyls content of P-PE.

For this purpose, the intensities of [fatty alkenyl PEA + H]$^+$, whose *m/z* values are presented in the first row of Table 1, were extracted from mass spectra obtained before hydrolysis. In Fig. 9, the [fatty alkenyl PEA + H]$^+$ intensities (dark orange bars) are compared with the DMAs composition obtained by GC-FID (blue bars). The two methods provide comparable results for estimating fatty alkenyls content of P-PE.

4.5.2. P-PE and P-PC

We hypothesized that ions P are characteristic of fatty alkenyls for all P-PLs. We thus extracted the intensities of ions P, whose *m/z* values as presented in the second column of Table 1, from all samples containing P-PLs. The ion P intensities are presented as light orange bars in Fig. 9.

Concerning PE from heart and brain, the results obtained using ion P intensities are consistent with those from [fatty alkenyl PEA + H]$^+$ intensities. For PE from liver, where P-PEs only represent only 9%, ions P could not be extracted with measurable intensities. As shown in Fig. 7, the ions P are significantly less intense (about six times) than the corresponding [fatty alkenyl PEA + H]$^+$ ions. This suggests that [fatty alkenyl PEA + H]$^+$ ions should be preferred to evaluate P-PE's fatty alkenyl composition.

Concerning the PC from heart, the ion P appears to be the only ion allowing direct access to the fatty alkenyls composition. Despite the low intensity of ions P in the full scan spectrum, the pre-

dicted fatty alkenyl composition for PC heart is close to that determined by GC-FID.

5. Conclusion

The proof of concept developed on TGs for predicting the FAs composition from in-source produced ions B intensities in NP-LC-APPI$^+$-HRMS [25] has been successfully implemented on PLs. Our study also shows that the more widespread APCI ion source can be used as an alternative to APPI.

The response factors of the ions B were found to be homogeneous within all PLs classes. Moreover, ions B response factors appear to be consistent for saturated, mono- and di-unsaturated FAs. Thus, in the general case of diacyl-PLs and their corresponding lyso-PLs, a direct reading of the ions B relative intensities directly predicted the composition of the corresponding FAs.

We have shown that the method can also be implemented in the case of extracts containing both diacyl-PLs and P-PLs. In this case, we propose to carry out a second analysis after acid hydrolysis of the sample. During this reaction, only the vinyl ether bonds are hydrolyzed. The ions B from the lyso-PLs thus formed provide information on the FAs in position *sn*-2 of the P-PLs. The intact diacyl-PLs can then also be analyzed at their usual retention time.

P-PLs are rich in PUFAs located in the *sn*-2 position of the glycerol backbone. A weighting factor two times higher was applied to ions B corresponding to FAs with $\geq$ 3 unsaturation number to account for their lesser response compared to ions B from other FAs. This quick correction resulted in a composition similar to that obtained by GC-FID.

We also showed that the fatty alkenyls composition of P-PLs could be assessed from ions [fatty alkenyl PEA + H]$^+$ and ions P relative intensities. The results obtained this way compare favorably with the composition of DMAs obtained by GC-FID.

Compared to the GC-FID analyses conventionally used, our method requires no (or negligible) sample processing. In addition, a single analysis gives access to the FAs composition by lipid class of glycero- (TG [26]) and glycerophospholipids (PG, PE, PA, PI, CL, PS and PC) and their corresponding lyso forms. Our approach allows differentiating FAs from diacyl-PLs and P-PLs, which is not possible with the GC-FID analysis of FAMES.

Declaration of Competing Interest

The authors declare that they have no known competing financial interests or personal relationships that could have appeared to influence the work reported in this paper.

CRediT authorship contribution statement

Sonia Abreu: Conceptualization, Methodology, Validation, Formal analysis, Investigation, Writing – original draft, Visualization, Writing – review & editing. **Sylvie Héron:** Writing – review & editing. **Audrey Solgadi:** Resources. **Bastien Prost:** Resources. **Jessica Dalloux-Chioccioli:** Formal analysis. **Alice Kermarrec:** Formal analysis, Writing – review & editing. **Anne Meynier:** Formal analysis, Writing – review & editing. **Justine Bertrand-Michel:** Formal analysis, Writing – review & editing. **Alain Tchapla:** Writing – review & editing. **Pierre Chaminade:** Resources, Project administration, Supervision, Writing – review & editing.

Acknowledgments

We would like to thank the reviewers for helping us to improve the clarity and correctness of our manuscript and, especially, for the helpful suggestions made regarding the fragmentation of plasmalogens.

Supplementary materials

Supplementary material associated with this article can be found, in the online version, at doi:10.1016/j.chroma.2022.463093.

References

[1] A. Delobel, D. Touboul, O. Laprévote, Structural characterization of phosphatidylcholines by atmospheric pressure photoionization mass spectrometry, Eur. J. Mass Spectrom. 11 (2005) 409–417, doi:10.1255/ejms.760.
[2] D.B. Goodenowe, L.L. Cook, J. Liu, Y. Lu, D.A. Jayasinghe, P.W.K. Ahiahonu, D. Heath, Y. Yamazaki, J. Flax, K.F. Krenitsky, D.L. Sparks, A. Lerner, R.P. Friedland, T. Kudo, K. Kamino, T. Morihara, M. Takeda, P.L. Wood, Peripheral ethanolamine plasmalogen deficiency: a logical causative factor in Alzheimer's disease and dementia, J. Lipid Res. 48 (2007) 2485–2498, doi:10.1194/jlr.P700023-JLR200.
[3] E. Fahy, S. Subramaniam, R.C. Murphy, M. Nishijima, C.R.H. Raetz, T. Shimizu, F. Spener, G. van Meer, M.J.O. Wakelam, E.A. Dennis, Update of the LIPID MAPS comprehensive classification system for lipids, J. Lipid Res. 50 (2009) S9–S14, doi:10.1194/jlr.R800095-JLR200.
[4] E.J. Murphy, R. Stephens, M. Jurkowitz-Alexander, L.A. Horrocks, Acidic hydrolysis of plasmalogens followed by high-performance liquid chromatography, Lipids 28 (1993) 565–568, doi:10.1007/BF02536090.
[5] F. Dorninger, S. Forss-Petter, J. Berger, From peroxisomal disorders to common neurodegenerative diseases – the role of ether phospholipids in the nervous system, FEBS Lett. 591 (2017) 2761–2788, doi:10.1002/1873-3468.12788.
[6] G. Dacremont, G. Vincent, Assay of plasmalogens and polyunsaturated fatty acids (PUFA) in erythrocytes and fibroblasts, J. Inherit. Metab. Dis. 18 (1995) 6, doi:10.1007/BF00711431.
[7] G. Liebisch, E. Fahy, J. Aoki, E.A. Dennis, T. Durand, C.S. Ejsing, M. Fedorova, I. Feussner, W.J. Griffiths, H. Köfeler, A.H. Merrill, R.C. Murphy, V.B. O'Donnell, O. Oskolkova, S. Subramaniam, M.J.O. Wakelam, F. Spener, Update on LIPID MAPS classification, nomenclature, and shorthand notation for MS-derived lipid structures, J. Lipid Res. 61 (2020) 1539–1555, doi:10.1194/jlr.S120001025.
[8] G. van Meer, D.R. Voelker, G.W. Feigenson, Membrane lipids: where they are and how they behave, Nat. Rev. Mol. Cell Biol. 9 (2008) 112–124, doi:10.1038/nrm2330.
[9] H. Goldfine, The appearance, disappearance and reappearance of plasmalogens in evolution, Prog. Lipid Res. 49 (2010) 493–498, doi:10.1016/j.plipres.2010.07.003.
[10] H.W. Mueller, J.T. O'Flaherty, D.G. Greene, M.P. Samuel, 1-0-Alkyl-linked glycerophospholipids of human neutrophils: distribution of arachidonate and other acyl residues in the ether-linked and diacyl species, J. Lipid Res. 25 (1984) 6, doi:10.1016/S0022-2275(20)37812-3.
[11] J. Jouhet, J. Lupette, O. Clerc, L. Magneschi, M. Bedhomme, S. Collin, S. Roy, E. Maréchal, F. Rébeillé, LC-MS/MS versus TLC plus GC methods: consistency of glycerolipid and fatty acid profiles in microalgae and higher plant cells and effect of a nitrogen starvation, PLoS One. 12 (2017) e0182423, doi:10.1371/journal.pone.0182423.
[12] J. Koch, K. Lackner, Y. Wohlfarter, S. Sailer, J. Zschocke, E.R. Werner, K. Watschinger, M.A. Keller, Unequivocal mapping of molecular ether lipid species by LC–MS/MS in plasmalogen-deficient mice, Anal. Chem. 92 (2020) 11268–11276, doi:10.1021/acs.analchem.0c01933.
[13] K. Nagy, V.V. Brahmbhatt, O. Berdeaux, L. Bretillon, F. Destaillats, N. Acar, Comparative study of serine-plasmalogens in human retina and optic nerve: identification of atypical species with odd carbon chains, J. Lipid Res. 53 (2012) 776–783, doi:10.1194/jlr.D022962.
[14] K. Yang, Z. Zhao, R.W. Gross, X. Han, Shotgun lipidomics identifies a paired rule for the presence of isomeric ether phospholipid molecular species, PLoS One 2 (2007) e1368, doi:10.1371/journal.pone.0001368.
[15] K.A.Z. Berry, R.C. Murphy, Electrospray ionization tandem mass spectrometry of glycerophosphoethanolamine plasmalogen phospholipids, J. Am. Soc. Mass Spectrom. 15 (2004) 1499–1508, doi:10.1016/j.jasms.2004.07.009.
[16] M. Gaudin, L. Imbert, D. Libong, P. Chaminade, A. Brunelle, D. Touboul, O. Laprévote, Atmospheric pressure photoionization as a powerful tool for large-scale lipidomic studies, J. Am. Soc. Mass Spectrom. 23 (2012) 869–879, doi:10.1007/s13361-012-0341-y.
[17] M. He, C.X. Qin, X. Wang, N.Z. Ding, Plant unsaturated fatty acids: biosynthesis and regulation, Front. Plant Sci. 11 (2020) 390, doi:10.3389/fpls.2020.00390.
[18] M. Holčapek, P. Jandera, P. Zderadička, L. Hruba, Characterization of triacylglycerol and diacylglycerol composition of plant oils using high-performance liquid chromatography–atmospheric pressure chemical ionization mass spectrometry, J. Chromatogr. A 1010 (2003) 195–215, doi:10.1016/s0021-9673(03)01030-6.
[19] M. Pulfer, R.C. Murphy, Electrospray mass spectrometry of phospholipids, Mass Spectrom. Rev. 22 (2003) 332–364, doi:10.1002/mas.10061.
[20] N. Acar, O. Berdeaux, P. Juaneda, S. Grégoire, S. Cabaret, C. Joffre, C.P. Creuzot-Garcher, L. Bretillon, A.M. Bron, Red blood cell plasmalogens and docosahexaenoic acid are independently reduced in primary open-angle glaucoma, Exp. Eye Res. 89 (2009) 840–853, doi:10.1016/j.exer.2009.07.008.
[21] N. Nagan, R.A. Zoeller, Plasmalogens: biosynthesis and functions, Prog. Lipid Res. 40 (2001) 199–229, doi:10.1016/S0163-7827(01)00003-0.
[22] N.E. Braverman, A.B. Moser, Functions of plasmalogen lipids in health and disease, Biochim. Biophys. Acta BBA Mol. Basis Dis. 1822 (2012) 1442–1452, doi:10.1016/j.bbadis.2012.05.008.

[23] Q. Lin, D. Zhang, Y. Xia, Analysis of ether glycerophosphocholines at the level of C=C locations from human plasma, Analyst 145 (2020) 513–522, doi:10.1039/C9AN01515A.
[24] R.A. Klein, Mass spectrometry of the phosphatidylcholines: fragmentation processes for dioleoyl and stearoyl-oleoyl glycerylphosphorylcholine, J. Lipid Res. 12 (1971) 628–634, doi:10.1016/S0022-2275(20)39483-9.
[25] S. Abreu, A. Solgadi, P. Chaminade, Optimization of normal phase chromatographic conditions for lipid analysis and comparison of associated detection techniques, J. Chromatogr. A (2017), doi:10.1016/j.chroma.2017.07.063.
[26] S. Abreu, S. Heron, A. Solgadi, F. Joffre, A. Tchapla, P. Chaminade, Rapid assessment of triacylglycerol fatty acyls composition by LC-APPI+-HRMS using monoacylglycerol like fragments intensities, Anal. Chim. Acta 1178 (2021) 338809, doi:10.1016/j.aca.2021.338809.
[27] S. Anjos, E. Feiteira, F. Cerveira, T. Melo, A. Reboredo, S. Colombo, R. Dantas, E. Costa, A. Moreira, S. Santos, A. Campos, R. Ferreira, P. Domingues, M.R.M. Domingues, Lipidomics reveals similar changes in serum phospholipid signatures of overweight and obese pediatric subjects, J. Proteome Res. 18 (2019) 3174–3183, doi:10.1021/acs.jproteome.9b00249.
[28] S. Mawatari, Y. Okuma, T. Fujino, Separation of intact plasmalogens and all other phospholipids by a single run of high-performance liquid chromatography, Anal. Biochem. 370 (2007) 54–59, doi:10.1016/j.ab.2007.05.020.
[29] S. Paul, G.I. Lancaster, P.J. Meikle, Plasmalogens: a potential therapeutic target for neurodegenerative and cardiometabolic disease, Prog. Lipid Res. 74 (2019) 186–195, doi:10.1016/j.plipres.2019.04.003.
[30] S. Wallner, E. Orsó, M. Grandl, T. Konovalova, G. Liebisch, G. Schmitz, Phosphatidylcholine and phosphatidylethanolamine plasmalogens in lipid loaded human macrophages, PLoS One. 13 (2018) e0205706, doi:10.1371/journal.pone.0205706.
[31] S. Yamashita, A. Honjo, M. Aruga, K. Nakagawa, T. Miyazawa, Preparation of marine plasmalogen and selective identification of molecular species by LC-MS/MS, J. Oleo Sci. 63 (2014) 423–430, doi:10.5650/jos.ess13188.
[32] S.J. Kim, N. Kim, E.H. Koh, H.J. Yoo, Identification of ethanolamine plasmalogens from complex lipid mixtures by MS/MS and Ag adduction, Anal. Sci. 28 (2012) 1207–1212, doi:10.2116/analsci.28.1207.
[33] T. Cajka, O. Fiehn, Comprehensive analysis of lipids in biological systems by liquid chromatography-mass spectrometry, TrAC Trends Anal. Chem. 61 (2014) 192–206, doi:10.1016/j.trac.2014.04.017.
[34] T.H. Pham, M. Zaeem, T.A. Fillier, M. Nadeem, N.P. Vidal, C. Manful, S. Cheema, M. Cheema, R.H. Thomas, Targeting modified lipids during routine lipidomics analysis using HILIC and C30 reverse phase liquid chromatography coupled to mass spectrometry, Sci. Rep. 9 (2019) 5048, doi:10.1038/s41598-019-41556-9.
[35] T.J. Leiker, R.M. Barkley, R.C. Murphy, Analysis of diacylglycerol molecular species in cellular lipid extracts by normal-phase LC-electrospray mass spectrometry, Int. J. Mass Spectrom. 305 (2011) 103–108, doi:10.1016/j.ijms.2010.09.008.
[36] W.R. Morrison, L.M. Smith, Preparation of fatty acid methyl esters and dimethylacetals from lipids with boron fluoride methanol, J. Lipid Res. 5 (1964) 600–608, doi:10.1016/S0022-2275(20)40190-7.
[37] Wm.C. Byrdwell, Dual parallel mass spectrometers for analysis of sphingolipid, glycerophospholipid and plasmalogen molecular species, Rapid Commun. Mass Spectrom. 12 (1998) 256–272, doi:10.1002/(SICI)1097-0231(19980314)12:5(256::AID-RCM149)3.0.CO;2-8.
[38] X. Li, Q. He, H. Hou, S. Zhang, X. Zhang, Y. Zhang, X. Wang, L. Han, K. Liu, Targeted lipidomics profiling of marine phospholipids from different resources by UPLC-Q-exactive orbitrap/MS approach, J. Chromatogr. B 1096 (2018) 107–112, doi:10.1016/j.jchromb.2018.08.018.
[39] Y. Otoki, K. Nakagawa, S. Kato, T. Miyazawa, MS/MS and LC-MS/MS analysis of choline/ethanolamine plasmalogens via promotion of alkali metal adduct formation, J. Chromatogr. B 1004 (2015) 85–92, doi:10.1016/j.jchromb.2015.09.012.
[40] Y. Wang, S. Hinz, O. Uckermann, P. Hönscheid, W. von Schönfels, G. Burmeister, A. Hendricks, J.M. Ackerman, G.B. Baretton, J. Hampe, M. Brosch, C. Schafmayer, A. Shevchenko, S. Zeissig, Shotgun lipidomics-based characterization of the landscape of lipid metabolism in colorectal cancer, Biochim. Biophys. Acta BBA Mol. Cell Biol. Lipids 1865 (2020) 158579, doi:10.1016/j.bbalip.2019.158579.
[41] Y. Zhou, N. Yu, J. Zhao, Z. Xie, Z. Yang, B. Tian, Advances in the biosynthetic pathways and application potential of plasmalogens in medicine, Front. Cell Dev. Biol. 8 (2020) 765, doi:10.3389/fcell.2020.00765.
[42] Z. Ni, G. Angelidou, M. Lange, R. Hoffmann, M. Fedorova, LipidHunter identifies phospholipids by high-throughput processing of LC-MS and shotgun lipidomics datasets, Anal. Chem. 89 (2017) 8800–8807, doi:10.1021/acs.analchem.7b01126.

Erratum bibliographie

[1] G. Liebisch, E. Fahy, J. Aoki, E.A. Dennis, T. Durand, C.S. Ejsing, M. Fedorova, I. Feussner, W.J. Griffiths, H. Köfeler, A.H. Merrill, R.C. Murphy, V.B. O'Donnell, O. Oskolkova, S. Subramaniam, M.J.O. Wakelam, F. Spener, Update on LIPID MAPS classification, nomenclature, and shorthand notation for MS-derived lipid structures, J. Lipid Res. 61 (2020) 1539–1555. https://doi.org/10.1194/jlr.S120001025.

[2] M. Pulfer, R.C. Murphy, Electrospray mass spectrometry of phospholipids, Mass Spectrom. Rev. 22 (2003) 332–364. https://doi.org/10.1002/mas.10061.

[3] G. van Meer, D.R. Voelker, G.W. Feigenson, Membrane lipids: where they are and how they behave, Nat. Rev. Mol. Cell Biol. 9 (2008) 112–124. https://doi.org/10.1038/nrm2330.

[4] T. Cajka, O. Fiehn, Comprehensive analysis of lipids in biological systems by liquid chromatography-mass spectrometry, TrAC Trends Anal. Chem. 61 (2014) 192–206. https://doi.org/10.1016/j.trac.2014.04.017.

[5] K.A.Z. Berry, R.C. Murphy, Electrospray ionization tandem mass spectrometry of glycerophosphoethanolamine plasmalogen phospholipids, J. Am. Soc. Mass Spectrom. 15 (2004) 1499–1508. https://doi.org/10.1016/j.jasms.2004.07.009.

[6] N. Nagan, R.A. Zoeller, Plasmalogens: biosynthesis and functions, Prog. Lipid Res. 40 (2001) 199–229. https://doi.org/10.1016/S0163-7827(01)00003-0.

[7] E. Fahy, S. Subramaniam, R.C. Murphy, M. Nishijima, C.R.H. Raetz, T. Shimizu, F. Spener, G. van Meer, M.J.O. Wakelam, E.A. Dennis, Update of the LIPID MAPS comprehensive classification system for lipids, J. Lipid Res. 50 (2009) S9–S14. https://doi.org/10.1194/jlr.R800095-JLR200.

[8] Y. Zhou, N. Yu, J. Zhao, Z. Xie, Z. Yang, B. Tian, Advances in the Biosynthetic Pathways and Application Potential of Plasmalogens in Medicine, Front. Cell Dev. Biol. 8 (2020) 765. https://doi.org/10.3389/fcell.2020.00765.

[9] N.E. Braverman, A.B. Moser, Functions of plasmalogen lipids in health and disease, Biochim. Biophys. Acta BBA - Mol. Basis Dis. 1822 (2012) 1442–1452. https://doi.org/10.1016/j.bbadis.2012.05.008.

[10] K. Nagy, V.V. Brahmbhatt, O. Berdeaux, L. Bretillon, F. Destaillats, N. Acar, Comparative study of serine-plasmalogens in human retina and optic nerve: identification of atypical species with odd carbon chains, J. Lipid Res. 53 (2012) 776–783. https://doi.org/10.1194/jlr.D022962.

[11] S. Paul, G.I. Lancaster, P.J. Meikle, Plasmalogens: A potential therapeutic target for neurodegenerative and cardiometabolic disease, Prog. Lipid Res. 74 (2019) 186–195. https://doi.org/10.1016/j.plipres.2019.04.003.

[12] F. Dorninger, S. Forss-Petter, J. Berger, From peroxisomal disorders to common neurodegenerative diseases – the role of ether phospholipids in the nervous system, FEBS Lett. 591 (2017) 2761–2788. https://doi.org/10.1002/1873-3468.12788.

[13] S. Wallner, E. Orsó, M. Grandl, T. Konovalova, G. Liebisch, G. Schmitz, Phosphatidylcholine and phosphatidylethanolamine plasmalogens in lipid loaded human macrophages, PLOS ONE. 13 (2018) e0205706. https://doi.org/10.1371/journal.pone.0205706.

[14] N. Acar, O. Berdeaux, P. Juaneda, S. Grégoire, S. Cabaret, C. Joffre, C.P. Creuzot-Garcher, L. Bretillon, A.M. Bron, Red blood cell plasmalogens and docosahexaenoic acid are independently reduced in primary open-angle glaucoma, Exp. Eye Res. 89 (2009) 840–853. https://doi.org/10.1016/j.exer.2009.07.008.

[15] H. Goldfine, The appearance, disappearance and reappearance of plasmalogens in evolution, Prog. Lipid Res. 49 (2010) 493–498. https://doi.org/10.1016/j.plipres.2010.07.003.
[16] H.W. Mueller, J.T. O'Flaherty, D.G. Greene, M.P. Samuel, 1-0-Alkyl-linked glycerophospholipids of human neutrophils: distribution of arachidonate and other acyl residues in the ether-linked and diacyl species, J. Lipid Res. 25 (1984) 6. https://doi.org/10.1016/S0022-2275(20)37812-3.
[17] J. Koch, K. Lackner, Y. Wohlfarter, S. Sailer, J. Zschocke, E.R. Werner, K. Watschinger, M.A. Keller, Unequivocal Mapping of Molecular Ether Lipid Species by LC–MS/MS in Plasmalogen-Deficient Mice, Anal. Chem. 92 (2020) 11268–11276. https://doi.org/10.1021/acs.analchem.0c01933.
[18] T.H. Pham, M. Zaeem, T.A. Fillier, M. Nadeem, N.P. Vidal, C. Manful, S. Cheema, M. Cheema, R.H. Thomas, Targeting Modified Lipids during Routine Lipidomics Analysis using HILIC and C30 Reverse Phase Liquid Chromatography coupled to Mass Spectrometry, Sci. Rep. 9 (2019) 5048. https://doi.org/10.1038/s41598-019-41556-9.
[19] Q. Lin, D. Zhang, Y. Xia, Analysis of ether glycerophosphocholines at the level of C=C locations from human plasma, The Analyst. 145 (2020) 513–522. https://doi.org/10.1039/C9AN01515A.
[20] Y. Wang, S. Hinz, O. Uckermann, P. Hönscheid, W. von Schönfels, G. Burmeister, A. Hendricks, J.M. Ackerman, G.B. Baretton, J. Hampe, M. Brosch, C. Schafmayer, A. Shevchenko, S. Zeissig, Shotgun lipidomics-based characterization of the landscape of lipid metabolism in colorectal cancer, Biochim. Biophys. Acta BBA - Mol. Cell Biol. Lipids. 1865 (2020) 158579. https://doi.org/10.1016/j.bbalip.2019.158579.
[21] X. Li, Q. He, H. Hou, S. Zhang, X. Zhang, Y. Zhang, X. Wang, L. Han, K. Liu, Targeted lipidomics profiling of marine phospholipids from different resources by UPLC-Q-Exactive Orbitrap/MS approach, J. Chromatogr. B. 1096 (2018) 107–112. https://doi.org/10.1016/j.jchromb.2018.08.018.
[22] S. Anjos, E. Feiteira, F. Cerveira, T. Melo, A. Reboredo, S. Colombo, R. Dantas, E. Costa, A. Moreira, S. Santos, A. Campos, R. Ferreira, P. Domingues, M.R.M. Domingues, Lipidomics Reveals Similar Changes in Serum Phospholipid Signatures of Overweight and Obese Pediatric Subjects, J. Proteome Res. 18 (2019) 3174–3183. https://doi.org/10.1021/acs.jproteome.9b00249.
[23] Z. Ni, G. Angelidou, M. Lange, R. Hoffmann, M. Fedorova, LipidHunter Identifies Phospholipids by High-Throughput Processing of LC-MS and Shotgun Lipidomics Datasets, Anal. Chem. 89 (2017) 8800–8807. https://doi.org/10.1021/acs.analchem.7b01126.
[24] J. Jouhet, J. Lupette, O. Clerc, L. Magneschi, M. Bedhomme, S. Collin, S. Roy, E. Maréchal, F. Rébeillé, LC-MS/MS versus TLC plus GC methods: Consistency of glycerolipid and fatty acid profiles in microalgae and higher plant cells and effect of a nitrogen starvation, PLOS ONE. 12 (2017) e0182423. https://doi.org/10.1371/journal.pone.0182423.
[25] S. Abreu, S. Heron, A. Solgadi, F. Joffre, A. Tchapla, P. Chaminade, Rapid assessment of triacylglycerol fatty acyls composition by LC-APPI+-HRMS using monoacylglycerol like fragments intensities, Anal. Chim. Acta. 1178 (2021) 338809. https://doi.org/10.1016/j.aca.2021.338809.
[26] S. Abreu, A. Solgadi, P. Chaminade, Optimization of normal phase chromatographic conditions for lipid analysis and comparison of associated detection techniques, J. Chromatogr. A. (2017). https://doi.org/10.1016/j.chroma.2017.07.063.

[27] A. Delobel, D. Touboul, O. Laprévote, Structural Characterization of Phosphatidylcholines by Atmospheric Pressure Photoionization Mass Spectrometry, Eur. J. Mass Spectrom. 11 (2005) 409–417. https://doi.org/10.1255/ejms.760.
[28] M. Gaudin, L. Imbert, D. Libong, P. Chaminade, A. Brunelle, D. Touboul, O. Laprévote, Atmospheric Pressure Photoionization as a Powerful Tool for Large-Scale Lipidomic Studies, J. Am. Soc. Mass Spectrom. 23 (2012) 869–879. https://doi.org/10.1007/s13361-012-0341-y.
[29] W.R. Morrison, L.M. Smith, Preparation of fatty acid mathyl esters and dimethylacetals from lipids with boron fluoride methanol, J. Lipid Res. 5 (1964) 600–608. https://doi.org/10.1016/S0022-2275(20)40190-7.
[30] M. Holčapek, P. Jandera, P. Zderadička, L. Hruba, Characterization of triacylglycerol and diacylglycerol composition of plant oils using high-performance liquid chromatography–atmospheric pressure chemical ionization mass spectrometry, J. Chromatogr. A. 1010 (2003) 195–215. https://doi.org/10.1016/s0021-9673(03)01030-6.
[31] E.J. Murphy, R. Stephens, M. Jurkowitz-Alexander, L.A. Horrocks, Acidic hydrolysis of plasmalogens followed by high-performance liquid chromatography, Lipids. 28 (1993) 565–568. https://doi.org/10.1007/BF02536090.
[32] S. Mawatari, Y. Okuma, T. Fujino, Separation of intact plasmalogens and all other phospholipids by a single run of high-performance liquid chromatography, Anal. Biochem. 370 (2007) 54–59. https://doi.org/10.1016/j.ab.2007.05.020.
[33] R.A. Klein, Mass spectrometry of the phosphatidylcholines: fragmentation processes for dioleoyl and stearoyl-oleoyl glycerylphosphorylcholine, J. Lipid Res. 12 (1971) 628–634. https://doi.org/10.1016/S0022-2275(20)39483-9.
[34] Wm.C. Byrdwell, Dual parallel mass spectrometers for analysis of sphingolipid, glycerophospholipid and plasmalogen molecular species, Rapid Commun. Mass Spectrom. 12 (1998) 256–272. https://doi.org/10.1002/(SICI)1097-0231(19980314)12:5<256::AID-RCM149>3.0.CO;2-8.
[35] S.J. Kim, N. Kim, E.H. Koh, H.J. Yoo, Identification of Ethanolamine Plasmalogens from Complex Lipid Mixtures by MS/MS and Ag Adduction, Anal. Sci. 28 (2012) 1207–1212. https://doi.org/10.2116/analsci.28.1207.
[36] Y. Otoki, K. Nakagawa, S. Kato, T. Miyazawa, MS/MS and LC-MS/MS analysis of choline/ethanolamine plasmalogens via promotion of alkali metal adduct formation, J. Chromatogr. B. 1004 (2015) 85–92. https://doi.org/10.1016/j.jchromb.2015.09.012.
[37] S. Yamashita, A. Honjo, M. Aruga, K. Nakagawa, T. Miyazawa, Preparation of Marine Plasmalogen and Selective Identification of Molecular Species by LC-MS/MS, J. Oleo Sci. 63 (2014) 423–430. https://doi.org/10.5650/jos.ess13188.
[38] K. Yang, Z. Zhao, R.W. Gross, X. Han, Shotgun Lipidomics Identifies a Paired Rule for the Presence of Isomeric Ether Phospholipid Molecular Species, PLoS ONE. 2 (2007) e1368. https://doi.org/10.1371/journal.pone.0001368.
[39] T.J. Leiker, R.M. Barkley, R.C. Murphy, Analysis of diacylglycerol molecular species in cellular lipid extracts by normal-phase LC-electrospray mass spectrometry, Int. J. Mass Spectrom. 305 (2011) 103–108. https://doi.org/10.1016/j.ijms.2010.09.008.
[40] M. He, C.-X. Qin, X. Wang, N.-Z. Ding, Plant Unsaturated Fatty Acids: Biosynthesis and Regulation, Front. Plant Sci. 11 (2020) 390. https://doi.org/10.3389/fpls.2020.00390.
[41] G. Dacremont, G. Vincent, Assay of plasmalogens and polyunsaturated fatty acids (PUFA) in erythrocytes and fibroblasts, J Inherit Metab Dis. 18 (1995) 6. https://doi.org/10.1007/BF00711431.
[42] D.B. Goodenowe, L.L. Cook, J. Liu, Y. Lu, D.A. Jayasinghe, P.W.K. Ahiahonu, D. Heath, Y. Yamazaki, J. Flax, K.F. Krenitsky, D.L. Sparks, A. Lerner, R.P. Friedland, T.

Kudo, K. Kamino, T. Morihara, M. Takeda, P.L. Wood, Peripheral ethanolamine plasmalogen deficiency: a logical causative factor in Alzheimer's disease and dementia, J. Lipid Res. 48 (2007) 2485–2498. https://doi.org/10.1194/jlr.P700023-JLR200.

3. Conclusion

L'étude a montré que la méthode des ions B développée initialement sur la classe de TGs est également applicable aux différentes classes des PLs, avec certaines précautions.

Lorsque les extraits de PLs (PE œuf/soja ; PC œuf/cerveau/foie/soja ; PG œuf ; CL cœur ; PS cerveau ; PI soja ; PA œuf ; LPE œuf et LPC œuf) sont constitués exclusivement de diacyl-PLs, la méthode est directement utilisable.

Globalement, ces extraits contiennent de faibles teneurs en FAs polyinsaturés. L'utilisation de coefficients pondérateurs n'a pas été nécessaire pour corriger l'intensité des ions B. Les régressions de Deming ont mis en évidence que les résultats obtenus par la méthode de référence et par notre méthode n'étaient statistiquement pas différents (au risque de 5%).

Ce résultat démontre que dans notre étude, ni la nature de la tête polaire des PLs, ni la nature des FAs de même que la variation de composition de la phase mobile due au gradient d'élution n'ont un impact statistiquement significatif sur la formation des ions B.

Lors des premières analyses menées par GC-FID, la présence de P-PLs n'a pas été anticipée dans quatre extraits (PE cœur/foie/cerveau et PC cœur). Lors de la transestérification, les chaînes alkényles des P-PLs produisent des DMAs. Les DMAs peuvent être facilement confondus avec des FAMEs sur les chromatogrammes [178]. Ces extraits ont été analysés avec la méthode de Morrison et Smith [174], pour l'obtention de valeurs de référence fiables.

Les deux sous-classes, diacyl-PLs et P-PLs, contenues simultanément dans ces extraits, sont coélués chromatographiquement avec la méthode NPLC-APCI-HRMS. Or, les ions fragments produits par ces deux sous-classes, ne sont pas formés au même degré. L'utilisation des ions B n'est donc pas utilisable dans ces conditions, il est de ce fait impératif de séparer les diacyl-PLs et les P-PLs.

Un traitement rapide des échantillons est proposé dans l'étude pour pallier cette difficulté. Les extraits contenant des P-PLs ont été soumis à des vapeurs d'acide chlorhydrique concentré. Lors de cette étape, les liaisons éther vinyliques sont hydrolysées tandis que les liaisons esters restent intactes. Les P-PLs sont transformés en Lyso-PLs et en aldéhydes. La distribution des FAs estérifiés sur les P-PLs est accessible à travers l'analyse des Lyso-PLs formés. Les diacyl-PLs n'étant plus coélués avec les P-PLs, la distribution des FAs est accessible. La distinction de la distribution des FAs de diacyl-PLs et P-PLs est un avantage supplémentaire de cette méthode par rapport à la GC-FID.

Ces quatre extraits de PLs, contiennent des pourcentages en FAs polyinsaturés importants (C20 :4, C20 :3, C22 :6, C22 :5 et 22:4). Cependant, compte tenu du faible nombre d'extraits, il n'a pas été possible de calculer les coefficients pondérateurs pour corriger les intensités des ions B correspondants. Par comparaison avec l'étude précédente, un coefficient 2 a été appliqué à l'ensemble des intensités des ions B. Cette correction a permis d'obtenir des résultats comparables à ceux obtenus par GC-FID.

La fragmentation des P-PE et P-PC a également été explorée. Les P-PE étant naturellement plus abondants que les P-PC, il a été possible de trouver des informations sur leur fragmentation dans la littérature. Cependant, aucune information n'a pu être trouvée sur la fragmentation des P-PC lors de l'utilisation d'une source APPI ou APCI en mode positif.
La fragmentation du standard PC P-18 :0/18 :1 a été explorée et un schéma de fragmentation a été proposé dans cet article.

A l'issue de ce travail, nous avons également mis en évidence des ions spécifiques des P-PLs, permettant d'accéder à la distribution des alkényls gras, à l'image des ions B pour accéder à la distribution des FAs.

CHAPITRE VIII. REAJUSTEMENT DES LIPIDES DANS LES SOUCHES PRODUCTRICES D'ACIDES GRAS A CHAINES IMPAIRES DE *YARROWIA LIPOLYTICA*

1. Introduction

Au cours de cette thèse, nous avons collaboré avec le Dr Jean-Marc Nicaud, Directeur de l'équipe Biologie Intégrative du Métabolisme lipidique microbien BIMLip de l'institut MICALIS (INRA-AgroParisTech, à Jouy-en-Josas) sur le réajustement des lipides dans les souches productrices d'acides gras à chaînes impaires de *Yarrowia lipolytica*.

L'équipe BIMLip entreprend une approche fondamentale de biologie systémique et d'ingénierie génétique du métabolisme lipidique des levures oléagineuses et en particulier de *Yarrowia lipolytica*. Les applications concernent les biocarburants, les biolipides, les bioplastiques et la chimie blanche. Les travaux de l'équipe BIMLip s'articulent autour de 3 axes majeurs : le métabolisme des lipides ; la biologie synthétique et la valorisation.

Dans ce travail collaboratif, le profil lipidique de la souche obese L de *Yarrowia lipolytica* est comparé à celui de la souche obese LP (modifiée génétiquement pour la production de FAs à chaînes impaires). Les échantillons correspondent à des triplicatas de cultures, réalisés à trois temps (72 h, 144 h et 216 h). Le BIMLip possède un GC-FID, avec lequel il détermine la composition des FAs totaux pour contrôler la production des souches en FAs. Cependant, ces analyses ne permettent pas de déterminer si les FAs impairs sont localisés spécifiquement sur la classe des TGs, répartis sur l'ensemble des classes ou bien répartis d'une autre manière. Cette information est importante pour la compréhension du métabolisme de ces levures.

Cette collaboration a donné lieu à l'article « Lipid Readjustment in Yarrowia lipolytica Odd-Chain Fatty Acids Producing Strains » publié dans Biomolecules. L'article est présenté ci-après.

2. Publication 4

Les données supplémentaires liées à cette publication sont présentées en Annexe IV.

biomolecules

MDPI

Article

Lipid Readjustment in *Yarrowia lipolytica* Odd-Chain Fatty Acids Producing Strains

Sonia Abreu [1,†], Young-Kyoung Park [2,†], Camilla Pires de Souza [2], Lea Vidal [2], Pierre Chaminade [1,*] and Jean-Marc Nicaud [2,*]

[1] Lipides: Systèmes Analytiques et Biologiques, Université Paris-Saclay, 91400 Orsay, France; sonia.abreu@universite-paris-saclay.fr
[2] Micalis Institute, INRAE, AgroParisTech, Université Paris-Saclay, 78350 Jouy-en-Josas, France; yk16.park@gmail.com (Y.-K.P.); camilla.pires-de-souza@inrae.fr (C.P.d.S.); lea.vidal@inrae.fr (L.V.)
* Correspondence: pierre.chaminade@universite-paris-saclay.fr (P.C.); jean-marc.nicaud@inrae.fr (J.-M.N.)
† These authors equally contributed to this work.

Abstract: *Yarrowia lipolytica* is a promising oleaginous yeast for producing unusual lipids, such as odd-chain fatty acids (OCFA). Their diverse applications and low natural production make OCFA particularly interesting. In recent studies, inhibiting the catabolic pathway of precursor, boosting precursor pools, and optimizing substrate combination greatly improved the production of OCFA in *Y. lipolytica*. We explored the lipid readjustment of OCFA in engineered *Y. lipolytica* strains. NPLC-Corona-CAD® evidenced a time-dependent overproduction of free fatty acids, diglycerides, and phosphatidylcholine (PC) in obese LP compared to obese L. Phosphatidylethanolamine (PE) and phosphatidylinositol, largely overproduced in obese LP at 72 h compared to obese L, vanished at 216 h. The fatty acyls (FAs) composition of glycero- and glycerophospholipids was determined by NPLC-APPI$^+$-HRMS from in-source generated monoacylglycerol-like fragment ions. C18:1 and C17:1 were predominant acylglycerols in obese L and obese LP, respectively. Phosphatidic acid, PE, and PC exhibited similar FAs composition but differed in their molecular species distributions. Cardiolipin (CL) is known to contain mostly C18:2 FAs corresponding to the composition in obese L, 50% of C18:2, and 35% of C18:1. In obese LP, both FAs dropped to drop to 20%, and C17:1 were predominant, reaching 55%. We hypothesize that CL-modified composition in obese LPs may alter mitochondrial function and limit lipid production.

Keywords: *Yarrowia lipolytica*; OCFA; lipid profile; lipidome; normal-phase liquid chromatography; metabolic readjustments

check for updates

Citation: Abreu, S.; Park, Y.-K.; Pires de Souza, C.; Vidal, L.; Chaminade, P.; Nicaud, J.-M. Lipid Readjustment in *Yarrowia lipolytica* Odd-Chain Fatty Acids Producing Strains. *Biomolecules* **2022**, *12*, 1026. https://doi.org/10.3390/biom12081026

Academic Editor: Naoko Goto-Inoue

Received: 21 June 2022
Accepted: 20 July 2022
Published: 25 July 2022

Publisher's Note: MDPI stays neutral with regard to jurisdictional claims in published maps and institutional affiliations.

Copyright: © 2022 by the authors. Licensee MDPI, Basel, Switzerland. This article is an open access article distributed under the terms and conditions of the Creative Commons Attribution (CC BY) license (https://creativecommons.org/licenses/by/4.0/).

1. Introduction

In recent years, *Yarrowia lipolytica* has emerged as a favorable chassis for the production of unusual lipids [1,2]. Its oleaginous phenotype, the comprehensive studies on its lipid metabolism, and the advancement of synthetic biology tools provided a huge opportunity to improve the unusual lipid production at high titer, rate, and yield in *Y. lipolytica* [3–6]. Unusual lipids have received increasing attention as target products of metabolic engineering due to their wide range of applications in industry. Odd chain fatty acids (OCFAs), a type of unusual lipids, have shown various applications in the food, medical, and chemical industries. OCFA can be used as a biomarker of obesity, dietary fiber intake, and the risk of coronary heart disease [7–10]. *cis*-9-heptadecenoic acid (C17:1) has anti-inflammatory effects and can help treat psoriasis, allergies, and autoimmune diseases [11]. As well as, *cis*-9-heptadecenoic acid is known to have antagonistic activity against powdery mildew (a plant disease) [12]. OCFA and its derivatives have high value as precursors for flavor and fragrance, hydraulic fluids, plasticizers, coatings, and others [12–15].

Despite their broad applications, the natural production of OCFA is very limited [6,16]. In order to improve the production of OCFA, metabolic engineering and optimization of

production conditions were shown in several studies [17]. In recent studies, the production of OCFA in *Y. lipolytica* was greatly improved by inhibiting the catabolic pathway of precursor, boosting precursor pools, and optimizing substrate combination [1,5]. From the engineered strain, 1.87 g/L of OCFA, which was 62% of total lipids, was produced. The composition of fatty acids was also significantly changed, resulting from this genetic engineering. Indeed, in the engineered strain, the ratio of oleic acid (C18:1, main FA produced by *Y. lipolytica*) was only about 15% of total lipids, while more than 45% was heptadecenoic acid (C17:1) [1].

In most studies, the production of lipid is determined by GC-FID analysis after the transesterification of fatty acyl chains [18]. This method is straightforward and robust to quantify the fatty acids and assess the chain length and the degree of saturation. However, this method is not capable of assessing the lipidome, i.e., understanding the distribution of lipids in different classes and the flexibility of the lipidome according to environmental stress or genetic modification. It is known that the lipidome (membrane and metabolic energy storage) is flexible and can be readjusted [19,20]. Therefore, exploring the dynamic modification of lipidome is very important to understand the mechanism of stress response and adaptation of microorganisms. Hein and Hayen investigated the adaptive changes of glycerophospholipids (GP) under various environmental conditions with five phylogenetically different yeasts, including *Y. lipolytica* [21]. It was observed that the GP profiles were significantly different, showing characteristic genetic traits and phylogenetic relationships reflected in the GP profile of the organism. More recently, the lipidome adjustment in *Y. lipolytica* upon different cultivation conditions was explored [22]. Remarkable changes in the composition and the degree of saturation of fatty acids were observed due to the increase in the temperature. Modification of fatty acid composition of some membrane phospholipids was shown at changing pH and temperature. The study reflects the flexibility of lipid composition of *Y. lipolytica* in adaptation to environmental conditions. Apart from the environmental change, the readjustment of lipidome depending on genetic engineering is not explored in *Y. lipolytica* so far.

The recent development of mass spectrometry has paved the way for a more comprehensive and quantitative assessment of lipidome [23]. Through LC-MS and LC with Corona-CAD® detection, notable variations of lipid class composition were observed in modified *Streptomyces* bacteria strains [24–26]. In another study, we showed that the FAs distribution of TAGs and PLs could be assessed from the relative intensities of ions $[MG+H-H_2O]^+$ produced in-source using $APCI^+$ (or $APPI^+$) ionization. This approach allows access to the FAs distribution by lipid class without pretreatment of the lipid extracts, which greatly simplifies the analyses. LC-MS coupling (MS^2 and MS^3) was also used for lipid class and molecular species identification [27,28].

In this study, we aimed to explore the lipid readjustment of OCFA in engineered *Y. lipolytica* strains employing the LC-MS method recently developed for lipidomic analysis. First, we assessed the lipid readjustment by comparing chromatographic lipid class analysis profiles obtained by LC with Corona-CAD® detection. Second, we evaluated the lipid rearrangement by comparing the FAs distribution of lipid classes as measured by LC-MS according to the up-to-date methodology.

2. Materials and Methods

2.1. Strains and Media Composition

Y. lipolytica strains, JMY7775 (obese L), and JMY7780 (obese LP) previously constructed in Park et al. [1] were used in this study. Rich medium (YPD) for strain activation and preculture was prepared with 1% (*w*/*v*) yeast extract, 2% (*w*/*v*) peptone, and 2% (*w*/*v*) glucose. For lipid accumulation, minimal media (YNBD2P0.5A1) was prepared with 0.17% (*w*/*v*) yeast nitrogen base without amino acids and ammonium sulfate (YNBww), 0.15% (*w*/*v*) NH_4Cl, 50 mM KH_2PO_4–Na_2HPO_4 (pH 6.8), 2% (*w*/*v*) glucose, 0.5% (*w*/*v*) propionate and 1% (*w*/*v*) acetate.

2.2. Culture Conditions

OCFA biosynthesis experiments were carried out in minimal media under nitrogen-limited conditions, and the cultures were prepared as follows: an initial pre-culture was established by inoculating in 10 mL of YPD medium and grown overnight at 28 °C and 180 rpm. The cells were washed with sterile distilled water and used inoculating to 50 mL of minimal medium in 250 mL Erlenmeyer flasks with initial OD 0.1. The cultures were then incubated at 28 °C and 180 rpm for 8 days. All cultivations were made in three biological replicates.

In order to determine the dry cell weight (DCW), 2 mL of the culture was taken from the flasks, washed, and lyophilized in a pre-weighed tube. The differences in mass corresponded to the mg of cells in 2 mL of culture.

2.3. Lipid Extraction and Analysis by GC-FID

Lipids were extracted from freeze-dried cells (around 20 mg) by transmethylation described by Browse et al. [18]. The methylated FA (FAMEs) were then analyzed using gas chromatography equipped with a flame ionization detector (GC-FID, Varian 3900, Walnut Creek, CA, USA) and a Varian FactorFour vf-23 ms column where the bleed specification at 260 °C is 3 pA (30 m, 0.25 mm, 0.25 µm).

The FAMEs were identified via comparisons with commercial standards (FAME32, Supelco, Bellefonte, PA, USA) and quantified using the internal standard, 100 µg of commercial dodecanoic acid (Sigma-Aldrich, St. Louis, MO, USA). Commercial standards of OCFAs (Odd Carbon Straight Chains Kit containing 9 FAs, OC9, Supelco, Bellefonte, PA, USA,) were converted into their FAMEs using the same method employed with the yeast samples. They were then analyzed by GC to identify the OCFAs from the yeast samples. For each data point, we used three biological replicates and calculated average and standard deviation values.

2.4. Lipid Extraction and Analysis by LC-MS and LC-Corona-CAD®

Lipid extraction was carried out by a modified Folch's method [29] from three independent cultures of *Y. lipolytica* strains JMY7775 and JMY7780. A 4.5 mL volume of chloroform/methanol (1:2) was added to 10 mg of lyophilized *Y. lipolytica* strains and vortexed for 30 s. The mixture was allowed to stay at ambient temperature for 1 h before addition of 1.25 mL of water and vortexing for 30 s. The phase separation was achieved by centrifugation (1000× *g* for 10 min). The (lower) organic phase was collected, and the (upper) aqueous phase was re-extracted by adding 2 mL of chloroform/methanol (85:15). The two organic phases were pooled and evaporated under a stream of nitrogen at room temperature. The dry residue was dissolved in 900 µL of isooctane/chloroform (4:1) before analysis.

The chromatographic conditions of the lipid class analysis have been described previously [30]. The separation was performed with an Inertsil Silica (150 mm × 2.1 mm I.D, 5 mm) column (GL Sciences Inc., Tokyo, Japan) fitted to a Dionex U-3000 RSLC (Thermo Fisher Scientific, Waltham, MA, USA) liquid chromatograph. A quaternary solvent gradient was used to elute all the lipid classes present in the sample by increasing the order of polarity, with slight modifications in the solvent program as presented in [27], where two isocratic steps were introduced to improve PLs separation. The column temperature was set at 25 °C (instead of 40 °C) for the same purpose. The flow rate was set at 0.8 mL/min.

Lipid class identification was verified by coupling chromatographic separation to mass spectrometry. MS analyses were performed with an LTQ-Orbitrap Velos Pro (Thermo Fisher Scientific, Waltham, MA, USA) equipped with an APCI ion source piloted by the Xcalibur software. The MS^2 and MS^3 spectra were obtained in data-dependent acquisition (DDA) mode as described previously [30]. The injected volume was increased to 10 µL (instead of 2 µL) to improve the detection.

The TAG, DAG, GlcADG, and PL FAs distribution is determined with the method described in [27,28]. Briefly, the % FAs are obtained by direct measurement of the %

intensities of ions B ([MAG+H-H2O]$^+$) for each lipid class molecular species distribution analyzed. In order to facilitate the identification, the *m/z* were compared to the database LIPID MAPS®. MS2 spectra allowed distinguishing isomers.

Lipid profiles were compared by coupling the chromatographic separation to a Corona-CAD® detector (ESA, Chelmsford, MA, USA) [30]. An injected volume of 2 µL was used for these analyses. The signal was acquired with a Chromeleon data station (Thermo Fisher Scientific, Villebon-sur-Yvette, France). Corona-CAD® is a universal detector used for liquid chromatography and described in [31]. The differences in the composition of the lipid classes in the samples are expressed as peak areas.

3. Results

3.1. Metabolic Pathways for Lipid Synthesis and Lipid Readjustments

Pathways for lipid synthesis and degradation are well explored in *Y. lipolytica* as a model oleaginous yeast so far [4,32]. The synthesis of phospholipids in *Y. lipolytica* is identified based on the pathway of *Saccharomyces cerevisiae* [33].

De novo lipid synthesis starts from acetyl-CoA and malonyl-CoA building blocks. Fatty acid synthase enzymatic complex (FAS) produces an acyl-CoA pool using acetyl-CoA as an initiation molecule and malonyl-CoA as an elongation unit. The released acyl-CoAs go through further modification, elongation, and/or desaturation, resulting in various fatty acids with different chain lengths and the degree of saturation. These acyl-CoA pools are condensed with glycerol-3-phosphate to generate lysophosphatidic acid (LPA), then phosphatidic acid (PA), diacylglycerol (DAG), and finally triacylglycerol (TAG) via the Kennedy pathway. TAG is then incorporated into the lipid body (LB) specialized compartment for neutral lipid storage.

Glycerophospholipids known to compose the plasma membrane have different classes depending on their head group. Each class is synthesized through a different pathway, as depicted in Figure 1. Phosphatidylserine (PS), phosphatidylethanolamine (PE), and phosphatidylcholine (PC) are synthesized through the CDP-DAG pathway. PC has an alternative pathway from DAG, too. CDP-DAG is also a precursor of phosphatidylinositol (PI) and cardiolipin (CL), as well as the products of the CDP-DAG pathway.

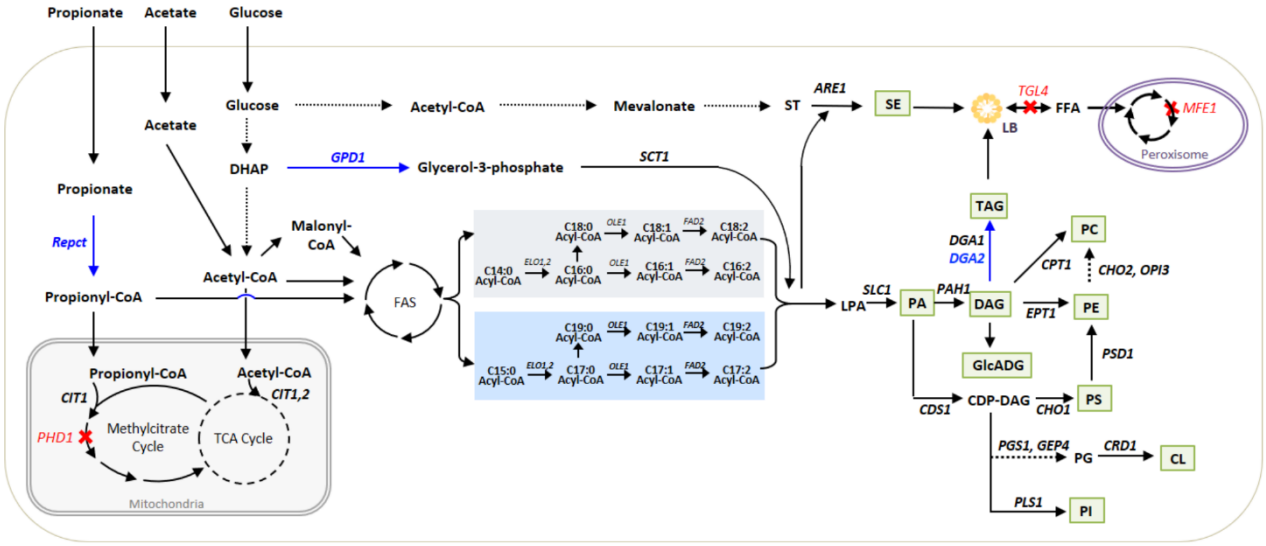

Figure 1. The engineering strategy used in this study to improve the accumulation of odd-chain fatty acids are described in the pathway. The overexpressed genes in the *Y. lipolytica* strain used in this study

are written in blue, and corresponding paths are depicted with blue arrows. The deleted genes are written in red, and corresponding paths are depicted with red cross. The lipid class detected in this study are written in green box. The multiple steps in the pathway are depicted as dashed line. Even-chain acyl-CoA pools are in the grey box, and odd-chain acyl-CoA pools are in the blue box. SE—sterol ester; ST—sterol; LPA—lysophosphatidic acid; PA—phosphatidic acid; DAG—diacylglycerol; TAG—triacylglycerol; GlcADG—1,2-diacyl-3-O-α-glucuronosylglycerol; CDP-DAG—cytidine diphosphate-diacylglycerol; PC—phosphatidylcholine; PE—phosphatidylethanolamine; PS—phosphatidylserine; PG—phosphatidylglycerol; CL—cardiolipin; PI—phosphatidylinositol; LB—lipid body; FFA—free fatty acid.

Sterol (ST) is synthesized from acetyl-CoA through the mevalonate pathway, then converted to sterol ester (SE), which is known as a storage form of lipids in the cell.

The fatty acids stored in the lipid body can be mobilized and degraded through the β-oxidation pathway, resulting in the release of acetyl-CoA (relevant pathways and genes were well explained in the review [4,32]).

3.2. Odd-Chain Fatty Acid Production by Obese L and Obese LP Strains

In this study, two *Y. lipolytica* strains (obese L and obese LP) engineered to accumulate a high amount of lipids, mostly TAG, were used. The metabolic modification includes the deletion of *MFE1* and *TGL4* to inhibit TAG remobilization and degradation, the overexpression of *GPD1* and *DGA2* to push and pull TAG biosynthesis, and the overexpression of *LPD1* to enhance the storage of TAG (obese L strain). The OCFA-producing strain (obese LP strain) has a unique modification to improve OCFA synthesis, the introduction of the *PCT* from *Ralstonia eutropha* to boost the propionyl-CoA pool [1]. In order to improve OCFA synthesis, the condition of cultivation, especially the combination of carbon sources and the C/N ratio, was optimized in the same study. Thus, obese L and obese LP strains were cultivated with a substrate combination of 2% (*w*/*v*) glucose, 0.5% (*w*/*v*) propionate, and 1% (*w*/*v*) acetate and the ratio C/N = 45 for the analysis of lipid readjustment in this study. Samples for lipid analysis and lipidomic analysis were harvested at 72 h, 144 h, and 216 h (Figure 2). First, to verify biomass and lipid content, samples from 216 h were analyzed by GC-FID as described previously [1]. Results showed that the major FA produced from the control strain (Obese L) was oleic acid (C18:1), while the obese LP strain produced mostly heptadecenoic acid (C17:1), which is consistent with the previous study. The ratio of OCFA to total lipid was 5.07% in the obese L strain, while more than 50% of lipids were OCFA in the obese LP strain, as described in Table 1. Around 35% of lipids were heptadecenoic acid (C17:1), the major OCFA, in the obese LP strain. There was no significant difference in substrate utilization between the two strains, Figure S1).

Table 1. Biomass and lipid content from obese L and obese LP strains. The samples harvested at 216 h were used for the analysis of GC-FID.

Samples	DCW (g/L)	Lipid Content % (g/g DCW)	Lipids (g/L)	OCFA /Total Lipids (%)	C17:1 /Total lipids (%)	C17:1/C18:1 (%)
Obese L	8.48	21.46	1.82	5.07	2.30	5.47
Obese LP	6.07	23.92	1.45	50.86	35.29	197.98

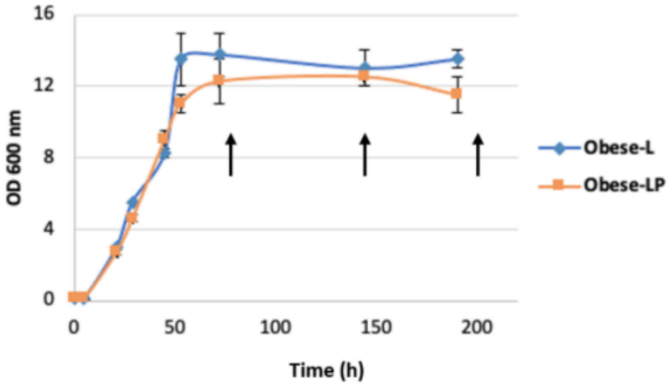

Figure 2. Growth and time-point sampling for lipidomic analysis. Two strains obese L (JMY7775) and obese LP (JMY7780) were grown in YNBDPA media at 28 °C. Samples for lipidomic analysis were taken at 72 h, 144 h, and 216 h (arrow). The corresponding samples were named L-72, L-144, L-216 and LP-72, LP-144, LP-216, respectively. Growth A600 is adapted from Park et al., 2021.

3.3. LC-Corona-CAD® and LC-MS Analyses

The lipid samples from the obese L and obese LP strains, at the three time points, were analyzed by LC-Corona-CAD® a in triplicates and were named one to three. Results from sample one, collected at 144 h of cultivation, are shown in Figure 3. Twelve different lipid classes were separated and identified using this chromatographic method. Results are from three independent extractions. Chromatogram corresponds to sample one at 144 h for the strain obese L (obese L1-144) and obese LP (obese LP1-144). TAG is the primary lipid class in *Y. lipolytica*. In Figure 3, the TAG peak (measured at 900 mV) is truncated to allow the observation of other lipid classes, which are SE, DAG, FFA, GlcCer, GlcADG, PE, PA, PI, CL, and PC. DAGs are eluted as a double peak (1,3 DAG and 1,2 DAG); however, the literature describes changes in stereochemistry during analysis that do not reflect the true stereochemistry in the sample [34]. For this reason, the data from the two peaks were summed, and the stereochemistry was not taken into account. The LC-MS data allowed identifying a small amount of ST co-eluted with the first DAG peak. Peaks related to impurities present in the solvents or plastic (Erucamide) [35] are also observed, with no impact on the analysis.

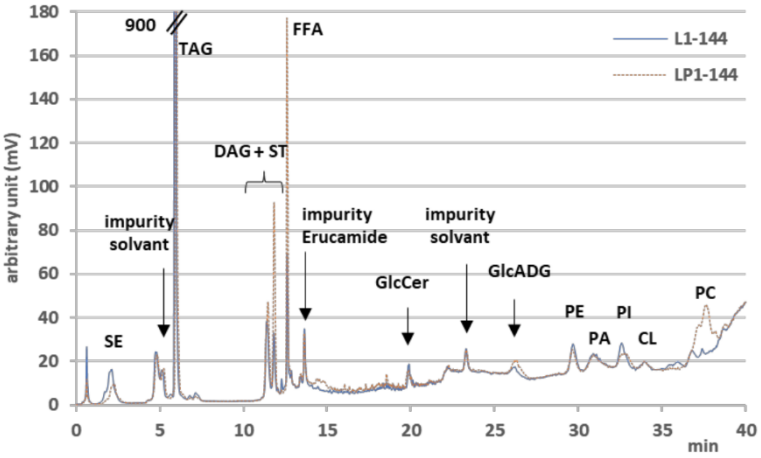

Figure 3. LC-Corona-CAD® lipid profiles from obese L1-144 and obese LP1-144. SE—sterol esters; TAG—triacylglycerols; DAG—diacylglycerols; ST—sterols, FFA—free fatty acids; GlcCer—glucosylceramides; GlcADG—glycosyldiacylglycerols; PE—phosphatidylethanolamines; PA—phosphatidic acids; PI—phosphatidylinositols; CL—cardiolipins; PC—phosphatidylcholines.

In the following figures, the ordering of the lipid classes corresponds to the order of elution. FAs and lipid molecular species will be presented in increasing molecular masses.

3.3.1. Storage Lipid Profiles during Odd-Chain Fatty Acid Production

Figure 4 represents the peak areas of the storage lipid classes as obtained in LC-Corona-CAD®.

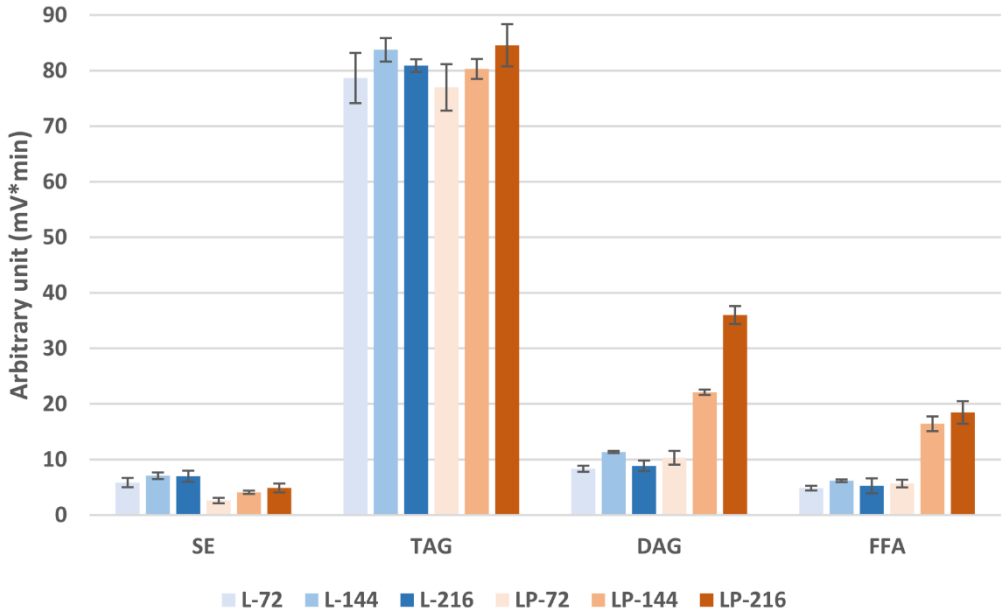

Figure 4. Comparison of the storage lipid content in the obese L and obese LP over time. SE—sterol esters; TAG—triacylglycerols; DAG—diacylglycerols; FFA—free fatty acids. Mean values are displayed (n = 3, ± SD).

TAG amounts are comparable between the two strains and do not vary significantly over time, as described in Figure 4. Similarly, the amounts of SEs, DAGs, and FFAs were similarly maintained over the cultivation time in the obese L strain. On the contrary, the OCFA-producing strain (obese LP), the odd-chain-producing strain, presents a time-dependent increase, in particular for DAGs and FFAs. SE levels are lower in obese LP compared to the control, suggesting limitation in the Kennedy pathway. Alternatively, this increase in DAG and FFA may result from the induction of the expression of lipase genes, such as the *LIP2* gene coding for the main extracellular lipase Lip2p, or the expression of intracellular lipases coding genes such as *LIP1*, *LIP3*, and *LIP5*, or the induction of the TAG remobilization pathway by increasing the expression of the genes coding for the intracellular TAG-lipases Tgl3p and/or Tgl4p, involved in TAG remobilization.

LC-MS analyses allow access to the FA distribution of most lipid classes. The distribution of FAs of TAGs and DAGs is obtained from the relative intensities of ions $[MG+H-H_2O]^+$ [27,28]. In the case of free FFAs, where this approach cannot be implemented, the relative intensities of the $[RCOO]^-$ ions are presented. The FA distribution is presented in Figure 5.

Obese LP produces significantly more OCFAs than obese L for these three reserve lipids. The majority of FA is C17:1 in obese LP and C18:1 in obese L. In general, all even FAs decrease in favor of mainly C17:1 in obese LP. Moreover, in obese LP, TAGs, and DAGs, unsaturated FAs (C17:1 and C18:2) increase while saturated FAs (C16:0, C17:0, C18:0, and C19:0) decrease.

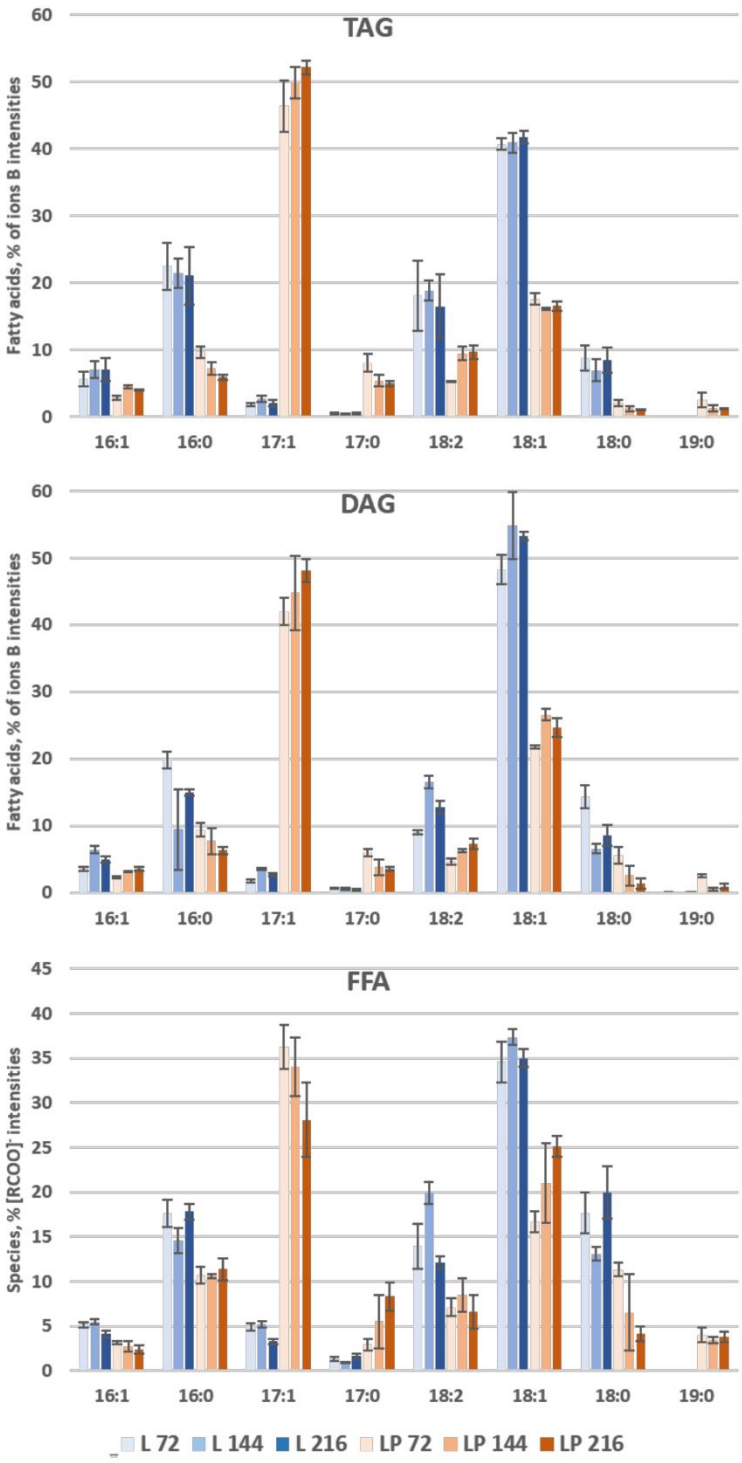

Figure 5. Comparison of the storage lipid composition in the obese L and obese LP over time. Lipid profiles in % FA per classes for TAG and DAG and % $[RCOO]^-$ Intensities for FFA. Mean values are displayed (n = 3, ±SD). Lipid species below 3% are not indicated.

SE mass spectra obtained for obese L and obese LP at 144 h in positive and negative ionization modes are presented in Figure S2. In positive mode, SE directly loses their FA, and the majority ion corresponds to $[M\text{-}FA+H\text{-}H_2O]^+$ [36]. This ion gives information on the sterol nucleus but does not allow for formally identifying the sterol among the numerous existing isomers. The nature of the sterols nuclei naturally present in *Y. lipolytica* SEs has already been investigated in the literature [37–39]. The identification of the sterols nuclei is presented in Table S1, and the distribution of $[M\text{-}FA+H\text{-}H_2O]^+$ ions are presented in Figure S3. The most abundant SE contains ergosta 5,7 dienol, corresponding to ergosterol with two π-bonds and an additional methyl group on the B-ring and acyl chain. High intensities corresponding to ergosterol and episterol are also measured. The distribution of sterol nuclei in SE is slightly different depending on the strain. Obese LP has a higher proportion of ergosta 5,7 dienol and ergosterol and a lower proportion of episterol and lanosterol than obese L.

In negative mode, the fragment ions $[RCOO]^-$ of the full scan mass spectra may, to some extent, indicate the distribution of esterified FAs on the SEs. Obese L1-144 and obese LP1-144 spectra are presented in Figure S4. These spectra show a similarity in the distribution of FAs in this class and those of other storage lipids.

Under our analytical conditions, it is not possible to formally identify the molecular species of SE, TAG, and DAG.

3.3.2. Membrane Lipid Profiles during Odd-Chain Fatty Acid Production

Figure 6 represents the peak areas obtained in LC-Corona-CAD® of the membrane lipids of the different samples. ST are omitted in this figure since their abundance is very low, and the ST peak is partially coeluted with DAGs.

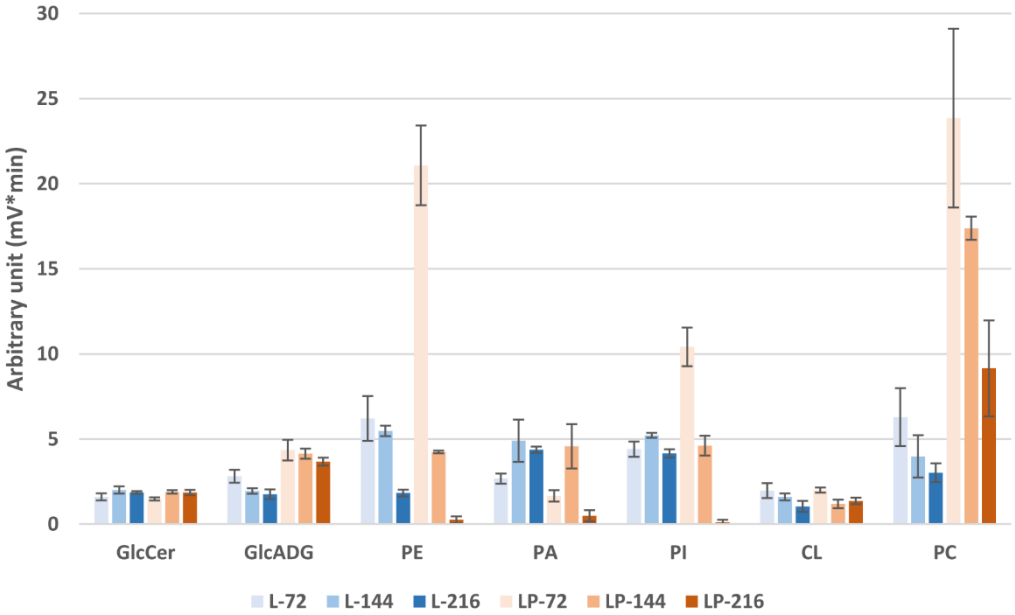

Figure 6. Comparison of membrane lipid composition in the obese L and obese LP over time. Error bars represent the standard deviation of triplicates. Mean values are displayed (n = 3, ±SD). Lipid classes below 3% are not indicated.

At 72 h, obese LP contains much higher PE, PI, and PC amounts than obese L. These amounts decrease drastically at 144 h and 216 h. At 216 h, PE and PI have almost disappeared from the LC-Corona-CAD® profiles. However, the PC remains at a high level compared to obese L.

In obese L, PE and PC decrease less significantly, and PI remains stable over time. PA is the only PL whose amount increases between 72 and 144 h in both strains. CL is present at the same amount in both strains and a decrease with time is visible in both strains.

The amounts of GlcCer are stable over time and comparable between the two strains. The amounts of GlcADG are higher in obese LP. A slight decrease is observed in both strains.

The distribution of FAs in PLs determined by LC-MS [27,28] is presented in Figure 7, left side. At 216 h, the amounts of PE, PA, and PI in obese LP are too low to be exploited by LC-MS. Obese LP produces significantly more OCFAs than obese L in the membranes. The major OCFA is consistently C17:1 in obese LP and C18:1 in obese L, except for CL (mainly C18:2). C17:0 is predominantly detected in PI (3% and 7%). C19:0 represents less than 0.1% of the FAs in PLs, whereas it could represent up to 3% of the FAs in storage lipids. In general, all even FAs decrease in favor of mainly C17:1 in obese LP. The distribution in FAs is comparable between PE, PA, and PC. PI differentiates itself by a higher % of C16:0 and CL by a higher percentage of C18:2. CL is mainly localized in mitochondria and predominantly contains C18:2 FAs [40].

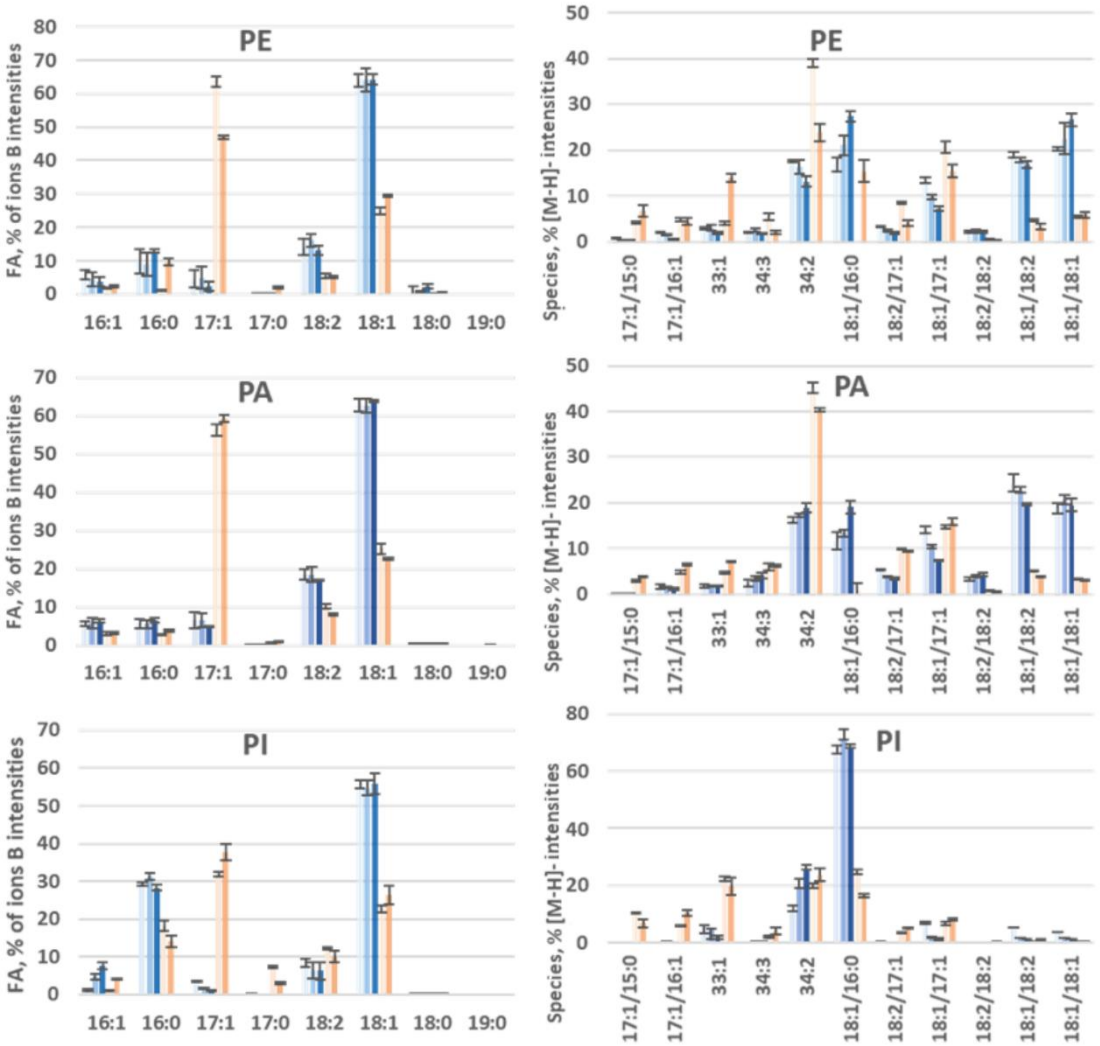

Figure 7. *Cont.*

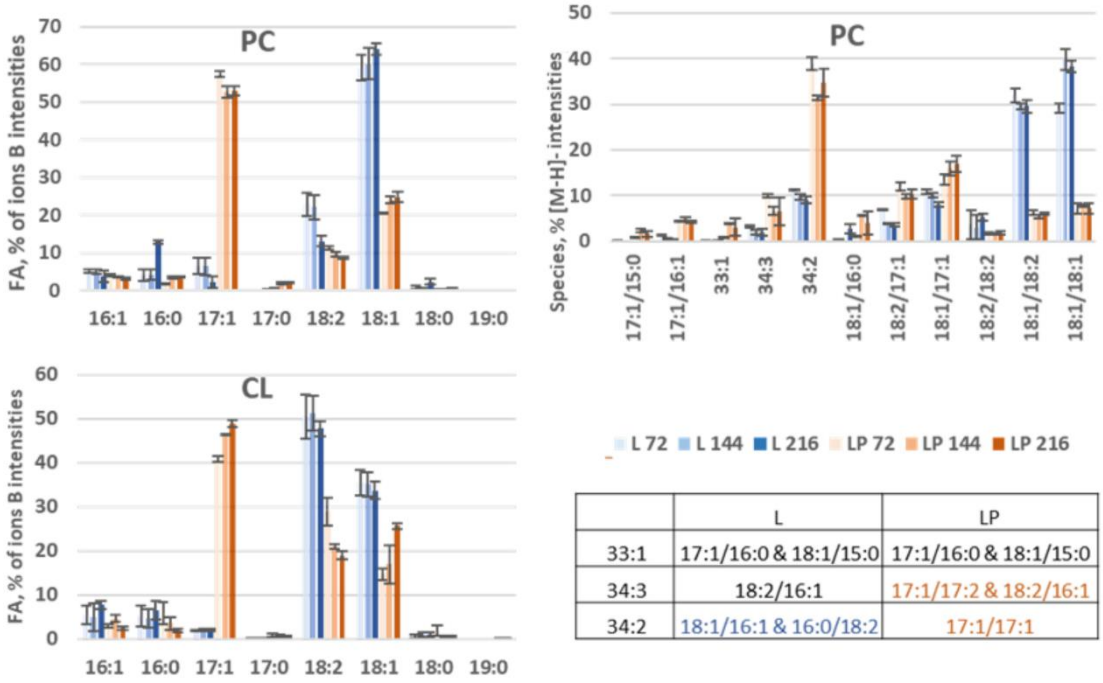

	L	LP
33:1	17:1/16:0 & 18:1/15:0	17:1/16:0 & 18:1/15:0
34:3	18:2/16:1	17:1/17:2 & 18:2/16:1
34:2	18:1/16:1 & 16:0/18:2	17:1/17:1

Figure 7. Comparison of the FA profiles in PL classes during OCFA production in the obese L and obese LP over time. On the left side, histograms represent the FA profiles expressed as % of total fatty acids. On the right side, histograms represent the % intensity of PLs molecular species (calculated from their $[M\text{-}H]^-$). Species noted 33:1, 34:3 and 34:2 correspond to isobaric species differing according to strains. The corresponding molecular species are indicated in the table.

3.3.3. Species Distribution

- PLs

The molecular species distribution, shown on the right side of Figure 7, was determined from the intensity of $[M\text{-}H]^-$ ions for all PLs and, specifically for PC, $[M^\circ]^-$. FAs identification was performed from the MS^2 mass spectra of the corresponding ions. An example of a full scan and MS^2 mass spectrum of the most abundant ion for obese L and obese LP at 144 h of each PL class is shown in Figure S5–S12. Table S2–S5 present the identification of the $[M\text{-}H]^-$ or $[M^\circ]^-$ of PLs. As the ionization of PLs is dependent on the nature of the FAs and the physiochemical environment [41], the concordance of these data with those obtained by ions B [27,28] was investigated. Therefore, the FAs distribution was recalculated from the results issued from the distribution of molecular species, and the results are presented in Figure S13. The distributions of FAs calculated in this way and those obtained by B ions show the same trends for all PLs. An overestimation is observed for the C17:1 of PI, which is explained by the presence of isobaric molecular species of PI (17:1/17:1), not taken into account in the calculation. This overall agreement of the two methods provides reasonable confidence in the molecular species distribution data. CL is the only PL studied containing four FAs; the molecular species representation for this class is presented differently in the following.

The species noted in 33:1, 34:3, and 34:2 correspond to isobar molecular species; the correspondence is given in the box of Figure 7. All molecular species in obese L containing C17:1 are more abundant in obese LP (at the detriment of the other species). The 17:1/17:1, almost non-existent in obese L, represents the most abundant molecular species in obese LP except in the PI, where it is at the same level as 18:1/16:0 and 17:1/16:0. There are no single predominant molecular species in obese L, except in the PI with PI (18:1/16:0). On the other hand, although the distribution of FAs is similar for PE, PA, and PC, the distribution in

terms of molecular species is not uniform. In obese L, PC is distinguished by two majority species, PC (18:1/18:2) and PC (18:1/18:1), whereas in PE and PA, there are four majority species. In addition, PC has a very low percentage of 18:1/16:0 compared to other PLs. In obese LP, the distribution of species in PA and PC are close. The majority species is the (17:1/17:1), whereas, in the PE, four molecular species are in the majority representing about 20%.

- CL

For CL, a full scan mass spectrum is presented for each strain in Figure S14. Molecular species are identified by the number of carbons shown at the bottom of the figure and by the number of unsaturations shown at the top of the ion intensities. Examples of the most likely molecular species (based on the distribution of the previously determined FAs) are given as a guide. Fragmentation could not be exploited due to the low intensities of $[M-H]^-$ ions. The spectra show that obese L contains predominantly two molecular species, C72:7 and C72:6 (probably corresponding to CL (18:2/18:2/18:2/18:1), and CL (18:2/18:2/18:1/18:1). Obese LP has a wider distribution with shorter chains due to the abundance of C17:1.

- GlcADG

The FA and molecular species distribution of GlcADG are presented in Figure 8. The distributions are very similar to those found for PI. This is probably related to their chemical structures, which are also very close. The mass spectra are presented in Figure S15, and the MS^2 of the majority $[M-H]^-$ ion is shown in Figure S16.

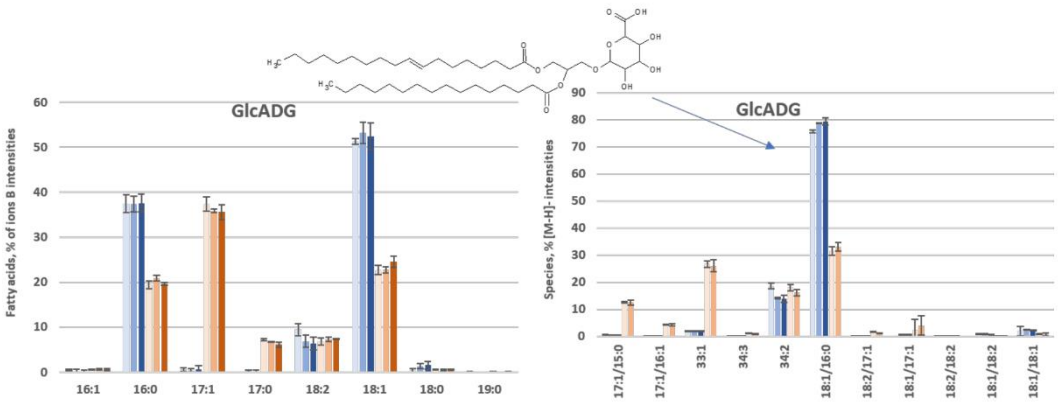

Figure 8. Comparison of %FA profiles in the GlcADG during OCFA production in the obese L (Blue) and obese LP (orange) over time (72, 144 and 216 h).

- GlcCer

Since GlcCer does not contain a glycerol backbone but a sphingoid base, the FAs distribution cannot be estimated from the ion B measurement. The obese L and obese LP mass spectra at 144 h in negative and positive ionization mode are shown in Figure S17. GlcCer ionizes as $[M-H]^-$ and $[M+H-H2O]^+$, respectively. According to the LIPID MAPS® MS Data Bulk Search tool, the $[M+H-H2O]^+$ ion at 710.552 *m/z*, which is predominant in both strains, is consistent with a HexCer 35:2;O_3. This structure is in agreement with the observations of Bal and coworkers [42], who reported that the sphingolipids synthesized by *Y. lipolytica* are GlcCer with a long chain base C18, desaturated at C4 and C8 positions and methylated at C9, and an amide-bonded C16 FA hydroxylated at the C2 position.

In obese LP, the $[M+H-H2O]^+$ ion at 724.568 *m/z* is also very abundant (60% of the intensity of the major ion). By analogy, we hypothesize that its structure contains a C17 FA instead of C16.

- ST

LC-MS allows selectively extracting the spectrum of ST from their coelution with DAGs. For STs, a mass spectrum for obese L and LP at 144 h in positive mode (in the range [360–400]) is shown in Figure S18. The only ST in both strains is ergosterol ($[M+H-H_2O]^+$ ion at *m/z* 379.335. The intensities are of the same order of magnitude in both strains. The same observation was made for the other time points (data not shown). In contrast to SE, which contains a diversity of sterol nuclei, free STs are exclusively composed of ergosterol.

4. Discussion

Y. lipolytica is widespread in nature. This yeast has often been found to inhabit dairy products, cheese, contaminated milk, fermented vegetables, poultry, sausages and meat products, and marine ecosystems, including high saline waters, as well as in environments rich in hydrophobic substrates [43,44].

This yeast was shown to be well adapted to efficiently utilize hydrophobic substrates such as n-alkanes, fatty acids, fats, and oils [45–47], which correlate with its ecologic niches such as sewage, industrial wastewaters, oil-polluted soil, and seawater [44].

This non-conventional strictly aerobic ascomycetous yeast, generally regarded as safe (GRAS) by the American Food and Drug Administration (FDA), has been exploited in several biotechnological, environmental, and industrial applications. Some examples include heterologous hosts for producing pharmaceutically and industrially relevant proteins, enzymes, organic acids, biofuels, and bioremediation of industrial and environmental waste.

The capacity of *Y. lipolytica* to degrade very efficiently hydrophobic substrates, for which it has a specific metabolic pathway, made this yeast a promising chassis as a cell factory for producing lipid and lipid derivatives.

The oleaginous yeast *Y. lipolytica* is a particularly attractive platform for the sustainable industrial production of lipid-derived fuels and chemicals [3] and the production of usual and unusual lipids [4].

Over the past several years, great progress has been made to improve lipid and lipid-derivatives production by *Y. lipolytica* [48–50]. Different strategies have been used for increasing lipid accumulation and recovery from *Y. lipolytica* [51,52].

Several engineered strains have been generated to over-accumulate specific fatty acids, such as the high oleic acid producing strains, where oleic acid represents more than 90% of the fatty acids [53], 6.5% of conjugated linoleic acid [54], Cyclopropane fatty acids reach 22% [55], 10-methyl branched fatty acids represent 37% [56] and odd chain fatty acids content was improved from 46.8% up to 62% [1,5].

The results of our study show about a 22% lipid content in our condition for both strains (obese and OCFA producing strains). Similar lipid content was previously reported by Sekova and coworkers [22] and in our previous reports [1]. Additional genetic modifications could be introduced to further improve the lipid content in odd-chain-producing strains, as those described in the recent review by El kantar and Koubaa [52].

Few lipidome analyses were previously reported; Hein and Hayen reported the comparison of lipidome in different yeast [21]. Furthermore, Sekova and coworkers [22] reported a lipidome analysis of the *Y. lipolytica* wild-type strain W29 at two temperatures of culture (29 °C and 38 °C) and two pH (5.5 and 9). A high level of DAG was observed at 38 °C (20–30% of storage lipid), which were not present at a lower temperature. A two-fold decrease in the FFA level was reported (from 40% to about 20%). The optimal lipid content of cell dry weight was 23% at pH 5.5, 29 °C, while it represents only 14,4% at pH 9, 38 °C at the expense of a two-fold higher level of cytosol sugar (a mean of 4.4% at 29 °C, up to a mean of 10.4% at 38 °C). Our study shows no changes in TAG level in obese L versus obese LP (Figure 4); however, an increase in DAG and FAA in the obese LP during cultivation suggests a lipid readjustment induced by stress resulting from the OCFA production. Such lipid readjustments were induced by temperature stress but not pH stress [22].

A transitory lipid readjustment during OCFA production was mainly observed in the membrane lipid composition at the PE, PI, and PC levels and was mainly seen at 72 h of

culture (Figure 6). In contrast, Sekova and coworkers did not observe PE readjustment but observed an increase in PC at 38 °C [22]. We may hypothesize that such transitory readjustment may occur upon temperature stress if a lipidomic analysis has been performed during the culture time. Alternatively, we could speculate that the temperature stress response may be different from the membrane fatty acid profile response.

This lipidomic study is the first implementation of the FAs distribution assessment by NPLC-HRMS as proposed by [27,28]. According to this method, the FAs distributions of glycero- and glycerophospholipid classes are assessed from their insource fragmentation acquired during the lipid classes chromatographic separation. This information is comparable with the classical methodology, which consists of a TLC separation followed by a GC-FID FAMEs analysis as used in Sekova et al.'s study [22]. This new methodology is simple to implement and much more rapid than the classical one but does not provide information about unsaturation positions. It provides the FAs with relative distribution, the most frequently reported result, but not a quantitation of individual FAs. This rapid method of FAs distribution assessment is advantageous when an important number of samples is to be analyzed. This allowed us to perform a kinetic study at three different times and to evidence the PE readjustment. Furthermore, the lipid extract can be analyzed without pretreatment or sample denaturation. The whole information is accessible, and a non-targeted analysis can be conducted.

Studies using HILIC [38] or RPLC [57] coupled with ESI-MS are comparable to our approach in their implementation but do not allow assessing the FAs distribution of lipid classes. In both HILIC and RPLC studies, GC-MS complementary analyses were conducted to evaluate the total FAs distributions. This total FAs distribution is less informative than the per-class distribution.

As previously indicated, the objective of our lipidomic approach was to evaluate the readjustment of OCFAs in two engineered *Y. lipolytica* strains. For this purpose, an NPLC-Corona-CAD® analysis [30] allowed a detailed analysis of the relative contents of the different lipid classes with a time-dependent over-expression of FFAs, DAGs, and PCs in obese LP compared to obese L. As proposed in two recent studies [27,28], coupling the NPLC method to APCI+-HRMS allows the assessment of the distribution of FAs, namely the different glycero- and glycerophospholipid classes. This approach offers an important degree of detail for each of these lipid classes and allows, if necessary, to compare this distribution to that of the molecular species. Thus, we were able to verify that TAG and DAG had a similar FA distribution with C18:1 as the majority FA in obese L, which C17:1 replaces in obese LP. The observation is similar in the PL classes, although more subtle differences can be noted. Thus, the distribution of FAs in PA, PE, and PC are similar and close to those of TAG and DAG, with here also a predominance of C18:1 in obese L replaced by C17:1 in obese LP. In obese L, C18:1 is distributed in three main species (PC (18:1/16:0), PC (18:1/18:1), and PC (18:1/18:2)) of equal importance, while C17:1 is found overwhelmingly in PC (34:2) in obese LP. CL and PI show differences from the other classes of PLs. In obese L, PI shows a distribution of FAs where C18:1 is in the majority associated with a high proportion of C16:0, which leads to the presence of the very majority species PI (18:1/16:0). In contrast, in obese LP, FA C17:1 alongside C16:0 and C18:1 leads to a complete redistribution of these FAs within the molecular species. Concerning CL, C18:2 is in the majority in obese L next to C18:1, while these two FAs remain present although halved in favor of C17:1 in obese LP.

CL is known to undergo a remodeling favoring C18:2 incorporation [58]. A high level of C18:2 is correlated with an effective mitochondrial function. CL is primarily located in the inner membrane of mitochondria, notably in the cristae region [59].

When an aberrant distribution of CL FAs is observed, as in Barth's syndrome [60,61], mitochondrial function is impaired, including energy production and protein transport. In the case of obese LP, the distribution of CL FAs is strongly altered; it is reasonable to assume that this may negatively affect the development of these strains.

Based on the experimental evidence, we conclude that *Y. lipolytica* can use different kinds of lipid readjustment responses for long-term adaptation to unfavorable environmental conditions and upon unusual fatty acids production.

Based on the modification in FA profiles and phospholipid type and profiles, it is worth noticing that lipid readjustments take place rapidly. Accumulation of unusual lipids in *Y. lipolytica* leads to dramatic metabolic readjustments of lipid profiles and crucial changes in the membrane lipids and sterols.

The flexibility and the readjustments of lipid and phospholipids upon OCFA synthesis demonstrate that *Y. lipolytica* has the capacity to modulate and induce lipid readjustment. This confirms that *Y. lipolytica* has high potential as a workhorse microorganism for producing unusual lipids.

Supplementary Materials: The following are available online at https://www.mdpi.com/article/10.3390/biom12081026/s1, Figure S1: Substrates consumption during cultivation. Figure S2: SE mass spectra of obese L and obese LP at 144 h. Figure S3: Distribution of $[M\text{-}FA\text{+}H\text{-}H2O]^+$ ions and corresponding stérols in SE fraction. Figure S4: SE mass spectra in obese L and obese LP at 144 h, zoom *m/z* [225–300]. Figure S5: PE mass spectra in obese L and obese LP at 144 h. Figure S6: MS^2 spectra of ions @714.55 of detected PE. Figure S7: PA mass spectra in obese L and obese LP at 144 h. Figure S8: MS^2 spectra of ions @671.46 of detected PA in obese L and obese LP at 144 h. Figure S9: PI mass spectra in obese L and obese LP at 144 h. Figure S10: MS^2 spectra of ions @833.52 of detected PI in obese L and obese LP at 144 h. Figure S11: PC mass spectra in obese L and obese LP at 144 h. Figure S12: MS^2 spectra of ions @757.50 of detected PC in obese L and obese LP at 144 h. Figure S13: Obese L and obese LP (at 144 h) FA distribution of PLs classes calculated from Ion B intensities (green bars) or from molecular species intensities (yellow bars). Figure S14: CL mass spectra in obese L and obese LP at 144 h. Figure S15: GlcADG mass spectra in obese L and obese LP at 144 h. Figure S16: MS^2 spectra of ions @769.54 of detected GlcADG in obese L and obese LP at 144 h. Figure S17: GlcCER mass spectra in obese L and obese LP at 144 h. Figure S18: ST Mass spectra of Ergosterol in obese L and obese LP at 144 h. Table S1: Identification of sterol motifs present in SE. Table S2: Identification of molecular species present in PE. Table S3: Identification of molecular species present in PA. Table S4: Identification of molecular species present in PI. Table S5: Identification of molecular species present in PC.

Author Contributions: Conceptualization, J.-M.N., Y.-K.P. and P.C.; methodology, S.A., P.C. and Y.-K.P.; formal analysis, S.A. and Y.-K.P.; writing—original draft preparation, Y.-K.P., S.A., C.P.d.S. and L.V.; writing—review and editing, P.C., Y.-K.P. and J.-M.N.; supervision, P.C. and J.-M.N.; funding acquisition, J.-M.N. All authors have read and agreed to the published version of the manuscript.

Funding: Young-Kyoung Park and Camilla Pires de Souza received grants from the project YaLiOl supported by the ANR grant "ANR-20-CE43-0007" of the French National Research Agency (ANR) in France. Lea Vidal received grants from the project Val2O supported by the UPSaclay in the frame of the Investments for the future managed by the Agence Nationale de la Recherche under the "Investissements d'avenir" program with the reference Poc in Labs 2020-1011.

Data Availability Statement: Mass spectrometry data are available upon request to P. Chaminade.

Acknowledgments: The authors acknowledge Audrey Solgadi and Bastien Prost from IPSIT, SAMM Facility, for their support in mass spectrometric analysis. We also thank the Région Ile de France for the financial support of this facility.

Conflicts of Interest: The authors declare no conflict of interest. The funders had no role in the design of the study; in the collection, analyses, or interpretation of data; in the writing of the manuscript, or in the decision to publish the results.

Abbreviations

ACPT	acyl-ACP thioesterase
AcTAGs	acetylated TAGs
C/N ratio	carbon to nitrogen ratio
CFA	cyclopropanated fatty acid
CL	cardiolipin
CLA	conjugated linoleic acid
DacT	diacylglycerol acetyltransferase
DAG	diacylglycerol
DCW	dry cell weight
DHA	docosahexaenoic acid
DPA	docosapentaenoic acid
ECFA	even-chain fatty acid
EPA	eicosapentaenoic acid
ER	endoplasmic reticulum
FA	fatty acyl
FAEE	fatty acid ethyl ester
FAME	fatty acid methyl ester
FAS	fatty acid synthase
FFA	free fatty acid
GPL	glycerophospholipids
KAS	beta-ketoacyl-ACP synthase
KS	ketoacyl synthase
LA	linoleic acid
LB	lipid body
LCFA	long-chain fatty acid
LPA	lysophosphatidic acid
MAG	monoacylglycerol
MCFA	medium-chain fatty acid
MFE	multi-functional enzyme
MPT	malonyl/palmitoyl transacylase
OCFA	odd chain fatty acids
PA	phosphatidic acid
PC	phosphatidylcholne
PCT	propionyl-CoA transferase
PE	phosphatidylethanolamine
PG	phosphatidylglycerol
PI	phosphatidylinositol
PKT	polyketide synthase
PPP	pentose phosphate pathway
PS	phosphtidylserine
PUFA	polyunsaturated fatty acid
RA	ricinoleic acid
SCFASEST	short-chain fatty acidsterol estersterol
TAG	triacylglycerol
TALEN	transcription activator-like effector nuclease
VLCFA	very long-chain fatty acid
WT	wild-type

References

1. Park, Y.-K.; Bordes, F.; Letisse, F.; Nicaud, J.-M. Engineering precursor pools for increasing production of odd-chain fatty acids in *Yarrowia lipolytica*. *Metab. Eng. Commun.* **2021**, *12*, e00158. [CrossRef] [PubMed]
2. Czerwiec, Q.; Idrissitaghki, A.; Imatoukene, N.; Nonus, M.; Thomasset, B.; Nicaud, J.-M.; Rossignol, T. Optimization of cyclopropane fatty acids production in *Yarrowia lipolytica*. *Yeast* **2019**, *36*, 143–151. [CrossRef] [PubMed]
3. Ledesma-Amaro, R.; Nicaud, J.-M. *Yarrowia lipolytica* as a biotechnological chassis to produce usual and unusual fatty acids. *Prog. Lipid Res.* **2016**, *61*, 40–50. [CrossRef] [PubMed]

4. Park, Y.-K.; Nicaud, J.-M. Metabolic Engineering for Unusual Lipid Production in *Yarrowia lipolytica*. *Microorganisms* **2020**, *8*, 1937. [CrossRef] [PubMed]
5. Park, Y.-K.; Dulermo, T.; Ledesma-Amaro, R.; Nicaud, J.-M. Optimization of odd chain fatty acid production by *Yarrowia lipolytica*. *Biotechnol. Biofuels* **2018**, *11*, 158. [CrossRef] [PubMed]
6. Diedrich, M.; Henschel, K.-P. The natural occurrence of unusual fatty acids. Part 1. Odd numbered fatty acids. *Food /Nahrung.* **1990**, *34*, 935–943. [CrossRef]
7. Forouhi, N.G.; Koulman, A.; Sharp, S.J.; Imamura, F.; Kröger, J.; Schulze, M.B.; Crowe, F.L.; Huerta, J.M.; Guevara, M.; Beulens, J.W.; et al. Differences in the prospective association between individual plasma phospholipid saturated fatty acids and incident type 2 diabetes: The EPIC-InterAct case-cohort study. *Lancet Diabetes Endocrinol.* **2014**, *2*, 810–818. [CrossRef]
8. Pfeuffer, M.; Jaudszus, A. Pentadecanoic and Heptadecanoic Acids: Multifaceted Odd-Chain Fatty Acids. *Adv. Nutr. Int. Rev. J.* **2016**, *7*, 730–734. [CrossRef]
9. Khaw, K.-T.; Friesen, M.D.; Riboli, E.; Luben, R.; Wareham, N. Plasma Phospholipid Fatty Acid Concentration and Incident Coronary Heart Disease in Men and Women: The EPIC-Norfolk Prospective Study. *PLoS Med.* **2012**, *9*, e1001255. [CrossRef]
10. Jenkins, B.; West, J.A.; Koulman, A. A Review of Odd-Chain Fatty Acid Metabolism and the Role of Pentadecanoic Acid (C15:0) and Heptadecanoic Acid (C17:0) in Health and Disease. *Molecules* **2015**, *20*, 2425–2444. [CrossRef]
11. Degwert, J.; Jacob, J.; Steckel, F. Use of cis-9-heptadecenoic Acid for Treating Psoriasis and Allergies. U.S. Patent 5,708,028A, 24 March 1994.
12. Avis, T.; Boulanger, R.R.; Bélanger, R.R. Synthesis and Biological Characterization of (Z)-9-Heptadecenoic and (Z)-6-Methyl-9-Heptadecenoic Acids: Fatty Acids with Antibiotic Activity Produced by Pseudozyma flocculosa. *J. Chem. Ecol.* **2000**, *26*, 987–1000. [CrossRef]
13. Clausen, C.A.; Coleman, R.D.; Yang, V.W. Fatty Acid–Based Formulations for Wood Protection against Mold and Sapstain. *For. Prod. J.* **2010**, *60*, 301–304. [CrossRef]
14. Köckritz, A.; Blumenstein, M.; Martin, A. Catalytic cleavage of methyl oleate or oleic acid. *Eur. J. Lipid Sci. Technol.* **2010**, *112*, 58–63. [CrossRef]
15. Fitton, A.; Goa, K.L. Azelaic Acid: A Review of its Pharmacological Properties and Therapeutic Efficacy in Acne and Hyperpigmentary Skin Disorders. *Drugs* **1991**, *41*, 780–798. [CrossRef]
16. Řezanka, T.; Sigler, K. Odd-numbered very-long-chain fatty acids from the microbial, animal and plant kingdoms. *Prog. Lipid Res.* **2009**, *48*, 206–238. [CrossRef]
17. Zhang, L.-S.; Liang, S.; Zong, M.-H.; Yang, J.-G.; Lou, W.-Y. Microbial synthesis of functional odd-chain fatty acids: A review. *World J. Microbiol. Biotechnol.* **2020**, *36*, 35. [CrossRef]
18. Browse, J.; McCourt, P.J.; Somerville, C.R. Fatty acid composition of leaf lipids determined after combined digestion and fatty acid methyl ester formation from fresh tissue. *Anal. Biochem.* **1986**, *152*, 141–145. [CrossRef]
19. Ejsing, C.S.; Sampaio, J.L.; Surendranath, V.; Duchoslav, E.; Ekroos, K.; Klemm, R.W.; Simons, K.; Shevchenko, A. Global analysis of the yeast lipidome by quantitative shotgun mass spectrometry. *Proc. Natl. Acad. Sci. USA* **2009**, *106*, 2136–2141. [CrossRef]
20. Klose, C.; Surma, M.A.; Gerl, M.J.; Meyenhofer, F.; Shevchenko, A.; Simons, K. Flexibility of a Eukaryotic Lipidome—Insights from Yeast Lipidomics. *PLoS ONE* **2012**, *7*, e35063. [CrossRef]
21. Hein, E.-M.; Hayen, H. Comparative Lipidomic Profiling of *S. cerevisiae* and Four Other Hemiascomycetous Yeasts. *Metabolites* **2012**, *2*, 254–267. [CrossRef]
22. Sekova, V.Y.; Dergacheva, D.I.; Isakova, E.P.; Gessler, N.N.; Tereshina, V.M.; Deryabina, Y.I. Soluble Sugar and Lipid Readjustments in the *Yarrowia lipolytica* Yeast at Various Temperatures and pH. *Metabolites* **2019**, *9*, 307. [CrossRef] [PubMed]
23. Navas-Iglesias, N.; Carrasco-Pancorbo, A.; Cuadros-Rodríguez, L. From lipids analysis towards lipidomics, a new challenge for the analytical chemistry of the 21st century. Part II: Analytical lipidomics. *TrAC Trends Anal. Chem.* **2009**, *28*, 393–403. [CrossRef]
24. Lejeune, C.; Abreu, S.; Chaminade, P.; Dulermo, T.; David, M.; Werten, S.; Virolle, M.-J. Impact of Phosphate Availability on Membrane Lipid Content of the Model Strains, Streptomyces lividans and Streptomyces coelicolor. *Front. Microbiol.* **2021**, *12*, 623919. [CrossRef] [PubMed]
25. Zhang, J.; Liang, Q.; Xu, Z.; Cui, M.; Zhang, Q.; Abreu, S.; David, M.; Lejeune, C.; Chaminade, P.; Virolle, M.-J.; et al. The Inhibition of Antibiotic Production in Streptomyces coelicolor Over-Expressing the TetR Regulator SCO3201 Is Correlated with Changes in the Lipidome of the Strain. *Front. Microbiol.* **2020**, *11*, 1399. [CrossRef] [PubMed]
26. David, M.; Lejeune, C.; Abreu, S.; Thibessard, A.; Leblond, P.; Chaminade, P.; Virolle, M.-J. Negative Correlation between Lipid Content and Antibiotic Activity in Streptomyces: General Rule and Exceptions. *Antibiotics* **2020**, *9*, 280. [CrossRef]
27. Abreu, S.; Heron, S.; Solgadi, A.; Joffre, F.; Tchapla, A.; Chaminade, P. Rapid assessment of triacylglycerol fatty acyls composition by LC-APPI$^+$ -HRMS using monoacylglycerol like fragments intensities. *Anal. Chim. Acta* **2021**, *1178*, 338809. [CrossRef] [PubMed]
28. Abreu, S.; Héron, S.; Solgadi, A.; Prost, B.; Dalloux-Chioccioli, J.; Kermarrec, A.; Meynier, A.; Bertrand-Michel, J.; Tchapla, A.; Chaminade, P. Rapid assessment of fatty acyls chains of phospholipids and plasmalogens by atmospheric pressure chemical ionization in positive mode and high-resolution mass spectrometry using in-source generated monoacylglycerol like fragments intensities. *J. Chromatogr. A* **2022**, *1673*, 463093. [CrossRef] [PubMed]
29. Folch, J.; Lees, M.; Stanley, G.H.S. A Simple Method for the Isolation and Purification of Total Lipides from Animal Tissues. *J. Biol. Chem.* **1957**, *226*, 497–509. [CrossRef]

30. Abreu, S.; Solgadi, A.; Chaminade, P. Optimization of normal phase chromatographic conditions for lipid analysis and comparison of associated detection techniques. *J. Chromatogr. A* **2017**, *1514*, 54–71. [CrossRef] [PubMed]
31. Dixon, R.W.; Peterson, D.S. Development and testing of a detection method for liquid chromatography based on aerosol charging. *Anal. Chem.* **2002**, *74*, 2930–2937. [CrossRef]
32. Beopoulos, A.; Cescut, J.; Haddouche, R.; Uribelarrea, J.-L.; Molina-Jouve, C.; Nicaud, J.-M. *Yarrowia lipolytica* as a model for bio-oil production. *Prog. Lipid Res.* **2009**, *48*, 375–387. [CrossRef] [PubMed]
33. Koch, B.; Schmidt, C.; Daum, G. Storage lipids of yeasts: A survey of nonpolar lipid metabolism in *Saccharomyces cerevisiae*, *Pichia pastoris*, and *Yarrowia lipolytica*. *FEMS Microbiol. Rev.* **2014**, *38*, 892–915. [CrossRef] [PubMed]
34. Leiker, T.J.; Barkley, R.M.; Murphy, R.C. Analysis of diacylglycerol molecular species in cellular lipid extracts by normal-phase LC-electrospray mass spectrometry. *Int. J. Mass Spectrom.* **2011**, *305*, 103–108. [CrossRef]
35. Jug, U.; Naumoska, K.; Metličar, V.; Schink, A.; Makuc, D.; Vovk, I.; Plavec, J.; Lucas, K. Interference of oleamide with analytical and bioassay results. *Sci. Rep.* **2020**, *10*, 2163. [CrossRef]
36. Rozenberg, R.; Ruibal-Mendieta, N.L.; Petitjean, G.; Cani, P.; Delacroix, D.L.; Delzenne, N.M.; Meurens, M.; Quetin-Leclercq, J.; Habib-Jiwan, J.-L. Phytosterol analysis and characterization in spelt (*Triticum aestivum* ssp. *spelta* L.) and wheat (*T. aestivum* L.) lipids by LC/APCI-MS. *J. Cereal Sci.* **2003**, *38*, 189–197. [CrossRef]
37. Langseter, A.M.; Dzurendova, S.; Shapaval, V.; Kohler, A.; Ekeberg, D.; Zimmermann, B. Evaluation and optimisation of direct transesterification methods for the assessment of lipid accumulation in oleaginous filamentous fungi. *Microb. Cell Factories* **2021**, *20*, 59. [CrossRef] [PubMed]
38. Walker, C.; Ryu, S.; Trinh, C.T. Exceptional Solvent Tolerance in *Yarrowia lipolytica* Is Enhanced by Sterols. *Metab. Eng.* **2019**, *54*, 83–95. [CrossRef]
39. Ta, T.M.N. Mécanismes Physiologiques et Biologiques Induits Chez Yarrowia Lipolytyica en Réponse à des Modifications de L'environnement Physico-Chimique des Cellules. Ph.D. Thesis, Alimentation et Nutrition, Université de Bourgogne, Bourgogne, France, 2010. Available online: https://tel.archives-ouvertes.fr/tel-00575589 (accessed on 20 July 2022).
40. Han, X.; Yang, K.; Yang, J.; Cheng, H.; Gross, R.W. Shotgun lipidomics of cardiolipin molecular species in lipid extracts of biological samples. *J. Lipid Res.* **2006**, *47*, 864–879. [CrossRef]
41. Khoury, S.; El Banna, N.; Tfaili, S.; Chaminade, P. A study of inter-species ion suppression in electrospray ionization-mass spectrometry of some phospholipid classes. *Anal. Bioanal. Chem.* **2016**, *408*, 1453–1465. [CrossRef]
42. Bal, J.; Lee, H.-J.; Cheon, S.A.; Lee, K.J.; Oh, D.-B.; Kim, J.-Y. Ylpex5 mutation partially suppresses the defective hyphal growth of a *Yarrowia lipolytica* ceramide synthase mutant, Yllac1, by recovering lipid raft polarization and vacuole morphogenesis. *Fungal Genet. Biol.* **2013**, *50*, 1–10. [CrossRef]
43. Madzak, C. Engineering *Yarrowia lipolytica* for Use in Biotechnological Applications: A Review of Major Achievements and Recent Innovations. *Mol. Biotechnol.* **2018**, *60*, 621–635. [CrossRef] [PubMed]
44. Mamaev, D.; Zvyagilskaya, R. *Yarrowia lipolytica*: A multitalented yeast species of ecological significance. *FEMS Yeast Res.* **2021**, *21*, foab008. [CrossRef] [PubMed]
45. Fickers, P.; Benetti, P.-H.; Waché, Y.; Marty, A.; Mauersberger, S.; Smit, M.S.; Nicaud, J.-M. Hydrophobic substrate utilisation by the yeast, and its potential applications. *FEMS Yeast Res.* **2005**, *5*, 527–543. [CrossRef] [PubMed]
46. Thevenieau, F.; Le Dall, M.-T.; Nthangeni, B.; Mauersberger, S.; Marchal, R.; Nicaud, J.-M. Characterization of *Yarrowia lipolytica* mutants affected in hydrophobic substrate utilization. *Fungal Genet. Biol.* **2007**, *44*, 531–542. [CrossRef] [PubMed]
47. Thevenieau, F.; Beopoulos, A.; Desfougeres, T.; Sabirova, J.; Albertin, K.; Zinjarde, S.; Nicaud, J.M. Uptake and assimilation of hydrophobic substrates by the oleaginous yeast *Yarrowia lipolytica*. In *Handbook of Hydrocarbon and Lipid Microbiology*; Timmis, K.N., Ed.; Springer: Berlin/Heidelberg, Germany, 2009.
48. Blazeck, J.; Hill, A.; Liu, L.; Knight, R.; Miller, J.; Pan, A.; Otoupal, P.; Alper, H.S. Harnessing *Yarrowia lipolytica* lipogenesis to create a platform for lipid and biofuel production. *Nat. Commun.* **2014**, *5*, 3131. [CrossRef]
49. Lazar, Z.; Liu, N.; Stephanopoulos, G. Holistic Approaches in Lipid Production by *Yarrowia lipolytica*. *Trends Biotechnol.* **2018**, *36*, 1157–1170. [CrossRef]
50. Liu, H.; Song, Y.; Fan, X.; Wang, C.; Lu, X.; Tian, Y. *Yarrowia lipolytica* as an Oleaginous Platform for the Production of Value-Added Fatty Acid-Based Bioproducts. *Front. Microbiol.* **2021**, *11*, 608662. [CrossRef]
51. Kamineni, A.; Consiglio, A.L.; MacEwen, K.; Chen, S.; Chifamba, G.; Shaw, A.J.; Tsakraklides, V. Increasing lipid yield in *Yarrowia lipolytica* through phosphoketolase and phosphotransacetylase expression in a phosphofructokinase deletion strain. *Biotechnol. Biofuels* **2021**, *14*, 113. [CrossRef]
52. El Kantar, S.; Khelfa, A.; Vorobiev, E.; Koubaa, M. Strategies for increasing lipid accumulation and recovery from *Y. lipolytica*: A review. *OCL* **2021**, *28*, 51. [CrossRef]
53. Tsakraklides, V.; Kamineni, A.; Consiglio, A.L.; MacEwen, K.; Friedlander, J.; Blitzblau, H.G.; Hamilton, M.A.; Crabtree, D.V.; Su, A.; Afshar, J.; et al. High-oleate yeast oil without polyunsaturated fatty acids. *Biotechnol. Biofuels* **2018**, *11*, 131. [CrossRef]
54. Imatoukene, N.; Verbeke, J.; Beopoulos, A.; Taghki, A.I.; Thomasset, B.; Sarde, C.-O.; Nonus, M.; Nicaud, J.-M. A metabolic engineering strategy for producing conjugated linoleic acids using the oleaginous yeast *Yarrowia lipolytica*. *Appl. Microbiol. Biotechnol.* **2017**, *101*, 4605–4616. [CrossRef] [PubMed]
55. Imatoukene, N.; Back, A.; Nonus, M.; Thomasset, B.; Rossignol, T.; Nicaud, J.-M. Fermentation process for producing CFAs using *Yarrowia lipolytica*. *J. Ind. Microbiol. Biotechnol.* **2020**, *47*, 403–412. [CrossRef] [PubMed]

56. Blitzblau, H.G.; Consiglio, A.L.; Teixeira, P.; Crabtree, D.V.; Chen, S.; Konzock, O.; Chifamba, G.; Su, A.; Kamineni, A.; MacEwen, K.; et al. Production of 10-methyl branched fatty acids in yeast. *Biotechnol. Biofuels* **2021**, *14*, 12. [CrossRef] [PubMed]
57. Pomraning, K.R.; Wei, S.; Karagiosis, S.A.; Kim, Y.-M.; Dohnalkova, A.C.; Arey, B.W.; Bredeweg, E.L.; Orr, G.; Metz, T.O.; Baker, S.E. Comprehensive Metabolomic, Lipidomic and Microscopic Profiling of *Yarrowia lipolytica* during Lipid Accumulation Identifies Targets for Increased Lipogenesis. *PLoS ONE* **2015**, *10*, e0123188. [CrossRef] [PubMed]
58. Abe, M.; Hasegawa, Y.; Oku, M.; Sawada, Y.; Tanaka, E.; Sakai, Y.; Miyoshi, H. Mechanism for Remodeling of the Acyl Chain Composition of Cardiolipin Catalyzed by *Saccharomyces cerevisiae* Tafazzin. *J. Biol. Chem.* **2016**, *291*, 15491–15502. [CrossRef]
59. Falabella, M.; Vernon, H.J.; Hanna, M.G.; Claypool, S.M.; Pitceathly, R.D. Cardiolipin, Mitochondria, and Neurological Disease. *Trends Endocrinol. Metab.* **2021**, *32*, 224–237. [CrossRef]
60. Barth, P.G.; Wanders, R.J.A.; Vreken, P.; Janssen, E.A.M.; Lam, J.; Baas, F. X-linked cardioskeletal myopathy and neutropenia (Barth syndrome) (MIM 302060). *J. Inherit. Metab. Dis.* **1999**, *22*, 555–567. [CrossRef]
61. Valianpour, F.; Mitsakos, V.; Schlemmer, D.; Towbin, J.A.; Taylor, J.M.; Ekert, P.G.; Thorburn, D.R.; Munnich, A.; Wanders, R.J.A.; Barth, P.G.; et al. Monolysocardiolipins accumulate in Barth syndrome but do not lead to enhanced apoptosis. *J. Lipid Res.* **2005**, *46*, 1182–1195. [CrossRef]

3. Conclusion

L'identification des lipides a été relativement simple, puisque seuls les glucuronosyl diacylglycérol (GlcADG) n'avaient jamais été analysés avec notre méthode séparative. Les GlcADG sont des glycolipides des membranes végétales spécialement formés dans des conditions d'appauvrissement en phosphate. Les lipides de réserves identifiés se composent de SE, TGs, DG et FFA et les lipides de membranes se composent de GlcCer, GlcADG, PE, PA, PI, CL et PC.

Pour les lipides de réserve, les analyses ont mis en évidence que les quantités de TGs sont comparables entre les deux souches et ne varient pas de manière significative dans le temps. Les quantités de SE, DG et FFA sont également restées constantes dans la souche obese L. Au contraire, dans la souche productrice de FAs impaires (LP obese), une augmentation avec le temps a été observée pour les DG et les FFA. Cela peut résulter de l'action de TG-lipases intracellulaires impliquées dans la remobilisation des TGs. Des niveaux de SE plus faibles chez les LP obese par rapport au contrôle, ont également été observés, suggérant une limitation de la voie de Kennedy.

La distribution des FAs des TGs et des DG a été évaluée avec la méthode des ions B. Pour les FFA les % des intensités des ions $[RCOO]^-$ ont été explorés. La répartition des FAs pour ces trois classes de lipides est relativement homogène et les mêmes tendances sont observées. Les écarts types évalués sur les triplicata sont également homogènes. Ces informations confortent l'extension du concept aux DG.

Pour ces trois classes, le FA majoritaire chez obese L est le C18:1 et pour obese LP le C17:1. D'une manière générale, les modifications génétiques ont induit une diminution des FAs pairs en faveur principalement de C17:1.

Les *m/z* des ions B correspondant aux FAs C19 :1, C19 :2 et C17 :2 ont été recherchés avec succès sur les spectres de masse des échantillons, afin de compléter les informations sur les voies métaboliques de *Yarrowia lipolytica*. Ces FAs minoritaires ont été ajoutés au schéma métabolique avec les enzymes nécessaires à leur synthèse.

Pour les lipides de membrane, les analyses ont mis en évidence des réajustements de lipides importants avec le temps chez obese LP. À 72 h, obese LP contient des quantités de PE, PI et PC beaucoup plus élevées que la souche obese L. Ces quantités diminuent considérablement à 144 h et 216 h. A 216 h, PE et PI ont quasiment disparu des profils LC-Corona-CAD®.

Comme pour les lipides de stockage, les lipides de membrane chez obese L contiennent majoritairement du C18 :1 alors que les obese LP contiennent principalement du C17 :1. La même tendance générale est observée avec la diminution de tous les FA pairs chez obese LP au profit principalement de C17 :1.

Une exception est observée pour la CL, dont la teneur en C18 :2 est majoritaire (50%) chez obese L. La forte proportion de C18 :2 dans la classe de CL (principalement localisé dans les mitochondries) est habituelle dans les extraits biologiques et participe au bon fonctionnement de la mitochondrie. Chez obese LP le C17 :1 devient majoritaire (≈45%) et le C18 :2 ne représente plus qu'environ 20%. Nous avons donc émis l'hypothèse que la modification de la composition de la CL chez les LP obèses pouvait altérer la fonction mitochondriale et limiter la production de lipides.

Le PE, PA et PC présentent une distribution en FAs proche. Le PI et le GlcADG ont également une distribution proche et se distinguent par une proportion en C16 :0 plus importante.

La distribution des espèces moléculaires des classes de PLs a également été recherchée. Pour cela l'intensité des ions $[M\text{-}H]^-$ des PE, PA, PI et GlcADG ainsi que l'intensité des ions $[M^{\bullet}]^-$ du PC ont été étudiés. Les FAs substitués sur le glycérol ont été identifiés grâce aux ions $[RCOO]^-$ issus de la MS^2.

Les données montrent qu'à partir d'une distribution en FAs similaire (PE, PA et PC), les classes de PLs peuvent avoir une distribution en espèces moléculaires très différentes. Le PE et le PA possèdent 4 espèces moléculaires majoritaires (représentant chacune 20%), tandis que le PC possède 2 espèces moléculaires majoritaires (représentant respectivement 30% et 40%).

Une similitude de distribution est observée pour les espèces moléculaires de PI et de GlcADG. Les résultats obtenus pour le GlcADG sont apparus cohérents (distribution et écart type) avec ceux obtenus pour les autres lipides. Notre méthode semble également applicable à cette classe de lipide.

Pour les PLs (hors CL) la distribution en FAs a été recalculée à partir des espèces moléculaires. Les résultats trouvés sont similaires à ceux obtenus avec l'utilisation des ions B. Cette concordance est sans doute à mettre en relation avec la diversité de FAs présents dans les échantillons (homogènes en nombre de carbones et comportant peu d'insaturations).

La méthode des ions B a mis en évidence que les souches *Yarrowia lipolytica* modifiées produisent des FAs à chaînes impaires dans l'ensemble des classes lipidiques, et cela, de manière relativement homogène.

DISCUSSION ET CONCLUSION GENERALE

L'analyse des lipides représente un intérêt majeur dans de nombreux domaines, dont celui de la nutrition et de la santé. Les analyses « omiques » sont en plein essor pour tenter d'appréhender la complexité du vivant dans son ensemble. Les analyses lipidomiques, sous-partie de la métabolomique, focalisent leur champ d'investigation sur les lipides. Cependant, la grande diversité naturelle de cette catégorie de molécules, induit des défis analytiques. Les difficultés sont principalement liées à la variabilité de la réponse des instruments en fonction de l'espèce lipidique et de son environnement chimique ainsi qu'au manque de standards pouvant corriger cette variabilité. Malgré des moyens importants pour la mise en œuvre de ces méthodes, l'obtention de résultats quantitatifs et exhaustifs fiables est pour le moment difficile à atteindre.

En 2017, nous avons publié une méthode globale de séparation de lipides par classe (NPLC) pouvant être couplée à différents détecteurs (DEDL, Corona et MS). Cette méthode est régulièrement couplée au DEDL par d'autres auteurs, pour accéder à la distribution des lipides par classe. Dans plusieurs études, une analyse des FAMEs par GC-FID est réalisée pour l'obtention de la distribution des FAs totaux. Cependant, la distribution des FAs par classe n'est jamais recherchée, malgré son intérêt évident. La séparation et l'isolement des classes lipidiques représente une contrainte importante pour de nombreux laboratoires.

Les travaux menés au cours de cette thèse ont démontré, au travers de trois publications, que l'évaluation de la distribution des acyles gras estérifiés (FAs) des glycérolipides et PLs était accessible grâce aux ions fragments $[MG+H-H_2O]^+$ (ions B) produits en source lors des analyses NPLC-APPI/APCI-HRMS.

Ce traitement original des données permet d'accéder à des informations complémentaires à celles classiquement obtenues avec ce type de méthodes. La comparaison des données

(distribution des FAs/distribution d'espèces moléculaires) peut mettre en exergue d'éventuels biais analytiques.

Dans un premier temps, les bases méthodologiques de notre approche ont été posées à travers l'étude de la classe des TGs issus d'huiles végétales. Le développement ainsi que la validation du concept ont fait l'objet d'une première publication dans **Analytica Chimica Acta** [21].

La dépendance de la fragmentation en source des TGs envers la nature des FAs qui les composent est connue, elle empêche l'accès à l'ensemble des espèces moléculaires à partir de l'ion $[M+H]^+$. Cette difficulté est généralement surmontée par l'utilisation d'adduits (notamment NH_4^+) pour stabiliser les TGs. Cette stratégie n'a pas été mise en œuvre dans nos travaux. Cependant, l'étude de l'ionisation de standards de TGs homogènes a mis en exergue l'omniprésence des ions B sur les spectres de masse, quel que soit la nature des FAs des TGs. L'intensité des ions B est globalement homogène et représente 1 à 2% de l'intensité de l'ion $[DG+H-H_2O]^+$ (ions A) le plus intense. Cette observation ouvre la possibilité d'accéder à la distribution des FAs de l'ensemble des TGs.

La spécificité de notre approche repose sur la capacité de l'appareillage à séparer les ions B des ions quasi isobares issus de la fragmentation des TGs. Nous avons établi une liste de 41 FAs couramment rencontrés dans les échantillons naturels et calculé la valeur des rapports *m/z* des ions B correspondants. L'écart minimal entre ces *m/z* et ceux des ions théoriquement issus de la fragmentation des TGs indique qu'une résolution (FWHM) minimale du spectromètre de masse de 60 000 @ *m/z* 400 est nécessaire pour garantir la spécificité de notre approche.

Contrairement à la GC-FID, notre méthode ne permet pas de différencier les FAs isomères, ceux-ci sont donc regroupés dans l'étude. L'utilisation de la mobilité ionique, couplée à la spectrométrie de masse, pourrait être envisagée pour accéder à cette information. Cette

technologie en plein essor permet une séparation supplémentaire des ions par leur taille, forme, charge et masse, ce qui s'avère particulièrement intéressant dans ce contexte [64].

La distribution des intensités des ions B des huiles végétales a été déterminée par FIA et NPLC-APPI$^+$-HRMS. Ces deux modes d'élution permettent à l'ensemble des ions B d'une même classe lipidique d'être élués simultanément sous un même pic chromatographique. Cette condition est un prérequis pour l'emploi de notre méthode. Dans le cas de la FIA comme de la NPLC, les intensités des ions B sont apparues sensiblement proportionnelles aux teneurs en FAs mesurées par GC-FID (valeurs prises en références), à l'exception de l'ion B(18 :3) dont l'intensité est deux fois plus faible qu'attendue.

La prédiction de la distribution des FAs à partir de la mesure de l'intensité des ions B a ensuite été affinée par le calcul de coefficients de pondération affectés à chaque ion B. Dix huiles ont été utilisées pour cette calibration et dix autres huiles ont été utilisées pour la validation de la méthode. Les régressions de Deming ont permis de conclure que les résultats obtenus par GC-FID et la méthode des ions B n'étaient pas statistiquement différents. Les limites de détection des deux méthodes sont également similaires. Tous les FAs présent à plus de 0.2% dans les huiles (GC-FID) ont été détectés par la méthode des ions B.

L'approche de l'évaluation de la distribution des FAs, par la mesure de l'intensité des ions B, à ensuite été étendue à la catégorie des phospholipides (PLs). La source d'ionisation APCI, plus couramment utilisée que l'APPI, a été choisie pour ce travail. Comme pour les TGs, les PLs s'ionisent en source sous la forme d'ion $[M+H]^+$ et se fragmentent en ions A puis en ions B. Cette étude a été publiée dans **Journal of Chromatography A** [22].

De façon analogue à l'étude sur les TGs, 17 standards commerciaux de PLs issus d'extraits naturels répartis en 9 classes différentes ont été sélectionnés. La distribution des FAs a été mesurée par GC-FID pour l'obtention de valeurs de références.

Pour les 13 standards de PLs comportant uniquement des diacyl-PLs, les régressions de Deming ont montré que les résultats obtenus avec notre méthode n'étaient statistiquement pas différents de ceux obtenus par la méthode de référence. Le recours à des coefficients de pondération n'a pas été nécessaire pour corriger l'intensité des ions B.

Ce résultat montre que la nature de la tête polaire, la nature des FAs (avec de faibles teneurs en FAs polyinsaturés) et le gradient d'élution employé n'ont pas influencé la formation des ions B.

Pour les 4 standards (PE cœur/foie/cerveau et PC cœur) contenant simultanément des diacyl-PLs et des plasmalogènes (P-PLs) deux difficultés ont dû être surmontées.

La première difficulté a été la prise en compte des P-PLs par les analyses GC-FID. Lors de la transestérification, les P-PLs produisent des FAMEs issus des FAs et des diméthylacétals (DMAs) issus des alkényls gras. Il est impératif d'identifier correctement l'ensemble de ces composés sur les chromatogrammes afin d'obtenir respectivement la distribution des FAs et des alkényls gras.

La deuxième difficulté a été la prise en compte des P-PLs lors des analyses NPLC-APCI-HRMS. L'ion B d'un FA n'a pas le même degré de formation selon que celui-ci est porté par un diacyl-PL ou un P-PL. La méthode que nous proposons n'est donc pas directement applicable lorsque ces deux sous-classes sont présentes simultanément sous le même pic chromatographique.

Les extraits contenant des mélanges d'acyl-PLs/P-PLs ont été soumis à une oxydation par des vapeurs d'acide chlorhydrique concentré. Cette oxydation rompt spécifiquement les liaisons éthers vinyliques, les P-PLs sont alors convertis en Lyso-PLs et aldéhydes. Après ce traitement, les deux sous-classes ne sont plus coéluées lors de l'analyse NPLC-APCI-HRMS. Cette stratégie permet d'accéder indépendamment à la distribution des FAs issus des acyl-PLs et des P-PLs, ce qui n'est pas possible par GC-FID.

Les quatre extraits contenant des P-PLs contiennent également une forte proportion de FAs polyinsaturés, dont les intensités des ions B doivent être corrigées par des coefficients pondérateurs. Le faible nombre d'échantillons ne permet pas le calcul de ces coefficients. Par analogie avec l'étude sur les TGs, un coefficient 2 est appliqué aux intensités des ions B des FAs polyinsaturés. Avec cette correction, la distribution des FAs calculée selon l'intensité des ions B correspond aux valeurs obtenues par GC-FID.

Par analogie avec les ions B, nous avons également identifié deux ions permettant d'évaluer la distribution des alkényls gras des P-PE et P-PC. La distribution de ces ions a été comparée avec succès à la distribution des DMAs. Des spectres de masse du PC P-18:0/18:1 ont également été réalisés et un schéma de fragmentation a été proposé pour compléter les informations disponibles dans la littérature.

Nous avons eu l'opportunité de mettre en œuvre notre nouveau concept lors d'une étude collaborative sur le réajustement des lipides dans les souches productrices de FAs à chaînes impaires de *Yarrowia Lipolytica*, publiée dans **Biomolecules** [23].

Dans cette étude, une souche de *Yarrowia Lipolytica* a été modifiée génétiquement pour favoriser la production de FAs inhabituels à chaînes impaires. Le profil lipidique de cette souche a été comparé à celui de la souche sauvage à trois temps de développement.

Les profils lipidiques obtenus par NPLC-Corona CAD® ont mis en évidence une forte proportion de TGs dans l'ensemble des échantillons, ainsi qu'un réajustement important du PE, PI et PC au cours du temps chez la souche modifiée.

La méthode des ions B a mis en exergue une surproduction du C17 :1 (et autres FAs impairs) au détriment des FAs pairs chez les souches modifiées. Cette surproduction a été observée pour toutes les classes de lipides de manière relativement homogène.

La meilleure spécificité de l'utilisation des ions B par rapport à la GC-FID (utilisée par nos co-auteurs) a permis d'apporter des informations supplémentaires quant à la présence de certains FAs minoritaires. Ceux-ci ont été ajoutés au schéma métabolique de cette levure.

Les FAs présents dans les échantillons de *Yarrowia Lipolytica* sont homogènes en nombre de carbones (16 à 19) et comportent peu d'insaturations (maximum 2). Cette configuration est idéale pour la mise en œuvre de la méthode des ions B et pour l'évaluation de la distribution des espèces moléculaires.

L'évaluation de la distribution des espèces moléculaires de PLs a été réalisée en mode négatif via les ions $[M\text{-}H]^-$ et les ions $[M^\bullet]^-$ pour le PC. Chaque spectre MS^2 a été étudié pour identifier les FAs substitués. Cette étape pourrait être optimisée par l'utilisation de logiciels libres tels que MS-Dial.

Dans certains cas, des espèces moléculaires isobares sont présentes, le résultat est alors exprimé en « nombre de carbones/nombre d'insaturations ». Même si les résultats obtenus avec la méthode des ions B sont globalement moins informatifs, ils présentent l'avantage d'accéder à la distribution complète des FAs et de fournir un résultat global simple à appréhender.

Par le calcul, nous avons montré que les distributions des FAs obtenue à partir des ions B et par les espèces moléculaires étaient cohérentes. Cette similitude est sans doute à mettre en relation avec la nature des FAs présents et de la source utilisée. La source APCI est moins sujette aux problèmes de suppression d'ionisation que la source ESI (très majoritairement utilisée dans les études lipidomiques). Il serait intéressant d'évaluer l'intensité de tous les ions formés en source (APCI/APPI/ESI) par des standards de PLs comportant un nombre variable d'insaturations, afin de déterminer si la formation des ions B serait moins sensible au nombre d'insaturations que la formation des espèces moléculaires.

L'évaluation des espèces moléculaires reste essentielle. Dans ce travail, nous avons observé à travers les classes de PE, PA et PC qu'à partir d'une même distribution de FAs, les espèces moléculaires formées (combinaison de 2 FAs) n'étaient pas toujours les mêmes.
La position des FAs (*sn*-1/*sn*-2), non étudiée dans ce travail, est également un élément essentiel dans l'établissement des schémas métaboliques, car les phospholipases ont des sites d'action spécifiques (phospholipase A1 en *sn*-1, phospholipase A2 en *sn*-2, etc.).

Les distributions des espèces moléculaires des TGs et des DGs n'ont pas été étudiées, car dans nos conditions d'analyse ces lipides se fragmentent de manière trop importante en source. L'utilisation de phases mobiles apolaires empêche l'utilisation de sels pour la formation d'adduit stabilisant les lipides sous leur forme entière. Dans ce contexte, la méthode des ions B représente l'unique accès à la distribution des FAs.

Cette étude a également permis de mettre en œuvre la méthode des ions B sur deux nouvelles classes de lipides non étudiés dans les deux articles précédents (DGs et glycosyldiacylglycérols -GlcADG). La cohérence de leurs distributions avec celles trouvées pour les autres lipides permet d'avoir une confiance raisonnable quant à l'extrapolation de la méthode.

A l'heure actuelle, aucune méthode n'est idéale pour appréhender la complexité des lipides dans leur contexte biologique. La complémentarité des techniques et des méthodes reste pour le moment une stratégie nécessaire.

La GC-FID est la technique de choix pour l'obtention de la distribution des FAs totaux d'un échantillon. Elle permet des résultats quantitatifs fiables et une différenciation des FAs isomères. Sa mise en œuvre nécessite cependant certaines précautions.
Si l'échantillon contient plusieurs classes de lipides, il est nécessaire d'utiliser des réactifs appropriés pour que l'ensemble des classes soit totalement transestérifié. Il faut également tenir compte de la présence éventuelle de composés pouvant aboutir à la formation d'autres

composés que les FAMEs, comme dans le cas des P-PLs et la formation des DMAs.

Les FAMEs sont identifiés par la comparaison de leur temps de rétention à ceux de standards pris en référence. Cela suppose l'accès à l'ensemble des standards, ce qui n'est pas toujours possible, notamment dans le cas des FAs inhabituels. D'autre part, il peut y avoir des pics interférents avec des temps de rétention identiques ou proches. Dans ce cas, l'interprétation des résultats peut se révéler erronée. A l'opposé, l'identification des ions B repose sur la mesure à haute résolution de leur rapport *m/z* ce qui est à la fois spécifique et pratique. Dans le cadre de ce travail de thèse, la confrontation des résultats obtenus par la méthode des ions B à ceux obtenus par la GC-FID a permis à plusieurs reprises d'identifier des problèmes d'interprétation des données GC-FID.

L'utilisation de la TLC (et autres techniques séparatives) en amont de l'utilisation de la GC-FID permet de relier la distribution des FAs aux classes de lipides. Cependant, ces séparations restent sous-employées à cause d'une mise en œuvre relativement contraignante lorsque celles-ci sont réalisées manuellement, ou de l'investissement nécessaire dans des équipements supplémentaires lorsque celles-ci sont en partie automatisées.

La GC-MS est également une technique de choix pour l'obtention de la distribution des FAs totaux. Lors de l'analyse des FAMEs, les réponses obtenues par GC-MS sont généralement plus variables que celles obtenues par FID [179]. Cependant, la GC-MS présente de nombreux avantages, tel que l'accès à des informations structurales, la possibilité d'extraire des ions lors de coélutions et l'utilisation de standards internes deutérés pour des quantifications absolues (attribution d'une quantité ou d'une concentration à partir de la réponse analytique) hautement sensibles [188].

La LC-MS est la technique de choix pour les analyses lipidomiques quantitatives. Pour certains lipides spécifiques tels que les stérols [189], les acides gras ou dérivés [190], les bases sphingoïdes et dérivés [191], etc. dont les standards analytiques purs sont disponibles, une

quantification absolue est possible[18].

Pour les catégories de lipides contenant une grande variabilité d'espèces moléculaires tels que les sphingolipides, glycérolipides ou PLs, il n'est pas possible d'accéder à un standard analytique pur par espèce moléculaire, la quantification ne peut être que relative malgré tous les efforts analytiques pouvant être mis en œuvre [18]. Des efforts sont réalisés pour caractériser de manière la plus exhaustive possible des matériaux de références, tel que le «NIST SRM 1950 – Metabolites in Frozen Human Plasma » pour évaluer l'exactitude de ces approches [116,192].

LIPID MAPS et le consortium Lipidomics Standards Initiative (LSI) [96] ont établi une collaboration afin de créer des lignes directrices pour les principaux flux de travail en lipidomique et pour harmoniser la communication et le stockage des données. L'une des préconisations proposées pour quantifier les lipides complexes (sphingolipides, glycérolipides ou PLs) consiste à utiliser plusieurs standards marqués par classe de lipides pour tenir compte des effets liés aux groupements polaires, aux longueurs de chaînes carbonées, aux insaturations et fonctionnalisations sur l'extraction des lipides et leur réponse par spectrométrie de masse. Cette recommandation pourrait être mise en œuvre avec la méthode utilisant les ions B dans la mesure où les carbones deutérés sont positionnés, soit sur le glycérol soit sur l'ensemble des FAs du standard. Dans ces conditions, les valeurs des *m/z* des ions B (standard/échantillon) peuvent être discriminées.

Il est également préconisé d'éluer simultanément les standards et les espèces moléculaires correspondantes pour que l'ionisation se fasse dans les mêmes conditions. Cela suppose de travailler par « shotgun lipidomics » [104,105] ou avec une méthode permettant une séparation de lipides par classe (NPLC, HILIC, SFC). Cette recommandation est totalement en adéquation avec l'utilisation de notre méthode.

Dans ce travail de thèse, la source ESI n'a pas été utilisée, car les solvants mis en œuvre pour

la séparation NPLC ne sont pas compatibles, contrairement aux solvants utilisés lors des séparations HILIC et SFC. Il serait donc intéressant d'étudier la transposition de notre méthode aux séparations HILIC-ESI et SFC-ESI. La transposition à la SFC semble particulièrement intéressante, car cette technique permet une séparation de lipides comparable à celle obtenue avec notre méthode, mais avec un temps réduit (6 min [52]), une consommation limitée en solvant et une compatibilité avec les trois sources d'ionisation (ESI, APCI et APPI) [50]. L'ESI est reconnue pour son ionisation « plus douce » que les sources APCI et APPI, mais une optimisation des énergies pourrait être étudiée afin de favoriser la formation des ions B en source [193]. De même, la compatibilité de notre méthode avec l'utilisation de sels permettant la formation d'adduit (NH_4^+) serait intéressante à explorer, notamment pour les TGs.

Ce travail de thèse répond à une demande à laquelle notre laboratoire est souvent confronté, celui de pouvoir évaluer la distribution des FAs par classe de lipides. Nous avons montré, avec les instruments à notre disposition, le potentiel des ions B pour l'évaluation de la distribution des FAs des glycérolipides et PLs lors des analyses NPLC-APPI/APCI-HRMS. Nous avons également proposé des axes d'amélioration, comme l'utilisation de la mobilité ionique pour accéder à l'isomérie des FAs, mais aussi des axes de transposition pour étendre son champ d'application. Cette méthode est compatible avec les développements lipidomiques moyennant le respect de certains critères liés à l'utilisation des standards internes deutérés et aux conditions d'ionisation en source permettant la formation des ions B.

REFERENCES BIBLIOGRAPHIQUES

[1] J. Adrian, J. Potus, R. Frangne, La science alimentaire de A à Z, 3e éd, New York Éd. Tec & doc, Paris Londres, 2002.

[2] G.O. Burr, M.M. Burr, A new deficiency disease produced by the rigid exclusion of fat from the diet, J. Biol. Chem. 82 (1929) 345–367. https://doi.org/10.1016/S0021-9258(20)78281-5.

[3] G.O. Burr, M.M. Burr, On the nature and rôle of the fatty acids essential in nutrition, J. Biol. Chem. 86 (1930) 587–621. https://doi.org/10.1016/S0021-9258(20)78929-5.

[4] D. Steinberg, Thematic review series: The Pathogenesis of Atherosclerosis. An interpretive history of the cholesterol controversy: part I, J. Lipid Res. 45 (2004) 1583–1593. https://doi.org/10.1194/jlr.R400003-JLR200.

[5] D. Steinberg, Thematic review series: The Pathogenesis of Atherosclerosis. An interpretive history of the cholesterol controversy: part II:the early evidence linking hypercholesterolemia to coronary disease in humans, J. Lipid Res. 46 (2005) 179–190. https://doi.org/10.1194/jlr.R400012-JLR200.

[6] P.W.F. Wilson, Lipids and Vascular Disease: A Framingham Perspective, Glob. Heart. 8 (2013) 25. https://doi.org/10.1016/j.gheart.2012.12.009.

[7] P.C. Calder, Functional Roles of Fatty Acids and Their Effects on Human Health, J. Parenter. Enter. Nutr. 39 (2015) 18S-32S. https://doi.org/10.1177/0148607115595980.

[8] A.P. Simopoulos, The importance of the ratio of omega-6/omega-3 essential fatty acids, Biomed. Pharmacother. 56 (2002) 365–379. https://doi.org/10.1016/S0753-3322(02)00253-6.

[9] S. Stender, A. Astrup, J. Dyerberg, Ruminant and industrially produced *trans* fatty acids: health aspects, Food Nutr. Res. 52 (2008) 1651. https://doi.org/10.3402/fnr.v52i0.1651.

[10] A. Ascherio, W.C. Willett, Health effects of trans fatty acids, Am. J. Clin. Nutr. 66 (1997) 1006S-1010S. https://doi.org/10.1093/ajcn/66.4.1006S.

[11] G. van Meer, D.R. Voelker, G.W. Feigenson, Membrane lipids: where they are and how they behave, Nat. Rev. Mol. Cell Biol. 9 (2008) 112–124. https://doi.org/10.1038/nrm2330.

[12] G. Maulucci, O. Cohen, B. Daniel, A. Sansone, P.I. Petropoulou, S. Filou, A. Spyridonidis, G. Pani, M. De Spirito, C. Chatgilialoglu, C. Ferreri, K.E. Kypreos, S. Sasson, Fatty acid-related modulations of membrane fluidity in cells: detection and implications, Free Radic. Res. 50 (2016) S40–S50. https://doi.org/10.1080/10715762.2016.1231403.

[13] R. Mallick, S. Basak, A.K. Duttaroy, Fatty acids and evolving roles of their proteins in neurological, cardiovascular disorders and cancers, Prog. Lipid Res. 83 (2021) 101116. https://doi.org/10.1016/j.plipres.2021.101116.

[14] O. Quehenberger, A.M. Armando, A.H. Brown, S.B. Milne, D.S. Myers, A.H. Merrill, S. Bandyopadhyay, K.N. Jones, S. Kelly, R.L. Shaner, C.M. Sullards, E. Wang, R.C. Murphy, R.M. Barkley, T.J. Leiker, C.R.H. Raetz, Z. Guan, G.M. Laird, D.A. Six, D.W. Russell, J.G. McDonald, S. Subramaniam, E. Fahy, E.A. Dennis, Lipidomics reveals a remarkable diversity of lipids in human plasma, J. Lipid Res. 51 (2010) 3299–3305. https://doi.org/10.1194/jlr.M009449.

[15] LIPID MAPS® Lipidomics Gateway, (n.d.). http://www.lipidmaps.org/ (accessed March 21, 2020).

[16] E. Fahy, S. Subramaniam, R.C. Murphy, M. Nishijima, C.R.H. Raetz, T. Shimizu, F. Spener, G. van Meer, M.J.O. Wakelam, E.A. Dennis, Update of the LIPID MAPS

comprehensive classification system for lipids, J. Lipid Res. 50 (2009) S9–S14. https://doi.org/10.1194/jlr.R800095-JLR200.
[17] T. Cajka, O. Fiehn, Comprehensive analysis of lipids in biological systems by liquid chromatography-mass spectrometry, TrAC Trends Anal. Chem. 61 (2014) 192–206. https://doi.org/10.1016/j.trac.2014.04.017.
[18] S. Khoury, C. Canlet, M. Lacroix, O. Berdeaux, J. Jouhet, J. Bertrand-Michel, Quantification of Lipids: Model, Reality, and Compromise, Biomolecules. 8 (2018) 174. https://doi.org/10.3390/biom8040174.
[19] J. Jouhet, J. Lupette, O. Clerc, L. Magneschi, M. Bedhomme, S. Collin, S. Roy, E. Maréchal, F. Rébeillé, LC-MS/MS versus TLC plus GC methods: Consistency of glycerolipid and fatty acid profiles in microalgae and higher plant cells and effect of a nitrogen starvation, PLOS ONE. 12 (2017) e0182423. https://doi.org/10.1371/journal.pone.0182423.
[20] S. Abreu, A. Solgadi, P. Chaminade, Optimization of normal phase chromatographic conditions for lipid analysis and comparison of associated detection techniques, J. Chromatogr. A. (2017). https://doi.org/10.1016/j.chroma.2017.07.063.
[21] S. Abreu, S. Heron, A. Solgadi, F. Joffre, A. Tchapla, P. Chaminade, Rapid assessment of triacylglycerol fatty acyls composition by LC-APPI+-HRMS using monoacylglycerol like fragments intensities, Anal. Chim. Acta. 1178 (2021) 338809. https://doi.org/10.1016/j.aca.2021.338809.
[22] S. Abreu, S. Héron, A. Solgadi, B. Prost, J. Dalloux-Chioccioli, A. Kermarrec, A. Meynier, J. Bertrand-Michel, A. Tchapla, P. Chaminade, Rapid assessment of fatty acyls chains of phospholipids and plasmalogens by atmospheric pressure chemical ionization in positive mode and high-resolution mass spectrometry using in-source generated monoacylglycerol like fragments intensities, J. Chromatogr. A. 1673 (2022) 463093. https://doi.org/10.1016/j.chroma.2022.463093.
[23] S. Abreu, Y.-K. Park, C. Pires de Souza, L. Vidal, P. Chaminade, J.-M. Nicaud, Lipid Readjustment in Yarrowia lipolytica Odd-Chain Fatty Acids Producing Strains, Biomolecules. 12 (2022) 1026. https://doi.org/10.3390/biom12081026.
[24] C. Lejeune, S. Abreu, P. Chaminade, T. Dulermo, M. David, S. Werten, M.-J. Virolle, Impact of Phosphate Availability on Membrane Lipid Content of the Model Strains, Streptomyces lividans and Streptomyces coelicolor, Front. Microbiol. 12 (2021) 623919. https://doi.org/10.3389/fmicb.2021.623919.
[25] M. David, C. Lejeune, S. Abreu, A. Thibessard, P. Leblond, P. Chaminade, M.-J. Virolle, Negative Correlation between Lipid Content and Antibiotic Activity in Streptomyces: General Rule and Exceptions, Antibiotics. 9 (2020) 280. https://doi.org/10.3390/antibiotics9060280.
[26] J. Zhang, Q. Liang, Z. Xu, M. Cui, Q. Zhang, S. Abreu, M. David, C. Lejeune, P. Chaminade, M.-J. Virolle, D. Xu, The Inhibition of Antibiotic Production in Streptomyces coelicolor Over-Expressing the TetR Regulator SCO3201 IS Correlated With Changes in the Lipidome of the Strain, Front. Microbiol. 11 (2020) 1399. https://doi.org/10.3389/fmicb.2020.01399.
[27] M. Nič, J. Jirát, B. Košata, A. Jenkins, A. McNaught, eds., IUPAC Compendium of Chemical Terminology: Gold Book, 2.1.0, IUPAC, Research Triagle Park, NC, 2009. https://doi.org/10.1351/goldbook.
[28] R.W. Gross, The evolution of lipidomics through space and time, Biochim. Biophys. Acta BBA - Mol. Cell Biol. Lipids. 1862 (2017) 731–739. https://doi.org/10.1016/j.bbalip.2017.04.006.

[29] R. Wang, B. Li, S.M. Lam, G. Shui, Integration of lipidomics and metabolomics for in-depth understanding of cellular mechanism and disease progression, J. Genet. Genomics. (2019) S1673852719302000. https://doi.org/10.1016/j.jgg.2019.11.009.
[30] E. Fahy, S. Subramaniam, H.A. Brown, C.K. Glass, A.H. Merrill, R.C. Murphy, C.R.H. Raetz, D.W. Russell, Y. Seyama, W. Shaw, T. Shimizu, F. Spener, G. van Meer, M.S. VanNieuwenhze, S.H. White, J.L. Witztum, E.A. Dennis, A comprehensive classification system for lipids, J. Lipid Res. 46 (2005) 839–862. https://doi.org/10.1194/jlr.E400004-JLR200.
[31] F.-F. Hsu, Mass spectrometry-based shotgun lipidomics – a critical review from the technical point of view, Anal. Bioanal. Chem. 410 (2018) 6387–6409. https://doi.org/10.1007/s00216-018-1252-y.
[32] H.W. Mueller, J.T. O'Flaherty, D.G. Greene, M.P. Samuel, 1-0-Alkyl-linked glycerophospholipids of human neutrophils: distribution of arachidonate and other acyl residues in the ether-linked and diacyl species, (n.d.) 6.
[33] L.A. Scherrer, Subcellular distribution, molecular dynamics and catabolism of plasmalogens in myocardium, (n.d.) 9.
[34] A.A. Farooqui, L.A. Horrocks, Book Review: Plasmalogens: Workhorse Lipids of Membranes in Normal and Injured Neurons and Glia, The Neuroscientist. 7 (2001) 232–245. https://doi.org/10.1177/107385840100700308.
[35] N.E. Braverman, A.B. Moser, Functions of plasmalogen lipids in health and disease, Biochim. Biophys. Acta BBA - Mol. Basis Dis. 1822 (2012) 1442–1452. https://doi.org/10.1016/j.bbadis.2012.05.008.
[36] N. Dalal, R. Jalandra, M. Sharma, H. Prakash, G.K. Makharia, P.R. Solanki, R. Singh, A. Kumar, Omics technologies for improved diagnosis and treatment of colorectal cancer: Technical advancement and major perspectives, Biomed. Pharmacother. 131 (2020) 110648. https://doi.org/10.1016/j.biopha.2020.110648.
[37] G. Polo, A.P. Burlina, T.B. Kolamunnage, M. Zampieri, C. Dionisi-Vici, P. Strisciuglio, M. Zaninotto, M. Plebani, A.B. Burlina, Diagnosis of sphingolipidoses: a new simultaneous measurement of lysosphingolipids by LC-MS/MS, Clin. Chem. Lab. Med. CCLM. 55 (2017). https://doi.org/10.1515/cclm-2016-0340.
[38] A. Zarrouk, M. Debbabi, M. Bezine, E.M. Karym, A. Badreddine, O. Rouaud, T. Moreau, M. Cherkaoui-Malki, M. El Ayeb, B. Nasser, M. Hammami, G. Lizard, Lipid Biomarkers in Alzheimer's Disease, Curr. Alzheimer Res. 15 (2018) 303–312. https://doi.org/10.2174/1567205014666170505101426.
[39] P.A. Vorkas, G. Isaac, A. Holmgren, E.J. Want, J.P. Shockcor, E. Holmes, M.Y. Henein, Perturbations in fatty acid metabolism and apoptosis are manifested in calcific coronary artery disease: An exploratory lipidomic study, Int. J. Cardiol. 197 (2015) 192–199. https://doi.org/10.1016/j.ijcard.2015.06.048.
[40] G. Lee, M. Hasan, O.-S. Kwon, B.H. Jung, Identification of Altered Metabolic Pathways during Disease Progression in EAE Mice via Metabolomics and Lipidomics, Neuroscience. 416 (2019) 74–87. https://doi.org/10.1016/j.neuroscience.2019.07.029.
[41] C. Lu, J.A. Napier, T.E. Clemente, E.B. Cahoon, New frontiers in oilseed biotechnology: meeting the global demand for vegetable oils for food, feed, biofuel, and industrial applications, Curr. Opin. Biotechnol. 22 (2011) 252–259. https://doi.org/10.1016/j.copbio.2010.11.006.
[42] P.J. Horn, C. Benning, The plant lipidome in human and environmental health, Science. 353 (2016) 1228–1232. https://doi.org/10.1126/science.aaf6206.
[43] J. Folch, M. Lees, G.H.S. Stanley, A Simple Method for the Isolation and Purification of Total Lipides from Animal Tissues, J. Biol. Chem. 226 (1957) 497–509.
[44] E.G. Bligh, W.J. Dyer, A rapid method of total lipid extraction and purification, (n.d.) 7.

[45] V. Matyash, G. Liebisch, T.V. Kurzchalia, A. Shevchenko, D. Schwudke, Lipid extraction by methyl-tert-butyl ether for high-throughput lipidomics, J. Lipid Res. 49 (2008) 1137–1146. https://doi.org/10.1194/jlr.D700041-JLR200.
[46] L. Löfgren, M. Ståhlman, G.-B. Forsberg, S. Saarinen, R. Nilsson, G.I. Hansson, The BUME method: a novel automated chloroform-free 96-well total lipid extraction method for blood plasma, J. Lipid Res. 53 (2012) 1690–1700. https://doi.org/10.1194/jlr.D023036.
[47] M. Lange, Z. Ni, A. Criscuolo, M. Fedorova, Liquid Chromatography Techniques in Lipidomics Research, Chromatographia. (2018). https://doi.org/10.1007/s10337-018-3656-4.
[48] D.R. Stoll, P.W. Carr, Two-Dimensional Liquid Chromatography: A State of the Art Tutorial, Anal. Chem. 89 (2017) 519–531. https://doi.org/10.1021/acs.analchem.6b03506.
[49] E. Cífková, R. Hájek, M. Lísa, M. Holčapek, Hydrophilic interaction liquid chromatography–mass spectrometry of (lyso)phosphatidic acids, (lyso)phosphatidylserines and other lipid classes, J. Chromatogr. A. 1439 (2016) 65–73. https://doi.org/10.1016/j.chroma.2016.01.064.
[50] L. Laboureur, M. Ollero, D. Touboul, Lipidomics by Supercritical Fluid Chromatography, Int. J. Mol. Sci. 16 (2015) 13868–13884. https://doi.org/10.3390/ijms160613868.
[51] E. Lesellier, C. West, The many faces of packed column supercritical fluid chromatography – A critical review, J. Chromatogr. A. 1382 (2015) 2–46. https://doi.org/10.1016/j.chroma.2014.12.083.
[52] M. Lísa, M. Holčapek, High-Throughput and Comprehensive Lipidomic Analysis Using Ultrahigh-Performance Supercritical Fluid Chromatography–Mass Spectrometry, Anal. Chem. 87 (2015) 7187–7195. https://doi.org/10.1021/acs.analchem.5b01054.
[53] L. Yang, H. Nie, F. Zhao, S. Song, Y. Meng, Y. Bai, H. Liu, A novel online two-dimensional supercritical fluid chromatography/reversed phase liquid chromatography–mass spectrometry method for lipid profiling, Anal. Bioanal. Chem. 412 (2020) 2225–2235. https://doi.org/10.1007/s00216-019-02242-x.
[54] M.K. Parr, B. Wüst, J. Teubel, J.F. Joseph, Splitless hyphenation of SFC with MS by APCI, APPI, and ESI exemplified by steroids as model compounds, J. Chromatogr. B. 1091 (2018) 67–78. https://doi.org/10.1016/j.jchromb.2018.05.017.
[55] P. Arpino, Couplages chromatographiques avec la spectrométrie de masse. III, Tech. Anal. (2015). https://doi.org/10.51257/a-v1-p1492.
[56] Monégier, Bertrand, Électrospray, Tech. Ing. (1997).
[57] R. Kostiainen, T.J. Kauppila, Effect of eluent on the ionization process in liquid chromatography–mass spectrometry, J. Chromatogr. A. 1216 (2009) 685–699. https://doi.org/10.1016/j.chroma.2008.08.095.
[58] S.-S. Cai, J.A. Syage, Atmospheric pressure photoionization mass spectrometry for analysis of fatty acid and acylglycerol lipids, J. Chromatogr. A. 1110 (2006) 15–26. https://doi.org/10.1016/j.chroma.2006.01.050.
[59] M. Mann, J.B. Fenn, Electrospray Mass Spectrometry: Principles and Methods, in: D.M. Desiderio (Ed.), Mass Spectrom., Springer US, Boston, MA, 1992: pp. 1–35. https://doi.org/10.1007/978-1-4899-1173-5_1.
[60] F.W. Röllgen, E. Bramer-Weger, L. Bütfering, Field ion emission from liquid solutions: ion evaporation against electrohydrodynamic disintegration, J. Phys. Colloq. 48 (1987) C6-253-C6-256. https://doi.org/10.1051/jphyscol:1987641.

[61] S. Khoury, N.E. Banna, S. Tfaili, P. Chaminade, A study of inter-species ion suppression in electrospray ionization-mass spectrometry of some phospholipid classes, Anal. Bioanal. Chem. 408 (2016) 1453–1465. https://doi.org/10.1007/s00216-015-9245-6.
[62] R. King, R. Bonfiglio, C. Fernandez-Metzler, C. Miller-Stein, T. Olah, Mechanistic investigation of ionization suppression in electrospray ionization, J. Am. Soc. Mass Spectrom. 11 (2000) 942–950. https://doi.org/10.1016/S1044-0305(00)00163-X.
[63] D. Volmer, L.L. Jessome, Ion Suppression: A Major Concern in Mass Spectrometry, LCGC N. Am. 24 (2006) 498–510.
[64] J.E. Kyle, X. Zhang, K.K. Weitz, M.E. Monroe, Y.M. Ibrahim, R.J. Moore, J. Cha, X. Sun, E.S. Lovelace, J. Wagoner, S.J. Polyak, T.O. Metz, S.K. Dey, R.D. Smith, K.E. Burnum-Johnson, E.S. Baker, Uncovering biologically significant lipid isomers with liquid chromatography, ion mobility spectrometry and mass spectrometry, The Analyst. 141 (2016) 1649–1659. https://doi.org/10.1039/C5AN02062J.
[65] Ruwan Kurulugama, K. Imatani, L. Taylor, The Agilent Ion Mobility Q-TOF Mass Spectrometer System, (2013). https://www.agilent.com/cs/library/technicaloverviews/public/5991-3244EN.pdf (accessed April 23, 2020).
[66] Quadrupole Mass Spectrometry and its Applications, Elsevier, 1976. https://doi.org/10.1016/C2013-0-04436-2.
[67] R.E. March, An Introduction to Quadrupole Ion Trap Mass Spectrometry, J. Mass Spectrom. 32 (1997) 351–369. https://doi.org/10.1002/(SICI)1096-9888(199704)32:4<351::AID-JMS512>3.0.CO;2-Y.
[68] M. Guilhaus, Special feature: Tutorial. Principles and instrumentation in time-of-flight mass spectrometry. Physical and instrumental concepts, J. Mass Spectrom. 30 (1995) 1519–1532. https://doi.org/10.1002/jms.1190301102.
[69] R.A. Zubarev, A. Makarov, Orbitrap Mass Spectrometry, Anal. Chem. 85 (2013) 5288–5296. https://doi.org/10.1021/ac4001223.
[70] A.G. Marshall, C.L. Hendrickson, G.S. Jackson, Fourier transform ion cyclotron resonance mass spectrometry: A primer, Mass Spectrom. Rev. 17 (1998) 1–35. https://doi.org/10.1002/(SICI)1098-2787(1998)17:1<1::AID-MAS1>3.0.CO;2-K.
[71] S. Schuchardt, A. Sickmann, Protein identification using mass spectrometry: A method overview, in: S. Baginsky, A.R. Fernie (Eds.), Plant Syst. Biol., Birkhäuser Basel, Basel, 2007: pp. 141–170. https://doi.org/10.1007/978-3-7643-7439-6_7.
[72] V. Cunsolo, V. Muccilli, R. Saletti, S. Foti, Mass spectrometry in food proteomics: a tutorial: MS-based approaches in food proteomics, J. Mass Spectrom. 49 (2014) 768–784. https://doi.org/10.1002/jms.3374.
[73] K. Strupat, O. Scheibner, M. Bromirski, High-Resolution, Accurate-Mass Orbitrap Mass Spectrometry – Definitions, Opportunities, and Advantages, (2016).
[74] A.G. Brenton, A.R. Godfrey, Accurate mass measurement: Terminology and treatment of data, J. Am. Soc. Mass Spectrom. 21 (2010) 1821–1835. https://doi.org/10.1016/j.jasms.2010.06.006.
[75] T.F. Scientific, Orbitrap Velos Pro Hardware Manual, (n.d.) 202.
[76] L. Imbert, R.G. Ramos, D. Libong, S. Abreu, P.M. Loiseau, P. Chaminade, Identification of phospholipid species affected by miltefosine action in Leishmania donovani cultures using LC-ELSD, LC-ESI/MS, and multivariate data analysis, Anal. Bioanal. Chem. 402 (2012) 1169–1182. https://doi.org/10.1007/s00216-011-5520-3.
[77] L. Xiang, L. Zhu, Y. Huang, Z. Cai, Application of Derivatization in Fatty Acids and Fatty Acyls Detection: Mass Spectrometry-Based Targeted Lipidomics, Small Methods. 4 (2020) 2000160. https://doi.org/10.1002/smtd.202000160.

[78] C. Bennaceur, C. Afonso, S. Alves, A. Bossée, J.-C. Tabet, Instrumental Dependent Dissociations of ***n*** -Propyl/Isopropyl Phosphonate Isomers: Evaluation of Resonant and Non-Resonant Vibrational Activations, J. Am. Soc. Mass Spectrom. 24 (2013) 1260–1270. https://doi.org/10.1007/s13361-013-0656-3.
[79] S. Ickert, J. Riedel, S. Beck, M.W. Linscheid, Negative nucleotide ions as sensitive probes for energy specificity in collision-induced fragmentation in mass spectrometry, Rapid Commun. Mass Spectrom. 32 (2018) 597–603. https://doi.org/10.1002/rcm.8062.
[80] M. Raetz, R. Bonner, G. Hopfgartner, SWATH-MS for metabolomics and lipidomics: critical aspects of qualitative and quantitative analysis, Metabolomics. 16 (2020) 71. https://doi.org/10.1007/s11306-020-01692-0.
[81] Bernhard Drotleff, Carlos Calderón Castro, Malgorzata Cebo, Kristina Dittrich, Xiaoqing Fu, Michael Lämmerhofer, Untargeted LC–MS Lipidomics with Data Independent Acquisition using Sequential Window Acquisition of All Theoretical Fragment-Ion Spectra, LCGC Eur. 34 (2021). www.chromatographyonline.com.
[82] M.A. Kochen, M.C. Chambers, J.D. Holman, A.I. Nesvizhskii, S.T. Weintraub, J.T. Belisle, M.N. Islam, J. Griss, D.L. Tabb, Greazy: Open-Source Software for Automated Phospholipid Tandem Mass Spectrometry Identification, Anal. Chem. 88 (2016) 5733–5741. https://doi.org/10.1021/acs.analchem.6b00021.
[83] C.A. Smith, E.J. Want, G. O'Maille, R. Abagyan, G. Siuzdak, XCMS: Processing Mass Spectrometry Data for Metabolite Profiling Using Nonlinear Peak Alignment, Matching, and Identification, (n.d.) 9.
[84] F. Giacomoni, G.L. Corguille, M. Monsoor, M. Landi, P. Pericard, M. Tremblay-Franco, S. Goulitquer, Workflow4Metabolomics: a collaborative research infrastructure for computational metabolomics, (n.d.) 3.
[85] G. Gürdeniz, M. Kristensen, T. Skov, L.O. Dragsted, The Effect of LC-MS Data Preprocessing Methods on the Selection of Plasma Biomarkers in Fed vs. Fasted Rats, Metabolites. 2 (2012) 77–99. https://doi.org/10.3390/metabo2010077.
[86] H. Tsugawa, K. Ikeda, M. Takahashi, A. Satoh, Y. Mori, H. Uchino, N. Okahashi, Y. Yamada, I. Tada, P. Bonini, Y. Higashi, Y. Okazaki, Z. Zhou, Z.-J. Zhu, J. Koelmel, T. Cajka, O. Fiehn, K. Saito, M. Arita, M. Arita, A lipidome atlas in MS-DIAL 4, Nat. Biotechnol. 38 (2020) 1159–1163. https://doi.org/10.1038/s41587-020-0531-2.
[87] J.P. Koelmel, N.M. Kroeger, C.Z. Ulmer, J.A. Bowden, R.E. Patterson, J.A. Cochran, C.W.W. Beecher, T.J. Garrett, R.A. Yost, LipidMatch: an automated workflow for rule-based lipid identification using untargeted high-resolution tandem mass spectrometry data, BMC Bioinformatics. 18 (2017) 331. https://doi.org/10.1186/s12859-017-1744-3.
[88] H.C. Köfeler, T.O. Eichmann, R. Ahrends, J.A. Bowden, N. Danne-Rasche, E.A. Dennis, M. Fedorova, W.J. Griffiths, X. Han, J. Hartler, M. Holčapek, R. Jirásko, J.P. Koelmel, C.S. Ejsing, G. Liebisch, Z. Ni, V.B. O'Donnell, O. Quehenberger, D. Schwudke, A. Shevchenko, M.J.O. Wakelam, M.R. Wenk, D. Wolrab, K. Ekroos, Quality control requirements for the correct annotation of lipidomics data, Nat. Commun. 12 (2021) 4771. https://doi.org/10.1038/s41467-021-24984-y.
[89] T. Sangster, H. Major, R. Plumb, A.J. Wilson, I.D. Wilson, A pragmatic and readily implemented quality control strategy for HPLC-MS and GC-MS-based metabonomic analysis, The Analyst. 131 (2006) 1075. https://doi.org/10.1039/b604498k.
[90] T. Kind, K.-H. Liu, D.Y. Lee, B. DeFelice, J.K. Meissen, O. Fiehn, LipidBlast in silico tandem mass spectrometry database for lipid identification, Nat. Methods. 10 (2013) 755–758. https://doi.org/10.1038/nmeth.2551.
[91] X. Chen, Y. Yin, Z. Zhou, T. Li, Z.-J. Zhu, Development of a combined strategy for accurate lipid structural identification and quantification in ion-mobility mass

spectrometry based untargeted lipidomics, Anal. Chim. Acta. 1136 (2020) 115–124. https://doi.org/10.1016/j.aca.2020.08.048.
[92] J.P. Koelmel, C.Z. Ulmer, C.M. Jones, R.A. Yost, J.A. Bowden, Common cases of improper lipid annotation using high-resolution tandem mass spectrometry data and corresponding limitations in biological interpretation, Biochim. Biophys. Acta BBA - Mol. Cell Biol. Lipids. 1862 (2017) 766–770. https://doi.org/10.1016/j.bbalip.2017.02.016.
[93] S.M. Lam, H. Tian, G. Shui, Lipidomics, en route to accurate quantitation, Biochim. Biophys. Acta. (2017). https://doi.org/10.1016/j.bbalip.2017.02.008.
[94] S. Fan, T. Kind, T. Cajka, S.L. Hazen, W.H.W. Tang, R. Kaddurah-Daouk, M.R. Irvin, D.K. Arnett, D.K. Barupal, O. Fiehn, Systematic Error Removal Using Random Forest for Normalizing Large-Scale Untargeted Lipidomics Data, Anal. Chem. 91 (2019) 3590–3596. https://doi.org/10.1021/acs.analchem.8b05592.
[95] Guideline-bioanalytical-method-validation, (2015).
[96] Lipidomics Standards Initiative Consortium, Lipidomics needs more standardization, Nat. Metab. 1 (2019) 745–747. https://doi.org/10.1038/s42255-019-0094-z.
[97] M.H. Philipsen, S. Sämfors, P. Malmberg, A.G. Ewing, Relative quantification of deuterated omega-3 and -6 fatty acids and their lipid turnover in PC12 cell membranes using TOF-SIMS, J. Lipid Res. 59 (2018) 2098–2107. https://doi.org/10.1194/jlr.M087734.
[98] A. Suarez-Trujillo, K. Huff, C. Ramires Ferreira, T.J. Paschoal Sobreira, K.K. Buhman, T. Casey, High-fat-diet induced obesity increases the proportion of linoleic acyl residues in dam serum and milk and in suckling neonate circulation, Biol. Reprod. 103 (2020) 736–749. https://doi.org/10.1093/biolre/ioaa103.
[99] L.M. Ingram, M.C. Finnerty, M. Mansoura, C.-W. Chou, B.S. Cummings, Identification of lipidomic profiles associated with drug-resistant prostate cancer cells, Lipids Health Dis. 20 (2021) 15. https://doi.org/10.1186/s12944-021-01437-5.
[100] M. Lange, M. Fedorova, Evaluation of lipid quantification accuracy using HILIC and RPLC MS on the example of NIST® SRM® 1950 metabolites in human plasma, Anal. Bioanal. Chem. 412 (2020) 3573–3584. https://doi.org/10.1007/s00216-020-02576-x.
[101] D. Wolrab, M. Chocholoušková, R. Jirásko, O. Peterka, V. Mužáková, H. Študentová, B. Melichar, M. Holčapek, Determination of one year stability of lipid plasma profile and comparison of blood collection tubes using UHPSFC/MS and HILIC-UHPLC/MS, Anal. Chim. Acta. 1137 (2020) 74–84. https://doi.org/10.1016/j.aca.2020.08.061.
[102] B. Su, L.F. Bettcher, W.-Y. Hsieh, D. Hornburg, M.J. Pearson, N. Blomberg, M. Giera, M.P. Snyder, D. Raftery, S.J. Bensinger, K.J. Williams, A DMS Shotgun Lipidomics Workflow Application to Facilitate High-Throughput, Comprehensive Lipidomics, J. Am. Soc. Mass Spectrom. 32 (2021) 2655–2663. https://doi.org/10.1021/jasms.1c00203.
[103] K.A. Lippa, J.J. Aristizabal-Henao, R.D. Beger, J.A. Bowden, C. Broeckling, C. Beecher, W. Clay Davis, W.B. Dunn, R. Flores, R. Goodacre, G.J. Gouveia, A.C. Harms, T. Hartung, C.M. Jones, M.R. Lewis, I. Ntai, A.J. Percy, D. Raftery, T.B. Schock, J. Sun, G. Theodoridis, F. Tayyari, F. Torta, C.Z. Ulmer, I. Wilson, B.K. Ubhi, Reference materials for MS-based untargeted metabolomics and lipidomics: a review by the metabolomics quality assurance and quality control consortium (mQACC), Metabolomics. 18 (2022) 24. https://doi.org/10.1007/s11306-021-01848-6.
[104] C.S. Ejsing, J.L. Sampaio, V. Surendranath, E. Duchoslav, K. Ekroos, R.W. Klemm, K. Simons, A. Shevchenko, Global analysis of the yeast lipidome by quantitative shotgun mass spectrometry, Proc. Natl. Acad. Sci. 106 (2009) 2136–2141.
[105] L. Lu, C. Hu, Y. Zhao, L. He, J. Zhou, H. Li, Y. Du, Y. Wang, C. Wen, X. Han, Y. Fan, Shotgun Lipidomics Revealed Altered Profiles of Serum Lipids in Systemic Lupus

Erythematosus Closely Associated with Disease Activity, Biomolecules. 8 (2018) 105. https://doi.org/10.3390/biom8040105.
[106] X. Han, R.W. Gross, Shotgun lipidomics: Electrospray ionization mass spectrometric analysis and quantitation of cellular lipidomes directly from crude extracts of biological samples, Mass Spectrom. Rev. 24 (2005) 367–412. https://doi.org/10.1002/mas.20023.
[107] X. Han, R.W. Gross, Electrospray ionization mass spectroscopic analysis of human erythrocyte plasma membrane phospholipids., Proc. Natl. Acad. Sci. 91 (1994) 10635–10639. https://doi.org/10.1073/pnas.91.22.10635.
[108] M. Koivusalo, P. Haimi, L. Heikinheimo, R. Kostiainen, P. Somerharju, Quantitative determination of phospholipid compositions by ESI-MS: effects of acyl chain length, unsaturation, and lipid concentration on instrument response, J. Lipid Res. 42 (2001) 663–672. https://doi.org/10.1016/S0022-2275(20)31176-7.
[109] T. Hofmann, C. Schmidt, Instrument response of phosphatidylglycerol lipids with varying fatty acyl chain length in nano-ESI shotgun experiments, Chem. Phys. Lipids. 223 (2019) 104782. https://doi.org/10.1016/j.chemphyslip.2019.05.007.
[110] X. Wang, P. Cong, Q. Chen, Z. Li, J. Xu, C. Xue, Characterizing the phospholipid composition of six edible sea cucumbers by NPLC-Triple TOF-MS/MS, J. Food Compos. Anal. 94 (2020) 103626. https://doi.org/10.1016/j.jfca.2020.103626.
[111] M. Lísa, E. Cífková, M. Khalikova, M. Ovčačíková, M. Holčapek, Lipidomic analysis of biological samples: Comparison of liquid chromatography, supercritical fluid chromatography and direct infusion mass spectrometry methods, J. Chromatogr. A. 1525 (2017) 96–108. https://doi.org/10.1016/j.chroma.2017.10.022.
[112] A. Kij, K. Kus, I. Czyzynska-Cichon, S. Chlopicki, M. Walczak, Development and validation of a rapid, specific and sensitive LC-MS/MS bioanalytical method for eicosanoid quantification - assessment of arachidonic acid metabolic pathway activity in hypertensive rats, Biochimie. 171–172 (2020) 223–232. https://doi.org/10.1016/j.biochi.2020.03.010.
[113] R. Berkecz, M. Lísa, M. Holčapek, Analysis of oxylipins in human plasma: Comparison of ultrahigh-performance liquid chromatography and ultrahigh-performance supercritical fluid chromatography coupled to mass spectrometry, J. Chromatogr. A. 1511 (2017) 107–121. https://doi.org/10.1016/j.chroma.2017.06.070.
[114] Z. Pataj, G. Liebisch, G. Schmitz, S. Matysik, Quantification of oxysterols in human plasma and red blood cells by liquid chromatography high-resolution tandem mass spectrometry, J. Chromatogr. A. 1439 (2016) 82–88. https://doi.org/10.1016/j.chroma.2015.11.015.
[115] J.A. Bowden, A. Heckert, C.Z. Ulmer, C.M. Jones, J.P. Koelmel, L. Abdullah, L. Ahonen, Y. Alnouti, A.M. Armando, J.M. Asara, T. Bamba, J.R. Barr, J. Bergquist, C.H. Borchers, J. Brandsma, S.B. Breitkopf, T. Cajka, A. Cazenave-Gassiot, A. Checa, M.A. Cinel, R.A. Colas, S. Cremers, E.A. Dennis, J.E. Evans, A. Fauland, O. Fiehn, M.S. Gardner, T.J. Garrett, K.H. Gotlinger, J. Han, Y. Huang, A.H. Neo, T. Hyötyläinen, Y. Izumi, H. Jiang, H. Jiang, J. Jiang, M. Kachman, R. Kiyonami, K. Klavins, C. Klose, H.C. Köfeler, J. Kolmert, T. Koal, G. Koster, Z. Kuklenyik, I.J. Kurland, M. Leadley, K. Lin, K.R. Maddipati, D. McDougall, P.J. Meikle, N.A. Mellett, C. Monnin, M.A. Moseley, R. Nandakumar, M. Oresic, R. Patterson, D. Peake, J.S. Pierce, M. Post, A.D. Postle, R. Pugh, Y. Qiu, O. Quehenberger, P. Ramrup, J. Rees, B. Rembiesa, D. Reynaud, M.R. Roth, S. Sales, K. Schuhmann, M.L. Schwartzman, C.N. Serhan, A. Shevchenko, S.E. Somerville, L. St. John-Williams, M.A. Surma, H. Takeda, R. Thakare, J.W. Thompson, F. Torta, A. Triebl, M. Trötzmüller, S.J.K. Ubhayasekera, D. Vuckovic, J.M. Weir, R. Welti, M.R. Wenk, C.E. Wheelock, L. Yao, M. Yuan, X.H. Zhao, S. Zhou, Harmonizing lipidomics: NIST interlaboratory comparison exercise for lipidomics using

SRM 1950–Metabolites in Frozen Human Plasma, J. Lipid Res. 58 (2017) 2275–2288. https://doi.org/10.1194/jlr.M079012.
[116] M. Ghorasaini, Y. Mohammed, J. Adamski, L. Bettcher, J.A. Bowden, M. Cabruja, K. Contrepois, M. Ellenberger, B. Gajera, M. Haid, D. Hornburg, C. Hunter, C.M. Jones, T. Klein, O. Mayboroda, M. Mirzaian, R. Moaddel, L. Ferrucci, J. Lovett, K. Nazir, M. Pearson, B.K. Ubhi, D. Raftery, F. Riols, R. Sayers, E.J.G. Sijbrands, M.P. Snyder, B. Su, V. Velagapudi, K.J. Williams, Y.B. de Rijke, M. Giera, Cross-Laboratory Standardization of Preclinical Lipidomics Using Differential Mobility Spectrometry and Multiple Reaction Monitoring, Anal. Chem. 93 (2021) 16369–16378. https://doi.org/10.1021/acs.analchem.1c02826.
[117] J.W. Thompson, K.J. Adams, J. Adamski, Y. Asad, D. Borts, J.A. Bowden, G. Byram, V. Dang, W.B. Dunn, F. Fernandez, O. Fiehn, D.A. Gaul, A.F. Hühmer, A. Kalli, T. Koal, S. Koeniger, R. Mandal, F. Meier, F.J. Naser, D. O'Neil, A. Pal, G.J. Patti, H. Pham-Tuan, C. Prehn, F.I. Raynaud, T. Shen, A.D. Southam, L. St. John-Williams, K. Sulek, C.G. Vasilopoulou, M. Viant, C.L. Winder, D. Wishart, L. Zhang, J. Zheng, M.A. Moseley, International Ring Trial of a High Resolution Targeted Metabolomics and Lipidomics Platform for Serum and Plasma Analysis, Anal. Chem. 91 (2019) 14407–14416. https://doi.org/10.1021/acs.analchem.9b02908.
[118] K.E. Christensen, O.V. Malysheva, S. Carlin, F. Matias, A.J. MacFarlane, R.L. Jacobs, M.A. Caudill, R. Rozen, Mild Choline Deficiency and MTHFD1 Synthetase Deficiency Interact to Increase Incidence of Developmental Delays and Defects in Mice, Nutrients. 14 (2021) 127. https://doi.org/10.3390/nu14010127.
[119] F.S. Teixeira, S.S.M.P. Vidigal, L.L. Pimentel, P.T. Costa, D. Tavares-Valente, J. Azevedo-Silva, M.E. Pintado, J.C. Fernandes, L.M. Rodríguez-Alcalá, Phytosterols and Novel Triterpenes Recovered from Industrial Fermentation Coproducts Exert In Vitro Anti-Inflammatory Activity in Macrophages, Pharmaceuticals. 14 (2021) 583. https://doi.org/10.3390/ph14060583.
[120] A. Bassot, J. Chen, K. Takahashi-Yamashiro, M.C. Yap, C.S. Gibhardt, G.N.T. Le, S. Hario, Y. Nasu, J. Moore, T. Gutiérrez, L. Mina, H. Mast, A. Moses, R. Bhat, K. Ballanyi, H. Lemieux, R. Sitia, E. Zito, I. Bogeski, R.E. Campbell, T. Simmen, The endoplasmic reticulum kinase PERK interacts with the oxidoreductase ERO1 to metabolically adapt mitochondria, Cell Rep. (2022) 111899. https://doi.org/10.1016/j.celrep.2022.111899.
[121] F.S. Teixeira, L.L. Pimentel, S.S.M.P. Vidigal, P.T. Costa, M.E. Pintado, L.M. Rodríguez-Alcalá, Suitability of Solvent-Assisted Extraction for Recovery of Lipophilic Phytochemicals in Sugarcane Straw and Bagasse, Foods. 11 (2022) 2661. https://doi.org/10.3390/foods11172661.
[122] H.Chr. Eilertsen, G.K. Eriksen, J.-S. Bergum, J. Strømholt, E. Elvevoll, K.-E. Eilertsen, E.S. Heimstad, I.H. Giæver, L. Israelsen, J.B. Svenning, L. Dalheim, R. Osvik, E. Hansen, R.A. Ingebrigtsen, T. Aspen, G.-H. Wintervoll, Mass Cultivation of Microalgae: I. Experiences with Vertical Column Airlift Photobioreactors, Diatoms and CO2 Sequestration, Appl. Sci. 12 (2022) 3082. https://doi.org/10.3390/app12063082.
[123] K. Uehara, J. Sostre-Colón, M. Gavin, D. Santoleri, K.-A. Leonard, R.L. Jacobs, P.M. Titchenell, Activation of Liver mTORC1 Protects Against NASH via Dual Regulation of VLDL-TAG Secretion and De Novo Lipogenesis, Cell. Mol. Gastroenterol. Hepatol. 13 (2022) 1625–1647. https://doi.org/10.1016/j.jcmgh.2022.02.015.
[124] L. Dalheim, J.B. Svenning, H.C. Eilertsen, T. Vasskog, R.L. Olsen, Stability of lipids during wet storage of the marine diatom Porosira glacialis under semi-preserved conditions at 4 and 20 °C, J. Appl. Phycol. (2020). https://doi.org/10.1007/s10811-020-02292-0.

[125] J.B. Svenning, L. Dalheim, T. Vasskog, L. Matricon, B. Vang, R.L. Olsen, Lipid yield from the diatom Porosira glacialis is determined by solvent choice and number of extractions, independent of cell disruption, Sci. Rep. 10 (2020) 22229. https://doi.org/10.1038/s41598-020-79269-z.
[126] Z. Hou, L.A. Fuiman, Incorporation of dietary lipids and fatty acids into red drum Sciaenops ocellatus eggs, Comp. Biochem. Physiol. B Biochem. Mol. Biol. (2021) 110694. https://doi.org/10.1016/j.cbpb.2021.110694.
[127] H.Chr. Eilertsen, E. Elvevoll, I.H. Giæver, J.B. Svenning, L. Dalheim, R.A. Svalheim, B. Vang, S. Siikavuopio, R. Dragøy, R.A. Ingebrigtsen, E. Hansen, A. Hustad, K.-E. Eilertsen, Inclusion of photoautotrophic cultivated diatom biomass in salmon feed can deter lice, PLOS ONE. 16 (2021) e0255370. https://doi.org/10.1371/journal.pone.0255370.
[128] L. Dalheim, J.B. Svenning, R.L. Olsen, In vitro intestinal digestion of lipids from the marine diatom Porosira glacialis compared to commercial LC n-3 PUFA products, PLOS ONE. 16 (2021) e0252125. https://doi.org/10.1371/journal.pone.0252125.
[129] J.-F. Montero-Bullon, S.S. Aveiro, T. Melo, T. Martins-Marques, D. Lopes, B. Neves, H. Girão, M. Rosário M Domingues, P. Domingues, Cardiac phospholipidome is altered during ischemia and reperfusion in an ex vivo rat model, Biochem. Biophys. Rep. 27 (2021) 101037. https://doi.org/10.1016/j.bbrep.2021.101037.
[130] C. Martín-Sierra, S. Colombo, R. Martins, P. Laranjeira, T. Melo, A.M. Abrantes, R.C. Oliveira, J.G. Tralhão, M.F. Botelho, E. Furtado, P. Domingues, M.R. Domingues, A. Paiva, Tumor Resection Induces Alterations on Serum Phospholipidome of Liver Cancer Patients, Lipids. 55 (2020) 185–191. https://doi.org/10.1002/lipd.12221.
[131] A. Burgos, J. Szymanski, B. Seiwert, T. Degenkolbe, M.A. Hannah, P. Giavalisco, L. Willmitzer, Analysis of short-term changes in the Arabidopsis thaliana glycerolipidome in response to temperature and light: Arabidopsis glycerolipids in abiotic stress, Plant J. 66 (2011) 656–668. https://doi.org/10.1111/j.1365-313X.2011.04531.x.
[132] T. Liu, J. Chen, F. Xu, X. He, S. Yang, Y. Zhu, W. Li, G. Zheng, Analysis of changes in the Panax notoginseng glycerolipidome in response to long-term chilling and heat, Plant Divers. 42 (2020) 102–110. https://doi.org/10.1016/j.pld.2019.11.002.
[133] F. Wei, B. Fanella, L. Guo, X. Wang, Membrane glycerolipidome of soybean root hairs and its response to nitrogen and phosphate availability, Sci. Rep. 6 (2016) 36172. https://doi.org/10.1038/srep36172.
[134] S. Wu, C. Hu, X. Yang, Q. Tan, S. Yao, Y. Zhou, X. Wang, X. Sun, Molybdenum induces alterations in the glycerolipidome that confer drought tolerance in wheat, J. Exp. Bot. 71 (2020) 5074–5086. https://doi.org/10.1093/jxb/eraa215.
[135] G. Zheng, L. Li, W. Li, Glycerolipidome responses to freezing- and chilling-induced injuries: examples in Arabidopsis and rice, BMC Plant Biol. 16 (2016) 70. https://doi.org/10.1186/s12870-016-0758-8.
[136] V. Gros, J. Lupette, J. Jouhet, Extraction and Quantification of Lipids from Plant or Algae, in: E. Maréchal (Ed.), Plastids, Springer US, New York, NY, 2018: pp. 213–240. https://doi.org/10.1007/978-1-4939-8654-5_15.
[137] H. Abida, L.-J. Dolch, C. Meï, V. Villanova, M. Conte, M.A. Block, G. Finazzi, O. Bastien, L. Tirichine, C. Bowler, F. Rébeillé, D. Petroutsos, J. Jouhet, E. Maréchal, Membrane Glycerolipid Remodeling Triggered by Nitrogen and Phosphorus Starvation in *Phaeodactylum tricornutum*, Plant Physiol. 167 (2015) 118–136. https://doi.org/10.1104/pp.114.252395.
[138] C. Degraeve-Guilbault, C. Bréhélin, R. Haslam, O. Sayanova, G. Marie-Luce, J. Jouhet, F. Corellou, Glycerolipid Characterization and Nutrient Deprivation-Associated

Changes in the Green Picoalga *Ostreococcus tauri*, Plant Physiol. 173 (2017) 2060–2080. https://doi.org/10.1104/pp.16.01467.
[139] A. Sergeeva, T. Mettler-Altmann, H. Liu, H. Mai, P. Bauer, Glycerolipid profile differences between perennial and annual stem zones in the perennial model plant *Arabis alpina*, Plant Direct. 5 (2021). https://doi.org/10.1002/pld3.302.
[140] O. Montero, M. Velasco, J. Miñón, E.A.N. Marks, A. Sanz-Arranz, C. Rad, Differential Membrane Lipid Profiles and Vibrational Spectra of Three Edaphic Algae and One Cyanobacterium, Int. J. Mol. Sci. 22 (2021) 11277. https://doi.org/10.3390/ijms222011277.
[141] X. Zhao, X. Qiu, Very Long Chain Polyunsaturated Fatty Acids Accumulated in Triacylglycerol Are Channeled From Phosphatidylcholine in Thraustochytrium, Front. Microbiol. 10 (2019) 645. https://doi.org/10.3389/fmicb.2019.00645.
[142] Y. Nakamura, Y. Liu, Y.-C. Lin, Floral glycerolipid profiles in homeotic mutants of Arabidopsis thaliana, Biochem. Biophys. Res. Commun. 450 (2014) 1272–1275. https://doi.org/10.1016/j.bbrc.2014.06.115.
[143] Anses, Actualisation des apports nutritionnels conseillés pour les acides gras., 2011. https://www.anses.fr/fr/system/files/NUT2006sa0359Ra.pdf (accessed April 6, 2022).
[144] X. Han, Lipidomics for studying metabolism, Nat. Rev. Endocrinol. 12 (2016) 668–679. https://doi.org/10.1038/nrendo.2016.98.
[145] R.A. Coleman, It takes a village: channeling fatty acid metabolism and triacylglycerol formation via protein interactomes, J. Lipid Res. 60 (2019) 490–497. https://doi.org/10.1194/jlr.S091843.
[146] M.C.F. Messias, G.C. Mecatti, D.G. Priolli, P. de Oliveira Carvalho, Plasmalogen lipids: functional mechanism and their involvement in gastrointestinal cancer, Lipids Health Dis. 17 (2018). https://doi.org/10.1186/s12944-018-0685-9.
[147] Lamiquiz-Moneo, Civeira, Gómez-Coronado, Blanco-Vaca, Villafuerte-Ledesma, Gil, Amigó, Mateo-Gallego, Cenarro, Lipid Profile Rather Than the LCAT Mutation Explains Renal Disease in Familial LCAT Deficiency, J. Clin. Med. 8 (2019) 1860. https://doi.org/10.3390/jcm8111860.
[148] V. Senanayake, D.B. Goodenowe, Plasmalogen deficiency and neuropathology in Alzheimer's disease: Causation or coincidence?, Alzheimers Dement. Transl. Res. Clin. Interv. 5 (2019) 524–532. https://doi.org/10.1016/j.trci.2019.08.003.
[149] H. Xicoy, B. Wieringa, G.J.M. Martens, The Role of Lipids in Parkinson's Disease, Cells. 8 (2019) 27. https://doi.org/10.3390/cells8010027.
[150] M. Mapstone, A.K. Cheema, M.S. Fiandaca, X. Zhong, T.R. Mhyre, L.H. MacArthur, W.J. Hall, S.G. Fisher, D.R. Peterson, J.M. Haley, M.D. Nazar, S.A. Rich, D.J. Berlau, C.B. Peltz, M.T. Tan, C.H. Kawas, H.J. Federoff, Plasma phospholipids identify antecedent memory impairment in older adults, Nat. Med. 20 (2014) 415–418. https://doi.org/10.1038/nm.3466.
[151] R. Laaksonen, K. Ekroos, M. Sysi-Aho, M. Hilvo, T. Vihervaara, D. Kauhanen, M. Suoniemi, R. Hurme, W. März, H. Scharnagl, T. Stojakovic, E. Vlachopoulou, M.-L. Lokki, M.S. Nieminen, R. Klingenberg, C.M. Matter, T. Hornemann, P. Jüni, N. Rodondi, L. Räber, S. Windecker, B. Gencer, E.R. Pedersen, G.S. Tell, O. Nygård, F. Mach, J. Sinisalo, T.F. Lüscher, Plasma ceramides predict cardiovascular death in patients with stable coronary artery disease and acute coronary syndromes beyond LDL-cholesterol, Eur. Heart J. 37 (2016) 1967–1976. https://doi.org/10.1093/eurheartj/ehw148.
[152] G. Lin, L. Wang, P.C. Marcogliese, H.J. Bellen, Sphingolipids in the Pathogenesis of Parkinson's Disease and Parkinsonism, Trends Endocrinol. Metab. 30 (2019) 106–117. https://doi.org/10.1016/j.tem.2018.11.003.

[153] P.J. Meikle, S.A. Summers, Sphingolipids and phospholipids in insulin resistance and related metabolic disorders, Nat. Rev. Endocrinol. 13 (2017) 79–91. https://doi.org/10.1038/nrendo.2016.169.
[154] J. Fernández-Irigoyen, P. Cartas-Cejudo, M. Iruarrizaga-Lejarreta, E. Santamaría, Alteration in the Cerebrospinal Fluid Lipidome in Parkinson's Disease: A Post-Mortem Pilot Study, Biomedicines. 9 (2021) 491. https://doi.org/10.3390/biomedicines9050491.
[155] J. Dyerberg, H.O. Bang, N. Hjørne, Fatty acid composition of the plasma lipids in Greenland Eskimos, Am. J. Clin. Nutr. 28 (1975) 958–966. https://doi.org/10.1093/ajcn/28.9.958.
[156] afssa, Acides gras de la famille oméga 3 et système cardiovasculaire: intérêt nutritionnel et allégations, 2002. https://www.anses.fr/fr/system/files/NUT-Ra-omega3.pdf (accessed February 16, 2022).
[157] S. Jovanovic, D. Dietrich, J. Becker, M. Kohlstedt, C. Wittmann, Microbial production of polyunsaturated fatty acids — high-value ingredients for aquafeed, superfoods, and pharmaceuticals, Curr. Opin. Biotechnol. 69 (2021) 199–211. https://doi.org/10.1016/j.copbio.2021.01.009.
[158] P. Bajpai, P.K. Bajpai, Eicosapentaenoic acid (EPA) production from microorganisms: a review, J. Biotechnol. 30 (1993) 161–183. https://doi.org/10.1016/0168-1656(93)90111-Y.
[159] A. Patel, D. Karageorgou, E. Rova, P. Katapodis, U. Rova, P. Christakopoulos, L. Matsakas, An Overview of Potential Oleaginous Microorganisms and Their Role in Biodiesel and Omega-3 Fatty Acid-Based Industries, Microorganisms. 8 (2020) 434. https://doi.org/10.3390/microorganisms8030434.
[160] Y. Gong, X. Wan, M. Jiang, C. Hu, H. Hu, F. Huang, Metabolic engineering of microorganisms to produce omega-3 very long-chain polyunsaturated fatty acids, Prog. Lipid Res. 56 (2014) 19–35. https://doi.org/10.1016/j.plipres.2014.07.001.
[161] T.-T. Zhang, J. Xu, Y.-M. Wang, C.-H. Xue, Health benefits of dietary marine DHA/EPA-enriched glycerophospholipids, Prog. Lipid Res. 75 (2019) 100997. https://doi.org/10.1016/j.plipres.2019.100997.
[162] X.Q. Su, J. Wang, A.J. Sinclair, Plasmalogens and Alzheimer's disease: a review, Lipids Health Dis. 18 (2019) 100. https://doi.org/10.1186/s12944-019-1044-1.
[163] S. Paul, G.I. Lancaster, P.J. Meikle, Plasmalogens: A potential therapeutic target for neurodegenerative and cardiometabolic disease, Prog. Lipid Res. 74 (2019) 186–195. https://doi.org/10.1016/j.plipres.2019.04.003.
[164] W.A. Wannes, B. Mhamdi, J. Sriti, B. Marzouk, Glycerolipid and fatty acid distribution in pericarp, seed and whole fruit oils of Myrtus communis var. italica, Ind. Crops Prod. 31 (2010) 77–83. https://doi.org/10.1016/j.indcrop.2009.09.006.
[165] L. Boudière, Analyse de l'homéostasie des lipides membranaires d'Arabidopsis thaliana par une stratégie de génétique chimique exploitant une nouvelle classe d'analogues du diacylglycérol, Université de Grenoble, 2014.
[166] C.-Y. Yu, V.C. Nguyen, L. Chuang, K. Kanehara, Membrane glycerolipid equilibrium under endoplasmic reticulum stress in Arabidopsis thaliana, Biochem. Biophys. Res. Commun. 500 (2018) 103–109. https://doi.org/10.1016/j.bbrc.2018.03.025.
[167] D. Dannenberger, G. Nuernberg, K. Nuernberg, K. Will, N. Schauer, M. Schmicke, Effects of diets supplemented with n –3 or n –6 PUFA on pig muscle lipid metabolites measured by non-targeted LC–MS lipidomic profiling, J. Food Compos. Anal. 56 (2017) 47–54. https://doi.org/10.1016/j.jfca.2016.11.015.
[168] C. He, Z. Sun, X. Qu, J. Cao, X. Shen, C. Li, A comprehensive study of lipid profiles of round scad (Decapterus maruadsi) based on lipidomic with UPLC-Q-Exactive Orbitrap-MS, Food Res. Int. 133 (2020) 109138. https://doi.org/10.1016/j.foodres.2020.109138.

[169] Q. Ren, Y. Ma, R. Wang, Y. Ma, T. Niu, Triacylglycerol Composition of Butterfat Fractions Determines Its Gastrointestinal Fate and Postprandial Effects: Lipidomic Analysis of Tri-, Di-, and Mono-acylglycerols and Free Fatty Acids, J. Agric. Food Chem. 69 (2021) 11033–11042. https://doi.org/10.1021/acs.jafc.1c03291.
[170] A.H. Banskota, A. Jones, J.P.M. Hui, R. Stefanova, I.W. Burton, Analysis of Polar Lipids in Hemp (Cannabis sativa L.) By-Products by Ultra-High Performance Liquid Chromatography and High-Resolution Mass Spectrometry, (2022) 17.
[171] V. Ollivier, D. Ollivier, J. Artaud, Analyse des lipides, (2015) 28.
[172] A. Sehl, L. Couëdelo, L. Fonseca, C. Vaysse, M. Cansell, A critical assessment of transmethylation procedures for n-3 long-chain polyunsaturated fatty acid quantification of lipid classes, Food Chem. 251 (2018) 1–8. https://doi.org/10.1016/j.foodchem.2018.01.060.
[173] A.I. Ostermann, M. Müller, I. Willenberg, N.H. Schebb, Determining the fatty acid composition in plasma and tissues as fatty acid methyl esters using gas chromatography – a comparison of different derivatization and extraction procedures, Prostaglandins Leukot. Essent. Fatty Acids. 91 (2014) 235–241. https://doi.org/10.1016/j.plefa.2014.10.002.
[174] W.R. Morrison, L.M. Smith, Preparation of fatty acid mathyl esters and dimethylacetals from lipids with boron fluoride methanol, J. Lipid Res. 5 (1964) 600–608. https://doi.org/10.1016/S0022-2275(20)40190-7.
[175] P. Castro-Gómez, J. Fontecha, L.M. Rodríguez-Alcalá, A high-performance direct transmethylation method for total fatty acids assessment in biological and foodstuff samples, Talanta. 128 (2014) 518–523. https://doi.org/10.1016/j.talanta.2014.05.051.
[176] W.W. Christie, J.L. Sébédio, P. Juanéda, A practical guide to the analysis of conjugated linoleic acid (CLA), (2001) 7.
[177] S. Khoury, V. Gudziol, S. Grégoire, S. Cabaret, S. Menzel, L. Martine, E. Mézière, V. Soubeyre, T. Thomas-Danguin, X. Grosmaitre, L. Bretillon, O. Berdeaux, N. Acar, T. Hummel, A.M. Le Bon, Lipidomic profile of human nasal mucosa and associations with circulating fatty acids and olfactory deficiency, Sci. Rep. 11 (2021) 16771. https://doi.org/10.1038/s41598-021-93817-1.
[178] P. Gómez-Cortés, V. Rodríguez-Pino, A.L.M. Marín, M.A. de la Fuente, Identification and quantification of dimethyl acetals from plasmalogenic lipids in lamb intramuscular fat under different derivatization procedures, J. Chromatogr. B. 1120 (2019) 24–28. https://doi.org/10.1016/j.jchromb.2019.04.049.
[179] E.D. Dodds, M.R. McCoy, L.D. Rea, J.M. Kennish, Gas chromatographic quantification of fatty acid methyl esters: Flame ionization detection vs. Electron impact mass spectrometry, Lipids. 40 (2005) 419–428. https://doi.org/10.1007/s11745-006-1399-8.
[180] M.A. Bromke, A. Hochmuth, T. Tohge, A.R. Fernie, P. Giavalisco, A. Burgos, L. Willmitzer, Y. Brotman, Liquid chromatography high-resolution mass spectrometry for fatty acid profiling, Plant J. 81 (2015) 529–536. https://doi.org/10.1111/tpj.12739.
[181] J.J. Kamphorst, J. Fan, W. Lu, E. White, J.D. Rabinowitz, Liquid Chromatography–High Resolution Mass Spectrometry Analysis of Fatty Acid Metabolism, Anal. Chem. 83 (2011) 9114–9122. https://doi.org/10.1021/ac202220b.
[182] E. Koch, M. Wiebel, C. Hopmann, N. Kampschulte, N.H. Schebb, Rapid quantification of fatty acids in plant oils and biological samples by LC-MS, Anal. Bioanal. Chem. 413 (2021) 5439–5451. https://doi.org/10.1007/s00216-021-03525-y.
[183] A.I. Ostermann, E. Koch, K.M. Rund, L. Kutzner, M. Mainka, N.H. Schebb, Targeting esterified oxylipins by LC–MS - Effect of sample preparation on oxylipin pattern, Prostaglandins Other Lipid Mediat. 146 (2020) 106384. https://doi.org/10.1016/j.prostaglandins.2019.106384.

[184] C. Buré, A. Solgadi, S. Yen-Nicolaÿ, T. Bardeau, D. Libong, S. Abreu, P. Chaminade, P. Subra-Paternault, M. Cansell, Electrospray mass spectrometry as a tool to characterize phospholipid composition of plant cakes, Eur. J. Lipid Sci. Technol. (2016) n/a-n/a. https://doi.org/10.1002/ejlt.201500345.
[185] M. Cansell, T. Bardeau, E. Morvan, A. Grélard, C. Buré, P. Subra-Paternault, Phospholipid Profiles of Oleaginous Pressed Cakes Using NMR and Gas Chromatography, J. Am. Oil Chem. Soc. 94 (2017) 1219–1223. https://doi.org/10.1007/s11746-017-3022-y.
[186] M. Holčapek, P. Jandera, P. Zderadička, L. Hruba, Characterization of triacylglycerol and diacylglycerol composition of plant oils using high-performance liquid chromatography–atmospheric pressure chemical ionization mass spectrometry, J. Chromatogr. A. 1010 (2003) 195–215. https://doi.org/10.1016/s0021-9673(03)01030-6.
[187] A. Delobel, D. Touboul, O. Laprévote, Structural Characterization of Phosphatidylcholines by Atmospheric Pressure Photoionization Mass Spectrometry, Eur. J. Mass Spectrom. 11 (2005) 409–417. https://doi.org/10.1255/ejms.760.
[188] O. Quehenberger, A.M. Armando, E.A. Dennis, High sensitivity quantitative lipidomics analysis of fatty acids in biological samples by gas chromatography–mass spectrometry, Biochim. Biophys. Acta BBA - Mol. Cell Biol. Lipids. 1811 (2011) 648–656. https://doi.org/10.1016/j.bbalip.2011.07.006.
[189] J.G. McDonald, D.D. Smith, A.R. Stiles, D.W. Russell, A comprehensive method for extraction and quantitative analysis of sterols and secosteroids from human plasma, J. Lipid Res. 53 (2012) 1399–1409. https://doi.org/10.1194/jlr.D022285.
[190] D. Balgoma, J. Larsson, J. Rokach, J.A. Lawson, K. Daham, B. Dahlén, S.-E. Dahlén, C.E. Wheelock, Quantification of Lipid Mediator Metabolites in Human Urine from Asthma Patients by Electrospray Ionization Mass Spectrometry: Controlling Matrix Effects, Anal. Chem. 85 (2013) 7866–7874. https://doi.org/10.1021/ac401461b.
[191] T. Lan, H. Bi, W. Liu, X. Xie, S. Xu, H. Huang, Simultaneous determination of sphingosine and sphingosine 1-phosphate in biological samples by liquid chromatography–tandem mass spectrometry, J. Chromatogr. B. 879 (2011) 520–526. https://doi.org/10.1016/j.jchromb.2011.01.015.
[192] Z. Cao, T.C. Schmitt, V. Varma, D. Sloper, R.D. Beger, J. Sun, Evaluation of the Performance of Lipidyzer Platform and Its Application in the Lipidomics Analysis in Mouse Heart and Liver, J. Proteome Res. 19 (2020) 2742–2749. https://doi.org/10.1021/acs.jproteome.9b00289.
[193] J. Xue, X. Domingo-Almenara, C. Guijas, A. Palermo, M.M. Rinschen, J. Isbell, H.P. Benton, G. Siuzdak, Enhanced in-Source Fragmentation Annotation Enables Novel Data Independent Acquisition and Autonomous METLIN Molecular Identification, Anal. Chem. 92 (2020) 6051–6059. https://doi.org/10.1021/acs.analchem.0c00409.
[194] S. Lewenza, R. Falsafi, M. Bains, P. Rohs, J. Stupak, G.D. Sprott, R.E.W. Hancock, The olsA gene mediates the synthesis of an ornithine lipid in Pseudomonas aeruginosa during growth under phosphate-limiting conditions, but is not involved in antimicrobial peptide susceptibility: Phosphate-free membrane lipids, FEMS Microbiol. Lett. 320 (2011) 95–102. https://doi.org/10.1111/j.1574-6968.2011.02295.x.
[195] M. Sandoval-Calderón, Z. Guan, C. Sohlenkamp, Knowns and unknowns of membrane lipid synthesis in streptomycetes, Biochimie. 141 (2017) 21–29. https://doi.org/10.1016/j.biochi.2017.05.008.
[196] E.R. Olukoshi, N.M. Packter, Importance of stored triacylglycerols in Streptomyces: possible carbon source for antibiotics, Microbiology. 140 (1994) 931–943. https://doi.org/10.1099/00221287-140-4-931.

[197] N.M. Packter, E.R. Olukoshi, Ultrastructural studies of neutral lipid localisation inStreptomyces, Arch. Microbiol. 164 (1995) 420–427. https://doi.org/10.1007/BF02529740.
[198] C. Banchio, H. Gramajo, A Stationary-Phase Acyl-Coenzyme A Synthetase of *Streptomyces coelicolor* A3(2) Is Necessary for the Normal Onset of Antibiotic Production, Appl. Environ. Microbiol. 68 (2002) 4240–4246. https://doi.org/10.1128/AEM.68.9.4240-4246.2002.
[199] W. Wang, S. Li, Z. Li, J. Zhang, K. Fan, G. Tan, G. Ai, S.M. Lam, G. Shui, Z. Yang, H. Lu, P. Jin, Y. Li, X. Chen, X. Xia, X. Liu, H.K. Dannelly, C. Yang, Y. Yang, S. Zhang, G. Alterovitz, W. Xiang, L. Zhang, Harnessing the intracellular triacylglycerols for titer improvement of polyketides in Streptomyces, Nat. Biotechnol. 38 (2020) 76–83. https://doi.org/10.1038/s41587-019-0335-4.
[200] Y. Chen, J. Metz, R.K. Miller-Xavier, G. Wang, Unlocking a new target for streptomycetes strain improvement, Synth. Syst. Biotechnol. 5 (2020) 33–34. https://doi.org/10.1016/j.synbio.2020.02.001.
[201] D. Xu, N. Seghezzi, C. Esnault, M.-J. Virolle, Repression of Antibiotic Production and Sporulation in Streptomyces coelicolor by Overexpression of a TetR Family Transcriptional Regulator□, APPL Env. MICROBIOL. 76 (2010) 13.
[202] T.L. Foley, B.S. Young, M.D. Burkart, Phosphopantetheinyl transferase inhibition and secondary metabolism: PPTase inhibition and secondary metabolism, FEBS J. 276 (2009) 7134–7145. https://doi.org/10.1111/j.1742-4658.2009.07425.x.
[203] A. Craney, C. Ozimok, S.M. Pimentel-Elardo, A. Capretta, J.R. Nodwell, Chemical Perturbation of Secondary Metabolism Demonstrates Important Links to Primary Metabolism, Chem. Biol. 19 (2012) 1020–1027. https://doi.org/10.1016/j.chembiol.2012.06.013.

ANNEXES

ANNEXE I. SUPPLEMENTAIRES PUBLICATION 1

Journal of Chromatography A, 1514 (2017) 54–71

Contents lists available at ScienceDirect

Journal of Chromatography A

journal homepage: www.elsevier.com/locate/chroma

Optimization of normal phase chromatographic conditions for lipid analysis and comparison of associated detection techniques

Sonia Abreu[a], Audrey Solgadi[b], Pierre Chaminade[a,*]

[a] Lip(Sys)², Chimie Analytique Pharmaceutique (FKA EA4041 Groupe de Chimie Analytique de Paris-Sud), Univ. Paris-Sud, Université Paris-Saclay, F-92290 Châtenay-Malabry, France
[b] SAMM, UMS IPSIT, Université Paris Sud, Université Paris-Saclay, Chatenay-Malabry, France

ARTICLE INFO

Article history:
Received 7 November 2016
Received in revised form 7 July 2017
Accepted 18 July 2017
Available online 24 July 2017

Keywords:
Lipids
Normal-phase liquid chromatography
Evaporative light scattering detector
Charged aerosol detector
Atmospheric pressure photoionization
LC/MS

ABSTRACT

One important challenge in lipid class analysis is to develop a method suitable or, at least adaptable, for a vast diversity of samples. In the current study, an improved normal-phase liquid chromatography (NPLC) method allowed analyzing the lipid classes present in mammalian, vegetable as well as microorganism (yeast and bacteria) lipid samples. The method effectively separated 30 lipid classes or subclasses with a special focus on medium polarity lipids. The separation was carried out with bare silica stationary phase and was coupled to evaporative light scattering detection (ELSD), charged aerosol detection (Corona-CAD®) and mass spectrometry. Solutions are provided to circumvent technical issues (such as pumping solvents of low viscosity, solvent purity, rinsing step). The influence of mobile phase composition and addition of ionic modifiers on the chromatographic behavior of particular lipid classes is documented. A comparison between ELSD and Corona-CAD® confirmed the interest of this later detector for samples with a wide range of concentration of different lipids. Three common atmospheric pressure ionization interfaces were used for coupling the NPLC separation to a LTQ Velos Pro® mass spectrometer. The comparison of the chromatographic profiles showed that atmospheric pressure chemical ionization (APCI) and atmospheric pressure photoionization (APPI) are both suitable to detect the different lipid classes whereas APPI allows a better sensitivity for lipids at low-concentration.

© 2017 Elsevier B.V. All rights reserved.

1. Introduction

Lipidomics has emerged with the growing progress in mass spectrometry and bioinformatics. This is a complex field of activity since more than 40 000 unique lipid structures are listed in the LIPIDMAPS database nowadays [1,2]. Analytical techniques for lipidomics represent a very dynamic and motivating area as the lipid composition of animal or vegetal tissue is influenced by external factors (such as metabolic state or diet) and as research methods have still to be developed. New technologies and/or new developments in analytical sciences are now addressing lipid analysis to promote alternative and original separation techniques coupled with mass spectrometry. An important review about LC/MS based lipid analysis was published by Cajka & Fiehn [3] in 2014. They analyzed 185 original research papers and covered the technical approaches involved in lipidomics. The scope ranges from sample preparation to data treatment and encompasses mass spectrometry and separation techniques.

Several interesting findings can be extracted from this article. First, the diversity of the biological samples addressed by these 185 studies: plasma and serum represent 39% of the samples, animal tissue 23% and cells 22%, only 3% are plant tissues and other matrix represent 13%. Second, when LC/MS is used, reversed-phase liquid chromatography (RPLC), normal phase liquid chromatography (NPLC) and hydrophilic interaction chromatography (HILIC) are the most important techniques and correspond respectively to 71, 19 and 8% of the studies. It is worthy to note that RPLC and HILIC take advantage of improved sub-2-μm or fused core 2.6–2.8 μm particle size stationary phases whereas NPLC methods use classical 3–5 μm. In the vast majority of cases, narrow bore columns (2.1 mm I.D.) are used whatever is the retention mechanism. RPLC and HILC benefit from the high water content and water miscible solvents used as mobile phase that facilitate the coupling with MS. HILIC is presented as an alternative to NPLC with a better reproducibility and a better compatibility with MS. Finally, this review pointed out the dominant position of electrospray ionization mass spectrometry (ESI) in lipidomic studies, most of time used in positive mode.

* Corresponding author.
E-mail address: pierre.chaminade@u-psud.fr (P. Chaminade).

http://dx.doi.org/10.1016/j.chroma.2017.07.063
0021-9673/© 2017 Elsevier B.V. All rights reserved.

SUPPORTING INFORMATION

Abbreviations	
ASG	acylated steryl glycosides
CE	cholesteryl esters
Cer	ceramides
CL	cardiolipins
Chol	cholesterol
DG	diacylglycerols
DGDG	digalactosyldiglycerols
DAGE	diacylglycerol ethers
DPG	diphosphatidylglycerol
FA	fatty acids
FAlc	fatty acids alcohol
FAME	fatty acids methylesters
GlcCer	glucosylceramides
HexCER	hexosylceramide
IPA	isopropanol
IPC	inositol phosphoceramide
LPA	lysophosphatidic acids
LPC	lysophosphatidylcholines
MG	monoacylglycerols
MGDG	monogalactosyldiglycerols
NAPE	N-Acylphosphatidylethanolamines
PA	phosphatidic acids
PC	phosphatidylcholines
PE	phosphatidylethanolamines
PG	phosphatidylglycerols
PI	phosphatidylinositols
PL	phospholipids
PS	phosphatidylserines
SE	sterol ester
SG	steryl glycosides
SM	sphingomyelins
SQ	squalene
ST	sterols
TG	triacylglycerols
WE	wax ester
NALPE	N-Acylphosphatidylethanolamines

Table S- 1. Lipid name abbreviations used in the manuscript.

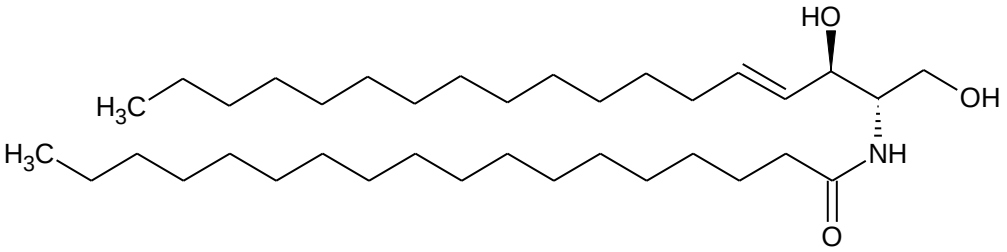

CerII (Cer(d18:1/18:0))

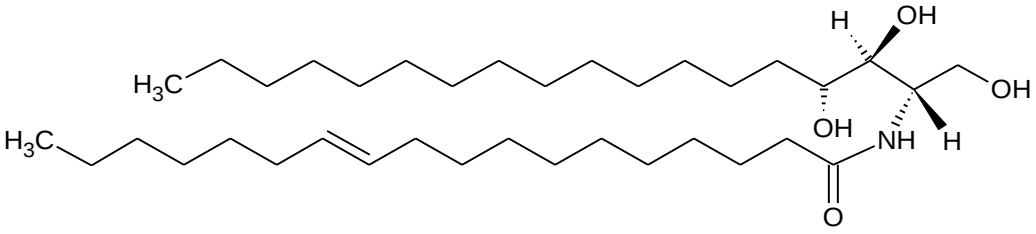

CerIIIb (Cer(t18:0/18:1))

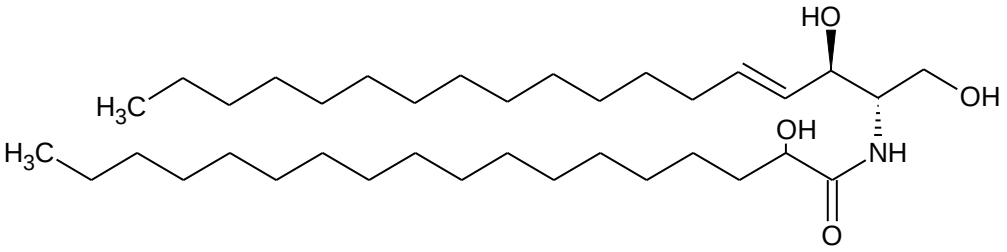

CerV (Cer(d18:1/18:0(2OH)))

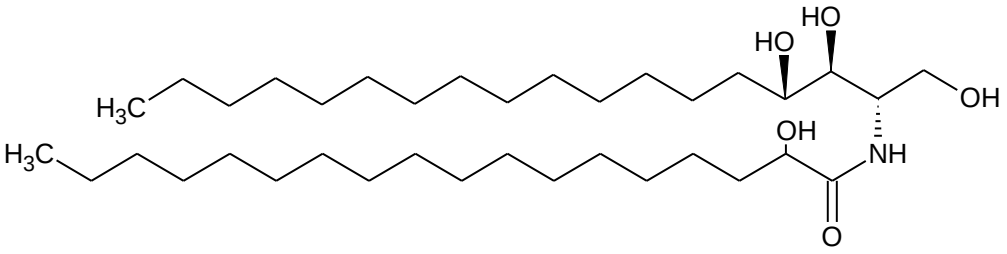

CerVI (Cer(t18:0/18:0(2OH)))

Figure S-1. Structures of ceramide standards.

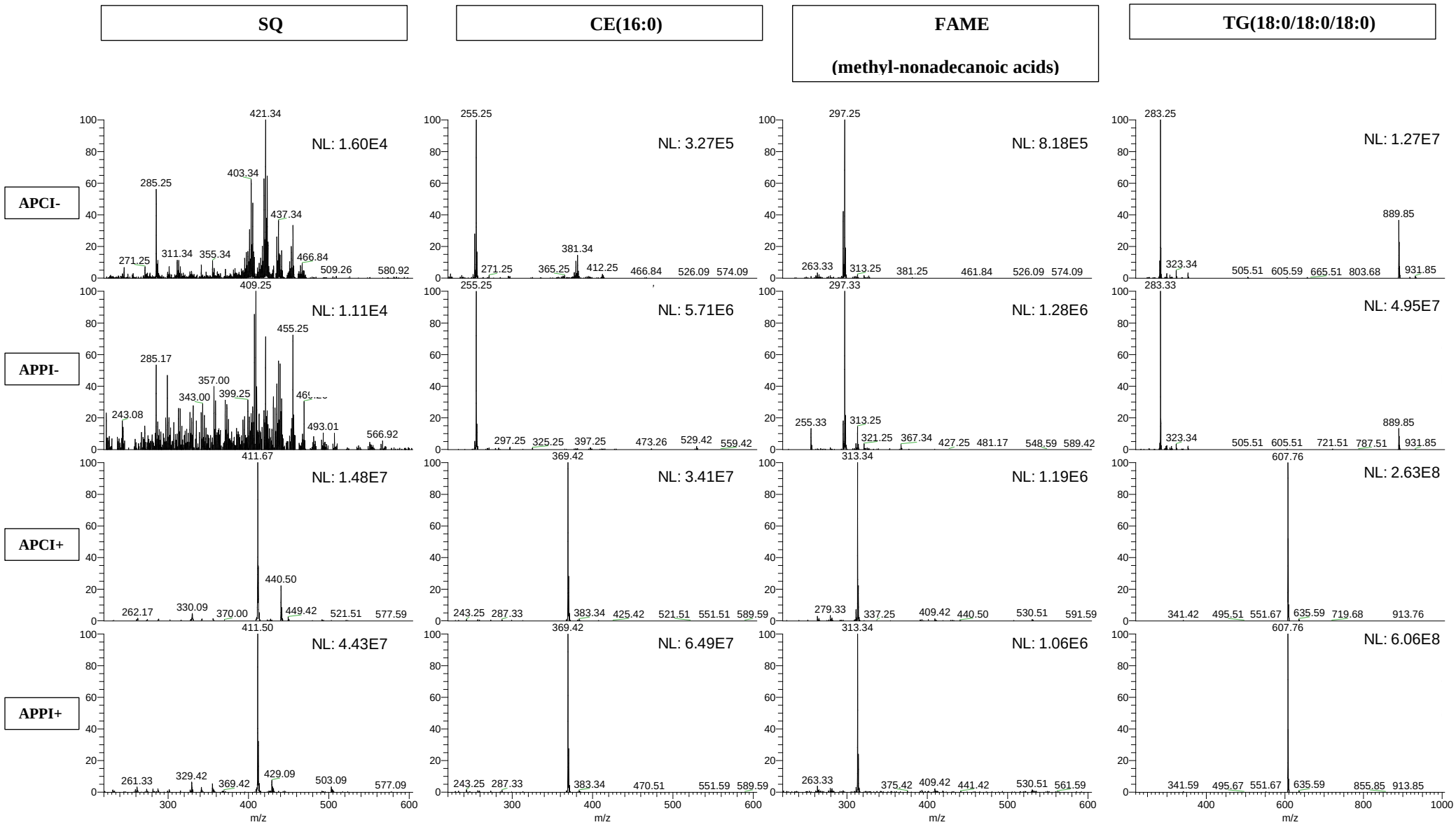
SQ
CE(16:0)
FAME
(methyl-nonadecanoic acids)
TG(18:0/18:0/18:0)
APCI-
APPI-
APCI+
APPI+
NL: 1.60E4
NL: 3.27E5
NL: 8.18E5
NL: 1.27E7
NL: 1.11E4
NL: 5.71E6
NL: 1.28E6
NL: 4.95E7
NL: 1.48E7
NL: 3.41E7
NL: 1.19E6
NL: 2.63E8
NL: 4.43E7
NL: 6.49E7
NL: 1.06E6
NL: 6.06E8
m/z

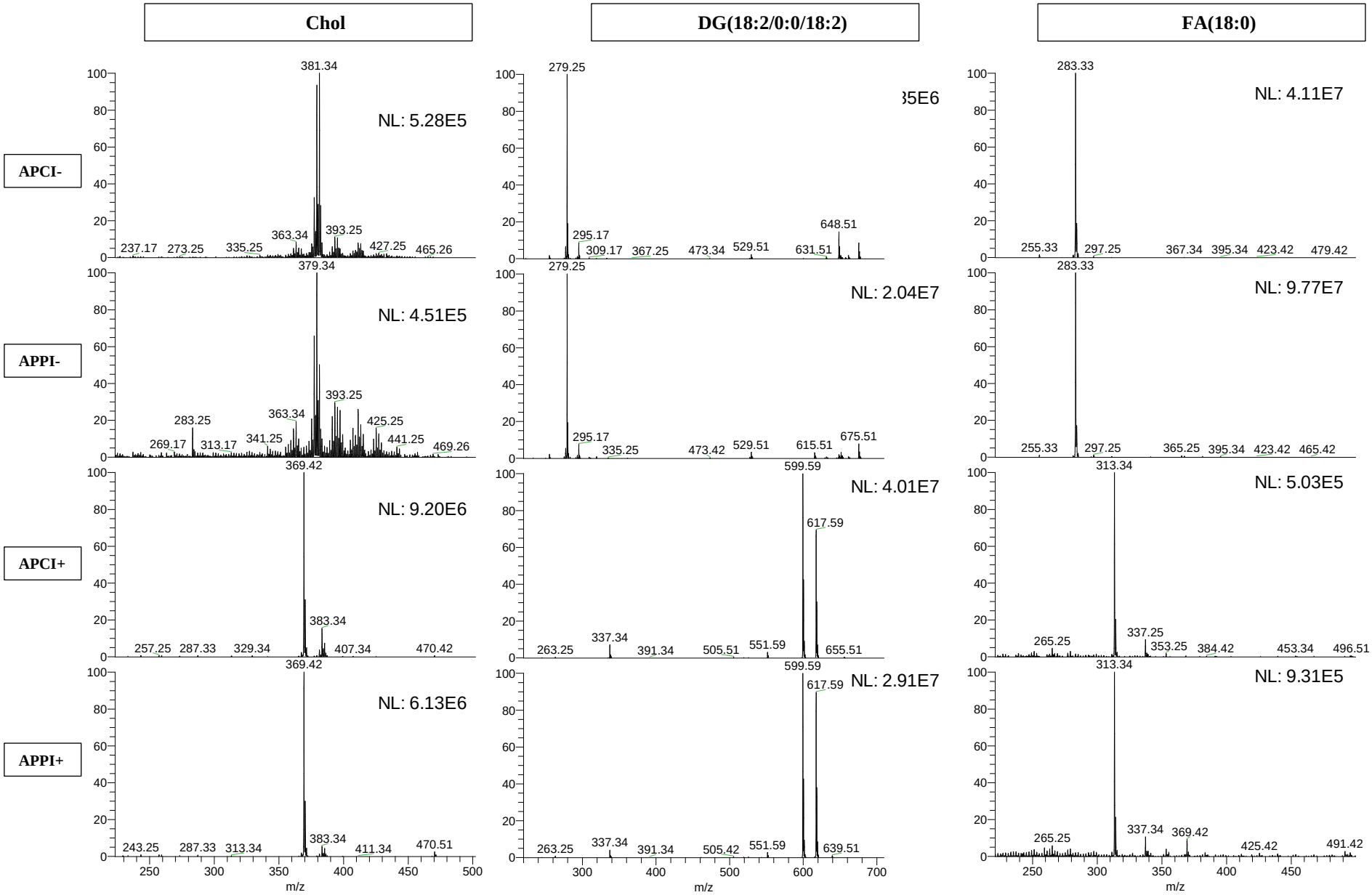
Chol
DG(18:2/0:0/18:2)
FA(18:0)
APCI-
APPI-
APCI+
APPI+
NL: 5.28E5
NL: 4.51E5
NL: 9.20E6
NL: 6.13E6
NL: 2.04E7
NL: 4.01E7
NL: 2.91E7
NL: 4.11E7
NL: 9.77E7
NL: 5.03E5
NL: 9.31E5
m/z

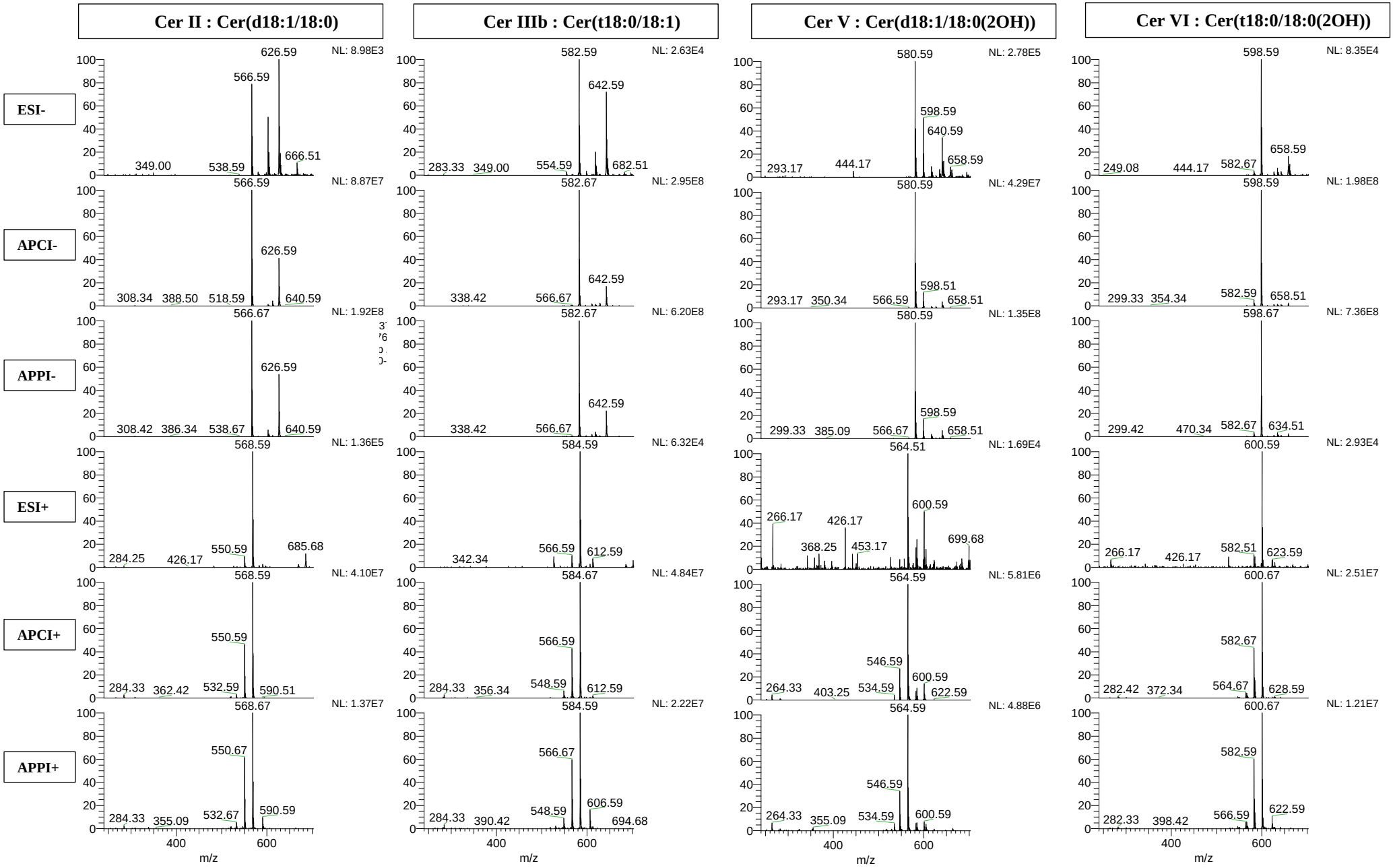
Cer II : Cer(d18:1/18:0)
Cer IIIb : Cer(t18:0/18:1)
Cer V : Cer(d18:1/18:0(2OH))
Cer VI : Cer(t18:0/18:0(2OH))
ESI-
APCI-
APPI-
ESI+
APCI+
APPI+
m/z

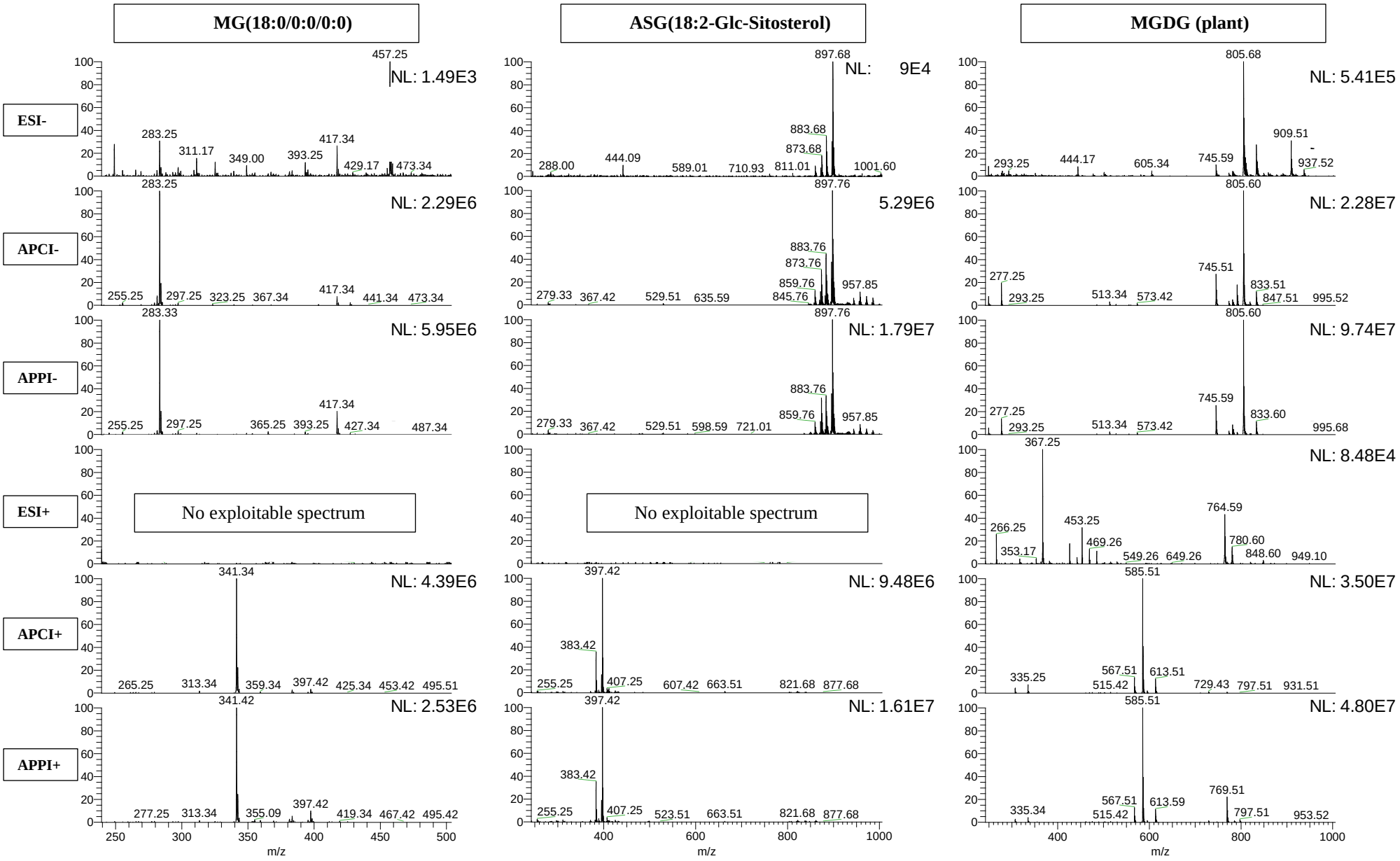
MG(18:0/0:0/0:0)
ASG(18:2-Glc-Sitosterol)
MGDG (plant)
ESI-
APCI-
APPI-
ESI+
APCI+
APPI+
No exploitable spectrum
No exploitable spectrum
NL: 1.49E3
NL: 9E4
NL: 5.41E5
NL: 2.29E6
5.29E6
NL: 2.28E7
NL: 5.95E6
NL: 1.79E7
NL: 9.74E7
NL: 8.48E4
NL: 4.39E6
NL: 9.48E6
NL: 3.50E7
NL: 2.53E6
NL: 1.61E7
NL: 4.80E7
m/z
m/z
m/z

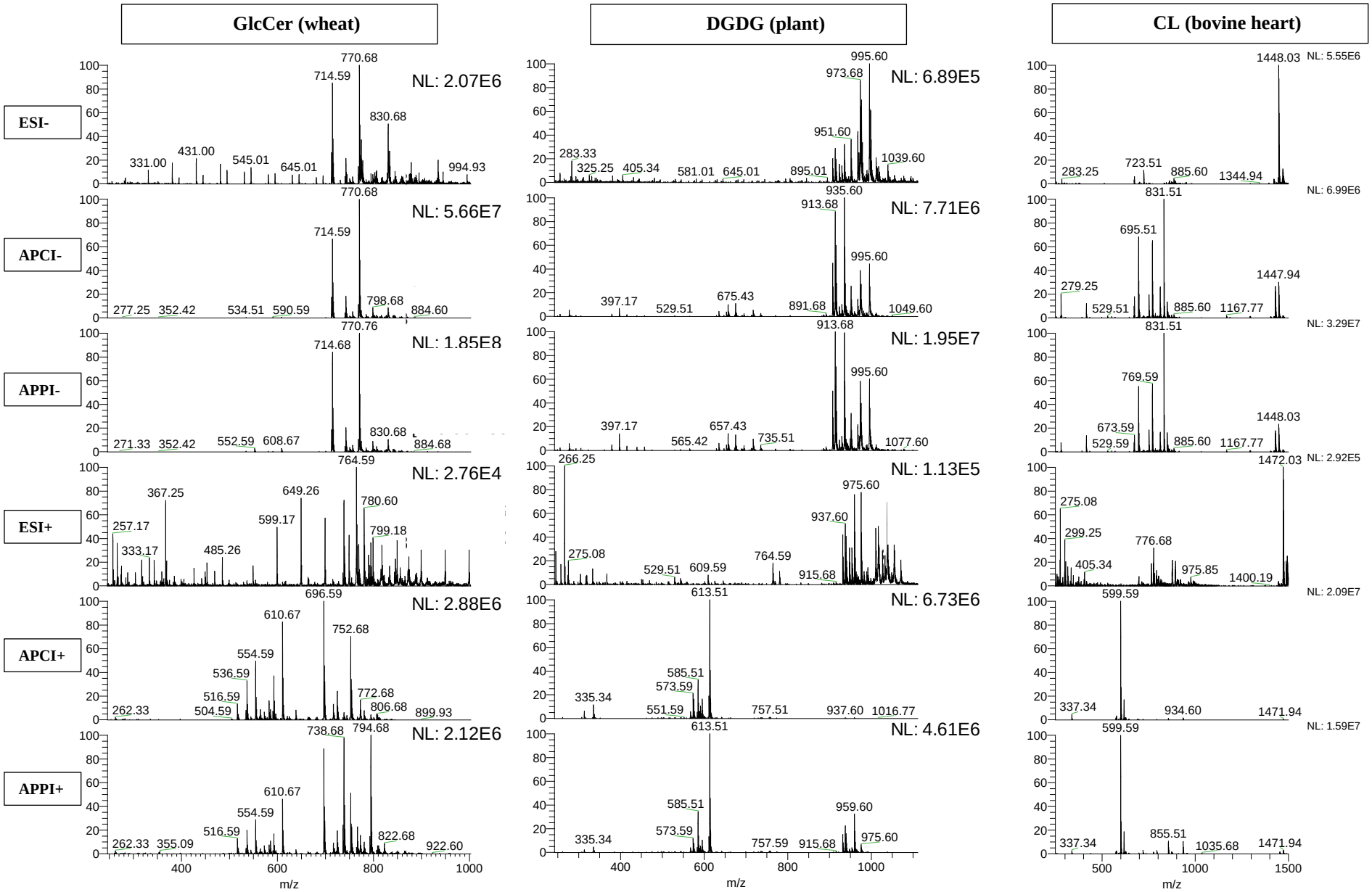
GlcCer (wheat)
DGDG (plant)
CL (bovine heart)
ESI-
APCI-
APPI-
ESI+
APCI+
APPI+
NL: 2.07E6
NL: 5.66E7
NL: 1.85E8
NL: 2.76E4
NL: 2.88E6
NL: 2.12E6
NL: 6.89E5
NL: 7.71E6
NL: 1.95E7
NL: 1.13E5
NL: 6.73E6
NL: 4.61E6
NL: 5.55E6
NL: 6.99E6
NL: 3.29E7
NL: 2.92E5
NL: 2.09E7
NL: 1.59E7
m/z

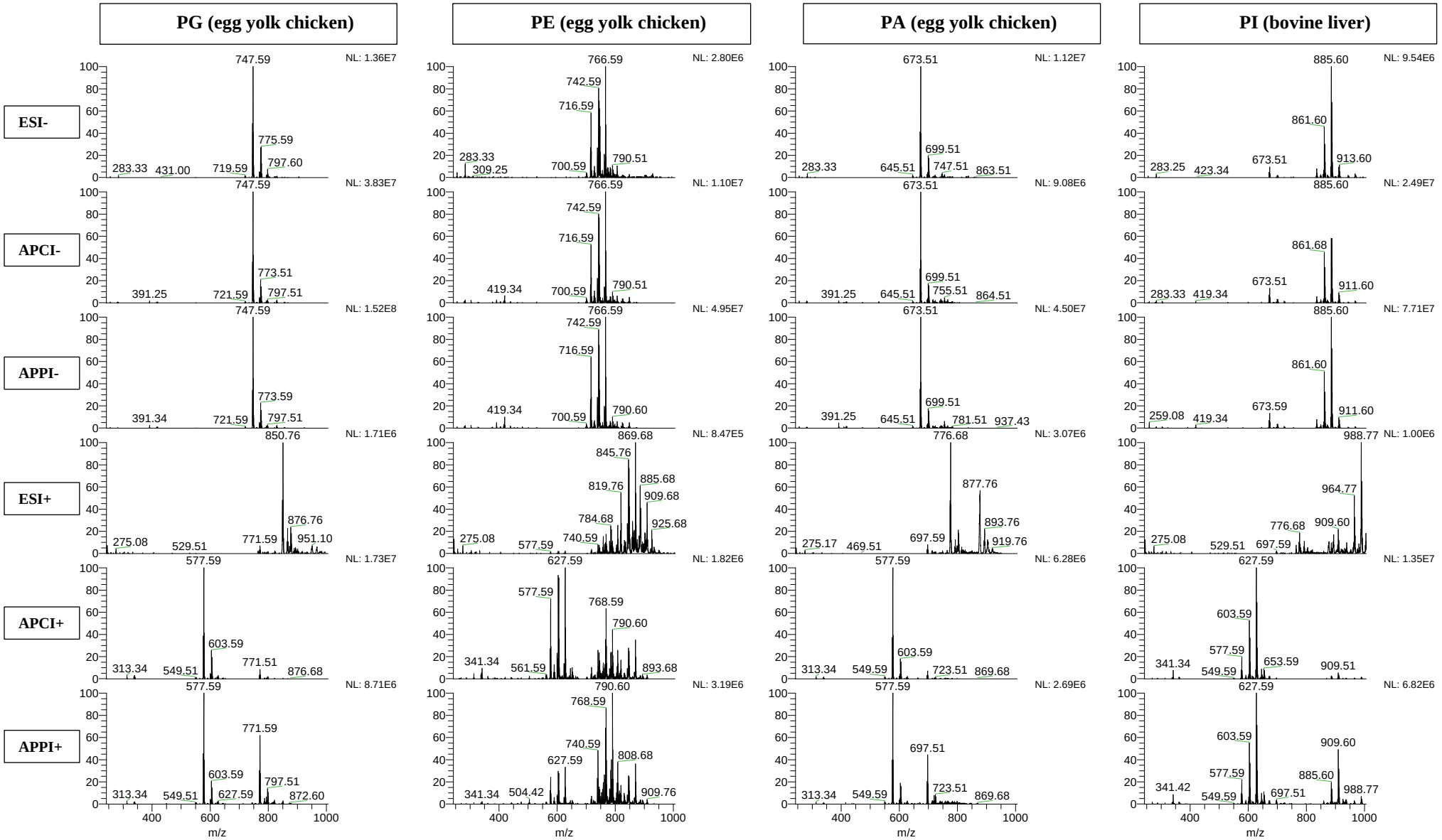
PG (egg yolk chicken)
PE (egg yolk chicken)
PA (egg yolk chicken)
PI (bovine liver)
ESI-
APCI-
APPI-
ESI+
APCI+
APPI+
m/z

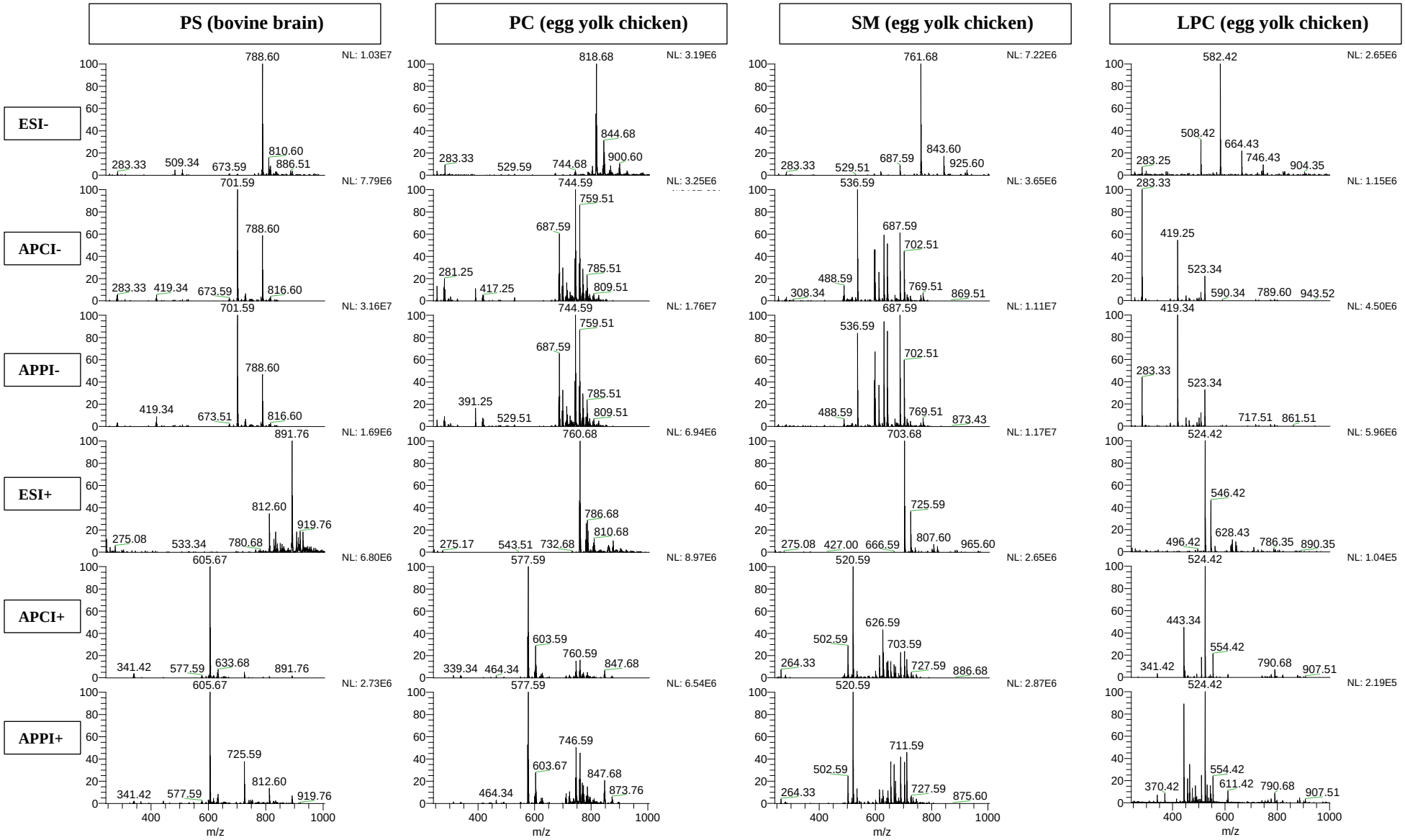

Figure S-2**.** LC/MS Full scan mass spectra obtained with the three API sources in negative and positive mode for each lipid standard used in the study.

Cer II : Cer(d18:1/18:0)

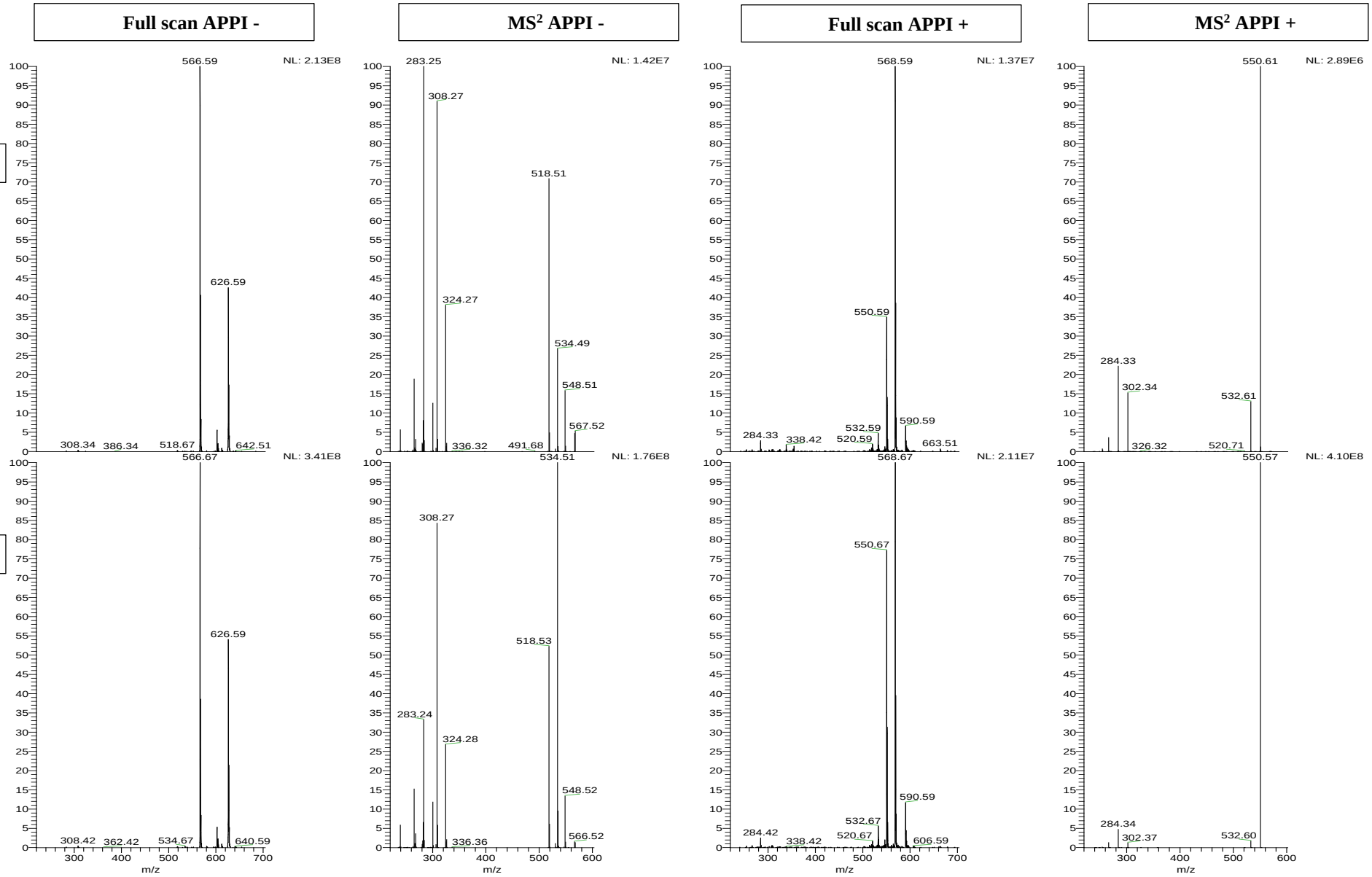

Cer V : Cer(d18:1/18:0(2OH))

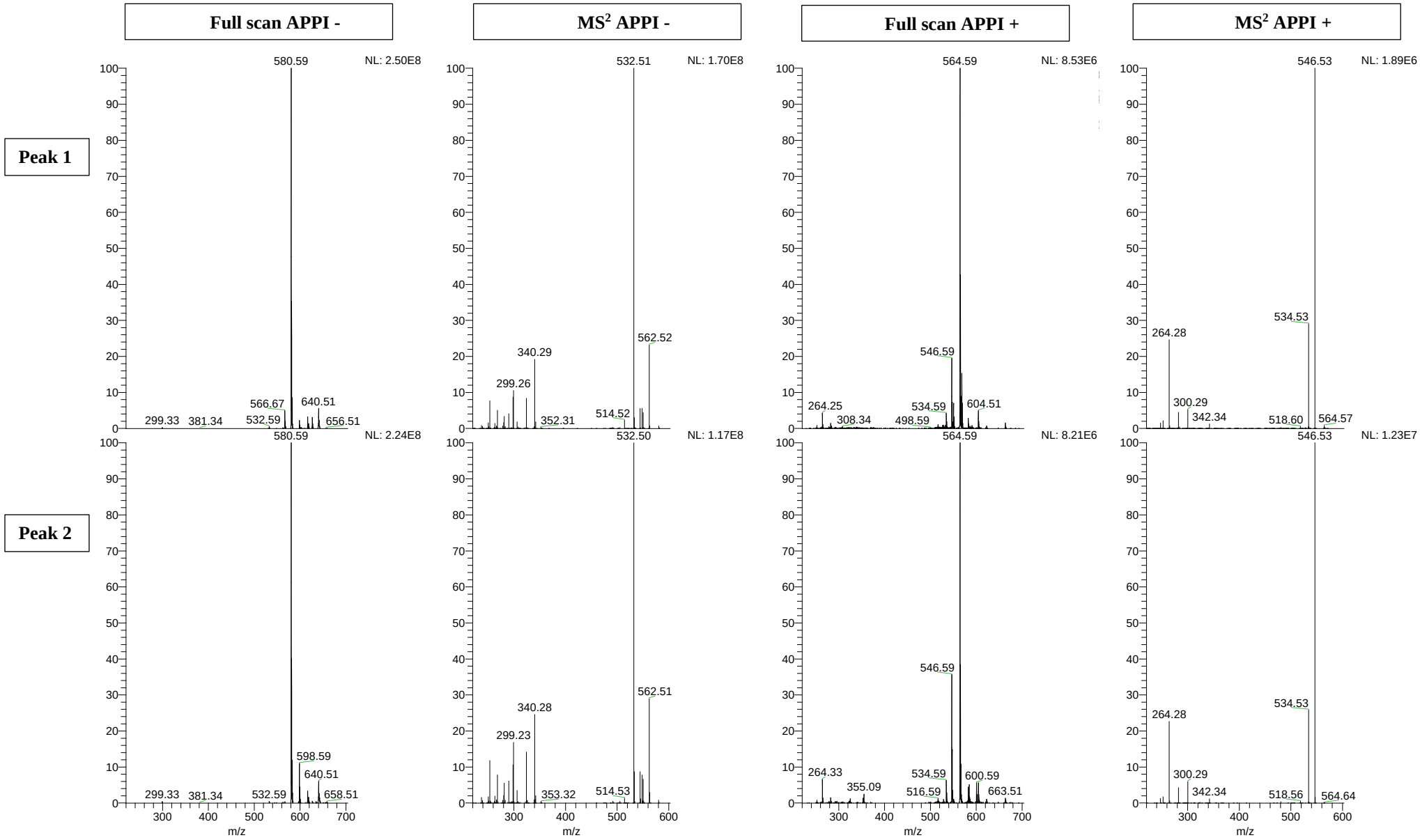

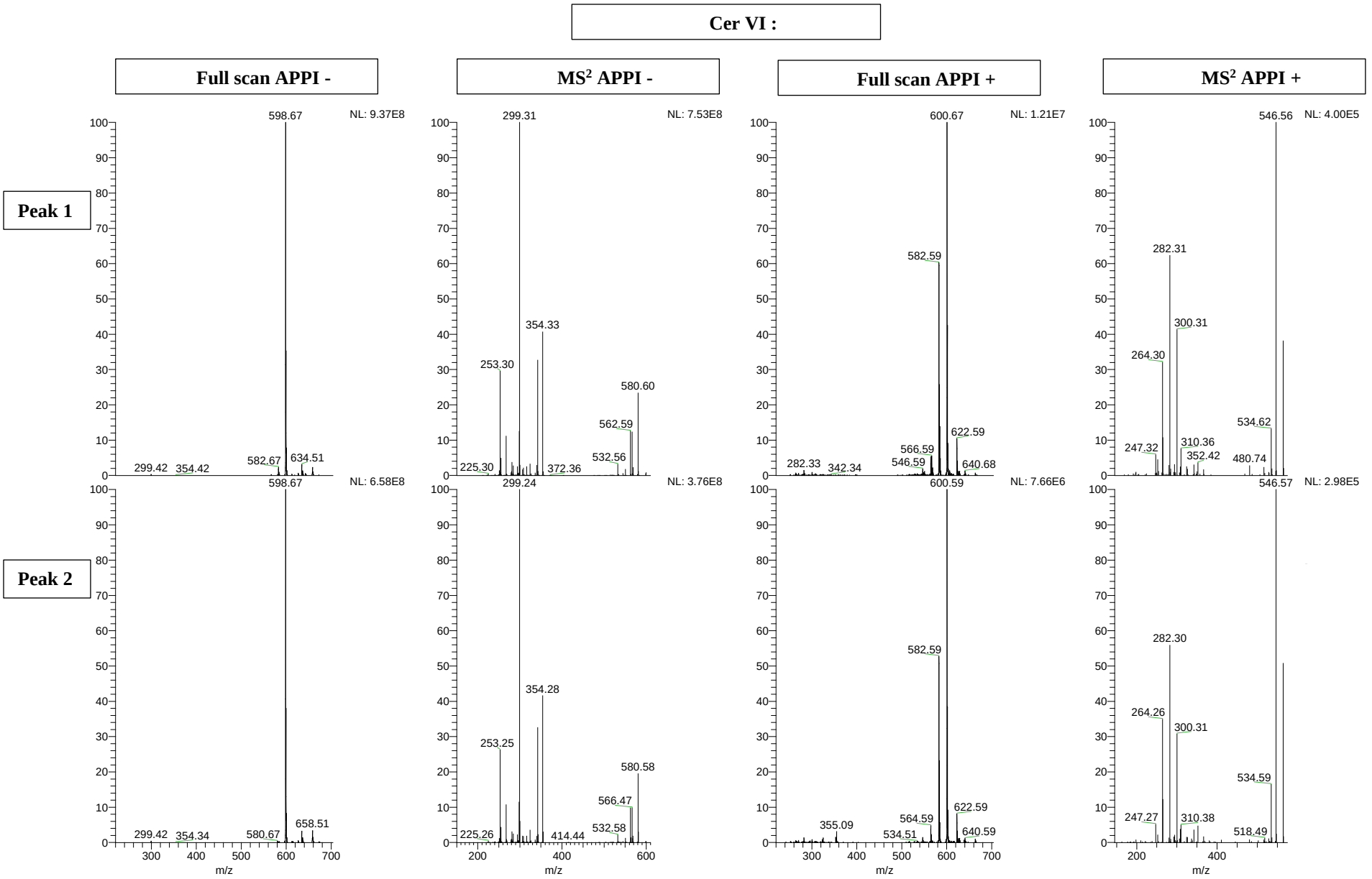

Figure S-3. LC/MS APPI Full Scan and MS² spectra in negative and positive mode for the two peaks obtained with either CerV and VI or CerII.

ANNEXE II. SUPPLEMENTAIRES PUBLICATION 2

Analytica Chimica Acta 1178 (2021) 338809

Contents lists available at ScienceDirect

Analytica Chimica Acta

journal homepage: www.elsevier.com/locate/aca

Rapid assessment of triacylglycerol fatty acyls composition by LC-APPI$^+$-HRMS using monoacylglycerol like fragments intensities

Sonia Abreu [a], Sylvie Heron [b, 1], Audrey Solgadi [c], Florent Joffre [d], Alain Tchapla [b, 1], Pierre Chaminade [a, *]

[a] Université Paris-Saclay, Lipides: Systèmes Analytiques et Biologiques, 92290, Chatenay-Malabry, France
[b] Université Paris-Saclay, ICP – CNRS UMR 8000, (LETIAM), 91400, Orsay, France
[c] Université Paris-Saclay, Inserm, CNRS, Ingénierie et Plateformes Au Service de l'Innovation Thérapeutique, IPSIT-SAMM, 92290, Chatenay-Malabry, France
[d] ITERG, 33610, Canejan, France

HIGHLIGHTS

- Fatty acyls distribution of triacylglycerols is estimated from their APPI $^+$-HRMS spectra.
- Monoacylglycerol like fragments (Ions B) are produced by in source fragmentation of triacylglycerols.
- The fatty acyls composition of triacylglycerols (TG) can be deduced from Ion B intensities.
- Coupling with flow injection (TG in plant oils) or NPLC (TG in complex samples) is achieved without prior sample preparation.

GRAPHICAL ABSTRACT

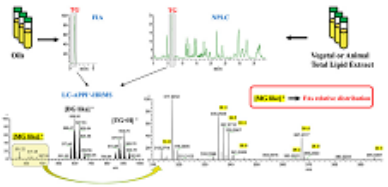

ARTICLE INFO

Article history:
Received 19 May 2021
Accepted 27 June 2021
Available online 1 July 2021

Keywords:
Lipids
Triacylglycerols
Fatty acids composition
Normal phase chromatography
Orbitrap mass spectrometry
Atmospheric pressure photoionization

ABSTRACT

We present a new analytical approach for the analysis of triacylglycerol fatty acyls distribution by normal phase liquid chromatography (NPLC) coupled with APPI$^+$-HRMS. The NPLC method used allows the separation of more than 30 classes of lipids. The energy of the APPI$^+$ source enables the formation of low-intensity ions B fragments ($[RC = O+74]^+$ <3%), characteristic of lipids with a glycerol esterified by one or more fatty acyls. We found the relative intensities of ions B were close to the fatty acyl distribution. To establish the proof of concept, we decided to focus on the triacylglycerols (TGs) class, the major component of plant oils. By either NPLC or FIA, the TGs class appeared as a single peak. In our experimental conditions, ions B are always present in the mass spectra of TGs and each ion B is specific to a fatty acyl group. The Orbitrap mass spectrometer featured high enough resolution and accuracy to identify ions B and distinguish them from other TG fragment ions. A further adjustment of the fatty acyls relative quantities calculation from ions B intensities was computed using weighting coefficients of ions B response. The methodology was developed and validated using plant oils characterized by a GC-FID reference method. NPLC-APPI$^+$-HRMS method offers the advantage of analyzing the fatty acyl composition of complex lipid extracts without the need for sample preparation.

© 2021 Elsevier B.V. All rights reserved.

* Corresponding author.
E-mail address: pierre.chaminade@universite-paris-saclay.fr (P. Chaminade).
[1] Former address: Université Paris-Saclay, EA 7357, Lip(Sys)^2, LETIAM, IUT Orsay, Plateau de Moulon, 91400, Orsay, France.

https://doi.org/10.1016/j.aca.2021.338809
0003-2670/© 2021 Elsevier B.V. All rights reserved.

1. Introduction

Fatty acids consist of an aliphatic hydrocarbon chain, variable in

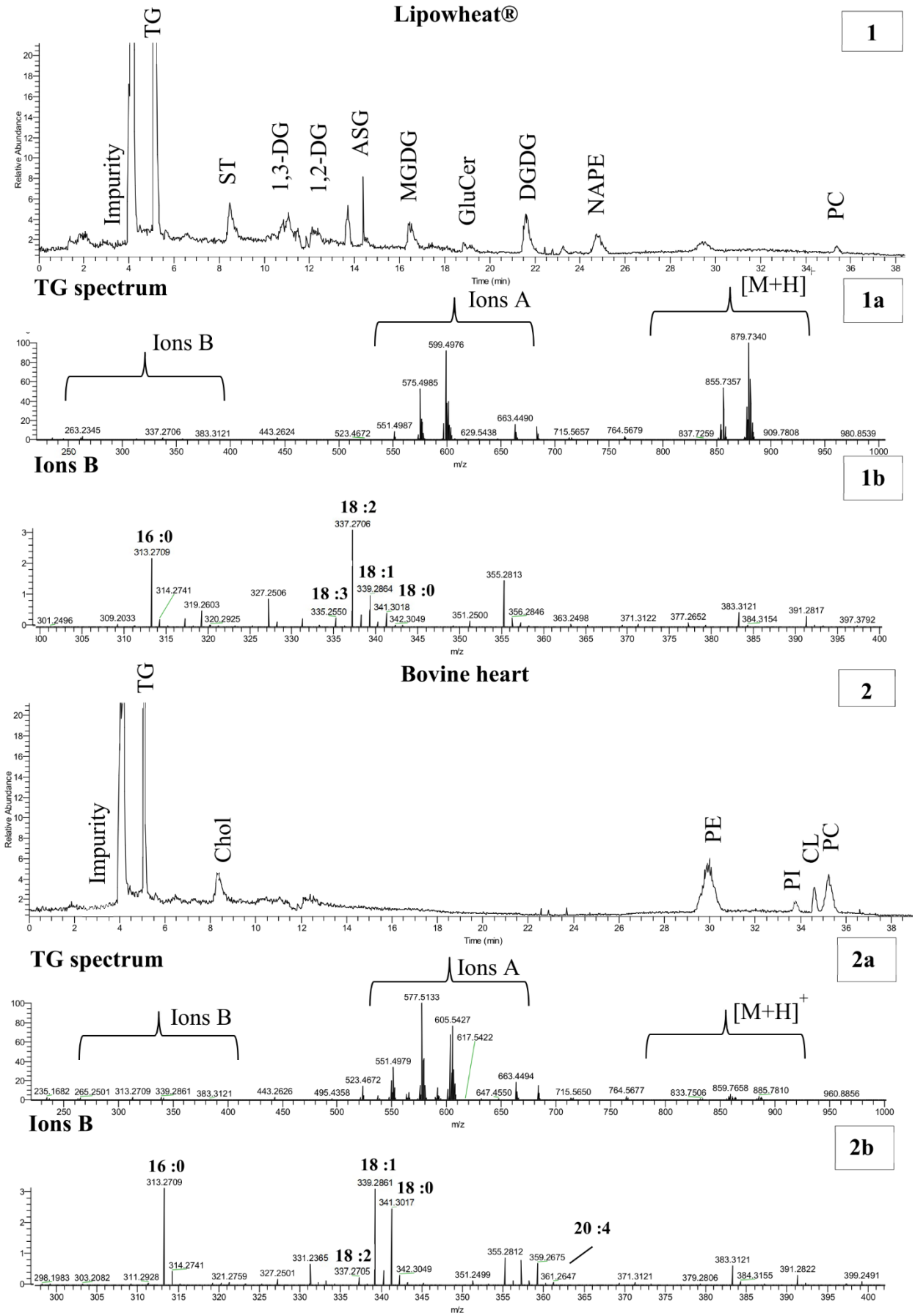
Lipowheat®
1
TG
Impurity
ST
1,3-DG
1,2-DG
ASG
MGDG
GluCer
DGDG
NAPE
PC
Relative Abundance
Time (min)
TG spectrum
Ions A
[M+H]
1a
Ions B
599.4976
575.4985
879.7340
855.7357
663.4490
551.4987
263.2345
337.2706
383.3121
443.2624
523.4672
629.5438
715.5657
764.5679
837.7259
909.7808
980.8539
m/z
Ions B
1b
18 :2
337.2706
16 :0
313.2709
18 :1
339.2864
18 :3
335.2550
18 :0
341.3018
314.2741
319.2603
320.2925
327.2506
342.3049
355.2813
356.2846
Bovine heart
2
TG
Impurity
Chol
PE
PI
CL
PC
Time (min)
TG spectrum
Ions A
577.5133
605.5427
617.5422
[M+H]+
Ions B
551.4979
523.4672
663.4494
235.1682
265.2501
313.2709
339.2861
383.3121
443.2626
495.4358
647.4550
715.5650
764.5677
833.7506
859.7658
885.7810
960.8856
2b
16 :0
313.2709
18 :1
339.2861
18 :0
341.3017
20 :4
18 :2
337.2705
314.2741
331.2365
342.3049
355.2812
359.2675
383.3121
391.2822
298.1983
303.2082
311.2928
321.2759
327.2501
351.2499
361.2647
371.3121
379.2806
384.3155
399.2491

Figure S1: Profile of Lipowheat® and total bovine heart extract obtained by NPLC-APPI$^+$-HRMS.

Chromatogram 1 shows a NPLC-APPI$^+$ chromatogram of Lipowheat®, extracted from wheat where TGs are majoritary. A zoomed view in figure S1-1 allows to visualize the other lipid classes: sterols (ST), diacylglycerols (DG), acylated steryl glucoside (ASG), monogalactosyldiglycerols (MGDG), glucosylceramides (GlcCer), digalactosyldiglycerols (DGDG), N-Acylphosphatidylethanolamines (NAPE) and phosphatidylcholines (PC). The mass spectrum of the TGs is shown in figure S1-1a. The $[M+H]^+$ and ions A, of comparable intensities, represent the most abundant ions. The intensities of the ions B are very low, representing less than 3% of the intensity of the majority ions, Figure S1-1b. The ion B corresponding to the presence of the linoleic FAs is the most intense, followed by the ions B corresponding to the palmitic, oleic, linolenic and stearic FAs.

Chromatogram 2 corresponds to a total lipid extract from bovine liver. In this animal sample, TGs are also in the majority, a zoomed view in figure S1-2 allows to visualize the presence of cholesterol (Chol), phosphatidylethanolamines (PE), phosphatidylinositols (PI), cardiolipins (CL) and PC. On the TGs spectrum in figure S1-2a, ions A are in the majority whereas $[M+H]^+$ ions are barely visible. Here also, in figure S1-2b, the intensities of the ions B represent less than 3% of the intensity of the majority ions. Ions B corresponding to C16:0, C18:1 and C16:0 FAs are in the majority, lower intensities are found for ions B corresponding to linoleic and arachidonic FAs.

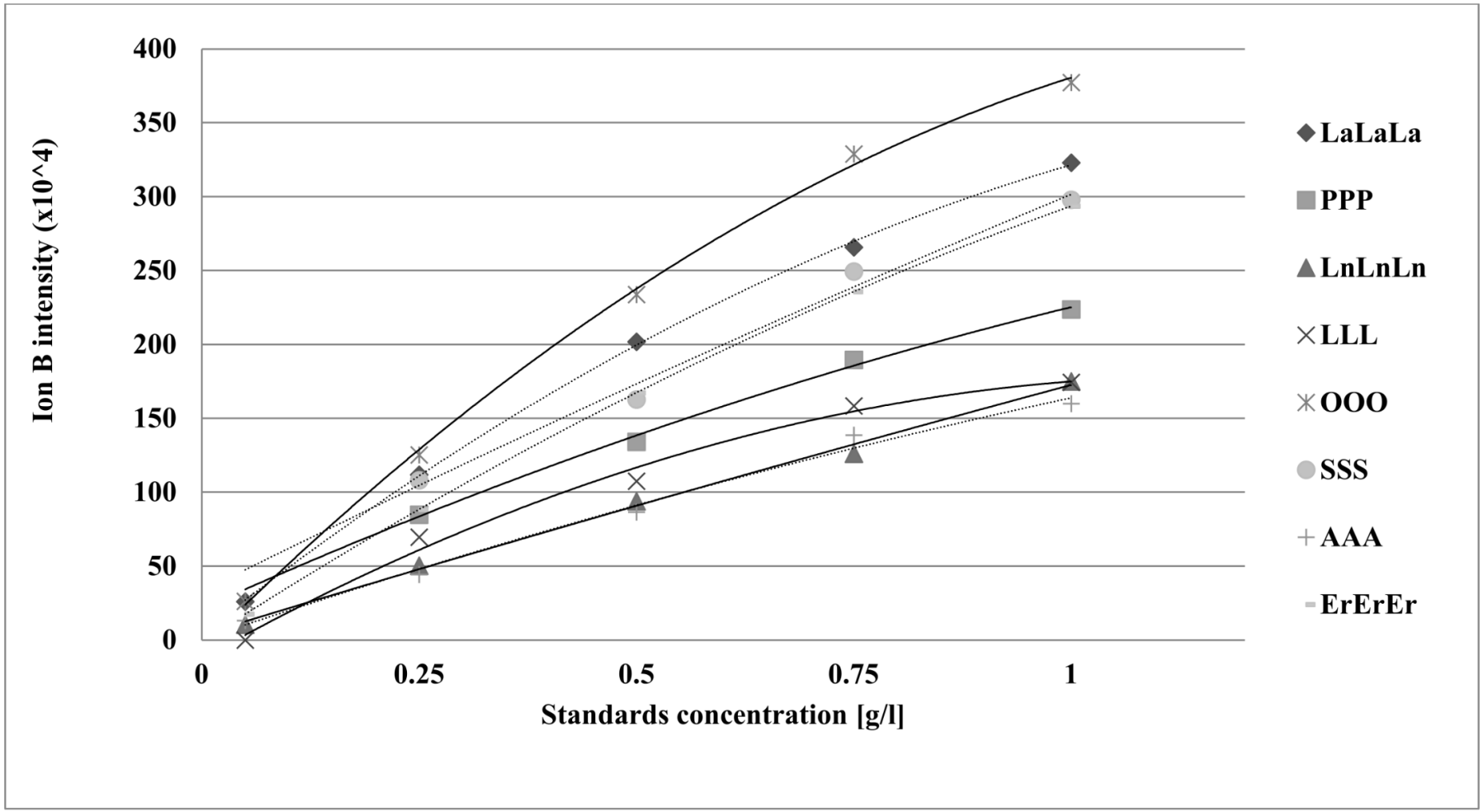

Figure S2: Relationship between ion B intensity and homotriacylglycerols concentrations. Results obtained in FIA-APPI^{+}-HRMS.

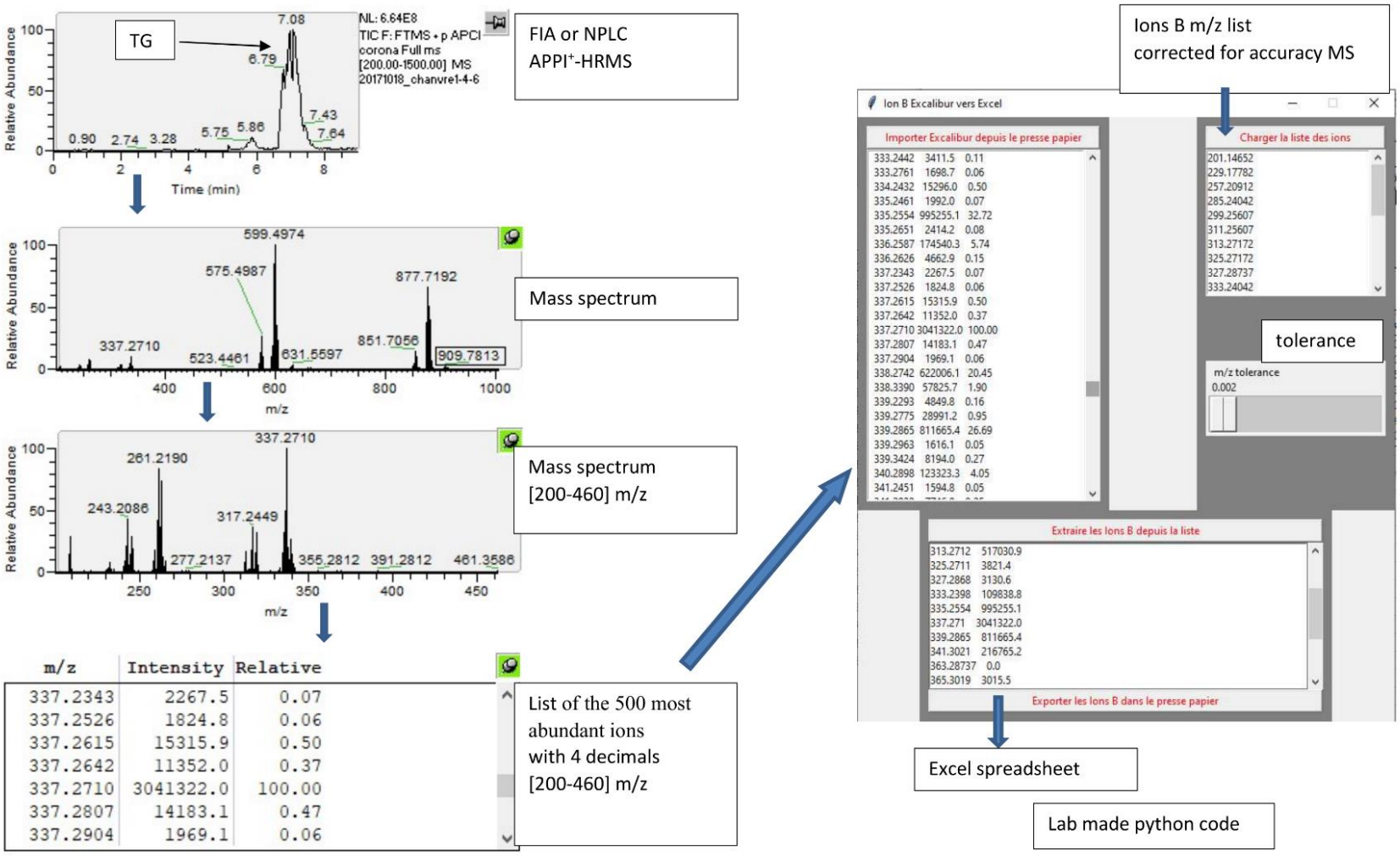

Figure S3: Ions B extraction.

```
        for j in range(0,nb_val_ex-1):
            if mz[j] >= (mz_IonB[i]-mz_tol) and mz[j]<= (mz_IonB[i]+mz_tol):
                aux = str(mz[j])+' '+str(intens[j])
                IonB_listbox.insert(END,aux)

aux=str(mz[j])+'\t'+str(intens[j])+'\r'
                line_string=line_string+aux
                pas_trouve = False
        if pas_trouve == True:
            aux = str(mz_IonB[i])+' '+str(0.00)
            IonB_listbox.insert(END,aux)

aux=str(mz_IonB[i])+'\t'+str(0.00)+'\r'
            line_string=line_string+aux
    return

def exporter_les_ions():
    global line_string
    #line_string ='1.23\t3.4\r9.78\t6.33\r'
    fenetre.clipboard_clear()
    fenetre.clipboard_append(line_string)
    return

fenetre = Tk()

fenetre.geometry("600x675+10+10")
fenetre.title("Ion B Excalibur vers Excel")
fenetre.positionfrom("user")
fenetre.resizable(False, False)

base_frame =Frame(fenetre,bg="grey", width=600, height=300, padx=10, pady=10)
base_frame.pack(side ="bottom", fill=Y)

extraire_les_ions_button = Button(base_frame, text="Extraire les Ions B depuis la liste", fg="red", command=extraire_les_ions)
extraire_les_ions_button.pack(expand=1, fill = X, side="top")

exporter_les_ions_button = Button(base_frame, text="Exporter les Ions B dans le presse papier", fg="red", command=exporter_les_ions)
exporter_les_ions_button.pack(expand=1, fill = X, side="bottom")

IonB_scrollbar = Scrollbar(base_frame, orient=VERTICAL)
IonB_listbox = Listbox(base_frame, width=70, yscrollcommand=IonB_scrollbar.set)
IonB_scrollbar.config(command=IonB_listbox.yview)
IonB_scrollbar.pack(side=RIGHT, fill=Y)
IonB_listbox.pack()

right_frame = Frame(fenetre,bg="grey", width=350, height=375, padx=10, pady=10)
right_frame.pack(side ="right", fill=Y)
left_frame = Frame(fenetre,bg="grey", width=250, height=375, padx=10, pady=10)
left_frame.pack(side ="left", fill=Y)
```

```
copy_from_clipboard_button =
Button(left_frame, text="Importer
Excalibur depuis le presse papier",
fg="red",
command=copy_from_clipboard)

copy_from_clipboard_button.pack(expand
="false", fill = "x", side="top")

ascenseur = Scrollbar(left_frame,
orient=VERTICAL)

boiteliste = Listbox(left_frame, width=40,
yscrollcommand=ascenseur.set)

ascenseur.config(command=boiteliste.yvie
w)

ascenseur.pack(side=RIGHT, fill=Y)

boiteliste.pack(fill=Y, expand=1)


load_ion_list_button = Button(right_frame,
text="   Charger la liste des ions   ",
fg="red", command=load_ion_list)

load_ion_list_button.pack(expand="false",
fill = "x", side="top")

mz_tol_scale =
Scale(right_frame,label="m/z
tolerance",width=40,from_=0.001, to=0.2,
resolution=0.001, orient=HORIZONTAL)

mz_tol_scale.set(0.005)

mz_tol_scale.pack(side="bottom",
fill=X,expand=1)


scrollbar = Scrollbar(right_frame,
orient=VERTICAL)

listbox = Listbox(right_frame,
width=30,yscrollcommand=scrollbar.set)

scrollbar.config(command=listbox.yview)

scrollbar.pack(side=RIGHT, fill=Y)

listbox.pack()

listbox.insert(END,"La liste des ions B est
vide,")

listbox.insert(END," copier la liste dans le
")

listbox.insert(END,"presse papier et
Charger")

listbox.insert(END,"la liste")


fenetre.mainloop()
```

Figure S4: Python code. Please cite the present article if you use this Python code.

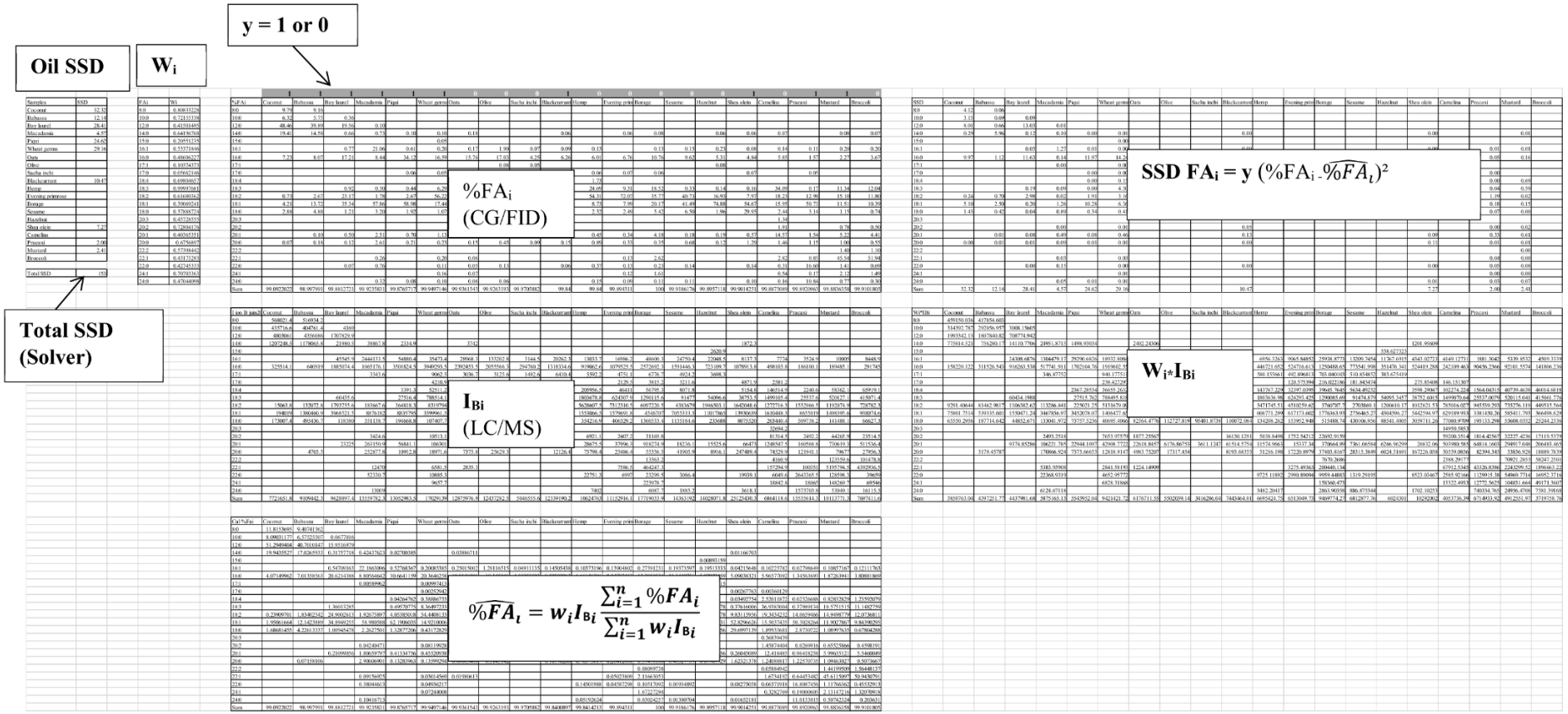

Figure S 5: Excel spreadsheet.

In the Excel spreadsheet it is necessary to input the FA composition of the oils selected for calibration as determined by GC-FID, then to input the corresponding intensities of ion B for each FA and start by specifying an arbitrary value for Wi. The Solver function is then used to adjust the w_i coefficients by minimizing the total SSD between experimental and calculated FA%. In the Excel sheet, a line noted “y-values” with y being zero or one, determines which sample belong to the calibration or validation set. The oils used for calibration have their SSD multiplied by 1 and those for validation multiplied by 0.

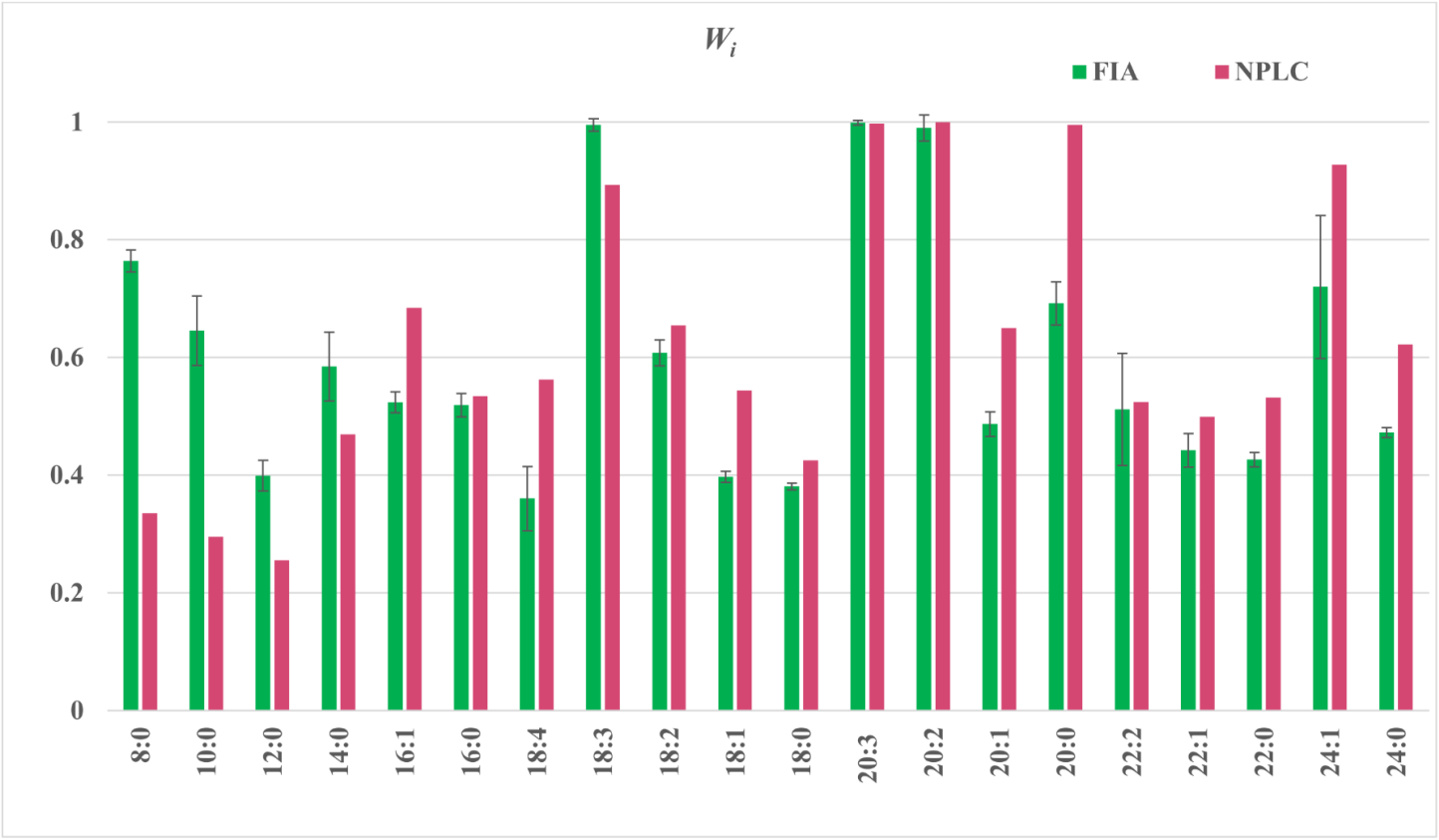

FA	8:0	10:0	12:0	14:0	16:1	16:0	18:4	18:3	18:2	18:1	18:0	20:3	20:2	20:1	20:0	22:2	22:1	22:0	24:1	24:0
NB	2	3	4	9	8	10	1	8	10	10	10	1	2	9	10	1	4	7	3	6
%Min	9.16	0.36	0.10	0.06	0.08	1.57	2.71	0.16	0.73	4.21	1.15	1.34	0.78	0.10	0.07	1.40	0.26	0.06	0.17	0.08
%Max	9.79	6.32	48.46	19.41	21.06	34.12	2.71	34.09	46.63	58.98	29.95	1.34	1.91	14.57	2.61	1.40	45.54	16.60	2.12	10.84

Figure S6: Weighting coefficient.

Weighting coefficient to be applied to ions B according to the calculations made by FIA (green) and NPLC (red) on calibration set. NB is the number of occurrences of each ion B in the samples. %Min and %Max are the minimum and maximum % values reported for each FA using GC-FID. NB equals 1 for C18:4, C20:3 and C22:2 which means these FAs where reported by GC-FID in only one oil sample. However, their corresponding ion B was measured in other samples using either FIA or NPLC and a standard deviation could be calculated.

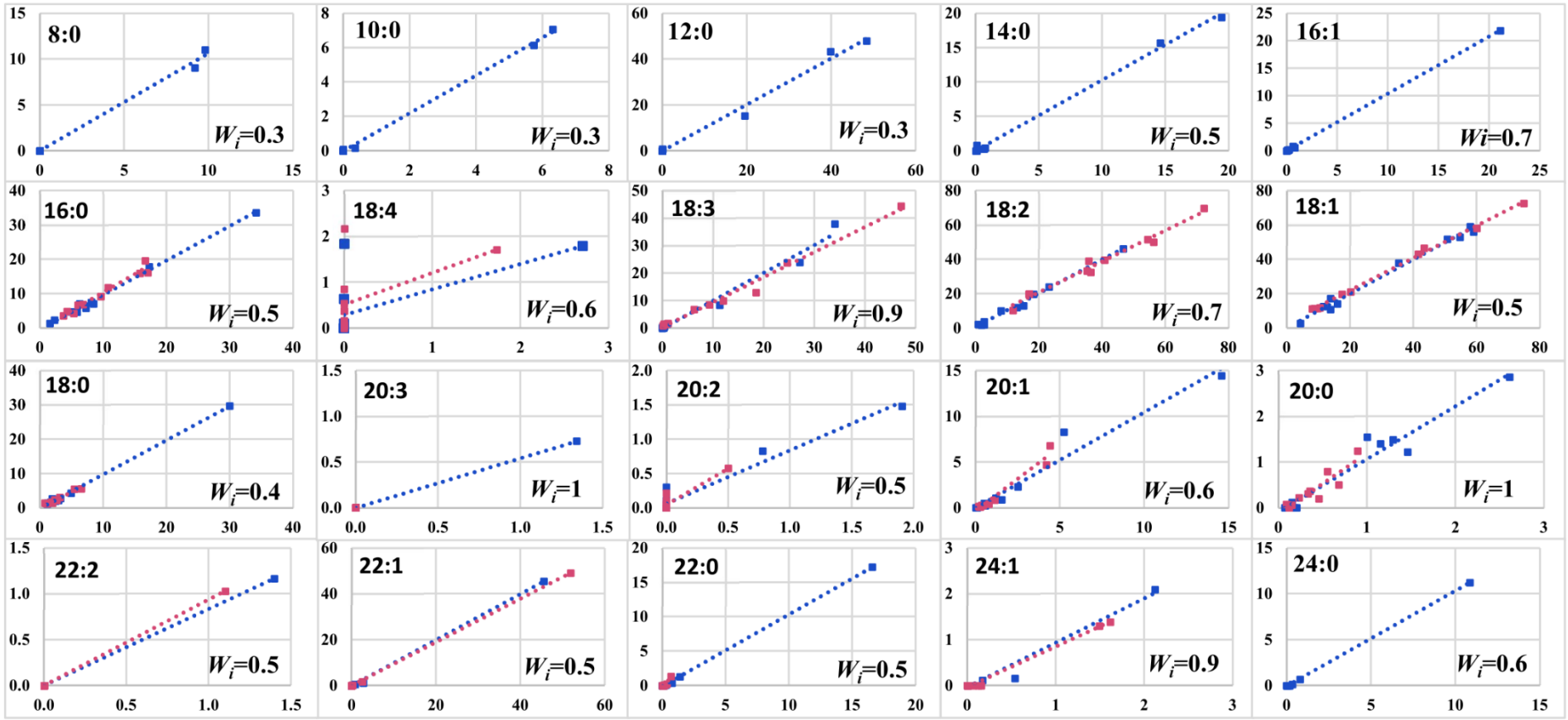

Figure S7: NPLC-APPI$^+$-HRMS individual FA prediction and validation.

Regression lines for predicted (Y-axis) *vs* GC-FID (X-axis). Blue lines are for the calibration set and red lines for the validation set.

Table S1: Isobaric ions mass difference calculation (^{12}C only considered).

Ion B	**$C_3H_6O_2+(C_nH_{2n-1}O)$**						**$C_3H_6O_2+(C_nH_{2n-5}O)$**		**$C_3H_6O_2+(C_nH_{2n-9}O)$**	**$C_3H_6O_2+(C_nH_{2n-11}O)$**
$[M+H]^+$	**$C_3H_6O_3+(C_{n-3}H_{2n-13}O_3)$**									**$C_3H_6O_3+(C_{n-4}H_{2n-11}O_3)$**
$[M+H-H_2O]^+$		**$C_3H_6O_3+(C_{n-2}H_{2n-9}O_3)$**								
Ion A			**$C_3H_5O_2+(C_{n-1}H_{2n-4}O_2)$**							
Ion B - H_2O				**$C_3H_6O_2+(C_{n+2}H_{2n-9})$**			**$C_3H_6O_2+(C_{n+1}H_{2n-1})$**			
Ion C					**$(C_{n+6}H_{2n+1}O)$**			**$(C_{n+5}H_{2n+9}O)$**		
Ion C - H_2O						**$(C_{n+7}H_{2n+5})$**			**$(C_{n+6}H_{2n+9})$**	
Δ struct (ion B-ion x)	**3C + 12H - 3O**	**2C + 8H - 2O**	**1C + 4H - 1O**	**-2C + 8H + 1O**	**-3C + 4H + 2O**	**-4C + 3O**	**-1C - 4H + 1O**	**-2C - 8H + 2O**	**-3C - 12H + 3O**	**+4C - 3O**
| Δ u.m.a |	**0.109155**	**0.072770**	**0.036385**	**0.057515**	**0.021130**	**0.015255**	**0.036385**	**0.072770**	**0.109155**	**0.015255**
Example										
Ion B	**B(24:0)**	**B(26:0)**	**B(21:0)**	**B(18:0)**	**B(14:0)**	**B(15:0)**	**B(18:2)**	**B(18:2)**	**B(18:4)**	**B(22:5)**
Ion X	**[TG(17:2/2:0/2:0)+H]$^+$**	**[TG(8:0/8:0/8:0)+H-H2O]$^+$**	**A(10:0/10:0)**	**B(20:5)-H2O**	**C(20:5)**	**C(22:3)-H2O**	**B(19:0)-H2O**	**C(23:0)**	**C(24:0)-H2O**	**[TG(6:0/6:0/6:0)+H]$^+$**

Table S2: Relative intensities of characteristic homotriacylglycerols ions in the ionization source.

TG	Double bonds	$[M+H]^+$	$[M+H- H_2O]^+$	Ion A	Ion B	Ion B - H_2O	Ion C	Ion C - H_2O
LaLaLa	**0**	**0**	**0**	**100**	**1.26**	**0**	**nd**	**nd**
PPP	**0**	**0**	**0**	**100**	**1.11**	**0**	**0**	**0**
SSS	**0**	**0**	**0**	**100**	**1.21**	**0**	**0**	**0**
AAA	**0**	**0**	**0**	**100**	**1.26**	**0**	**0**	**0**
OOO	**3**	**9.4**	**0.54**	**100**	**1.96**	**0.1**	**1.14**	**0.15**
ErErEr	**3**	**11.91**	**0.41**	**100**	**1.8**	**1.13**	**2.7**	**0.08**
LLL	**6**	**100**	**1.65**	**75.37**	**1.76**	**0.67**	**1.43**	**0.53**
LnLnLn	**9**	**100**	**1.63**	**52.03**	**1.27**	**1.11**	**1.54**	**0.43**

* nd, not detected.

Table S3: FAs Composition of plants oils obtained by GC-FID, (values > 3% are shaded).

Symbol	FA	Coconut	Babassu	Bay laurel	Macadamia	Piqui	Wheat germ	Oats	Olive	Sacha Inhi	Blackurrant	Hemp	Evening primose	Borage	Sesame	Hazelnut	Shea Olein	Camelina	Pracaxi	Mustard	Broccoli
Co	6:0	0.89	0.85																		
Cy	8:0	9.79	9.16																		
C	10:0	6.32	5.75	0.36	<0.05	<0.05	<0.05	<0.05			<0.05						<0.05		<0.05	<0.05	
La	12:0	48.46	39.89	19.56	0.10	<0.05	<0.05	<0.05			<0.05						<0.05		<0.05	<0.05	<0.05
	12:1																				
My	14:1																				
M	14:0	19.41	14.58	0.66	0.73	0.10	0.10	0.18	<0.05	<0.05	0.06	<0.05	0.06	0.08	<0.05	0.06	0.06	0.07	<0.05	0.08	0.07
Bo	15:0	<0.05	<0.05	<0.05	<0.05		0.05	<0.05			<0.05	<0.05	<0.05			<0.05	<0.05	<0.05		<0.05	<0.05
Po	16:1 (n-7)		<0.05	0.77	20.76	0.61	0.20	0.17	1.90	0.07	0.09	0.13	<0.05	0.13	0.15	0.23	0.08	0.14	0.11	0.20	0.20
	16:1 (n-9)				0.30																
P	16:0	7.23	8.07	17.21	8.44	34.12	16.59	15.76	17.03	4.25	6.26	6.01	6.76	10.76	9.62	5.31	4.84	5.85	1.57	2.27	3.67
Mr	17:1 (n-8)								0.08	0.05	<0.05	<0.05	<0.05			0.08		<0.05			
Ma	17:0			<0.05	<0.05	0.06	0.05	0.05	<0.05	0.10	0.06	0.06	0.07	0.06	<0.05	<0.05	0.07	<0.05	0.05	<0.05	<0.05
St	18:4 (n-3)										2.71	1.73									
γLn	18:3 (n-6)										14.25	4.62	8.96	18.35							
Ln	18:3 (n-3)		<0.05	0.92	0.30	0.44	6.29	1.11	0.68	47.14	12.89	20.08	0.35	0.17	0.33	0.14	0.16	34.09	0.17	11.34	12.04
L	18:2 (n-6)	0.73	2.67	23.17	1.78	2.67	56.22	36.33	16.76	35.20	46.63	54.31	72.07	35.77	40.73	16.93	7.97	18.23	12.98	15.10	11.80
O	18:1 (n-9)	4.16	13.40	33.64	54.10	57.37	16.31	42.55	57.21	9.08	13.08	7.91	7.30	19.66	40.61	73.46	53.92	15.01	50.34	10.49	9.55
As	18:1 (n-7)	0.05	0.33	1.70	3.76	1.61	1.13	0.82	2.74	0.62	0.70	0.82	0.69	0.51	0.88	1.42	0.68	0.94	0.39	1.03	0.84
	18:1 (trans)																0.08				
S	18:0	2.88	4.88	1.21	3.20	1.92	1.07	1.82	2.64	3.09	1.70	2.32	2.49	5.42	6.50	1.96	29.95	2.44	3.14	1.15	0.74
Bi	20:3 (n-3)																	1.34			
Dh	20:2 (n-6)																	1.91		0.78	0.50
Ga	20:1 (n-11)										0.13						0.10			5.22	4.41
Go	20:1 (n-9)		0.10	0.50	2.51	0.70	1.13	0.76	0.25	0.28	1.06	0.45	0.34	4.18	0.18	0.19	0.46	14.57	1.54		
A	20:0	0.07	0.18	0.12	2.61	0.21	0.23	0.15	0.45	0.09	0.15	0.89	0.33	0.35	0.68	0.12	1.29	1.46	1.15	1.00	0.55
Di	22:2 (n-6)																			1.40	1.10
Er	22:1 (n-9)				0.26		0.20	0.06				<0.05	0.13	2.62				2.82	0.85	44.44	50.96
	22:1 (n-7)																			1.10	0.98
B	22:0		<0.05	0.07	0.76	<0.05	0.11	0.05	0.13		0.06	0.37	0.13	0.23	0.14	<0.05	0.14	0.31	16.60	1.41	0.69
Ne	24:1 (n-9)						0.16	0.07					0.12	1.61				0.54	0.17	2.12	1.49
Lg	24:0		<0.05	<0.05	0.32	0.08	0.10	0.06	0.06		<0.05	0.15	0.09	0.11	0.11		0.10	0.16	10.84	0.77	0.30

Table S4: Deming regression.

Deming regression coefficients (slope and intercept) with their standard error and critical probabilities associated with hypothesis testing (slope = 1.0 and intercept = 0.0). Degrees of freedom and coefficient of determination (R^2) are also indicated for each regression.

FIA/APPI⁺ HRMS

Calibration Set									Validation Set								
FA	**df**	**Intercept**	**std err**	**Pr(>|t|)**	**Slope**	**std err**	**Pr(>|t|)**	**R^2**	**FA**	**df**	**Intercept**	**std err**	**Pr(>|t|)**	**coeff**	**std err**	**Pr(>|t|)**	**R^2**
16:1	**6**	**-0.07**	**0.04**	**0.12**	**1.04**	**0.13**	**0.78**	**0.9998**	**16:1**	**7**	**0.06**	**0.35**	**0.86**	**0.62**	**2.30**	**0.87**	**0.9892**
16:0	**8**	**1.01**	**1.98**	**0.62**	**0.98**	**0.34**	**0.94**	**0.9432**	**16:0**	**8**	**0.28**	**0.64**	**0.68**	**1.19**	**0.11**	**0.11**	**0.9792**
18:3	**6**	**-0.22**	**0.31**	**0.50**	**1.01**	**0.07**	**0.92**	**0.9946**	**18:3**	**8**	**0.30**	**0.58**	**0.62**	**0.95**	**0.03**	**0.12**	**0.9824**
18:2	**8**	**0.56**	**0.61**	**0.38**	**0.98**	**0.04**	**0.64**	**0.9957**	**18:2**	**8**	**2.69**	**1.48**	**0.11**	**0.91**	**0.03**	**0.03**	**0.9932**
18:1	**8**	**-0.47**	**0.80**	**0.57**	**1.02**	**0.03**	**0.60**	**0.9963**	**18:1**	**8**	**0.87**	**0.56**	**0.16**	**0.94**	**0.01**	**0.00**	**0.9979**
18:0	**8**	**-0.32**	**0.21**	**0.16**	**1.01**	**0.07**	**0.94**	**0.9988**	**18:0**	**8**	**-0.14**	**0.25**	**0.58**	**1.01**	**0.06**	**0.86**	**0.9767**
20:1	**6**	**-0.15**	**0.59**	**0.81**	**1.05**	**0.33**	**0.89**	**0.9810**	**20:1**	**8**	**-0.32**	**0.16**	**0.09**	**1.39**	**0.33**	**0.27**	**0.8981**
20:0	**6**	**-0.04**	**0.06**	**0.54**	**1.10**	**0.07**	**0.23**	**0.9797**	**20:0**	**8**	**-0.06**	**0.02**	**0.01**	**0.99**	**0.05**	**0.90**	**0.9754**
22:0	**6**	**-0.04**	**0.06**	**0.54**	**1.10**	**0.07**	**0.23**	**0.9993**	**22:0**	**8**	**-0.06**	**0.02**	**0.01**	**0.99**	**0.05**	**0.90**	**0.9551**
24:0	**3**	**-0.16**	**0.10**	**0.20**	**1.02**	**0.21**	**0.93**	**0.9997**	**24:0**	**3**	**-0.08**	**0.03**	**0.06**	**0.81**	**0.20**	**0.41**	**0.9857**

NPLC/APPI⁺ HRMS

Calibration Set									Validation Set								
FA	**df**	**Intercept**	**std err**	**Pr(>|t|)**	**Slope**	**std err**	**Pr(>|t|)**	**R^2**	**FA**	**df**	**Intercept**	**std err**	**Pr(>|t|)**	**coeff**	**std err**	**Pr(>|t|)**	**R^2**
16:1	**6**	**0.07**	**0.07**	**0.37**	**1.04**	**0.31**	**0.91**	**0.9997**	**16:1**	**7**	**0.16**	**0.86**	**0.86**	**0.73**	**5.61**	**0.96**	**0.9461**
16:0	**8**	**-0.23**	**0.39**	**0.57**	**1.00**	**0.04**	**0.97**	**0.9931**	**16:0**	**8**	**0.26**	**0.63**	**0.69**	**0.98**	**0.07**	**0.82**	**0.9430**
18:3	**6**	**-0.74**	**0.89**	**0.44**	**1.04**	**0.17**	**0.80**	**0.9740**	**18:3**	**8**	**0.01**	**0.73**	**0.99**	**0.92**	**0.07**	**0.30**	**0.9884**
18:2	**8**	**0.29**	**0.64**	**0.66**	**1.00**	**0.03**	**0.90**	**0.9910**	**18:2**	**8**	**1.91**	**2.10**	**0.39**	**0.93**	**0.04**	**0.17**	**0.9804**
18:1	**8**	**0.32**	**2.04**	**0.88**	**0.99**	**0.05**	**0.88**	**0.9890**	**18:1**	**8**	**3.21**	**0.57**	**0.00**	**0.94**	**0.02**	**0.02**	**0.9972**
18:0	**8**	**-0.13**	**0.40**	**0.75**	**0.99**	**0.15**	**0.96**	**0.9976**	**18:0**	**8**	**0.17**	**0.41**	**0.68**	**0.89**	**0.15**	**0.48**	**0.9585**
20:1	**6**	**-0.15**	**1.01**	**0.88**	**1.09**	**0.61**	**0.89**	**0.9389**	**20:1**	**8**	**-0.34**	**0.15**	**0.06**	**1.45**	**0.31**	**0.18**	**0.9186**
20:0	**4**	**-0.15**	**2.00**	**0.94**	**1.29**	**1.65**	**0.87**	**0.8200**	**20:0**	**7**	**-0.24**	**0.13**	**0.11**	**1.52**	**0.23**	**0.06**	**0.5525**
22:0	**4**	**-0.15**	**2.00**	**0.94**	**1.29**	**1.65**	**0.87**	**0.9998**	**22:0**	**7**	**-0.24**	**0.13**	**0.11**	**1.52**	**0.23**	**0.06**	**0.2605**
24:0									**24:0**	**2**	**-0.24**	**0.16**	**0.28**	**2.30**	**1.12**	**0.37**	**0.7514**

Table S5: Comparison of the composition of plant oils by the GC-FID method and ion B methods after applying w_i coefficients.

	Coconut			Babassu			Bay laurel			Macadamia			Piqui			Wheat germs			Oats		
FA	**GC**	**FIA**	**NPLC**	**GC**	**FIA**	**NPLC**	**GC**	**FIA**	**NPLC**	**GC**	**FIA**	**NPLC**	**GC**	**FIA**	**NPLC**	**GC**	**FIA**	**NPLC**	**GC**	**FIA**	**NPLC**
8:0	9.79	12.06	11.02	9.16	8.13	9.09						0.02									
10:0	6.32	7.77	7.08	5.75	5.97	6.15	0.36	0.07	0.17			0.10			0.03						
12:0	48.46	50.57	48.02	39.89	41.05	43.36	19.56	15.53	15.32	0.10	0.01	0.72			0.81			0.10			
14:0	19.41	19.48	19.44	14.58	16.63	15.73	0.66	0.30	0.28	0.73	0.39	0.41	0.10	0.02	0.80	0.10	0.02	0.04	0.18	0.06	0.06
16:1							0.77	0.52	0.59	21.06	21.81	21.89	0.61	0.50	0.84	0.20	0.22	0.37	0.17	0.24	0.62
16:0	7.23	4.86	5.83	8.07	8.02	7.47	17.21	22.17	17.87	8.44	9.23	7.14	34.12	31.22	33.66	16.59	20.81	19.65	15.76	19.70	15.95
18:4								0.02	0.10					0.02			0.21	0.38		0.09	0.16
18:3			0.38				0.92	1.27	1.54	0.30	0.09	0.14	0.44	0.42	0.56	6.29	8.32	6.80	1.11	2.54	1.75
18:2	0.73	0.24	2.27	2.67	1.81	2.12	23.17	24.24	24.14	1.78	1.95	1.84	2.67	3.86	3.89	56.22	53.56	50.18	36.33	34.56	32.53
18:1	4.21	2.13	2.85	13.72	12.79	10.85	35.34	34.42	38.01	57.86	58.51	59.21	58.98	61.76	56.15	17.44	15.16	19.88	43.37	40.49	46.72
18:0	2.88	1.98	2.20	4.88	4.53	4.23	1.21	1.08	1.37	3.20	2.47	2.71	1.92	1.42	2.64	1.07	0.54	1.17	1.82	1.54	1.66
20:3																					
20:2											0.02						0.13	0.10		0.03	
20:1				0.10			0.50	0.24	0.49	2.51	2.10	2.27	0.70	0.47	0.48	1.13	0.58	0.86	0.76	0.50	0.42
20:0	0.07			0.18	0.05		0.12			2.61	2.75	2.85	0.21	0.13		0.23	0.14	0.22	0.15	0.10	0.06
22:2																					
22:1										0.26	0.08	0.09				0.20	0.03	0.09	0.06	0.01	
22:0							0.07			0.76	0.30	0.38		0.01		0.11	0.06	0.03	0.05		
24:1											0.02					0.16	0.07		0.07		
24:0										0.32	0.11	0.13	0.08			0.10	0.01	0.06	0.06		
	Olive			**Sacha inchi**			**Blackurrant**			**Hemp**			**Evening primrose**			**Borage**			**Sesame**		
FA	**GC**	**FIA**	**NPLC**	**GC**	**FIA**	**NPLC**	**GC**	**FIA**	**NPLC**	**GC**	**FIA**	**NPL**	**GC**	**FIA**	**NPLC**	**GC**	**FIA**	**NPLC**	**GC**	**FIA**	**NPLC**
8:0																					
10:0																					
12:0																					
14:0			0.04			0.02	0.06					0.02	0.06	0.01		0.08	0.01	0.03			
16:1	1.90	1.22	1.47	0.07	0.05	0.11	0.09	0.13	0.15	0.13	0.12	0.19		0.11	0.17	0.13	0.26	0.29	0.15	0.14	0.23
16:0	17.03	18.96	16.20	4.25	5.00	4.89	6.26	9.49	7.14	6.01	7.36	7.24	6.76	8.85	6.89	10.76	14.07	11.85	9.62	11.76	9.24
18:4		0.04	0.07		1.38	2.18	2.71	1.08	1.79	1.73	1.08	1.66		0.26	0.38		0.25	0.54		0.04	0.05
18:3	0.68	0.96	1.42	47.14	44.90	44.52	27.15	25.53	23.94	24.69	26.61	23.42	9.31	9.69	8.53	18.52	13.62	13.03	0.33	1.44	1.49
18:2	16.76	18.63	19.90	35.20	35.29	33.38	46.63	45.60	46.29	54.31	51.78	50.85	72.07	67.89	69.75	35.77	38.77	39.13	40.73	38.55	39.61
18:1	59.94	57.44	58.27	9.69	10.15	11.59	13.78	14.82	17.36	8.73	9.44	12.13	7.99	9.75	11.26	20.17	18.81	21.17	41.49	40.82	43.11
18:0	2.64	2.14	2.26	3.09	2.97	3.06	1.70	1.69	1.66	2.32	2.12	2.57	2.49	2.51	2.19	5.42	5.49	5.46	6.50	6.40	5.49
20:3																					
20:2					0.01			0.32	0.30		0.05	0.06		0.08	0.05		0.30	0.22		0.02	
20:1	0.25	0.13	0.08	0.28	0.15	0.12	1.19	1.03	1.06	0.45	0.25	0.27	0.34	0.26	0.26	4.18	4.38	4.69	0.18	0.12	0.13
20:0	0.45	0.36	0.20	0.09	0.03	0.08	0.15	0.10	0.12	0.89	0.82	1.14	0.33	0.29	0.31	0.35	0.34	0.36	0.68	0.55	0.50
22:2																	0.06				
22:1												0.01	0.13	0.06	0.05	2.62	1.92	1.72			
22:0	0.13	0.01					0.06	0.01		0.37	0.16	0.18	0.13	0.04	0.04	0.23	0.10	0.09	0.14	0.01	0.05
24:1													0.12	0.01		1.61	1.58	1.39			
24:0	0.06									0.15	0.03	0.07	0.09			0.11	0.02	0.04	0.11		

	Hazelnut			Shea olein			Camelina			Pracaxi			Mustard			Broccoli		
FA	**GC**	**FIA**	**NPLC**	**GC**	**FIA**	**NPLC**	**GC**	**FIA**	**NPLC**	**GC**	**FIA**	**NPLC**	**GC**	**FIA**	**NPLC**	**GC**	**FIA**	**NPLC**
8:0																		
10:0																		
12:0																		
14:0	**0.06**			**0.06**		**0.04**	**0.07**						**0.08**		**0.05**	**0.07**	**0.01**	
16:1	**0.23**	**0.17**	**0.34**	**0.08**	**0.04**	**0.18**	**0.14**	**0.08**	**0.18**	**0.11**	**0.06**	**0.09**	**0.20**	**0.09**	**0.25**	**0.20**	**0.14**	**0.23**
16:0	**5.31**	**6.36**	**4.32**	**4.84**	**5.13**	**4.79**	**5.85**	**6.41**	**4.74**	**1.57**	**1.48**	**1.46**	**2.27**	**2.39**	**2.42**	**3.67**	**4.41**	**3.68**
18:4		**0.01**			**0.01**			**1.25**	**1.84**		**0.01**			**0.50**	**0.63**		**0.57**	**0.85**
18:3	**0.14**	**0.81**	**0.89**	**0.16**	**0.34**	**0.46**	**34.09**	**35.52**	**37.92**	**0.17**	**0.38**	**0.33**	**11.34**	**10.33**	**8.42**	**12.04**	**10.32**	**10.03**
18:2	**16.93**	**19.39**	**20.06**	**7.97**	**9.45**	**10.09**	**18.23**	**18.58**	**19.84**	**12.98**	**13.77**	**12.03**	**15.10**	**14.18**	**13.03**	**11.80**	**11.26**	**10.37**
18:1	**74.88**	**71.19**	**72.69**	**54.67**	**53.06**	**52.96**	**15.95**	**15.45**	**14.20**	**50.73**	**50.48**	**51.75**	**11.51**	**11.87**	**12.66**	**10.39**	**9.54**	**11.88**
18:0	**1.96**	**1.68**	**1.43**	**29.95**	**29.82**	**29.63**	**2.44**	**1.96**	**1.94**	**3.14**	**2.86**	**2.73**	**1.15**	**1.15**	**1.08**	**0.74**	**1.14**	**1.39**
20:3							**1.34**	**0.80**	**0.73**					**0.03**				
20:2							**1.91**	**1.98**	**1.48**		**0.04**	**0.11**	**0.78**	**0.79**	**0.82**	**0.50**	**0.62**	**0.57**
20:1	**0.19**	**0.14**	**0.16**	**0.57**	**0.36**	**0.24**	**14.57**	**14.53**	**14.39**	**1.54**	**1.16**	**0.88**	**5.22**	**6.88**	**8.26**	**4.41**	**6.61**	**6.77**
20:0	**0.12**	**0.03**		**1.29**	**1.60**	**1.48**	**1.46**	**1.40**	**1.22**	**1.15**	**1.23**	**1.40**	**1.00**	**1.14**	**1.55**	**0.55**	**0.57**	**0.79**
22:2								**0.06**					**1.40**	**1.33**	**1.17**	**1.10**	**1.47**	**1.03**
22:1							**2.82**	**1.46**	**1.18**	**0.85**	**0.66**	**0.52**	**45.54**	**45.53**	**45.48**	**51.94**	**51.26**	**49.20**
22:0				**0.14**	**0.06**		**0.31**	**0.11**	**0.07**	**16.60**	**16.64**	**17.24**	**1.41**	**1.06**	**1.28**	**0.69**	**0.54**	**1.34**
24:1							**0.54**	**0.27**	**0.15**	**0.17**	**0.20**	**0.12**	**2.12**	**2.12**	**2.10**	**1.49**	**1.28**	**1.30**
24:0				**0.10**	**0.03**		**0.16**	**0.04**		**10.84**	**10.91**	**11.22**	**0.77**	**0.50**	**0.69**	**0.30**	**0.17**	**0.46**

ANNEXE III. SUPPLEMENTAIRES PUBLICATION 3

Journal of Chromatography A 1673 (2022) 463093

Contents lists available at ScienceDirect

Journal of Chromatography A

journal homepage: www.elsevier.com/locate/chroma

Rapid assessment of fatty acyls chains of phospholipids and plasmalogens by atmospheric pressure chemical ionization in positive mode and high-resolution mass spectrometry using in-source generated monoacylglycerol like fragments intensities

Sonia Abreu[a], Sylvie Héron[b], Audrey Solgadi[c], Bastien Prost[c], Jessica Dalloux-Chioccioli[d,e], Alice Kermarrec[f], Anne Meynier[f], Justine Bertrand-Michel[d,e], Alain Tchapla[b], Pierre Chaminade[a,*]

[a] Lipides: Systèmes Analytiques et Biologiques, Université Paris-Saclay, Chatenay-Malabry 92290, France
[b] ICP - CNRS UMR 8000, (LETIAM), Université Paris-Saclay, Orsay 91400, France
[c] Inserm, CNRS, Ingénierie et Plateformes Au Service de l'Innovation Thérapeutique, IPSIT-SAMM, Université Paris-Saclay, Chatenay-Malabry 92290, France
[d] I2MC, INSERM, Université Toulouse III -Paul Sabatier (UPS), Université de Toulouse, Toulouse, France
[e] MetaboHUB-MetaToul, National Infrastructure of Metabolomics and Fluxomics, Toulouse 31077, France
[f] INRAE, UR BIA, Nantes F-44316, France

ARTICLE INFO

Article history:
Received 2 March 2022
Revised 23 April 2022
Accepted 25 April 2022
Available online 27 April 2022

Keywords:
Phospholipids
Plasmalogens
Fatty acyls composition
Normal phase chromatography
Atmospheric pressure chemical ionization

ABSTRACT

We recently published a new concept using monoacylglycerol-like fragments $[MG+H-H_2O]^+$ (ions B) produced in-source by atmospheric pressure photoionization in positive mode and high-resolution mass spectrometry for the determination of the fatty acyl (FA) composition of triacylglycerols (TGs) from plant oils. This study extends the concept to the phospholipids (PLs) category and shows that the APCI$^+$ source can also be used. Moreover, the coupling with NP-LC allows to simultaneously analyze different PLs classes in the same sample. We compared the relative intensities of the ions B produced in-source to the % composition of FAs determined by GC-FID. In the case of PLs from natural extracts composed exclusively of diacyl-PLs, the relative intensities of ions B are close to the % of the FAs obtained by GC-FID. This approach is not directly useable for extracts containing plasmalogens (P-PLs). For these PLs, acidic hydrolysis by HCl fumes allows hydrolyzing selectively vinyl ether functions to form lyso-PLs. The analysis of hydrolyzed extracts makes it possible to obtain the composition of P-PLs FAs thanks to the lyso-PLs thus formed, while the diacyl-PLs composition remains unchanged. Unlike GC-FID FAs determination, this approach allows a distinction between the diacyl-PLs and P-PLs FAs composition. We also found that the ion B intensities were consistent among the PL classes (PG, PE, PA, PI, CL, PS and PC) and lyso- forms (LPE and LPC). In the case of the diacyl-PLs extracts analyzed, no statistically significant differences were found between the PLs FAs compositions calculated from ion B intensities and the corresponding GC-FID data. A weighting coefficient was applied to correct ion B intensities issued from polyunsaturated FAs with three or more double bonds. The fatty alkenyls composition of P-PLs could also be calculated from the % intensities of specific ions.

© 2022 Elsevier B.V. All rights reserved.

1. Introduction

Phospholipids (PLs) are a family of lipids (termed as the glycerophospholipids category in the Lipidmaps Lipid Classification System [1]), composed of a glycerol skeleton substituted in position *sn*-1 by a radyl, in *sn*-2 by a fatty acyl (FA) and in position *sn*-3 by a phosphate ester group [2]. The polar head in *sn*-3 defines the PL class. The type of radyl in *sn*-1 (ester, vinyl ether or ether) defines the subclass. The structure, name, and abbreviation of the different PL classes and the *sn*-1 and *sn*-2 substituents are shown in Fig. 1.

PLs are the main constituents of biological membranes (cells and organelles), but their role in biochemistry is only partially understood [3]. Diacyl-PLs are the most abundant in living beings and are the most commonly studied [4] for this reason.

* Corresponding author.
E-mail address: pierre.chaminade@universite-paris-saclay.fr (P. Chaminade).

https://doi.org/10.1016/j.chroma.2022.463093
0021-9673/© 2022 Elsevier B.V. All rights reserved.

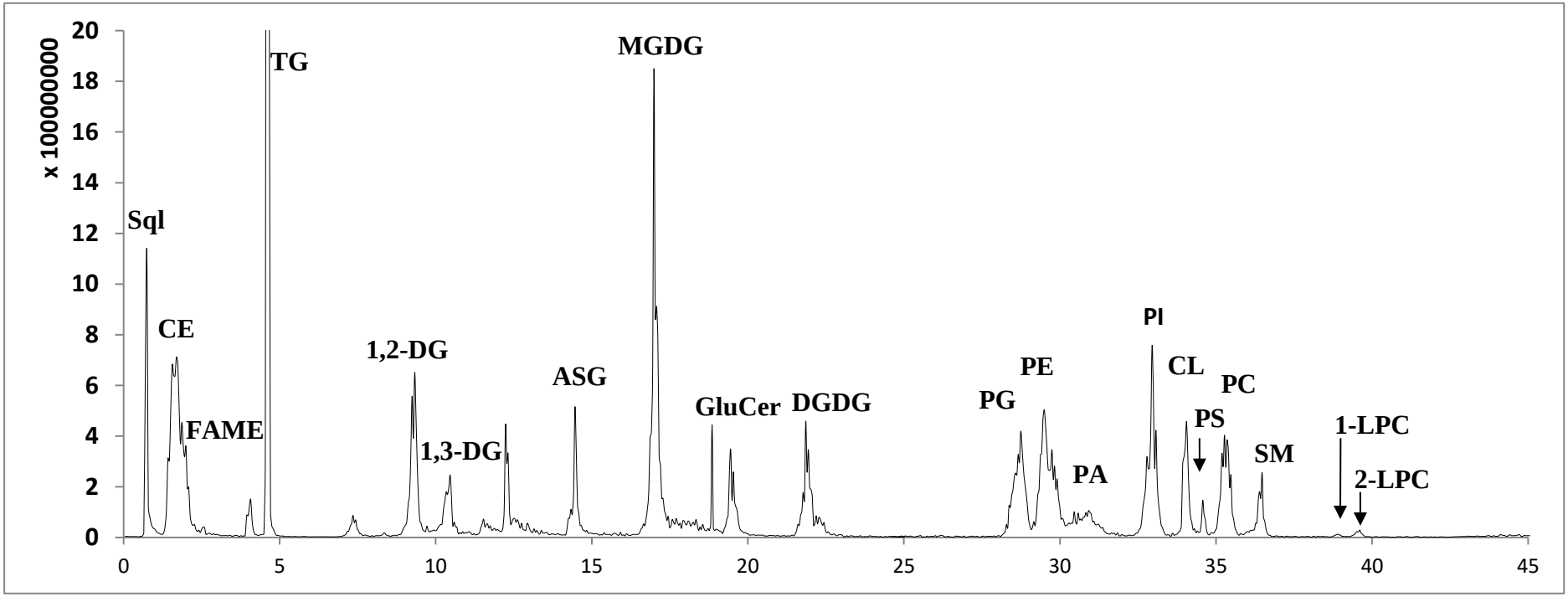

Figure S 8: NP-LC-APCI$^+$ MS chromatogram of 22 lipid standard at an individual concentration of 0.5 g/L. SQ-squalene, CE-cholesteryl esters, FAME-fatty acids methylesters, TG-triacylglycerols, Chol-cholesterol, DG-diacylglycerols, FA-fatty acids, ASG-acylated steryl glycosides, MGDG-monogalactosyldiglycerols, GlcCer-glucosylceramides, DGDG-digalactosyldiglycerols, PG-phosphatidylglycerols, PE-phosphatidylethanolamines, PA-phosphatidic acids, PI-phosphatidylinositols, CL-cardiolipins, PS-phosphatidylserines, PC-phosphatidylcholines, SM-sphingomyelins, LPC-lysophosphatidylcholines.

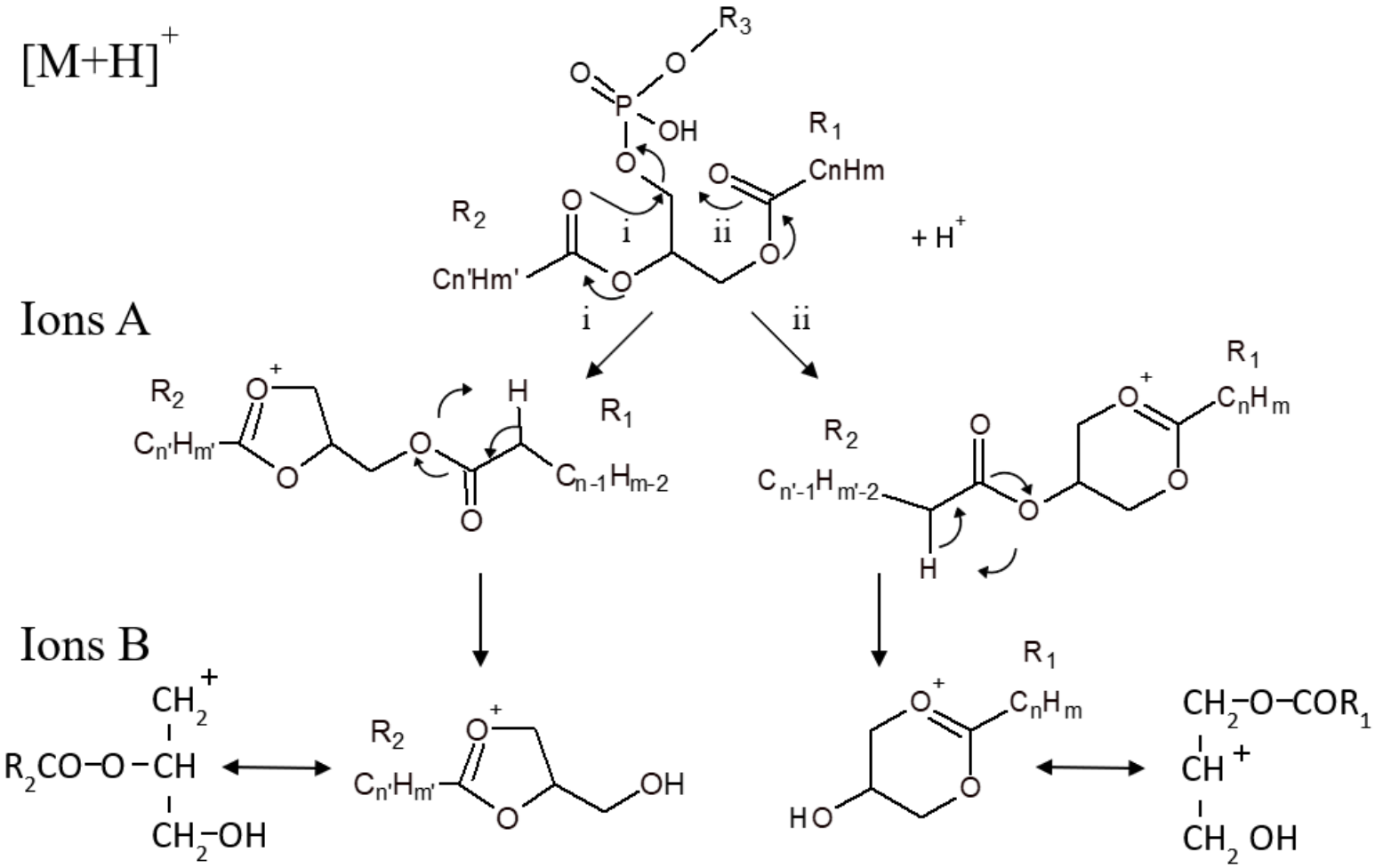

Figure S 9: Fragmentation process, of the diacyl-PLs produces the ions A and B in source APPI$^+$ and APCI$^+$ [27,33].

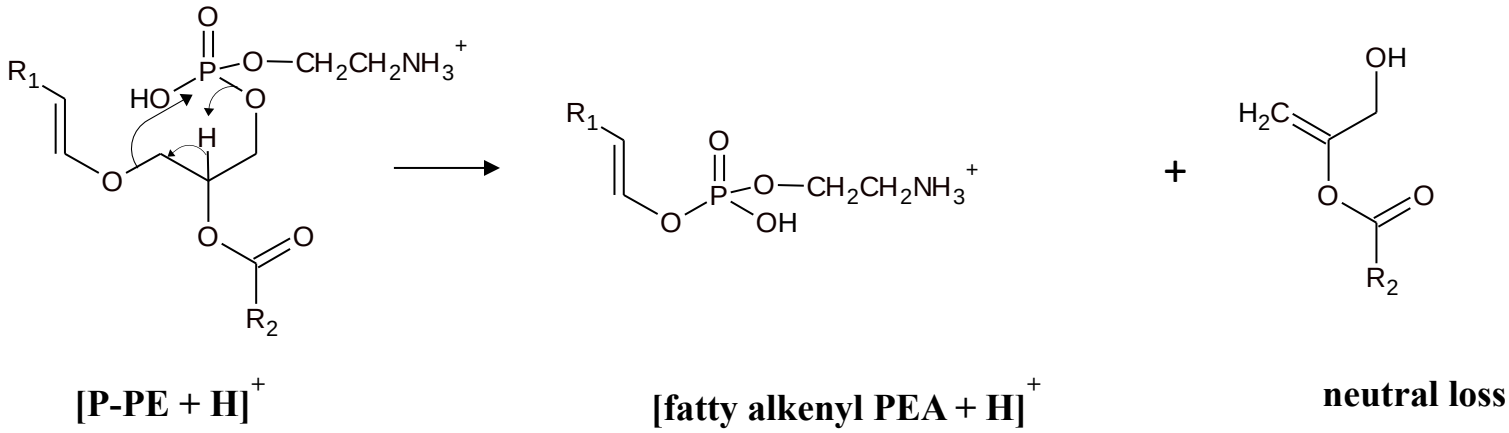

Figure S 10: Formation of the [fatty alkenyl PEA + H]$^+$ ion from the fragmentation of P-PE [5].

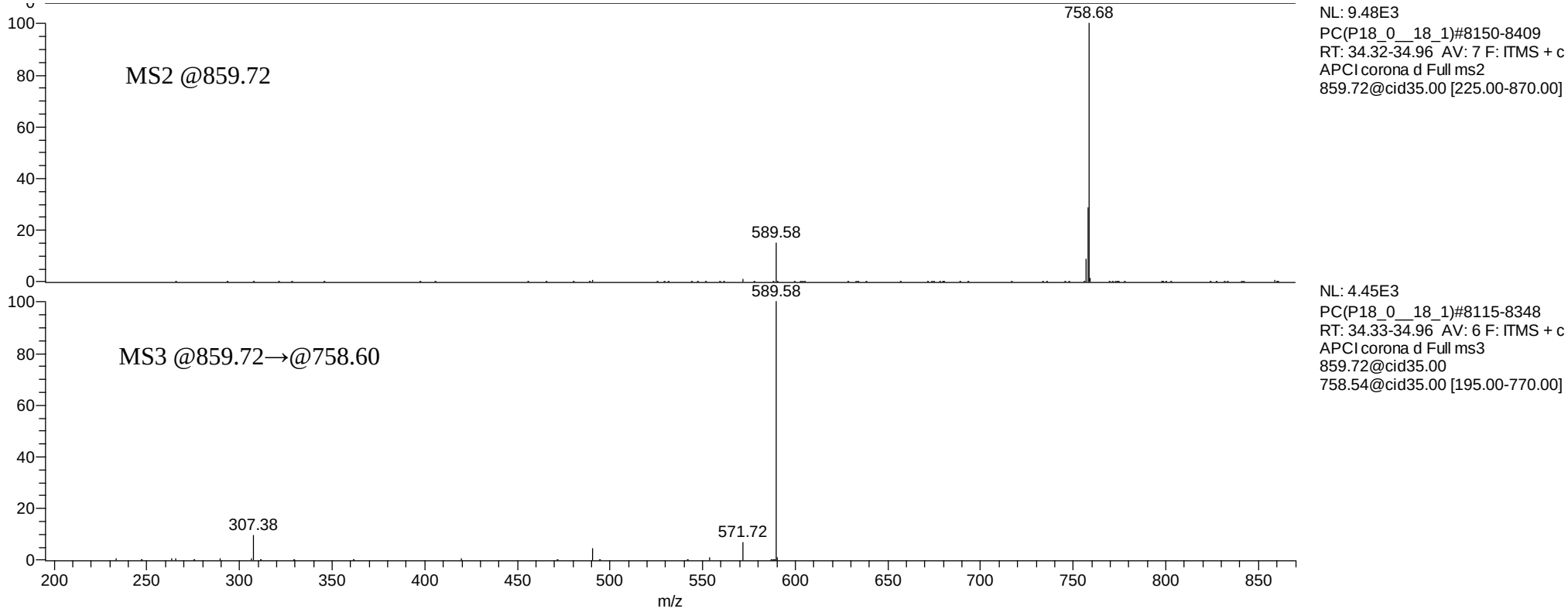

Figure S 11: MS^2 and MS^3 of the ion at *m/z* 859.72 of PC P-18:0/18:1.

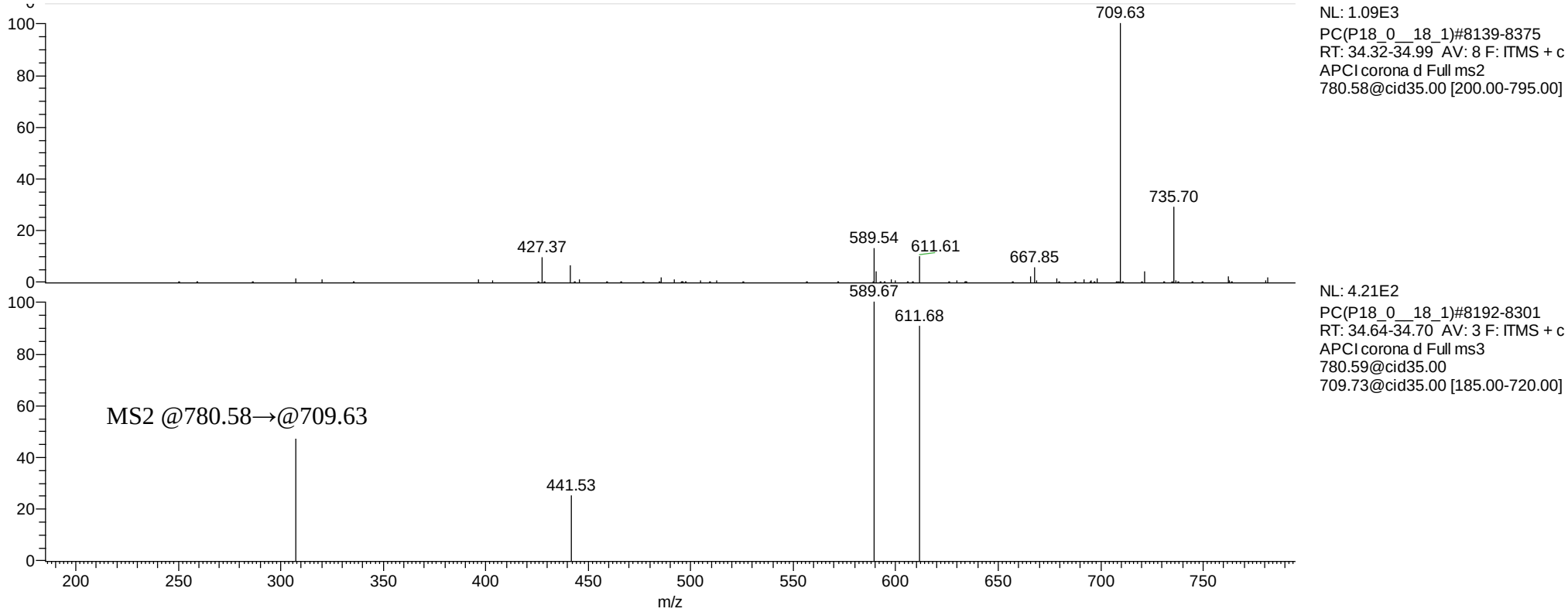

Figure S 12: MS² and MS3 of the ion at m/z 780.58 of PC P-18:0/18:1.

MS2 @780.58

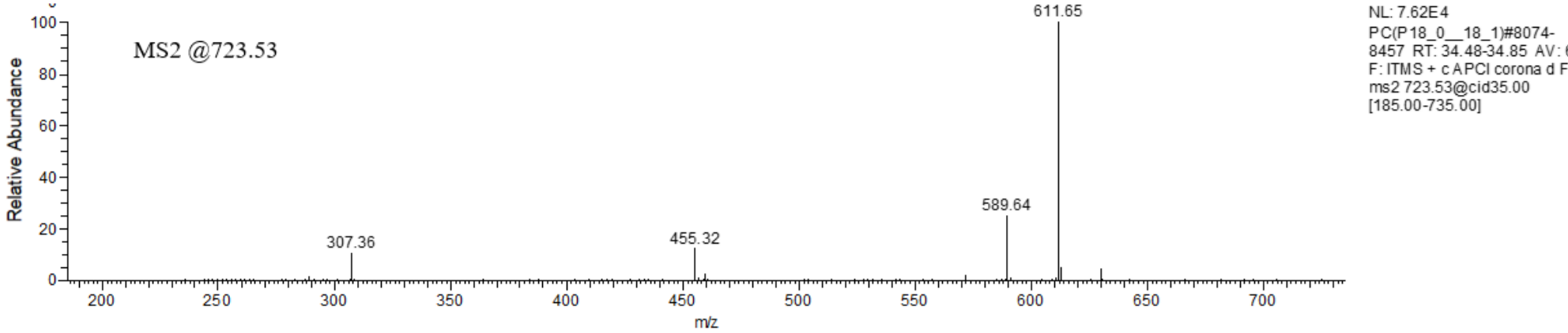

Figure S 13: MS² of the ion at *m/z* 723.53 of PC P-18:0/18:1.

Table S6: Quaternary gradient mobile phase composition. A, isooctane : ethyl acetate (99.8:0.2, v/v); B, acetone : ethyl acetate (2:1, v/v) containing 0.15% acetic acid (v/v); C, 2-propanol : water (85:15, v/v) containing 0.043% acetic acid (v/v) and 0.104% triethylamine (v/v); D, ethyl acetate.

Time	Percent solvent				Flow-rate
(min)	A	B	C	D	(mL/min)
0	100	0	0	0	0.8
1.5	100	0	0	0	0.8
1.6	97	3	0	0	0.8
9	94	6	0	0	0.8
11	70	30	0	0	0.8
14	45	55	0	0	0.8
15	45	55	0	0	0.8
16	40	55	5	0	0.8
20	35	55	10	0	0.8
20.1	33	50	17	0	0.8
25	38	45	17	0	0.8
25.1	48	35	17	0	0.8
30	53	30	17	0	0.8
36	53	30	17	0	0.8
40	40	10	50	0	0.8
46	40	10	50	0	0.8
46.1	0	100	0	0	0.8
49	0	100	0	0	0.8
49.1	50	0	0	50	0.8
52	50	0	0	50	0.8
54	100	0	0	0	0.8
60	100	0	0	0	0.8

The shaded area corresponds to modifications of the original solvent program.

Table S7: Percent FAs composition of PLs extracts as measured by GC-FID FAMEs analysis, results from Laboratory 1.

	PC				PE		PI	PS	CL	PG	PA	LPC	LPE
FAs	**Egg**	**Brain**	**Soy**	**Liver**	**Egg**	**Soy**	**Soy**	**Brain**	**Heart**	**Egg**	**Egg**	**Egg**	**Egg**
8:0													
10:0													
11:0													
12:0											**0.1**		
13:0													
14:0	**0.2**	**0.4**	**1.3**	**0.1**	**0.8**	**0.1**	**0.2**	**0.2**	**0.4**	**0.6**	**0.2**	**0.3**	
15:0			**0.1**	**0.1**	**0.1**				**0.1**				
16:0	**29.1**	**25.3**	**18.9**	**12.7**	**21.6**	**17.9**	**32.1**	**1.9**	**3.0**	**30.9**	**31.2**	**60.6**	**34.2**
17:0	**0.2**	**0.5**	**0.5**	**1.1**	**0.5**	**0.1**	**0.3**	**0.2**	**0.1**	**0.3**	**0.2**	**0.4**	**0.6**
18:0	**14.8**	**24.3**	**11.9**	**35.3**	**30.6**	**2.9**	**8.9**	**47.6**	**4.4**	**19.3**	**13.2**	**36.9**	**60.0**
20:0		**0.2**	**0.2**			**0.2**		**0.3**	**0.1**	**0.1**		**0.2**	
21:0													
22:0		**0.1**	**0.1**			**0.5**		**0.3**					
23:0													
24:0		**0.1**	**0.1**						**0.1**	**0.1**	**0.1**		
MUFA													
14:1n-7													
15:1n-7													
16:1n-9	**0.1**	**0.8**	**0.2**			**0.1**				**0.2**	**0.2**		
16:1n-7				**0.4**				**0.1**					
17:1n-7													
18:1n-9c	**31.2**	**30.6**	**13.4**	**16.2**	**19.5**	**6.9**	**5.1**	**21.7**	**2.3**	**29.9**	**34.7**	**1.3**	**1.6**
18:1n-9t	**1.3**	**8.3**	**1.6**			**0.9**	**1.3**		**4.1**	**1.2**	**1.3**		
18:1n-7				**1.3**	**1.0**			**4.2**				**0.2**	**0.5**
20:1n-9	**0.2**	**0.8**	**0.1**					**1.5**	**0.1**	**0.1**	**0.1**		
22:1n-9		**0.2**	**0.1**					**0.4**				**0.1**	**3.0**
24:1n-9													
PUFA													
16:2n-6													
16:2n-4													
16:3		**0.3**	**0.1**	**0.3**	**0.3**	**0.1**			**0.1**				
16:4n-3				**0.1**									
18:2n-6c	**16.7**	**0.9**	**46.7**	**10.8**	**10.7**	**63.7**	**46.6**	**0.2**	**82.3**	**12.8**	**15.8**		
18:2n-6t													
18:3n-6				**0.2**									
18:3n-3	**0.1**	**0.1**	**4.5**	**0.6**		**6.4**	**5.5**		**0.7**	**0.1**	**0.2**		
18:4n-3		**0.3**		**0.2**						**0.1**			
20:2n-6	**0.2**	**0.2**		**0.4**	**0.5**			**0.6**	**0.4**	**0.2**	**0.2**		
20:3n-3													
20:3n-6	**0.3**	**0.3**		**7.3**	**0.5**			**0.5**	**0.7**	**0.3**	**0.2**		
20:4n-6	**3.7**	**3.8**	**0.1**	**6.6**	**11.0**	**0.1**		**2.4**	**0.9**	**2.7**	**2.0**		
20:5n-3				**0.7**									
22:2n-6													
22:3n-3													
22:4n-6	**0.2**	**0.9**			**0.5**	**0.1**		**5.5**					
22:5n-3	**0.1**	**0.1**	**0.2**	**4.3**	**0.1**			**0.3**		**0.1**			
22:6n-3	**1.6**	**1.7**		**1.0**	**2.1**	**0.1**		**12.0**		**1.0**	**0.5**		

Table S8: Percent FAs composition of PLs extracts as measured by GC-FID FAMEs and DMAs analysis, results from Laboratory 2.

FA	PE heart	PE brain	PE liver	PC heart
8:0				
10:0				
11:0				
12:0				
13:0			0.1	
14:0			0.3	0.1
14:1				
15:0			0.1	0.2
15:1				
DMA 16:0	6.3	6.6	2.6	15.7
DMA 16:1	0.3		0.4	0.6
16:0	1.0	3.3	6.2	17.3
16:1n-9		0.4	0.2	0.2
16:1n-7				
16:2				
16:3				
16:4				
17:0	0.2	0.2	0.1	0.1
17:1			0.1	
DMA 18:0	14.1	11.3	1.2	4.2
DMA 18:1n-9	1.7	7.0	0.3	0.4
DMA 18:1n-7	1.7	9.4	0.1	1.2
18:0	23.2	11.8	37.1	5.3
18:1n-9	1.8	18.0	9.0	6.2
18:1n-7	0.5	2.7	0.6	1.9
18:2n-6t	19.1		9.2	32.7
18:2n-6		0.3		
18:3n-6	0.2		0.3	0.4
18:3n-3			0.2	0.1
18:4n-3				
20:0	0.1	0.3	0.1	0.2
20:1	0.1	2.2	0.3	0.3
20:2	0.1		0.1	0.2
20:3n-6	1.9	0.4	3.3	2.3
20:4n-6	23.5	8.7	15.4	5.5
21:0			0.2	
20:3n-3	0.2		0.1	
20:4n-3				
20:5n-3	0.7		0.4	0.2
22:0		0.2		
22:1	0.8	1.9	1.2	2.4
22:2		0.9		
22:4n-6	0.1	2.8	0.7	
22:5n-6	0.9	0.3	3.7	0.7
22:5n-3	0.5	5.8	4.3	0.4
22:6n-3	0.1	4.7	1.3	
24:0	0.7	0.9	0.8	1.0
24:1				
SAT	25.1	16.7	44.9	24.1
MONO	3.3	25.1	11.3	11.0
N-6	45.7	12.4	32.6	41.6
N-3	1.6	10.5	6.3	0.8
PUFA	47.4	23.8	39.0	42.6
N-6/N-3	28.7	1.2	5.2	54.8
FAs (%)	75.7	65.6	95.3	77.7
DMAs (%)	24.1	34.3	4.6	22.2

	PE heart	PE brain	PE liver	PC heart
% P-PLs	48.3	68.6	9.2	44.5

ANNEXE IV. SUPPLEMENTAIRES PUBLICATION 4

biomolecules

MDPI

Article

Lipid Readjustment in *Yarrowia lipolytica* Odd-Chain Fatty Acids Producing Strains

Sonia Abreu [1,†], Young-Kyoung Park [2,†], Camilla Pires de Souza [2], Lea Vidal [2], Pierre Chaminade [1,*] and Jean-Marc Nicaud [2,*]

[1] Lipides: Systèmes Analytiques et Biologiques, Université Paris-Saclay, 91400 Orsay, France; sonia.abreu@universite-paris-saclay.fr
[2] Micalis Institute, INRAE, AgroParisTech, Université Paris-Saclay, 78350 Jouy-en-Josas, France; yk16.park@gmail.com (Y.-K.P.); camilla.pires-de-souza@inrae.fr (C.P.d.S.); lea.vidal@inrae.fr (L.V.)
* Correspondence: pierre.chaminade@universite-paris-saclay.fr (P.C.); jean-marc.nicaud@inrae.fr (J.-M.N.)
† These authors equally contributed to this work.

Abstract: *Yarrowia lipolytica* is a promising oleaginous yeast for producing unusual lipids, such as odd-chain fatty acids (OCFA). Their diverse applications and low natural production make OCFA particularly interesting. In recent studies, inhibiting the catabolic pathway of precursor, boosting precursor pools, and optimizing substrate combination greatly improved the production of OCFA in *Y. lipolytica*. We explored the lipid readjustment of OCFA in engineered *Y. lipolytica* strains. NPLC-Corona-CAD® evidenced a time-dependent overproduction of free fatty acids, diglycerides, and phosphatidylcholine (PC) in obese LP compared to obese L. Phosphatidylethanolamine (PE) and phosphatidylinositol, largely overproduced in obese LP at 72 h compared to obese L, vanished at 216 h. The fatty acyls (FAs) composition of glycero- and glycerophospholipids was determined by NPLC-APPI+-HRMS from in-source generated monoacylglycerol-like fragment ions. C18:1 and C17:1 were predominant acylglycerols in obese L and obese LP, respectively. Phosphatidic acid, PE, and PC exhibited similar FAs composition but differed in their molecular species distributions. Cardiolipin (CL) is known to contain mostly C18:2 FAs corresponding to the composition in obese L, 50% of C18:2, and 35% of C18:1. In obese LP, both FAs dropped to drop to 20%, and C17:1 were predominant, reaching 55%. We hypothesize that CL-modified composition in obese LPs may alter mitochondrial function and limit lipid production.

Keywords: *Yarrowia lipolytica*; OCFA; lipid profile; lipidome; normal-phase liquid chromatography; metabolic readjustments

check for updates

Citation: Abreu, S.; Park, Y.-K.; Pires de Souza, C.; Vidal, L.; Chaminade, P.; Nicaud, J.-M. Lipid Readjustment in *Yarrowia lipolytica* Odd-Chain Fatty Acids Producing Strains. *Biomolecules* 2022, *12*, 1026. https://doi.org/10.3390/biom12081026

Academic Editor: Naoko Goto-Inoue

Received: 21 June 2022
Accepted: 20 July 2022
Published: 25 July 2022

Publisher's Note: MDPI stays neutral with regard to jurisdictional claims in published maps and institutional affiliations.

Copyright: © 2022 by the authors. Licensee MDPI, Basel, Switzerland. This article is an open access article distributed under the terms and conditions of the Creative Commons Attribution (CC BY) license (https://creativecommons.org/licenses/by/4.0/).

1. Introduction

In recent years, *Yarrowia lipolytica* has emerged as a favorable chassis for the production of unusual lipids [1,2]. Its oleaginous phenotype, the comprehensive studies on its lipid metabolism, and the advancement of synthetic biology tools provided a huge opportunity to improve the unusual lipid production at high titer, rate, and yield in *Y. lipolytica* [3–6]. Unusual lipids have received increasing attention as target products of metabolic engineering due to their wide range of applications in industry. Odd chain fatty acids (OCFAs), a type of unusual lipids, have shown various applications in the food, medical, and chemical industries. OCFA can be used as a biomarker of obesity, dietary fiber intake, and the risk of coronary heart disease [7–10]. *cis*-9-heptadecenoic acid (C17:1) has anti-inflammatory effects and can help treat psoriasis, allergies, and autoimmune diseases [11]. As well as, *cis*-9-heptadecenoic acid is known to have antagonistic activity against powdery mildew (a plant disease) [12]. OCFA and its derivatives have high value as precursors for flavor and fragrance, hydraulic fluids, plasticizers, coatings, and others [12–15].

Despite their broad applications, the natural production of OCFA is very limited [6,16]. In order to improve the production of OCFA, metabolic engineering and optimization of

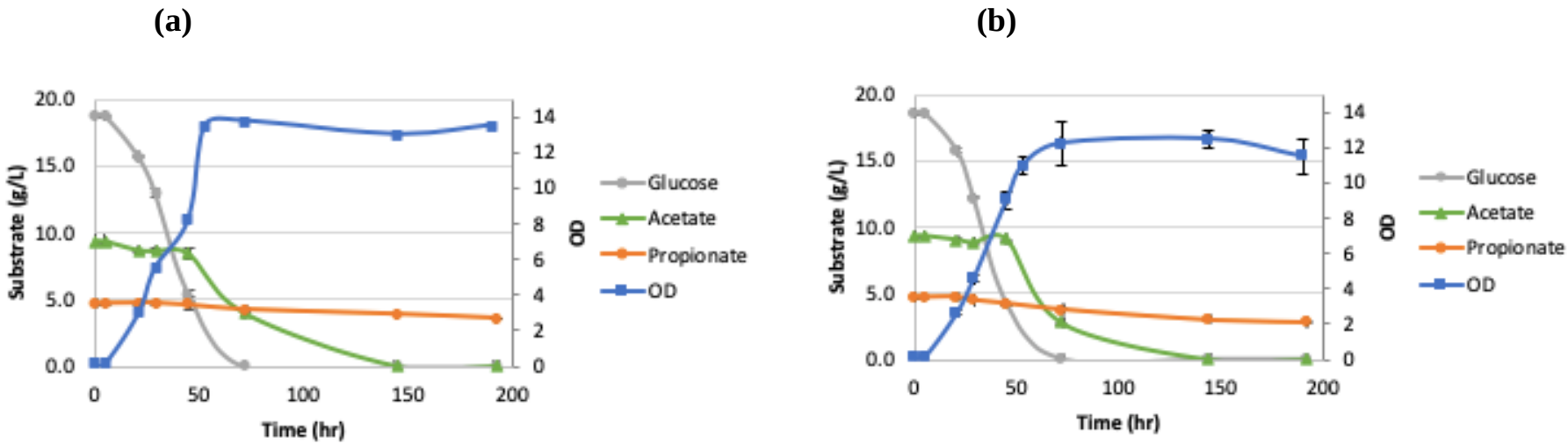

Figure S1. The consumption of substrates during the cultivation. (a) control, obese-L strain, (b) OCFA-producer, obese-LP strain. Averages and standard deviations were obtained from two replicate experiments. This data was published in Park et al. 2021.

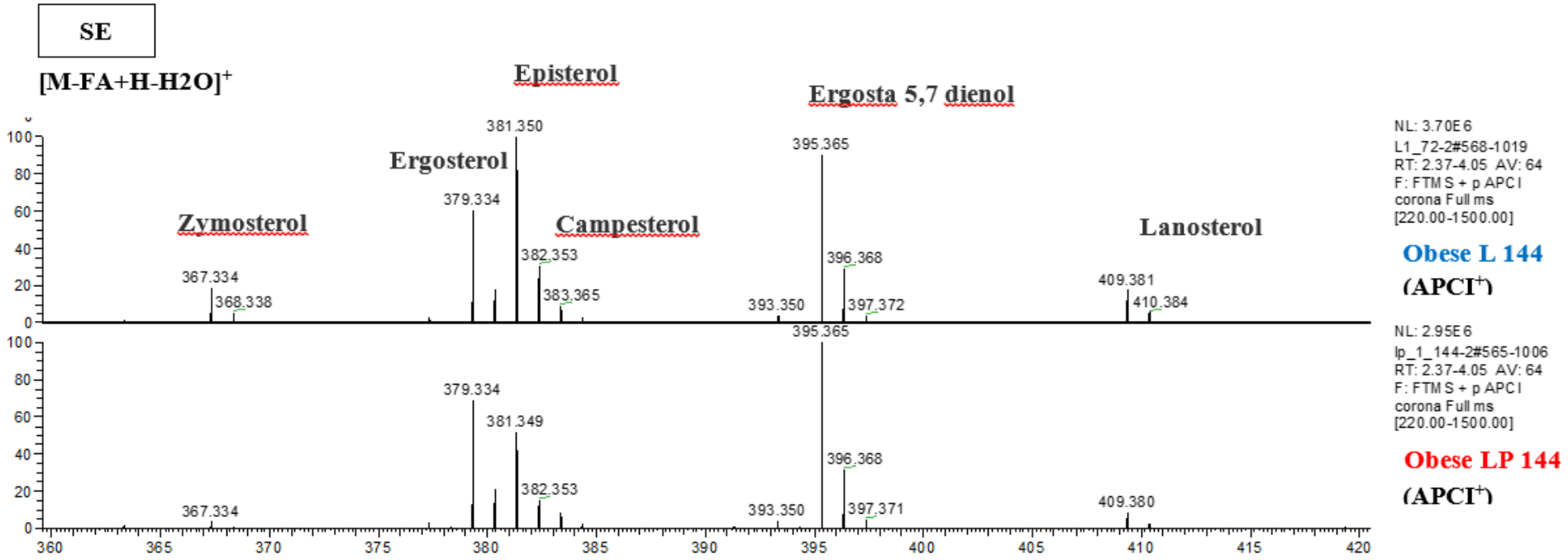

Figure S2. SE mass spectra of obese L and obese LP at 144 hours. The obseved ions correspond to $[M\text{-}FA+H\text{-}H2O]^+$.

Table S6. Identification of sterol nuclei present in SE. The m/z observed were imput in the Lipid Maps database (column 1). The corresponding matched mass are indicated in column 2. The delta mass, the name, the formula and the corresponding Ion are indicated in column 4 to 5, respectively. In column 7, the putative corresponding sterols according to the Lipid Maps and the identified Yarrowia lipolytica sterols by Walker et al. (2019) are indicated.

Input Mass	**Matched Mass**	**Delta**	**Name**	**Formula**	**Ion**	**Sterols (putative identity)**
367.334	367.3359	0.0019	ST 27:2;O	C27H44O	[M+H-H2O]+	Zymosterol
377.319	377.3203	0.0013	ST 28:4;O	C28H42O	[M+H-H2O]+	Ergosta-5,7,22E,24(28)-tetraenol
379.335	379.3359	0.0009	ST 28:3;O	C28H44O	[M+H-H2O]+	Ergosterol
381.35	381.3516	0.0016	ST 28:2;O	C28H46O	[M+H-H2O]+	Episterol / Fecosterol
383.365	383.3672	0.0022	ST 28:1;O	C28H48O	[M+H-H2O]+	Campesterol
393.35	393.3516	0.0016	ST 29:3;O	C29H46O	[M+H-H2O]+	
395.365	395.3672	0.0022	ST 29:2;O	C29H48O	[M+H-H2O]+	Ergosta 5,7 dienol
409.381	409.3829	0.0019	ST 30:2;O	C30H50O	[M+H-H2O]+	Lanosterol

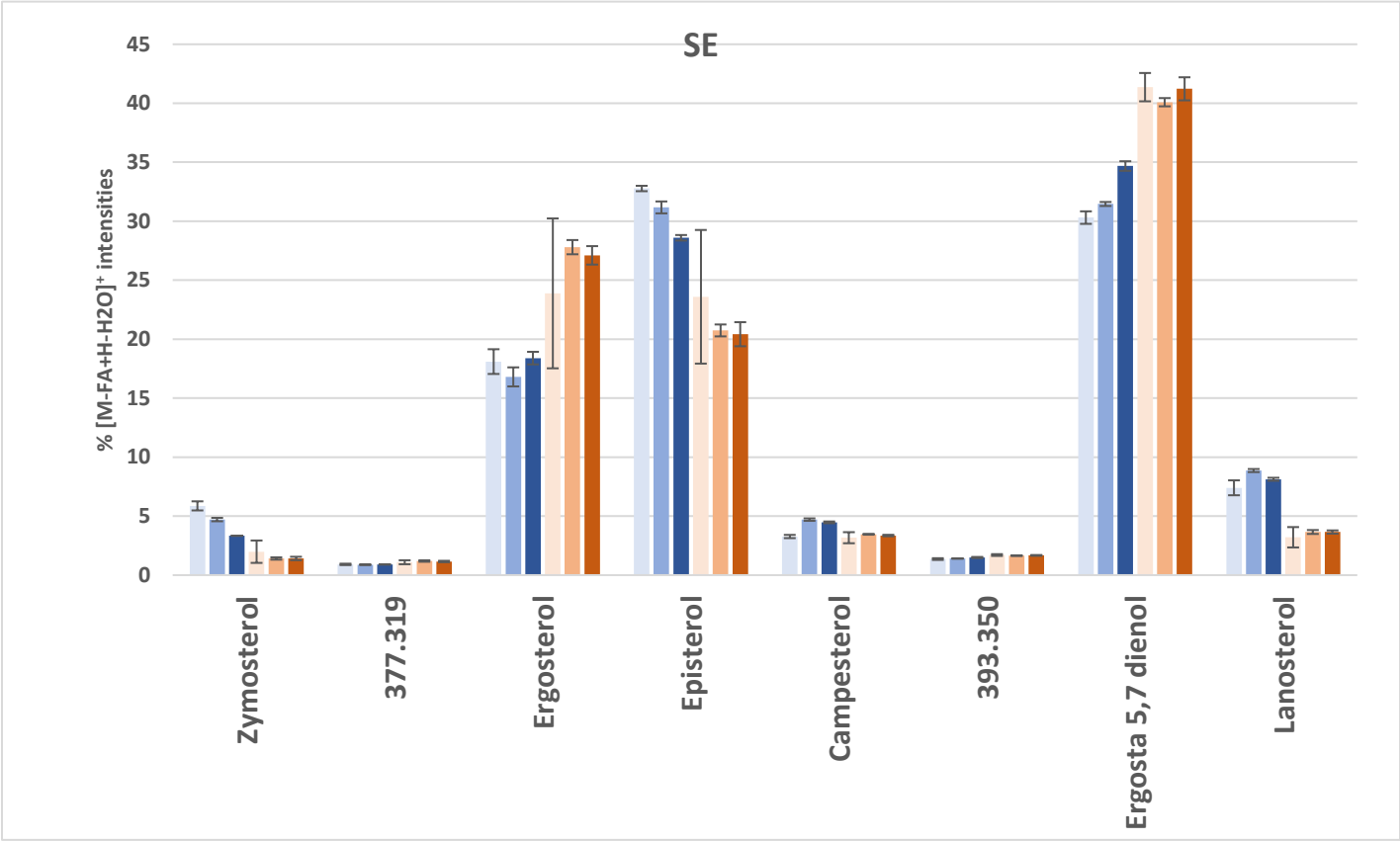

Figure S3. Distribution of $[M\text{-}FA+H\text{-}H2O]^+$ ions and corresponding sterols in SE fraction in the obese L (blue) and obese LP (orange) at 72, 144 and 216 hours..

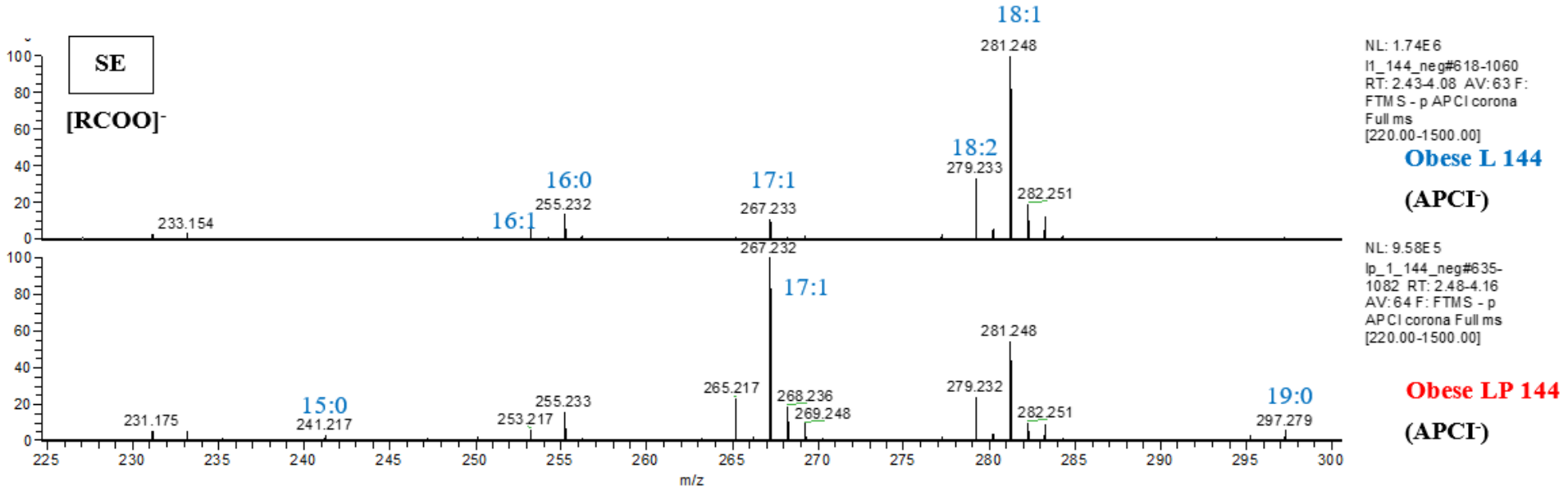

Figure S4. SE mass spectra in obese L and obese LP at 144 hours, zoomed in the m/z [225-300] region. The observed $[RCOO]^-$, allowing to determine the esterified FA in the sterols.

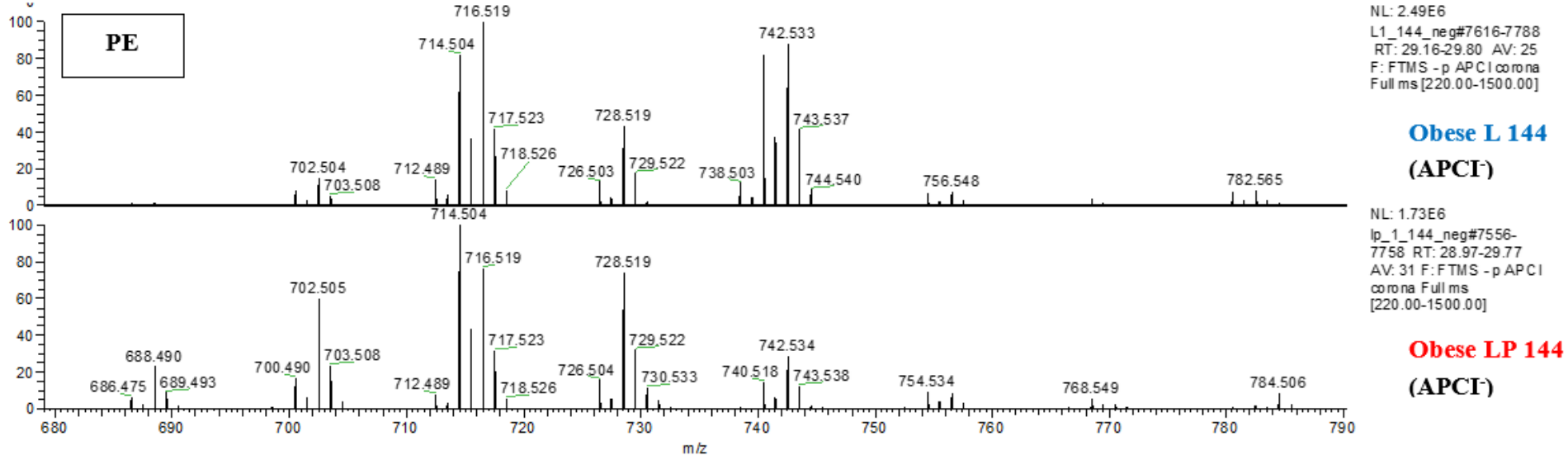

Figure S5. PE mass spectra in obese L and obese LP at 144 hours.

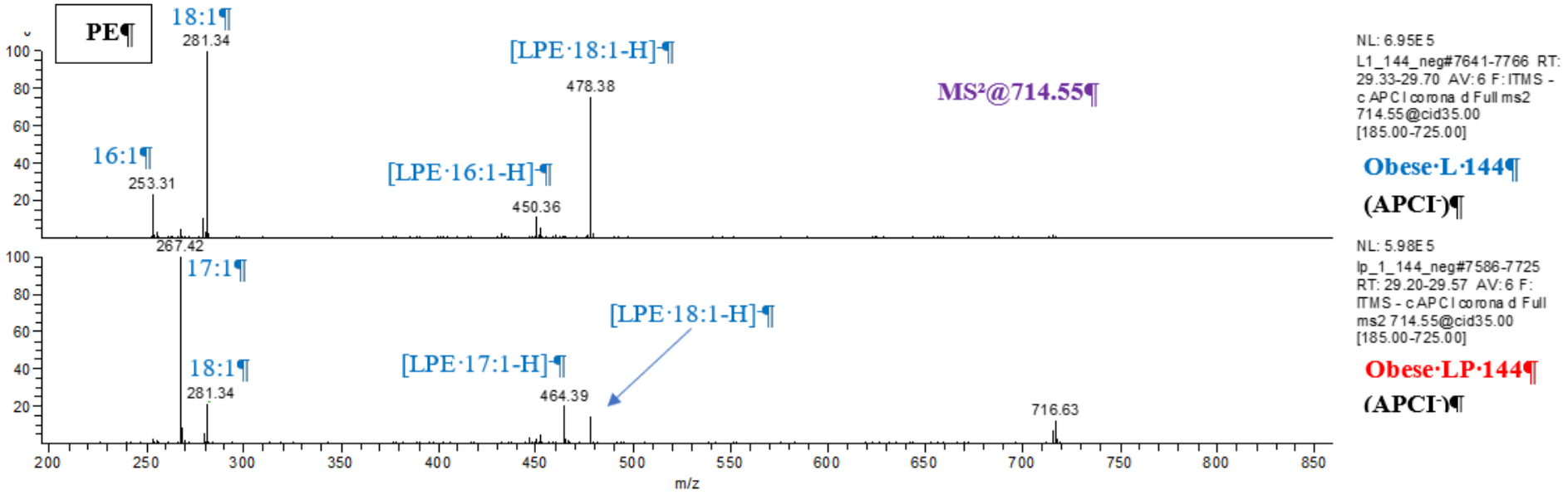

Figure S6. MS² spectra of ions @714.55 of PE in obese L and obese LP at 144 hours.

PE

Table S7. Identification of molecular species present in PE. The m/z observed were imput in the Lipid Maps database (column 1). The corresponding matched mass are indicated in column 2. The delta mass, the name, the formula and the corresponding Ion are indicated in column 3 to 6, respectively. In column 7 and 8, the main molecular species identified according to their name and MS^2 are indicated for obese L and obese LP, respectively.

Input Mass	Matched Mass	Delta	Name	Formula	Ion	Obese L	Obese LP
686.4746	686.4766	0.002	PE 32:2	C37H70NO8P	$[M-H]^-$		17:1/15:1
688.4897	688.4923	0.0026	PE 32:1	C37H72NO8P	$[M-H]^-$		17:1/15:0
700.4898	700.4923	0.0025	PE 33:2	C38H72NO8P	$[M-H]^-$	17:1/16:1	17:1/16:1 & 18:1-15:1
702.5048	702.5079	0.0031	PE 33:1	C38H74NO8P	$[M-H]^-$	17:1/16:0 & 18:1/15:0	17:1/16:0 & 18:1-15:0
712.4894	712.4923	0.0029	PE 34:3	C39H72NO8P	$[M-H]^-$	18:2/16:1	17:1-17:2
714.5043	714.5079	0.0036	PE 34:2	C39H74NO8P	$[M-H]^-$	18:1/16:1 &	17:1/17:1
716.5188	716.5236	0.0048	PE 34:1	C39H76NO8P	$[M-H]^-$	18:1/16:0	17:1/17:0 & 18:1/16:0
726.5035	726.5079	0.0044	PE 35:3	C40H74NO8P	$[M-H]^-$	18:2/17:1	18:2/17:1 & 18:1/17:2
728.5188	728.5236	0.0048	PE 35:2	C40H76NO8P	$[M-H]^-$	18:1/17:1	18:1/17:1
730.5331	730.5392	0.0061	PE 35:1	C40H78NO8P	$[M-H]^-$	18:2-18:2	18:1/17:0 & 18:0/17:1
740.5184	740.5236	0.0052	PE 36:3	C41H76NO8P	$[M-H]^-$	18:1/18:2	18:1/18:2
742.5342	742.5392	0.005	PE 36:2	C41H78NO8P	$[M-H]^-$	18:1-18:1	18:1/18:1

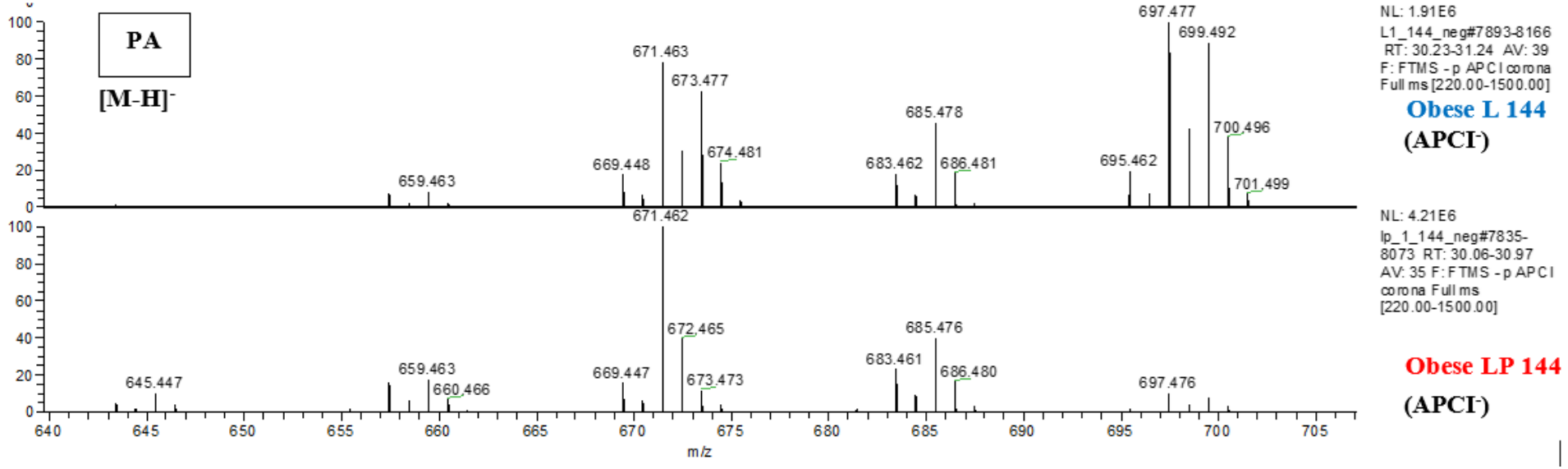

Figure S7. PA mass spectra in obese L and obese LP at 144 hours.

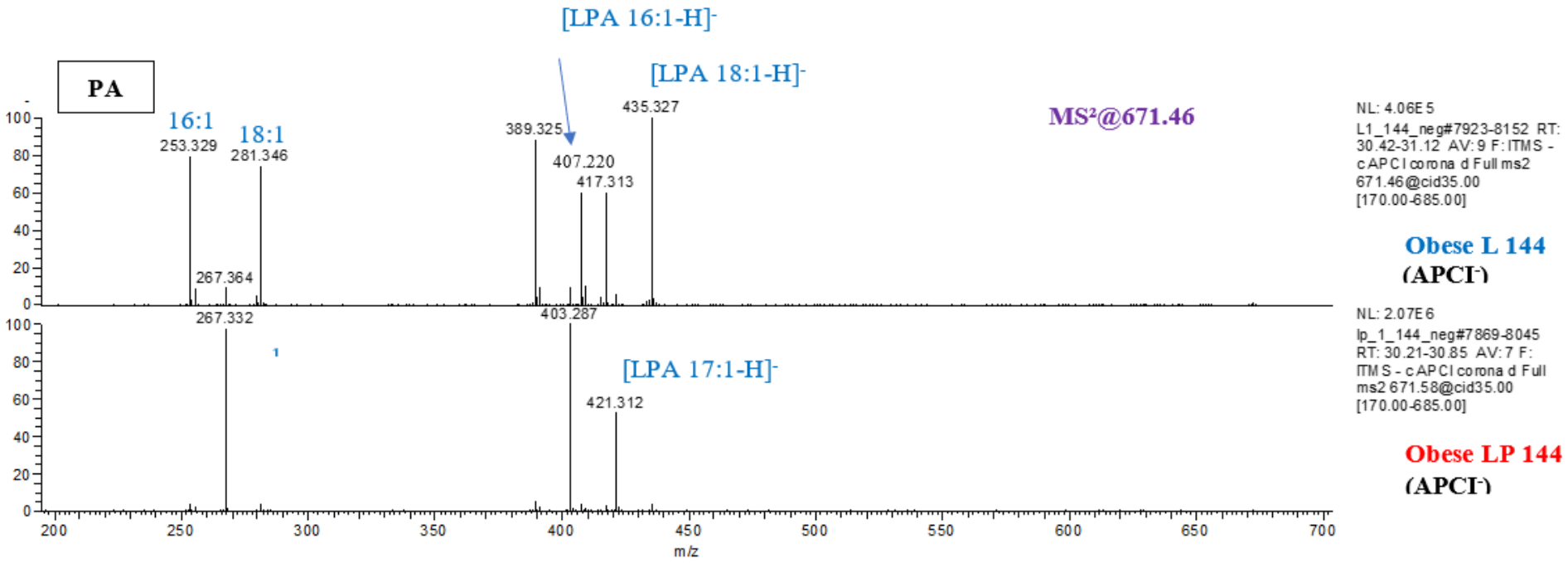

Figure S8. MS² spectra of ions @671.46 of PA in obese L and obese LP at 144 hours.

PA

Table S8. Identification of molecular species present in PA. The m/z observed were imput in the Lipid Maps database (column 1). The corresponding matched mass are indicated in column 2. The delta mass, the name, the formula and the corresponding Ion are indicated in column 3 to 6, respectively. In column 7 and 8, the main molecular species identified according to their name and MS^2 are indicated for obese L and obese LP, respectively.

Input Mass	Matched Mass	Delta	Name	Formula	Ion	L	LP
645.4470	645.4501	0.0031	PA 32:1	C35H67O8P	$[M-H]^-$		15:0/17:1
657.4481	657.4501	0.002	PA 33:2	C36H67O8P	$[M-H]^-$	17:1/16:1	17:1/16:1
659.4634	659.4657	0.0023	PA 33:1	C36H69O8P	$[M-H]^-$	17:1/16:0 & 18:1/15:0	16:0/17:1
669.4482	669.4501	0.0019	PA 34:3	C37H67O8P	$[M-H]^-$	18:2/16:1	17:1/17:2
671.4634	671.4657	0.0023	PA 34:2	C37H69O8P	$[M-H]^-$	18:1/16:1	17:1/17:1
673.4781	673.4814	0.0033	PA 34:1	C37H71O8P	$[M-H]^-$	18:1/16:0	17:1/17:0 & 16:0/18:1
683.463	683.4657	0.0027	PA 35:3	C38H69O8P	$[M-H]^-$	18:2/17:1	17:1/18:2
685.4783	685.4814	0.0031	PA 35:2	C38H71O8P	$[M-H]^-$	18:1/17:1	17:1/18:1
695.4627	695.4657	0.003	PA 36:4	C39H69O8P	$[M-H]^-$	18:2/18:2	18:2/18:2 & 17:2/19:2
697.4778	697.4814	0.0036	PA 36:3	C39H71O8P	$[M-H]^-$	18:1/18:2	18:2/18:1
699.4924	699.497	0.0046	PA 36:2	C39H73O8P	$[M-H]^-$	18:1/18:1	18:1/18:1

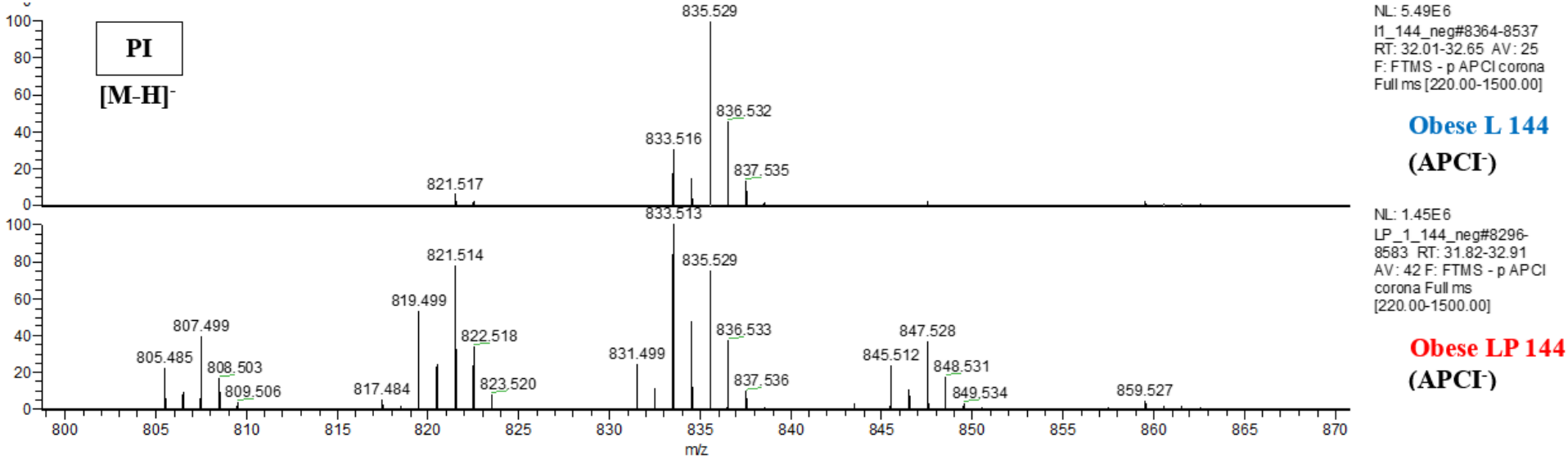

Figure S9.: PI mass spectra in obese L and obese LP at 144 hours.

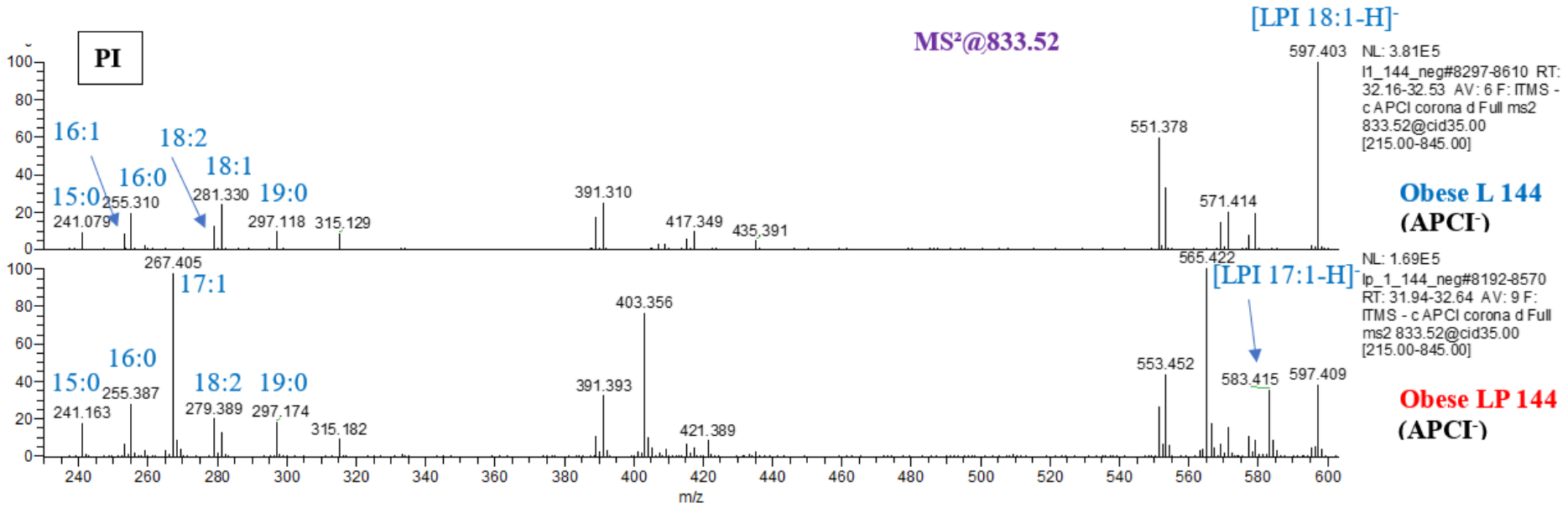

Figure S10. MS² spectra of ions @833.52 of PI in obese L and obese LP at 144 hours.

PI

Table S9. Identification of molecular species present in PI. The m/z observed were imput in the Lipid Maps database (column 1). The corresponding matched mass are indicated in column 2. The delta mass, the name, the formula and the corresponding Ion are indicated in column 3 to 6, respectively. In column 7 and 8, the main molecular species identified according to their name and MS^2 are indicated for obese L and obese LP, respectively.

Input Mass	Matched Mass	Delta	Name	Formula	Ion	L	LP	
805.4846	805.4873	0.0027	PI 32:2	C41H75O13P	$[M-H]^-$		17:1/15:1	
807.4993	807.5029	0.0036	PI 32:1	C41H77O13P	$[M-H]^-$		17:1/15:0	
817.4839	817.4873	0.0034	PI 33:3	C42H75O13P	$[M-H]^-$		18:2/15:1	
819.4992	819.5029	0.0037	PI 33:2	C42H77O13P	$[M-H]^-$		17:1/16:1 & 15:0/18:2	
821.5141	821.5186	0.0045	PI 33:1	C42H79O13P	$[M-H]^-$	17:1/16:0 & 18:1/15:0	16:0/17:1 & 18:1/15:0	
831.4985	831.5029	0.0044	PI 34:3	C43H77O13P	$[M-H]^-$		17:1/17:2 & 18:2/16:1	
833.5133	833.5186	0.0053	PI 34:2	C43H79O13P	$[M-H]^-$	16:0/18:2 & 16:1/18:1	17:1/17:1	
835.5293	835.5342	0.0049	PI 34:1	C43H81O13P	$[M-H]^-$	18:1/16:0	17:1/17:0 & 16:0/18:1	
843.4977	843.5029	0.0052	PI 35:4	C44H77O13P	$[M-H]^-$		17:2/18:2	
845.5124	845.5186	0.0062	PI 35:3	C44H79O13P	$[M-H]^-$	18:2/17:1	17:1/18:2	
847.5279	847.5342	0.0063	PI 35:2	C44H81O13P	$[M-H]^-$	18:1/17:1	17:1/18:1	
849.5435	849.5499	0.0064	PI 35:1	C44H83O13P	$[M-H]^-$	18:2-18:2	17:1/18:0 & 18:1/17:0	
857.5125	857.5186	0.0061	PI 36:4	C45H79O13P	$[M-H]^-$		18:2/18:2	

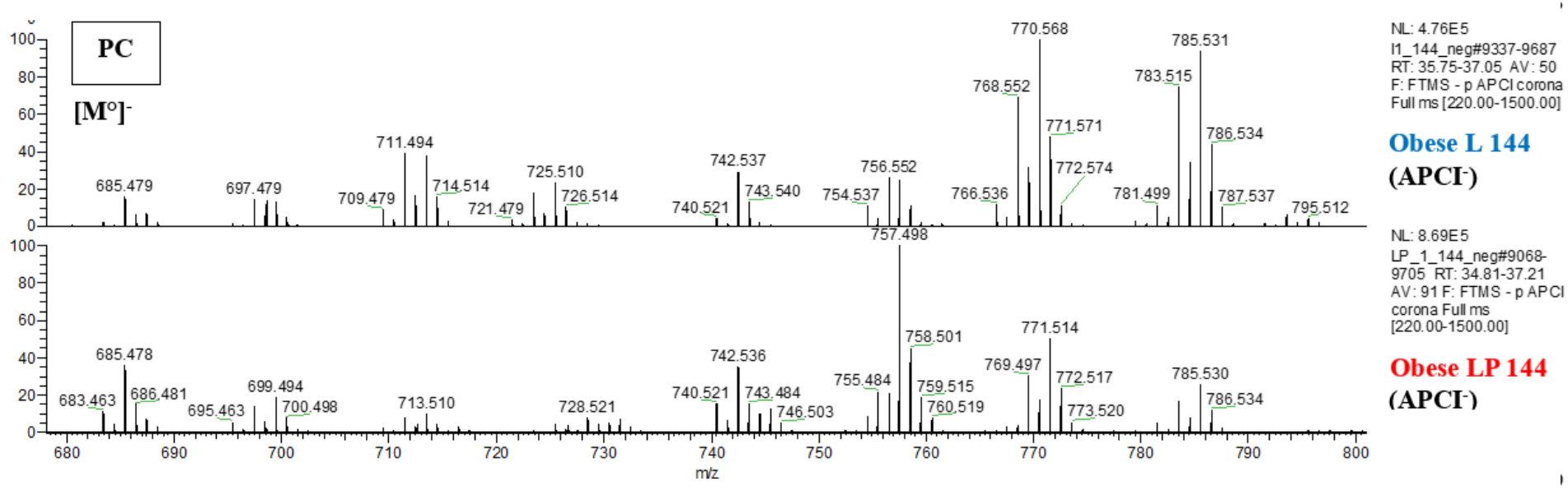

Figure S11. PC mass spectra in obese L and obese LP at 144 hours.

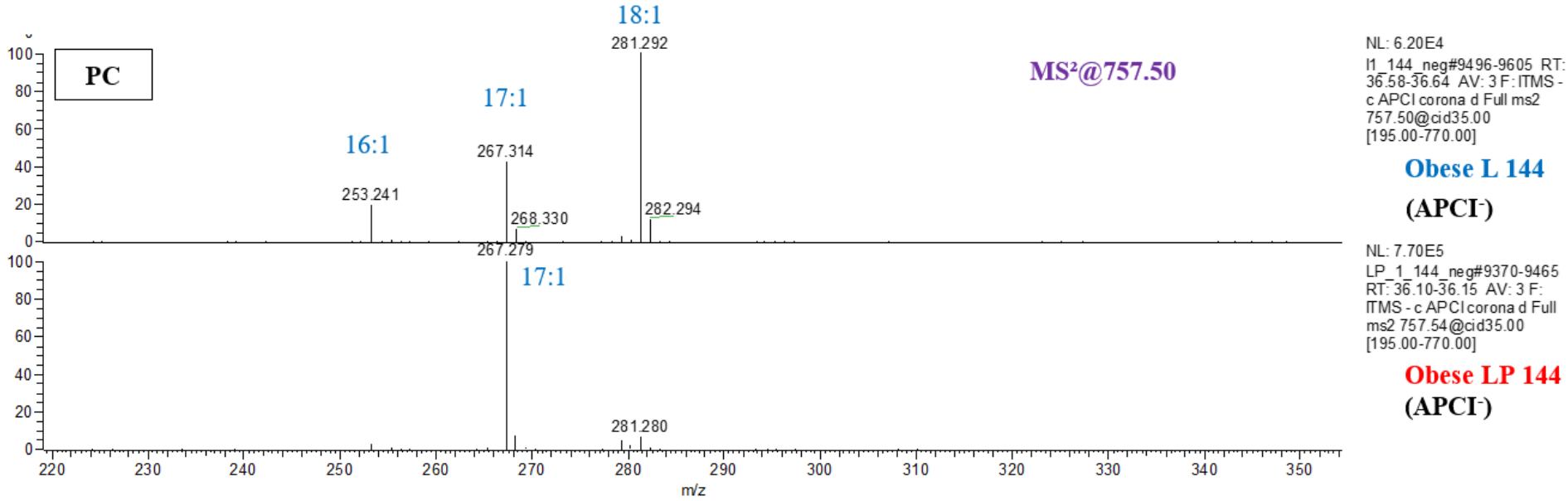

Figure S12. MS² spectra of ions @757.50 of PC in obese L and obese LP at 144 hours.

PC

Table S10. Identification of molecular species present in PC. Manual identification of the observed m/z (column 1). The corresponding PC species and the main molecular species identified according to their MS^2 are indicated for obese L and obese LP in column 4 and 5, respectively.

LIPID MAPS®, does not allow a PC search via ions $[M°]^-$.

Mass	Name	Ion	L	LP
729.4678	PC(32:2)	$[M°]^-$		
731.4818	PC(32:1)	$[M°]^-$		15:0/17:1
741.4678	PC(33:3)	$[M°]^-$		
743.4828	PC(33:2)	$[M°]^-$	17:1/16:1	17:1/16:1
745.4974	PC(33:1)	$[M°]^-$	17:1/16:0 & 18:1/15:0	16:0/17:1
755.4829	PC(34:3)	$[M°]^-$	18:2/16:1	17:1/17:2
757.4978	PC(34:2)	$[M°]^-$	18:1/16:1	17:1/17:1
759.5132	PC(34:1)	$[M°]^-$	18:1/16:0	17:1/17:0 & 16:0/18:1
767.4825	PC(35:4)	$[M°]^-$		
769.4972	PC(35:3)	$[M°]^-$	18:2/17:1	17:1/18:2
771.5134	PC(35:2)	$[M°]^-$	18:1/17:1	17:1/18:1
773.5298	PC(35:1)	$[M°]^-$		
781.4962	PC(36:4)	$[M°]^-$	18:2/18:2	18:2/18:2 & 17:2/19:2
783.5121	PC(36:3)	$[M°]^-$	18:1/18:2	18:2/18:1
785.5296	PC(36:2)	$[M°]^-$	18:1/18:1	18:1/18:1

Figure S13. Obese-L and obese-LP (at 144 hours) FA distribution of PLs classes calculated from Ion B intensities (green bars) or from molecular species intensities (yellow bars).

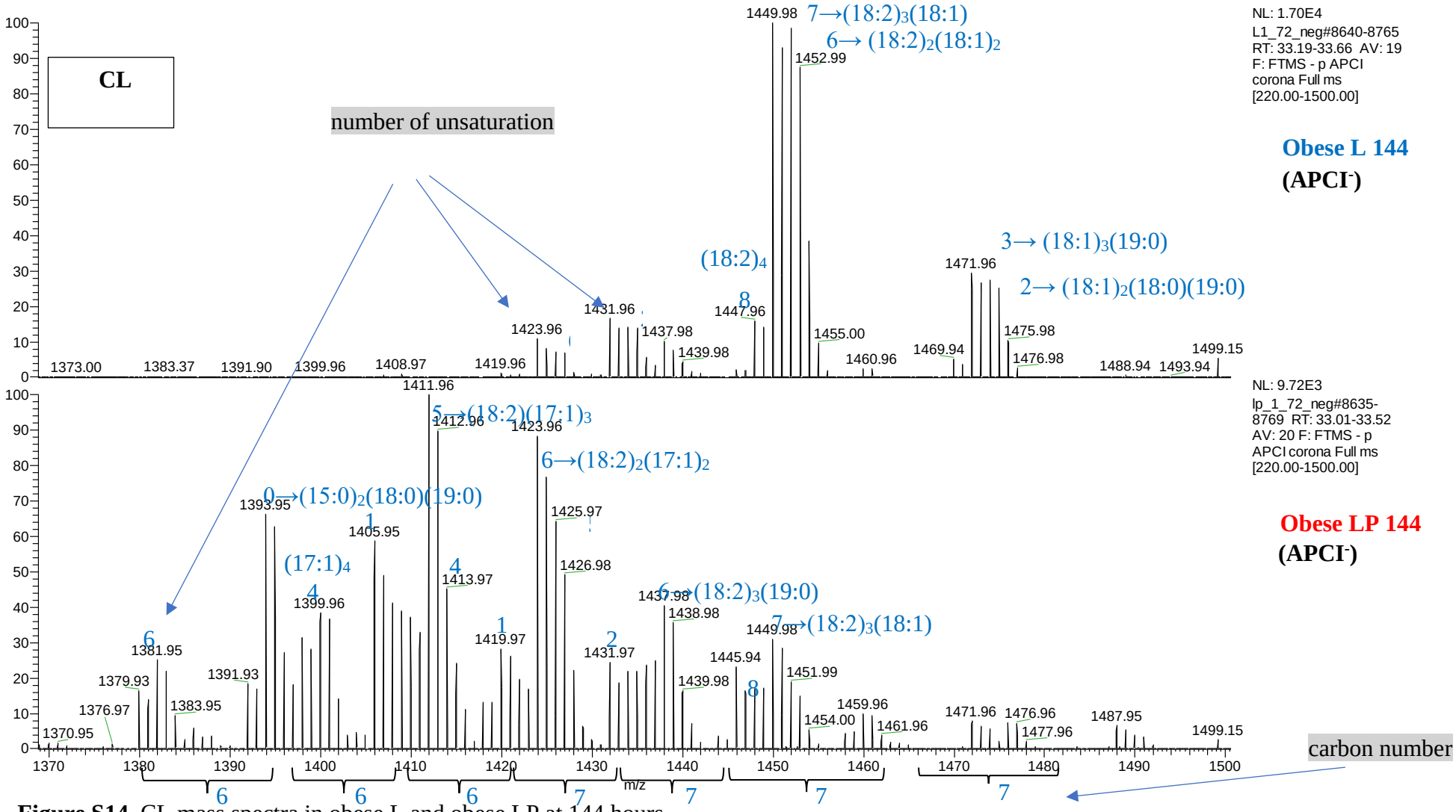

Figure S14. CL mass spectra in obese L and obese LP at 144 hours.

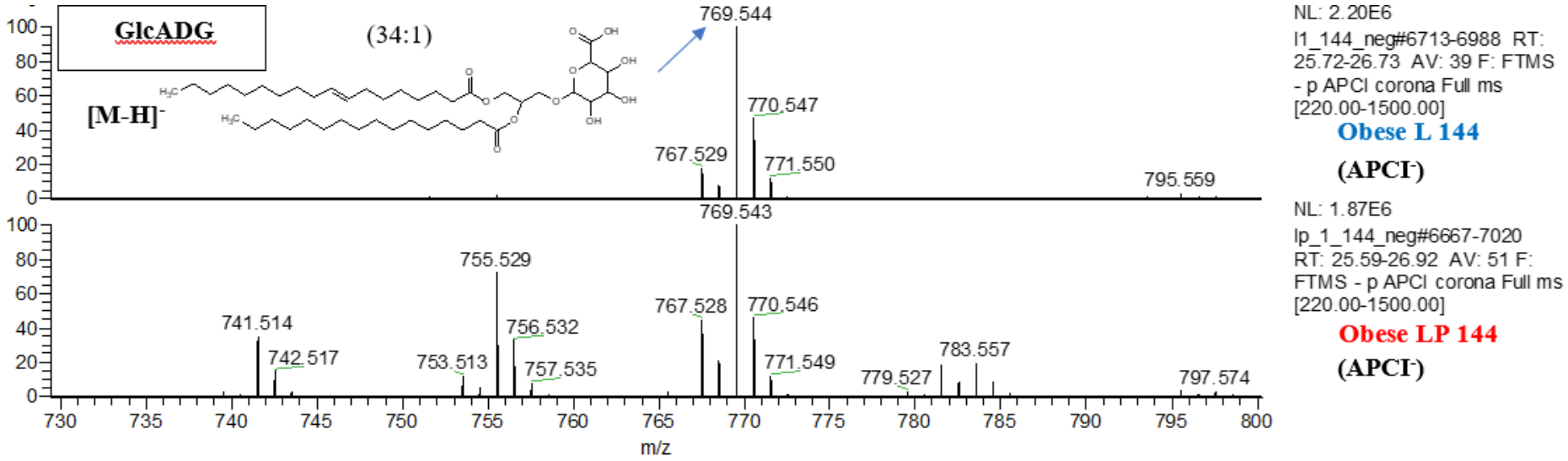

Figure S15. GlcADG mass spectra in obese L and obese LP at 144 hours.

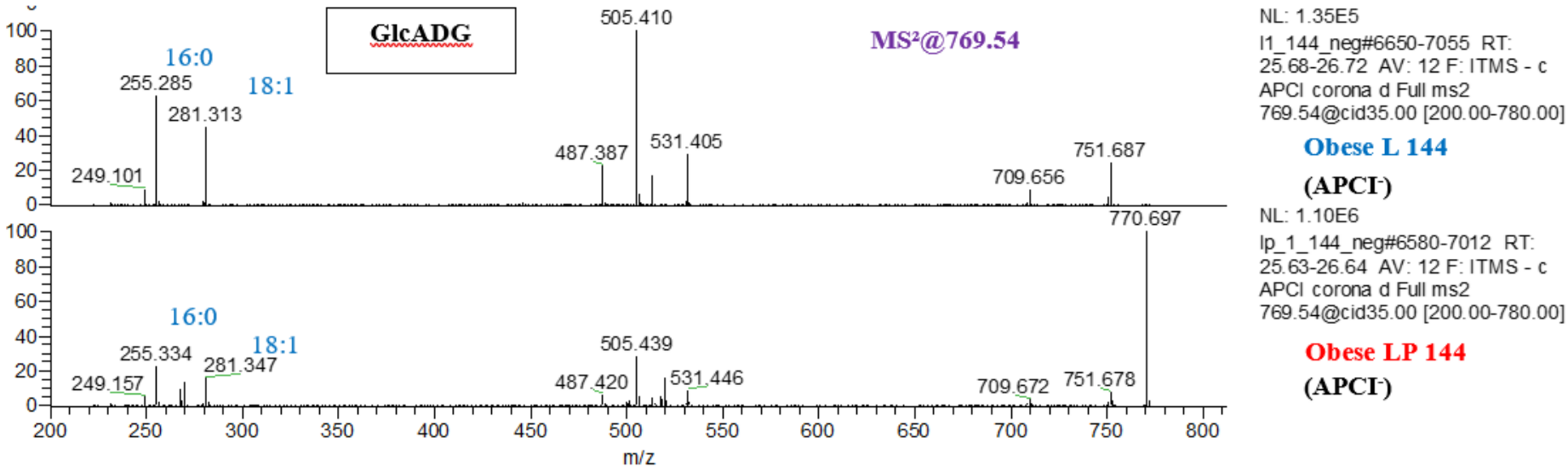

Figure S16. MS² spectra of ions @769.54 of GlcADG in obese L and obese LP at 144 hours.

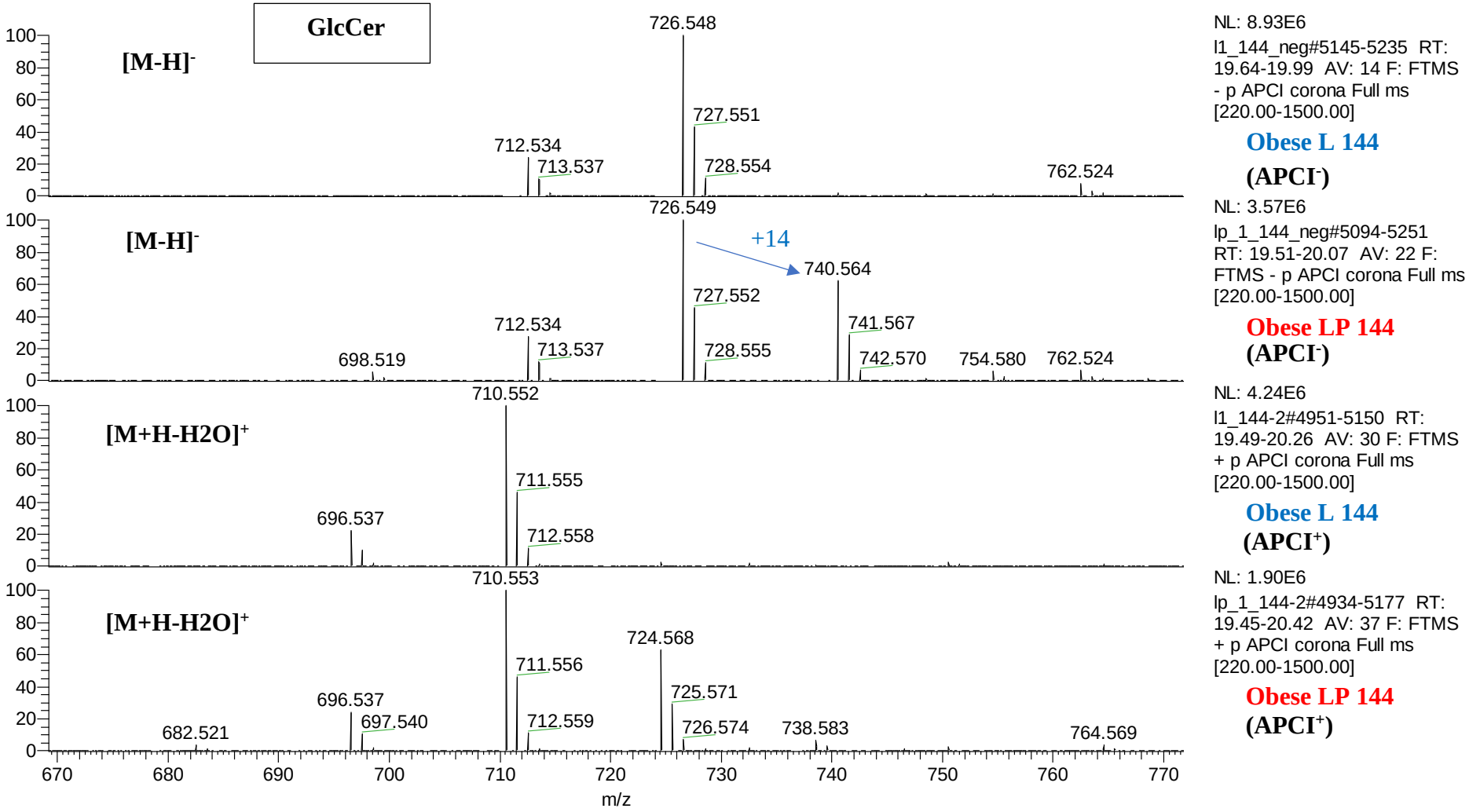

Figure S17: GlcCER mass spectra in obese L and obese LP at 144 hours.

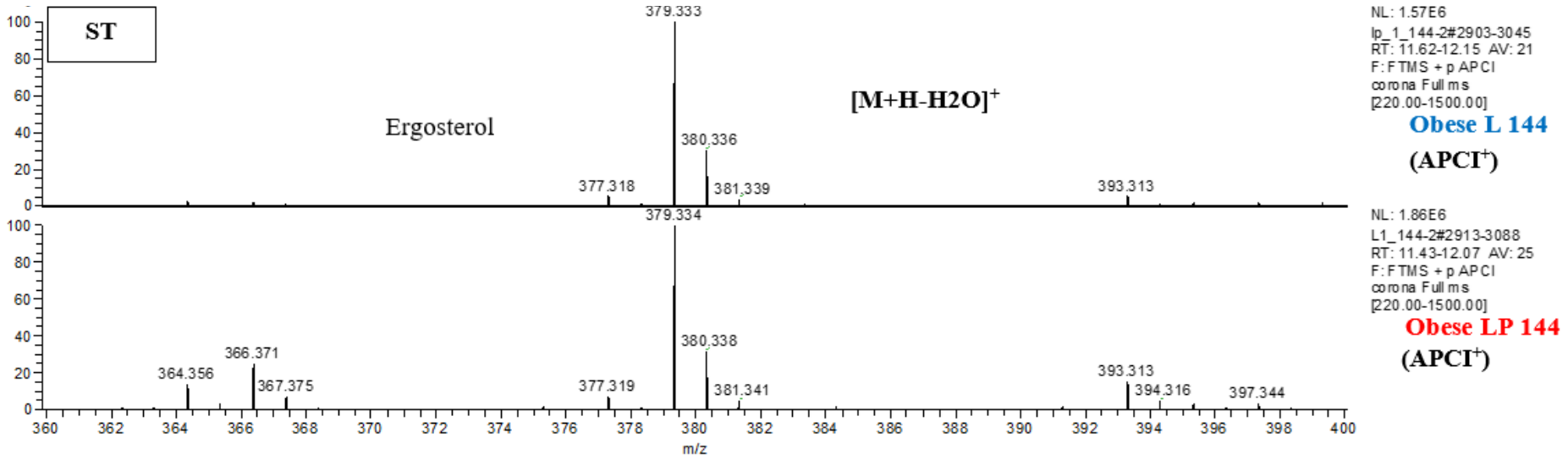

Figure S1814. ST Mass spectra of Ergosterol in obese L and obese LP at 144 hours.

Collaboration sur l'étude des lipides chez les bactéries du genre Streptomyces

Les annexes V-VII sont consacrées à l'étude des lipides des bactéries du genre *Streptomyces*, réalisée dans le cadre de trois collaborations avec le Dr Marie-Joëlle Virolle, directrice de l'équipe " Métabolisme Energétique des *Streptomyces* " (MES), à l'Institut de Biologie Intégrative de la Cellule (I2BC) de l'Université Paris-Saclay.

Ces travaux ont été réalisés parallèlement au projet de thèse, dans le cadre de mon activité d'Ingénieure d'Etude. Nous avons établi le profil lipidique par classe, de différentes souches de *Streptomyces*, grâce au couplage NPLC-HRMS [20]**. Il n'a pas été nécessaire d'évaluer la distribution des FAs, mais nous avons souhaité incorporer ces trois études en annexes du manuscrit, car elles permettent d'illustrer l'apport et la puissance de la combinaison des approches lipidomiques et génétiques dans l'élucidation de la fonction in vivo des enzymes impliquées dans le métabolisme des lipides.**

Le groupe MES étudie la régulation et la biosynthèse d'antibiotique chez deux souches modèles phylogénétiquement proches, *S. coelicolor* et *S. lividans*. En particulier les liens entre les TGs de réserve (métabolisme primaire) et la production d'antibiotiques (métabolisme dit secondaire/spécialisé). Ces deux souches présentent des voies de biosynthèse similaires pour la production de trois antibiotiques (CDA (calcium-dependent antibiotic), RED (undecylprodigiosin) et ACT (actinorhodin)), mais les expriment différemment. Les capacités d'accumulation des TGs de ces deux souches sont également différentes. Pour mieux comprendre les différences de biosynthèse, le groupe MES mène des manipulations génétiques et des analyses « omique » comparatives de ces deux souches et de mutants dérivés. Les

analyses comparatives sont parfois réalisées par des laboratoires partenaires, comme dans le cas présent.

Cette collaboration a donné lieu à deux articles publiés dans le journal « Frontiers in microbiology » [24,26] et à un article publié dans le journal « Antibiotics » [25].

Les premières analyses ont été réalisées sur les souches sauvages de *S. coelicolor* et *S. lividans* pour appréhender les échantillons. Puis les analyses se sont étendues à des souches modifiées génétiquement ou soumises à différentes conditions de cultures. Dans l'étude [25] la souche *Streptomyces antibioticus* a également été étudiée.

Notre principal défi a été de caractériser par NPLC-HRMS certains lipides ou métabolites spécifiques de ces bactéries, jamais étudiés dans notre laboratoire.
C'est le cas des phosphatidylinositol mannosides (PIMs), famille de glycolipides présents dans la paroi cellulaire des actinobactéries.
C'est également le cas des ornithines lipides (OL), lipides membranaires sans phosphore répandus chez les eubactéries.
D'autre part, des métabolites tels que certains antibiotiques sont extraits lors de l'extraction de Folch et visibles sur les chromatogrammes. Ces métabolites ont donc été également caractérisés et leurs données exploitées. Les données NPLC-HRMS ont principalement servi à l'identification des lipides en vue des analyses NPLC-Corona-CAD® pour l'obtention de la distribution des lipides par classe.

Le choix des journaux n'a pas permis de présenter en détail le travail réalisé par spectrométrie de masse. Nous prévoyons de ce fait de publier ultérieurement cet aspect des travaux. Le but est de proposer une publication à mi-chemin entre une revue et un article, qui regrouperait l'ensemble des données NPLC-HRMS nécessaires pour l'exploration des extraits lipidiques des *Streptomyces*.

Dans l'article [24] la contribution de la lipidomique a été considérée comme équivalente à celles de la génétique et de la microbiologie. Cette égalité d'apport, s'est traduit par la position en 1er auteur exæquo des deux ingénieures de chaque équipe (Clara Lejeune et moi-même).

Dans les articles [25,26] notre niveau de contribution a été moins important, mais l'impact de nos données a été fondamental dans l'élucidation des processus métaboliques des souches étudiées.

Les trois articles sont présentés en Annexes V-VII.

ANNEXE V. IMPACT DE LA DISPONIBILITE DU PHOSPHATE SUR LA TENEUR EN LIPIDES MEMBRANAIRES DES SOUCHES MODELES, *STREPTOMYCES LIVIDANS* ET *STREPTOMYCES COELICOLOR*

1. Introduction

Dans la publication Lejeune et al. (2021) [24], nous avons étudié l'impact de la disponibilité du phosphate (Pi) sur la teneur en lipides membranaires des souches modèles *Streptomyces lividans* et *Streptomyces coelicolor*.

Chez les espèces *Streptomyces*, comme chez d'autres bactéries, les PLs de la membrane bactérienne constituent un réservoir majeur de phosphore. En condition de privation en phosphate, les bactéries développent diverses stratégies pour remplacer leurs PLs par des lipides sans phosphore afin de récupérer et d'économiser le phosphate [194]. Chez *Streptomyces*, ce sont principalement les ornithines lipides (OL) qui sont synthétisées. La synthèse nécessite deux étapes enzymatiques comme illustré sur la Figure 60, extraite de l'étude de Sandoval-Calderón, et al. (2017) [195].

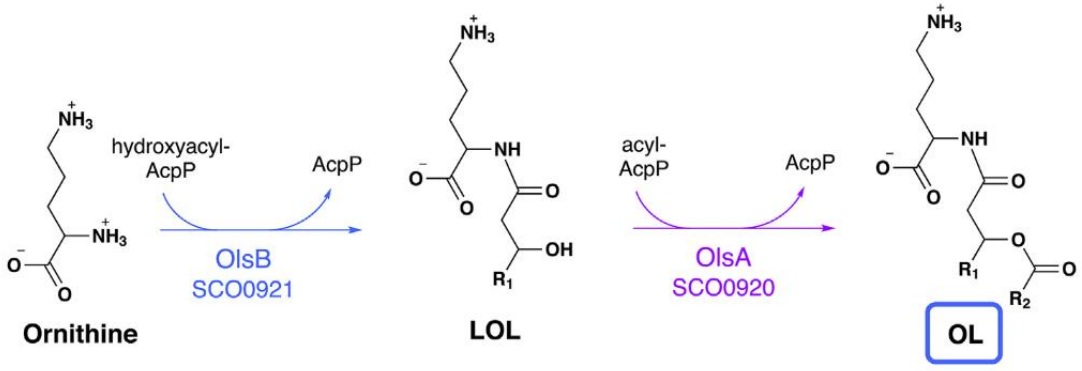

Figure 60: Biosynthèse des lipides d'ornithine (OL) chez *S. coelicolor* [195].

Sur la Figure 60, la participation de sco0921 à la synthèse d'OL en tant que N-acyltransférase a été vérifiée expérimentalement (indiquée en bleu), et l'activité de sco0920 en tant que O-acyltransférase est fortement étayée par des preuves bio-informatiques (indiquée en violet) – d'après la légende originale de la figure.

Le rôle des opérons sco0921 et sco0920 impliqués dans la synthèse des OLs a également été approfondi dans notre étude. Pour cela, ces opérons ont été tour à tour : délétés (Δ), délétés puis complémentés (compl) et sur-exprimés (over-expr).

2. Publication 5

frontiers in Microbiology

ORIGINAL RESEARCH
published: 22 February 2021
doi: 10.3389/fmicb.2021.623919

Impact of Phosphate Availability on Membrane Lipid Content of the Model Strains, *Streptomyces lividans* and *Streptomyces coelicolor*

Clara Lejeune[1†], Sonia Abreu[2†], Pierre Chaminade[2], Thierry Dulermo[1,3], Michelle David[1], Sebastiaan Werten[4] and Marie-Joelle Virolle[1*]

[1] CEA, CNRS, Institute for Integrative Biology of the Cell (I2BC), Université Paris-Saclay, Gif-sur-Yvette, France, [2] Lipides, Systèmes Analytiques et Biologiques, Université Paris-Saclay, Châtenay-Malabry, France, [3] Lesaffre International, Marcq-en-Baroeul, France, [4] Institute of Biological Chemistry, Biocenter, Medical University of Innsbruck, Innsbruck, Austria

In this issue we demonstrated that the phospholipid content of *Streptomyces lividans* varies greatly with Pi availability being was much lower in Pi limitation than in Pi proficiency whereas that of *Streptomyces coelicolor* varied little with Pi availability. In contrast the content in phosphate free ornithine lipids was enhanced in both strains in condition of phosphate limitation. Ornithine lipids biosynthesis starts with the *N*-acylation of ornithine to form lyso-ornithine that is then *O*-acylated to yield ornithine lipid. The operon *sco1222-23* was proposed to be involved in the conversion of specific amino acids into ornithine in condition of phosphate limitation whereas the *sco0921-20* operon encoding *N*- and *O*-acyltransferase, respectively, was shown to be involved in the biosynthesis of these lipids. The expression of these two operons was shown to be under the positive control of the two components system PhoR/PhoP and thus induced in phosphate limitation. The expression of *phoR/phoP* being weak in *S. coelicolor*, the poor expression of these operons resulted into a fivefold lower ornithine lipids content in this strain compared to *S. lividans*. In the deletion mutant of the *sco0921-20* operon of *S. lividans*, lyso-ornithine and ornithine lipids were barely detectable and TAG content was enhanced. The complementation of this mutant by the *sco0921-20* operon or by *sco0920* alone restored ornithine lipids and TAG content to wild type level and was correlated with a twofold increase in the cardiolipin content. This suggested that SCO0920 bears, besides its broad *O*-acyltransferase activity, an *N*-acyltransferase activity and this was confirmed by the detection of lyso-ornithine in this strain. In contrast, the complementation of the mutant by *sco0921* alone had no impact on ornithine lipids, TAG nor cardiolipin content but was correlated with a high lyso-ornithine content. This confirmed that SCO0921 is a strict *N*-acyltransferase. However, interestingly, the over-expression of the *sco0921-20* operon or of *sco0921* alone in *S. coelicolor*, led to an almost total disappearance of phosphatidylinositol that was correlated with an enhanced DAG and TAG content. This suggested that SCO0921 also acts as a phospholipase C, degrading phosphatidylinositol to indirectly supply of phosphate in condition of phosphate limitation.

Keywords: phospholipids, ornithine lipids, triacylglycerol, acyltransferase, hemolysin, phospholipase C, phosphatidylinositol, phosphate limitation

OPEN ACCESS

Edited by:
Hari S. Misra, Bhabha Atomic Research Centre (BARC), India

Reviewed by:
Stefano Donadio, Naicons Srl, Italy
Juan F. Martin, Universidad de León, Spain

****Correspondence:***
Marie-Joelle Virolle
marie-joelle.virolle@i2bc.paris-saclay.fr

[†] These authors have contributed equally to this work

Specialty section:
This article was submitted to Microbial Physiology and Metabolism, a section of the journal Frontiers in Microbiology

Received: *30 October 2020*
Accepted: *22 January 2021*
Published: *22 February 2021*

Citation:
Lejeune C, Abreu S, Chaminade P, Dulermo T, David M, Werten S and Virolle M-J (2021) Impact of Phosphate Availability on Membrane Lipid Content of the Model Strains, Streptomyces lividans and Streptomyces coelicolor. Front. Microbiol. 12:623919. doi: 10.3389/fmicb.2021.623919

INTRODUCTION

In *Streptomyces* species, as in other bacteria, the phospholipids of the bacterial membrane constitute a major phosphorus reservoir and, in condition of phosphate deprivation, bacteria have evolved various strategies to replace their phospholipids by phosphorus-free lipids in order to retrieve and save phosphate. Phosphorus-free lipids include glycolipids, amino lipids (ornithine, glycine, lysine, glutamine, serine…), sulfolipids, and betaine lipids (Benning et al., 1995; Geiger et al., 1999; Lewenza et al., 2011; Diercks et al., 2015; Sohlenkamp, 2016; Lev et al., 2019). In *Streptomyces*, the most common of these lipids are ornithine lipids (OL) whose synthesis requires two enzymatic steps (Sandoval-Calderón et al., 2015, 2017). The first step was proposed to be catalyzed by SCO0921 (OlsB), a supposedly very specific *N*-acyltransferase that transfers the first acyl chain onto the NH_2 group of ornithine to yield lyso-ornithine (Weissenmayer et al., 2002; Gao et al., 2004; Sandoval-Calderón et al., 2015; Sohlenkamp, 2016). Subsequently, the *O*-acyltransferase SCO0920 (OlsA) was proposed to transfer the second acyl chain onto the hydroxyl group of the acyl moiety of the lyso-ornithine lipid (LOL) to yield OL (Weissenmayer et al., 2002; Gao et al., 2004; Sandoval-Calderón et al., 2015; Sohlenkamp, 2016). In many *Streptomyces* species including *Streptomyces coelicolor* (*SC*) and *Streptomyces lividans* (*SL*), these two genes form an operon under the positive control of the two component system (TCS) PhoR/PhoP (Weissenmayer et al., 2002; Gao et al., 2004; Martín et al., 2012; Sandoval-Calderón et al., 2015).

Streptomyces coelicolor and *S. lividans* are phylogenetically very closely related model strains showing nonetheless very contrasted metabolic features (Esnault et al., 2017). *S. lividans* is a weak antibiotic producer characterized by a glycolytic metabolism promoting triacylglycerol (TAG) accumulation whereas *S. coelicolor* is a strong antibiotic producer characterized by an oxidative metabolism incompatible with TAG accumulation (Esnault et al., 2017). Recent studies indicate that these drastically different metabolic features are, at least in part, due to the weaker expression of the two components system PhoR/PhoP in *S. coelicolor* compared to *S. lividans* (Millan-Oropeza et al., 2020). This TCS governs the adaptation of the bacteria to low phosphate availability *via* the positive and negative control it exerts on phosphate and nitrogen assimilation, respectively (Martín et al., 2017). The consequences of low and high phosphate (Pi) availability on the lipid composition of the membranes of these two model strains was assessed and revealed that the phospholipids content was reduced in condition of Pi limitation in *S. lividans* whereas that of *S. coelicolor* varies little with phosphate availability. In contrast the OL content was enhanced in condition of Pi limitation in both strains. Ornithine biosynthesis was previously shown to involve the *sco0921-20* operon whose expression is under the positive control of PhoR/PhoP and thus induced in condition of phosphate limitation (Martín et al., 2012; Sandoval-Calderón et al., 2015) and our data confirmed this statement. Furthermore, we identified an operon (*sco1222-23*) encoding enzymes putatively involved in the conversion of arginine, proline and glutamate into ornithine in condition of phosphate limitation and we demonstrated that the expression of this operon was also under the positive control of PhoR/PhoP. At last, we assessed the consequences of deletion or over-expression of the *sco0921-20* operon on the lipidome of *S. lividans* and *S. coelicolor*. The complementation of the *sco0921-20* operon deletion mutants by an ectopic copy of this operon, or by *sco0920* or *sco0921* alone, gave clue of unexpected additional functions of these two enzymes.

MATERIALS AND METHODS

Bacterial Strains, Media and Culture Conditions

Bacteria strains used in this study were *S. lividans* TK24 (*SL*, Ruckert, 2015) and *S. coelicolor* M145 (*SC*, Bentley, 2002). These strains were grown on SFM medium (Kieser et al., 2000) to obtain spores. Modified R2YE agar medium (Kieser et al., 2000), devoided of sucrose and with no phosphate added (condition of phosphate limitation, 1 mM free phosphate final as determined by PiBlueTM test from BioAssay Systems) and supplemented with glucose 50 mM, was used for solid-grown cultures of these strains. 10^6 spores of each strain were plated on the surface of cellophane disks (Focus Packaging & Design Ltd, Louth, United Kingdom) laid down on the surface of R2YE agar medium and incubated at 28°C in darkness for 72 h. Mycelial lawns of each of the four replicate of the different strains were collected with a spatula, washed twice with deionized water, lyophilized and weighted.

Lipid Extraction and Characterization by LC/Corona-CAD and LC/MS

Lipid extraction was performed by a procedure derived from Folch's method (Folch et al., 1957) from four independent cultures of *Streptomyces antibioticus* DSM 41,481 and DSM 40,868. A defined volume (4.5 mL) of chloroform/methanol (1:2) was added to 10 mg of lyophilized *Streptomyces* mycelium and vortexed for 30 s. The mixture was left at ambient temperature for 1 h, then 1.25 mL of water was added, and the mixture was vortexed for 30 s. The mixture was then centrifuged (1000 × *g* for 10 min) to obtain phase separation. The lower organic phase was collected, and the upper aqueous phase was submitted to a second extraction by adding 2 mL of chloroform/methanol (85:15). The two organic phases were pooled and evaporated under a stream of nitrogen at room temperature. The dry residue was dissolved in 400 µL of isooctane/chloroform (4:1) before analysis. The chromatographic conditions have been described previously (Abreu et al., 2017). Briefly, lipid class analysis was performed with an Inertsil Silica (150 mm × 2.1 mm I.D, 5 µm) column (GL Sciences Inc., Tokyo, Japan) thermostated at 40°C. The HPLC instrumentation consisted of the system Dionex U-3000 RSLC (Thermofisher, Villebon, France). A quaternary solvent gradient was used to elute all the lipid classes present in the sample by increasing the order

of polarity. Lipid class identification was verified by coupling the chromatographic separation to mass spectrometry. MS analyses were performed with a LTQ-Orbitrap Velos Pro (Thermo Fisher Scientific) equipped with an APPI ion source. The MS2 and MS3 spectra were obtained in data-dependent acquisition (DDA) mode. Lipid detection was performed using a Corona-CAD system (ESA, Chelmsford, MA, United States) (Abreu et al., 2017); the signal was acquired with a Chromeleon data station (Thermo Fisher Scientific, Villebon-sur-Yvette, France). Corona-CAD is a universal detector used for liquid chromatography and described in Dixon and Peterson (2002). The differences in the composition of the lipid classes in the samples are expressed as peak areas. All the data were subjected to Anova test using R 3.3.2 (R Core Team, 2013) and the "multcompView" package (Graves et al., 2019). The results obtained are presented as the mean ± standard error; a p-value <0.05 was considered as statistically significant. The letters above the histograms indicate the significance of the differences. When two histograms bear two different letters that mean that they are statistically significantly different but when they show the same letter that means that they are not statistically significantly different ($p > 0,05$; Tukey-adjusted comparisons).

Due to their low amount in samples, LOL could not be detected by LC-Corona-CAD analysis. They had to be detected and quantified using LC/MS by extracting their specific mass from the total ion current. The peak areas of $[M\text{-}H]^-$ @m/z 371.3; 385.3; 399.3; 425.3 corresponding to C15:0, C16:0, C17:0, and C19:1 3-hydroxy fatty acids where summed up and shown in **Figure 4**.

RNA Preparation and qRT-PCR Experiments

RNA was isolated from mycelia obtained from *S. lividans* TK24 (*SL*), wild type, its *phoP* mutant and *S. coelicolor* M145 (*SC*) grown for 40 h at 28°C on the solid R2YE medium with no K_2HPO_4 added (containing 1 mM free phosphate from elements of the media as determined with PiBlue™ Phosphate Assay Kit from BioAssays Systems). In order to preserve RNA integrity, the mycelium was immediately freezed in liquid nitrogen in a solution containing denaturating guanidinium thiocyanate buffer RA1 (Macherey-Nagel, Hoerdt, France), phenol-chloroform and ß-mercaptoethanol (a reducing agent). The cells were then lysed and homogenized in the presence of glass beads (diameter < 106 µm) using a Fast-Prep apparatus (Savant Instruments). Total RNA was purified using the Nucleospin RNA Kit (Macherey-Nagel, Hoerdt, France), according to the manufacturer's instructions. To remove residual DNA, a DNAse TURBO™ treatment (Invitrogen) was performed at 37°C for one hour and total RNA was purified with the Nucleospin RNA Clean-Up kit (Macherey-Nagel, Hoerdt, France). The RNA concentrations were quantified using the Nanodrop 2000 spectrophotometer (Thermo Scientific). The integrity of the RNAs was verified using the Agilent 2100 bioanalyzer with the eukaryote total RNA 6000 Nano assay (Agilent Technologies). A total of 1 µg of total RNA was reverse transcribed in a 20 µL final reaction volume using the High Capacity cDNA Reverse Transcription Kit (Life Technologies) with RNase inhibitor and random primers following the manufacturer's instructions. Quantitative PCR was performed on a QuantStudio 12K Flex Real-Time PCR System (Life Technologies) with a SYBR green detection protocol. A total of 3 ng of cDNA were mixed with Fast SYBR Green Master Mix and 750 nM of each primer in a final volume of 10 µL. The reaction mixture was loaded on 384 well microplates and submitted to 40 cycles of PCR (95°C/20 sec; [95°C/1 s; 60°C/20 s] X40) followed by a fusion cycle to analyze the melting curve of the PCR products. A qPCR analysis in the absence of a reverse transcription step was performed on all RNA samples to check the absence of any DNA contamination. Primers were designed using the Primer-Blast tool from NCBI and the Primer Express 3.0 software (Life Technologies) (**Supplementary Table S1**). Specificity and the absence of multi-locus matching at the primer site were verified by BLAST analysis. The amplification efficiencies of primers were generated using the slopes of standard curves obtained by a 10-fold dilution series. Amplification specificity for each real-time PCR reaction was confirmed by analysis of the dissociation curves. Each sample measurement was made in duplicate and four independent RNA biological samples were prepared for each condition. Determined cycle threshold (Ct) values were then exploited for further analysis. Cycle threshold is defined as the calculated cycle number at which the PCR product crosses the threshold of detection. This value tells how many cycles it took to detect the signal from your samples. Seven most stable reference genes were selected by GenEx software (MultiD) and the geometric mean of the five most stable genes (Glk/SCO2126, AspS/SCO3795, GyrA/SCO3873, GyrB/SCO3874, and RpoB/SCO4654) was used to normalize the data (HrdB/SCO5820 and RecG/SCO5566 were excluded). The determination of the relative gene expression ratio was achieved using the ΔΔCt method using three biological replicates (Pfaffl, 2001). The values of ΔΔCt of *SC* and of the *phoP* mutant of *SL* were normalized and standardized by log transforming, mean centering and autoscaling (Willems et al., 2008). All data were subjected to the Student test and the results were presented as the mean of delta-delta-Ct with error bars representing 95% confidence interval.

Deletion and Over-Expression of the *sco0921-20* Operon or of *sco0920* or *sco0921* Alone in Wild Type and *sco0921-20* Deletion Mutants of *S. lividans* TK24 and *S. coelicolor* M145

All strains and plasmids used for these constructs are listed in **Supplementary Table S2**. DNA fragments were amplified by PCR from genomic DNA of *SL* and *SC* prepared as described previously (Sambrook and Russell, 2001), using primers listed in **Supplementary Table S3**. Primers used for PCR amplification and gene sequence analysis (Sci-Ed Software) were designed with Clone Manager Professional 9 software and purchased from IDT (Integrated DNA

Technologies, Leuven, France). PCR amplifications were performed in a Techne ^{3}Prime thermal cycler with Phusion High-Fidelity DNA polymerase (ThermoFisher Scientific, Illkirch Graffenstaden, France). PCR conditions were: 30 s at 98°C, then 10 s at 98°C for 30 cycles, followed by 30 s at 65°C then 6 min at 72°C. PCR fragments were purified with a NucleoSpin® PCR clean-up Gel extraction Kit (Macherey-Nagel, Hoerdt, France).

In order to delete the *sco0921-20* operon in *SL* and *SC*, approximately 1 kb DNA fragments flanking this operon were amplified by PCR from genomic DNA of *SL* and *SC* prepared as described previously (Sambrook and Russell, 2001). The resulting PCR fragments were digested with adequate restriction enzymes, *HindIII* and *XbaI* for upstream region, *EcoRI* and *BamHI* for downstream region, and the apramycin resistance cassette (apra^{R}, recovered from pW60 plasmid; Li et al., 1997) with *XbaI* and *EcoRI* restriction enzymes (ThermoFisher Scientific, Illkirch Graffenstaden, France). These three fragments were ligated into the plasmid pOSV400 (Boubakri et al., 2015) cut by the *HindIII* and *BamHI* sites, in presence of T4 DNA Ligase (5 U/μL, ThermoFisher Scientific, Illkirch Graffenstaden, France). The resulting plasmid was called pOSV400-UD-*sco0921-20-apra*^{R}.

In order to over-express the *sco0921-20* operon or *sco0920* or *sco0921* alone, the amplified PCR fragments were purified and digested with *HindIII* and *PstI* (ThermoFisher Scientific, Illkirch Graffenstaden, France) were ligated behind the constitutive promoter *ermE** (Siegl et al., 2013) into the plasmid pOSV557, a derivative of pOSV010 carrying the *ermE** promoter (Juguet et al., 2009). The resulting three plasmids were called pOSV557-*sco0921-20*, pOSV557-*sco0921*, and pOSV557-*sco0920*.

The latter as well as pOSV400-UD-*sco0921-20-apra*^{R} used for the deletion of the *sco0921-20* operon were transferred into competent *Escherichia coli* DH5α (Hanahan, 1983) by transformation using standard procedures (Kieser et al., 2000), purified and sequenced for structural verification. The plasmids were then transformed by electroporation into *E. coli* ET12567 pUZ8002 (Gust et al., 2004). The resulting *E. coli* ET12567 pUZ8002 strains were used to introduce the recombinant plasmids by conjugation into *SC* and *SL* using standard procedures (Kieser et al., 2000).

After 1 week of sporulation at 28°C, the ex-conjugants *sco0921-20* disruptive mutants, apramycin-resistant and hygromycin-sensitive, resulting from the transformation of pOSV400-UD-*sco0921-20-apra*^{R}, were spotted on the solid medium HT (Kieser et al., 2000) containing apramycin (30 μg mL^{-1}) and hygromycin (50 μg mL^{-1}). The replacement of the *sco0921-20* operon by apra^{R} cassette in the genome of the mutant strains was confirmed by PCR using primers shown in **Supplementary Table S3**.

Concerning the three constructions used for over-expression, the hygromycin-resistant ex-conjugants were selected on the solid medium HT (Kieser et al., 2000) containing hygromycin (50 μg mL^{-1}). The integration of the *sco0921-20* operon, of *sco0920* or of *sco0921* alone into the genome of the target strains was verified by PCR *via* amplification of the sequences surrounding the *attL* and *attR* sites using primers shown in **Supplementary Table S3**.

Assay of Extracellular Actinorhodin (ACT) Production

Extracellular actinorhodin (ACT) was quantified from four individual plates of each strain grown on the conditions described above. After 72 h of incubation, mycelia were scrapped off the cellophane disks of each plate with a spatula and lyophilized in order to assess their mass. The R2YE agar medium (Kieser et al., 2000) present below the surface of cellophane disks was cut into small pieces and allowed to diffuse in 10 mL water for 2 h at 4°C. The first eluate was transferred into a new tube, and 10 mL of water was added again to the agar medium and allowed to diffuse for 2 h at 4°C. The second eluate was pooled with the first eluate, and 10 mL of water was added again to the agar medium and allowed to diffuse for 1 h at 4°C. The last eluates were pooled to the other two (30 mL final). Three mL of HCl (3 M) were added to 6 mL of the final eluate. The mixture was incubated on ice for one night to allow ACT precipitation. Precipitated ACT was collected by centrifugation (13,000 *g* for 30 min). Supernatants were discarded and the ACT pellets were suspended in 1 mL of KOH 1 M. Optical density of the solution was determined at 640 nm in a Shimadzu UV-1800 spectrophotometer using KOH 1 M as blank (Kieser et al., 2000).

Protein Sequence Analysis

The Conserved Domain Database (Lu et al., 2020) was used to detect known functional domains. Alignment of SCO0921 with representative members of COG3176, a family of putative hemolysins, was performed with MAFFT (Katoh et al., 2019).

RESULTS

Impact of Phosphate Availability on the Lipidome of *S. lividans* and *S. coelicolor*

In order to assess the impact of phosphate availability on the lipid and fatty acid content of *SL* and *SC*, cultures of these strains grown for 72 h on solid R2YE limited or proficient in phosphate was analyzed by LC/Corona-CAD (Abreu et al., 2017). The results are shown in **Figure 1**.

In *S. lividans* (*SL*), the content in the phospholipids, phosphatidyl inositol (PI), phosphatidyl ethanolamine (PE) and cardiolipin (CL) was, respectively, 189, 8.8, and 2.4 fold higher in Pi proficiency than in Pi limitation. In contrast in *S. coelicolor* (*SC*) the content in PE and CL did not change with Pi availability whereas the PI content of *SC* was only 1.6 fold higher in Pi proficiency than in Pi limitation (versus 189 fold for *SL*). In Pi proficiency, PE, PI and CL were, respectively, 2.3, 2, and 1.1 fold more abundant in *SL* than in *SC* (**Figures 1c** and **d**). In Pi limitation, PI, PE and CL were, respectively, 53.5, 3.1, and 1.8 fold more abundant in *SC* than in *SL*. These data thus revealed a default of PL biosynthesis in *SC* even in Pi proficiency. This might be due to reduced Pi availability in *SC* linked to the weak expression of the genes of the Pho regulon involved in Pi supply in this strain (Millan-Oropeza et al., 2020). Furthermore, the 189 fold lower PI content of *SL* in condition of Pi limitation compared to Pi proficiency suggested that this very low PI content did not

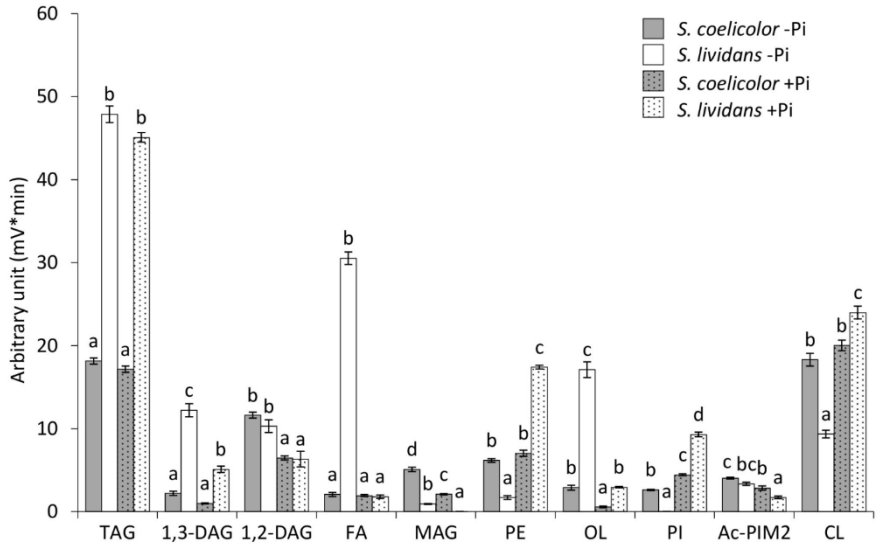

FIGURE 1 | LC/Corona-CAD analysis of the total lipid content of *S. lividans* TK24 (white histograms) and *S. coelicolor* M145 (gray histograms) grown for 72 h at 28°C on solid R2YE medium with glucose (50 mM) as the main carbon source and containing either 1 mM (Pi limitation, plain histograms) or 5 mM phosphate (Pi proficiency, dotted histograms).TAG, triacylglycerol; DAG, diacylglycerol (1,2 or 1,3); FA, fatty acids; MAG, monoacylglycerol; PE, phosphatidylethanolamine; OL, ornithine lipids; PI, phosphatidylinositol; Ac-PIM2, acetylated phosphatidylinositol mannoside 2; CL, cardiolipid. Means values are shown as histograms with error bars representing standard error. Means sharing a letter are not significantly different ($P > 0.05$; Tukey-adjusted comparisons).

rely exclusively on reduced synthesis but also onto enhanced degradation of this specific phospholipid. The 53.5 higher PI content of *SC* compared to *SL* in Pi limitation suggested that the putative degradation of this specific phospholipid might be dependent of PhoR/PhoP that is known to be weakly expressed in *SC* (Millan-Oropeza et al., 2020). We will see later in the manuscript that SCO0921 might be involved in this process.

The higher PL content of *SL* in condition of Pi proficiency was accompanied by lower content of all biosynthetic intermediates FA (14.8 fold), MAG (22.1 fold), 1,2-DAG (1.7 fold), and 1,3-DAG (1.8 fold) in Pi proficiency than in Pi limitation. In *SC*, the content in MAG and DAG was also lower in Pi proficiency than in Pi limitation whereas that of the FA was similar in both Pi conditions. In Pi limitation, the FA content of *SL* was much higher (12.9 fold) than that of *SC*. This is consistent with the glycolytic (acetylCoA generating) versus oxidative (acetylCoA consuming) metabolism of *SL* and *SC*, respectively (Esnault et al., 2017). Furthermore, the abundance of free FA in *SL* in condition of Pi limitation, compared to the condition of Pi proficiency, might indicate insufficient glycerol 3P generation in Pi limitation as suggested by Millan-Oropeza et al. (2020) as well as too low Pi availability for PL biosynthesis. The MAG content was 4.8 and 50.3 fold higher in *SC* than in *SL* in Pi limitation and proficiency, respectively, whereas in contrast the 1,3-DAG content of *SC* was 4.6 and 4.4 fold lower than that of *SL* in Pi limitation and proficiency, respectively. This higher abundance of MAG in *SC* compared to *SL* in Pi proficiency, that is correlated with a lower abundance of 1,3 DAG, might be related to the inability of *SC* to synthetize PL in this condition. All biosynthetic intermediates MAG, 1,2-DAG and 1,3-DAG, were less abundant in Pi proficiency than in Pi limitation in both strains but these differences were stronger in *SL* than in *SC*. These differences might also be due to more active PL synthesis in Pi proficiency than in Pi limitation in *SL* compared to *SC*.

The OL content of *SL* was 5.1 and 4.3 fold higher than that of *SC* in Pi limitation and proficiency, respectively. This is consistent with the PhoR/PhoP dependent induction of OL biosynthesis (Sandoval-Calderón et al., 2015). Since PhoR/PhoP is known to be weakly expressed in *SC* (Millan-Oropeza et al., 2020), induction of OL synthesis is not as strong in *SC* as in *SL* and thus results in a lower OL content in *SC* than in *SL*. However, OL synthesis remains inducible in condition of Pi limitation in *SC* since OL content was 3.9 fold higher in Pi limitation than in Pi proficiency in *SC* (versus 5.3 in *SL*).

The TAG content was 2.5 fold higher in *SL* than in *SC* in both Pi conditions confirming the previously reported higher ability of *SL* to store TAG compared to *SC* (Esnault et al., 2017). This is consistent with the glycolytic (acetylCoA generating) versus oxidative (acetylCoA consuming) metabolism of *SL* and *SC*, respectively (Esnault et al., 2017). However, unexpectedly the TAG content of the strains did not vary with Pi availability.

Altogether our data indicated that *SC* had a lower phospholipid and TAG content than *SL* and that its lipid content varies little with Pi availability, in contrast to *SL*. This is thought to be due to the previously reported oxidative metabolism of this strain that consumes acetylCoA (Esnault et al., 2017) as well as to its severe phosphate limitation linked to the weak expression of the TCS PhoR/PhoP in this strain (Millan-Oropeza et al., 2020). Interestingly this study revealed that the phosphatidylinositol (PI) is the phospholipid bearing

the greatest variation of content between the two strains and between the two Pi conditions. This suggested that this specific phospholipid might constitute a phosphate reserve.

The *sco921-20* and *sco1222-23* Operons Are Involved in Ornithine Lipids Biosynthesis and Their Expression Is Under the Positive Control of PhoR/PhoP

Ornithine lipids are phosphate free lipids synthesized in condition of phosphate limitation to surrogate a fraction of phospholipids, in order to save phosphate (Martín et al., 2012; Sandoval-Calderón et al., 2015). In *Streptomyces*, their biosynthesis is known to rely on the expression of the *sco0921-20* operon (Sandoval-Calderón et al., 2015) proposed to encode *N*- and *O*-acyltransferase, respectively. The expression of this operon was shown to be under the positive control the TCS PhoR/PhoP in *S. coelicolor* (Martín et al., 2012; Sandoval-Calderón et al., 2015) as was the expression of related operons in other bacteria (Benning et al., 1995; Geiger et al., 1999; Barbosa et al., 2018; Lev et al., 2019) and our data confirmed this statement. However, since OL biosynthesis also requires ornithine availability, we search and identified in our *S. lividans* and *S. coelicolor* proteomic data, an operon, *sco1222-23*, encoding proteins, putatively involved in the conversion of specific amino acids (Arg, Pro, and Glu) into ornithine, whose expression was much lower in *S. coelicolor* than in *S. lividans* (Millan-Oropeza et al., 2020). This suggested that the expression of this operon was under the positive control of PhoR/PhoP and we confirmed that it was indeed the case (**Figure 2A**). *sco1223* encodes a ornithine aminotransferase, related to RocD of *Bacillis subtilis*, involved in the conversion of pyrroline-5-carboxylate, originating from glutamate or proline degradation, into ornithine. *sco1222* encodes a protein of the aminohydrolase family that is possibly involved into the degradation of arginine into ornithine. The expression of the first gene of the operon,

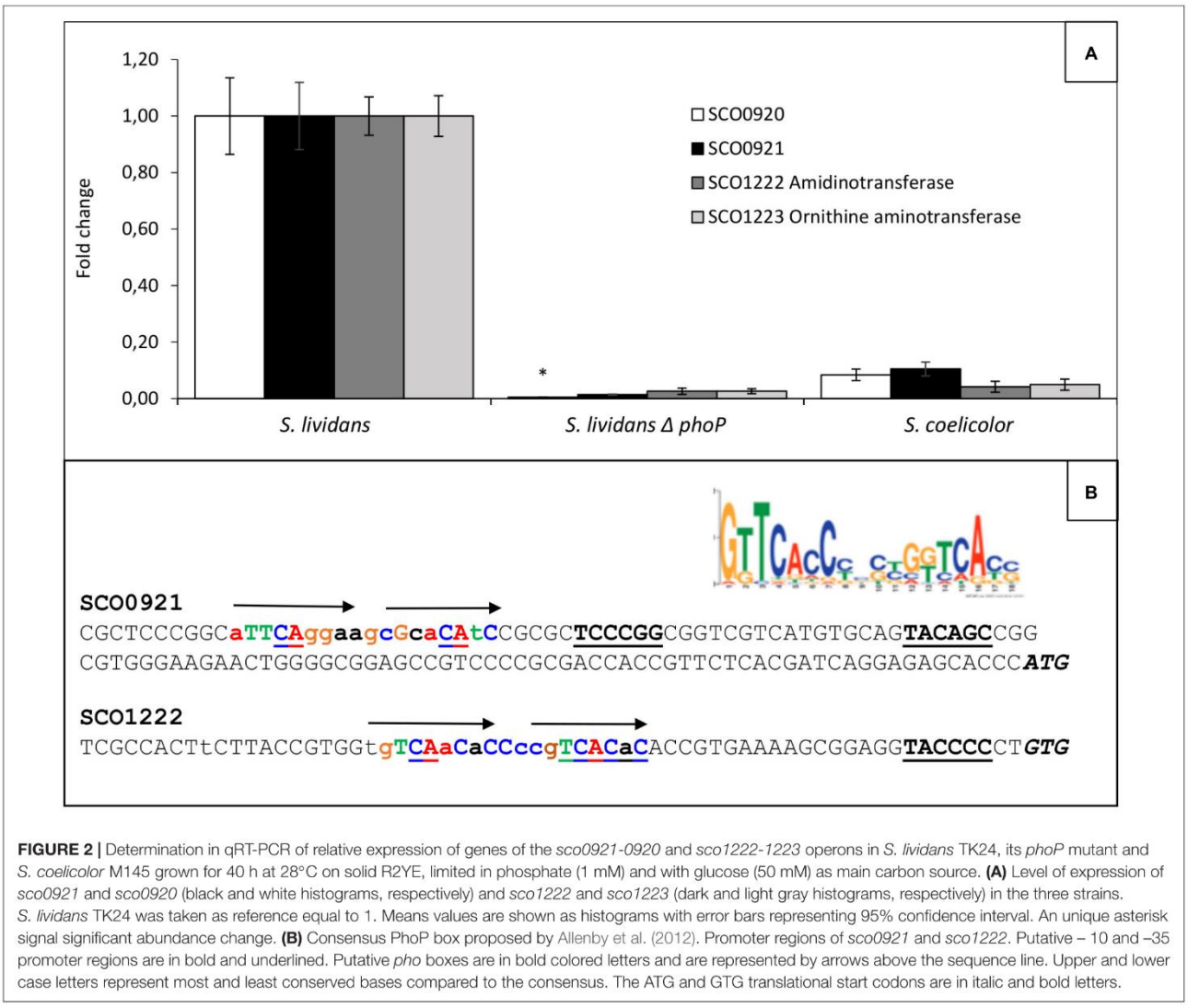

FIGURE 2 | Determination in qRT-PCR of relative expression of genes of the *sco0921-0920* and *sco1222-1223* operons in *S. lividans* TK24, its *phoP* mutant and *S. coelicolor* M145 grown for 40 h at 28°C on solid R2YE, limited in phosphate (1 mM) and with glucose (50 mM) as main carbon source. **(A)** Level of expression of *sco0921* and *sco0920* (black and white histograms, respectively) and *sco1222* and *sco1223* (dark and light gray histograms, respectively) in the three strains. *S. lividans* TK24 was taken as reference equal to 1. Means values are shown as histograms with error bars representing 95% confidence interval. An unique asterisk signal significant abundance change. **(B)** Consensus PhoP box proposed by Allenby et al. (2012). Promoter regions of *sco0921* and *sco1222*. Putative – 10 and –35 promoter regions are in bold and underlined. Putative *pho* boxes are in bold colored letters and are represented by arrows above the sequence line. Upper and lower case letters represent most and least conserved bases compared to the consensus. The ATG and GTG translational start codons are in italic and bold letters.

sco1222, was reported to be stimulated by arginine, independently on the presence of the ArgR regulator (Pérez-Redondo et al., 2012). The induction of the expression of this operon by arginine might thus be mediated by SCO1221, a regulator of the AsnC-familly encoded by a gene located just upstream this operon. Putative Pho boxes were detected in the promoter region of the first genes of these two operons and are shown in **Figure 2B**. The expression of PhoR/PhoP being weak in *SC*

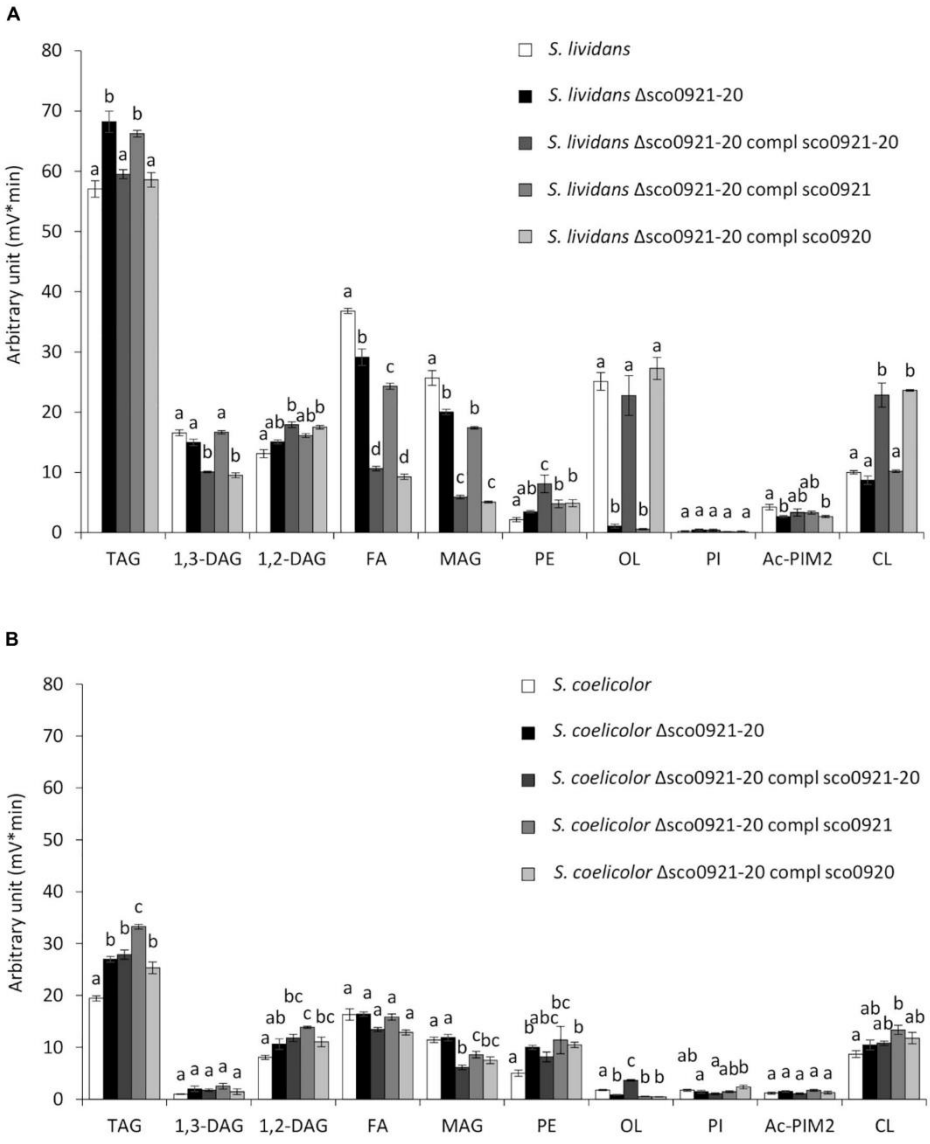

FIGURE 3 | LC/Corona-CAD analysis of the total lipid content of the *wt* strains of *S. lividans* TK24 and *S. coelicolor* M145 and of derivatives of these strains deleted for the *sco0921-20* operon et complemented by the *sco0921-20* operon or *sco0921* or *sco0920* alone whose expression was put under the control of the strong *ermE** promoter. Strains were grown for 72 h at 28°C on solid R2YE medium with glucose (50 mM) as the main carbon source and containing 1 mM phosphate (Pi limitation). **(A)** LC/Corona-CAD analysis of the total lipid content of *S. lividans* TK24 (white histograms), *S. lividans* TK24 deleted for the *sco0921-20* operon (black histograms), *S. lividans* TK24 deleted for the *sco0921-20* operon complemented by the *sco0921-20* operon (dark gray histograms), *S. lividans* TK24 deleted for the *sco0921-20* operon complemented by *sco0921* (medium gray histograms) and *S. lividans* TK24 deleted for the *sco0921-20* operon complemented by *sco0920* (light gray histograms). **(B)** LC/Corona-CAD analysis of the total lipid content of *S. coelicolor* M145 (white histograms), *S. coelicolor* M145 deleted for the *sco0921-20* operon (black histograms), *S. coelicolor* M145 deleted for the *sco0921-20* operon complemented by the *sco0921-20* operon (dark gray histograms), *S. coelicolor* M145 deleted for the *sco0921-20* operon complemented by *sco0921* (medium gray histograms) and *S. coelicolor* M145 deleted for the *sco0921-20* operon complemented by *sco0920* (light gray histograms). TAG, triacylglycerol; DAG, diacylglycerol (1,2 or 1,3); FA, fatty acids; MAG, monoacylglycerol; PE, phosphatidylethanolamine; OL, ornithine lipids; PI, phosphatidylinositol; Ac-PIM2, acetylated phosphatidylinositol mannoside 2; CL, cardiolipid. Means values are shown as histograms with error bars representing standard error. Means sharing a letter are not significantly different ($P > 0.05$; Tukey-adjusted comparisons).

compared to *SL* (Millan-Oropeza et al., 2020), the expression of these two operons is also weak in *SC* explaining the 5.1 fold lower OL content of this strain compared to *SL*, in phosphate limitation (**Figure 1c**).

Impact of the Deletion of the *sco0921-20* Operon and Its Complementation by the *sco921-20* Operon, *sco0921* or *sco0920* Alone on the Lipidome of *S. lividans* and *S. coelicolor*

The *sco0921-20* operon was deleted in *SL* and *SC* and the deletion mutants were complemented by a unique ectopic copy of the *sco0921-20* operon, or by *sco0920* or *sco0921* alone. The expression of these genes was put under the control of the strong *ermE** promoter (Siegl et al., 2013) and inserted at a unique position in the genome of the deletion mutant at the pSAM2 attB integration site (Boccard et al., 1989).

In *SL* grown in condition of Pi limitation, the deletion of the *sco0921-20* operon resulted in a 16.8 fold reduction of the OL content (**Figure 3A**). The reduction in OL content was correlated with a slightly higher TAG (1.1 fold) content accompanied by slightly lower content in biosynthetic intermediates such FA (1.2 fold) and MAG (1.2 fold) compared to the original strain (**Figure 3A**). This suggested that in absence of OL synthesis, acyl chains (FA) usually used for OL synthesis are being transferred by acyltransferases present in the bacteria, onto glycerol3P, MAG or DAG to synthesize TAG. The complementation of this mutant by the *sco0921-20* operon restored OL and TAG content to WT level but was also correlated with a significant increase in PE (1.8 fold) and CL (2.2 fold) content compared to the deletion mutant. This was accompanied by a lower content in the biosynthetic intermediates, FA (2.5 fold), MAG (3.2 fold), and 1,3-DAG (1.4 fold) (**Figure 3A**). Interestingly, the complementation of the deletion mutant by *sco0920* alone gave a lipid profile similar (except for PE) to that obtained with the complementation with the operon. In contrast, the complementation of the deletion mutant with *sco0921* alone of the deletion mutant had no impact on its PE, CL, TAG, 1,3-DAG, 1,2-DAG and MAG content (**Figure 3A**). Only a slight decrease in the FA content of this strain was noticed compared to the deletion mutant. These results unexpectedly suggested that SCO0920 might have both a *N*- and a broad *O*-acyltransferase activity and was able to transfer acyl chains to ornithine to synthetize lyso-ornithine (*N* acylation) as well as to achieve the *O*-acylation of lyso-ornithine and of other backbones such as precursors of cardiolipin.

In order to confirm this hypothesis lyso-ornithine was assayed in our strains by LC/MS (**Figure 4**). This study confirmed that LOL were detected in the *wt* strain but not in the *sco0921-20* deletion mutant whereas LOL were indeed detected in the mutant strain complemented by *sco0920* as well as by *sco0921*.This confirmed that SCO0920 bears *N*-acyltransferase activity besides its broad *O*-acyltransferase activity. The 2.3 lower LOL content of the mutant strain complemented by *sco0920* compared to that complemented by *sco0921* could be interpreted as the rapid conversion of LOL into OL by the *O*-acyltransferase function of *sco0920*. The presence of LOL in the mutant strain complemented by *sco0921* but the absence of OL in this strain confirmed that SCO0921 is a strict *N*-acyltransferase and has no *O*-acyltransferase function. The 11 fold lower LOL content of the mutant strain complemented by the *sco0921-20* operon compared to the *wt* strain might seem surprising (**Figure 4**). In

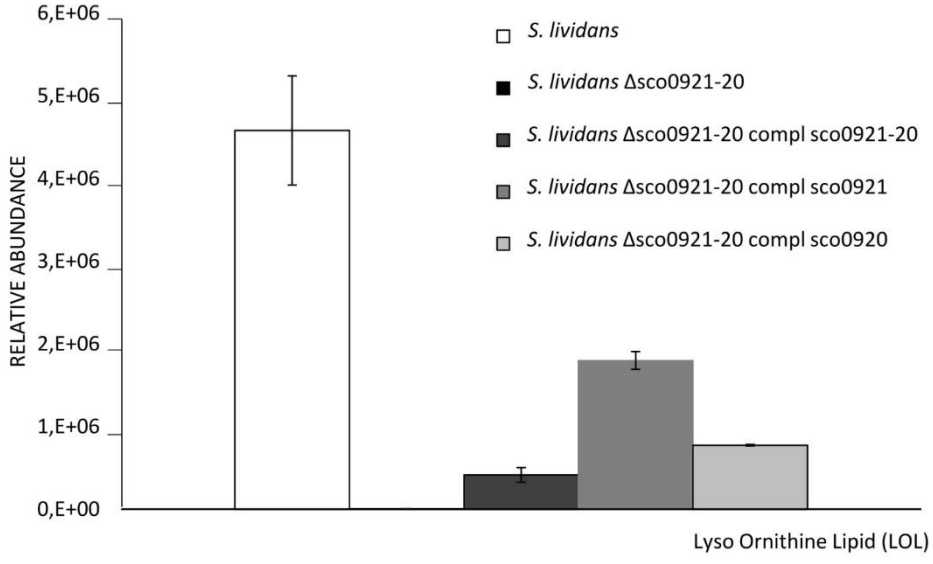

FIGURE 4 | Mass spec analysis of the total lyso ornithine content of *S. lividans* TK24 *wt* (white histograms), *S. lividans* TK24 deleted for the *sco0921-20* operon (black histograms invisible) and this deletion mutant complemented by the *sco0921-20* operon (dark gray histograms), *sco0921* alone (medium gray histograms) or *sco0920* alone (light gray histograms). Strains were grown for 72 h at 28°C on solid R2YE medium with glucose (50 mM) as the main carbon source and containing 1 mM phosphate (Pi limitation). Means values are shown as histograms with error bars representing standard error.

the *wt* strain the operon is expressed from its own regulated promoter whereas in the complemented mutant strain the operon is present at an ectopic position and its expression is under the control of the strong *ermE** promoter. We thus hypothesized that in the *wt* strain the level of expression of the first gene of the operon, *sco0921*, would be higher than that of the second one, *sco0920*. Consequently, in the *wt* strain the conversion of LOL into OL would be slowed down leading to LOL accumulation. In the complemented mutant both genes would be expressed at a high level from the strong *ermE** promoter, facilitating the rapid conversion of LOL into OL.

In *SC*, the deletion of the *sco0921-20* operon was correlated with a reduced content (1.8 fold) of the weak OL content of the strain and with higher TAG (1.3 fold) and PE (1.7 fold) content

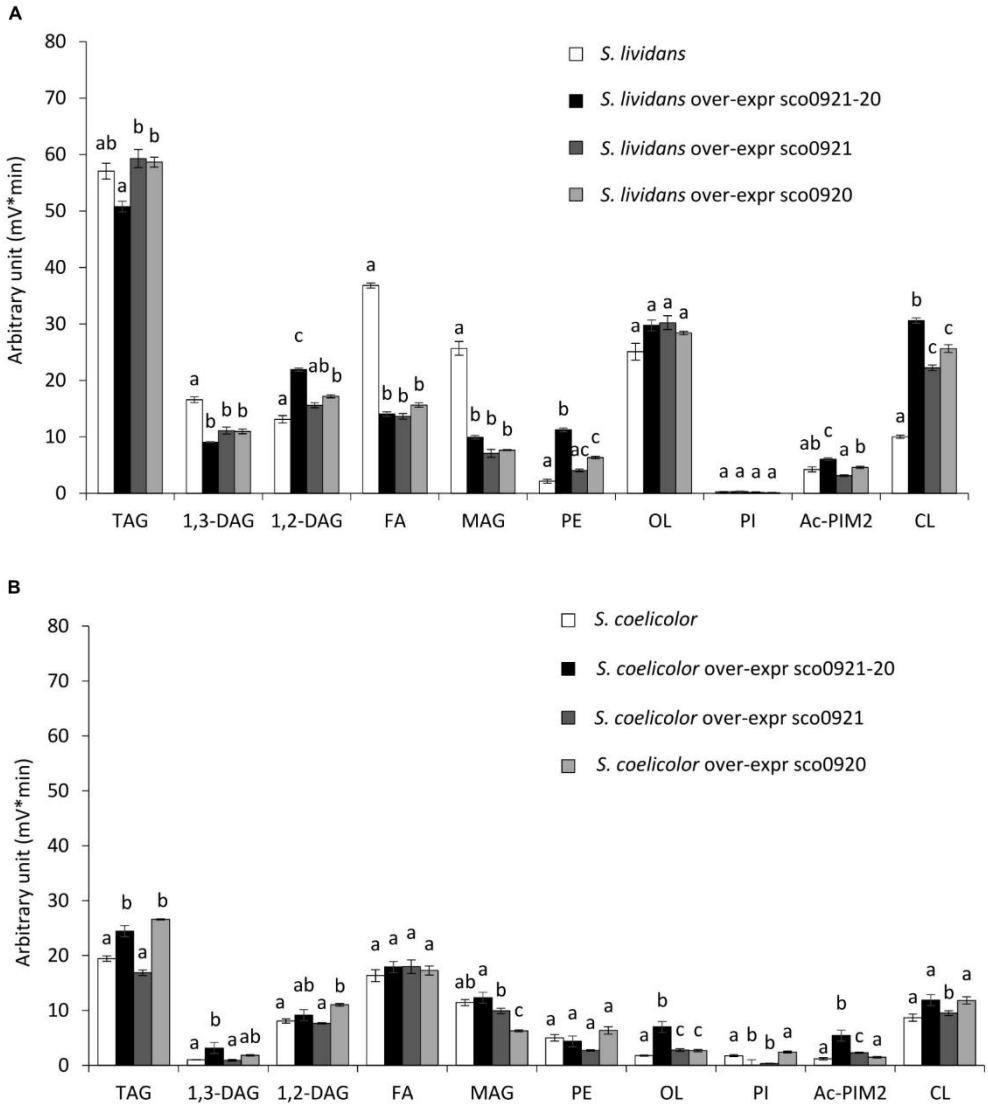

FIGURE 5 | LC/Corona-CAD analysis of the total lipid content of *wt* strains *S. lividans* TK24 and *S. coelicolor* M145 and of these strains over-expressing under the control of the strong *ermE** promoter, the *sco0921-20* operon or *sco0921* or *sco0920* alone. The strains were grown for 72 h at 28°C on solid R2YE medium with glucose (50 mM) as the main carbon source and containing 1mM phosphate (Pi limitation). **(A)** LC/Corona-CAD analysis of total lipid content of *S. lividans* TK24 (white histograms), *S. lividans* TK24 over-expressing the *sco0921-20* operon (black histograms), *S. lividans* TK24 over-expressing *sco0921* (dark gray histograms) and *S. lividans* TK24 over-expressing *sco0920* (light gray histograms). **(B)** LC/Corona-CAD analysis of the total lipid content of *S. coelicolor* M145 (white histograms), *S. coelicolor* M145 over-expressing the *sco0921-20* operon (black histograms), *S. coelicolor* M145 containing an extra copy of *sco0921* (dark gray histograms) and *S. coelicolor* M145 containing an extra copy of *sco0920* (light gray histograms). TAG, triacylglycerol; DAG, diacylglycerol (1,2 or 1,3); FA, fatty acids; MAG, monoacylglycerol; PE, phosphatidylethanolamine; OL, ornithine lipids; PI, phosphatidylinositol; Ac-PIM2, acetylated phosphatidylinositol mannoside 2; CL, cardiolipid. Means values are shown as histograms with error bars representing standard error. Means sharing a letter are not significantly different ($P > 0.05$; Tukey-adjusted comparisons).

(**Figure 3B**). This suggested that acyl chains not used for OL synthesis are being used for the biosynthesis of other lipids (TAG and PE) in this strain as in *SL*. This mutant was complemented by a unique ectopic copy of the *sco0921-20* operon, or of *sco0920* or of *sco0921* alone. The complementation of the deletion mutant by the *sco0921-20* operon was correlated with a 3.7 fold increase in the OL content. In contrast to what was seen for *SL*, the complementation of the *SC* deletion mutant with *sco0920* alone had no impact on the OL content. This might be due to the fact that the OL content of the deletion mutant of *SC* (**Figure 3B**) is very weak and its quantification is thus somehow unreliable being too close of the detection limit. The complementation of the *SC* deletion mutant with *sco0921* alone was not correlated either with an increase in the OL content but was correlated with a slight increase in 1,2-DAG (1.2 fold) and TAG (1.2 fold) content and a decrease in MAG content (1.2 fold) compared to the deletion mutant.

Impact of the Over-Expression of the *sco0921-20* Operon, of *sco0921* or of *sco0920* on the Lipidome of *S. lividans* and *S. coelicolor*

An extra copy of the *sco0921-20* operon or of *sco0921* or of *sco0920* alone expressed under the control of the *ermE** promoter (Siegl et al., 2013) was introduced at an ectopic position at the pSAM2 attB integration site (Boccard et al., 1989) in the genome of *S. lividans* and *S. coelicolor*. These two strains still have a native copy of this operon under the control of its own promoter but in *S. coelicolor* this native copy was shown to be weakly expressed (**Figure 2A**) so that is mainly the impact of the ectopic copies of these genes that is seen in this strain.

In *SC*, the over-expression of the *sco0921-20* operon led to an almost total disappearance of PI that was accompanied by a slight increase in the TAG (1.2 fold), 1,3-DAG (2.9 fold), OL (3.6 fold), and Ac-PIM2 content (3.7 fold) compared to the original strain (**Figure 5B**). The over-expression of *sco0921* alone was also correlated with a strong reduction (4.1 fold) in the PI content that, in contrast with the over-expression of the operon, was not correlated with an increase in the TAG nor 1,3-DAG content but was correlated with a slightly higher content in OL (1.4 fold) and Ac-PIM2 (1.6 fold) content. This suggested that SCO0921 might be responsible for the disappearance of PI. Since SCO0921 bears similarities with hemolysins (**Figure 6**) and hemolysins often bears phospholipase C activity (Maheswaran and Lindorfer, 1967; Pal et al., 1997), we propose that SCO0921 hydrolyzes PI into 1,2-DAG and inositol P. This specific lipid would thus somehow constitute a phosphorus reserve. The over-expression of *sco0920* alone was correlated with a clear increase in TAG (1.3 fold) and 1,2-DAG (1.3 fold) content and a decrease in MAG content (1.7 fold). This confirmed the O-acyltransferase function of this enzyme that otherwise had no impact on the PI content.

In *SL*, the presence of an extra ectopic copy of the *sco0921-20* operon led to an increase in CL (2.9 fold), PE (4.4 fold), Ac-PIM2 (1.2 fold), and 1,2-DAG (1.6 fold) content that was correlated with a decrease in FA (2.5 fold), MAG (2.4 fold),

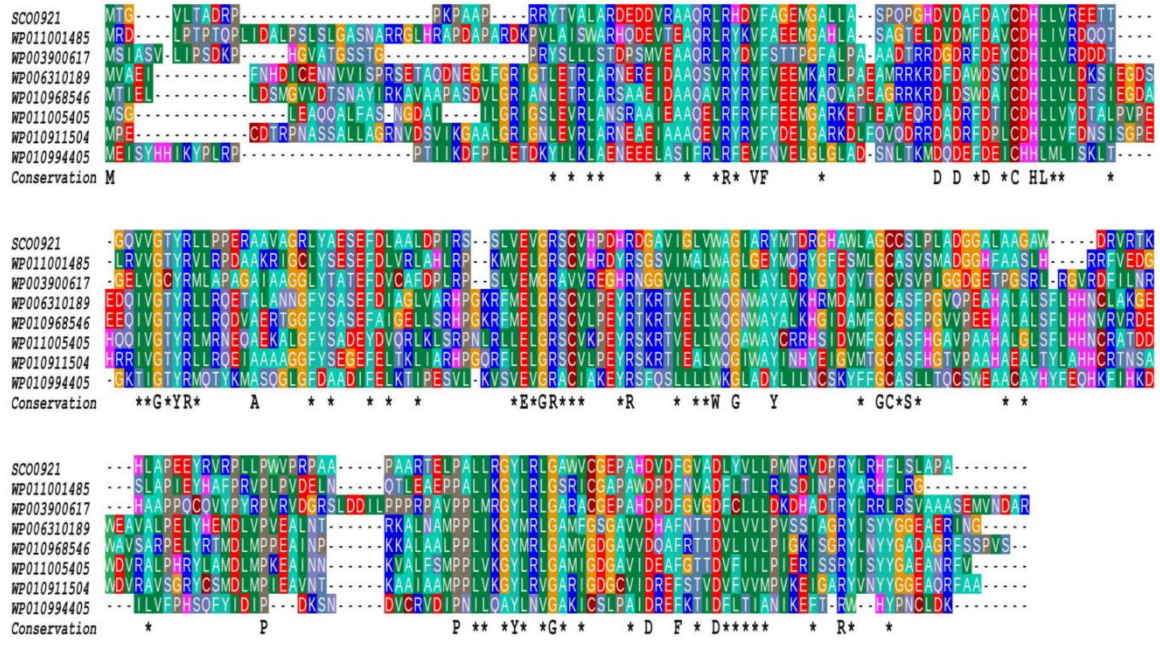

FIGURE 6 | Multiple sequence alignment of SCO0921 with representative members of COG3176, a Conserved Domain Database (CDD) family of putative hemolysins (Lu et al., 2020). The proteins aligned originate from Ralstonia (WP011001485), Mycobacterium tuberculosis (WP003900617), Agrobacterium (WP006310189, Rhizobiales (WP010968546), Brucella (WP011005405), Mesorhizobium (WP010911504), and Nostocaceae (WP010994405).The amino acids identical in all aligned sequences are indicated by a one letter code under the alignment whereas asterisks indicate conserved similarities.

and 1,3-DAG (1.8 fold) content compared to the original strain (**Figure 5A**). The presence of an extra ectopic copy of *sco0920* alone led to an increase in CL (2.4 fold), PE (2.4 fold), and 1,2-DAG (1.2 fold) content that was correlated with a decrease in FA (2.3 fold), MAG (3.2 fold), and 1,3-DAG (1.4 fold) content (**Figure 5A**). The presence of an extra ectopic copy of *sco0921* alone was correlated with an increase in CL (2.1 fold) content and a decrease in FA (2.6 fold), MAG (3.1 fold), and 1,3-DAG (1.4 fold) content (**Figure 5A**). One notices the three *S. lividans* strains over-expressing the *sco0921-20* operon, *sco0921* or *sco0920* alone showed similar trends. The native operon being highly expressed in this strain, the absence of one or the other function in the strains containing an extra ectopic copy of *sco0920* or *sco0921* is automatically compensated by the copy present in the native operon.

Impact of the Over-Expression of the *sco0921-20* Operon or of *sco0921* or *sco0920* Alone on Actinorhoddin Production in *S. coelicolor*

In Sandoval-Calderón et al. (2015), the authors mentioned that the disruption of *sco0921* by a transposon led to an early and enhanced ACT biosynthesis. The complementation of this mutant by the whole operon restored ACT production to wild type level but the authors did not provide any explanation for this interesting observation. We think that this observation is fully consistent with our hypothesis that SCO0921 acts as a phospholipase C involved in the cleavage of PI into inositol P and DAG. Inositol P would be dephosphorylated by broad specificity phosphatases induced in condition of phosphate limitation to provide phosphate. This Pi supply might be responsible for the observed repression of ACT biosynthesis. To verify this hypothesis, the *sco0921-20* operon, *sco0921* or *sco0920* alone, expressed from the strong *ermE** operon, were introduced into the native strain of *SC* and extracellular ACT production of these strains was assayed. Results shown in **Figure 7** indicated that the over-expression of the *sco0921-20* operon or of *sco0921* alone was correlated with a reduction of ACT biosynthesis compared to the wild strain whereas the over-expression of *sco0920* alone had no impact on ACT production. We proposed that the negative impact that *sco0921* over-expression has on ACT production might be due to its phospholipase C-like activity that indirectly allows the liberation of the Pi trapped into PI.

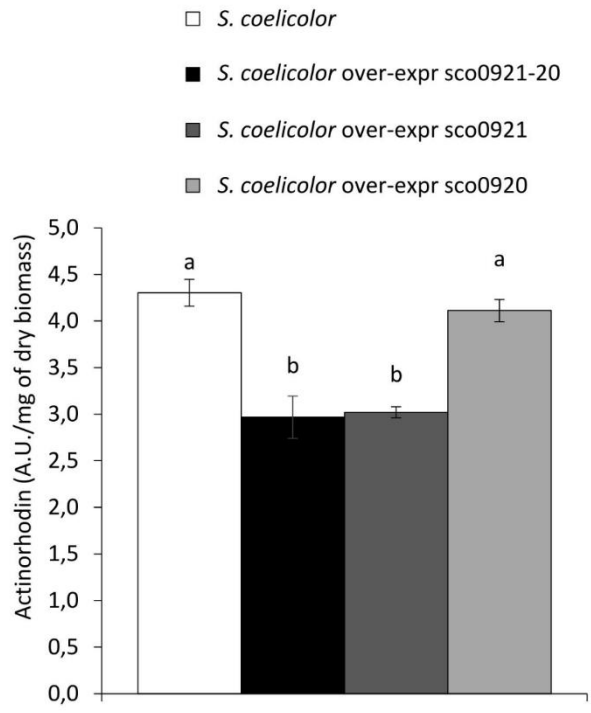

FIGURE 7 | Quantification of the extracellular actinorhodin in the culture medium of *S. coelicolor* (white histograms), *S. coelicolor* over-expressing the *sco0921-20* operon (black histograms), or *sco0921* (dark gray histograms) or *sco0920* (light gray histograms) alone. The strains were grown for 72 h at 28°C on solid agar modified R2YE medium with no phosphate added (conditions of phosphate limitation). Means values are shown as histograms with error bars representing standard error. Means sharing a letter are not significantly different ($P > 0.05$; Tukey-adjusted comparisons).

DISCUSSION

In this issue we demonstrated that in condition of phosphate (Pi) proficiency the phospholipid (PE, CL, and PI) content of *S. coelicolor* (*SC*) was lower than that of *S. lividans* (*SL*) and varied little with Pi availability. In contrast, the phospholipid content of *SL* varies greatly with Pi availability being was much lower in Pi limitation than in Pi proficiency. The limited variation of the phospholipid (PL) content in *SC* according to Pi availability might be due its characteristic oxidative metabolism that is known to consume acetylCoA and thus reduces acetylCoA availability (Esnault et al., 2017). It might also be due to the weak expression of the high (*pstSCAB*) and low (*sco4138/pitH2*) affinity phosphate transporters in this strain (Santos-Beneit et al., 2008) that is under the positive control of PhoR/PhoP that is poorly expressed in *SC* (Millan-Oropeza et al., 2020). The poor expression of these transporters in *SC* likely leads to a severe phosphate limitation.

In contrast the content in the phosphate-free OL of both strains increased in condition of Pi limitation. We demonstrated that the biosynthesis of OL requires mainly SCO0920, an enzyme encoded by the second gene of the *sco0921-20* operon. SCO0920 was shown to bear both *N*- and *O*-acyltransferase activities being thus more similar to OlsF of *Serratia proteamaculans*, *Vibrio cholerae*, and *Klebsiella pneumoniae* that also bears both *N*- and *O*-acyltransferase function (Vences-Guzmán et al., 2015; Barbosa et al., 2018; MetaCyc olsF, 2020) than to OlsA, a specific *O*-acyltransferase (Weissenmayer et al., 2002; Gao et al., 2004; Sandoval-Calderón et al., 2015; Sohlenkamp, 2016). Furthermore, our data indicated that SCO0920 is an *O*-acyltransferase with a broad substrate specificity since it is able to transfer acyl chains onto various backbones, besides LOL, such as precursors of TAG, PE, or CL.

Our experiments confirmed the previously reported strict *N*-acyltransferase activity of SCO0921 (Sandoval-Calderón et al., 2015) since the complementation the *sco0921-20* deletion

mutant by *sco0921* alone yielded LOL but not OL. Interestingly, the over-expression of *sco0921* in *SC* was correlated with an almost total disappearance of PI (**Figure 5B**). Since SCO0921 bears similarities with hemolysins that usually bear phospholipase C activity (Maheswaran and Lindorfer, 1967; Pal et al., 1997), we proposed that SCO0921 has phospholipase C activity and hydrolyzes PI into 1,2-DAG and inositol phosphate. The higher content in 1,2-DAG, in its isomerized form 1,3-DAG and in TAG directly derived from these precursors, in *SC* deleted for the operon and complemented by SCO0921 alone, is consistent with this hypothesis (**Figure 3B**). Similarly, the 53.5 fold lower PI content of *SL* compared to *SC* (**Figure 1c**) in conditions of Pi limitation that likely results from the cleavage of this specific lipid by SCO0921 whose expression is 13 fold higher in *SL* than in *SC* in condition of Pi limitation (**Figure 2A**) is also consistent with this hypothesis. Interestingly, a phospholipase C was also shown to be necessary for lipid remodeling during phosphorus limitation in the Gram negative bacteria, *Sinorhizobium meliloti* (Zavaleta-Pastor et al., 2010).

Inositol phosphate generated by the degradation of PI by SCO0921 is predicted to be dephosphorylated by various phosphatases induced in condition of phosphate scarcity, to provide phosphate. This specific lipid would thus constitute somehow a phosphorus reserve. The phosphate resulting indirectly from its degradation would repress actinorhoddin (ACT) production (Martín, 2004). Indeed ACT production was shown to be lower in the *SC* strains over-expressing the *sco0921-20* operon or *sco0921* alone in than in the *wt* strain or in the strain over-expressing *sco0920* alone (**Figure 7**). Consistently, Sandoval-Calderón et al. (2015) reported that ACT production occurred earlier and was enhanced in the *SC* strain deleted for the *sco0921-20* operon.

In conclusion, we wish to stress that, to our knowledge, our work is the first one to demonstrate that the combination of genetic and lipidomic approaches (Abreu et al., 2017) is an extremely useful and powerful approach to elucidate the *in vivo* function of enzymes involved in lipid metabolism.

DATA AVAILABILITY STATEMENT

The original contributions presented in the study are included in the article/**Supplementary Material**, further inquiries can be directed to the corresponding author/s.

AUTHOR CONTRIBUTIONS

CL, SA, and TD contributed to experimental materials and reagents, conception, execution of the experiments, data management, and reporting. MD executed the experiments. SW carried out protein alignements. M-JV, PC, SA, and CL were involved in the interpretation of the data and literature review. M-JV wrote the manuscript and provided financial support for the work. PC provided the tools and instruments that were vital for the project. PC, SA, SW and CL reviewed the manuscript before submission for both grammar and intellectual content. All authors contributed to the article and approved the submitted version.

FUNDING

This work was funded by several Institutions (CNRS and University Paris-Saclay) and grants including the ANRs PROBIO3 (https://www.inrae-transfert.fr/fr/102-8-projets/307-probio3) and Innovantibio (ANR-17-ASTR-0018) that covered the salaries of CL and TD as well as the cost of the analysis of the lipidome of the strains performed on the Lip(Sys)2 platform (http://www.lipsys2.universite-paris-saclay.fr/) and analysis of relative expression of genes using real-time quantitative PCR (RT-qPCR) and the 2 (-Delta Delta C(T)) method performed on the QPCR/TSA platform of ICSN (https://icsn.cnrs.fr/plateformes/qpcr). CNRS, Gif-sur-Yvette by Eric Jacquet and Naima Nhiri.

ACKNOWLEDGMENTS

We acknowledge the contribution of Eric Jacquet and Naima Nhiri from the QPCR/TSA platform of ICSN (https://icsn.cnrs.fr/plateformes/qpcr). CNRS, Gif-sur-Yvette for the analysis of relative expression of the studied genes using real-time quantitative PCR (RT-qPCR) and the 2 (-Delta Delta C(T)) method.

SUPPLEMENTARY MATERIAL

The Supplementary Material for this article can be found online at: https://www.frontiersin.org/articles/10.3389/fmicb.2021.623919/full#supplementary-material

REFERENCES

Abreu, S., Solgadi, A., and Chaminade, P. (2017). Optimization of normal phase chromatographic conditions for lipid analysis and comparison of associated detection techniques. *J. Chromatogr. A* 1514, 54–71. doi: 10.1016/j.chroma.2017.07.063

Allenby, N. E., Laing, E., Bucca, G., Kierzek, A. M., and Smith, C. P. (2012). Diverse control of metabolism and other cellular processes in *Streptomyces coelicolor* by the PhoP transcription factor: genome-wide identification of in vivo targets. *Nucleic Acids Res.* 40, 9543–9556.

Barbosa, L. C., Goulart, C. L., Avellar, M. M., Bisch, P. M., and von Kruger, W. M. A. (2018). Accumulation of ornithine lipids in *Vibrio cholerae* under phosphate deprivation is dependent on VC0489 (OlsF) and PhoBR system. *Microbiology (Reading)* 164, 395–399. doi: 10.1099/mic.0.000607

Benning, C., Huang, Z. H., and Gage, D. A. (1995). Accumulation of a novel glycolipid and a betaine lipid in cells of Rhodobacter sphaeroides grown under phosphate limitation. *Arch. Biochem. Biophys.* 317, 103–111. doi: 10.1006/abbi.1995.1141

Bentley, S. D. (2002). Complete genome sequence of the model actinomycete *Streptomyces coelicolor* A3(2. *Nature* 417, 141–147.

Boccard, F., Smokvina, T., Pernodet, J. L., Friedmann, A., and Guérineau, M. (1989). The integrated conjugative plasmid pSAM2 of *Streptomyces ambofaciens* is related to temperate bacteriophages. *EMBO J.* 8, 973–980.

Boubakri, H., Seghezzi, N., Duchateau, M., Gominet, M., Kofroňová, O., Benada, O., et al. (2015). The absence of pupylation (Prokaryotic Ubiquitin-like protein modification) affects morphological and physiological differentiation in *Streptomyces coelicolor*. *J. Bacteriol.* 197, 3388–3399. doi: 10.1128/JB.00591-15

Diercks, H., Semeniuk, A., Gisch, N., Moll, H., Duda, K. A., and Hölzl, G. (2015). Accumulation of novel glycolipids and ornithine lipids in Mesorhizobium loti under phosphate deprivation. *J. Bacteriol.* 197, 497–509. doi: 10.1128/JB.02004-14

Dixon, R. W., and Peterson, D. S. (2002). Development and testing of a detection method for liquid chromatography based on aerosol charging. *Anal. Chem.* 74, 2930–2937. doi: 10.1021/ac011208l

Esnault, C., Dulermo, T., Smirnov, A., Askora, A., David, M., Deniset-Besseau, A., et al. (2017). Strong antibiotic production is correlated with highly active oxidative metabolism in *Streptomyces coelicolor* M145. *Sci. Rep.* 7, 200. doi: 10.1038/s41598-017-00259-9

Folch, J., Lees, M., and Sloane Stanley, G. H. (1957). A simple method for the isolation and purification of total lipides from animal tissues. *J. Biol. Chem.* 226, 497–509.

Gao, J.-L., Weissenmayer, B., Taylor, A. M., Thomas-Oates, J., López-Lara, I. M., and Geiger, O. (2004). Identification of a gene required for the formation of lyso-ornithine lipid, an intermediate in the biosynthesis of ornithine-containing lipids. *Mol. Microbiol.* 53, 1757–1770. doi: 10.1111/j.1365-2958.2004.04240.x

Geiger, O., Röhrs, V., Weissenmayer, B., Finan, T. M., and Thomas-Oates, J. E. (1999). The regulator gene phoB mediates phosphate stress-controlled synthesis of the membrane lipid diacylglyceryl-N,N,N-trimethylhomoserine in Rhizobium (*Sinorhizobium*) meliloti. *Mol. Microbiol.* 32, 63–73. doi: 10.1046/j.1365-2958.1999.01325.x

Graves, S., Dorai-Raj, S., Piepho, H.-P., and Selzer, L. (2019). *multcompView: Visualizations of Paired Comparisons*. Available online at: https://CRAN.R-project.org/package=multcompView (accessed April 21, 2020).

Gust, B., Chandra, G., Jakimowicz, D., Yuqing, T., Bruton, C. J., and Chater, K. F. (2004). Lambda red-mediated genetic manipulation of antibiotic-producing *Streptomyces*. *Adv. Appl. Microbiol.* 54, 107–128. doi: 10.1016/S0065-2164(04)54004-2

Hanahan, D. (1983). Studies on transformation of *Escherichia coli* with plasmids. *J. Mol. Biol.* 166, 557–580. doi: 10.1016/s0022-2836(83)80284-8

Juguet, M., Lautru, S., Francou, F.-X., Nezbedová, S., Leblond, P., Gondry, M., et al. (2009). An iterative nonribosomal peptide synthetase assembles the pyrrole-amide antibiotic congocidine in Streptomyces ambofaciens. *Chem. Biol.* 16, 421–431. doi: 10.1016/j.chembiol.2009.03.010

Katoh, K., Rozewicki, J., and Yamada, K. D. (2019). MAFFT online service: multiple sequence alignment, interactive sequence choice and visualization. *Brief. Bioinform.* 20, 1160–1166.

Kieser, T., Bibb, M. J., Buttner, M. J., Chater, K. F., and Hopwood, D. A. (2000). *Practical Streptomyces genetics*. Norwich: Innes.

Lev, S., Rupasinghe, T., Desmarini, D., Kaufman-Francis, K., Sorrell, T. C., Roessner, U., et al. (2019). The PHO signaling pathway directs lipid remodeling in *Cryptococcus neoformans* via DGTS synthase to recycle phosphate during phosphate deficiency. *PLoS One* 14:e0212651. doi: 10.1371/journal.pone.0212651

Lewenza, S., Falsafi, R., Bains, M., Rohs, P., Stupak, J., Sprott, G. D., et al. (2011). The olsA gene mediates the synthesis of an ornithine lipid in *Pseudomonas aeruginosa* during growth under phosphate-limiting conditions, but is not involved in antimicrobial peptide susceptibility. *FEMS Microbiol. Lett.* 320, 95–102. doi: 10.1111/j.1574-6968.2011.02295.x

Li, X., Wang, W., and Lufkin, T. (1997). Dicistronic LacZ and alkaline phosphatase reporter constructs permit simultaneous histological analysis of expression from multiple transgenes. *BioTechniques* 23, 874–878, 880, 882. doi: 10.2144/97235st03

Lu, S., Wang, J., Chitsaz, F., Derbyshire, M. K., Geer, R. C., Gonzales, N. R., et al. (2020). CDD/SPARCLE: theconserved domain database in 2020. *Nucleic Acids Res.* 48, D265–D268. doi: 10.1093/nar/gkz991

Maheswaran, S. K., and Lindorfer, R. K. (1967). Staphylococcal beta-hemolysin. II. Phospholipase C activity of purified beta-hemolysin. *J. Bacteriol.* 94, 1313–1319.

Martín, J. F. (2004). Phosphate control of the biosynthesis of antibiotics and other secondary metabolites is mediated by the PhoR-PhoP system: an unfinished story. *J. Bacteriol.* 186, 5197–5201. doi: 10.1128/JB.186.16.5197-5201.2004

Martín, J. F., Rodríguez-García, A., and Liras, P. (2017). The master regulator PhoP coordinates phosphate and nitrogen metabolism, respiration, cell differentiation and antibiotic biosynthesis: comparison in *Streptomyces coelicolor* and *Streptomyces avermitilis*. *J. Antibiot.* 70, 534–541. doi: 10.1038/ja.2017.19

Martín, J. F., Santos-Beneit, F., Rodríguez-García, A., Sola-Landa, A., Smith, M. C. M., Ellingsen, T. E., et al. (2012). Transcriptomic studies of phosphate control of primary and secondary metabolism in Streptomyces coelicolor. *Appl. Microbiol. Biotechnol.* 95, 61–75. doi: 10.1007/s00253-012-4129-6

MetaCyc olsF (2020). Available online at: http://vm-trypanocyc.toulouse.inra.fr/gene?orgid=META&id=G-34498 (accessed May 14, 2020).

Millan-Oropeza, A., Henry, C., Lejeune, C., David, M., and Virolle, M.-J. (2020). Expression of genes of the Pho regulon is altered in *Streptomyces coelicolor*. *Sci. Rep.* 10, 8492. doi: 10.1038/s41598-020-65087-w

Pal, S., Guhathakurta, B., Sasmal, D., Mallick, R., and Datta, A. (1997). Purification and characterisation of a hemolysin with phospholipase C activity from *Vibrio cholerae* O139. *FEMS Microbiol. Lett.* 147, 115–120. doi: 10.1111/j.1574-6968.1997.tb10229.x

Pérez-Redondo, R., Rodríguez-García, A., Botas, A., Santamarta, I., Martín, J. F., and Liras, P. (2012). ArgR of *Streptomyces coelicolor* is a versatile regulator. *PLoS One* 7:e32697. doi: 10.1371/journal.pone.0032697

Pfaffl, M. W. (2001). A new mathematical model for relative quantification in real-time RT-PCR. *Nucleic Acids Res.* 29, e45. doi: 10.1093/nar/29.9.e45

R Core Team (2013). *A Language and Environment for Statistical Computing*. Vienna: R Foundation for Statistical Computing.

Ruckert, C. (2015). Complete genome sequence of *Streptomyces lividans* TK24. *J. Biotechnol.* 199, 21–22.

Sambrook, J., and Russell, D. W. (2001). *Molecular Cloning: A Laboratory Manual*. Cold Spring Harbor, NY: Cold Spring Harbor Laboratory Press.

Sandoval-Calderón, M., Guan, Z., and Sohlenkamp, C. (2017). Knowns and unknowns of membrane lipid synthesis in streptomycetes. *Biochimie* 141, 21–29. doi: 10.1016/j.biochi.2017.05.008

Sandoval-Calderón, M., Nguyen, D. D., Kapono, C. A., Herron, P., Dorrestein, P. C., and Sohlenkamp, C. (2015). Plasticity of *Streptomyces coelicolor* membrane composition under different growth conditions and during development. *Front. Microbiol.* 6:1465. doi: 10.3389/fmicb.2015.01465

Santos-Beneit, F., Rodríguez-García, A., Franco-Domínguez, E., and Martín, J. F. (2008). Phosphate-dependent regulation of the low- and high-affinity transport systems in the model actinomycete *Streptomyces coelicolor*. *Microbiology (Reading)* 154, 2356–2370. doi: 10.1099/mic.0.2008/019539-0

Siegl, T., Tokovenko, B., Myronovskyi, M., and Luzhetskyy, A. (2013). Design, construction and characterisation of a synthetic promoter library for fine-tuned gene expression in actinomycetes. *Metab. Eng.* 19, 98–106. doi: 10.1016/j.ymben.2013.07.006

Sohlenkamp, C. (2016). "Ornithine lipids and other amino acid-containing Acyloxyacyl lipids," in *Biogenesis of Fatty Acids, Lipids and Membranes*, ed. O. Geiger (Cham: Springer International Publishing), 1–14. doi: 10.1007/978-3-319-43676-0_13-1

Vences-Guzmán, M. Á, Guan, Z., Escobedo-Hinojosa, W. I., Bermúdez-Barrientos, J. R., Geiger, O., and Sohlenkamp, C. (2015). Discovery of a bifunctional acyltransferase responsible for ornithine lipid synthesis in *Serratia proteamaculans*. *Environ. Microbiol.* 17, 1487–1496. doi: 10.1111/1462-2920.12562

Weissenmayer, B., Gao, J.-L., López-Lara, I. M., and Geiger, O. (2002). Identification of a gene required for the biosynthesis of ornithine-derived lipids. *Mol. Microbiol.* 45, 721–733. doi: 10.1046/j.1365-2958.2002.03043.x

Willems, E., Leyns, L., and Vandesompele, J. (2008). Standardization of real-time PCR gene expression data from independent biological replicates. *Anal. Biochem.* 379, 127–129.

Zavaleta-Pastor, M., Sohlenkamp, C., Gao, J.-L., Guan, Z., Zaheer, R., Finan, T. M., et al. (2010). *Sinorhizobium meliloti* phospholipase C required for lipid remodeling during phosphorus limitation. *Proc. Natl. Acad. Sci. U.S.A.* 107, 302–307. doi: 10.1073/pnas.0912930107

Conflict of Interest: The authors declare that the research was conducted in the absence of any commercial or financial relationships that could be construed as a potential conflict of interest.

Copyright © 2021 Lejeune, Abreu, Chaminade, Dulermo, David, Werten and Virolle. This is an open-access article distributed under the terms of the Creative Commons Attribution License (CC BY). The use, distribution or reproduction in other forums is permitted, provided the original author(s) and the copyright owner(s) are credited and that the original publication in this journal is cited, in accordance with accepted academic practice. No use, distribution or reproduction is permitted which does not comply with these terms.

3. Conclusion

Les profils lipidiques des souches *S. lividans* et *S. coelicolor* cultivées en milieu limité et non limité en phosphate ont été analysés par LC-Corona-CAD®.

La teneur en OL lipides en condition de limitation en phosphate a augmenté dans les deux souches. Cependant, l'augmentation la plus importante a été observée chez *S. lividans.*

La discussion sur la variation des autres lipides (TGs et PLs) et les hypothèses métaboliques que cela suggère dépassent le cadre de ce travail.

Les analyses sur les souches modifiées (sco0920 et sco0921) ont montré que SCO0920 ne porte pas uniquement une activité O-acyltransférase comme suggéré dans l'étude Sandoval-Calderón, et al. [195], mais porte également une activité N-acyltransférase.

La délétion chez *S. lividans* de sco0921-20 suivi de la complémentation de sco0920 a permis d'observer une teneur en OL comparable à celle présente dans la souche sauvage. Pour valider la voie de synthèse, les intermédiaires de synthèse correspondant aux lyso ornithines lipides (LOL) ont été recherchés.

L'intensité du pic de LOL étant trop faible pour être détectée par Corona-CAD®, le courant ionique des *m/z* spécifiques des ions des LOL attendus a été étudié par NPLC-HRMS. La présence des LOL a bien été confirmée.

Nos expériences ont par ailleurs confirmé l'activité N-acyltransférase stricte précédemment rapportée de sco0921 [195], puisque la délétion de sco0921-20 suivi de la complémentation de sco0921 n'a pas permis d'observer la présence d'OL. Néanmoins, l'intermédiaire de synthèse LOL a bien été observé par NPLC-HRMS.

ANNEXE VI. CORRELATION NEGATIVE ENTRE LA TENEUR EN LIPIDES ET L'ACTIVITE ANTIBIOTIQUE CHEZ *STREPTOMYCES* : REGLE GENERALE ET EXCEPTIONS

1. Introduction

Dans l'article David et al. (2020) [25], nous avons cherché à déterminer s'il existait chez *Streptomyces* une corrélation négative entre la teneur totale en lipides et la capacité à produire des antibiotiques, comme cela avait été décrit chez *S. lividans* avec son mutant ppk [196,197] et avec *S. coelicolor* [198–200].

Pour déterminer si une telle corrélation négative pouvait être généralisée à d'autres espèces de *Streptomyces*, cinquante-quatre souches ont été prélevées au hasard et cultivées. Une analyse comparative des profils lipidiques et génomiques a été réalisée sur les deux souches ayant produit respectivement la teneur en lipides la plus élevée (Antibioticus DSM 41,481) et la plus faible (DSM 40,868).

2. Publication 6

antibiotics

MDPI

Article

Negative Correlation between Lipid Content and Antibiotic Activity in *Streptomyces*: General Rule and Exceptions

Michelle David [1,†], Clara Lejeune [1,†], Sonia Abreu [2], Annabelle Thibessard [3], Pierre Leblond [3], Pierre Chaminade [2] and Marie-Joelle Virolle [1,*]

1 Institute for Integrative Biology of the Cell (I2BC), CEA, CNRS, Université Paris-Saclay, 91198 Gif-sur-Yvette, France; michelle.david@i2bc.paris-saclay.fr (M.D.); clara.lejeune@i2bc.paris-saclay.fr (C.L.)
2 Lipides, Systèmes Analytiques et Biologiques, Université Paris-Saclay, 92296 Châtenay-Malabry, France; sonia.abreu@universite-paris-saclay.fr (S.A.); pierre.chaminade@universite-paris-saclay.fr (P.C.)
3 Université de Lorraine, INRAE, DynAMic, F-54000 Nancy, France; annabelle.thibessard@univ-lorraine.fr (A.T.); pierre.leblond@univ-lorraine.fr (P.L.)
* Correspondence: marie-joelle.virolle@i2bc.paris-saclay.fr
† These authors contributed equally to this work.

Received: 24 April 2020; Accepted: 20 May 2020; Published: 26 May 2020

check for updates

Abstract: Streptomycetes are well known antibiotic producers and are among the rare prokaryotes able to store carbon as lipids. Previous comparative studies of the weak antibiotic producer *Streptomyces lividans* with its *ppk* mutant and with *Streptomyces coelicolor*, which both produce antibiotics, suggested the existence of a negative correlation between total lipid content and the ability to produce antibiotics. To determine whether such a negative correlation can be generalized to other *Streptomyces* species, fifty-four strains were picked randomly and grown on modified R2YE medium, limited in phosphate, with glucose or glycerol as the main carbon source. The total lipid content and antibiotic activity against *Micrococcus luteus* were assessed for each strain. This study revealed that the ability to accumulate lipids was not evenly distributed among strains and that glycerol was more lipogenic than glucose and had a negative impact on antibiotic biosynthesis. Furthermore, a statistically significant negative Pearson correlation between lipid content and antibiotic activity could be established for most strains, but a few strains escape this general law. These exceptions are likely due to limits and biases linked to the type of test used to determine antibiotic activity, which relies exclusively on *Micrococcus luteus* sensitivity. They are characterized either by high lipid content and high antibiotic activity or by low lipid content and undetectable antibiotic activity against *Micrococcus luteus*. Lastly, the comparative genomic analysis of two strains with contrasting lipid content, and both named *Streptomyces antibioticus* (DSM 41,481 and DSM 40,868, which we found to be phylogenetically related to *Streptomyces lavenduligriseus*), indicated that some genetic differences in various pathways related to the generation/consumption of acetylCoA could be responsible for such a difference.

Keywords: *Streptomyces*; antibiotics; lipids; triacylglycerol; metabolism; glycerol; glucose

1. Introduction

The *Streptomyces* genus is a well-known producer of most antibiotics in current use and of a variety of other bioactive molecules useful to human health (e.g., anti-cancer and anti-inflammatory drugs) or agriculture (e.g., fungicides, pesticides, insecticides and herbicides) [1–4]. Furthermore, *Streptomyces* is one of the rare prokaryotes to have the ability to accumulate storage lipids of the triacylglycerol family when cultivated under nitrogen and/or phosphate limitation [5]. The biosynthesis of these molecules

requires the availability of glycerol3P and acetylCoA, both stemming from glycolysis. The condensation of acetylCoA results in fatty acid biosynthesis. The transfer of fatty acids on the glycerol backbone by glycerol3P acyl transferase (GPAT) yields diacylglycerol (DAG), a molecule precursor of polar membranous phospholipids as well as neutral lipids such as triacylglycerol (TAG). In previous studies, we demonstrated that, when grown on R2YE medium [6] limited in phosphate and containing glucose as the main carbon source, the weak antibiotic producer, *S. lividans*, had a high TAG content, indicative of a glycolytic metabolism [7]. By contrast, the *ppk* mutant of *S. lividans* and the closely related model strain, *S. coelicolor*—which both produce the same antibiotics—have a low TAG content compared to the wild type strain of *S. lividans* [7,8]. These two strains suffer energetic stress. *S. coelicolor* suffers energetic stress since the two component system PhoR/PhoP that positively controls the phosphate supply, necessary for ATP synthesis, is weakly expressed in this strain [9] whereas the *ppk* mutant suffers energetic stress since its lacks PPK, an important enzyme that regenerates ATP from ADP and polyphosphate [10,11]. In these two strains, similar homeostatic processes are triggered to restore their energetic balance [7,9]. Such processes include the activation of their TCA cycle, which yields reduced co-factors whose re-oxidation by the respiratory chain generates ATP. In these strains, with acetylCoA being used to feed the TCA cycle, it is not available to be stored as lipids [7,9]. The activation of the oxidative metabolism of these strains was shown to be correlated with the production of the antibiotics CDA (calcium dependent antibiotic), RED (undecylprodigiosin) and ACT (actinorhoddin) [7]. CDA and RED were proposed to create damage to the membrane, contributing to the cell death and lysis of a fraction of the population [7,12,13]. This would provide nutrients, and especially phosphate, to support the activation of the oxidative metabolism of the surviving population. Furthermore, since the onset of ACT biosynthesis was shown to coincide with an abrupt drop in the intracellular ATP concentration in *S. coelicolor*, ACT, like other molecules possessing quinone groups (melanine, humic acid etc.), was proposed to act as an electron acceptor [7]. In a context of low phosphate availability, ACT would reduce the electron flow through the respiratory chain, reducing respiration efficiency and thus ATP generation, in order to adjust it to low phosphate availability [7,12].

A putative link between TAG content and antibiotic activity was already anticipated twenty years ago by Olukoshi and Packter [14,15] in *S. lividans*. Furthermore, the impaired biosynthesis [16,17] or enhanced degradation [18–20] of fatty acids was indeed shown to be correlated with increased antibiotic biosynthesis in *S. coelicolor*. Similarly, enhanced spiramycin biosynthesis was correlated with lower lipid content in *S. ambofaciens* [21]. In order to determine whether these observations constituted a general rule for *Streptomyces* species, fifty-four randomly picked *Streptomyces* strains from our collection were grown on modified solid R2YE medium limited in phosphate with either glucose or glycerol as the main carbon source. Their total lipid content, on glucose or glycerol, was assessed by Fourier transformed infra-red spectroscopy (FTIRS) [22–24], and the measure of the diameter of the growth inhibition zones around four agar plugs of each strain gave an estimation of their antibiotic activity against *Micrococcus luteus* (Figure 1). This study confirmed the existence of a negative correlation between lipid content and antibiotic activity but with some exceptions commented on in the discussion. It also revealed that glycerol was more lipogenic than glucose but was not as good a carbon source as glucose to promote antibiotic activity. An explanation concerning this unexpected observation is also proposed in the discussion. Lastly, a comparative analysis of the genome of two *Streptomyces antibioticus* strains—DSM 41,481 and DSM 40,868, bearing among the highest and lowest lipid contents on glycerol—was carried out in an attempt to determine the genetic features responsible for their highly different lipid contents.

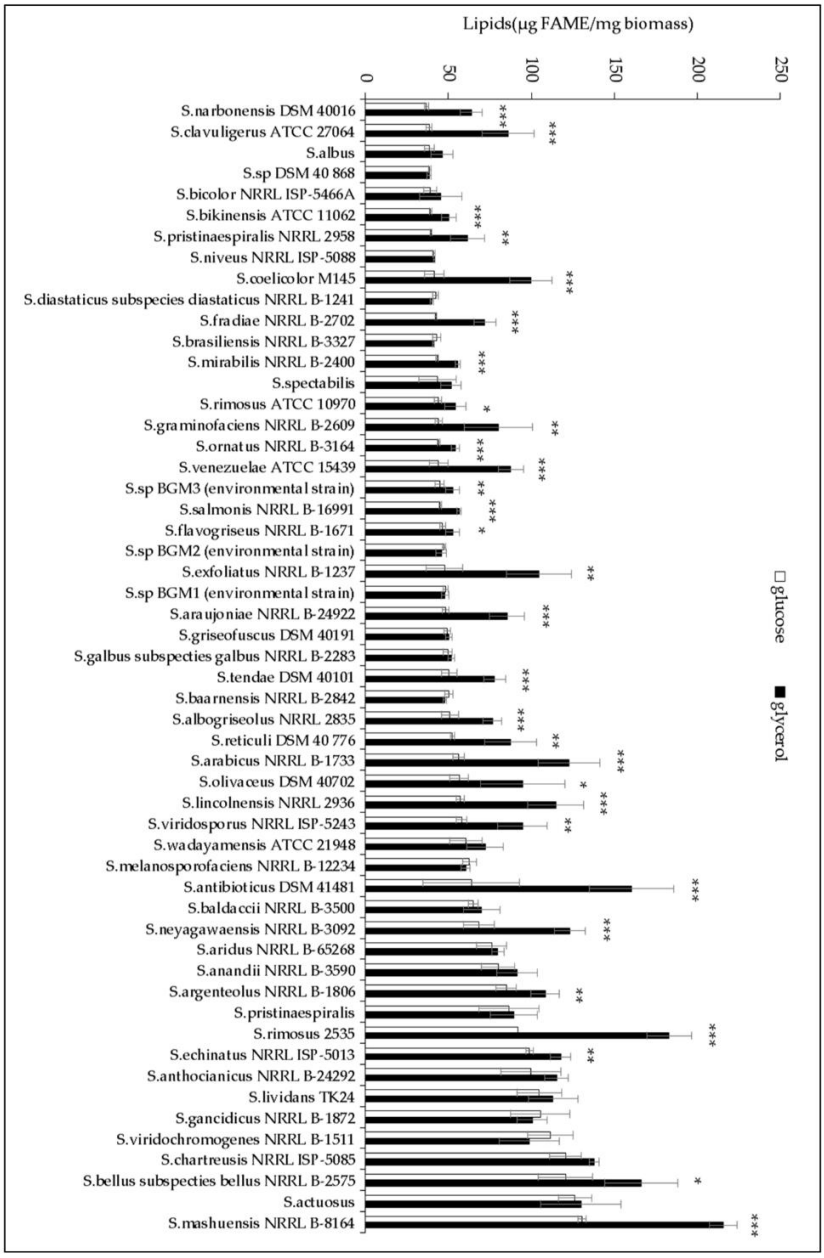

(**A**)

Figure 1. *Cont.*

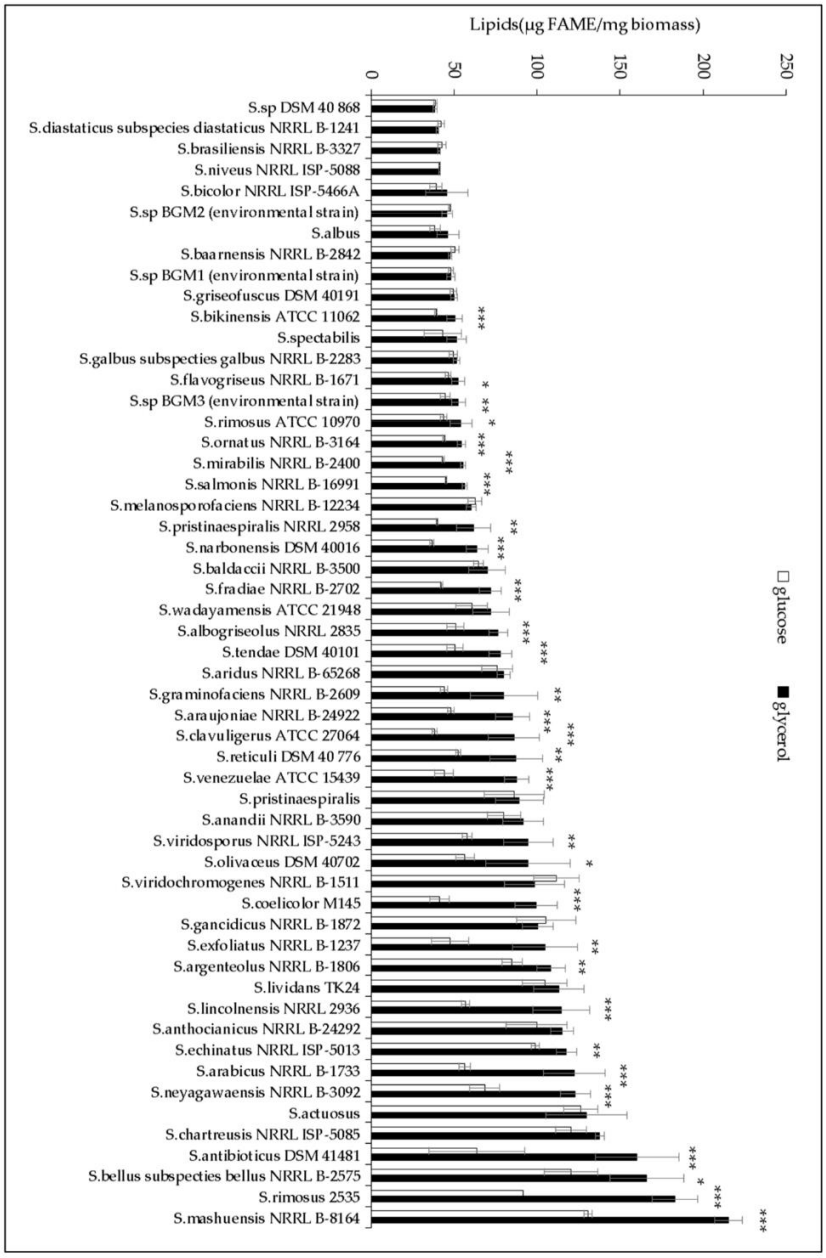

(**B**)

Figure 1. *Cont.*

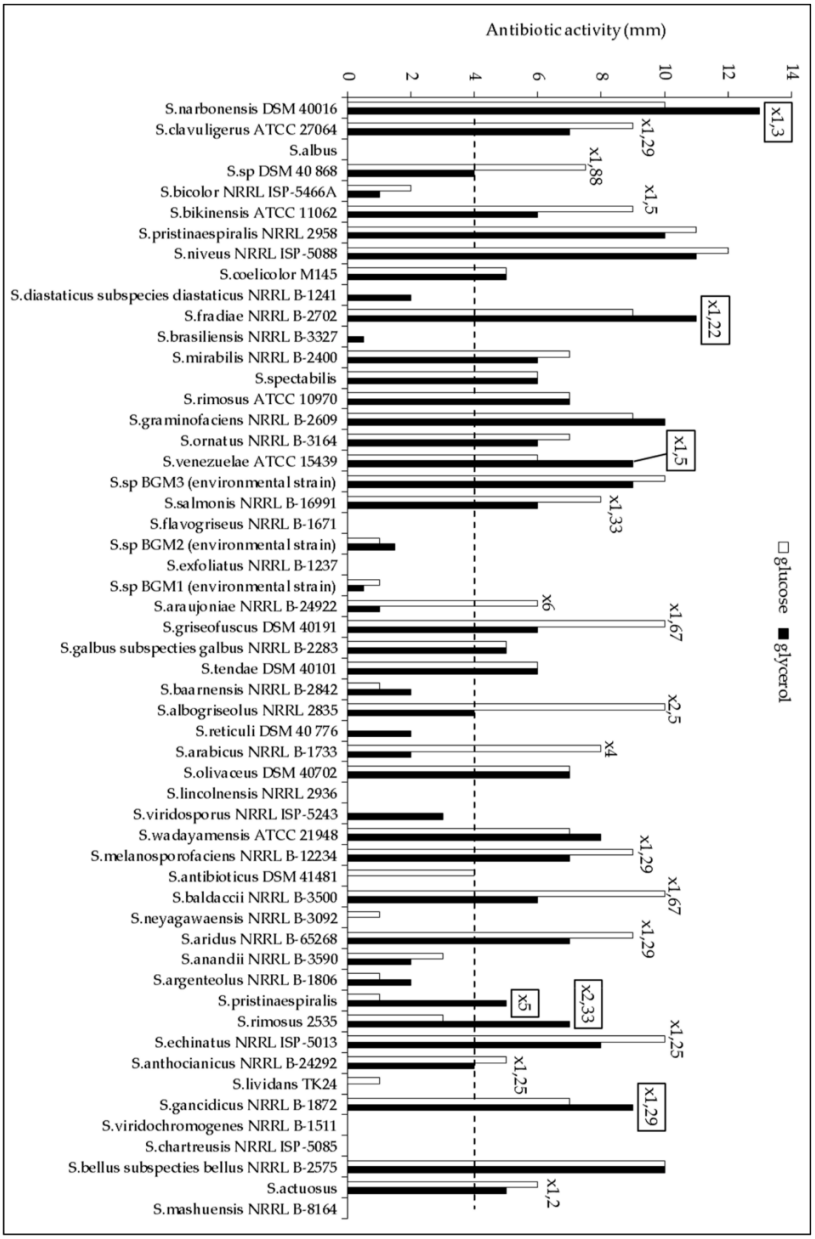

(**C**)

Figure 1. Total lipid/fatty methyl ester (FAME) content and antibiotic activity of *Streptomyces* strains. The strains were grown on modified solid R2YE limited in phosphate for 72 h at 28 °C with either glucose (white histograms) or glycerol (black histograms) as the main carbon source. Their total lipid/FAME content, determined with FTIRS, was ranked according to their increasing lipid/FAME content upon growth on (**A**) glucose or on (**B**) glycerol. Significant differences in lipid content between glucose- and glycerol-grown cultures are represented by an asterisk (ANOVA, *** = $p < 0.001$; ** = $p < 0.01$; * = $p < 0.05$). (**C**) Antibiotic activity of *Streptomyces* strains determined by the measurement of the diameters of the zones of growth inhibition of *Micrococcus luteus* around four agar plugs of each *Streptomyces* culture. Fold changes in antibiotic activity (>1.2 fold) between glucose and glycerol for inhibition zones > 4mm are shown above the histograms. The fold changes of the six cases where antibiotic activity was higher on glycerol than on glucose are boxed.

2. Results

2.1. The Lipid Content and Antibiotic Activity of the Streptomyces Strains Varies with the Nature of the Carbon Source Used for Growth

Fifty-four randomly picked *Streptomyces* strains from our collection were grown for 72 h at 28 °C on the surface of cellophane disks deposited on the surface of the modified (no sucrose added) R2YE medium [6] limited in phosphate and containing either glucose (50 mM) or glycerol (100 mM) as the main carbon source. The lipid content of the strains was determined using the fast and reliable FTIRS method [22–24]. The FTIRS values, expressed as arbitrary units, were converted into µg of Fatty Methyl Esters (FAME) per mg of dry mycelium using the converting equation established by Millan-Oropeza et al. (2017) [24]. Indeed, in the presence of methanol, fatty acids constitutive of all cellular lipids are esterified to yield FAME that can be accurately quantified by GC/MS [22–24]. The presence of antibiotic activity excreted in the agar medium was assessed by the measurement of the diameters of the zones of growth inhibition of *Micrococcus luteus* around four agar plugs of each *Streptomyces* strain tested. The strains were ranked according to their lipid/FAME content on glucose (Figure 1a) or glycerol (Figure 1b), and their antibiotic activity is shown in (Figure 1c). This study revealed that the average lipid content of the strains was highly variable, revealing their highly different metabolic features, and was usually higher on glycerol than on glucose (Figures 1 and 2). It also revealed that some strains have far lower lipid content on glucose than on glycerol (Figure 1b). These strains might have, like *S. coelicolor*, an oxidative metabolism yielding an insufficient amount of glycerol3P to support high lipid biosynthesis on glucose [9]. Thirty and fifteen strains (forty-five strains) had a medium (50–100 µg/mg) or high (>100 µg/mg) lipid content on glycerol whereas only twenty and seven strains (twenty-seven strains) had medium or high lipid content on glucose, respectively. Consistently, the number of strains bearing a low lipid content (<50 µg/mg) was 3 fold higher on glucose (twenty-seven strains) than on glycerol (nine strains) (Figure 2). This confirmed that glycerol was more lipogenic than glucose, likely because the generation of glycerol3P, a major lipid precursor, from glycerol is more direct than that from glucose (one step versus five steps).

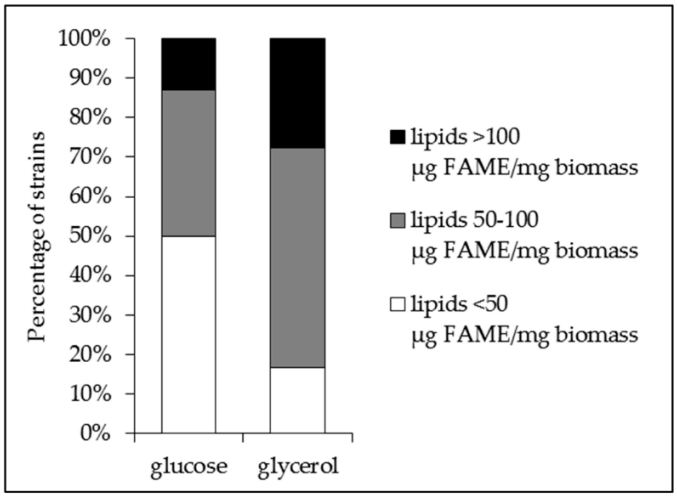

Figure 2. Percentage of *Streptomyces* strains grown for 72 h at 28 °C on solid modified R2YE limited in phosphate with either glucose (50 mM) or glycerol (100 mM) as the main carbon source bearing low (<50 µg FAME/mg biomass, white part); medium (50–100 µg FAME/mg biomass, grey part) and high (>100 µg FAME/mg biomass, black part) total lipid/FAME content.

This study also revealed that the antibiotic activity of the strains was also highly variable and was usually higher on glucose than on glycerol (Figure 3a,c). On glucose, fifteen strains gave halos of

inhibition >8 mm, and among them, nine (60%) had a low lipid content, five (33.3%) had a medium lipid content and one (6.7%) had a high lipid content. By contrast, on glycerol, only nine strains gave halos of inhibition >8 mm, and among them, only one (11.1%) had a low lipid content, six (66.7%) had a medium lipid content and two (22.2%) had a high lipid content (Figure 3a,c). Furthermore, among the thirty-four strains that gave inhibition halos with diameters greater than or equal to 4 mm, fourteen (41.2%) gave halos of similar size on both carbon sources, fourteen (41.2%) gave bigger halos on glucose than on glycerol and only six (17.6%) gave bigger halos on glycerol than on glucose (Figure 1c). This suggested that glycerol does not promote as good antibiotic activity as glucose. A hypothesis concerning the cause of this difference is proposed in the discussion.

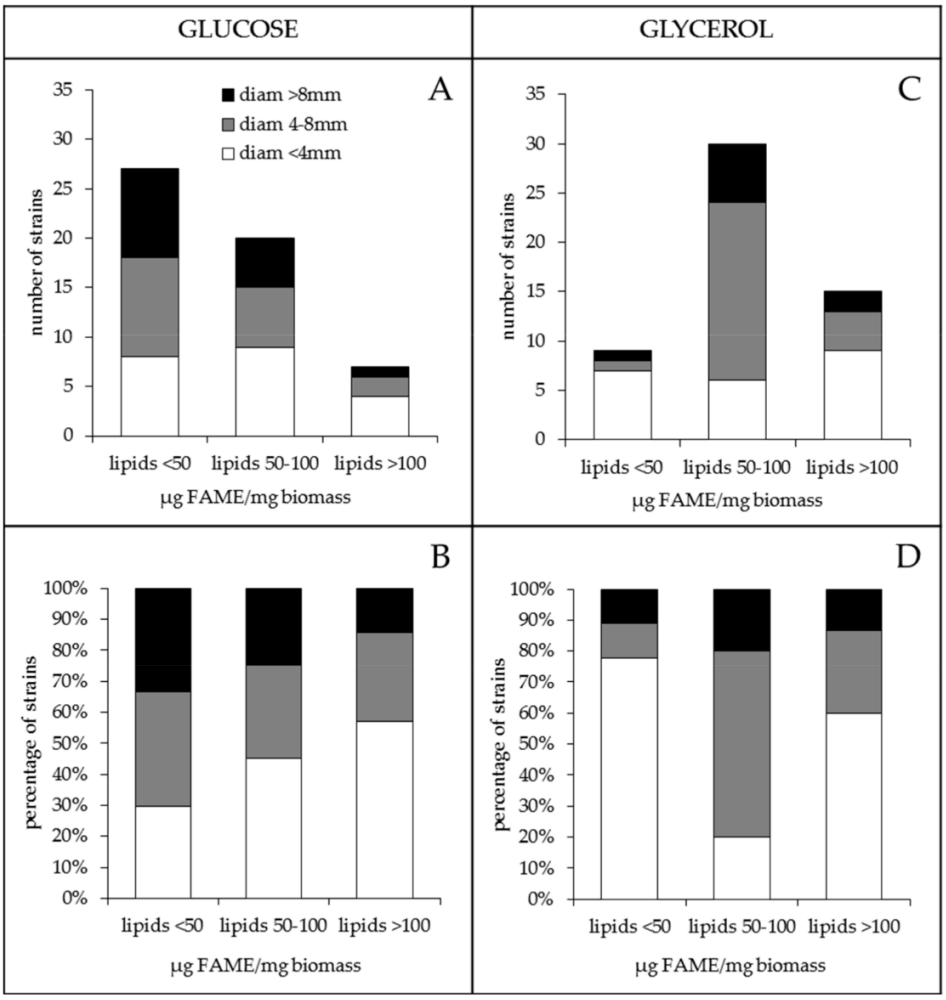

Figure 3. Classification of *Streptomyces* strains grown for 72 h at 28 °C on solid modified R2YE limited in phosphate, according to low (<50 µg FAME/mg biomass), medium (50–100 µg FAME/mg biomass) or high (>100 µg FAME/mg biomass) total lipid/FAME content, on glucose (**A**,**B**) and glycerol (**C**,**D**), respectively. Each lipid class is represented by an histogram, and the numbers (**A**,**B**) or percentages (**B**,**D**) of strains with weak (<4 mm), medium (4–8 mm) and strong (> 8 mm) antibiotic activity against *Micrococcus luteus* correspond to the white, grey and black parts of each histogram, respectively, on glucose (**A**,**B**) and glycerol (**C**,**D**).

Interestingly, on glucose, the proportion of strains yielding big halos of inhibition (>8 mm) decreases when the lipid content increases, and conversely, the proportion of strains yielding small

halos of inhibition (<4 mm) increases when the lipid content increases (Figure 3b). These features, that are consistent with a negative correlation existing between lipid content and antibiotic activity, are not seen on glycerol (Figure 3d).

2.2. A Statistically Significant Negative Pearson Correlation between Total Lipid Content and Antibiotic Activity Could Be Established with Some Exceptions

In order to determine whether a statistically significant negative correlation between total lipid content and antibiotic activity could be established for glucose but also for glycerol, the lipid content of each strain was plotted against its respective antibiotic activity and a linear regression curve was established (Figure 4a,c). This indicated that on R2YE glucose or glycerol, no strong negative Pearson correlation (p-value defined as <0.05) could be established between total lipid content and antibiotic activity since p-values of 0.135 and 0.227 were obtained for glucose and glycerol, respectively.

However, we noticed that if strains with extreme features were removed from our statistical analysis, a negative correlation between lipid content and antibiotic activity could be established. These strains were chosen by calculating quartiles. The graph (Figure 4a), representing the fifty-four strains grown on glucose, was divided into quartiles according to their lipid content (dashed vertical lines) and antibiotic activity (dashed horizontal lines). Each quartile contains 25% of each type of data. This delineated sixteen areas in which the strains had similar features concerning their lipid content and antibiotic activity. The three strains (*S. brasiliensis*, *S. diastaticus* subspecies *diastaticus* and *S. albus*) present in the lower corner area were in the quartiles bearing the lowest lipid content and no detectable antibiotic activity. By contrast, the three strains (*S. bellus* subspecies *bellus*, *S. echinatus* and *S. aridus*) present in upper corner area were in the quartiles bearing the highest lipid content and the highest antibiotic activity. The removal of these six strains with extreme features greatly improved the significance of the negative correlation between lipid content and antibiotic activity since statistically significant p-values of 0.002 and 0.013 (<0.05) and Pearson correlation coefficients of −0.432 and −0.355 were then obtained for glucose- and glycerol-grown cultures, respectively (Figure 4b,d).

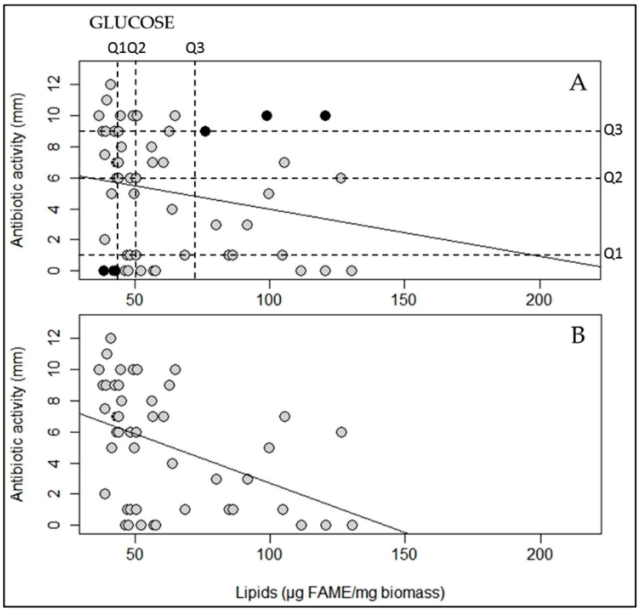

Figure 4. *Cont.*

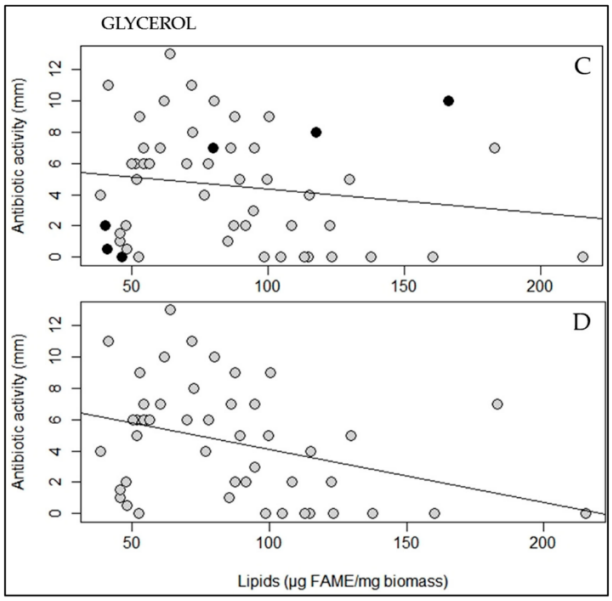

Figure 4. Lipid/FAME content of fifty-four *Streptomyces* strains grown on modified solid R2YE limited in phosphate for 72 h at 28 °C with (**A**) 50 mM glucose or (**C**) 100 mM glycerol as the main carbon source was plotted against their antibiotic activity, and linear regression lines were calculated (black lines). In (**A**,**C**), FAME content and antibiotic activity did not show a statistically significant negative Pearson correlation (coefficients of −0.206 and −0.167, *p*-values of 0.135 and 0.227 (> 0.05), on glucose and glycerol, respectively). In an attempt to enhance the amplitude of this negative correlation, six strains constituting exceptions (black spots) were removed. These strains were chosen as described in the text, and the vertical and horizontal dashed lines represent the quartiles (Q1, Q2 and Q3) of lipid content and antibiotic activity, respectively. The lipid/FAME content of the forty-eight remaining strains grown in the presence of (**B**) 50 mM glucose or (**D**) 100 mM glycerol was plotted against their antibiotic activity, and linear regression lines were calculated (black lines). In (**B**,**D**), the FAME content and the antibiotic activity show a statistically significant negative Pearson correlation (coefficients of −0.432 and −0.355, *p*-values of 0.002 and 0.013 (< 0.05), on glucose and glycerol, respectively).

2.3. Comparison of Streptomyces Antibioticus DSM 41,481 and DSM 40,868 Strains with Drastically Different Lipid Contents

In order to get a better understanding of the molecular basis for the huge difference in lipid content observed between strains, two strains named *Streptomyces antibioticus* DSM 41,481 (GenBank Acc. NZ_CM007717.1) and DSM 40,868 (ATCC 11,891, GenBank Acc. CP050504) that have among the highest and lowest lipid content, respectively, especially on glycerol, were studied in more detail.

The growth curves on R2YE glucose indicated that the strain DSM 41,481, bearing high lipid content, reached the stationary phase earlier and had a lower biomass yield than the strain DSM 40,868 (Figure 5a). The content in all lipid classes, and not only TAG as anticipated, was, on average, 2.5 fold higher in *S. antibioticus* DSM 41,481 than in DSM 40,868 (Figure 5c), consistent with FTIRS measurements [22–24]. Furthermore, the strain DSM 40,868 produced an antibiotic activity against *Micrococcus luteus*, whereas DSM 41,481 did not (Figure 5b). However, the production of antimycin by the strain DSM 41,481 was detected by LC/Corona-CAD (Figure 5d and Supplementary Figure S1), and the presence of an NRPS/PKS antimycin cluster in the genome of this strain was confirmed by anti-Smash [25] (Figure S2). In eukaryotes, antimycin impairs the correct functioning of the cytochrome c reductase, a key mitochondrial enzyme of the respiratory chain, and thus inhibits oxidative phosphorylation [26,27] *Streptomyces* is known to possess several cytochrome c reductases/oxidases

that could possibly be antimycin targets, but no report in the literature indicates that antimycin has an impact on the respiratory activity of *Streptomyces* producing strains. However, we think that it is likely that antimycin plays such a role in the producing strain since bio-active molecules often fulfill transient but important regulatory roles in their producer [12]. Furthermore, *Streptomyces* genomes are known to encode several eukaryotic-like enzymes as well as biosynthetic pathways directing the synthesis of molecules regulating their activity as well as that of their eukaryotic orthologs [28–30]. Since the strain DSM41481 stops growing earlier than the other strain, we cannot totally exclude that the antimycin produced by this strain alters the correct functioning of its oxidative metabolism, resulting in a reduction of TCA cycle activity. The latter would thus consume less acetylCoA, and an excess of acetylCoA would be stored as lipids.

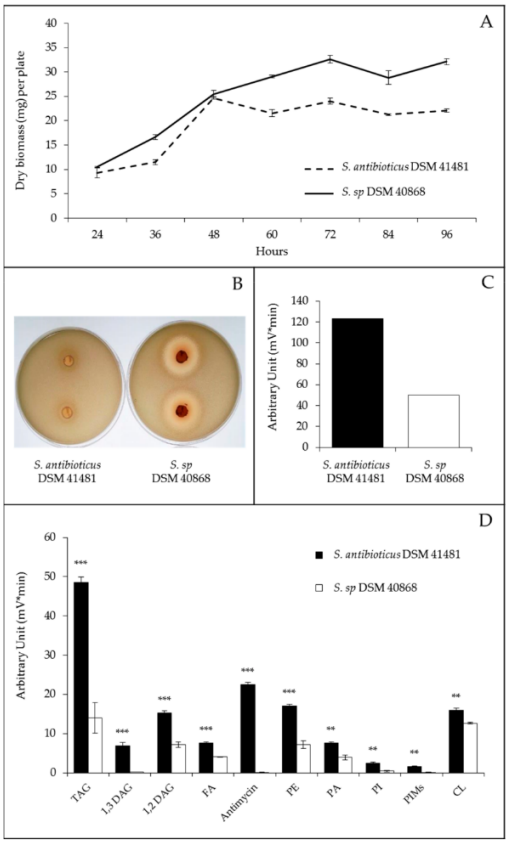

Figure 5. Cultures of *S. antibioticus* DSM 41,481 and *S. sp.* DSM 40,868 grown at 28 °C on solid R2YE limited in phosphate with glucose (50 mM) as the main carbon source. (**A**) Growth curves of *S. antibioticus* DSM 41,481 (dotted lines) and *S. sp.* DSM 40,868 (continuous lines); (**B**) Pictures of the zones of inhibition of *Micrococcus luteus* growth around agar plugs of 72 h-grown cultures of the *Streptomyces* strains; (**C**) Sum of all lipid classes (antimycin not included) in *S. antibioticus* DSM 41,481 (black histograms) and *S. sp.* DSM 40,868 (white histograms) according to LC/Corona-CAD data analysis; (**D**) Analysis of the total lipid contents in *S. antibioticus* DSM 41,481 (black histograms) and *Streptomyces sp.* DSM 40,868 (white histograms) grown for 72 h on solid R2YE glucose medium limited in phosphate according to LC/Corona-CAD. TAG stands for triacylglycerol; DAG, for diacylglycerol, FA for fatty acids; PE, for phosphatidylethanolamine; PA, for phosphatidic acid; PI, for phosphatidylinositol; PIMs, for phosphatidylinositol mannosides; and CL, for cardiolipid. Antimycin was detected in *S. antibioticus* DSM 41,481 but not in *Streptomyces sp.* DSM 40,868. Significant differences in lipid content between the two strains are represented by asterisks (ANOVA, *** = $p < 0.001$; ** = $p < 0.01$).

Since the two strains bear the same lipid classes, they most likely possess the same enzymes involved in the biosynthesis of the latter. As a consequence, the difference in their lipid content might be rather due to a difference in the availability of the necessary lipid precursor, acetylCoA. We thus examined, as a priority, through comparative genome analysis, genetic differences between the two strains in pathways involved in the generation, consumption or storage of acetylCoA that could be responsible for the high and low lipid contents of *Streptomyces antibioticus* DSM 41,481 and DSM 40,868, respectively.

2.4. Comparative Analysis of the Sequence of the Genome of Streptomyces Antibioticus DSM 41,481 and DSM 40,868

The genomes of the two strains of *S. antibioticus*—DSM 41,481 and DSM 40,868, called OSCP and OSBF in our collection—were fully sequenced thanks to a combination of Nanopore (Oxford Nanopore Technologies) and Illumina technologies. A hybrid assembly was generated to give a single contig per genome, of 8,473,575 bp and 9,195,693 bp for DSM 41,481 and DSM 40,868, respectively. They possess Terminal Inverted Repeats (TIR) of 26,378 bp and 13,483 bp, respectively. The genomic sequence of strain DSM 41,481 was almost identical to that present in the Genbank database (CM007717.1), with a very strong nucleotide identity over the whole genome (greater than 99.9%). Moreover, the two genomic sequences are fully collinear throughout (not shown). Due to the high quality of the sequencing performed in this work thanks to the dual technology used, we have deposited it in Genbank under the accession number CP050692.

In addition, the assignment of the strain DSM 40,868 to the species *S. antibioticus* was questioned by phylogenetic analyses carried out using the acquired genomic sequence. Indeed, its 16S rDNA sequence was identical to that of *S. lavenduligriseus* strain NBRC 13,405, while it bears only 96.47% identity with *S. antibioticus* DSM 41,481. Furthermore, a phylogenetic reconstruction showed that DSM 40,868 better clustered with *S. lavenduligriseus* strain NBRC 13,405 than with *S. antibioticus* strains. However, since DSM 40,868 is listed as *S. antibioticus* in both the DSMZ and ATCC website collections (DSM 40,868 is also registered as ATCC 11,891), re-naming this strain as *S. lavenduligriseus* would be confusing, so this strain was called *S. sp.* DSM 40,868, and its genome sequence was registered under the Genbank accession number CP050504. The annotation was performed using the RAST tool kit (RASTtk) [31], available on the Rapid Annotation using Subsystem Technology (RAST) platform. *S. antibioticus* DSM 41,481 included 7823 predicted coding DNA sequences (CDSs), while *Streptomyces* sp. DSM 40,868 contained 8637 CDSs. AntiSMASH was used to predict the presence of biosynthetic gene clusters [25]. Twenty-six and forty-six gene clusters were found in the genomes of *S. antibioticus* DSM 41,481 and *S. sp.* DSM 40,868, respectively (Figures S2–S4).

In the comparative analysis of the two genomes, we chose to consider only the reactions catalyzed by a single enzyme that was present in one species but absent in the other.

We first noticed that the enzyme 3.1.3.10 that catalyzes the dephosphorylation of glucose 1P to glucose does not exist in the high lipid-containing strain, *S. antibioticus* DSM 41,481 (Figure S5). The absence of this enzyme might eliminate a futile ATP-consuming cycle of the dephosphorylation/re-phosphorylation of glucose and would allow a more direct and efficient conversion of Glc1P to Glc6P, favorable for the generation of acetylCoA (Figure S5).

The presence in the strain DSM 41,481, but not in DSM 40,868, of the enzyme 1.1.1.83 that catalyzes the conversion of malate into pyruvate and of 2.3.1.54 (Figure S6) that catalyzes the conversion of pyruvate into acetylCoA (Figures S6 and S7) is likely to have a positive impact on acetylCoA availability and thus on the lipid content of DSM 41,481. Furthermore, two enzymes (1.1.99.2 and 2.8.3.12) converting 2-oxoglutarate into hydroxyglutarylCoA are present in the strain DSM 41,481 but absent in DSM 40,868 (Figure S6). Since hydroxyglutarylCoA can eventually lead to the synthesis of crotomyl and butanoylCoA, precursors of odd chain or branched fatty acids, its generation might thus have a positive impact on lipid content.

Concerning nitrogen metabolism, we noted the presence in DSM 40,868 but not in DSM 41,481 of a cyanate lyase (4.2.1.104) that catalyzes the reaction of cyanate with bicarbonate, yielding carbon dioxide and NH_4 (Figure S8). By contrast, we noted the presence in DSM 41,481 but not in DSM 40,868 of the enzyme 1.4.1.3 (Figure S9) that catalyzes the conversion of oxoglutarate into glutamate, consuming a molecule of NH_4. Since NH_4 is known to be inhibitory to lipid biosynthesis [32–34], its generation via the cyanate lyase in DSM 40,868 and its consumption, for glutamate generation, in DSM 41,481 might have negative and positive impacts on lipid accumulation in DSM 40,868 and DSM 41,481, respectively.

We also noticed that one of the multiple routes (catalyzed by the enzyme 1.1.1.169) involved in the conversion of 2-dehydropentoate into pentoate, a metabolite used for the biosynthesis of coenzyme A, is present in DSM 41,481 but absent in DSM 40,868 (Figure S10). Since coenzyme A is crucial to activate acetylCoA for fatty acid biosynthesis, the absence of this enzyme in DSM 40,868 might limit coenzyme A biosynthesis, contributing to its low lipid content.

Altogether, these genetic differences are consistent with the high and low lipid contents of *S. antibioticus* DSM 41,481 and *Streptomyces sp.* DSM 40,868, respectively. However, one cannot totally exclude that the main reason for the high lipid content of *S. antibioticus* DSM 41,481 is its production of antimycin as mentioned above.

3. Discussion

In this issue, we tried to determine whether a statistically significant negative Pearson correlation could be established between total lipid content and antibiotic activity in *Streptomyces* species, since previous studies suggested that such a correlation might exist [7]. The lipid content of a cell relies on its ability to synthetize glycerol3P and acetylCoA, which both stem mainly (but not exclusively) from glycolysis. AcetylCoA is a metabolic node that can have various fates. During active growth, it constitutes the main fuel of the TCA cycle, which generates the metabolic precursors of amino acids used for protein biosynthesis or other anabolic processes. However, if, for some reason (such as nitrogen or phosphate limitation), the TCA cycle and thus anabolic processes slow down, acetylCoA can then be stored as lipids, as in *S. lividans*, or used for polyketide antibiotics biosynthesis, as in *S. coelicolor*. In such a context of low anabolism, amino acids generated from intermediates of the TCA cycle can also be used for the biosynthesis of peptide antibiotics. Since the biosynthesis of these bioactive molecules directly or indirectly requires acetylCoA, their synthesis might be in direct competition with that of lipids. This could explain the negative correlation existing between these two processes, and these molecules can be seen as metabolic sinks when, in conditions of growth slowdown, the metabolites generated by anabolism exceed the needs of anabolism.

However, things might not be as simple as described above, since the biosynthesis of bioactive molecules is usually triggered by some specific physiological or environmental conditions, often linked to nutritional limitation and growth slowdown [12,35], and these molecules are believed to fulfill important regulatory roles for the producing bacteria in such contexts [12]. For instance, *S. coelicolor*, a strain characterized by an active oxidative metabolism consuming acetylCoA and thus bearing a low lipid content, produces antibiotics proposed to contribute to the regulation of its energetic metabolism [12]. Our data suggested that the existence of a negative correlation between lipid content and antibiotic activity, previously established for *S. coelicolor*, was also true for most *Streptomyces* strains, at least on R2YE glucose. However, the existence of exceptions to this general rule was noted. These strains either bear a low lipid content and undetectable antibiotic activity (Type I: *S. brasiliensis*, *S. diastaticus* subspecies *diastaticus* and *S. albus*) or a high lipid content and high antibiotic activity (Type II: *S. bellus* subspecies *bellus*, *S. echinatus* and *S. aridus*). One should be aware that assessing antibiotic activity via the measurement of the diameter of the growth inhibition zones of *Micrococcus luteus* might not reveal all antibiotic production. Indeed, the existence of Type I strains could be easily explained by the insensitivity of *Micrococcus luteus* to the antibiotic produced, which is thus not detected. This was exemplified by the production of antimycin by DSM41481, which has no impact on *Micrococcus* growth. By contrast, Type II strains may produce very small amounts of a specific

antibiotic that *Micrococcus luteus* is highly sensitive to or produce low levels of multiple antibiotics that synergistically impact *Micrococcus luteus* growth etc. Anyhow, if antibiotic biosynthesis is triggered in a strain with a low to medium lipid content, antibiotic biosynthesis is likely to have a significant impact on its lipid content, but such an impact will be hardly visible in a strain bearing high lipid content.

Furthermore, to explain the unexpected lower antibiotic activity on glycerol than on glucose, we propose that oxidative stress might be less severe on glycerol than on glucose since the catabolism of glycerol—and more precisely its conversion into dihydroxyacetone by a glycerol dehydrogenase or into glyceraldehyde by a glyceraldehyde reductase—generates more NADPH than the catabolism of glucose [36,37]. NADPH is an indispensable reduced co-factor necessary to combat and thus reduce oxidative stress [38], since some reports in the literature mention that the biosynthesis of specific antibiotics might be triggered by oxidative stress [39–43]. The biosynthesis of such antibiotics is thus expected to be reduced on glycerol. Antibiotics of this class (defined as class II in Virolle, 2020 [12]) are thought to have anti-oxidant functions via their ability to capture electrons from the respiratory chain to prevent the formation of ROS or NOS, but in doing so, they would also be inhibitory to respiration and thus toxic for living cells.

Lastly, the comparative genomic analysis of two strains—both named *Streptomyces antibioticus*, DSM 41,481 and DSM 40,868—that we found to be more phylogenetically related to *Streptomyces lavenduligriseus* indicated that some genetic differences in various pathways related to the generation/consumption of acetylCoA could be responsible for such differences.

4. Materials and Methods

4.1. Bacterial Strains, Media and Growth Conditions

Most of the fifty-four strains used in this study were ATCC/NRLL/DSM strains. The few that do not come from these collections (*S. albus*, *S. spectabilis*, *S. actuosus*, *S. coelicolor* M145, *S. lividans* TK24, *S. pristinaespiralis* and *S. rimosus* 2535) were generous gifts from John Innes Institute. Viable spores (10^6) of each strain were plated on the surface of four petri dishes (42 mm diameter) of solid modified R2YE medium [44] covered by a cellophane disk (Focus Packaging & Design Ltd., Louth, UK). No sucrose and no K_2HPO_4 were added to this modified solid R2YE medium supplemented with either glucose (50 mM) or glycerol (100 mM) as the main carbon sources. However, the determination of the content of free phosphate in this medium with a PiBlue phosphate assay kit (Gentaur, France) revealed a concentration of free Pi of 1 mM, corresponding to a situation of phosphate limitation. The plates were incubated for 72 h at 28 °C. After 72 h of incubation, mycelia were scraped off the cellophane disks of each plate with a spatula and lyophilized in order to assess their total lipid contents by Fourier transform infra- red spectroscopy (FTIRS) [22–24]. Four agar plugs of each plate were deposited on a lawn of the Actinobacteria *Micrococcus luteus* in order to determine the antibiotic activity of the *Streptomyces* strains against this strain that is known to be sensitive to most antibiotics [45,46]. The growth curves of *Streptomyces antibioticus* DSM 41,481 and *Streptomyces sp.* DSM 40,868, the two strains with extremely high and low total lipid contents, were obtained on the same R2YE medium (Figure 5a), and their lipid content was assessed by LC/Corona-CAD (Figure 5d).

4.2. Determination of Total Lipid Content Using Attenuated Total Reflectance-Fourier Transform Infra Red Spectroscopy (ATR-FTIRS) Measurements

In order to determine total lipid content, lyophilized mycelial samples of the *Streptomyces* strains were subjected to FTIR spectroscopy using a Bruker Vertex 70 FTIR spectrophotometer with a diamond ATR attachment (PIKE MIRacle crystal plate diamond ZnSe) and an MCT detector with a liquid nitrogen cooling system. A reference spectrum resulting from one hundred averaged scans obtained in absence of any sample on the Infra Red support was acquired before each sample analysis. Scans were conducted from 3600 cm^{-1} to 600 cm^{-1} with a spectral resolution of 4 cm^{-1}, with 100 averaged scans for each sample. This technique allows the establishment of spectral fingerprints of the complex biological

structures under investigation. The C-H stretching bands of the CH_2 of fatty acid chains (between 2959 and 2852 cm^{-1}) and the C=O ester stretching band of the ester carbonyl (band near 1740 cm^{-1}) are characteristic of lipids including mainly polar membrane lipids and neutral lipids such as TAG. The height of the sharp and distinct C=O ester stretching band of the ester carbonyl is especially relevant for monitoring the total intracellular lipid contents of the strains [23]. Furthermore, since the biomass protein content can be directly characterized by the amplitude of the Amide I absorption band (1650 cm^{-1}), all the FTIR spectra can be normalized to this band, allowing the comparison of the total lipid contents of the mycelial lawns of different strains. The total lipid contents of the strains assessed by FTIRS, expressed as arbitrary units, was converted into µg of Fatty Methyl Esters (FAME) per mg of dry mycelium using the converting equation established by Millan-Oropeza et al. (2017) [24]. Indeed, in the presence of methanol, fatty acids constitutive of all cellular lipids are esterified to yield FAME that can be accurately quantified by GC/MS [22–24]. The differences in the lipid contents of the strains were clear and highly reproducible.

4.3. Determination of the Antibiotic Activity of the Strains against Micrococcus Luteus

In order to determine the inhibitory impact that each *Streptomyces* strain had on *Micrococcus luteus* growth, four agar cylinders were taken aseptically from each of the replica plates using an appropriate device and were deposited onto the surface of LB agar plates, prepared as follows. Twenty-five microliters of a fresh culture of *Micrococcus luteus* (OD 600 nm of 0.4) were added to 3 mL of soft nutrient agar (SNA) that was poured onto the surface of the LB agar plate. As soon as the SNA containing *Micrococcus luteus* was solidified, the agar plugs were deposited on the surface of the plates and incubated 24 h at 37 °C. For each plate, the size of the four zones of inhibition was measured and reported in an Excel file, and the mean was calculated.

4.4. Statistical Analysis of the Correlation between the Lipid Content and Antibiotic Activity of Studied Streptomyces Strains

The total lipid contents of the strains were expressed as mean ± standard deviation in bar graphs and were subjected to the ANOVA test (Figure 1a,b). Correlation analyses between lipid content and antibiotic activity were achieved using Pearson correlation (Figure 4). All statistical methods and data representation were conducted in R 3.3.2 [47], using the "RVAideMemoire" package [48]; a p-value < 0.05 was considered as statistically significant.

4.5. Lipid Extraction and Characterization by LC/Corona-CAD and LC/MS

Lipid extraction was performed by a procedure derived from Folch's method [49] from four independent cultures of *Streptomyces antibioticus* DSM 41,481 and DSM 40,868. A defined volume (4.5 mL) of chloroform/methanol (1:2) was added to 10 mg of lyophilized *Streptomyces* mycelium and vortexed for 30 s. The mixture was left at ambient temperature for 1 hour, then 1.25 mL of water was added, and the mixture was vortexed for 30 s. The mixture was then centrifuged (1000× g for 10 min) to obtain phase separation. The lower organic phase was collected, and the upper aqueous phase was submitted to a second extraction by adding 2 mL of chloroform/methanol (85:15). The two organic phases were pooled and evaporated under a stream of nitrogen at room temperature. The dry residue was dissolved in 400 µL of isooctane/chloroform (4:1) before analysis. The chromatographic conditions have been described previously [50]. Briefly, lipid class analysis was performed with an Inertsil Silica (150 mm × 2.1 mm I.D, 5 µm) column (GL Sciences Inc., Tokyo, Japan) thermostated at 40 °C. The HPLC instrumentation consisted of the system Dionex U-3000 RSLC (Thermofisher, Villebon, France). A quaternary solvent gradient (Supplementary Table S1) was used to elute all the lipid classes present in the sample by increasing the order of polarity. Lipid class identification was verified by coupling the chromatographic separation to mass spectrometry. MS analyses were performed with a LTQ-Orbitrap Velos Pro (Thermo Fisher Scientific) equipped with an APPI ion source. The MS^2 and MS^3 spectra were obtained in data-dependent acquisition (DDA)

mode. Lipid detection was performed using a Corona-CAD system (ESA, Chelmsford, MA, USA) [50]; the signal was acquired with a Chromeleon data station (Thermo Fisher Scientific, Villebon-sur-Yvette, France). Corona-CAD is a universal detector used for liquid chromatography and described in Dixon and Peterson [51]. The differences in the composition of the lipid classes in the samples are expressed as peak areas. All the data were subjected to Student's t-test using R 3.3.2 [47] and the "multcompView" package [52]. The results obtained are presented as the mean ± standard error; a p-value < 0.05 was considered as statistically significant.

4.6. DNA Isolation, Genome Sequencing and Annotation

After growth in liquid Hickey-Tresner medium [6] at 30 °C for 30 h, DNA purification was performed using the salting-out method [6], followed by chloroform extraction. A hybrid assembly using Oxford Nanopore technology for scaffolding and Illumina technology for sequence improvement was performed. Nanopore reads were generated on a gridION system. The coverage was 30× and 67× for strains DSM 41,481 and DSM 40,868, respectively. The Illumina paired-end libraries were sequenced using a MiSeq system (Illumina). The coverages of the paired-end reads (length, 301 bp) ranged from 249× to 312×. The hybrid assembly was performed using Unicycler [53]. The accession numbers are CP050692 and CP050504 for *S. antibioticus* DSM 41,481 and *Streptomyces* sp. DSM 40,868, respectively. Sequencing and assembly were performed via the I2BC NGS platform (France). The automatic annotation of the genome sequences was achieved using the RAST tool kit (RASTtk [31]) available on the Rapid Annotation using Subsystem Technology (RAST) platform. Furthermore, the annotation files were used as the input for antiSMASH [25] in order to predict the biosynthetic gene clusters content of each genome. Biosynthetic pathways were mapped with KEGG, using the GHOSTZ search program and the BBH (bi-directional best hit) assignment method [54]. We used the default gene data set, to which we added the data sets available for five *Streptomyces* species (*Streptomyces coelicolor*, *Streptomyces avermitilis*, *Streptomyces griseus*, *Streptomyces scabiei* and *Streptomyces noursei*). The presence/absence of specific enzymatic steps was manually checked using BLAST searches [55].

Supplementary Materials: The following are available online at http://www.mdpi.com/2079-6382/9/6/280/s1, Figure S1: LC/Corona-CAD results of total lipid content in *Streptomcyces antibioticus* DSM 41,481 and *Streptomyces sp.* DSM 40,868 grown for 72 h on solid R2YE glucose medium limited in phosphate, Figure S2: Anti-Smash analysis of the genome of *Streptomyces antibioticus* DSM 41,481 (8,473,575 bp), Figure S3: Anti-smash analysis of the genome of *Streptomyces sp.* DSM 40,868 (registered in gene bank as *Streptomyces antibioticus* DSM 40,868 or ATCC 11,891) (9,195,693 bp), Figure S4: Chromosomal position of the biosynthetic gene clusters predicted by antiSMASH along the chromosome of *Streptomyces sp.* DSM 40,868 and *Streptomyces antibioticus* DSM 41,481. Metabolites synthetized by similar biosynthetic pathways are signaled by a vertical bar and named, Figure S5: Comparative analysis of glycolysis/gluconeogenesis pathway of DSM 40,868 and DSM 41,481, Figure S6: Comparative analysis of butanoate metabolism of DSM 40,868 and DSM 41,481, Figure S7: Comparative analysis of pyruvate metabolism of DSM 40,868 and DSM 41,481, Figure S8: Comparative analysis of nitrogen metabolism of DSM 40,868 and DSM 41,481, Figure S9: Comparative analysis of glutamine/glutamate metabolism of DSM 40,868 and DSM 41,481, Figure S10: Comparative analysis of pantothenate and CoA biosynthetic pathways of DSM 40,868 and DSM 41,481, Table S1: Quaternary gradient mobile phase composition.

Author Contributions: Conceptualization, M.-J.V.; methodology, M.D., S.A., A.T. and P.L.; validation, M.-J.V., C.L., S.A., P.C., A.T. and P.L.; formal analysis, C.L. and A.T.; investigation, M.D., C.L., S.A., A.T. and P.L.; resources, M.D., S.A., P.C., A.T. and P.L.; writing—original draft preparation, M.-J.V.; writing—review and editing, C.L., S.A., P.C., A.T. and P.L.; visualization, C.L. and A.T.; supervision, M.-J.V.; project administration, M.-J.V.; funding acquisition, M.-J.V. All authors have read and agreed to the published version of the manuscript.

Funding: This research was funded by dotation of the "Centre National de la Recherche Scientifique" CNRS (http://www.cnrs.fr) and University Paris Saclay (https://www.universite-paris-saclay.fr/en) as well as by the Investment for the Future "Biotechnologies et Bioressources" n°11-BTBR-0003 (PROBIO3), the ANR BioSound-IR (ANR-15-CE09-0002) and Innovantibio (ANR-17-ASTR-0018).

Acknowledgments: We thank Ariane Deniset-Besseau and Rolando Rebois (University of Paris-Saclay) for training and helping Michelle David to assess total lipid content of *Streptomyces* strains using "Attenuated Total Reflectance-Fourier Transform Infra Red Spectroscopy" (ATR-FTIRS).

Conflicts of Interest: The authors declare no conflict of interest.

References

1. Pham, J.V.; Yilma, M.A.; Feliz, A.; Majid, M.T.; Maffetone, N.; Walker, J.R.; Kim, E.; Cho, H.J.; Reynolds, J.M.; Song, M.C.; et al. A Review of the microbial production of bioactive natural products and biologics. *Front. Microbiol.* **2019**, *10*, 1404. [CrossRef]
2. Barka, E.A.; Vatsa, P.; Sanchez, L.; Gaveau-Vaillant, N.; Jacquard, C.; Klenk, H.-P.; Clément, C.; Ouhdouch, Y.; van Wezel, G.P. Taxonomy, physiology, and natural products of actinobacteria. *Microbiol. Mol. Biol. Rev.* **2016**, *80*, 1–43. [CrossRef]
3. Chater, K.F. Recent advances in understanding Streptomyces. *F1000Research* **2016**, *5*, 2795. [CrossRef]
4. Van Wezel, G.P.; McDowall, K.J. The regulation of the secondary metabolism of Streptomyces: New links and experimental advances. *Nat. Prod. Rep.* **2011**, *28*, 1311. [CrossRef]
5. Alvarez, H.M.; Steinbuchel, A. Triacylglycerols in prokaryotic microorganisms. *Appl. Microbiol. Biotechnol.* **2002**, *60*, 367–376. [CrossRef] [PubMed]
6. Kieser, T.; Bibb, M.J.; Buttner, M.J.; Chater, K.F.; Hopwood, D.A. *Practical Streptomyces Genetics*; Innes: Norwich, UK, 2000; ISBN 978-0-7084-0623-6.
7. Esnault, C.; Dulermo, T.; Smirnov, A.; Askora, A.; David, M.; Deniset-Besseau, A.; Holland, I.-B.; Virolle, M.-J. Strong antibiotic production is correlated with highly active oxidative metabolism in Streptomyces coelicolor M145. *Sci. Rep.* **2017**, *7*, 200. [CrossRef] [PubMed]
8. Le Maréchal, P.; Decottignies, P.; Marchand, C.H.; Degrouard, J.; Jaillard, D.; Dulermo, T.; Froissard, M.; Smirnov, A.; Chapuis, V.; Virolle, M.-J.; et al. Comparative proteomic analysis of Streptomyces lividans Wild-Type and ppk mutant strains reveals the importance of storage lipids for antibiotic biosynthesis. *Appl. Environ. Microbiol.* **2013**, *79*, 5907–5917. [CrossRef] [PubMed]
9. Millan-Oropeza, A.; Henry, C.; Lejeune, C.; David, M.; Virolle, M.-J. Expression of genes of the Pho regulon is altered in S. coelicolor. *Sci. Rep.* **2020**, *10*, 8492. [CrossRef] [PubMed]
10. Chouayekh, H.; Virolle, M.J. The polyphosphate kinase plays a negative role in the control of antibiotic production in Streptomyces lividans. *Mol. Microbiol.* **2002**, *43*, 919–930. [CrossRef] [PubMed]
11. Ghorbel, S. Regulation of ppk expression and in vivo function of Ppk in Streptomyces lividans TK24. *J. Bacteriol.* **2006**, *188*, 6269–6276. [CrossRef]
12. Virolle, M.-J. A challenging view: Antibiotics play a role in the regulation of the energetic metabolism of the producing bacteria. *Antibiotics* **2020**, *9*, 83. [CrossRef] [PubMed]
13. Tenconi, E.; Traxler, M.F.; Hoebreck, C.; Wezel, G.P.; Rigali, S. Production of prodiginines is part of a programmed cell death process in streptomyces coelicolor. *Front. Microbiol.* **2018**, *9*, 1742. [CrossRef] [PubMed]
14. Olukoshi, E.R.; Packter, N.M. Importance of stored triacylglycerols in Streptomyces: Possible carbon source for antibiotics. *Microbiology* **1994**, *140*, 931–943. [CrossRef] [PubMed]
15. Packter, N.M.; Olukoshi, E.R. Ultrastructural studies of neutral lipid localisation in Streptomyces. *Arch. Microbiol.* **1995**, *164*, 420–427. [CrossRef] [PubMed]
16. Foley, T.L.; Young, B.S.; Burkart, M.D. Phosphopantetheinyl transferase inhibition and secondary metabolism: PPTase inhibition and secondary metabolism. *FEBS J.* **2009**, *276*, 7134–7145. [CrossRef] [PubMed]
17. Craney, A.; Ozimok, C.; Pimentel-Elardo, S.M.; Capretta, A.; Nodwell, J.R. Chemical perturbation of secondary metabolism demonstrates important links to primary metabolism. *Chem. Biol.* **2012**, *19*, 1020–1027. [CrossRef] [PubMed]
18. Banchio, C.; Gramajo, H. A stationary-phase acyl-coenzyme A synthetase of streptomyces coelicolor A3(2) is necessary for the normal onset of antibiotic production. *Appl. Environ. Microbiol.* **2002**, *68*, 4240–4246. [CrossRef]
19. Wang, W.; Li, S.; Li, Z.; Zhang, J.; Fan, K.; Tan, G.; Ai, G.; Lam, S.M.; Shui, G.; Yang, Z.; et al. Harnessing the intracellular triacylglycerols for titer improvement of polyketides in Streptomyces. *Nat. Biotechnol.* **2020**, *38*, 76–83. [CrossRef]
20. Chen, Y.; Metz, J.; Miller-Xavier, R.K.; Wang, G. Unlocking a new target for streptomycetes strain improvement. *Synth. Syst. Biotechnol.* **2020**, *5*, 33–34. [CrossRef]
21. Schauner, C.; Dary, A.; Lebrihi, A.; Leblond, P.; Decaris, B.; Germain, P. Modulation of lipid metabolism and spiramycin biosynthesis in Streptomyces ambofaciens unstable mutants. *Appl. Environ. Microbiol.* **1999**, *65*, 2730–2737. [CrossRef]

22. Vitry, P.; Rebois, R.; Bourillot, E.; Deniset-Besseau, A.; Virolle, M.-J.; Lesniewska, E.; Dazzi, A. Combining infrared and mode synthesizing atomic force microscopy: Application to the study of lipid vesicles inside Streptomyces bacteria. *Nano Res.* **2016**, *9*, 1674–1681. [CrossRef]
23. Deniset-Besseau, A.; Prater, C.B.; Virolle, M.-J.; Dazzi, A. Monitoring TriAcylGlycerols accumulation by atomic force microscopy based infrared spectroscopy in streptomyces species for biodiesel applications. *J. Phys. Chem. Lett.* **2014**, *5*, 654–658. [CrossRef] [PubMed]
24. Millan-Oropeza, A.; Rebois, R.; David, M.; Moussa, F.; Dazzi, A.; Bleton, J.; Virolle, M.-J.; Deniset-Besseau, A. Attenuated total reflection fourier transform infrared (ATR FT-IR) for rapid determination of microbial cell lipid content: Correlation with gas chromatography-mass spectrometry (GC-MS). *Appl. Spectrosc.* **2017**, *71*, 2344–2352. [CrossRef] [PubMed]
25. Blin, K.; Wolf, T.; Chevrette, M.G.; Lu, X.; Schwalen, C.J.; Kautsar, S.A.; Suarez Duran, H.G.; de Los Santos, E.L.C.; Kim, H.U.; Nave, M.; et al. AntiSMASH 4.0-improvements in chemistry prediction and gene cluster boundary identification. *Nucleic Acids Res.* **2017**, *45*, W36–W41. [CrossRef]
26. Seipke, R.F.; Hutchings, M.I. The regulation and biosynthesis of antimycins. *Beilstein J. Org. Chem.* **2013**, *9*, 2556–2563. [CrossRef]
27. Joynt, R.; Seipke, R.F. A phylogenetic and evolutionary analysis of antimycin biosynthesis. *Microbiology (Reading, England)* **2018**, *164*, 28–39. [CrossRef]
28. Shanbhag, P.; Bhave, S.; Vartak, A.; Kulkarni-Almeida, A.; Mahajan, G.; Villanueva, I.; Davies, J. Screening of microbial extracts for anticancer compounds using streptomyces kinase inhibitor assay. *Nat. Prod. Commun.* **2015**, *10*, 1287–1291. [CrossRef]
29. Chevrette, M.G.; Gutiérrez-García, K.; Selem-Mojica, N.; Aguilar-Martínez, C.; Yañez-Olvera, A.; Ramos-Aboites, H.E.; Hoskisson, P.A.; Barona-Gómez, F. Evolutionary dynamics of natural product biosynthesis in bacteria. *Nat. Prod. Rep.* **2020**, *37*, 566–599. [CrossRef]
30. Yagüe, P.; Lopez-Garcia, M.T.; Rioseras, B.; Sanchez, J.; Manteca, A. New insights on the development of Streptomyces and their relationships with secondary metabolite production. *Curr. Trends Microbiol.* **2012**, *8*, 65–73.
31. Brettin, T.; Davis, J.J.; Disz, T.; Edwards, R.A.; Gerdes, S.; Olsen, G.J.; Olson, R.; Overbeek, R.; Parrello, B.; Pusch, G.D.; et al. RASTtk: A modular and extensible implementation of the RAST algorithm for building custom annotation pipelines and annotating batches of genomes. *Sci. Rep.* **2015**, *5*, 8365. [CrossRef]
32. Valledor, L.; Furuhashi, T.; Recuenco-Muñoz, L.; Wienkoop, S.; Weckwerth, W. System-level network analysis of nitrogen starvation and recovery in Chlamydomonas reinhardtii reveals potential new targets for increased lipid accumulation. *Biotechnol. Biofuels* **2014**, *7*, 171. [CrossRef] [PubMed]
33. Goncalves, E.C.; Koh, J.; Zhu, N.; Yoo, M.-J.; Chen, S.; Matsuo, T.; Johnson, J.V.; Rathinasabapathi, B. Nitrogen starvation-induced accumulation of triacylglycerol in the green algae: Evidence for a role for ROC40, a transcription factor involved in circadian rhythm. *Plant J.* **2016**, *85*, 743–757. [CrossRef] [PubMed]
34. Morin, N.; Cescut, J.; Beopoulos, A.; Lelandais, G.; Le Berre, V.; Uribelarrea, J.-L.; Molina-Jouve, C.; Nicaud, J.-M. Transcriptomic analyses during the transition from biomass production to lipid accumulation in the oleaginous yeast Yarrowia lipolytica. *PLoS ONE* **2011**, *6*, e27966. [CrossRef] [PubMed]
35. Liu, G.; Chater, K.F.; Chandra, G.; Niu, G.; Tan, H. Molecular regulation of antibiotic biosynthesis in streptomyces. *Microbiol. Mol. Biol. Rev.* **2013**, *77*, 112–143. [CrossRef]
36. Husain, A.; Sato, D.; Jeelani, G.; Soga, T.; Nozaki, T. Dramatic increase in glycerol biosynthesis upon oxidative stress in the anaerobic protozoan parasite Entamoeba histolytica. *PLoS Negl. Trop. Dis.* **2012**, *6*, e1831. [CrossRef]
37. Pahlman, A.K.; Granath, K.; Ansell, R.; Hohmann, S.; Adler, L. The yeast glycerol 3-phosphatases Gpp1p and Gpp2p are required for glycerol biosynthesis and differentially involved in the cellular responses to osmotic, anaerobic, and oxidative stress. *J. Biol. Chem.* **2001**, *276*, 3555–3563. [CrossRef]
38. Agledal, L.; Niere, M.; Ziegler, M. The phosphate makes a difference: Cellular functions of NADP. *Redox Rep.* **2010**, *15*, 2–10. [CrossRef]
39. Beites, T.; Oliveira, P.; Rioseras, B.; Pires, S.D.S.; Oliveira, R.; Tamagnini, P.; Moradas-Ferreira, P.; Manteca, Á.; Mendes, M.V. Streptomyces natalensis programmed cell death and morphological differentiation are dependent on oxidative stress. *Sci. Rep.* **2015**, *5*, 12887. [CrossRef]

40. Beites, T.; Pires, S.D.S.; Santos, C.L.; Osório, H.; Moradas-Ferreira, P.; Mendes, M.V. Crosstalk between ROS homeostasis and secondary metabolism in S. natalensis ATCC 27448: Modulation of pimaricin production by intracellular ROS. *PLoS ONE* **2011**, *6*, e27472. [CrossRef]
41. Miranda, R.U.; Gómez-Quiroz, L.E.; Mendoza, M.; Pérez-Sánchez, A.; Fierro, F.; Barrios-González, J. Reactive oxygen species regulate lovastatin biosynthesis in Aspergillus terreus during submerged and solid-state fermentations. *Fungal Biol.* **2014**, *118*, 979–989. [CrossRef]
42. Bibián, M.E.; Pérez-Sánchez, A.; Mejía, A.; Barrios-González, J. Penicillin and cephalosporin biosyntheses are also regulated by reactive oxygen species. *Appl. Microbiol. Biotechnol.* **2020**, *104*, 1773–1783. [CrossRef] [PubMed]
43. Prajapati, D.; Kumari, N.; Dave, K.; Chatupale, V.; Pohnerkar, J. Chromomycin, an antibiotic produced by Streptomyces flavisclerotic us might play a role in the resistance to oxidative stress and is essential for viability in stationary phase. *Environ. Microbiol.* **2019**, *21*, 814–826. [CrossRef] [PubMed]
44. Thompson, C.J.; Ward, J.M.; Hopwood, D.A. DNA cloning in Streptomyces: Resistance genes from antibiotic-producing species. *Nature* **1980**, *286*, 525–527. [CrossRef] [PubMed]
45. Young, M.; Artsatbanov, V.; Beller, H.R.; Chandra, G.; Chater, K.F.; Dover, L.G.; Goh, E.-B.; Kahan, T.; Kaprelyants, A.S.; Kyrpides, N.; et al. Genome sequence of the Fleming strain of Micrococcus luteus, a simple free-living actinobacterium. *J. Bacteriol.* **2010**, *192*, 841–860. [CrossRef]
46. Szczerba, I. Susceptibility to antibiotics of bacteria from genera Micrococcus, Kocuria, Nesterenkonia, Kytococcus and Dermacoccus. *Medycyna Doświadczalna i Mikrobiologia* **2003**, *55*, 75–80.
47. R.Core Team. *A Language and Environment for Statistical Computing*; R Foundation for Statistical Computing: Vienna, Austria, 2013.
48. Hervé, M. RVAideMemoire: Testing and Plotting Procedures for Biostatistics. R Package Version 0.9-75. 2020. Available online: https://CRAN.R-project.org/package=RVAideMemoire (accessed on 4 March 2020).
49. Folch, J.; Lees, M.; Sloane Stanley, G.H. A simple method for the isolation and purification of total lipides from animal tissues. *J. Biol. Chem.* **1957**, *226*, 497–509.
50. Abreu, S.; Solgadi, A.; Chaminade, P. Optimization of normal phase chromatographic conditions for lipid analysis and comparison of associated detection techniques. *J. Chromatogr. A* **2017**, *1514*, 54–71. [CrossRef]
51. Dixon, R.W.; Peterson, D.S. Development and testing of a detection method for liquid chromatography based on aerosol charging. *Anal. Chem.* **2002**, *74*, 2930–2937. [CrossRef]
52. Graves, S.; Piepho, H.-P.; Selzer, L.; Dorai-Raj, S. multcompView: Visualizations of Paired Comparisons. R Package Version 0.1-8. 2019. Available online: https://CRAN.Rproject.org/package=multcompView (accessed on 19 December 2019).
53. Wick, R.R.; Judd, L.M.; Gorrie, C.L.; Holt, K.E. Unicycler: Resolving bacterial genome assemblies from short and long sequencing reads. *PLoS Comput. Biol.* **2017**, *13*, e1005595. [CrossRef]
54. Moriya, Y.; Itoh, M.; Okuda, S.; Yoshizawa, A.C.; Kanehisa, M. KAAS: An automatic genome annotation and pathway reconstruction server. *Nucleic Acids Res.* **2007**, *35*, W182–W185. [CrossRef]
55. Altschul, S.F.; Gish, W.; Miller, W.; Myers, E.W.; Lipman, D.J. Basic local alignment search tool. *J. Mol. Biol.* **1990**, *215*, 403–410. [CrossRef]

© 2020 by the authors. Licensee MDPI, Basel, Switzerland. This article is an open access article distributed under the terms and conditions of the Creative Commons Attribution (CC BY) license (http://creativecommons.org/licenses/by/4.0/).

3. Conclusion

Les profils lipidiques obtenus par LC-Corona-CAD® ont montré que la teneur de l'ensemble des classes de lipides, et pas seulement les TGs comme anticipé, était en moyenne 2,5 fois plus élevée chez Antibioticus DSM 41,481. Ces résultats étaient concordants avec les mesures obtenues par FTIRS (Fourier-transform infrared spectroscopy).

D'autre part, la souche DSM 40,868 a produit une activité antibiotique contre Micrococcus luteus, contrairement au DSM 41,481. Ce test couramment utilisé pouvait laisser penser que la souche DSM 40,868 produisait plus d'antibiotiques. Cependant, la production d'antimycine a été détectée de manière importante seulement chez la souche DSM 41,481 par LC-Corona-CAD®. La présence d'un cluster antimycine NRPS/PKS dans le génome de cette souche a été confirmée par anti-Smash. Notre méthode a donc permis d'alerter sur les éventuels biais liés au type de test utilisé pour déterminer l'activité antibiotique, qui repose exclusivement sur la sensibilité de *Micrococcus luteus*.

Comme les analyses LC-Corona-CAD® ont montré que les deux souches contenaient les mêmes classes lipidiques, ces souches possèdent très probablement les mêmes enzymes impliquées dans la biosynthèse de ces lipides. En conséquence, la différence de leur teneur en lipides pourrait plutôt être due à une différence de disponibilité du précurseur lipidique nécessaire, l'acétyl-CoA. Nous avons donc examiné en priorité, par analyse comparative du génome, les différences génétiques entre les deux souches dans les voies impliquées dans la génération, la consommation ou le stockage de l'acétyl-CoA qui pourraient être responsables des teneurs élevées et faibles en lipides chez *Streptomyces antibiotiques* DSM 41,481 et DSM 40,868. L'analyse génomique a indiqué que certaines différences génétiques dans diverses voies

liées à la génération/consommation d'acétyl-CoA pourrait effectivement être responsable d'une telle différence.

ANNEXE VII. L'INHIBITION DE LA PRODUCTION D'ANTIBIOTIQUES CHEZ *STREPTOMYCES COELICOLOR* SUREXPRIMANT LE REGULATEUR TETR SCO3201 EST CORRELEE AUX MODIFICATIONS DU LIPIDOME DE LA SOUCHE

1. Introduction

Dans une étude précédente [201], nos co-auteurs (Xu et Virolle) ont montré que la surexpression du régulateur SCO3201 provoque l'inhibition de la production l'antibiotique polykétide bleu, l'actinorhodine (ACT) ainsi que la différenciation morphologique chez *Streptomyces coelicolor* M145.

Dans la présente étude [26], nous avons cherché à élucider les processus moléculaires sous-jacents à cette surexpression du régulateur SCO3201.

Pour cela, une analyse comparative des profils lipidiques et génomiques de la souche surexprimant SCO3201 (M145/pWHM3-*SCO3201*) et de la souche témoin contenant le plasmide vide (M145/pWHM3), a été réalisée.

2. Publication 7

Annexe VII.
L'inhibition de la production d'antibiotiques chez Streptomyces coelicolor surexprimant le régulateur TetR SCO3201 est corrélée aux modifications du lipidome de la souche

frontiers in Microbiology

ORIGINAL RESEARCH
published: 23 June 2020
doi: 10.3389/fmicb.2020.01399

The Inhibition of Antibiotic Production in *Streptomyces coelicolor* Over-Expressing the TetR Regulator SCO3201 IS Correlated With Changes in the Lipidome of the Strain

Jun Zhang[1†], Qiting Liang[1†], Zhongheng Xu[1], Miao Cui[1], Qizhong Zhang[1], Sonia Abreu[2], Michelle David[3], Clara Lejeune[3], Pierre Chaminade[2], Marie-Joelle Virolle[3*†] and Delin Xu[1*†]*

[1] Key Laboratory of Eutrophication and Red Tide Prevention of Guangdong Higher Education Institutes, Department of Ecology, School of Life Sciences and Technology, Engineering Research Center of Tropical and Subtropical Aquatic Ecological Engineering, Ministry of Education, Institute of Hydrobiology, Jinan University, Guangzhou, China, [2] Université Paris-Saclay, Lipides, Systèmes Analytiques et Biologiques, Châtenay-Malabry, France, [3] Group "Energetic Metabolism of Streptomyces", Institute for Integrative Biology of the Cell (I2BC), CEA, CNRS, Univ. Paris-Sud, INRA, University Paris-Saclay, Gif-sur-Yvette, France

In condition of over-expression, SCO3201, a regulator of the TetR family was previously shown to strongly inhibit antibiotic production and morphological differentiation in *Streptomyces coelicolor* M145. In order to elucidate the molecular processes underlying this interesting, but poorly understood phenomenon, a comparative analysis of the lipidomes and transcriptomes of the strain over-expressing *sco3201* and of the control strain containing the empty plasmid, was carried out. This study revealed that the strain over-expressing *sco3201* had a higher triacylglycerol content and a lower phospholipids content than the control strain. This was correlated with up- and down- regulation of some genes involved in fatty acids biosynthesis (*fab*) and degradation (*fad*) respectively, indicating a direct or indirect control of the expression of these genes by SCO3201. In some instances, indirect control might involve TetR regulators, whose encoding genes present in close vicinity of genes involved in lipid metabolism, were shown to be differentially expressed in the two strains. Direct interaction of purified His_6-SCO3201 with the promoter regions of four of such TetR regulators encoding genes (*sco0116*, *sco0430*, *sco4167,* and *sco6792*) was demonstrated. Furthermore, *fasR* (*sco2386*), encoding the activator of the main fatty acid biosynthetic operon, *sco2386-sco2390*, has been shown to be an illegitimate positive regulatory target of SCO3201. Altogether our data demonstrated that the *sco3201* over-expressing strain accumulates TAG and suggested that degradation of fatty acids was reduced in this strain. This is expected to result into a reduced acetyl-CoA availability that would impair antibiotic biosynthesis either directly or indirectly.

Keywords: ***Streptomyces coelicolor*, antibiotics, TetR regulator, fatty acid metabolism, RNA-seq**

OPEN ACCESS

Edited by:
Haike Antelmann,
Freie Universität Berlin, Germany

Reviewed by:
Yvonne Mast,
German Collection of Microorganisms and Cell Cultures GmbH (DSMZ), Germany
Ramón I. Santamaría,
Consejo Superior de Investigaciones Científicas (CSIC), Spain

***Correspondence:**
Qizhong Zhang
zhangqzdr@126.com
Marie-Joelle Virolle
marie-joelle.virolle@i2bc.paris-saclay.fr
Delin Xu
xudelin@live.com

†These authors have contributed equally to this work

Specialty section:
This article was submitted to Microbial Physiology and Metabolism, a section of the journal Frontiers in Microbiology

Received: *11 April 2020*
Accepted: *29 May 2020*
Published: *23 June 2020*

Citation:
Zhang J, Liang Q, Xu Z, Cui M, Zhang Q, Abreu S, David M, Lejeune C, Chaminade P, Virolle M-J and Xu D (2020) The Inhibition of Antibiotic Production in Streptomyces coelicolor Over-Expressing the TetR Regulator SCO3201 IS Correlated With Changes in the Lipidome of the Strain. Front. Microbiol. 11:1399. doi: 10.3389/fmicb.2020.01399

INTRODUCTION

Streptomyces are Gram-positive filamentous bacteria living in terrestrial, marine and fresh water ecosystems where they play essential biological roles (van der Meij et al., 2017). These bacteria have great industrial and economic importance since they produce most of the antibiotics in current use and a variety of other bioactive molecules useful to human health (e.g., anti-cancer and anti-inflammatory drugs), agriculture (e.g., fungicides, pesticides, insecticides, and herbicides), or industry (relevant enzymes) (Worthen, 2008; Barka et al., 2016; Baral et al., 2018). On solid medium, *Streptomyces* are characterized by a complex differentiation cycle that starts with the germination of a spore (Bobek et al., 2017), giving rise to a vegetative mycelium. However, when the bacteria faces conditions of nutritional stress, a programmed cell death (PCD) process is triggered (Flardh and Buttner, 2009; Manteca et al., 2010), resulting into the partial lysis of the vegetative mycelium that provides nutrients to support the development of an aerial mycelium (Mendez et al., 1985; Granozzi et al., 1990; Chater, 2006). Subsequently, the ends of the aerial hyphae tips differentiate into unigenomic spores that will disseminate in the environment. In solid-grown cultures, the production of secondary metabolites usually coincides with the onset of morphological differentiation indicating the existence of regulatory features common to these two processes (Chater, 2006; Liu et al., 2013; Wei et al., 2018). Regulatory cascades triggered by the sensing of extracellular and/or intracellular signals are involved in the control of the developmental program (Pereira et al., 2011). These include Ser/Thr/Tyr eukaryotic-like protein kinases or phosphatases (Petrickova and Petricek, 2003; Pereira et al., 2011), membrane-anchored sensory Histidine kinases from two-component systems (Rodriguez et al., 2013), as well as transcriptional regulators able to interact with specific ligands (Romero-Rodriguez et al., 2015). The latter class include regulators of the TetR family that bear a highly conserved helix-turn-helix (HTH) motif usually located in the N-terminal part of the protein involved in DNA binding, and a much more variable ligand-binding domain (Yu et al., 2010; Cuthbertson and Nodwell, 2013). TetR regulators act most often as transcriptional repressors since their binding site usually overlaps the promoter region of their target genes. However when their binding site is located upstream of the −35 promoter region of their regulatory targets, they can also act as activators (Cuthbertson and Nodwell, 2013). The behavior of the couple TetR/regulatory target is intrinsically complex and relies on the intracellular abundance of the specific ligand of the TetR regulator that usually hinders the interaction of the TetR with its target sites (Ahn et al., 2007). We have previously identified a TetR-like regulator SCO3201, whose over-expression in *S. coelicolor* caused inhibition of the biosynthesis of the blue polyketide antibiotic, actinorhodin (ACT) as well as of morphological differentiation of this strain (Xu et al., 2010). SCO3201 was proposed to govern the expression of genes encoding TetR-like regulators and/or of their regulatory targets but only in condition of over-expression since its disruption had no obvious phenotype (Xu et al., 2010). The ability of SCO3201 to control the expression of numerous "illegitimate" targets was attributed to the presence of a long N terminal extension, revealed by crystallographic studies, that would stabilize the interaction of SCO3201 with weakly similar binding sites (Xu et al., 2014). In this study, we performed a comparative RNA-Seq analysis of *S. coelicolor* carrying the empty vector (M145/pWHM3) or the *sco3201* over-expression construct (M145/pWHM3-*sco3201*). This study revealed that the expression of several pathways was affected by the over-expression of *sco3201*. Since a putative negative correlation between antibiotics biosynthesis and TAG content was previously reported (Le Marechal et al., 2013; Esnault et al., 2017), we mainly examined the consequences of *sco3201* over-expression on fatty acid metabolism.

MATERIALS AND METHODS

Streptomyces Strains and Culture Media

The wild-type strain of *S. coelicolor* M145 (Bentley et al., 2002) containing the empty high-copy-number plasmid pWHM3 (Vara et al., 1989) and the previously constructed strain overexpressing *sco3201* (*S. coelicolor* M145/pWHM3-*sco3201*) were used in this study (Xu et al., 2010). R2YE solid medium was used to cultivate *Streptomyces* strains. Thiostrepton (50 μg/ml) was added to the cultures when necessary.

Lipid Extraction and Analysis by LC/Corona-CAD and LC/MS

Lipid extraction was performed from four independent cultures of *S. coelicolor* M145/pWHM3 and *S. coelicolor* M145/pWHM3-*sco3201* using a procedure derived from the Folch's method (Folch et al., 1957). A defined volume (4.5 ml) of chloroform:methanol (1:2) was added to 10 mg of lyophilized *Streptomyces* mycelium and vortexed during 30 s. The mixture was left at ambient temperature for 1 h, then 1.25 ml of water was added. The mixture was vortexed 30 s then centrifuged (1000 g/10 min) to obtain phase separation. The lower organic phase was collected and the upper aqueous phase was submitted to a second extraction by adding 2 ml of chloroform: methanol (85:15). The two organic phases were pooled and evaporated under a stream of nitrogen at room temperature. The dry residue was dissolved in 400 μl of isooctane: chloroform (4:1) before analysis. The chromatographic conditions were as described previously (Folch et al., 1957). Briefly, lipid class analysis was performed with an Inertsil Silica (150 mm × 2.1 mm I.D, 5μm) column (GL Sciences Inc., Tokyo, Japan) thermostated at 40°C. The HPLC instrumentation consisted of system Dionex U-3000 RSLC (Thermo Fisher, Villebon, France). A quaternary solvent gradient (**Supplementary Table 2**) was used to elute the whole lipid classes present in the sample by increasing order of polarity. Lipid classes identification was verified by coupling the chromatographic separation to mass spectrometry. MS analyses were performed with a LTQ-Orbitrap Velos Pro (Thermo Fisher Scientific) equipped with an APPI ion source. The MS^2 and MS^3 spectra were obtained in data dependent acquisition (DDA) mode. Lipid detection was performed using a Corona-CAD system (ESA, Chelmsford, MA, United States) (Abreu et al., 2017); the signal was acquired with a Chromeleon

data station (Thermo Fisher Scientific, Villebon-sur-Yvette, France). Corona-CAD is an universal detector used in liquid chromatography and described by Dixon and Peterson (2002). The differences in composition of the lipid classes in the samples are expressed as peak areas. All data were subjected to the Student's *t*-test using R 3.3.2 and the "multcompView" package. The results obtained are presented as the mean ± standard deviation, a $p < 0.05$ was considered as statistically significant.

RNA Isolation, Transcriptome Analysis by RNA-Seq and qRT-PCR

10^7 spores of each strain were plated on cellophane discs laid on the surface of R2YE solid medium and incubated at 28°C for 24, 36, or 48 h. Mycelium was collected from three independent R2YE plates at various time points and total RNA was isolated using TRIzol-based reagent (Life Technologies, CA, United States) following the manufacturer's instructions. RNA integrity was confirmed by agarose gel electrophoresis, and the absence of genomic DNA was checked by Agilent 2100 RNA 6000 Nano kit. Ribosomal RNA were removed with a Ribo-Zero Magnetic Gold Kit (Epicentre Biotechnologies, Madison, WI, United States). Samples were sent to BaseClear, an independent and accredited service laboratory for DNA-based research to carry out transcriptome analysis by RNA-Seq. The sequences obtained on an Illumina sequencer were filtered for non-coding RNAs and analyzed with CLCbio bioinformatics software packages using the annotated *S. coelicolor* genome as reference (Bentley et al., 2002). Expression values were shown as reads/kb of exon model/million mapped reads, i.e., dividing the total number of exon reads (in this case one exon per reference sequence) by the number of mapped reads (in millions) times the exon length (in this case the length of the reference sequence).

All the differentially expressed genes of interest that were identified by RNA-Seq were subsequently validated by reverse transcription-PCR (qRT-PCR). For qRT-PCR, mtwo micrograms of each RNA samples was used as a template for cDNA synthesis with random primers, using the MLV Reverse Transcriptase (catalog no. M1705; Promega). The program for cDNA synthesis was 70°C/5 min, 42°C/60 min followed by 10 min at 72°C. Ten percent of the cDNA synthesis reaction mixture (2 μl) was used as a template for each subsequent PCR, using the gene-specific primer pairs listed in **Supplementary Table 1**. The PCR program used was as follows: (i) 95°C/1 min, (ii) 95°C/20 s (iii) 62°C/20 s, and (iv) 72°C/20 s with the second to the fourth steps repeated for 40 cycles. Negative controls were carried out without the addition of reverse transcriptase in order to demonstrate that amplified products were derived from RNA transcripts and not from chromosomal DNA.

The RNA seq dataset reported in the present study was deposited in the NCBI databases with accession number of PRJNA624242.

Electrophoretic Mobility Shift Assay (EMSA)

The promoter regions of *sco0116*, *sco0430*, *sco2386*, *sco2390*, *sco4167*, and *sco6792* were amplified from *S. coelicolor* M145 genomic DNA by PCR using primer pairs 0116F/0116R, 0430F/0430R, 2386F/2386R, 2390F/2390R, 4167F/4167R, and 6792F/6792R (**Supplementary Table 1**), respectively. The amplified PCR products were 5′ labeled with FITC (Fluoresceine IsoThioCyanate) by PCR using primer Plabel (**Supplementary Table 1**). Six-histidine-tagged SCO3201 (His_6-SCO3201) was purified from *E. coli* as previously described (Xu et al., 2010). EMSA was performed as described previously (Xu et al., 2010). Briefly, 0.522 pmol of each of the promoter regions was incubated with purified His_6-SCO3201 in various concentrations for 15 min at room temperature in binding buffer (10 mM Tris-HCl, 50 mM KCl, 1 mM DTT, pH 7.5) in a total volume of 20 μl. In order to assess binding specificity, competition assays were carried out using excess amounts of specific competitors of unlabeled *sco3201* promoter region or non-specific competitors of an unlabeled unrelated DNA probe, respectively. After incubation, the reaction mixtures were loaded on a 5% native polyacrylamide gel pre-run at 100 V for 30 min and run at 100 V for 90 min in running buffer (45 mM Tris-HCl, pH 8.3, 45 mM boric acid, 10 mM EDTA). The DNA signal was visualized by fluorescence imaging using a Bio-rad ChemiDoc MP (United States).

RESULTS

The Over-Expression of *sco3201* Alters the Lipidome of *S. coelicolor*

Since our previous results indicated the existence of a negative correlation between TAG content and antibiotic biosynthesis (Le Marechal et al., 2013; Esnault et al., 2017), analysis of the lipid content of M145/pWHM3 and M145/pWHM3-*sco3201* was carried out using LC/Corona-CAD (Abreu et al., 2017). This study revealed that the content in storage lipids of the triacylglycerol family (TAG) and of its direct precursor 1,3 diacylglycerol (DAG) were respectively 1.3 and 1.8-fold more abundant in M145/pWHM3-*sco3201* than in M145/pWHM3 (**Figure 1** and **Supplementary Figure 1**). The mixture Ornithine Lipid (OL)/Phosphatidic Acid (PA)/Monoacyl phosphatidylinositol dimannoside (Ac-PIM2) was also 1.3-fold more abundant in M145/pWHM3-*sco3201* than in M145/pWHM3. *S. coelicolor* is known to have a very low content in OL (Le Marechal et al., 2013; Esnault et al., 2017) and this study revealed that it has also a low PhosphatidylInositol Mannosides (PIM) and thus likely a low Ac-PIM2 content (**Figure 1** and **Supplementary Figure 1**). This suggested that the increase in the intensity of the OL/PA/Ac-PIM2 peak was likely due to an increase of its PA content, another direct precursor of TAG. Consistently, biosynthetic intermediates such as free fatty acids (FA) and monoacylglycerol (MAG), were respectively 1. 1-, and 1.3-fold less abundant in M145/pWHM3-*sco3201* than in M145/pWHM3. Indeed, FA are likely to be transferred by acyltransferases onto MAG to generate DAG than TAG.

In contrast, membranous phospholipids (PL) such as phosphatidylethanolamine (PE, 1.2-fold), phosphatidylinositol (PI, 1.3-fold), phosphatidylinositolmannosides (PIM, 5.7-fold)

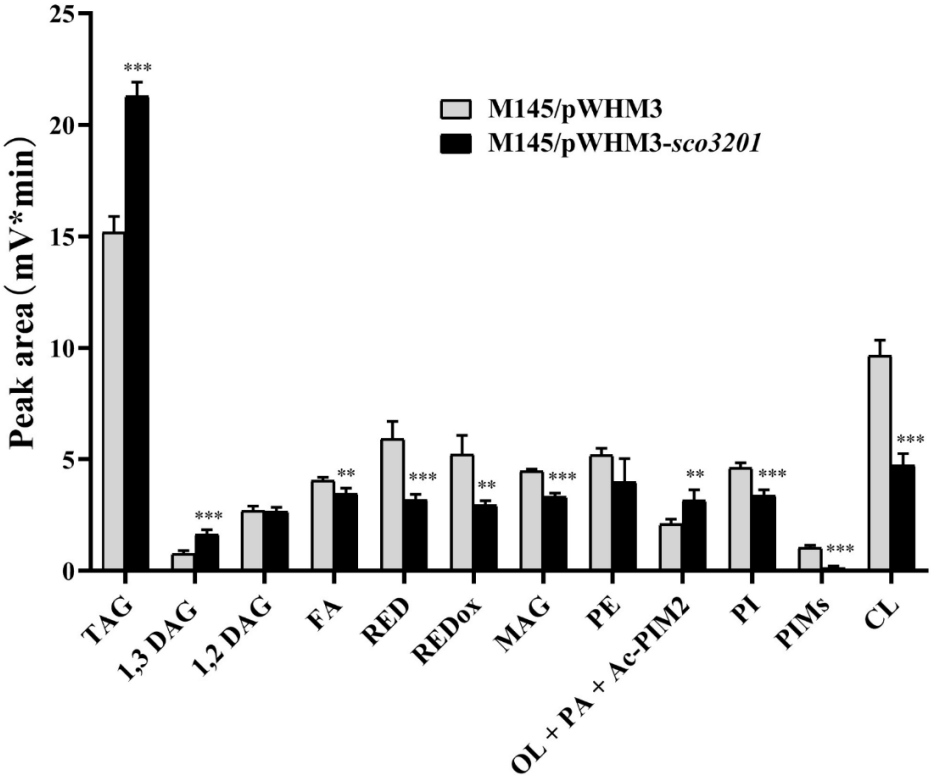

FIGURE 1 | Analysis of total lipid content of *S. coelicolor* M145/pWHM3 (black histograms) and *S. coelicolor* M145/pWHM3-*sco3201* (light gray histograms) by LC/MS expressed in arbitrary unit (mV*min) representing the peak area of each lipid specie detected by the Corona-CAD system used in this study. TAG stands for TriAcylGlycerol, DAG for DiAcylGlycerol, FA for Fatty Acids, RED for Undecylprodigiosin, REDox for oxidized Undecylprodigiosin, MAG for MonoAcylGlycerol, PE for PhosphatidylEthanolamine, OL for Ornithine Lipid, PA for Phosphatidic Acid, Ac-PIM2 for monoACyl PhosphatidylInositol diMannoside, PI for Phosphatidyl Inositol, PIMs for PhosphatidylInositol Mannosides and CL for CardioLipid. Significant difference of lipid content between the two strains are represented by an asterisk (ANOVA, ***$p < 0.001$; **$p < 0.01$).

and cardiolipin (CL, 1.9-fold) were all less abundant in M145/pWHM3-*sco3201* than in M145/pWHM3 (**Figure 1** and **Supplementary Figure 2**). This indicated that FA generated by the strain are rather being used for TAG than for PL biosynthesis.

Global Analysis of RNA-Seq Data Revealed a General Repressing Role of SCO3201

In order to determine the molecular processes underpinning the contrasted phenotypic features of the two strains, comparative RNA-sequence analysis (RNA-Seq) of the latter was carried out. Analysis of the data revealed that 121, 1191, and 1108 genes were differentially expressed at 24, 36, and 48 h, respectively, in the two strains. This represents approximately 1.5, 15, and 14% of the genes of *S. coelicolor*, respectively (**Figure 2**). Eighty three and sixty four percent of the differentially expressed genes were down-regulated at 36 and 48 h, respectively, indicating the preferential repressing role of SCO3201 (**Supplementary Data** and **Figure 2**). RNA-Seq data analysis revealed that the transcription of the TetR family regulator SCO3201 itself was 17-fold upregulated in M145/pWHM3-*sco3201*, indicating the successful overproduction of *sco3201* driven by the strong, constitutively expressed *ermE** promoter (**Supplementary Table 3**). RNA-Seq data analysis also revealed the differential expression of numerous genes belonging to various pathways of primary or specialized/secondary metabolism (**Table 1** and **Supplementary Table 4**). Pathways of primary metabolism include starch and sucrose metabolism, glycolysis, fatty acid biosynthesis (FAB) or degradation (FAD), TCA cycle and aromatic amino acids (phe, tyr, trp) biosynthesis or degradation. Detailed comments concerning pathways directing the synthesis and specialized/secondary metabolism are provided in the following section.

Annexe VII.

L'inhibition de la production d'antibiotiques chez Streptomyces coelicolor surexprimant le régulateur TetR SCO3201 est corrélée aux modifications du lipidome de la souche

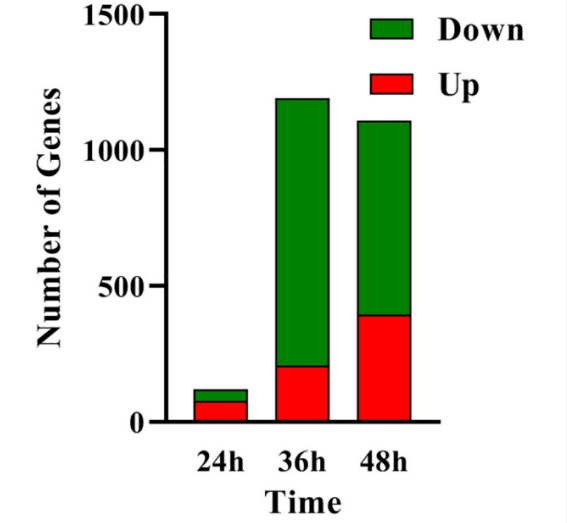

FIGURE 2 | RNA-Seq data: number of genes up- (in red) and down- (in green) regulated in M145/pWHM3-*sco3201* in comparison with M145/pWHM3 at 24, 36, and 48 h, respectively.

The Expression of Most Genes of Specialized/Secondary Metabolite Biosynthetic Pathways Was Down-Regulated in *S. coelicolor* Over-Expressing *sco3201*

The expression of 23 among the 28 known gene clusters that potentially direct the biosynthesis of secondary metabolites in *S. coelicolor* (Bentley et al., 2002; Challis and Hopwood, 2003) was down-regulated in the strain over-expressing *sco3201* (**Figure 3**). These included the pathways directing the biosynthesis of CDA (calcium-dependent antibiotic), RED (undecylprodigiosin), ACT (actinorhodin) and gray spore pigment (**Figure 3**; Feitelson et al., 1985; Malpartida and Hopwood, 1986; Kelemen et al., 1998; Bentley et al., 2002; Hojati et al., 2002).

The expression of 35 among the 39 genes of the CDA cluster (*sco3210-sco3249*) was down-regulated at 24 and 36 h (**Figure 3** and **Supplementary Data**), whereas the level of expression of the transcriptional activator CdaR (*sco3217*) (Ryding et al., 2002) remained unchanged at the three time points (**Supplementary Data**). Interestingly, the expression of the two component system AbsA (*sco3225*)/AbsA2 (*sco3226*) as well as that of *sco3222*, encoding a putative secreted phospholipase A2, and of *sco3216*, encoding a putative cation transport ATPase, was up-regulated in this strain, but only at 24 h (**Supplementary Data**).

The expression of the genes *sco5882* to *sco5898* of the RED biosynthetic gene cluster (*sco5877-sco5898*), was also clearly down-regulated in M145/pWHM3-*sco3201*, whereas the expression of the genes *sco5877* to *sco5881* including the two pathway-specific regulatory genes *redD* (*sco5877*)

TABLE 1 | RNA-Seq data: List of genes up- or down-regulated in M145/pWHM3-*sco3201* in comparison with M145/pWHM3.

Gene ID[a]	Protein name	logFC	
		36 h	48 h
Starch and sucrose metabolism			
sco0765	Secreted endoglucanase	0	−1.092
sco1879	Putative secreted pectinesterase	9.994	0
sco2228	Alpha-glucosidase	−1.867	−2.593
sco2649	Putative 4-alpha-glucanotransferase	−1.955	−1.337
sco3780	Putative threalose 6 phosphate hydrolase	−1.297	0
sco4285	Putative sugar kinase	−1.308	0
sco4288	Putative threalose 6 phosphate phosphatase	−2.402	0
sco4290	Putative possible trehalose-phosphate synthase	−1.697	0
sco5440	1,4-alpha-glucan branching enzyme	−1.787	−1.534
sco6110	Putative glucose kinase/N-acetylmannosamine kinase	−1.625	0
sco7020	Secreted alpha-amylase	−1.481	0
sco7332	1,4-alpha-glucan branching enzyme	0	−1.325
Glycolysis			
sco2119	6-phosphofructokinase	0	−1.946
sco4979	Putative phosphoenolpyruvate carboxykinase	0	1.559
sco5679	Glyceraldehyde 3-phosphate dehydrogenase	−1.370	0
sco6110	Putative sugar kinase	−1.625	0
sco6818	Phosphoglycerate mutase	1.347	0
sco7040	Glyceraldehyde-3-phosphate dehydrogenase	0	1.409
sco7511	Glyceraldehyde 3-phosphate dehydrogenase	0	3.915
Fatty acid biosynthesis			
sco0427	Putative acyltransferase	0	0
sco0428	**Putative TetR-family transcriptional regulator**	−1.053	1.789
sco0548	Putative 3-oxoacyl-(acyl-carrier-protein) synthase	−3.272	−3.765
sco1266	3-oxoacyl-[acyl-carrier-protein] synthase II	0	−2.142
sco1271	Putative 3-oxoacyl-[acyl-carrier-protein] synthase III	0	−1.831
sco1831	FabG-like 3-ketoacylACP reductase	−1.590	0
sco2131	Putative long chain fatty acid CoA ligase	0	1.214
sco2387	Malonyl CoA:acyl carrier protein malonyltransferase	0	1.004
sco3246	Putative 3-oxoacyl-[acyl carrier protein] synthase III	−1.856	2.109
sco3248	Putative 3-oxoacyl-[acyl carrier protein] synthase II	−2.040	2.242
sco4167	**Putative TetR-family transcriptional regulator**	−1.601	0
sco5886	3-oxoacyl-[acyl-carrier-protein] synthase II	−1.673	−1.702
sco5888	3-oxoacyl-ACP synthase III	−1.197	−1.713
sco6564	3-oxoacyl-[acyl-carrier-protein] synthase II	0	1.437
Fatty acid degradation			
sco0116	**Putative TetR-family transcriptional regulator**	1.139	0

(Continued)

TABLE 1 | Continued

Gene ID[a]	Protein name	logFC	
		36 h	48 h
sco0310	**Putative TetR-family transcriptional regulator**	1.048	0
sco3247	Putative acyl-CoA oxidase	−1.568	1.934
sco4502	Putative ketoacyl-CoA thiolase	−1.037	0
sco5399	Probable acetoacetyl-coA thiolase	1.111	0
sco6027	Acetyl-CoA acetyltransferase (thiolase)	1.068	1.342
sco6475	FadB-like enzyme	0	−1.366
sco6787	Probable acyl-CoA dehydrogenase	0	−1.804
sco6789	Putative fatty oxidation protein	0	−1.304
sco6790	Putative long chain fatty acid CoA ligase	0	−1.078
sco6792	**Putative TetR-family transcriptional regulator**	2.253	
TCA cycle			
sco5831	Putative citrate synthase-like protein	−1.238	0
sco4388	Putative citrate synthase	0	−1.786
sco1268	Acyltransferase of pyruvate/2-oxoglutarate dehydrogenase complex,	0	−1.518
sco1269	AcoB, pyruvate/2-oxoglutarate/dehydrogenase complex	0	−1.817
sco1270	AcoA, pyruvate/2-oxoglutarate/dehydrogenase complex (TPP)	−1.529	−4.042
sco3831	bkdA2, branched-chain alpha keto acid dehydrogenase subunit E1	−1.468	0
Oxidative stress			
sco0666	Catalase (EC 1.11.1.6).	−1.787	0
sco7590	Catalase	−1.555	−1.243
sco6204	Putative catalase	0	−1.179
Aromatic amino acids biosynthesis			
sco1859	Putative aminotransferase	−1.243	0
sco3210	Putative 2-dehydro-3-deoxyheptonate aldolase	−1.470	1.906
sco3211	Putative indoleglycerol phosphate synthase	−1.850	2.150
sco3212	Probable anthranilate phosphoribotransferase	−1.892	1.414
sco3213	Probable anthranilate synthase component II	−2.142	0
sco3214	Probable anthranilate synthase component I	−1.762	1.719
sco6819	3-phosphoshikimate 1-carboxyvinyltransferase.	1.425	0
Aromatic amino acids degradation			
sco0199	Putative alcohol dehydrogenase	0	5.466
sco1204	Putative aldehyde dehydrogenase	−1.344	0
sco1715	Putative homogentisate 1,2-dioxygenase	−1.336	0
sco2700	Tyrosinase (monophenol monooxygenase)	0	−1.967
sco2927	Putative 4-hydroxyphenylpyruvate dioxygenase	−1.824	0
sco3645	Putative hydrolase	−1.335	0
sco4681	Putative short chain dehydrogenase	0	−1.026
sco7035	Succinate-semialdehyde dehydrogenase	−1.550	−2.401

[a]*The TetR-family genes are in bold. "+": upregulated in M145/pWHM3-sco3201; "-": down-regulated in M145/pWHM3-sco3201. "0": No significant change detected between the two strains on the basis of RNA-Seq data.*

(Takano et al., 1992) and *redZ* (*sco5881*) (White and Bibb, 1997) remained unchanged (**Supplementary Data**).

The expression of 19 of the 21 genes of the ACT biosynthetic gene cluster (*sco5071-sco5092*) was down-regulated at 36 and 48 h, whereas the expression of the pathway specific TetR-like transcriptional factor ActII-1/AtrA (*sco5082*) as well as that of its regulatory target, ActII-ORF4 (*sco5085*), the activator of the ACT cluster (Uguru et al., 2005), remained unchanged (**Supplementary Data**).

The expression of other pathways such as those directing the synthesis of eicosapentaenoic acid (*sco0124-sco0129*), lantibiotic (*sco0267-sco0270*), THN/flaviolin (*sco1205-sco1208*), 5-hydroxyectoine (*sco1864-sco1867*), melanin (*sco2700-sco2701*), gray spore pigment (*sco5314-sco5320*), geosmin (*sco6073*), SapB (*sco6681-sco6685*), hopene (*sco6764-sco6769*), germicidin (*sco7221*), 2-methylisoborneol (*sco7700-sco7701*), the siderophores coelichelin (*sco0489-sco0499*), desferrioxamine (*sco2782-sco2785*), and putative siderophore encoded by *sco5799-sco5801* as well as the PKS encoding genes (*sco1265-sco1273*) and (*sco7670-sco7671*) was also down-regulated in M145/pWHM3-*sco3201* (**Figure 3**). The transcriptional activity of genes of the coelibactin cluster (*sco7681-sco7691*) was rather complex and puzzling, since the expression of *sco7681-sco7682* and *sco7691* as well as that of *sco7688* was up-regulated in M145/pWHM3-*sco3201* at 24 and 36 h, respectively, whereas the expression of *sco7687* and *sco7689* was up-regulated in the control strain at 36 h (**Figure 3**).

In contrast, the expression of the pathways directing the synthesis of the carotenoid pigment, isorenieratene (*sco0185-sco0191*), as well as that of the yellow pigment coelimycin P1 (*sco6273-sco6274*) and of another polyketide (*sco6826-sco6827*) was up-regulated in M145/pWHM3-*sco3201* at 48 and 36 h, respectively (**Figure 3**). The expression of four genes (*sco7681, sco7682, sco7688,* and *sco7691)* belonging to of the coelibactin cluster (*sco7681-sco7691*) was also up-regulated in M145/pWHM3-*sco3201* at 24 and 36 h, whereas the expression of two other genes (*sco7687* and *sco7689)* was up-regulated in the control strain at 36 h (**Figure 3**). This indicated a complex regulation of this pathway.

The Expression of Most Genes in Fatty Acid Biosynthesis (*fab*) Was Up-Regulated in the *sco3201* Over-Expressing Strain

Since the lipid content of the control strain and the strain over-expressing s*co3201* greatly varied, the expression of genes involved in fatty acid biosynthesis (*fab*) or degradation (*fad*) was examined in our RNA-Seq data. This revealed that a few *fab* and *fad* genes were differentially expressed in the two strains at 36 and/or 48 h (**Table 1** and **Figure 4**).

The expression of four *fab* genes was up-regulated whereas that of two was down-regulated in M145/pWHM3-*sco3201*. Up-regulated genes include *sco0117* encoding a FabG-like short-chain dehydrogenase/reductase (up-regulated by 2.3-fold at 72 h), *sco2131* encoding a putative long chain fatty acid CoA synthetase (up-regulated by 2.3-fold at 48 h), *sco4168* encoding

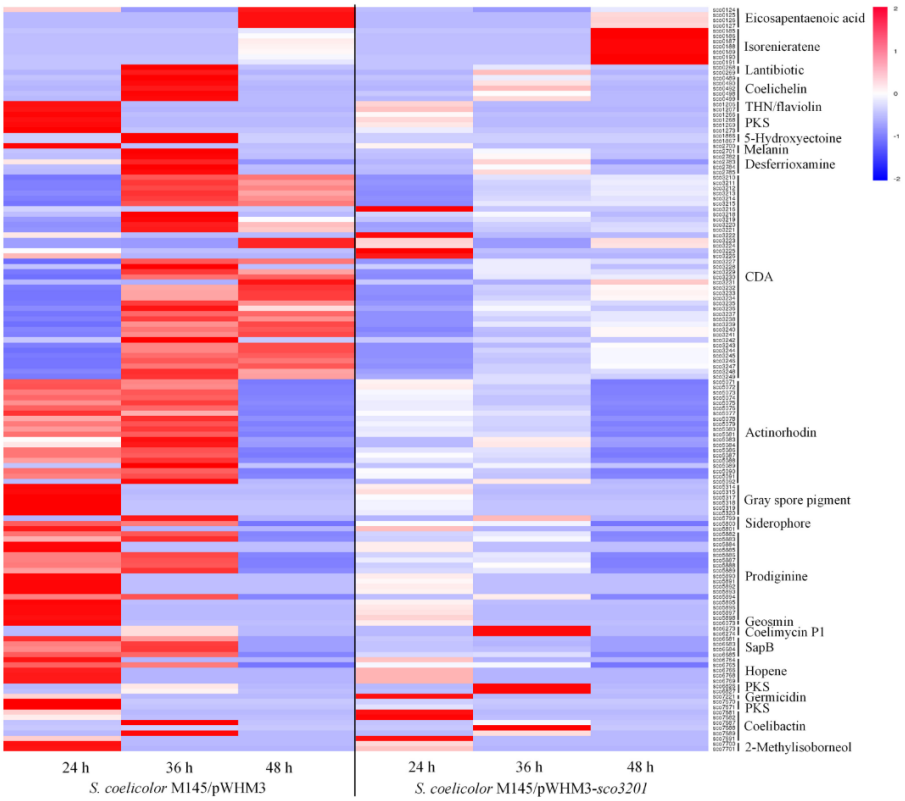

FIGURE 3 | Heat map of transcripts of gene clusters potentially directing the biosynthesis of secondary metabolites with significant abundance change (ANOVA, adjusted $p < 0.01$) between *S. coelicolor* M145/pWHM3-*sco3201* and the control strain *S. coelicolor* M145/pWHM3. RNA samples were prepared from cultures of the strains grown on modified R2YE solid medium for 24, 36, and 48 h, respectively. Only transcripts showing significant abundance change between the two strains (ANOVA, adjusted $p < 0.05$) are displayed. Clusters were named according to the nomenclature used previously (Jeong et al., 2016). Gene identifiers are indicated as SCO numbers for both strains. Relative transcript level was indicated on a color scale from red (high) to blue (low) in *S. coelicolor* M145/pWHM3-*sco3201*.

putative FabG-like protein (up-regulated by 2.4-fold at 72 h) and *sco6564* encoding a FabH2-like 3-oxoacyl-[acyl-carrier-protein] synthase II catalyzing the synthesis of 3-ketoacyl-ACP from malonyl-ACP (Revill et al., 2001) (up-regulated by 2.6-fold at 48 h) (**Figure 4** and **Table 1**). Furthermore, since the regulator FasR is known to be the activator of the major fatty acid biosynthetic operon, *fabDHPF* operon (Arabolaza et al., 2010), we tested its expression level in qRT-PCR and found that it was up-regulated (2.4-fold) in M145/pWHM3-*sco3201* as well as the genes known to be under its positive control, *sco2387* (2-fold) and *sco2390* (1.2-fold) (**Figure 4** and **Table 1**). The up-regulation of these genes is consistent with enhanced fatty acid biosynthesis and thus enhanced TAG content in M145/pWHM3-*sco3201*.

However, in contrast, the expression of some other *fab* genes was down-regulated in M145/pWHM3-*sco3201*. These include *sco0548* encoding a FabB2-like 3-oxoacyl-[acyl-carrier-protein] synthase and *sco1831* encoding a FabG-like 3-ketoacyl ACP reductase that were down-regulated 14- and 3-fold, at 48 and 36 h, respectively (**Table 1**).

In some of the cases mentioned above, genes encoding TetR regulators were present in the vicinity of *fab* genes/clusters and were also differentially expressed in the two strains as determined by qRT-PCR using RNA prepared from 24, 36, 48, and 72 h grown cultures of both strains. Our data revealed that the up-regulation (by 2.2-fold at 36 h) of the expression of the TetR encoding gene, *sco0116*, in M145/pWHM3-*sco3201*, was correlated with the up-regulation of its divergent gene *sco0117* (**Table 1** and **Figure 4**), whereas, in contrast, the down-regulation (by 0.8-fold at 72 h) of the expression of *sco0430* encoding another TetR regulator, was correlated with the up-regulation (by 1.9-fold at 72 h) of the expression of its divergent gene *sco0429* (**Figure 4**). Since TetR regulators often regulate the expression of their neighboring genes (Ramos et al., 2005; Cuthbertson and Nodwell, 2013), these observations could suggest that SCO0116 activates the expression of *sco0117* whereas SCO0430 represses that of *sco0429*. Such hypothesis is consistent with the positioning of the putative SCO3201 binding site in the promoter region of these genes, since a conserved BS was found to be located upstream of and

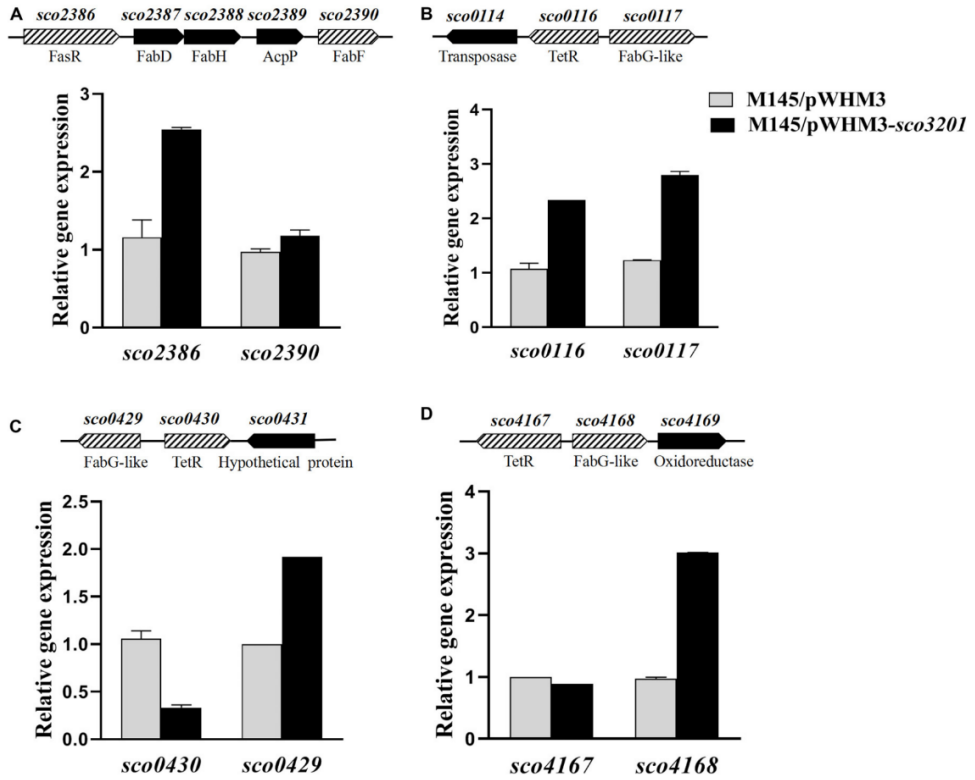

FIGURE 4 | Quantitative analysis of the transcriptional level of *fasR* (*sco2386*) and of putative TetR regulatory targets of SCO3201 (*sco0116*, *sco0430*, *sco4147*) and their neighboring genes by qRT-PCR in the control strain *S. coelicolor* M145/pWHM3 (black histograms) and in *S. coelicolor* M145/pWHM3-*sco3201* (gray histograms) at 72 h. Schematic representation of the genetic surroundings of each TetR regulator encoding gene is provided above each qRT-PCR results. SCO names and putative protein function are shown above and below the genetic maps, respectively. qRT-PCR analysis of the expression level of *sco2386* and *sco2390* **(A)**, *sco0116* and *sco0117* **(B)** *sco0430* and *sco429* **(C)**, and *sco4167* and *sco4168* **(D)**.

in overlap of the promoter regions of *sco0117* and *sco0429*, respectively (**Figure 5**). In contrast, the up-regulation of the expression of *sco4168* at 72 h was not correlated with any change in the level of expression of its neighboring TetR regulator encoding gene (**Figure 4**), suggesting that the latter (*sco4167*) does not regulate the expression of *sco4168*. The expression of *sco4168* might thus be regulated directly by SCO3201 or by another TetR regulator under the control of SCO3201.

The Expression of Most Genes Involved in Fatty Acid Degradation (*fad*) Was Down-Regulated in the *sco3201* Over-Expressing Strain

The expression of 6 *fad* genes (*sco3247*, *sco4502*, *sco6475*, *sco6787*, *sco6789*, and *sco6790*) was down-regulated in M145/pWHM3-*sco3201* whereas the expression of 2 *fad* genes *(sco5399 and sco6027)* was up-regulated (**Table 1** and **Supplementary Data**). *fad* genes whose expression was down-regulated include some genes of the *sco6785-sco6790* cluster, encoding proteins putatively involved in fatty acid degradation (FAD), such as *sco6787*/*acdH3* (acyl-CoA-dehydrogenase), *sco6789* (FadB/FadJ-like fatty acid oxidation protein) and *sco6790* (acyl-CoA ligase) (Yang et al., 1988; Menendez-Bravo et al., 2017), whose expression was 3. 5-, 2. 5-, and 2.1-fold down-regulated at 48 h, respectively (**Table 1** and **Supplementary Figure 2**). The down-regulation of the expression of these *fad* genes likely results into a less efficient degradation of fatty acid and thus into a reduced generation of acetyl-CoA and NADPH.

RNA-Seq analysis revealed that the expression of the gene, *sco6792*, encoding the TetR regulator present in the vicinity of this cluster was 4-fold up-regulated in M145/pWHM3-*sco3201* at 24 h (**Table 1** and **Supplementary Figure 2**). This suggests that this regulator represses the expression of genes of this cluster. However, the expression of another gene of this cluster, *sco6788*, encoding a putative thiolase was 2.3-fold up-regulated at 24 h (**Table 1** and **Supplementary Figure 2**) indicating a complex regulation of the expression of some genes of this cluster. Interestingly, the expression of two other thiolases encoding

Annexe VII.

L'inhibition de la production d'antibiotiques chez Streptomyces coelicolor surexprimant le régulateur TetR SCO3201 est corrélée aux modifications du lipidome de la souche

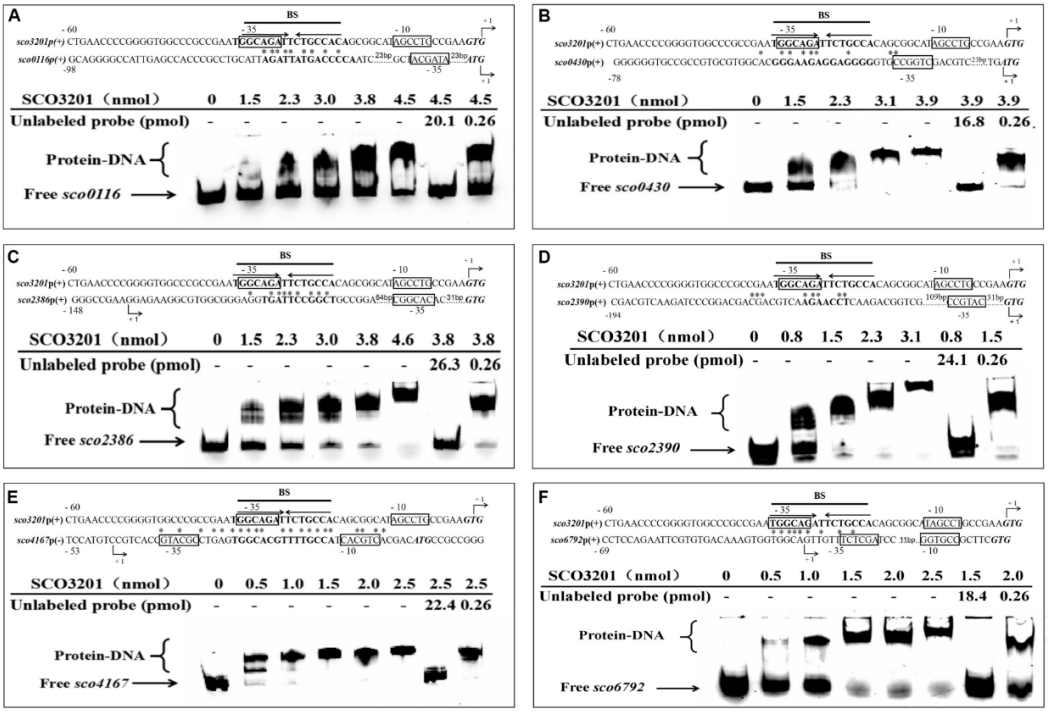

FIGURE 5 | Electrophoretic mobility shift assay of purified SCO3201 with its putative regulatory promoter targets: *sco0116* **(A)**, *sco0430* **(B)**, *sco2386* **(C)**, *sco2390* **(D)**, *sco4167* **(E)**, and *sco6792* **(F)**. In all cases, 0.522 pmol of FITC-labeled probe was used. The specific (unlabeled target promoters) and non-specific (irrelevant DNA) competitors were introduced in lane 7 and lane 8, respectively. BS indicates the core binding site of SCO3201. Putative −10 and −35 regions are boxed. The predicted transcriptional sites (PTS) are indicated by +1 with bent arrows. Translational start codons are in italic and bold. Consensus palindromic sequence of the SCO3201 binding motif is indicated by inverted arrows above the sequence line of the promoter region of *sco3201* on each EMSA result. The nucleotides conserved between the promoter region of a given gene and the BS of SCO3201 are marked by asterisks.

genes, *sco5399* and *sco6027* was also up-regulated (2.1- and 2.5-fold) at 36 and 48 h, respectively (**Table 1** and **Supplementary Figure 2**). These enzymes catalyze the biosynthesis of acyl-CoA from acyl chain and CoA or conversely the release of CoA from acyl-CoA. They are therefore involved in both biosynthetic and degradative pathways and their expression might thus be subjected to a specific regulation.

However, in some cases the putative regulatory interaction between a TetR regulator and its neighboring genes involved in lipid metabolism could not even be hypothesized. For instance, the expression of the TetR regulator encoding gene, *sco0310*, was 2-fold up-regulated in M145/pWHM3-*sco3201* (**Table 1** and **Supplementary Figure 2**), whereas the level of expression of its neighboring genes, *sco0311* encoding a FadD-like long-chain-fatty-acid-CoA ligase and *sco0312* encoding a FadE-like acyl-CoA dehydrogenase (Menendez-Bravo et al., 2017), was unchanged. Similarly, the expression of *sco6475*, encoding a FadB-like 3-hydroxyacyl-CoA dehydrogenase, was shown to be 2.6-fold down-regulated in M145/pWHM3-*sco3201* at 48 h (**Table 1** and **Supplementary Figure 2**), whereas the expression of its close-by TetR regulator encoding gene, *sco6474*, remained unchanged. This suggested that the expression of these genes might be controlled by other regulators under the control of SCO3201, since no SCO3201 binding site (BS) was detected in their promoter region.

Identification of SCO3201 Binding Sites in the Promoter Regions of Its Putative Regulatory Targets

In order to establish the ability of SCO3201 to interact with the promoter region of its putative targets genes defined above, the MEME program[1], was used to search the previously identified palindromic binding site of SCO3201 (BS: TGGCAGATTCTGCCA) (Xu et al., 2010) in the promoter regions of these genes. Putative operator sequences bearing similarity to SCO3201 binding site were discovered in the promoter regions of the TetR regulators encoding genes *sco0116*, *sco0430*, *sco4167*, and *sco6792* as well as in that of *fasR* (*sco2386*), encoding the positive regulator of the expression

[1]http://meme-suite.org/

of the major fatty acid biosynthetic operon, *fabD-H-acp-fabF operon* and of *fabF* (*sco2390*), a member of this operon (**Figure 5**; Arabolaza et al., 2010).

EMSA was performed using FITC-labeled target promoter regions and His_6-SCO3201 purified from *E. coli*. The results indicated that purified His_6-SCO3201 was able to specifically bind and delay the migration of the fragments carrying the promoter regions of these target genes (**Figure 5**). A competition assay was performed using excess amounts of unlabeled target promoter region to the reaction mixture. This successfully outcompeted the specific interactions and eliminated the presence of the delayed DNA fragments (**Figure 5**, lane 7). In contrast, when another DNA fragment (+11 to +444 relative to the translational start site of *sco3201*) was added, the delayed migration of the shifted bands remained, indicating the absence of competition (**Figure 5**, lane 8). Altogether, these data demonstrated the specificity of the interaction of SCO3201 with the promoter regions of these genes. The putative SCO3201 binding sites in the promoter regions of *sco0430* and *sco4167* overlapped their −35 promoter regions (**Figure 5**). The location of this BS was predicted to impair RNA polymerase binding leading to down-regulation of the expression of these genes. This prediction was verified by qRT-PCR experiment for *sco0430* but not for *sco4167* whose expression was similar in the two strains (**Figure 4**). Our EMSA results also demonstrated direct binding of SCO3201 to the promoters regions of *sco2386* (activator FasR) and *sco2390* (FabF-like), and the position of the BS of SCO3201, upstream of the −35 region (position of activator site), is consistent with the activation of the expression of these genes by SCO3201 as shown in **Figure 4**.

Our EMSA results thus demonstrated the specific binding of His_6-SCO3201 to the target promoter regions and most of them are consistent with RNA-Seq and qRT-PCR data. This indicated that, *in vivo* and in conditions of over-expression, SCO3201 likely regulates positively or negatively the expression of these genes.

DISCUSSION

The over-expression of *sco3201*, encoding a TetR regulator, was previously shown to inhibit antibiotic production and morphological differentiation in *S. coelicolor* (Xu et al., 2010). In this study, we demonstrated that these phenotypic changes were correlated with higher TAG content and lower phospholipid (PL) content as well as with the up-regulation of the *fab* genes and down-regulation of the *fad* genes found to be differentially expressed in the two strains (**Table 1** and **Figures 4**, **6**). This regulatory impact could be either direct or indirect, mediated by other TetR regulators present or not in the vicinity of *fab* or *fad* genes/clusters.

The enhanced TAG synthesis that requires enhanced fatty acid (FA) synthesis combined with predicted reduced FA degradation linked to down-regulation of the expression of *fad* genes is expected to lead to a reduction of acetyl-CoA availability in M145/pWHM3-*sco3201*. The enhanced TAG content and thus enhanced TAG biosynthesis in M145/pWHM3-*sco3201* might be responsible for the lower PL content since the biosynthesis of these two lipids classes use the same FA pool. Furthermore, PL being major phosphorus reservoirs, reduced PL synthesis is expected to lead to phosphorus saving leading to higher internal phosphate availability. Consequently, reduced availability of acetyl-CoA due to enhanced TAG synthesis and putative enhanced availability of internal phosphorus due to reduced PL synthesis might both contribute to the inhibition of the biosynthesis of the canonical antibiotics usually produced by this strain.

However, since other specialized metabolites requiring acetyl-CoA as precursors are being produced by the *sco3201* over-expressing strain, the poor acetyl-CoA availability might not be the main cause of the absence of biosynthesis of these antibiotics. The main cause might rather be related to the absence, in the *sco3201* over-expression strain, of the specific physiological signals involved in the triggering of the expression of the cognate biosynthetic pathways. The constitutive oxidative metabolism, characteristic of *S. coelicolor* and that of the *ppk* mutant of *S. lividans* mainly seen in condition of phosphate limitation, is linked to energetic stress (Esnault et al., 2017; Aaron et al., 2020; Virolle, 2020). Indeed, genes of the Pho regulon involved in phosphate supply were shown to be poorly expressed in *S. coelicolor* (Aaron et al., 2020) and the *ppk* mutant of *S. lividans* lacks a polyphosphate kinase, an important enzyme involved in the regeneration of ATP from ADP and polyphosphate (Chouayekh and Virolle, 2002; Ghorbel et al., 2006). In order to re-establish their energetic balance, these two strains activate, at least temporarily, their oxidative metabolism (Esnault et al., 2017). Acetyl-CoA is thus used to feed the TCA cycle and cannot be stored as TAG. An oxidative metabolism is known to generate ROS and NOS and the latter were proposed to play a role in the induction of antibiotic biosynthesis in this strain (Esnault et al., 2017; Virolle, 2020) as in other *Streptomyces* (Beites et al., 2011, 2015; Miranda et al., 2014; Prajapati et al., 2019). These bio-active molecules were proposed to fulfill specific functions in the producing bacteria (Esnault et al., 2017; Virolle, 2020). For instance, CDA and RED were proposed to create damage to the membrane contributing to cell death and lysis of a fraction of the population (Esnault et al., 2017; Tenconi et al., 2018; Virolle, 2020). This would provide nutriments, and especially phosphate, to support the activation of the oxidative metabolism of the surviving population. Furthermore, since the onset of ACT biosynthesis was shown to coincide with an abrupt drop in the intracellular ATP concentration in *S. coelicolor*, ACT, as other molecules possessing quinone groups (melanine, humic acid ...), was proposed to act as electron acceptor (Esnault et al., 2017). ACT would capture electrons of the respiratory chain and doing so would reduce oxidative stress as well as respiration efficiency to reduce ATP generation in order to adjust it to phosphate scarcity (Esnault et al., 2017; Virolle, 2020).

We propose that the activation of the oxidative metabolism that takes place in the native and control strains of *S. coelicolor* does not occur in the strain over-expressing *sco3201*. In that strain, acetyl-CoA availability is probably low since it is stored as TAG and its generation *via* FA degradation is down-regulated. This would impair sufficient feeding of the TCA cycle to support

Annexe VII.

L'inhibition de la production d'antibiotiques chez Streptomyces coelicolor surexprimant le régulateur TetR SCO3201 est corrélée aux modifications du lipidome de la souche

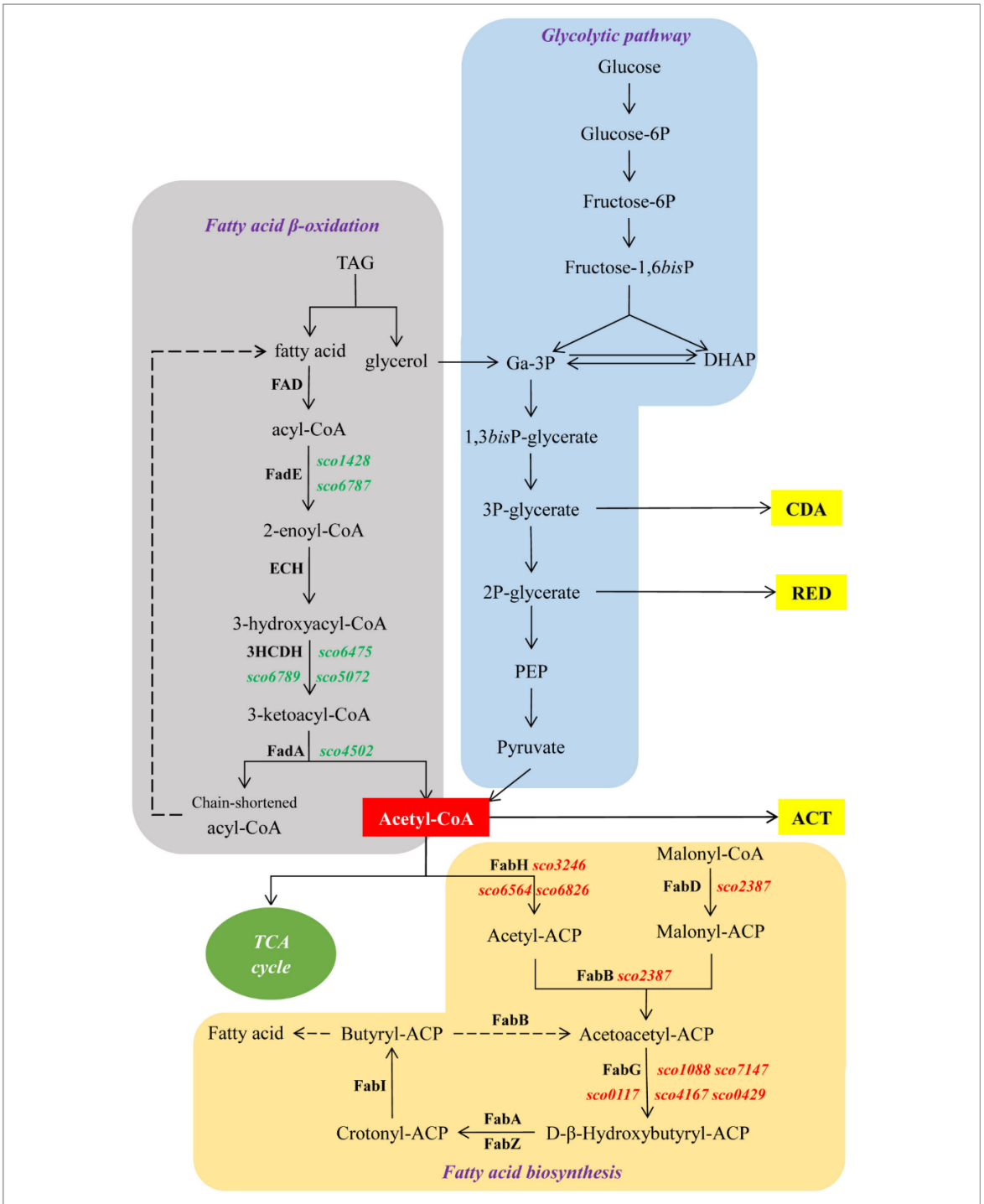

FIGURE 6 | Schematic representation of central metabolic pathways of *S. coelicolor*. In green and red, genes up- and down-regulated in M145/pWHM3-*sco3201*, respectively. Dashed arrows indicate multiple reactions.

an active oxidative metabolism. Furthermore, a putatively higher Pi availability due to reduced PL synthesis, might contribute to repress antibiotic biosynthesis in *Streptomyces* (Martin and Liras, 2012). This might be due to the fact that the activation of the oxidative metabolism does not take place in conditions of phosphate abundance, as demonstrated in the *ppk* mutant of *S. lividans* (Chouayekh and Virolle, 2002). Low acetyl-CoA availability and possibly also enhanced Pi availability are proposed to impede the activation of the oxidative metabolism of this strain. In consequence, the signals triggering the expression of the antibiotic biosynthetic pathways are not generated in this strain and the expression of these pathways is not activated. The hypothesis of the poor activation of the oxidative metabolism of this strain is supported by the fact that the expression of most genes of the TCA cycle was down-regulated in M145/pWHM3-*sco3201*, at least at 36 h (**Table 1**). In consequence, TCA might not provide sufficient precursors for amino acids biosynthesis and the expression of genes involved in amino acids metabolism as well as that of genes belonging to the clusters directing the biosynthesis of the antibiotics CDA and RED, was also down-regulated (**Figure 3**).

In contrast, genes of the biosynthetic pathways directing the synthesis of the carotenoid pigment, isorenieratene, the yellow pigment coelimycin P1 and of another polyketide encoded by the genes *sco6826-sco6827* were highly expressed in the *sco3201* over-expressing strain (**Figure 3**). The expression of these pathways is likely to be related to the specific physiological state of this strain. We propose that the strain over-expressing *sco3201* is depleted in NADPH since active fatty acid and thus TAG biosynthesis consumes NADPH and the latter is not regenerated by fatty acid degradation since *fad* genes expression was shown to be down-regulated in this strain. NADPH is a crucial co-factor for the activity of thioredoxins, enzymes involved in the reduction of non-native disulfide bonds formed in proteins in conditions of oxidative stress (Lu and Holmgren, 2014). Its consumption for other purpose might lead to the raise of a specific oxidative stress that might be responsible for the onset of the biosynthesis of isorenieratene, a carotenoid pigment known to possess anti-oxidant function (Galasso et al., 2017; Chen et al., 2019). The concomitant strong expression of the CPK cluster directing the synthesis of coelimycin P1 (Bednarz et al., 2019) and of another polyketide (*sco6826-sco6827*) in the *sco3201* over-expressing strain suggests that these molecules might have similar anti-oxidant function.

At last, it is noteworthy that whereas the expression of most biosynthetic genes of the CDA, RED, and ACT clusters was lower in M145/pWHM3-*sco3201* than in M145/pWHM3, the expression of their pathway-specific transcriptional activators (encoded by *cdaR*, *redD*, *redZ,* and *actII-ORF4*) remained at a similar level in both strains (**Figure 3**). This suggested that, these regulators are present but unable to fulfill their regulatory function in M145/pWHM3-*sco3201*. To be functional, these cluster-situlated regulators (CSR) require the binding of specific ligands that would be depleted in the *sco3201* over-expressing strain. Several reports in the literature mention that biosynthetic intermediates or even end-products of biosynthetic pathways interact with CSR and auto-control either positively, if poorly abundant, or negatively, if highly abundant, the expression of the corresponding pathway (Kong et al., 2019). If the expression level of the biosynthetic pathways is null in the strain over-expressing *sco3201,* positive regulation by intermediates or end products of the pathway cannot take place. Furthermore, gamma-butyrolactone synthetized by ScbA was shown to play a positive role in the regulation of the expression of the RED and ACT clusters (Takano et al., 2001; D'Alia et al., 2011) and our previous work indicated that SCO3201 represses *scbA* expression at least at early time points (Xu et al., 2010). A reduced butyrolactone synthesis in the *sco3201* over-expressing strain may thus also account for low ability of this strain to produce these antibiotics.

CONCLUSION

Our study contributed to elucidate the molecular processes underlying the inhibition of production of the canonical antibiotics usually produced by *S. coelicolor* in the strain over-expressing the TetR-regulator SCO3201. The absence of synthesis of these molecules was clearly correlated with an enhanced TAG content and a reduced PL content of this strain. This resulted into reduced acetyl-CoA availability as well as possibly enhanced internal phosphate availability that would preclude the activation of the oxidative metabolism of this strain that is thought to generate signaling molecules triggering the biosynthesis of the canonical antibiotics. Altogether, our results thus suggest that impaired TAG biosynthesis or enhanced TAG degradation would enhance acetyl-CoA availability and thus improve the feeding of the TCA cycle to support an active oxidative metabolism. Such strategies are promising to enhance antibiotic biosynthesis in *Streptomyces* species as already demonstrated by several published studies (Banchio and Gramajo, 2002; Foley et al., 2009; Craney et al., 2012; Chen et al., 2020).

DATA AVAILABILITY STATEMENT

The datasets presented in this study can be found in online repositories. The names of the repository/repositories and accession number(s) can be found in the article/**Supplementary Material**.

AUTHOR CONTRIBUTIONS

JZ contributed to experimental materials and reagents, execution of the experiments, and data management and reporting. QL, SA, and CL were involved in managing experimental materials and reagents and execution of the experiments. ZX executed the experiments. MC helped with data management and interpretation and literature review. QZ provided personnel, environmental and financial support, tools and instruments that were vital for the project, and constructed idea or hypothesis for research and manuscript. MD executed the experiments, managed and interpreted the data. PC contributed to data management and interpretation, reviewed the manuscript before submission for both grammar and intellectual content. M-JV

supervised the course of the project or article and reviewed the manuscript before submission. DX constructed idea and hypothesis for research, logical interpretation of the results, and constructed and drafted the whole manuscript. All authors contributed to the article and approved the submitted version.

FUNDING

This work was supported by the National Natural Science Foundation of China (No. 31300046), Guangdong Basic and Applied Basic Research Foundation (Nos. 2019A1515011791 and 2019A1515012112), the Natural Science Foundation of Guangdong Province (No. 2018A030313578), the Science and Technology Planning Project of Guangdong Province (No. [2019]170), the University Paris-Saclay, the CNRS, and the ANR-17-ASTR-0018 (Innovantibio).

SUPPLEMENTARY MATERIAL

The Supplementary Material for this article can be found online at: https://www.frontiersin.org/articles/10.3389/fmicb.2020.01399/full#supplementary-material

REFERENCES

Aaron, M.-O., Henry, C., Lejeune, C., David, M., and Virolle, M.-J. (2020). Expression of genes of the Pho regulon is altered in *Streptomyces coelicolor*. *Sci. Rep.* 10:8492.

Abreu, S., Solgadi, A., and Chaminade, P. (2017). Optimization of normal phase chromatographic conditions for lipid analysis and comparison of associated detection techniques. *J. Chromatogr. A* 1514, 54–71. doi: 10.1016/j.chroma.2017.07.063

Ahn, S. K., Tahlan, K., Yu, Z., and Nodwell, J. (2007). Investigation of transcription repression and small-molecule responsiveness by TetR-like transcription factors using a heterologous *Escherichia coli*-based assay. *J. Bacteriol.* 189, 6655–6664. doi: 10.1128/JB.00717-07

Arabolaza, A., D'Angelo, M., Comba, S., and Gramajo, H. (2010). FasR, a novel class of transcriptional regulator, governs the activation of fatty acid biosynthesis genes in *Streptomyces coelicolor*. *Mol. Microbiol.* 78, 47–63. doi: 10.1111/j.1365-2958.2010.07274.x

Banchio, C., and Gramajo, H. (2002). A stationary-phase acyl-coenzyme A synthetase of *Streptomyces coelicolor* A3(2) is necessary for the normal onset of antibiotic production. *Appl. Environ. Microbiol.* 68, 4240–4246. doi: 10.1128/aem.68.9.4240-4246.2002

Baral, B., Akhgari, A., and Metsa-Ketela, M. (2018). Activation of microbial secondary metabolic pathways: avenues and challenges. *Synth. Syst. Biotechnol.* 3, 163–178. doi: 10.1016/j.synbio.2018.09.001

Barka, E. A., Vatsa, P., Sanchez, L., Gaveau-Vaillant, N., Jacquard, C., Meier-Kolthoff, J. P., et al. (2016). Taxonomy, physiology, and natural products of actinobacteria. *Microbiol. Mol. Biol. Rev.* 80, 1–43. doi: 10.1128/MMBR.00019-15

Bednarz, B., Kotowska, M., and Pawlik, K. J. (2019). Multi-level regulation of coelimycin synthesis in *Streptomyces coelicolor* A3(2). *Appl. Microbiol. Biotechnol.* 103, 6423–6434. doi: 10.1007/s00253-019-09975-w

Beites, T., Oliveira, P., Rioseras, B., Pires, S. D., Oliveira, R., Tamagnini, P., et al. (2015). *Streptomyces natalensis* programmed cell death and morphological differentiation are dependent on oxidative stress. *Sci. Rep.* 5:12887. doi: 10.1038/srep12887

Beites, T., Pires, S. D., Santos, C. L., Osorio, H., Moradas-Ferreira, P., and Mendes, M. V. (2011). Crosstalk between ROS homeostasis and secondary metabolism in *S. natalensis* ATCC 27448: modulation of pimaricin production by intracellular ROS. *PLoS One* 6:e27472. doi: 10.1371/journal.pone.0027472

Bentley, S. D., Chater, K. F., Cerdeno-Tarraga, A. M., Challis, G. L., Thomson, N. R., James, K. D., et al. (2002). Complete genome sequence of the model actinomycete *Streptomyces coelicolor* A3(2). *Nature* 417, 141–147. doi: 10.1038/417141a

Bobek, J., Smidova, K., and Cihak, M. (2017). A waking review: old and novel insights into the spore germination in *Streptomyces*. *Front. Microbiol.* 8:2205. doi: 10.3389/fmicb.2017.02205

Challis, G. L., and Hopwood, D. A. (2003). Synergy and contingency as driving forces for the evolution of multiple secondary metabolite production by *Streptomyces* species. *Proc. Natl. Acad. Sci. U.S.A.* 100(Suppl. 2), 14555–14561. doi: 10.1073/pnas.1934677100

Chater, K. F. (2006). *Streptomyces* inside-out: a new perspective on the bacteria that provide us with antibiotics. *Philos. Trans. R. Soc. Lond. B Biol. Sci.* 361, 761–768. doi: 10.1098/rstb.2005.1758

Chen, Y., Guo, M., Yang, J., Chen, J., Xie, B., and Sun, Z. (2019). Potential TSPO ligand and photooxidation quencher isorenieratene from Arctic Ocean *Rhodococcus* sp. *B7740*. *Mar. Drugs* 17:316. doi: 10.3390/md17060316

Chen, Y., Metz, J., Miller-Xavier, R. K., and Wang, G. (2020). Unlocking a new target for streptomycetes strain improvement. *Synth. Syst. Biotechnol.* 5, 33–34. doi: 10.1016/j.synbio.2020.02.001

Chouayekh, H., and Virolle, M. J. (2002). The polyphosphate kinase plays a negative role in the control of antibiotic production in *Streptomyces lividans*. *Mol. Microbiol.* 43, 919–930. doi: 10.1046/j.1365-2958.2002.02557.x

Craney, A., Ozimok, C., Pimentel-Elardo, S. M., Capretta, A., and Nodwell, J. R. (2012). Chemical perturbation of secondary metabolism demonstrates important links to primary metabolism. *Chem. Biol.* 19, 1020–1027. doi: 10.1016/j.chembiol.2012.06.013

Cuthbertson, L., and Nodwell, J. R. (2013). The TetR family of regulators. *Microbiol. Mol. Biol. Rev.* 77, 440–475. doi: 10.1128/MMBR.00018-13

D'Alia, D., Eggle, D., Nieselt, K., Hu, W. S., Breitling, R., and Takano, E. (2011). Deletion of the signalling molecule synthase ScbA has pleiotropic effects on secondary metabolite biosynthesis, morphological differentiation and primary metabolism in *Streptomyces coelicolor* A3(2). *Microb. Biotechnol.* 4, 239–251. doi: 10.1111/j.1751-7915.2010.00232.x

Dixon, R. W., and Peterson, D. S. (2002). Development and testing of a detection method for liquid chromatography based on aerosol charging. *Anal. Chem.* 74, 2930–2937. doi: 10.1021/ac011208l

Esnault, C., Dulermo, T., Smirnov, A., Askora, A., David, M., Deniset-Besseau, A., et al. (2017). Strong antibiotic production is correlated with highly active oxidative metabolism in *Streptomyces coelicolor* M145. *Sci. Rep.* 7:200. doi: 10.1038/s41598-017-00259-9

Feitelson, J. S., Malpartida, F., and Hopwood, D. A. (1985). Genetic and biochemical characterization of the red gene cluster of *Streptomyces coelicolor* A3(2). *J. Gen. Microbiol.* 131, 2431–2441. doi: 10.1099/00221287-131-9-2431

Flardh, K., and Buttner, M. J. (2009). *Streptomyces* morphogenetics: dissecting differentiation in a filamentous bacterium. *Nat. Rev. Microbiol.* 7, 36–49. doi: 10.1038/nrmicro1968

Folch, J., Lees, M., and Sloane Stanley, G. H. (1957). A simple method for the isolation and purification of total lipides from animal tissues. *J. Biol. Chem.* 226, 497–509.

Foley, T. L., Young, B. S., and Burkart, M. D. (2009). Phosphopantetheinyl transferase inhibition and secondary metabolism. *FEBS J.* 276, 7134–7145. doi: 10.1111/j.1742-4658.2009.07425.x

Galasso, C., Corinaldesi, C., and Sansone, C. (2017). Carotenoids from marine organisms: biological functions and industrial applications. *Antioxidants* 6:96. doi: 10.3390/antiox6040096

Annexe VII.

L'inhibition de la production d'antibiotiques chez Streptomyces coelicolor surexprimant le régulateur TetR SCO3201 est corrélée aux modifications du lipidome de la souche

Ghorbel, S., Smirnov, A., Chouayekh, H., Sperandio, B., Esnault, C., Kormanec, J., et al. (2006). Regulation of *ppk* expression and in vivo function of Ppk in *Streptomyces lividans* TK24. *J. Bacteriol.* 188, 6269–6276. doi: 10.1128/JB.00202-06

Granozzi, C., Billetta, R., Passantino, R., Sollazzo, M., and Puglia, A. M. (1990). A breakdown in macromolecular synthesis preceding differentiation in *Streptomyces coelicolor* A3(2). *J. Gen. Microbiol.* 136, 713–716. doi: 10.1099/00221287-136-4-713

Hojati, Z., Milne, C., Harvey, B., Gordon, L., Borg, M., Flett, F., et al. (2002). Structure, biosynthetic origin, and engineered biosynthesis of calcium-dependent antibiotics from *Streptomyces coelicolor*. *Chem. Biol.* 9, 1175–1187. doi: 10.1016/s1074-5521(02)00252-1

Jeong, Y., Kim, J. N., Kim, M. W., Bucca, G., Cho, S., Yoon, Y. J., et al. (2016). The dynamic transcriptional and translational landscape of the model antibiotic producer *Streptomyces coelicolor* A3(2). *Nat. Commun.* 7:11605. doi: 10.1038/ncomms11605

Kelemen, G. H., Brian, P., Flärdh, K., Chamberlin, L., Chater, K. F., and Buttner, M. J. (1998). Developmental regulation of transcription of *whiE*, a locus specifying the polyketide spore pigment in *Streptomyces coelicolor* A3 (2). *J. Bacteriol.* 180, 2515–2521. doi: 10.1128/jb.180.9.2515-2521.1998

Kong, D., Wang, X., Nie, J., and Niu, G. (2019). Regulation of antibiotic production by signaling molecules in *Streptomyces*. *Front. Microbiol.* 10:2927. doi: 10.3389/fmicb.2019.02927

Le Marechal, P., Decottignies, P., Marchand, C. H., Degrouard, J., Jaillard, D., Dulermo, T., et al. (2013). Comparative proteomic analysis of *Streptomyces lividans* Wild-Type and *ppk* mutant strains reveals the importance of storage lipids for antibiotic biosynthesis. *Appl. Environ. Microbiol.* 79, 5907–5917. doi: 10.1128/AEM.02280-13

Liu, G., Chater, K. F., Chandra, G., Niu, G., and Tan, H. (2013). Molecular regulation of antibiotic biosynthesis in *Streptomyces*. *Microbiol. Mol. Biol. Rev.* 77, 112–143. doi: 10.1128/MMBR.00054-12

Lu, J., and Holmgren, A. (2014). The thioredoxin antioxidant system. *Free Radic. Biol. Med.* 66, 75–87. doi: 10.1016/j.freeradbiomed.2013.07.036

Malpartida, F., and Hopwood, D. A. (1986). Physical and genetic characterisation of the gene cluster for the antibiotic actinorhodin in *Streptomyces coelicolor* A3(2). *Mol. Gen. Genet.* 205, 66–73. doi: 10.1007/bf02428033

Manteca, A., Sanchez, J., Jung, H. R., Schwämmle, V., and Jensen, O. N. (2010). Quantitative proteomics analysis of *Streptomyces coelicolor* development demonstrates that onset of secondary metabolism coincides with hypha differentiation. *Mol. Cell. Proteomics* 9, 1423–1436. doi: 10.1074/mcp.M900449-MCP200

Martin, J. F., and Liras, P. (2012). Cascades and networks of regulatory genes that control antibiotic biosynthesis. *Subcell. Biochem.* 64, 115–138. doi: 10.1007/978-94-007-5055-5_6

Mendez, C., Brana, A. F., Manzanal, M. B., and Hardisson, C. (1985). Role of substrate mycelium in colony development in *Streptomyces*. *Can. J. Microbiol.* 31, 446–450. doi: 10.1139/m85-083

Menendez-Bravo, S., Paganini, J., Avignone-Rossa, C., Gramajo, H., and Arabolaza, A. (2017). Identification of FadAB complexes involved in fatty acid beta-oxidation in *Streptomyces coelicolor* and construction of a triacylglycerol overproducing strain. *Front. Microbiol.* 8:1428. doi: 10.3389/fmicb.2017.01428

Miranda, R. U., Gomez-Quiroz, L. E., Mendoza, M., Perez-Sanchez, A., Fierro, F., and Barrios-Gonzalez, J. (2014). Reactive oxygen species regulate lovastatin biosynthesis in *Aspergillus terreus* during submerged and solid-state fermentations. *Fungal Biol.* 118, 979–989. doi: 10.1016/j.funbio.2014.09.002

Pereira, S. F., Goss, L., and Dworkin, J. (2011). Eukaryote-like serine/threonine kinases and phosphatases in bacteria. *Microbiol. Mol. Biol. Rev.* 75, 192–212. doi: 10.1128/MMBR.00042-10

Petrickova, K., and Petricek, M. (2003). Eukaryotic-type protein kinases in *Streptomyces coelicolor*: variations on a common theme. *Microbiology* 149(Pt 7), 1609–1621. doi: 10.1099/mic.0.26275-0

Prajapati, D., Kumari, N., Dave, K., Chatupale, V., and Pohnerkar, J. (2019). Chromomycin, an antibiotic produced by *Streptomyces flaviscleroticus* might play a role in the resistance to oxidative stress and is essential for viability in stationary phase. *Environ. Microbiol.* 21, 814–826. doi: 10.1111/1462-2920.14515

Ramos, J. L., Martinez-Bueno, M., Molina-Henares, A. J., Teran, W., Watanabe, K., Zhang, X., et al. (2005). The TetR family of transcriptional repressors. *Microbiol. Mol. Biol. Rev.* 69, 326–356. doi: 10.1128/MMBR.69.2.326-356.2005

Revill, W. P., Bibb, M. J., Scheu, A. K., Kieser, H. J., and Hopwood, D. A. (2001). Beta-ketoacyl acyl carrier protein synthase III (FabH) is essential for fatty acid biosynthesis in *Streptomyces coelicolor* A3(2). *J. Bacteriol.* 183, 3526–3530. doi: 10.1128/JB.183.11.3526-3530.2001

Rodriguez, H., Rico, S., Diaz, M., and Santamaria, R. I. (2013). Two-component systems in *Streptomyces*: key regulators of antibiotic complex pathways. *Microb. Cell. Fact.* 12:127. doi: 10.1186/1475-2859-12-127

Romero-Rodriguez, A., Robledo-Casados, I., and Sanchez, S. (2015). An overview on transcriptional regulators in *Streptomyces*. *Biochim. Biophys. Acta* 1849, 1017–1039. doi: 10.1016/j.bbagrm.2015.06.007

Ryding, N. J., Anderson, T. B., and Champness, W. C. (2002). Regulation of the *Streptomyces coelicolor* calcium-dependent antibiotic by *absA*, encoding a cluster-linked two-component system. *J. Bacteriol.* 184, 794–805. doi: 10.1128/jb.184.3.794-805.2002

Takano, E., Chakraburtty, R., Nihira, T., Yamada, Y., and Bibb, M. J. (2001). A complex role for the gamma-butyrolactone SCB1 in regulating antibiotic production in *Streptomyces coelicolor* A3(2). *Mol. Microbiol.* 41, 1015–1028. doi: 10.1046/j.1365-2958.2001.02562.x

Takano, E., Gramajo, H. C., Strauch, E., Andres, N., White, J., and Bibb, M. J. (1992). Transcriptional regulation of the *redD* transcriptional activator gene accounts for growth-phase-dependent production of the antibiotic undecylprodigiosin in *Streptomyces coelicolor* A3(2). *Mol. Microbiol.* 6, 2797–2804. doi: 10.1111/j.1365-2958.1992.tb01459.x

Tenconi, E., Traxler, M. F., Hoebreck, C., van Wezel, G. P., and Rigali, S. (2018). Production of prodiginines is part of a programmed cell death process in *Streptomyces coelicolor*. *Front. Microbiol.* 9:1742. doi: 10.3389/fmicb.2018.01742

Uguru, G. C., Stephens, K. E., Stead, J. A., Towle, J. E., Baumberg, S., and McDowall, K. J. (2005). Transcriptional activation of the pathway-specific regulator of the actinorhodin biosynthetic genes in *Streptomyces coelicolor*. *Mol. Microbiol.* 58, 131–150. doi: 10.1111/j.1365-2958.2005.04817.

van der Meij, A., Worsley, S. F., Hutchings, M. I., and van Wezel, G. P. (2017). Chemical ecology of antibiotic production by actinomycetes. *FEMS Microbiol. Rev.* 41, 392–416. doi: 10.1093/femsre/fux005

Vara, J., Lewandowska-Skarbek, M., Wang, Y. G., Donadio, S., and Hutchinson, C. R. (1989). Cloning of genes governing the deoxysugar portion of the erythromycin biosynthesis pathway in *Saccharopolyspora erythraea* (*Streptomyces erythreus*). *J. Bacteriol.* 171, 5872–5881. doi: 10.1128/jb.171.11.5872-5881.1989

Virolle, M. J. (2020). A challenging view: antibiotics play a role in the regulation of the energetic metabolism of the producing bacteria. *Antibiotics* 9:83. doi: 10.3390/antibiotics9020083

Wei, J., He, L., and Niu, G. (2018). Regulation of antibiotic biosynthesis in actinomycetes: perspectives and challenges. *Synth. Syst. Biotechnol.* 3, 229–235. doi: 10.1016/j.synbio.2018.10.005

White, J., and Bibb, M. (1997). *bldA* dependence of undecylprodigiosin production in *Streptomyces coelicolor* A3(2) involves a pathway-specific regulatory cascade. *J. Bacteriol.* 179, 627–633. doi: 10.1128/jb.179.3.627-633.1997

Worthen, D. B. (2008). *Streptomyces* in nature and medicine: the antibiotic makers. *J. History Med. Allied Sci.* 63, 273–274. doi: 10.1093/jhmas/jrn016

Xu, D., Seghezzi, N., Esnault, C., and Virolle, M. J. (2010). Repression of antibiotic production and sporulation in *Streptomyces coelicolor* by overexpression of a TetR family transcriptional regulator. *Appl. Environ. Microbiol.* 76, 7741–7753. doi: 10.1128/AEM.00819-10

Xu, D., Waack, P., Zhang, Q., Werten, S., Hinrichs, W., and Virolle, M. J. (2014). Structure and regulatory targets of SCO3201, a highly promiscuous TetR-like

regulator of *Streptomyces coelicolor* M145. *Biochem. Biophys. Res. Commun.* 450, 513–518. doi: 10.1016/j.bbrc.2014.06.003

Yang, S. Y., Li, J. M., He, X. Y., Cosloy, S. D., and Schulz, H. (1988). Evidence that the *fadB* gene of the *fadAB* operon of *Escherichia coli* encodes 3-hydroxyacyl-coenzyme A (CoA) epimerase, delta 3-cis-delta 2-trans-enoyl-CoA isomerase, and enoyl-CoA hydratase in addition to 3-hydroxyacyl-CoA dehydrogenase. *J. Bacteriol.* 170, 2543–2548. doi: 10.1128/jb.170.6.2543-2548.1988

Yu, Z., Reichheld, S. E., Savchenko, A., Parkinson, J., and Davidson, A. R. (2010). A comprehensive analysis of structural and sequence conservation in the TetR family transcriptional regulators. *J. Mol. Biol.* 400, 847–864. doi: 10.1016/j.jmb.2010.05.062

Conflict of Interest: The authors declare that the research was conducted in the absence of any commercial or financial relationships that could be construed as a potential conflict of interest.

Copyright © 2020 Zhang, Liang, Xu, Cui, Zhang, Abreu, David, Lejeune, Chaminade, Virolle and Xu. This is an open-access article distributed under the terms of the Creative Commons Attribution License (CC BY). The use, distribution or reproduction in other forums is permitted, provided the original author(s) and the copyright owner(s) are credited and that the original publication in this journal is cited, in accordance with accepted academic practice. No use, distribution or reproduction is permitted which does not comply with these terms.

3. Conclusion

Les analyses menées par LC-Corona-CAD® ont montré que la souche surexprimant SCO3201 présentait des teneurs en TGs, DGs et PA plus importantes que la souche témoin contenant le plasmide vide. Les teneurs en DGs et PA sont expliquées par le fait que ces lipides sont des précurseurs des TGs. Au contraire, les teneurs en antibiotiques (RED et REDox) et en PLs (autres que PA) étaient toutes plus faibles.

Ces observations ont pu être corrélées avec la régulation à la hausse et à la baisse de certains gènes impliqués respectivement dans la biosynthèse des acides gras (fab) et la dégradation (fad), indiquant un contrôle direct ou indirect de l'expression de ces gènes par SCO3201.

L'accumulation de TGs suggère que les FAs sont consommés pour la synthèse des TGs. Cela suggère également que la dégradation des FAs pour produire de l'acétyl-CoA est réduite. Or la réduction de la disponibilité de l'acétyl-CoA et une disponibilité accrue du phosphate interne est connue pour empêcher l'activation du métabolisme oxydatif de cette souche censée générer des molécules de signalisation déclenchant la biosynthèse d'antibiotiques.

Nos résultats suggèrent donc qu'une amélioration de la biosynthèse des antibiotiques chez *Streptomyces* serait possible grâce à une altération de la biosynthèse des TGs ou une dégradation accrue des TGs. Cela améliorerait la disponibilité de l'acétyl-CoA et alimenterait le cycle de Krebs pour soutenir un métabolisme oxydatif actif. De telles stratégies sont prometteuses pour améliorer la biosynthèse des antibiotiques chez *Streptomyces*, [198,200,202,203].

université PARIS-SACLAY
ÉCOLE DOCTORALE
Sciences chimiques : molécules, matériaux, instrumentation et biosystèmes

Titre : Détermination de la composition des acyles gras des glycérolipides et glycérophospholipides par techniques séparatives couplées à la spectrométrie de masse haute résolution..... ....

Mots clés : acyles gras ; triacylglycérols ; phospholipides ; lipides ; chromatographie ; spectrométrie de masse

Résumé : Les acyles gras (FAs) représentent le principal élément constitutif des lipides complexes (glycérolipides / phospholipides / sphingolipides). Leur structure varie en fonction de leur fonctionnalisation, nombre de carbones, nombre et position d'insaturations. Cette variété est à l'origine du très grand nombre d'espèces lipidiques et de la complexité de leur analyse.

Les travaux menés au cours de cette thèse ont démontré, au travers de trois publications, que l'évaluation de la distribution FAs des glycérolipides et phospholipides était accessible grâce à l'intensité des ions fragments $[monoacylglycérol+H-H_2O]^+$ (ions B) produits en source APPI/APCI-HRMS, lors du couplage à la FIA ou la NPLC.

Les bases de ce nouveau concept ont été posées via l'étude des triglycérides d'huiles végétales.
Il a été observé que la distribution des intensités des ions B était directement reliée à la distribution des FAs, sauf pour le FA polyinsaturé C18:3.
Des coefficients de pondération des intensités des ions B ont été calculés pour compenser les différences d'ionisation. Globalement, un coefficient deux fois plus important a été appliqué aux intensités des ions B(18 :3) pour compenser sa plus faible intensité.

Le concept a ensuite été étendu aux phospholipides (PLs). Pour les extraits contenant uniquement des diacyl-PLs, la transposition est également directe. La nature de la tête polaire n'a pas eu d'influence sur la formation des ions B.

Pour les extraits contenant à la fois des diacyl-PLs et des plasmalogènes (fonction éther vinylique) une séparation préalable doit être réalisée. En effet, la formation des ions B n'a pas lieu au même degré pour ces deux sous-classes.
Une hydrolyse par des vapeurs d'acide chlorhydrique a permis de rompre spécifiquement les liaisons éthers vinyliques. Les plasmalogènes sont alors transformés en Lyso-PLs et aldéhydes.
Ces extraits ont également la particularité de contenir des teneurs importantes de FAs polyinsaturées. Par analogie avec l'étude des TGs, un coefficient pondérateur de deux a été appliqué aux intensités des ions B de ces FAs.

Pour accéder à la distribution des alkényls gras des plasmalogènes, un concept similaire à celui des ions B a été mis en œuvre avec succès.
De plus, un schéma de fragmentation a été proposé pour les plasmalogènes PC lors de l'utilisation de la source APCI.

Enfin, notre nouveau concept a été mis en œuvre sur des extraits lipidiques de souches *Yarrowia Lipolytica* (levure oléagineuse) modifiées pour favoriser la production de FAs à chaînes impaires. La distribution des FAs au sein de chaque classe de lipides a été évaluée et le concept a été étendu à deux autres classes de lipide (Diglycérides-DG et glucuronosyl diacylglycerol-GlcADG).